THERMODYNAMICS OF TRANSIENTLY PUMPED CO_2 GAS LASER PLASMAS

BY

MOUAYED AZIZ HASAN

B.Sc. (Mech. Eng.), M. Eng. (Mech. Eng.)

THESIS PRESENTED

FOR THE

DEGREE OF DOCTOR OF PHILOSOPHY

UNDER GENERAL REGULATIONS

MAY 1989

DEPARTMENT OF MECHANICAL ENGINEERING

FACULTY OF ENGINEERING

THE UNIVERSITY OF GLASGOW

ProQuest LLC.
789 East Eisenhower Parkway
P.O. Box 1346
Ann Arbor, MI 48106 – 1346

SYNOPSIS

Pulsed CO_2 lasers pumped by a self-sustained discharge have become very important and practical tools for materials processing. A high mean power pulsed CO_2 laser overcomes the instantaneous power intensity limitations inherent in CW operation which restricts performance, especially in metal machining. Design requirements include : simplicity of construction, reliability , high efficiency, low operating voltage , uniformity of the output beam, and the ability to vary the output parameters over a wide range. A major aim of this dissertation is to provide a fundamental physical understanding and data that will enable effective design.

The discharge parameters (i.e operating value of E/N, mean electron energy,ionisation and attachment coefficients, etc.), the plasma-chemical processes and CO_2 dissociation effects, the output pulse profile and intensity control are studied herein in order to maximise efficiency and optimise laser performance to the requirements of the workpiece.

The comprehensive computer simulations of the electron energy distribution function, discharge plasma parameters, plasma-chemical phenomena occuring in the discharge, and laser kinetic processes produce an exploratory tool that can provide essential data for developing a CO_2 laser capable of processing a wide range of engineering materials.

Experimental work is conducted to confirm the theoretical analysis of the discharge operating parameters.

To

My Wife Mahasin ,and To

My Children Mayada and Marwan

ACKNOWLEDGEMENT

I wish to express my sincere gratitude to Dr. C. R. Chatwin for his valuable advice, inspiration, constructive criticism and encouragement.

I owe a great debt to Professor B. F. Scott, Head of the department of mechanical engineering, for many stimulating discussions and advice throughout this work, and for the facilities provided in the department.

I also wish to thank the members of the Laser Group, in particular Mr. D. W. McDonald and Mr. I. Watson for their help and co-operation.

I am very grateful to my wife for her encouragement and forbearance during this work.

And last, but not least, I wish to acknowledge the financial support from The Government of The Republic of IRAQ, without which this work would not have been possible.

CONTENTS

CONTENT (CONT.).

CONTENT (CONT.).

CONTENT (CONT.).

CONTENT (CONT.).

CONTENT (CONT.).

CONTENT (CONT.).

LIST OF FIGURES

LIST OF FIGURES (CONT.)

LIST OF TABLES

LIST OF GRAPHS

LIST OF GRAPHS (CONT.)

CHAPTER ONE

INTRODUCTION

1.1 GENERAL:

Since laser action was first successfully demonstrated using a crystal of ruby as the active gain medium, solid state and gas systems have been developed to the point where lasers are now practical and economical tools for several industrial applications. New possibilities for improving materials processing (heat treatment, cutting, welding, deposition of special coatings, etc.) are enabled by the use of high power lasers. For laser machining, power intensities in the range 10^9 - 10^{12} w/m^2 are required to generate the necessary non-conduction limited heating. Below 10^9 w/m^2 the surface temperature rise is insufficient to cause significant surface damage; the incident energy is absorbed in a very thin surface layer ($\approx 10^{-8}$ m) resulting in heat treatment. Power intensities above 10^{12} w/m^2 produce highly absorbent plasma, hence energy absorption by the material is significantly reduced.

Laser systems capable of machining applications include both solid state and gas lasers. The two most commonly used lasers for materials processing are the Nd^{3+}:YAG and the CO_2 lasers. The fundamental advantage of solid state lasers is judged to be the combination of their high energy-generation parameters (up to 10 J per pulse, with an average generated power of up to 700 watts) and their ability to operate in various regimes - from ultrashort (picosecond length) pulses

to continuous operation (CW) -along with high power and reliability,[Prokhorov, 1.1]. However, an important drawback in solid state lasers is their low efficiency; a factor that limits mean power and hence applications, [Patel, 1.2].

CW CO_2 lasers are capable of operation in the multi-kilowatt range of output powers and exhibit high efficiency (up to 30 %), [Wilson and Hawkes, 1.3]. However, power intensities generated at the workpiece are below the damage thresholds of many engineering materials. This,together with thermal degradation of the optical system and the very high reflectivities exhibited by metals at the relatively long wavelength of the CO_2 laser, limit the industrial applications of the CW CO_2 lasers.

Consequently, the CO_2 laser can be designed to overcome these limitations by operating in a pulsed mode [Chatwin et al, 1.4]. High output pulse intensities can be generated with plateau powers (10 to 150 kW) and pulse durations controlled and matched to the processing requirements of materials by appropriate selection of: the input electrical pumping pulse, gas composition and pressure, and design parameters of the optical resonator. The relatively low mean output powers (2-5 kW) minimise thermal degradation of the optical system. Furthermore,high pulse repetition frequencies ($\approx$ 10 kHz) permit continuous machining because a steadily evaporating liquid phase ,at the workpiece, can be sustained [Vedenov et al, 1.5]. In addition, the interpulse period is sufficient to prevent the development of a plasma plume on and above the workpiece surface.

1.2 QUALITATIVE REQUIREMENTS FOR A STABLE PULSED CO_2 LASER FOR MATERIALS PROCESSING:

Extensive utilization of laser technology in industry is frequently inhibited by the failure of present day lasers to meet the rigorous requirements of industrial processes. Different industrial processes impose different requirements on the laser parameters, particularly the stability of the output power. For the majority of industrial applications the permissible variation in the laser output power P is in the range $\delta P \leq (3\text{-}5)\times10^{-2}$ P. The most rigorous demands are imposed by the processes of finishing cutting and thermal hardening where the permissible variation in the beam divergence is within -10^{-4} to 10^{-5} rad- for an unevenness of the cutting edge of less than 0.1 mm. For present-day CO_2 lasers, the beam divergence lies in the range 1-10 mrad. The process of welding also imposes strict conditions on the stability of the spatial location of the beam axis ; a fluctuation of the beam axis in the range -10^{-3} to 10^{-4}- is required for a beam axis displacement on the workpiece of less than 0.1 mm [Golubev and Lebedev, 1.6].

Fluctuations in the laser emission characteristics can be caused by an instability of the characteristics of the active medium. The properties of the active medium are determined by the average small signal gain,by the saturation parameter, and by its homogeneity throughout the laser cavity,[Sato and Miura, 1.7].

Inhomogeneities of the temperature hence density and composition of the active medium can arise due to

instabilities of the current in the discharge cavity and of the flow velocity. Furthermore, instability of the chemical composition of the active medium accompanied by variations in the output power can appear for a number of reasons.Since the overwhelming majority of present-day lasers operate with partial (0.1-1 %) continuous replenishment of the active mixture, an instability in the feed of fresh gas components will result in instability.A more serious cause of the power instability arises from a change in the chemical composition of the mixture due to chemical reactions taking place in the discharge,this results in changes in the CO_2 concentrations, gas temperature, rate of relaxation of the upper laser level , etc. It is because of plasma-chemical processes that the active medium gain falls with time; even with continuous gas-mixture replenishment rates of 0.1-1 % which are reasonable from the technical and cost points of view, the output power can fall by 10-20 % with time.

1.3 CHARACTERISTICS OF THE ELECTRIC DISCHARGE CO_2 LASER:

With the increasing realization of the potential of the CO_2 laser, within the broad field of industrial materials processing, there has been a continuing effort to improve its operating power and efficiency. To increase the average power and pulse power it is necessary to increase the gas pressure. However, when the pressure is increased, the glow discharge deteriorates and constriction occurs [Mesyats and Korolev, 1.8]. This leads to a lowering of the output pulse energy and to a consequent reduction in the average laser

power. High pulse repetition frequencies (>10^2 Hz) cause the same problem [Arutyunyan et al, 1.9]. The main cause of the discharge constriction is considered to be due to local temperature gradients which result in an inhomogeneous gas density in the discharge that leads to an inhomogeneous flow of discharge current.

In the discharge cavity the flowing gas mixture, which usually includes CO_2,N_2,and He, is converted into a weakly ionised glow discharge plasma. The mechanism of pumping the CO_2 molecules to the upper laser level (00°1) consists of exciting N_2 and CO_2 molecules by inelastic collisions with the electrons and the transfer of vibrational energy from N_2(v=1) to CO_2 . The near coincidence between the N_2(v=1) level and the CO_2(00°1) level (see figure 1.1) results in a very efficient energy transfer process [Patel, 1.2].

Several factors influence the performance of the pulsed CO_2 laser including the operating voltage, capacitance, gas mixture, pressure ranges for homogeneous discharge, the technique used to excite the gas and the changes in the chemical composition of the gas mixture. An important characteristic of the discharge is the parameter (E/N) which governs the electron energy distribution function (EEDF). Knowledge of the (EEDF) is necessary to obtain a more comprehensive understanding of the discharge kinetic processes and to make possible quantitative predictions of laser performance. The (EEDF) determines the excitation rates and efficiencies of the vibrational levels of CO_2 and N_2.It also determines other discharge plasma parameters ,e.g

ionisation and attachment coefficients, electron mean energy and drift velocity. In the operation of the CO_2 laser one important factor is the ratio $CO_2/(CO_2+N_2)$ which influences the formation of an arc-free discharge [Lavrentyuk et al, 1.10]. A stable discharge is, therefore,important to provide a homogeneous excitation of the active mixture. Several techniques have been used to improve discharge stability, e.g UV pre-ionisation with non-conventional electrodes [Biswas et al, 1.11], X-ray pre-ionisation [Krishnaswamy and Alcock, 1.12] , PIE (photoinitiated , impulse-enhanced , electrically excited) process [Nath et al, 1.13] , high frequency corona discharges [Akiyama et al, 1.14] , semiconductor pre-ionisation system [Stark and Crocker, 1.15], Pre-ionisation by α-particles [Glushchenko and Lavrentyuk, 1.16], and the addition of easily ionisable substances to the laser gas mixture [Aliev et al, 1.17]. The main objective of all these techniques is to provide the minimum sufficient electron density (10^4-10^5) necessary to obtain a homogeneous discharge [Yamabe et al, 1.18]. One of the major factors influencing this, is the oxygen content in the gas mixture. It is known that electrons strongly attach to O_2 molecules,hence the electron density becomes less than is necessary for a homogeneous arc-free discharge. In addition, changes in the chemical composition of the active gas mixture due to plasma-chemical reactions produce several species which have a deleterious effect on the discharge stability, and on the laser output power. Pace and Lacombe [1.19] have shown that the accumulated oxygen produced by

electron impact dissociation of carbon dioxide leads to the formation of large concentrations of negative ions (O^-,CO_3^-, CO_4^-). Nitrogen oxides (NO_x) are also known to easily form negative ions. Discharge instabilities,then, tend to develop due to the imbalance between charged particle production and loss processes in the discharge [Beverly,1.20]. Furthermore, species such as. CO,H_2,and H_2O have significant effects on the population and relaxation processes of the excited states of CO_2 [Smith et al,1.21] and therefore significantly affect the laser kinetic parameters [Siemsen, 1.22].

1.4 SCOPE OF THE PRESENT WORK:

This work is part of a continuing programme in the design and development of a high power, high P.R.F, CO_2 laser for materials processing applications. The following paragraphs summarise the scope of the work herein :

(1) Theoretical simulation of the gas discharge is described in Chapter 2. The Boltzmann transport equation is solved to determine the electron energy distribution function (EEDF). The operating characteristics of the discharge, the fractional power transferred to the various molecular energy levels and the transport parameters are predicted. The presence of CO in the discharge, its effect on the (EEDF) and transport parameters are examined.

(2) Theoretical simulation of the discharge plasma chemistry is considered in Chapter 3. Emphasis is directed toward identification of the most important chemical reactions occuring in the discharge. The dissociation of CO_2 is

examined and its control by gas additives are investigated.

(3) In Chapter 4 an 'eight-energy level' kinetic model is developed to simulate the performance of the CO_2 laser with the presence of CO in the discharge. This model gives profound insight into the kinetic processes occuring in the laser cavity and their relationships to the many interdependent design parameters.

(4) Experimental investigation of the gas discharge operation is presented in Chapter 5 . The operating characteristics of the glow discharge in several gas mixtures are determined; these results verified the predictions from the (EEDF) simulation. The effects of CO addition to the gas mixture on the operating characteristics of the discharge are investigated.

(5) General conclusions and recommendations for further work are given in Chapter 6.

REFERENCES

CHAPTER ONE

1.1 Prokhorov A M -'A new generation of solid-state lasers'- Sov. Phys. USP, Vol. 29 , 1986 (3).

1.2 Patel C K N - ' Lasers - Their Development and Applications at AT&T Bell Laboratories '- IEEE J. Q.E., Vol. 20 ,1984 (561) .

1.3 Wilson J and Hawkes J F B - ' Lasers - Principles and Applications '- Prentice Hall (U.K), 1987.

1.4 Chatwin C R, McDonald D W , and Scott B F -'Design of a High P.R.F Carbon Dioxide Laser for Processing High Damage Threshold Materials'- (to be published) .

1.5 Vedenov A A, Gladush G G, Drobyazko S V, Pavlovich Yu V, and Senatorov Yu M -' Physical laws governing the interaction of pulse-periodic CO_2 laser radiation with metals'- Sov. J. Q.E. , Vol. 15, 1985 (32).

1.6 Golubev V S and Lebedev F V -'Stability of the emission from fast-flow gas discharge industrial CO_2 laser'- Sov. J. Q.E. , Vol. 15, 1985 (437).

1.7 Sato H and Miura Y -' Line Shape Parameter Analysis of Individual Vibrational-Rotational Transitions in a CO_2 Laser Amplifier '- IEEE J. Q.E. , Vol. 19 , 1983 (410).

1.8 Mesyats G A and Korolev Yu D - ' High-pressure volume discharges in gas lasers'- Sov. Phys. USP, Vol. 29, 1986 (57) .

1.9 Arutyunyan R V , Baranov V Yu, Borisov V M, Vinnokhodov A Yu , and Kiryukhin Yu B - ' Influence of electrode processes on the constriction of a volume discharge in pulse-periodic lasers'- Sov. J. Q. E.,Vol.15, 1985(639).

1.10 Lavrentyuk V E, Podmoshenskii I V, and Belyatskii A F - 'Initiation of a self-sustained volume discharge in lasers by radioisotopes'- Sov. J.Q.E,Vol 16, 1986 (950).

1.11 Biswas D J , Abhinandan L, Chatterjee U K,and Nundy U - 'Operation of a UV pre-ionised TEA CO_2 laser utilising non-conventional electrodes'- J. Phys. E: Sci. Instrum., Vol 19, 1986 (372) .

1.12 Krishnaswamy J and Alcock A J -' X-ray preionisation of self-sustained,transverse excitation CO_2 laser discharges'- J. Appl. Phys. , Vol 58, 1985 (1719) .

1.13 Nath A K, Seguin H J J,and Seguin V A -' Optimization Studies of a Multikilowatt PIE CO_2 Laser'- IEEE J. Q.E , Vol 22 , 1986 (268).

1.14 Akiyama H, Takamatsu T, Yamabe C, and Horii K - Suppression of glow-to-arc transition in atmospheric pressure gas discharge of TEA CO_2 laser by high frequency corona discharges'- J. Phys. E: Sci. Instrum., Vol 17 , 1984 (1014).

1.15 Stark D S and Crocker A -' A Sealed, High-CO_2,High-PRF Semiconductor-Preionised TEA Laser Without a Solid Catalyst'- Opt. Commun. , Vol 48, 1984 (337).

1.16 Glushchenko Yu V and Lavrentyuk V E -' Pre-ionisation of a CO_2 laser gas mixture by α particles'- Sov. J. Q.E. ,Vol 16 , 1986 (1340).

1.17 Aliev A A, Appollonov V V, Akhunov N, Prokhorov A M, and Firsov K N -'Stability of a bulk self-sustained discharge in a CO_2-N_2-He mixtures of gases with easily ionizable additives'- Sov. J. Q.E. , Vol 15 ,1985 (700).

1.18 Yamabe C , Matsushita T , Sato S , and Horii K - 'Characteristics of a TEA CO_2 laser preionized by ultraviolet light'- J. Appl. Phys., Vol 51, 1980 (1345).

1.19 Pace P W and Lacombe M -' A Sealed High-Repetition-Rate TEA CO_2 Laser'- IEEE J. Q.E , Vol 14 , 1978 (263).

1.20 Beverly III R E -'Ion-aging effects on the dissociative attachment instability in CO_2 lasers'- Opt. Q.E.,Vol 14, 1982 (501).

1.21 Smith A L S, Sephton J P, and Scott G -'High-peak power extended lifetime sealed TEA CO_2 lasers' J. Phys. E: Sci. Instrum. , Vol 17, 1984 (590).

1.22 Siemsen K J-' Axial gain distribution in a CW CO_2 laser'-' Appl. Optics, Vol 19 , 1980 (818).

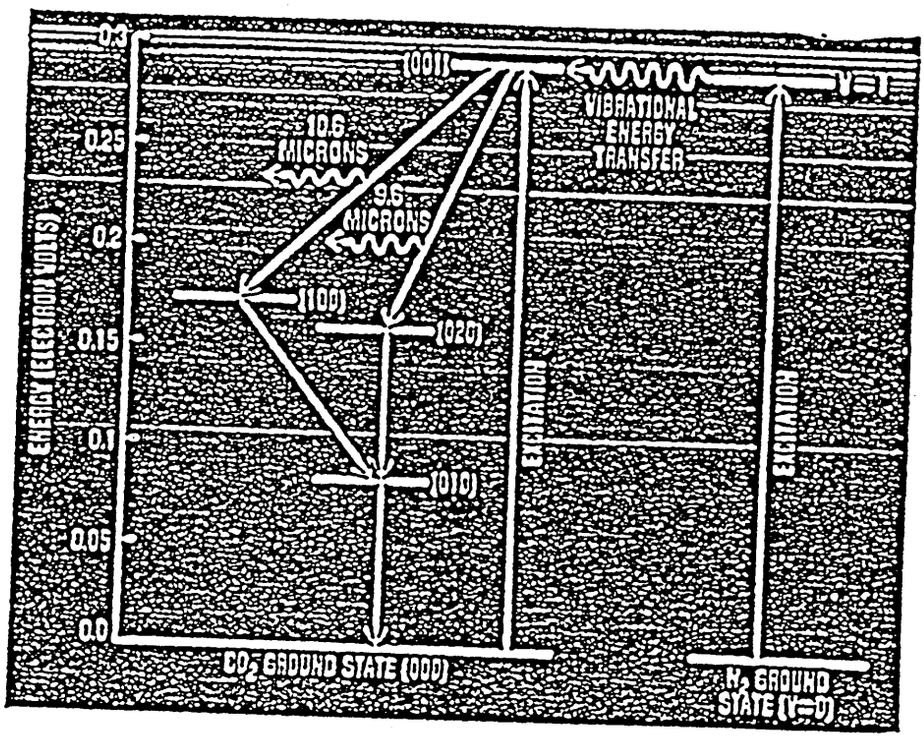

ENERGY LEVEL DIAGRAM FOR CO_2-N_2 SYSTEM [Ref. 1.2]

FIGURE (1.1)

CHAPTER TWO

THEORETICAL ANALYSIS OF THE GAS DISCHARGE PARAMETERS

2.1 INTRODUCTION

Optimal operation of CO_2 Lasers requires a thorough understanding of the gas discharge plasma kinetics: this necessitates a detailed knowledge of the electron energy distribution function (EEDF) . The electron energy distribution determines the fractional power transferred to the various molecular energy levels ,it also determines the various transport parameters which in turn control the development of the gas discharge. Thus, this knowledge is essential for laser performance simulation and the optimisation of output power and efficiency.

Several studies have been carried out to determine swarm parameters in CO_2 mixtures which usually contain CO_2,N_2, and He as their main constituents. The electron energy distribution in the discharge is described by the Boltzmann transport equation. Thus the swarm parameters may be calculated directly from a set of collision cross- sections by numerical solution of this equation. Extensive investigations have been undertaken over the past fifteen years and a number of investigators(Lowke et al [2.1],Sakai et al [2.2], Lakshminarasimha et al [2.3] , Kucukarpaci and Lucas [2.4] , Braglia et al [2.5],Rockwood and Green [2.6]) have used numerical methods to predict swarm parameters in laser gas mixtures in order to estimate the populations of

the laser energy levels. Experimental determination of some of these swarm parameters has been carried out by others (Sierra et al [2.7],Hasegawa et al [2.8],Davies [2.9], Haydon and McIntosh [2.10],Wedding [2.11],Braglia et al [2.12]).

In this chapter a theoretical model is developed to study the gas discharge parameters. It considers the influence of the electron energy distribution function on the transport parameters and the discharge development. The EEDF is determined by solving Boltzmann's transport equation for gas mixtures containing CO_2 ,N_2 ,and He. This model is a modification of that first developed by Smith et al [2.13] to calculate electron vibrational excitation rates for CO_2 gas mixtures . The basic features of the model are that it includes the effects of superelastic collisions on the EEDF. These effects were neglected in the work of Khahra [2.14]. It also includes the ionisation and electron attachment processes for CO_2 and N_2.The following transport parameters: average electron energy,electron drift velocity, ionisation and attachment coefficients are evaluated. The quantity of energy transferred through various excitation paths by collisions of electrons with molecules, and excitation efficiencies for different vibrational levels in the gas mixtures are also determined. The conditions that maximize the rate at which energy is transferred into vibrational excitation of the upper laser level are investigated. The operating characteristics of the gas discharge are predicted,and finally the effects of the addition of carbon

monoxide to the gas mixture on the distribution function and transport parameters are examined.This allows a profound understanding of the detailed mechanisms occuring within the CO_2 laser discharge,it provides the necessary data for both : simulation of the effects of dissociation , and prediction of the laser output pulse by solution of the molecular rate equations.

2.2 NOMENCLATURE

a attachment coefficient in gas discharge (cm^{-1}).

CS ionisation cross section (cm^2).

CSa attachment cross section (cm^2).

D diffusion coefficient (cm^2/sec).

E electric field (volt/cm).

$\dot{E}$ rate of energy transfer from electric field to electrons ($eV/cm^3.sec$).

e electron charge (1.602×10^{-19} C).

F excitation efficiency.

f electron energy distribution function ($eV^{-1/2}$) .

k_b Boltzmann constant $=1.30826 \times 10^{-23}$ (J/°K).

M mass of a molecule (gram).

m electron mass (gram).

N total molecular number density (cm^{-3}).

n species in the gas mixture.

n_e electron density in the discharge (cm^{-3}).

p gas pressure (Torr).

P_j vibrational excitation power delivered to level j ($eV.cm^3/sec$).

Q_i ionisation cross section (cm^2).

Q^n_j inelastic collision cross section for the jth level of n species in the mixture (cm^2).

Q^n_{-j} superelastic collision cross section for the jth level of n species in the mixture (cm^2).

Q^n_m momentum transfer cross section of species n (cm^2).

T temperature (°K).

t time (sec).

$\bar{U}$ average electron energy (eV).

u electron energy (eV).

u_j energy loss of the jth inelastic process in species n (eV).

V electron velocity (cm/sec).

X^n_j vibrational excitation rate for the jth excited state of species n (cm^3/sec).

V_d electron drift velocity (cm/sec).

ε electron energy (eV).

α ionisation coefficient (cm^{-1}).

μ electron mobilty (cm^2/sec.volt).

δ^n_j fraction of molecules of species n in the jth excited state.

δ_n fraction of molecules number density of species n.

2.3 ELEMENTARY PROCESSES IN CO_2 LASERS:

2.3.1 The CO_2 molecule:

The carbon dioxide molecule can be represented by a linear arrangement of two oxygen atoms and a carbon atom with the carbon atom in the middle. This is shown in figure (2.1). It can vibrate in three different modes, namely, the symmetric mode ($\nu 1$),the bending mode ($\nu 2$),and the asymmetric mode($\nu 3$).When discharge conditions are suitable for CO_2 laser action the principal energy levels are: 667.3 cm^{-1}(0.083 eV), 1285.5 cm^{-1}(0.16 eV) , 1388.3 cm^{-1}(0.17 eV) and 2349.3 cm^{-1} (0.29 eV).These are normally designated as $01^10,02^00,10^00$ and 00^01 respectively (see Appendix 2.I). The lower laser levels 02^00 and 10^00 are in strong Fermi resonance and are almost completely mixed,[Levine, 2.15]. Elementary processes in CO_2 lasers and the basic principles underlying laser action are described in Appendix 2.I.

2.3.2 Population Inversion In CO_2 Lasers:

Population inversion can be achieved by direct electronic excitation of molecules in the gas discharge. It may also be achieved by resonant transfer of energy between molecules in the gas system.

For a carbon dioxide laser , the important interaction between electrons and molecules are the inelastic collisions whereby energy is transferred from energetic electrons to both the CO_2 and N_2 molecules . In the resonant transfer process,the selective excitation of the upper laser

level(00°1) from the ground state by vibrationally excited N_2(V=1) occurs at a very rapid rate(1.9 x 10^4 $Torr^{-1}.sec^{-1}$) because of near coincidence between this level and CO_2(00°1). This resonance transfer produces a mixed state of N_2(v=1) and CO_2(00°1).By comparing the relaxation rate of this mixed state (110 $Torr^{-1}.sec^{-1}$) with that of the upper laser level in a pure CO_2 discharge (367 $Torr^{-1}.sec^{-1}$), it is seen that N_2 serves two purposes , firstly,it helps in the excitation of the upper laser level, and secondly,it increases the effective lifetime of CO_2(00°1). Cheo [2.15] has shown that the addition of a few Torr of N_2 pressure increases the effective lifetime of the upper laser level by almost a factor of two.

The addition of Helium causes an increase in the average electron energy, because helium has none of the inelastic vibrational losses that are present in N_2 and CO_2. This leads to a decrease in direct pumping of the lower laser level and an increase in the excitation of N_2 , hence an increase in the population of the upper laser level. It has been shown [Levine , 2.15] that efficient relaxation of the lower laser level occurs by collision with helium while the upper laser level lifetime is left unaffected.

2.3.3 Excitation Cross Section and Relaxation Rate Constants:

Measurements of rotational and vibrational excitation cross sections of carbon dioxide and nitrogen by inelastic collisions of electrons at low energies (0-3 eV) have been reviewed by Phelps [2.16]. Hake and Phelps [2.17] have shown that there exists a set of four resonances for the vibrational excitation of CO_2 molecules by electrons at 0.08,0.3,0.6, and 0.9 eV. The 0.3,0.6,and 0.9 eV energy loss processes are associated with the three levels of asymmetric mode, and 0.08 eV is associated with the lowest bending mode as shown in figure (2.2). For N_2 the total excitation cross - section has been investigated by Schulze [2.18] who showed that it reaches a maximum value (3×10^{-16} cm^2) at an electron energy of $\approx$ 2.3 eV (see figure (2.3)).

A comprehensive compilation of cross-section data has been made by Kieffer [2.19] for CO_2 ,CO,N_2 ,and He. Kieffer lists cross-section data for other gases. Table (2.1) lists the energy thresholds of 8 vibrational levels, dissociative attachment and ionisation process of CO_2 molecules; 8 vibrational levels and ionisation process of N_2.

Vibrational relaxation in different gas mixtures of CO_2 lasers has been extensively investigated by several workers. Relaxation via collisions are vital in achieving a population inversion in the gas system. A comprehensive survey of relaxation data for important processes in a CO_2 laser system has been made by Taylor and Bitterman [2.20]. Appendix 2.II shows different relaxation processes in CO_2.

2.4 THE BASIS OF THE MATHEMATICAL MODEL:

The mathematical connection between the microscopic behavior of electrons as described by electron-neutral particle scattering cross - sections and the macroscopic behavior of an electron swarm is given through the Boltzmann transport equation which may be written as :

$$\partial f/\partial t - (eE/m)\nabla_v f = (\partial f/\partial t)_{collision} \quad .....(2.1)$$

A detailed analysis of the equation is given by Smith and Thomson [2.21]. For conditions similar to those encountered in CO_2 lasers the Boltzmann equation is reduced to

$$(1/3)(E/N)^2 d/du\{(udf(u)/du)/\sum_n \delta_n Q^n_m(u)\} + 2md/du\{u(\sum_n(\delta_n Q^n_m(u)/M_n)f(u)\} + (2mk_bT/e)d/du\{u^2(\sum_n(\delta_n Q^n_m(u)/M_n))df(u)/du\}$$
$$+ \sum_j \sum_n \{(u+u_n)f(u+u_{jn})\delta_n Q^n_j(u+u_n) - uf(u)\delta_n Q^n_j(u)\}$$
$$+ \sum_j \sum_n \delta^n_j\{(u-u_{jn})f(u-u_{jn})\delta_n Q^n_{-j}(u-u_{jn}) - uf(u)\delta_n Q^n_{-j}(u)\} = 0$$
$$.....(2.2)$$

(see Appendix 2.IV for details).

The electron energy distribution function f(u) in equation (2.2) is normalized such that the fraction of electrons between energy u and u+du is given by $u^{1/2}$ f(u)du. Hence

$$\int_0^\infty u^{1/2} f(u)du = 1 \quad .....(2.3)$$

The first term on the left hand side in equation (2.2) contributes to the energy of the electrons gained from the applied electric field. The second and third terms interpret the elastic collisions of electrons with molecules,while the

fourth term represents the energy lost by electrons to the molecules in an inelastic collision process. The final term contributes to the energy of electrons gained from excited molecules in a superelastic collision process.

Having obtained the electron energy distribution function (EEDF),this can then be used to calculate various transport coefficients (drift velocity , average energy, diffusion coefficient and mobility) .The effective electron vibrational excitation rate for the jth excited state of species n is given by:

$$X^n{}_j=(2e/m)^{1/2}(u_{jn}/u_{1n})\int_0^\infty uf(u)Q^n{}_j(u)du \qquad .....(2.4)$$

In addition,the mobility (μ),diffusion coefficient (D), and drift velocity (V_d) are given respectively by:

$$\mu= (-1/3)(2e/m)^{1/2}\int_0^\infty (u/\Sigma_n\delta_n Q^n{}_m(u))(df/du)du \qquad .....(2.5)$$

$$D=(1/3)(2e/m)^{1/2}\int_0^\infty ((uf(u))/(\Sigma_n\delta_n Q^n{}_m(u)))du \qquad .....(2.6)$$

$$V_d=\mu E \qquad .....(2.7)$$

while the average electron energy is given by:

$$\bar{U}=(2/3)\int_0^\infty u^{3/2}f(u)du \qquad .....(2.8)$$

The Boltzmann transport equation (2.2) can be written in terms of the number density $n_e(u)$ of electrons with energy in the range u to u+du as:

$$n_e(u) = N\, u^{1/2}f(u) \qquad .....(2.9)$$

and the electron energy,ε, is specified in electron volts by

$$eu=\varepsilon \qquad .....(2.10)$$

Using equations (2.9) and (2.10), and partitioning the electron energy axis into K cells of width ε , the number density of electrons with energy between $(k-1)\Delta\varepsilon\equiv\varepsilon$ and $k\Delta\varepsilon\equiv\varepsilon$ is defined as n_{ek}.The Boltzmann equation is converted

to a set of K-coupled ordinary differential equations which can be represented by the following finite difference approximation:

$$a_{k-1}\, n_{ek-1} + b_{k+1} n_{ek+1} - (a_k+b_k) n_{ek}$$
$$+ \sum_j \sum_\eta N_n \,(R_{jn,k+m_{jn}}\, n_{e\,k+m_{jn}} - R_{jn,k}\, n_{ek})$$
$$+ \sum_j \sum_\eta N_n\, \delta^n{}_j \,(R'_{jn,k-m_{jn}}\, n_{e\,k-m_{jn}} - R'_{jn,k}\, n_{ek}) = 0 \qquad (2.11)$$

where

$$a_k = (2Ne^2/3m)(E/N)^2 (1/V^+{}_k/N)(1/\Delta\varepsilon)^2(\varepsilon^+{}_k + \tfrac{1}{4}\Delta\varepsilon) +$$
$$(\bar{V}^+{}_k/2\Delta\varepsilon)(\tfrac{1}{2}kT - \varepsilon^+{}_k + (2kT/\Delta\varepsilon)\varepsilon^+{}_k)$$

$$b_k = (2Ne^2/3m)(E/N)^2 (1/V^+{}_k/N)(1/\Delta\varepsilon)^2(\varepsilon^+{}_k - \tfrac{1}{4}\Delta\varepsilon) +$$
$$(\bar{V}^+{}_k/2\Delta\varepsilon)(\varepsilon^+{}_k - \tfrac{1}{2}kT + (2kT/\Delta\varepsilon)\varepsilon^+{}_k)$$

$$\bar{V}^+{}_k = 2mN(2\varepsilon^+{}_k/m)^{1/2} \sum_\eta [\delta_n\, Q^n{}_m(\varepsilon^+{}_k)/M_n]$$

$$V^+/N = (2\varepsilon^+{}_k/m)^{1/2} \sum_\eta \delta_n\, Q^n{}_m(\varepsilon^+{}_k)$$

$V(\varepsilon) = (2\varepsilon/m)^{1/2}$ is the electron velocity

$$R_{jn}(\varepsilon) = Q^n{}_j(\varepsilon)\, V(\varepsilon)$$

$$\varepsilon^-{}_{jn} = e\,u$$

$$R'_{jn}(\varepsilon) = ((\varepsilon+\varepsilon^-{}_{jn})/\varepsilon)\, Q^n_j\ (\varepsilon+\varepsilon^-{}_{jn})\, V(\varepsilon) = Q^n_{-j}(\varepsilon)\, V(\varepsilon)$$

In equation (2.11) :

m_{jn} is the nearest integer to $\varepsilon^-{}_{jn}/\Delta\varepsilon$,

a_k is the rate at which electrons in the kth energy cell are advanced to the (k+1)th cell,

b_k is the rate for electron demotion from the kth cell to the (k-1)th energy cell,

$R_{jn,k+m_{jn}}$ is the rate for electrons in the $(k+m_{jn})$ cell being degraded to the kth cell by transferring some of their translational energy to molecular excitation in an inelastic collision,

$R'_{jn,k-m_{jn}}$ is the rate for electrons in the $(k-m_{jn})$ cell being promoted to the kth cell by gaining energy from a molecule in a superelastic collision.

The total number density of electrons in the energy range $K\Delta\varepsilon$ is conserved by setting $a_k=0$,and in the lowest range $\Delta\varepsilon$,by setting $b_1=0$,and by setting equal to zero rates R_{jn} for which $k+m_{jn} > K$ and $k-m_{jn} < 1$.

Equation (2.11) may be written in matrix form as:

$$\sum_i C_i\, n_{ei} = 0 \qquad \text{.....(2.12)}$$

by setting $n_{ek} = 1$,the electron number density normalization is fixed arbitrarily and equation (2.12) is then solved by back substitution.

Electron vibrational excitation rates $X^n{}_j$ for excited state j of species n are calculated from:

$$X^n{}_j = (\varepsilon^*{}_{jn}/\varepsilon_{1n})(2e/m)^{1/2}(1/Ne^2)\sum_k(\varepsilon^+{}_k)n_{ek}\, Q^n{}_j(\varepsilon^+{}_k)\,\Delta\varepsilon \qquad \text{.....(2.13)}$$

these excitation rates are summed over the vibrational states j' of a particular mode to give effective excitation rates X_n for the modes:

$$X_n = \sum_j X^n{}_j \qquad \text{.....(2.14)}$$

The transport coefficients defined by equations (2.5) to (2.8) are calculated from:

$$V_d = [\{\sum_k(\bar{a}_k - \bar{b}_k)\, n_{ek}\,\Delta\varepsilon\}/\{E\sum_k n_{ek}\}] \qquad \text{.....(2.15)}$$

$$D=(1/3)(2/m)^{1/2}(N/n_{eo})\sum_k(\varepsilon^{1/2}n_{ek})/(\sum_k N_n\, Q^n{}_m(\varepsilon_k)) \qquad \text{.....(2.16)}$$

$$\mu = N\, V_d/E \qquad \text{.....(2.17)}$$

$$\bar{U}=(2/3Ne^2)\sum_k \varepsilon_k\, n_{ek}\,\Delta\varepsilon \qquad \ldots\ldots\ldots\ldots\ldots\ldots(2.18)$$

where:

$n_{eo} = \sum_k n_{ek}$ is the total electron number density,

$$\bar{a}_k =(2Ne^2/3m)(E/N)^2(1/V^+{}_k/N)(1/\Delta\varepsilon)^2(\varepsilon^+{}_k + \tfrac{1}{4}\Delta\varepsilon) \quad (2.19)$$

$$\bar{b}_k =(2Ne^2/3m)(E/N)^2(1/V^+{}_k/N)(1/\Delta\varepsilon)^2(\varepsilon^+{}_k - \tfrac{1}{4}\Delta\varepsilon) \quad (2.20)$$

A computer programme has been developed to solve the Boltzmann transport equation (2.2). The main interest in the solution is to obtain information regarding the excitation efficiencies of CO_2 and N_2 vibrational levels for various values of E/N and various mixtures. The average electron energy, the ionisation and attachment coefficients for corresponding conditions were also determined. The cross section data for CO_2 ,N_2 ,He, and CO collated by Kieffer [2.19] were used.

The model is a modification of that given by Smith et al [2.13],the major improvements being:

(i) the power delivered by each electron to vibrational level j of species n is determined by :

$$P_j=(2e/m)^{1/2}\delta_n\, u_{jn}\int_0^\infty uf(u)Q^n{}_j(u)du. \qquad \ldots\ldots(2.21)$$

which represents the rate at which electrons exchange energy with molecules.It strongly depends on the vibrational excitation rate for that level which is defined by equation (2.4).

Equation (2.21) can be written in terms of the solution to the distribution function as:

$$P_j = \delta_n\, \varepsilon^{\sim}{}_{jn}\, X^n{}_j$$

For particular mode of species n , the power transferred by electrons to molecules is:

$$P = \sum_j \delta_n \varepsilon^{-}_{jn} X^n_j$$

where the summation is made over all vibrational levels of that mode.

The rate of energy transfer from the electric field to the electrons is:

$$\dot{E} = (2e/m)^{1/2}((E/N)^2/3)\int_c^{\infty}[u(df(u)/du)/\sum_n \delta_n Q^n_m(u)]du \quad .....(2.22)$$

which can be written in terms of the solution to the distribution function as:

$$\dot{E} = \sum_k (\bar{a}_k - \bar{b}_k) n_{ek} \Delta\varepsilon$$

Hence the fractional power transfer to the jth vibrational level of species n is:

$$F_j = (P_j/\dot{E}) n_{eo} N \quad .....(2.23)$$

(ii) the CO_2 is an electronegative gas, hence, the electron attachment coefficient (a) should be derived as well as the ionisation coefficients for CO_2 and N_2 (α_{co2}, α_{N2}). These parameters are important for understanding the discharge development. The attachment coefficient can be represented by:

$$a = (2e/m)^{1/2}(N/V_d) \int_o^{\infty} Q_j u f(u) du \quad .....(2.24)$$

which can be written in terms of the solution to the distribution function as:

$$a = (2e/m)^{1/2}(N/V_d)\sum_k CSa_k(u_k)^{1/2}(n_{ek}/\sum_k n_{ek}) \quad ....(2.25)$$

The ionisation coefficient is defined in a way analogous to the attachment coefficient and can be written as:

$$\alpha = (2e/m)^{1/2}(N/V_d)\sum_k CS_k(u_k)^{1/2}(n_{ek}/\sum_k n_{ek}) \quad .....(2.26)$$

2.5 PREDICTED ELECTRON TRANSPORT PARAMETERS AND OPERATING CHARACTERISTICS OF THE DISCHARGE ; RESULTS AND DISCUSSION :

2.5.1 Electron energy distribution:

The Boltzmann equation (2.2) has been solved numerically over a range of E/N values typical of those for efficient pumping of carbon dioxide lasers in a number of gas mixtures which are of special importance for high-power CO_2 lasers. Values of E/N between $2 - 9 \times 10^{-16}$ volt.cm^2 are considered because the experimental values of E/N for the gas mixtures under consideration ,lie within this range. Calculated electron energy distributions are shown in graphs (2.1 to 2.6) for different gas mixtures. The graphs demonstrate the influence of different discharge parameters on the distribution function . The EEDF is strongly affected by changing either the parameter E/N or the gas mixture.Graph (2.1) shows that as the E/N value of the discharge increases, the high energy part of the distribution function and the average electron energy both increase. This is simply because of the increasing applied electric field, hence the electrons gain more energy from the field. In mixtures with less helium (graph 2.2) or with more nitrogen content(graphs 2.3 and 2.4),this effect is reduced.

The effects of varying the gas mixture on the electron energy distribution function are shown in graphs(2.5 and 2.6). With more helium in the mixture, the high energy part of the distribution function increases since helium has

none of the inelastic vibrational losses that are present in CO_2 and N_2. On the other hand, as the proportion of nitrogen in the gas mixture increases so too does the inelastic vibrational losses since nitrogen has large vibrational excitation cross sections. This prevents the electrons from reaching higher energies, therefore the high energy part of the distribution function decreases.

The effect of superelastic collisions (i.e collisions of electrons with excited molecules) on the distribution function is shown in graphs(2.7 to 2.9). In these collisions ,a certain fraction of the energy previously lost by electrons in collisions with neutral molecules is returned to the electrons. Therefore the electric field is not the only energy source for the electrons. It can be seen from graph (2.7) that by including superelastic collisions,the high energy part of the distribution function slightly increases as some electrons gain energy from excited molecules in the discharge. When E/N increases, as shown by comparing graphs (2.8) and (2.9), the effect of superelastic collisions on the EEDF decreases. This is mainly due to the decreasing population of the vibrationally excited N_2 and CO_2 molecules in the discharge as their vibrational excitation cross sections decrease rapidly with increasing electron energy. At $E/N = 2\times10^{-16}$ volt.cm^2 the percentage increase in the electron energy is $\approx 3.5\%$,whereas at $E/N = 4\times10^{-16}$ volt.cm^2 the increase is $\approx 1.1\%$. For values of $E/N \geq 5\times10^{-16}$ volt.cm^2 the increase in the electron energy is less than 0.5 % . It is, therefore , assumed that for values of $E/N \geq 2\times10^{-16}$ volt.cm^2

superelastic collisions can safely be neglected as their effects are insignificant compared with that of other inelastic collisions. The same assumption has been made by Lowke et al [2.1] and Khahra [2.14] throughout their work. However, at lower values of E/N superelastic collisions are extremely important [Belousova,2.22],due to large population of the CO_2 (10^00 and 01^10) levels.

2.5.2 Average electron energy:

Graph (2.10) shows that the average electron energy in the discharge increases with the increase in the helium content in the gas mixture for a particular CO_2 : N_2 ratio. This is because helium has none of the inelastic vibrational losses that are present in N_2 and CO_2. In addition, since no electronic excitation of helium occurs below 19.7 eV, electrons in the discharge can reach higher energies. This effect is similar to that of increasing the E/N value for the discharge as discussed in 2.5.1 ,where the high energy part of the distribution function and the average electron energy both increase. Thus,the discharge will operate at a lower value of E/N with more helium content in the mixture.

The average electron energy in the discharge decreases with the addition of N_2 to the gas mixture,as shown in graph (2.11). It also decreases with increasing proportion of CO_2 in the gas mixture as shown in graph (2.12). This effect is greater with N_2 than with CO_2 as the vibrational excitation cross sections for N_2(V=1-8) are larger than that for CO_2 (00^01 , 10^00 , and 01^10) level over the range of electron energies considered (see figures 2.2 and 2.3), hence an

increasing content of N_2 in the mixture leads to an increasing number of energetic electrons being taken out of the discharge and thus decreases the average electron energy,[Khahra ,2.14]. A similar effect is indicated by reducing the E/N value for the discharge as discussed in 2.5.1. Thus,the discharge will operate at a higher value of E/N with more N_2 in the mixture.

The present values of the average electron energy show good agreement with those of Khahra[2.14],though they are few per cent lower, particularly at higher values of E/N due to different cross section data used in the calculations.

2.5.3 Excitation efficiencies:

Graph (2.13) shows the input power per molecule delivered into the upper laser level $CO_2(00^o1)$ and the first eight vibrational levels of $N_2(V=1-8)$ for a 1:1:8 mixture . The input power delivered to both the upper laser level and vibrational levels of nitrogen increases with increasing E/N. However, the power fed to vibrational levels of nitrogen falls off more rapidly than that of the upper laser level. The reason is that the excitation rate for $N_2(V=1-8)$,as predicted by equation (2.13) falls off with increasing E/N (i.e. increasing average electron energy) more rapidly than in CO_2 ,as shown in graph (2.14). The total excitation effeciency is the sum of the contributions from both N_2 and CO_2 ,this is shown in graph (2.20). There is good agreement with the results reported by Lowke et al [2.1]. For a 1:1:8 mixture at E/N= 3×10^{-16} volt.cm^2,Lowke et al and Khahra [2.14] obtained excitation efficiencies of 44% and 35%

respectively, compared with 42.8% in the present work. The discrepency is due to the different cross sections used,in addition, Khahra used cross sections for only the first four vibrational levels of N_2. The effect of increasing the helium content of the gas mixture on the excitation efficiency of $CO_2(00°1)$ and $N_2(v=1-8)$ levels is shown in graphs (2.15) and (2.16) respectively. Increasing the proportion of helium leads to an increase in the average electron energy,thus electron energies sufficient to excite the $CO_2(00°1)$ and $N_2(v=1-8)$ occur at a lower E/N for mixture with high helium content than for a mixture with less helium(as discussed in 2.5.2 ,graph 2.10). On the other hand, the increase in helium content doesn't alter the total excitation efficiency of N_2 and CO_2 ,as shown in graph (2.17). This is in agreement with the results of Lowke et al [2.1], and Khahra [2.14]. The effect of increasing the nitrogen content in the gas mixture on the excitation effeciency of $CO_2(00°1)$ is shown in graph (2.18). As the nitrogen proportion increases ,the excitation effeciency of $CO_2(00°1)$ decreases due to the decrease in the average electron energy which means decreasing excitation cross sections for $CO_2(00°1)$. Whereas,the effect of varying the proportion of nitrogen in the gas mixture on the excitation effeciency of $N_2(v=1-8)$ is indicated in graph (2.19). The excitation efficiency increases with increasing amount of nitrogen. This is simply due to the presence of more nitrogen in the mixture which has a higher excitation cross section. The combined excitation efficiency of $N_2(v=1-8)$ +

$CO_2(00°1)$ levels is increased with the addition of nitrogen to the mixture, as shown in graph(2.20). The reason is that more energy is coupled into the excitation of $N_2(v=1-8)$ levels, hence less energy is being wasted in the excitation of bending and stretching modes of CO_2.

2.5.4 Ionisation and attachment coefficients:

Graphs (2.21) shows the ionisation and attachment rates for a 1:1:8 gas mixture at different values of E/N . The ionisation rate for carbon dioxide is about two orders of magnitude greater than that of nitrogen since the ionisation threshold for CO_2(13.3 eV) is lower than that for N_2(15.5 eV) and ionisation cross-sections for CO_2 are larger, [KucuKarpaci and Lucas ,2.4]. The attachment rate represents the process:

$$CO_2 + e \longrightarrow CO + O^-$$

as nitrogen does not form negative ions. The ionisation and attachment rates increase with increasing E/N as a result of increasing electron energy, but at higher values of E/N the attachment rate levels off , as shown in the graph, because the attachment cross sections pass a maximum with increasing electron energy. Graphs (2.22 to 2.25) show the specific ionisation and attachment coefficients (α/N , a/N) at different values of E/N,and for several gas mixtures . The agreement between these results,the theoretical results of Lowke et al [2.1], and experimental results of Haydon and McIntosh [2.10] is very good . It should be noted that the experimental data gives lower values than the calculated results of both Lowke et al and the present work.This is due

to the fact that theoretical investigations of the electron swarm parameters, made using Boltzmann's energy equation and the measured collision cross-section values under estimate the magnitude of the drift velocity and hence over estimate the values of the ionisation coefficient. Graph (2.26) shows the electron drift velocty at different values of E/N. The drift velocity increases almost linearly with increasing E/N as the electrons gain more energy from the applied electric field. The agreement between the present results and those of Lakshminarasimha et al [2.3] is excellent. On the other hand, the agreement between these theoretical predictions and the experimental results of Sierra et al [2.7] is fair. The divergence between the two approaches increases at higher values of E/N. This can be explained as following: the drift velocity of electrons in molecular gases is very roughly a linear function of E/N, and as E/N increases the mean swarm energy changes rapidly, the main source of energy loss transfers from vibrational to electronic excitational collisions. At higher values of E/N ,ionisation ocurrs, the newly-formed electrons start at the bottom of the energy distribution. The distribution is modified by the increasingly large proportion of fast electrons,hence the observed drift velocity increases faster than expected. It can be seen from graphs (2.22 and 2.23) that variation in the percentage of helium in the gas mixture has more influence on the values of α/N than do variations in the proportion of N_2. This is primarily because the helium plays a dominant role in determining the

electron energy distribution function and hence the average electron energy. As the percentage of helium is increased so too does the value of α/N,whereas the value of α/N decreases with increasing amount of N_2 in the mixture.

The specific attachment coefficient (a/N) is plotted against E/N for different gas mixtures in graphs (2.24 and 2.25). There is good agreement between present results ,the theoretical results of Lowke et al [2.1] and experimental values of Alger and Rees[2.23]. The graph shows that the a/N curve passes a maximum as E/N rises. This seems to indicate that at higher values of E/N (see graph 2.1) an increasing number of electrons have energies which are too high to allow an attachment to take place. The quasi-steady operating value of E/N for the gas discharge can be adequately predicted by a simple balance of electron production and attachment rates[Denes and Lowke 2.24]. The intersection of the curves representing the calculated dependences of α/N and a/N on E/N presented in graph (2.27) effectively give the quasi - steady operating value of E/N for the gas mixture shown. However,discharges which operate at a characteristic quasi- steady value of E/N are found to be attachment dominated, [Nighan and Wiegand,2.25]. Table (2.2) lists predicted values of specific ionisation and attachment coefficients , and electron drift velocity at different values of E/N for several gas mixtures.While Table (2.3) lists predicted quasi-steady operating values of E/N for these gas mixtures,graphs (2.28) and (2.29) are included as examples of how to obtain the operating values of E/N.

2.6 EFFECTS OF THE ADDITION OF CO :

In a CO_2 laser discharge ,carbon monoxide is formed due to the dissociation of carbon dioxide. Vibrational excitation cross sections for CO are comparable to that of N_2,hence for electron energies corresponding to typical CO_2 laser discharges ,CO is expected to be a vibrational energy reservoir and an alternative pumping channel for the upper laser level.

As mentioned earlier , for efficient operation of the gas discharge the distribution of electron energy should be such that it is most favorable for excitation of $N_2(V=1-8)$ and $CO_2(00^01)$ but not $CO_2(01^10)$. The effects of carbon monoxide on excitation and relaxation processes of different energy levels in the gas system have been investigated by various workers. Smith et al [2.26] have investigated the effects of addition of several gases.Belousova et al[2.22] have studied the vibrational excitation and energy balance in a CO electrical discharge.Effects of CO on the discharge stability have been examined by Nagai et al [2.27]. Ono and Teii [2.28] have studied both theoretically and experimentally the influence of CO on the electron temperature and negative ion formation in CO_2 mixture gas discharges. Recently, Wedding [2.11] has investigated various electron transport parameters in a (CO_2 : N_2 : He : CO) gas mixture. It has usually been seen that a small amount of CO is effective for the deactivation of the lower laser level (Appendix 2.II) and for excitation to the upper laser level (Appendix

2.III).Furthermore,the carbon monoxide affects the discharge through detachment processes such as:

$$CO + O^- \longrightarrow CO_2 + e$$

$$CO + CO_3^- \longrightarrow 2CO_2 + e$$

which release more low energy electrons and reduce negative ion densities in the discharge (to be discussed in chapter 3) hence the discharge can run at a lower value of E/N , [Smith et al,2.26]. The effects of addition of CO to the gas mixture on the electron energy distribution function and transport parameters are reported in the following sections.

The calculations have been made using the first eight vibrational excitation levels of CO which have a near resonance energy transfer with the CO_2(oon) levels , [Braglia et al, 2.5].

2.6.1 Electron energy distribution function and average electron energy :

Graph (2.30) shows the effects of added CO on the electron energy distribution function in a 1:1:8 gas mixture. It clearly indicates that CO addition decreases both the high energy part of the distribution function and the average electron energy due to large cross sections for vibrational excitation of CO molecules. Thus,the increasing relative concentration of CO prevents electrons from reaching energies greater than about 2 eV and only a small number of electrons are able to exceed this value. The decreasing electron energy reduces vibrational excitation of nitrogen (see figure 2.3 where the cross section curve

has a maximum at about 2.3 eV). On the other hand,the CO vibrational excitation cross section is broader and has a maximum at about 0.5 eV lower in energy than N_2(see Appendix 2.III) ,hence the initial decrease in the electron energy caused by the addition of small concentration of CO (i.e $\approx$ 3%) produces more CO(v=1) molecules in the discharge which are available for transferring their vibrational energy to CO_2 molecules . This , partially compensates for the decrease in vibrational excitation of N_2. Further addition of CO to the gas mixture largely reduces the average electron energy as shown in graph (2.31) , thus reduces the vibrational excitation of both CO and N_2.

Graph(2.32) shows the effects of added CO,as a substitute for N_2,on the distribution function and the average electron energy. The high energy part of the distribution function and the average electron energy are reduced with added CO. It can be seen that when the proportion of CO is about 30% of that of N_2,the effect is relatively small since the vibrational excitation cross section for CO and N_2 are comparable in the electron energy range of 1.9-2.4 eV (see figures 2.3 and A2.III.1). When the CO fraction becomes equal to or greater than that of N_2,the decrease in the average electron energy is relatively large.

Graph (2.33) shows the effects of added CO , as a substitue for CO_2 ,on the distribution function and the average electron energy. As the proportion of CO in the gas mixture increases, the high energy part of the distribution function and the average electron energy are reduced due to

large cross sections for vibrational excitation of CO. By comparing graphs (2.32) and (2.33) ,it can be seen that the decrease in the high energy part of the distribution function and the average electron energy is greater when CO is added as a substitute for CO_2 than as a substitute for N_2 ,because the vibrational excitation cross sections for N_2 are larger than that for CO_2. Thus, as the carbon dioxide is replaced by CO which has large cross sections,this together with large cross sections for N_2 both greatly reduce the electron energy in the discharge as shown in graph (2.33). It also reduces the vibrational excitation of N_2(v=1-8) . It is therefore essential to control the proportion of added CO to the gas mixture in order to obtain consistent results.

2.6.2 Excitation efficiencies:

Graph (2.34) shows the effect of CO addition on the vibrational excitation rates for a 1:1:8 gas mixture. The addition of 2% CO to the gas mixture reduces the excitation rates for N_2(v=1-8) as a result of the decreasing electron energy in the gas discharge, since vibrational excitation cross sections for N_2(v=1-8) fall off rapidly with decreasing electron energy as shown in figure (2.3). Whereas the effect on the vibrational excitation rate for CO_2(00°1) level is relatively small as the cross sections for this level fall off slowly with decreasing electron energy as shown in figure (2.2).

The net power input to vibrational excitation of N_2(v=1-8) ,CO(v=1-8) and CO_2(00°1) levels are shown in graph (2.35).

The power delivered to N_2 and CO_2 molecules are slightly decreased with addition of 2% CO due to decreasing excitation rates. The power delivered to CO molecules produces a further pumping channel of the $CO_2(00°1)$ level through resonant energy transfer process (see Appendix 2.III). In addition, this leads to less energy wasted in the excitation of bending and stretching modes of CO_2.

The effects of added CO on the excitation efficiency for $N_2(v=1-8)$ and $CO_2(00°1)$ levels are shown in graphs(2.36 and 2.37). It can be seen that the maximum vibrational excitation of $N_2(v=1-8)$ with CO addition occurs at a higher value of E/N than that for a mixture without CO due to the decrease in the average electron energy. Graph (2.38) shows the excitation efficiency for CO(v=1-8) and graph (2.39) shows the total excitation efficiency for the mixture (i.e $N_2(v=1-8)$ + $CO_2(00°1)$ + CO(v=1-8)). The behaviour shown is similar to that in the work of Braglia et al[2.5],though they include the excitation of the first ten vibrational levels of CO in their calculations.

2.6.3 Ionisation and attachment coefficients:

Graphs (2.40) and (2.41) show the ionisation and attachment rates for a 1:1:8 gas mixture with 2% added CO at different values of E/N. The ionisation rate for CO is greater than that of N_2 because it has lower ionisation threshold (14.0 eV). Whereas attachment rate for CO is less than that for carbon dioxide since the attachment threshold for CO(9.2 eV) is greater than that for CO_2(3.85 eV) and

attachment cross-sections for CO are smaller,[Kieffer,2.19]. The behaviour shown in these graphs is similar to that reported by Nighan and Wiegand [2.25].

The effects of CO addition to the gas mixture on the specific ionisation and attachment coefficients are shown in graphs (2.42 and 2.43).It can be seen that the ionisation and attachment coefficients are larger in the ternary mixture than in the quaternary mixture. This is because the addition of CO to the gas mixture reduces the average electron energy and the high energy part of the distribution function,hence the ionisation and attachment rates are reduced. This trend is in agreement with the results of Braglia et al[2.12].

2.7 CONCLUSIONS:

(1) For values of E/N > $2x10^{-16}$ volt.cm^2 , superelastic collisions can be neglected as their effects on the EEDF are insignificant compared with other inelastic processes.

(2) The effect of increasing the proportion of He in the gas mixture is to increase the electron energy for a given E/N (graph 2.10). Thus, the E/N for maximum efficiency (graph 2.17) and the operating value of E/N for self-sustained discharge(graph 2.28)are both reduced.

(3) The predicted laser excitation efficiency increases as the ratio of N_2 to CO_2 is increased(graph 2.19),because then power is fed into N_2 vibrational levels instead of being lost in the excitation of bending and stretching modes of CO_2.

(4) Increasing the proportion of He in the mixture increases the ionisation and attachment coefficients as a result of increasing electron energy (graphs 2.22 and 2.24).

(5) Increasing the ratio of N_2 to CO_2 reduces the electron energy for a given value of E/N (graph 2.11). Thus, the E/N for maximum efficiency , (graph 2.20), and the operating value of E/N for the discharge (graph 2.29), are both increased, while the ionisation and attachment coefficients are both reduced ,(graphs 2.23 and 2.25).

(6) Addition of CO to the gas mixture reduces the electron energy for a given E/N (graph 2.32). Thus, the E/N for maximum efficiency and the operating value of E/N are both increased. Whereas, the ionisation and attachment coefficients are both reduced (graphs 2.42 and 2.43).

REFERENCES

CHAPTER TWO

2.1 Lowke J J,Phelps A V and Irwin B W - 'Predicted electron transport coefficients and operating characteristics of CO_2 -N_2 -He laser mixture '-J.Appl.Phys. ,Vol 44 , 1973(4664).

2.2 Sakai Y,Keneko S, Tagashira H and sakamoto S - 'A Boltzmann equation analysis of electron swarm parameters in CO_2 laser mixtures'- J.Phys. D: Appl.Phys.,Vol 12, 1979(23).

2.3 Lakshminarasimha CS,Lucas J,Moruzzi JL and Spalding IJ - 'Electron swarm parameters in CO_2 laser gas mixtures' - J.Phys.D:Appl.Phys.,Vol 9,1976(1727).

2.4 KucuKarpaci H N and Lucas J - 'Simulation of electron swarm parameters in carbon dioxide and nitrogen for high E/N'-J.Phys.D: Appl.Phys., Vol 12,1979 (2123).

2.5 Braglia G L,Bruzzese R and Caraffini G L - 'An analysis on the electron motion in the laser mixture CO_2-N_2-He -CO '- Lettre al Nuovo Cimento , Vol 25 , 1979 (139).

2.6 Rockwood S D and Greene A E -'Numerical solution of the Boltzmann transport equation'- Comp. Phys. Commun., Vol 19, 1980(377).

2.7 Sierra RA,Brooks HL,Sommerer AJ,Foltyn SR and Nygaard KJ -'Effective swarm parameters and transport coefficients in CO_2 laser mixtures '- J.Phys. D: Appl. Phys., Vol 14, 1981 (1791).

2.8 Hasegawa H,Sato Y,Murai K,Shimozuma M and Tagashira H-'Measurements of the ionisation coefficients in binary and ternary mixtures of CO_2,N_2 and He '- J.Phys. D: Appl.Phys., Vol 18, 1985 (1361).

2.9 Davies D Kenneth -'Ionisation and attachment coefficients in CO_2: N_2: He and pure CO_2 '- J.Appl. Phys., Vol 49(1), 1978 (127).

2.10 Haydon S C and McIntosh A I - ' Investigation of ionisation growth in gas mixtures '- J.Phys. D: Appl. Phys., Vol 11,1978 (1859) .

2.11 Wedding A B - 'Electron swarm parameters in a CO_2-N_2-He-CO gas mixture '-J.Phys. D: Appl. Phys., Vol 18, 1985 (2351).

2.12 Braglia G L ,Romano 1 and Roznerski W -'Electron drift velocity in CO_2 laser mixtures'-Nuovo Cimento, series 1 D, 1983 (898).

2.13 Thomson R M,Smith K and Davies A R-'BOLTZ: a code to solve the transport equation for electron distributions and then calculate transport coefficients and vibrational excitation rates in gases with applied fields'- Comput. Phys. Commun. ,11, 1976 (369) .

2.14 Khahra JS -Ph.D Thesis,University of Birmingham,1976.

2.15 Levine A K - 'A Series of advances in lasers ', Vol 3, Chap(II) ,Marcel Dekker Inc., New York, 1971.

2.16 Phelps A V -'Rotational and vibrational excitation of molecules by low-energy electrons'- Rev. Mod. Phys. , Vol 40 , 1968 (399).

2.17 Hake R D and Phelps A V -'Momentum transfer and inelastic collision cross-sections for electrons in O_2 ,CO and CO_2'- Phys. Rev., Vol 158, 1967 (70).

2.18 Schulz G J -'Vibrational excitation of N_2,CO_2 and H_2 by electron impact '- Phys. Rev. , Vol 135 , 1964 (A988) .

2.19 Kieffer L J-Joint Institute for Laboratory Astrophysics Information Center, Report 13, Sept. 1973.

2.20 Taylor R L and Bitterman S - 'Survey of vibrational relaxation data for processes important in the CO_2 -N_2 laser system '- Rev. Mod. Phys., Vol 41 , 1969 (29) .

2.21 Smith K and Thomson R M - 'Computer Modelling of Gas Lasers '- Plenum Press, New York, 1978.

2.22 Belousova I M , Liukonen R A , and Leonov S N - 'Vibrational excitation rate levels and energy balance in an electrical-discharge carbon monoxide laser'-Sov. Phys. Tech. Phys.,Vol 23, 1978 (1345).

2.23 Alger S R and Rees J A - 'Ionisation , attachment and negative ion reactions in carbon dioxide'- J.Phys. D: Appl. Phys. , Vol9 ,1976 (2359).

2.24 Denes LJ and Lowke JJ -'V-I characteristics of pulsed CO_2 laser discharges'- Appl. Phys. Lett., Vol 23, 1973, (130).

2.25 Nighan W L and Wiegand W J -'Influence of negative-ion processes on steady-state properties and striations in molecular gas discharges '- Phys. Rev., Vol 10, 1974(922).

2.26 Smith A L S, Bett T H and Browne P G -'The effects of gas additives on TEA CO_2 lasers'-IEEE J.QE., Vol 11 ,1975 (335).

2.27 Nagai H, Hishii M, Shibayama K, Nagai A and Akiba T - 'High-pressure sealed CW CO_2 laser with high efficiency '- IEEE J.QE., Vol 18, 1982 (416).

2.28 Ono S and Teii S -'Vibrational temperature in a weakly ionised CO_2-N_2-He discharge '- J.Phys.D:Appl. Phys, Phys., Vol 18, 1985 ,(441).

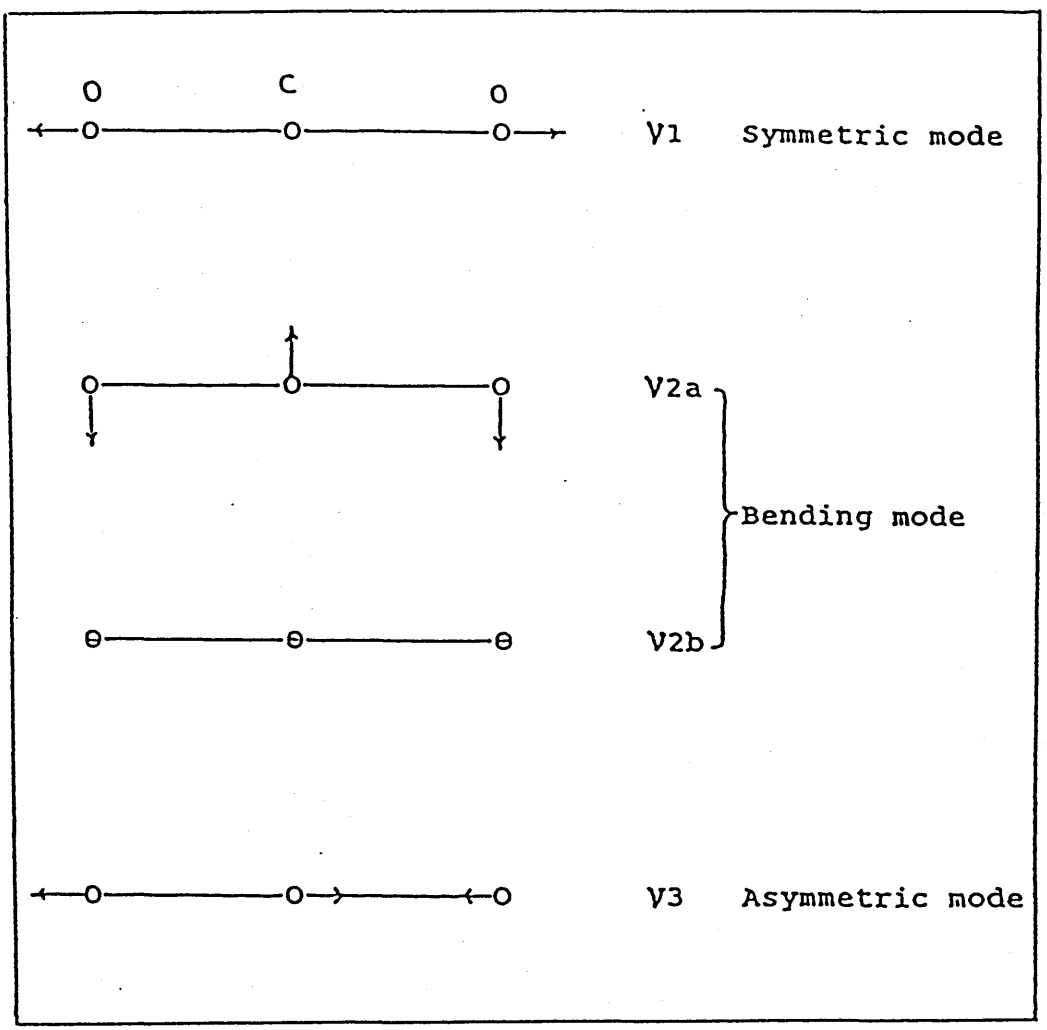

VIBRATIONAL MODES OF THE CO_2 MOLECULE

FIGURE (2.1)

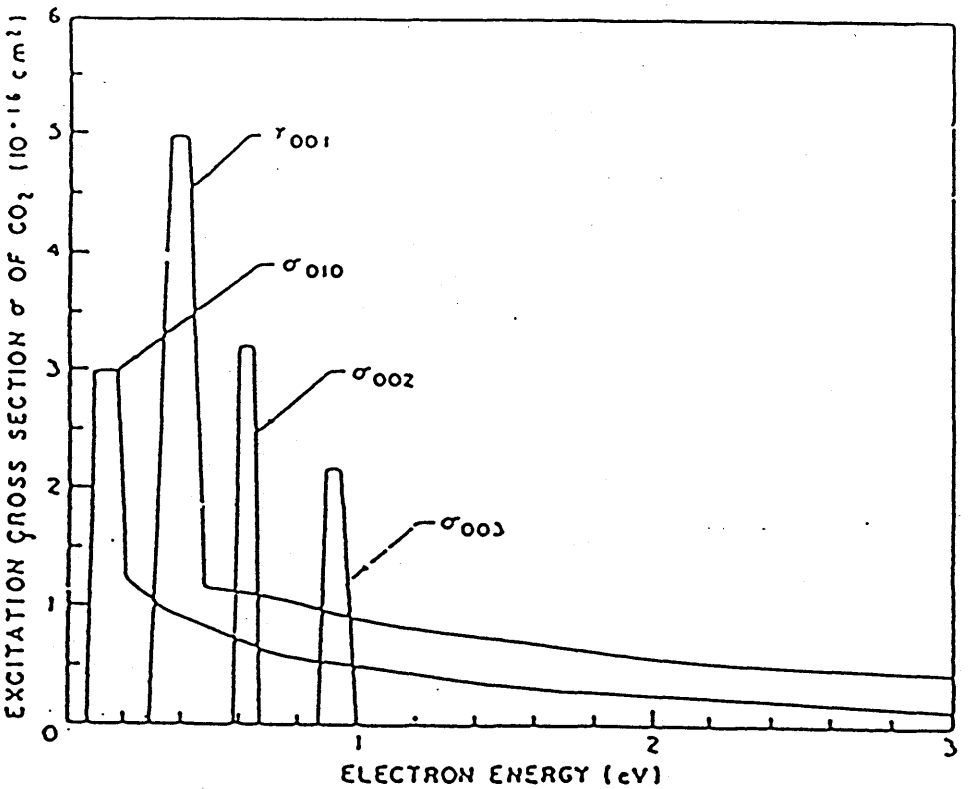

CROSS SECTION FOR VIBRATIONAL EXCITATION OF CO_2 BY ELECTRON IMPACT [REF. 2.17]

FIGURE (2.2)

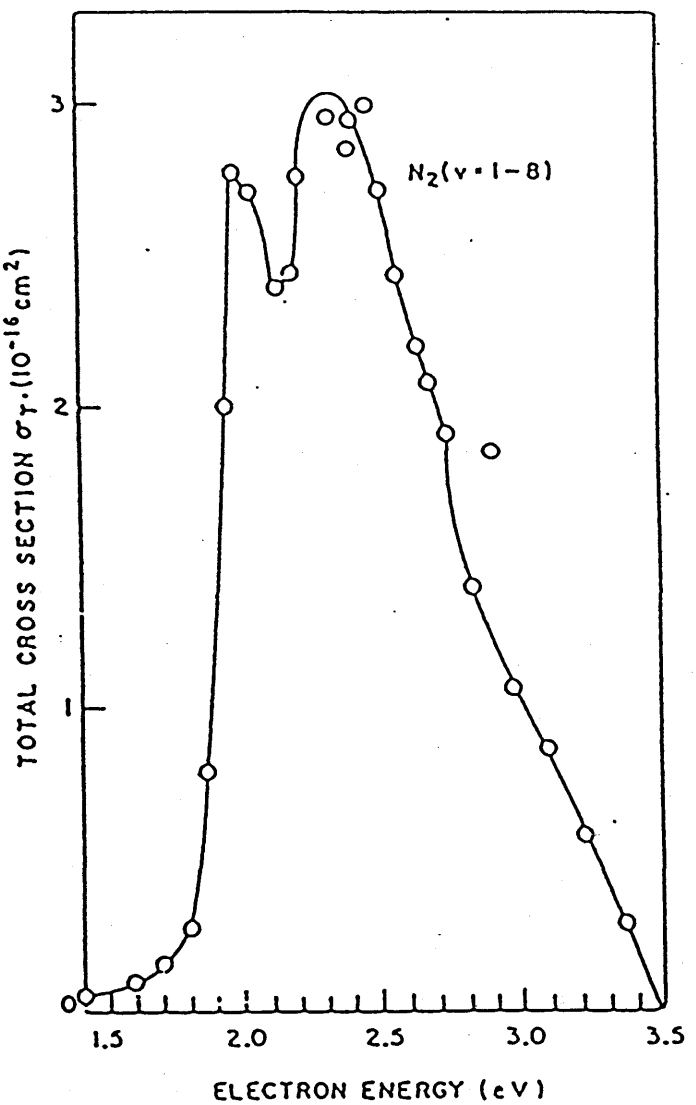

TOTAL EFFECTIVE CROSS SECTION FOR VIBRATIONAL EXCITATION OF N_2(V=1-8) BY ELECTRON IMPACT [REF. 2.18]

FIGURE (2.3)

TABLE (2.1)

ENERGY THRESHOLDS FOR CO_2 AND N_2 (*)

Process / Level	Threshold (eV)	
	CO_2	N_2
Vibrational Excitation:		
V=1	0.083	0.290
V=2	0.167	0.590
V=3	0.252	0.880
V=4	0.291	1.170
V=5	0.339	1.470
V=6	0.422	1.760
V=7	0.505	2.060
V=8	2.500	2.350
Ionisation	13.300	15.500
Attachment	3.850	___

(*) Reference: Kieffer [2.19]

TABLE (2.2)

PREDICTED VALUES OF (α/N) , (a/N) AND (V_a)

SPECIFIC IONISATION COEFFICIENT (α/N)

E/N x 10^{-16} ($V.Cm^2$)	GAS MIXTURES / α/N (cm^2) 1:1:0	1:1:1	1:1:2
2.0	0.28317×10^{-30}	0.55850×10^{-26}	0.85033×10^{-24}
3.0	0.80435×10^{-25}	0.43321×10^{-22}	0.10377×10^{-20}
4.0	0.30400×10^{-22}	0.28205×10^{-20}	0.26715×10^{-19}
5.0	0.91109×10^{-21}	0.29198×10^{-19}	0.15943×10^{-18}
6.0	0.79107×10^{-20}	0.12510×10^{-18}	0.47907×10^{-18}
7.0	0.34398×10^{-19}	0.33181×10^{-18}	0.99686×10^{-18}
8.0	0.98358×10^{-19}	0.66215×10^{-18}	0.16705×10^{-17}
9.0	0.21476×10^{-18}	0.11030×10^{-17}	0.24409×10^{-17}
10.0	0.39095×10^{-18}	0.16282×10^{-17}	0.32538×10^{-17}

(continued on next page)

(Table 2.2 cont.)

SPECIFIC ATTACHMENT COEFFICIENT (a/N)

E/N $x10^{-16}$ (V.Cm²)	GAS MIXTURES / a/N (cm²) 1:1:0	1:1:1	1:1:2
2.0	$0.21829x10^{-23}$	$0.17316x10^{-21}$	$0.15507x10^{-20}$
3.0	$0.51914x10^{-21}$	$0.76667x10^{-20}$	$0.28768x10^{-19}$
4.0	$0.63619x10^{-20}$	$0.41008x10^{-19}$	$0.98853x10^{-19}$
5.0	$0.25317x10^{-19}$	$0.97932x10^{-19}$	$0.18062x10^{-18}$
6.0	$0.58263x10^{-19}$	$0.15975x10^{-18}$	$0.24795x10^{-18}$
7.0	$0.98994x10^{-19}$	$0.21324x10^{-18}$	$0.29454x10^{-18}$
8.0	$0.14041x10^{-18}$	$0.25412x10^{-18}$	$0.32321x10^{-18}$
9.0	$0.17790x10^{-18}$	$0.28292x10^{-18}$	$0.33869x10^{-18}$
10.0	$0.20944x10^{-18}$	$0.30182x10^{-18}$	$0.34512x10^{-18}$

(continued on next page)

(Table 2.2 cont.)

ELECTRON DRIFT VELOCITY (V_d)

E/N $x10^{-16}$ ($V.Cm^2$)	GAS MIXTURES / V_d (cm/sec) 1:1:0	1:1:1	1:1:2
2.0	$0.6061x10^7$	$0.5839x10^7$	$0.5675x10^7$
3.0	$0.7145x10^7$	$0.7034x10^7$	$0.6970x10^7$
4.0	$0.8087x10^7$	$0.8107x10^7$	$0.8117x10^7$
5.0	$0.8525x10^7$	$0.8605x10^7$	$0.8661x10^7$
6.0	$0.9737x10^7$	$0.1003x10^8$	$0.1025x10^8$
7.0	$0.1050x10^8$	$0.1096x10^8$	$0.1130x10^8$
8.0	$0.1125x10^8$	$0.1188x10^8$	$0.1234x10^8$
9.0	$0.1200x10^8$	$0.1279x10^8$	$0.1336x10^8$
10.0	$0.1274x10^8$	$0.1369x10^8$	$0.1436x10^8$

(continued on next page)

(Table 2.2 cont.)

SPECIFIC IONISATION COEFFICIENT (α/N)

E/N $x10^{-16}$ (V.cm^2)	GAS MIXTURES / α/N (cm^2)		
	1:1:4	1:1:6	1:1:8
2.0	$0.15063x10^{-21}$	$0.22221x10^{-20}$	$0.11796x10^{-19}$
3.0	$0.25783x10^{-19}$	$0.13245x10^{-18}$	$0.36165x10^{-18}$
4.0	$0.25138x10^{-18}$	$0.78131x10^{-18}$	$0.15673x10^{-17}$
5.0	$0.82973x10^{-18}$	$0.19617x10^{-17}$	$0.33297x10^{-17}$
6.0	$0.18148x10^{-17}$	$0.35645x10^{-17}$	$0.53971x10^{-17}$
7.0	$0.29709x10^{-17}$	$0.51650x10^{-17}$	$0.72461x10^{-17}$
8.0	$0.41858x10^{-17}$	$0.66525x10^{-17}$	$0.88155x10^{-17}$
9.0	$0.53615x10^{-17}$	$0.79494x10^{-17}$	$0.10073x10^{-16}$
10.0	$0.64414x10^{-17}$	$0.90313x10^{-17}$	$0.11034x10^{-16}$

(continued on next page)

(Table 2.2 cont.)

SPECIFIC ATTACHMENT COEFFICIENT (a/N)

E/N $x10^{-16}$ (V.cm²)	GAS MIXTURES / a/N (cm²) 1:1:4	1:1:6	1:1:8
2.0	$0.14237x10^{-19}$	$0.44075x10^{-19}$	$0.87809x10^{-19}$
3.0	$0.10473x10^{-18}$	$0.19621x10^{-18}$	$0.28384x10^{-18}$
4.0	$0.22503x10^{-18}$	$0.33008x10^{-18}$	$0.41183x10^{-18}$
5.0	$0.31102x10^{-18}$	$0.39974x10^{-18}$	$0.45932x10^{-18}$
6.0	$0.36341x10^{-18}$	$0.42800x10^{-18}$	$0.46665x10^{-18}$
7.0	$0.38566x10^{-18}$	$0.42978x10^{-18}$	$0.45334x10^{-18}$
8.0	$0.39099x10^{-18}$	$0.41918x10^{-18}$	$0.43202x10^{-18}$
9.0	$0.38665x10^{-18}$	$0.40293x10^{-18}$	$0.40825x10^{-18}$
10.0	$0.37707x10^{-18}$	$0.38456x10^{-18}$	$0.38457x10^{-18}$

(continued on next page)

(Table 2.2 cont.)

ELECTRON DRIFT VELOCITY (V_d)

E/N $x10^{-16}$ (V.cm^2)	GAS MIXTURES / V_d (cm/sec)		
	1:1:4	1:1:6	1:1:8
2.0	$0.5483x10^7$	$0.5353x10^7$	$0.5246x10^7$
3.0	$0.6863x10^7$	$0.6772x10^7$	$0.6697x10^7$
4.0	$0.8121x10^7$	$0.8112x10^7$	$0.8108x10^7$
5.0	$0.9301x10^7$	$0.9397x10^7$	$0.9471x10^7$
6.0	$0.1056x10^8$	$0.1077x10^8$	$0.1092x10^8$
7.0	$0.1177x10^8$	$0.1208x10^8$	$0.1231x10^8$
8.0	$0.1295x10^8$	$0.1337x10^8$	$0.1368x10^8$
9.0	$0.1412x10^8$	$0.1463x10^8$	$0.1503x10^8$
10.0	$0.1526x10^8$	$0.1588x10^8$	$0.1636x10^8$

(continued on next page)

(Table 2.2 cont.)

SPECIFIC IONISATION COEFFICIENT (α/N)

E/N $\times 10^{-16}$ (V.cm^2)	GAS MIXTURES / α/N (cm^2)		
	1:2:0	1:2:1	1:2:2
2.0	0.99565×10^{-30}	0.10415×10^{-26}	0.71712×10^{-25}
3.0	0.12178×10^{-24}	0.11114×10^{-22}	0.17372×10^{-21}
4.0	0.34673×10^{-22}	0.95411×10^{-21}	0.70088×10^{-20}
5.0	0.93546×10^{-21}	0.12277×10^{-19}	0.56586×10^{-19}
6.0	0.78183×10^{-20}	0.61901×10^{-19}	0.20894×10^{-18}
7.0	0.33593×10^{-19}	0.18510×10^{-18}	0.50227×10^{-18}
8.0	0.95841×10^{-19}	0.40371×10^{-18}	0.93443×10^{-18}
9.0	0.20943×10^{-18}	0.71915×10^{-18}	0.14766×10^{-17}
10.0	0.38176×10^{-18}	0.11178×10^{-17}	0.20915×10^{-17}

(continued on next page)

(Table 2.2 cont.)

SPECIFIC ATTACHMENT COEFFICIENT (a/N)

E/N $x10^{-16}$ (V.cm²)	GAS MIXTURES / a/N (cm²) 1:2:0	1:2:1	1:2:2
2.0	$0.24349x10^{-23}$	$0.61952x10^{-22}$	$0.42761x10^{-21}$
3.0	$0.45633x10^{-21}$	$0.34325x10^{-20}$	$0.11394x10^{-19}$
4.0	$0.51921x10^{-20}$	$0.21737x10^{-19}$	$0.50122x10^{-19}$
5.0	$0.20456x10^{-19}$	$0.59671x10^{-19}$	$0.10941x10^{-18}$
6.0	$0.47827x10^{-19}$	$0.10852x10^{-18}$	$0.17021x10^{-18}$
7.0	$0.83191x10^{-19}$	$0.15721x10^{-18}$	$0.22078x10^{-18}$
8.0	$0.12075x10^{-18}$	$0.19906x10^{-18}$	$0.25802x10^{-18}$
9.0	$0.15605x10^{-18}$	$0.23191x10^{-18}$	$0.28313x10^{-18}$
10.0	$0.18670x10^{-18}$	$0.25604x10^{-18}$	$0.29864x10^{-18}$

(continued on next page)

(Table 2.2 cont.)

ELECTRON DRIFT VELOCITY (V_d)

E/N $x10^{-16}$ (V.cm²)	GAS MIXTURES / V_d (cm/sec)		
	1:2:0	1:2:1	1:2:2
2.0	$0.5208x10^7$	$0.5124x10^7$	$0.5089x10^7$
3.0	$0.6161x10^7$	$0.6257x10^7$	$0.6351x10^7$
4.0	$0.7104x10^7$	$0.7341x10^7$	$0.7527x10^7$
5.0	$0.8003x10^7$	$0.8363x10^7$	$0.8637x10^7$
6.0	$0.8867x10^7$	$0.9351x10^7$	$0.9712x10^7$
7.0	$0.9712x10^7$	$0.1032x10^8$	$0.1076x10^8$
8.0	$0.1054x10^8$	$0.1127x10^8$	$0.1180x10^8$
9.0	$0.1137x10^8$	$0.1221x10^8$	$0.1282x10^8$
10.0	$0.1219x10^8$	$0.1313x10^8$	$0.1381x10^8$

(continued on next page)

(Table 2.2 cont.)

SPECIFIC IONISATION COEFFICIENT (α/N)

E/N $\times 10^{-16}$ (V.cm^2)	GAS MIXTURES / α/N (cm^2)		
	1:2:4	1:2:6	1:2:8
2.0	0.10275×10^{-22}	0.17947×10^{-21}	0.11743×10^{-20}
3.0	0.42373×10^{-20}	0.25820×10^{-19}	0.83151×10^{-19}
4.0	0.68515×10^{-19}	0.24440×10^{-18}	0.55371×10^{-18}
5.0	0.31873×10^{-18}	0.83146×10^{-18}	0.15395×10^{-17}
6.0	0.82205×10^{-18}	0.17561×10^{-17}	0.28607×10^{-17}
7.0	0.15431×10^{-18}	0.28747×10^{-17}	0.42883×10^{-17}
8.0	0.24006×10^{-17}	0.40496×10^{-17}	0.56636×10^{-17}
9.0	0.33154×10^{-17}	0.51861×10^{-17}	0.69013×10^{-17}
10.0	0.42274×10^{-17}	0.62292×10^{-17}	0.79659×10^{-17}

(continued on next page)

(Table 2.2 cont.)

SPECIFIC ATTACHMENT COEFFICIENT (a/N)

E/N $x10^{-16}$ (V.cm^2)	GAS MIXTURES / a/N (cm^2)		
	1:2:4	1:2:6	1:2:8
2.0	$0.39066x10^{-20}$	$0.13552x10^{-19}$	$0.30286x10^{-19}$
3.0	$0.44341x10^{-19}$	$0.93439x10^{-19}$	$0.14935x10^{-18}$
4.0	$0.12538x10^{-18}$	$0.20341x10^{-18}$	$0.27334x10^{-18}$
5.0	$0.20816x10^{-18}$	$0.28875x10^{-18}$	$0.35073x10^{-18}$
6.0	$0.27033x10^{-18}$	$0.33929x10^{-18}$	$0.38679x10^{-18}$
7.0	$0.30969x10^{-18}$	$0.36337x10^{-18}$	$0.39712x10^{-18}$
8.0	$0.33124x10^{-18}$	$0.37065x10^{-18}$	$0.39328x10^{-18}$
9.0	$0.34053x10^{-18}$	$0.36808x10^{-18}$	$0.38224x10^{-18}$
10.0	$0.34191x10^{-18}$	$0.36004x10^{-18}$	$0.36784x10^{-18}$

(continued on next page)

(Table 2.2 cont.)

ELECTRON DRIFT VELOCITY (V_d)

E/N $x10^{-16}$ (V.cm²)	GAS MIXTURES / V_d (cm/sec)		
	1:2:4	1:2:6	1:2:8
2.0	$0.5078x10^7$	$0.5084x10^7$	$0.5085x10^7$
3.0	$0.6489x10^7$	$0.6566x10^7$	$0.6603x10^7$
4.0	$0.7776x10^7$	$0.7918x10^7$	$0.8002x10^7$
5.0	$0.9001x10^7$	$0.9221x10^7$	$0.9366x10^7$
6.0	$0.1019x10^8$	$0.1050x10^8$	$0.1071x10^8$
7.0	$0.1137x10^8$	$0.1176x10^8$	$0.1203x10^8$
8.0	$0.1252x10^8$	$0.1299x10^8$	$0.1334x10^8$
9.0	$0.1365x10^8$	$0.1421x10^8$	$0.1462x10^8$
10.0	$0.1475x10^8$	$0.1539x10^8$	$0.1587x10^8$

(continued on next page)

(Table 2.2 cont.)

SPECIFIC IONISATION COEFFICIENT (α/N)

E/N $\times 10^{-16}$ ($V.cm^2$)	GAS MIXTURES / α/N (cm^2)		
	1:3:0	1:3:1	1:3:2
2.0	0.20784×10^{-29}	0.43418×10^{-27}	0.15996×10^{-25}
3.0	0.15782×10^{-24}	0.52711×10^{-23}	0.56737×10^{-22}
4.0	0.38098×10^{-22}	0.51546×10^{-21}	0.29612×10^{-20}
5.0	0.96320×10^{-21}	0.74142×10^{-20}	0.28709×10^{-19}
6.0	0.78418×10^{-20}	0.40846×10^{-19}	0.12083×10^{-18}
7.0	0.33356×10^{-19}	0.13078×10^{-18}	0.31926×10^{-18}
8.0	0.94840×10^{-19}	0.30054×10^{-18}	0.63686×10^{-18}
9.0	0.20707×10^{-18}	0.55733×10^{-18}	0.10608×10^{-17}
10.0	0.37746×10^{-18}	0.89390×10^{-18}	0.15652×10^{-17}

(continued on next page)

(Table 2.2 cont.)

SPECIFIC ATTACHMENT COEFFICIENT (a/N)

E/N $x10^{-16}$ (V.cm^2)	GAS MIXTURES / a/N (cm^2)		
	1:3:0	1:3:1	1:3:2
2.0	$0.28784x10^{-23}$	$0.36383x10^{-22}$	$0.19558x10^{-21}$
3.0	$0.44822x10^{-21}$	$0.22102x10^{-20}$	$0.63739x10^{-20}$
4.0	$0.47942x10^{-20}$	$0.15116x10^{-19}$	$0.32143x10^{-19}$
5.0	$0.18582x10^{-19}$	$0.44472x10^{-19}$	$0.77921x10^{-19}$
6.0	$0.43532x10^{-19}$	$0.85757x10^{-19}$	$0.13116x10^{-18}$
7.0	$0.76375x10^{-19}$	$0.13016x10^{-18}$	$0.18033x10^{-18}$
8.0	$0.11197x10^{-18}$	$0.17089x10^{-18}$	$0.22000x10^{-18}$
9.0	$0.14604x10^{-18}$	$0.20471x10^{-18}$	$0.24930x10^{-18}$
10.0	$0.17609x10^{-18}$	$0.23093x10^{-18}$	$0.26946x10^{-18}$

(continued on next page)

(Table 2.2 cont.)

ELECTRON DRIFT VELOCITY (V_d)

E/N $x10^{-16}$ (V.cm²)	GAS MIXTURES / V_D (cm²) 1:3:0	1:3:1	1:3:2
2.0	$0.4711x10^7$	$0.4702x10^7$	$0.4718x10^7$
3.0	$0.5672x10^7$	$0.5815x10^7$	$0.5945x10^7$
4.0	$0.6630x10^7$	$0.6887x10^7$	$0.7102x10^7$
5.0	$0.7545x10^7$	$0.7907x10^7$	$0.8203x10^7$
6.0	$0.8431x10^7$	$0.8897x10^7$	$0.9273x10^7$
7.0	$0.9303x10^7$	$0.9871x10^7$	$0.1032x10^8$
8.0	$0.1016x10^8$	$0.1083x10^8$	$0.1135x10^8$
9.0	$0.1103x10^8$	$0.1178x10^8$	$0.1237x10^8$
10.0	$0.1187x10^8$	$0.1271x10^8$	$0.1336x10^8$

(contined on next page)

(Table 2.2 cont.)

SPECIFIC IONISATION COEFFICIENT (α/N)

E/N $\times 10^{-16}$ (V.cm^2)	GAS MIXTURES / α/N (cm^2)		
	1:3:4	1:3:6	1:3:8
2.0	0.16106×10^{-23}	0.28107×10^{-22}	0.20026×10^{-21}
3.0	0.11687×10^{-20}	0.74415×10^{-20}	0.26066×10^{-19}
4.0	0.26578×10^{-19}	0.99684×10^{-19}	0.24191×10^{-18}
5.0	0.15394×10^{-18}	0.41946×10^{-18}	0.81957×10^{-18}
6.0	0.45960×10^{-18}	0.10172×10^{-17}	0.17292×10^{-17}
7.0	0.95515×10^{-18}	0.18317×10^{-17}	0.28298×10^{-17}
8.0	0.15998×10^{-17}	0.27653×10^{-17}	0.39854×10^{-17}
9.0	0.23359×10^{-17}	0.37331×10^{-17}	0.51027×10^{-17}
10.0	0.31108×10^{-17}	0.46749×10^{-17}	0.61281×10^{-17}

(continued on next page)

(Table 2.2 cont.)

SPECIFIC ATTACHMENT COEFFICIENT (a/N)

E/N $x10^{-16}$ ($V.cm^2$)	GAS MIXTURES / a/N (cm^2) 1:3:4	1:3:6	1:3:8
2.0	$0.15985x10^{-20}$	$0.56925x10^{-20}$	$0.13419x10^{-19}$
3.0	$0.23869x10^{-19}$	$0.52551x10^{-19}$	$0.88703x10^{-19}$
4.0	$0.80672x10^{-19}$	$0.13741x10^{-18}$	$0.19374x10^{-18}$
5.0	$0.15141x10^{-18}$	$0.21954x10^{-18}$	$0.27728x10^{-18}$
6.0	$0.21388x10^{-18}$	$0.27878x10^{-18}$	$0.32791x10^{-18}$
7.0	$0.25981x10^{-18}$	$0.31469x10^{-18}$	$0.35275x10^{-18}$
8.0	$0.28972x10^{-18}$	$0.33307x10^{-18}$	$0.36090x10^{-18}$
9.0	$0.30707x10^{-18}$	$0.33976x10^{-18}$	$0.35915x10^{-18}$
10.0	$0.31545x10^{-18}$	$0.33909x10^{-18}$	$0.35183x10^{-18}$

(continued on next page)

(Table 2.2 cont.)

ELECTRON DRIFT VELOCITY (V_d)

E/N $x10^{-16}$ (V.cm^2)	GAS MIXTURES / V_d (cm/sec) 1:3:4	1:3:6	1:3:8
2.0	$0.4774x10^7$	$0.4831x10^7$	$0.4878x10^7$
3.0	$0.6153x10^7$	$0.6301x10^7$	$0.6402x10^7$
4.0	$0.7428x10^7$	$0.7648x10^7$	$0.7796x10^7$
5.0	$0.8641x10^7$	$0.8933x10^7$	$0.9136x10^7$
6.0	$0.9820x10^7$	$0.1018x10^8$	$0.1044x10^8$
7.0	$0.1097x10^8$	$0.1141x10^8$	$0.1173x10^8$
8.0	$0.1211x10^8$	$0.1262x10^8$	$0.1299x10^8$
9.0	$0.1322x10^8$	$0.1380x10^8$	$0.1423x10^8$
10.0	$0.1430x10^8$	$0.1495x10^8$	$0.1545x10^8$

TABLE (2.3)

PREDICTED QUASI-STEADY OPERATING VALUES OF E/N

Gas Mixture	E/N $x10^{-16}$ (volt.cm^2)
1:1:0	8.6269
1:1:1	6.3216
1:1:2	5.1362
1:1:4	3.9048
1:1:6	3.2509
1:1:8	2.8423
1:2:0	8.4119
1:2:1	6.7464
1:2:2	5.7279
1:2:4	4.5307
1:2:6	3.8389
1:2:8	3.3681
1:3:0	8.2972
1:3:1	6.9925
1:3:2	6.1096
1:3:4	4.9815
1:3:6	4.2835
1:3:8	3.7891

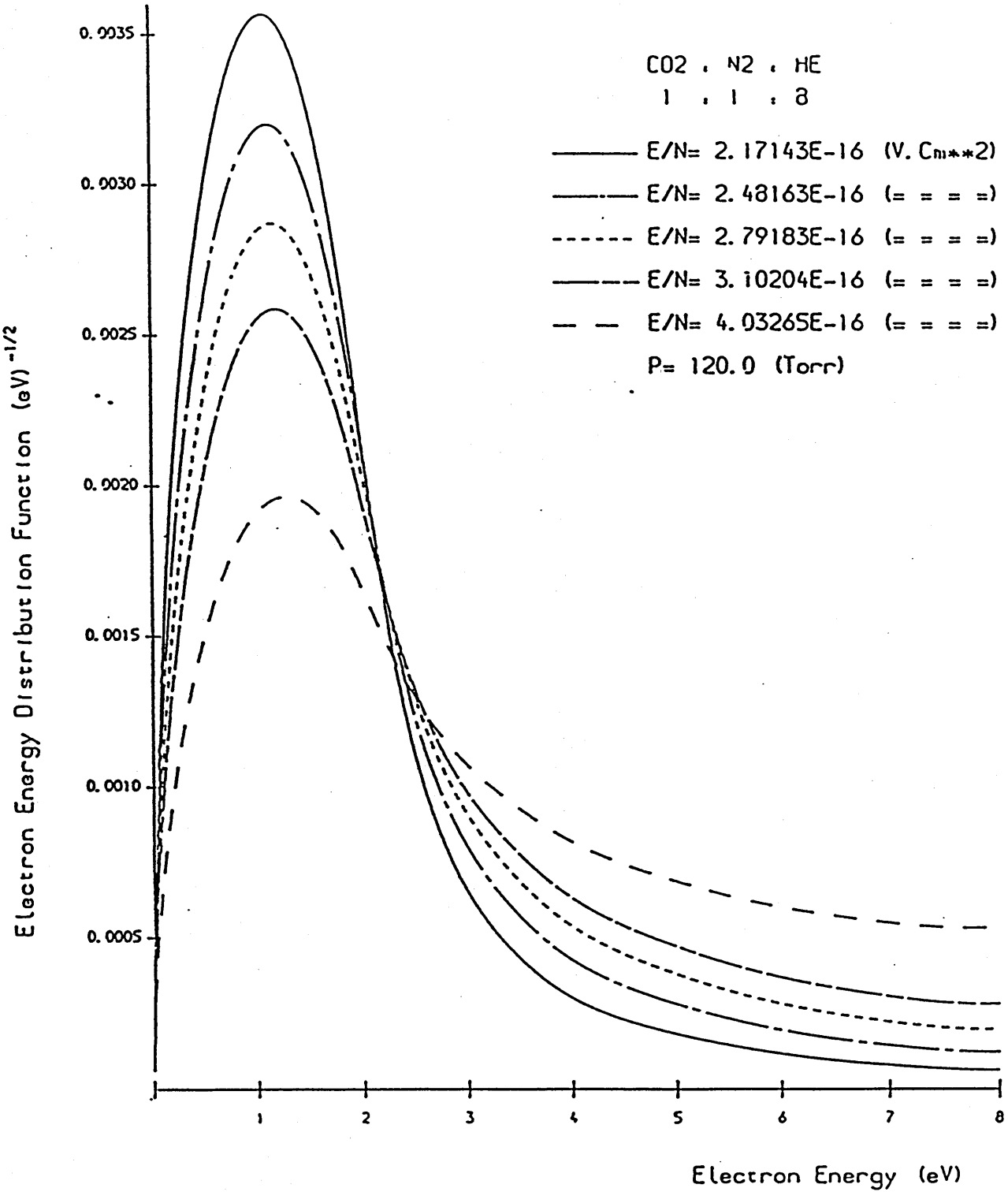

GRAPH OF ELECTRON ENERGY DISTRIBUTION FUNCTION

GRAPH (2.1)

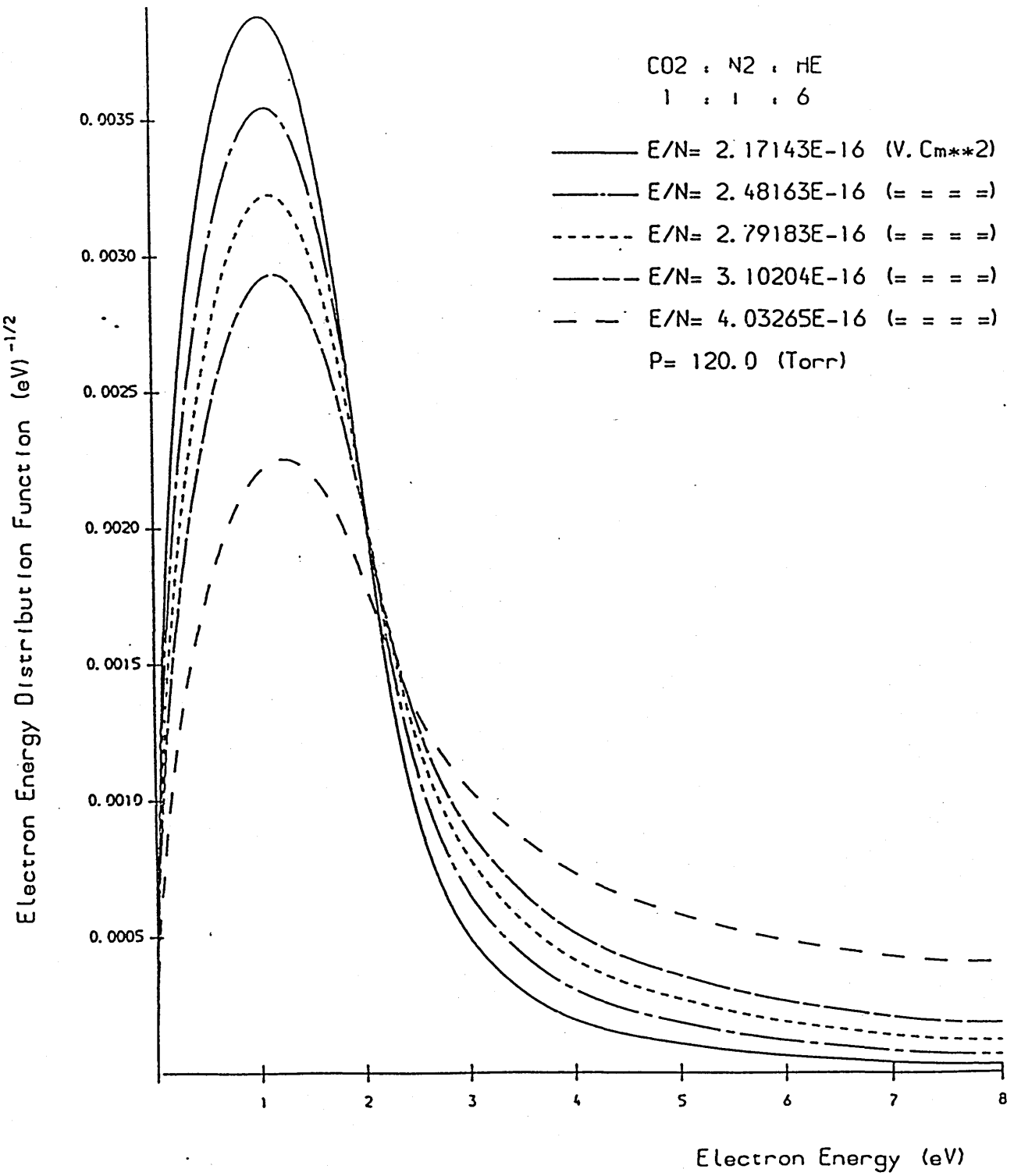

GRAPH OF ELECTRON ENERGY DISTRIBUTION FUNCTION

GRAPH (2.2)

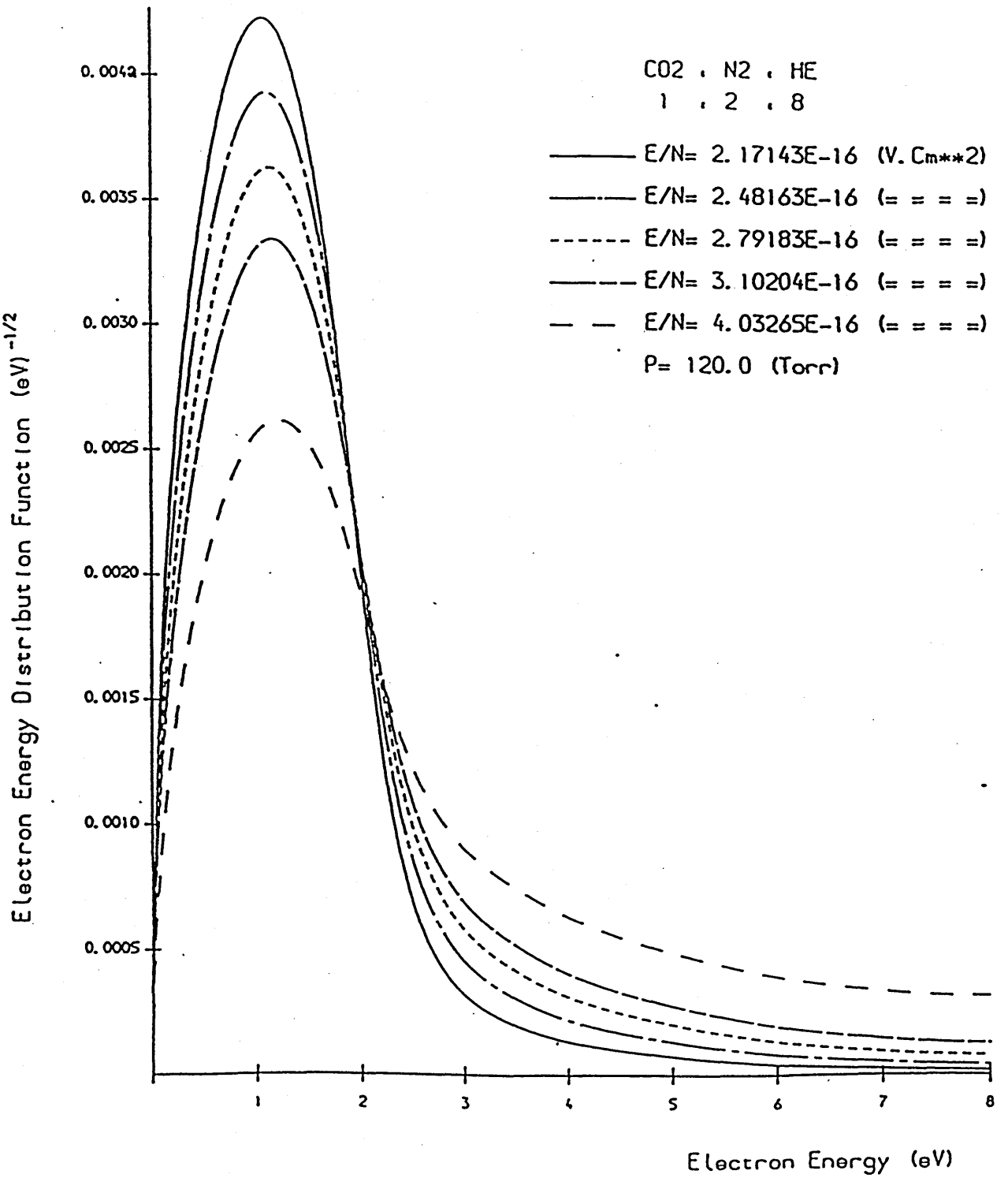

GRAPH OF ELECTRON ENERGY DISTRIBUTION FUNCTION

GRAPH (2.3)

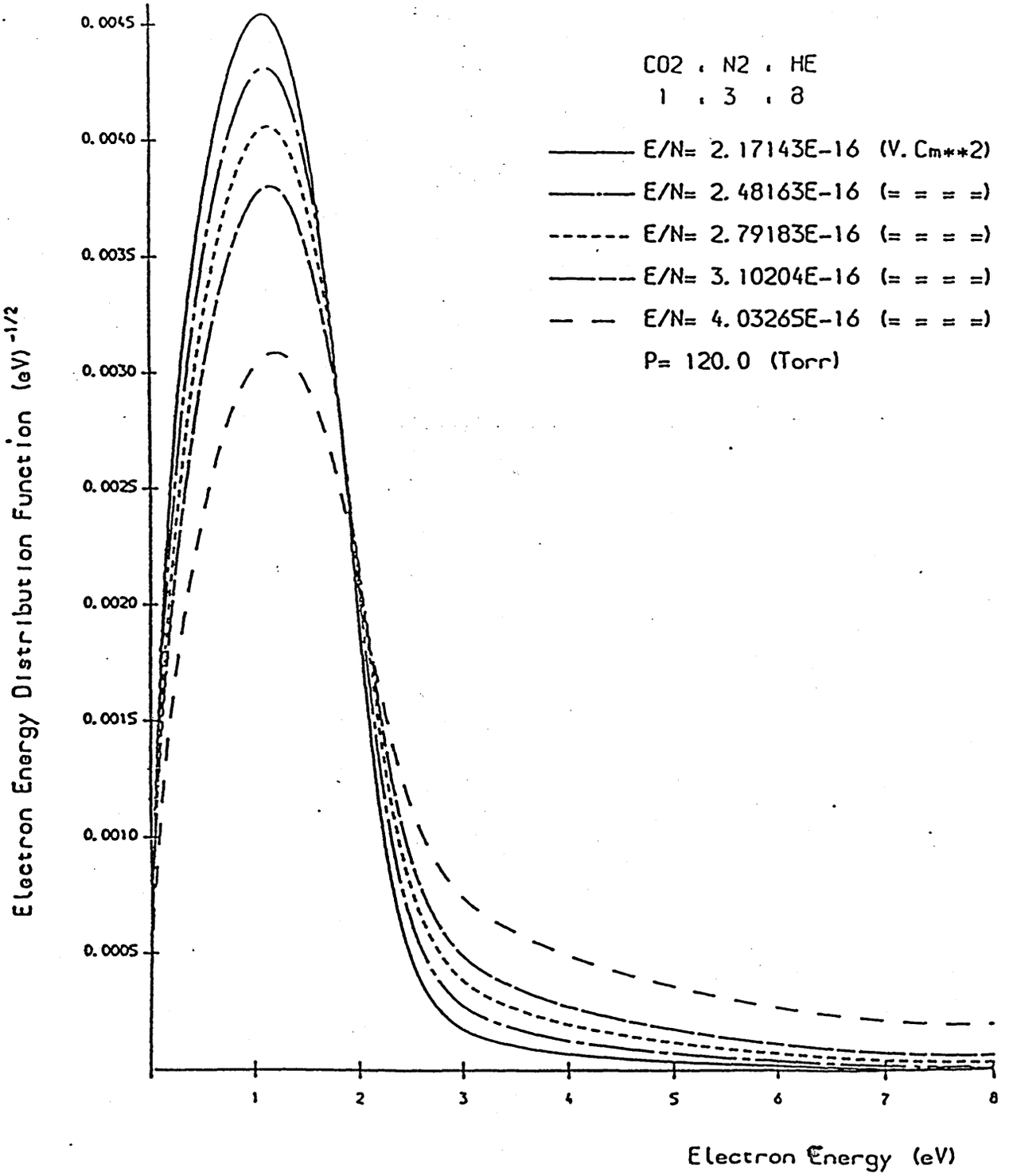

GRAPH OF ELECTRON ENERGY DISTRIBUTION FUNCTION

GRAPH (2.4)

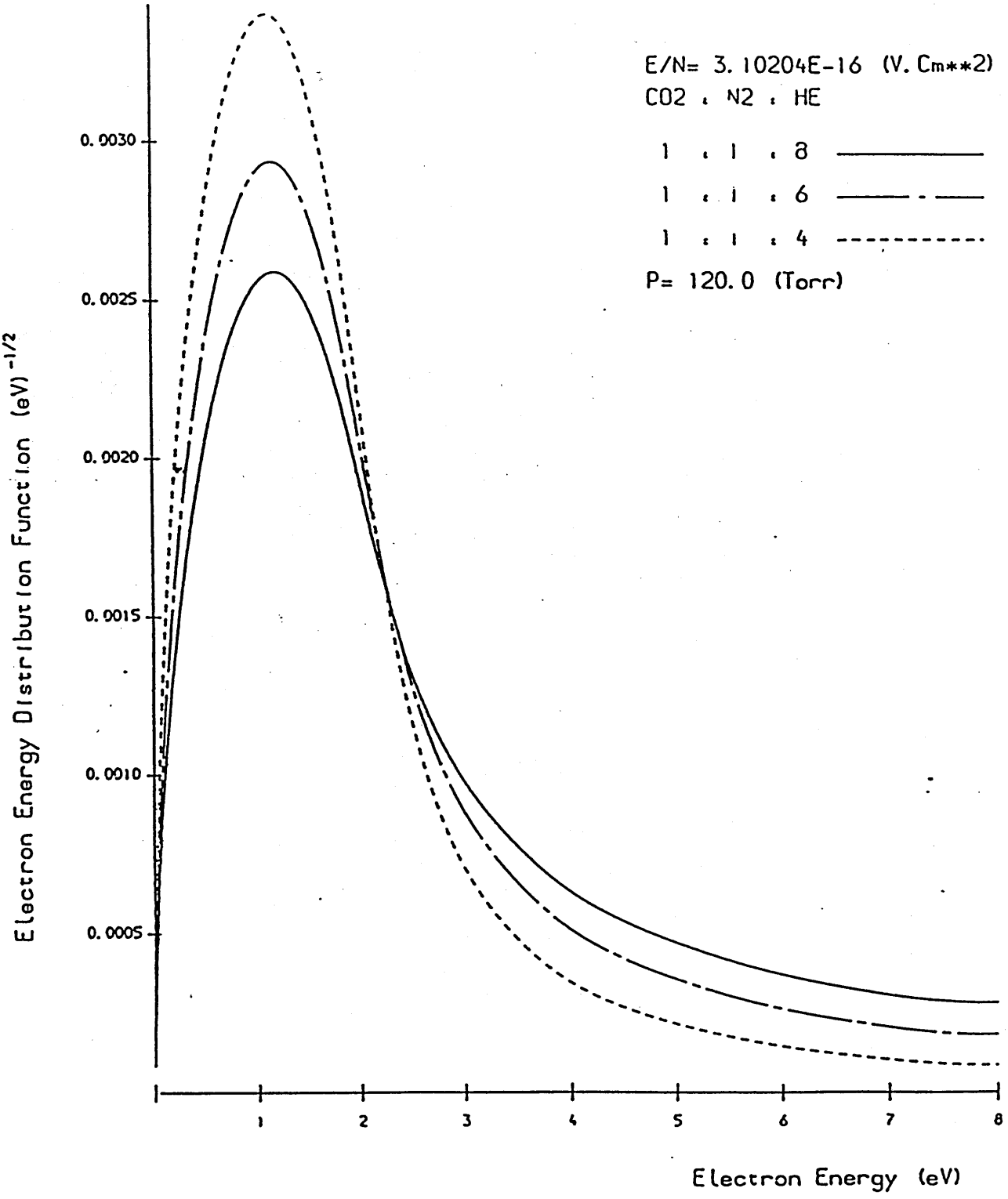

GRAPH OF ELECTRON ENERGY DISTRIBUTION FUNCTION

GRAPH (2.5)

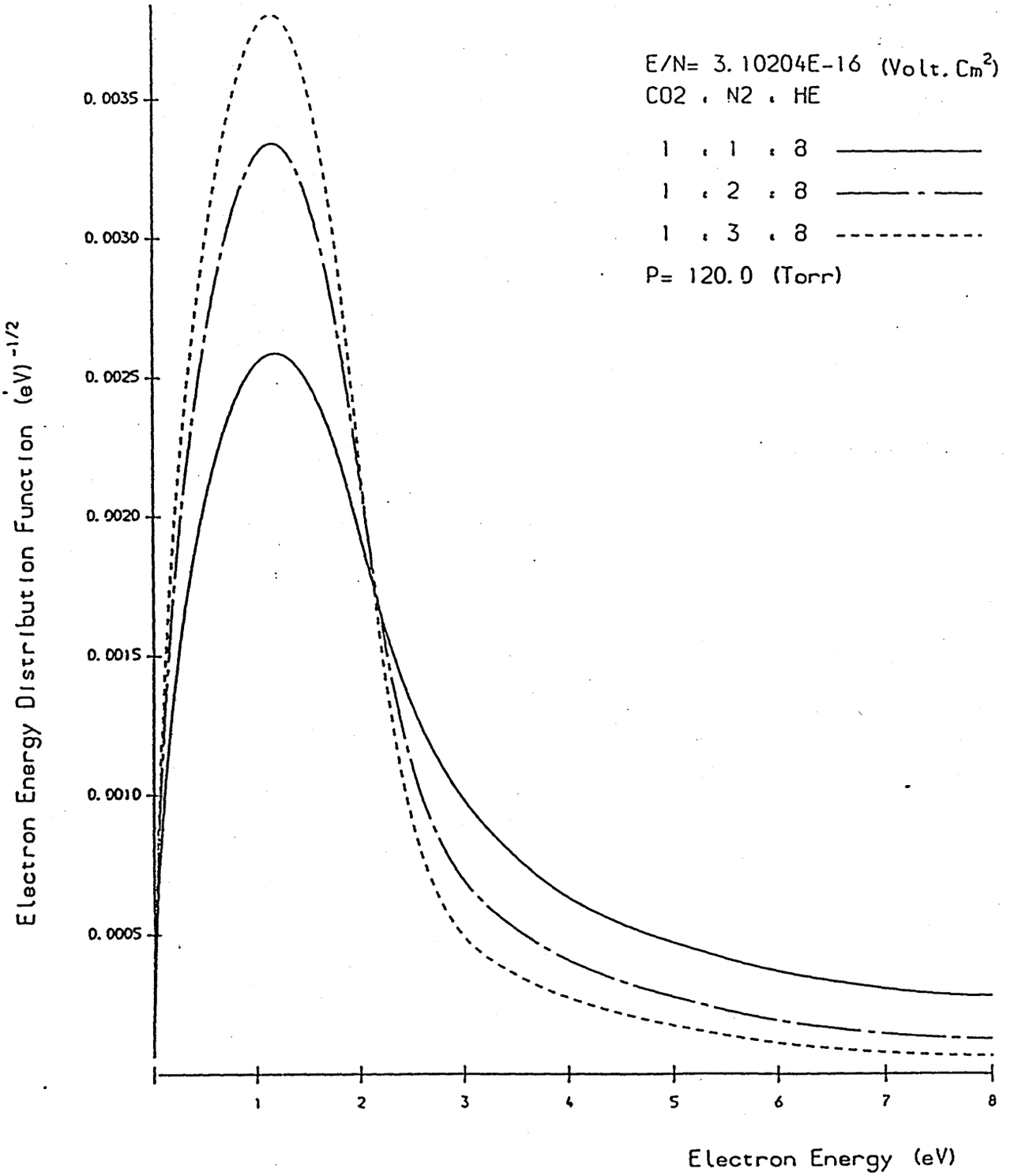

GRAPH OF ELECTRON ENERGY DISTRIBUTION FUNCTION

GRAPH (2.6)

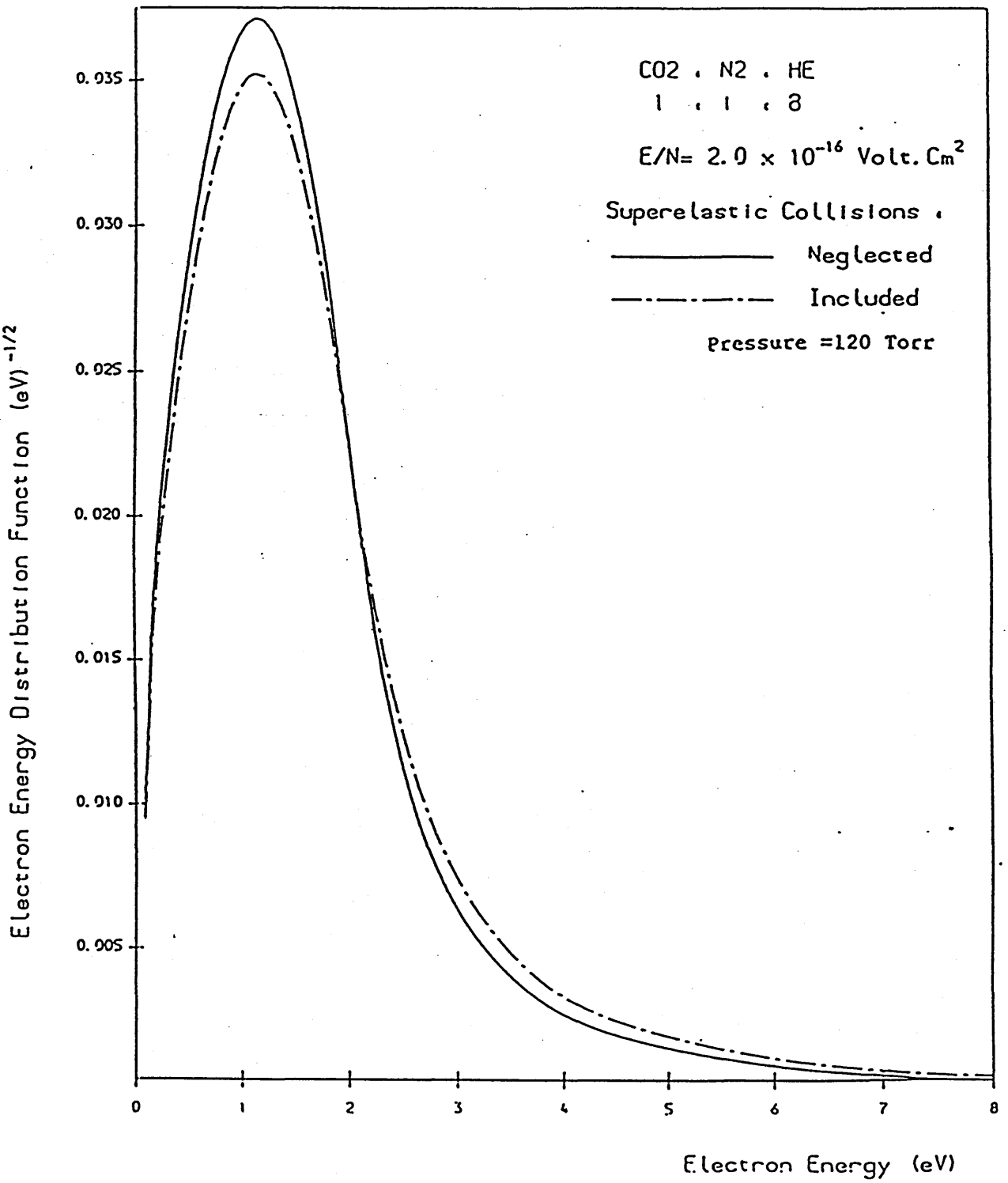

GRAPH OF ELECTRON ENERGY DISTRIBUTION FUNCTION

GRAPH (2.7)

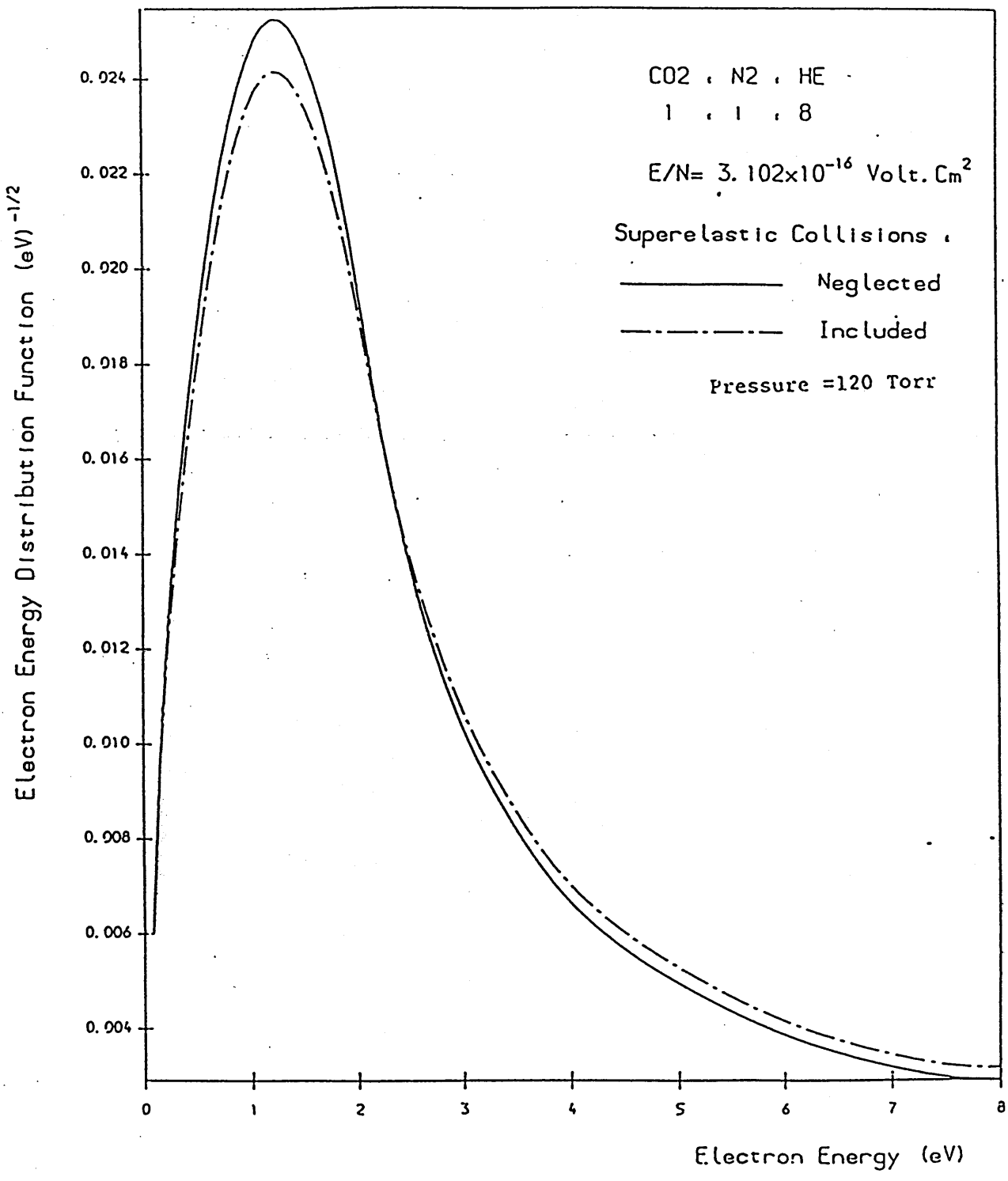

GRAPH OF ELECTRON ENERGY DISTRIBUTION FUNCTION

GRAPH (2.8)

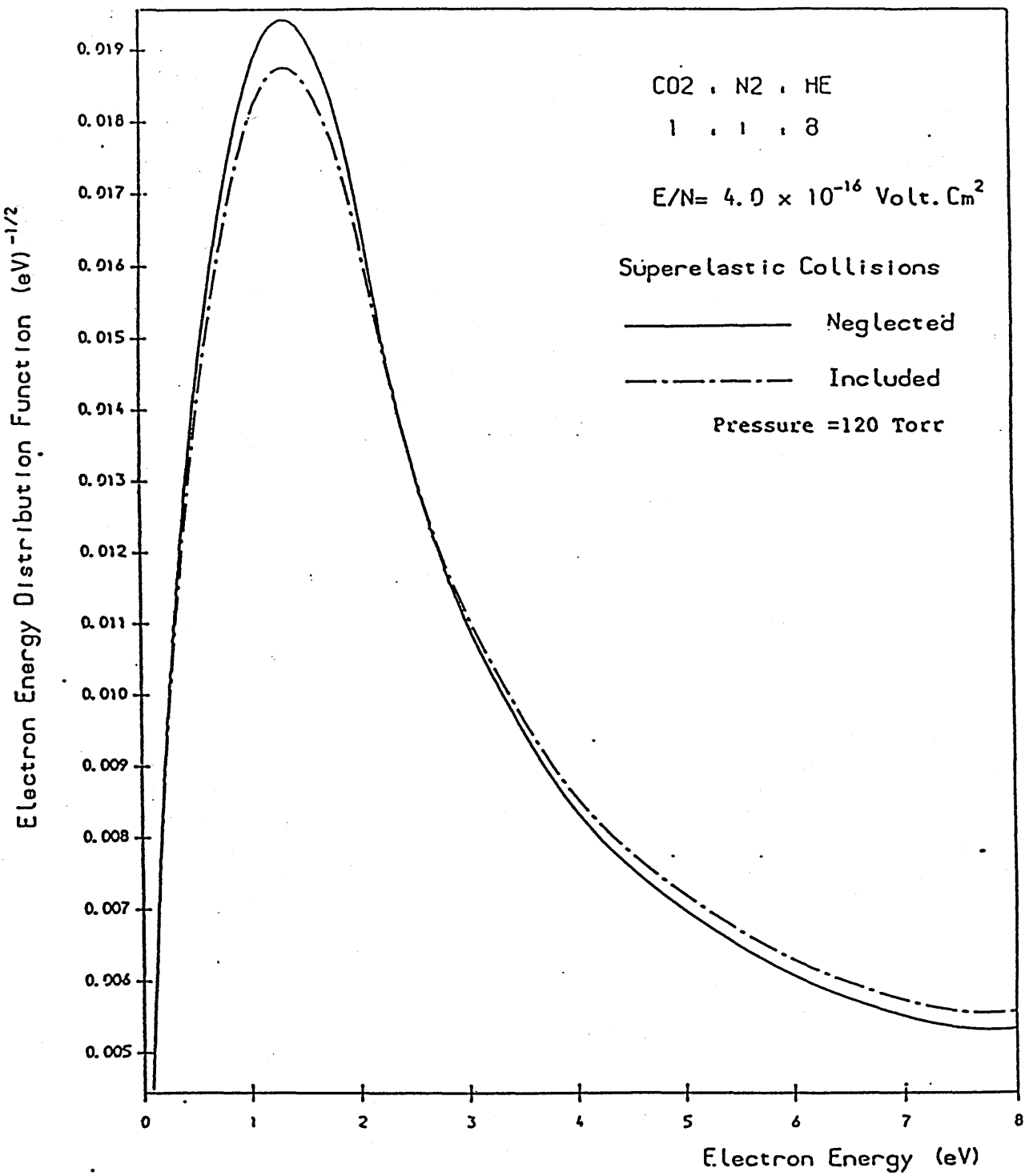

GRAPH OF ELECTRON ENERGY DISTRIBUTION FUNCTION

GRAPH (2.9)

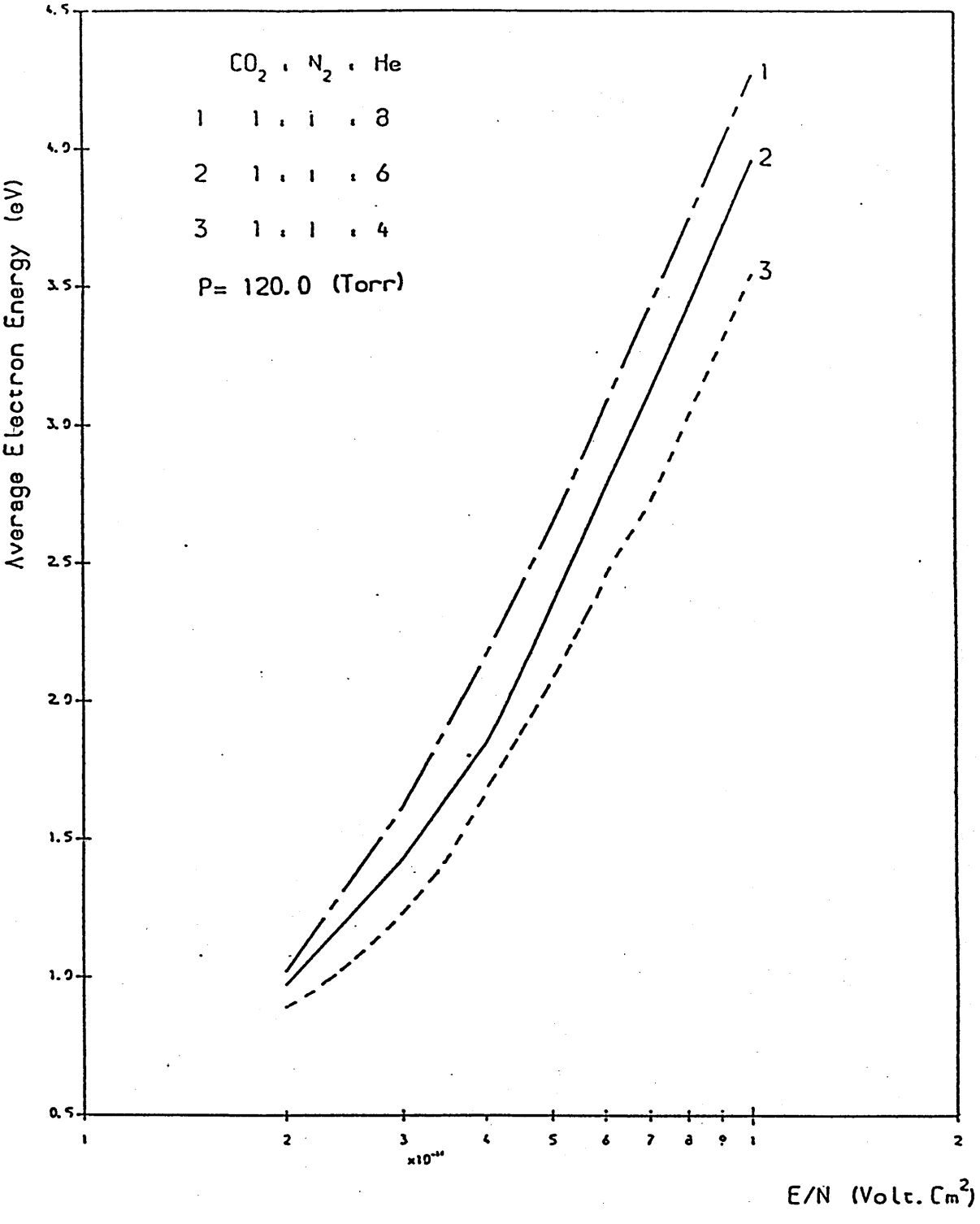

GRAPH OF AVERAGE ELECTRON ENERGY VERSUS E/N

GRAPH (2.10)

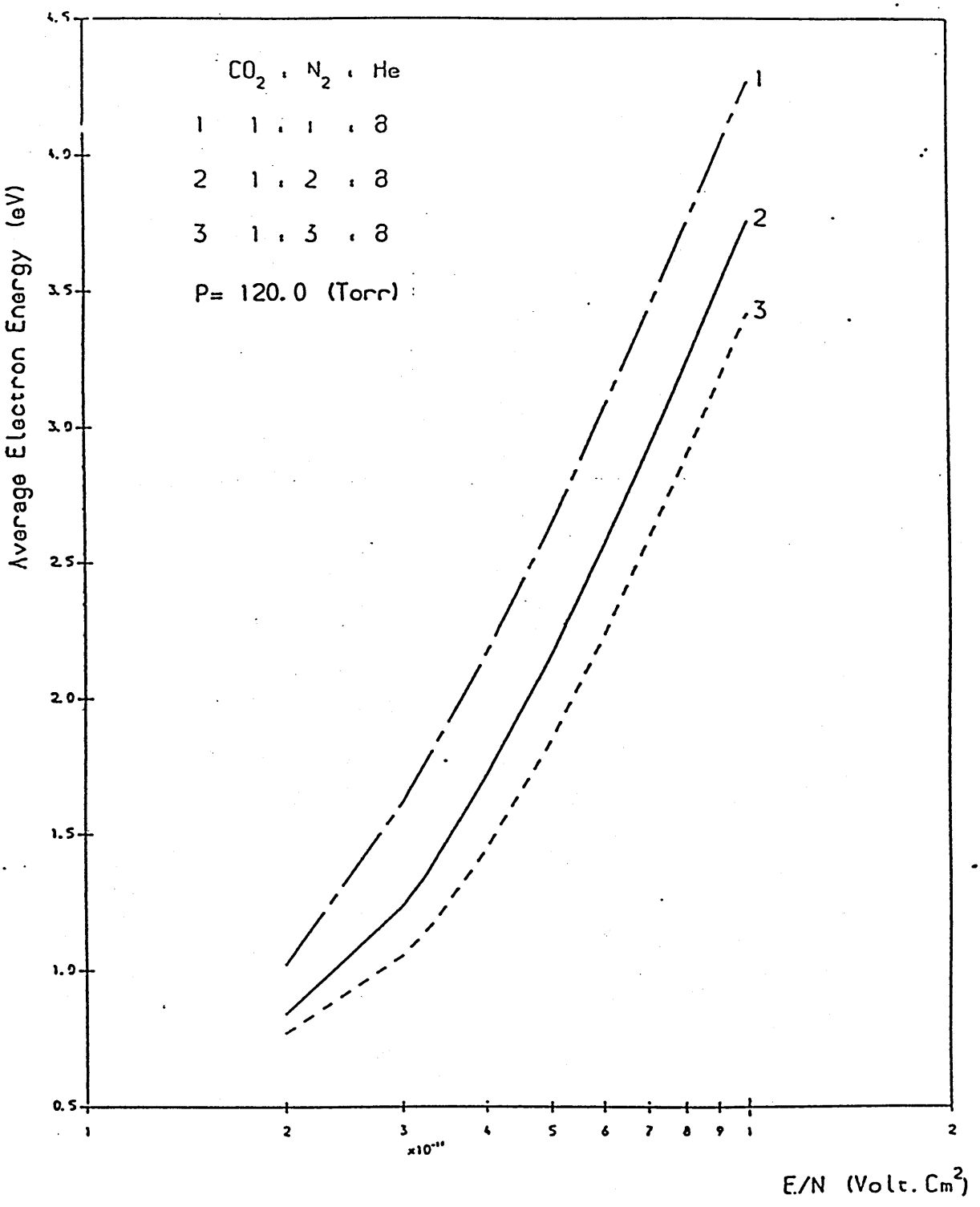

GRAPH OF AVERAGE ELECTRON ENERGY VERSUS E/N

GRAPH (2.11)

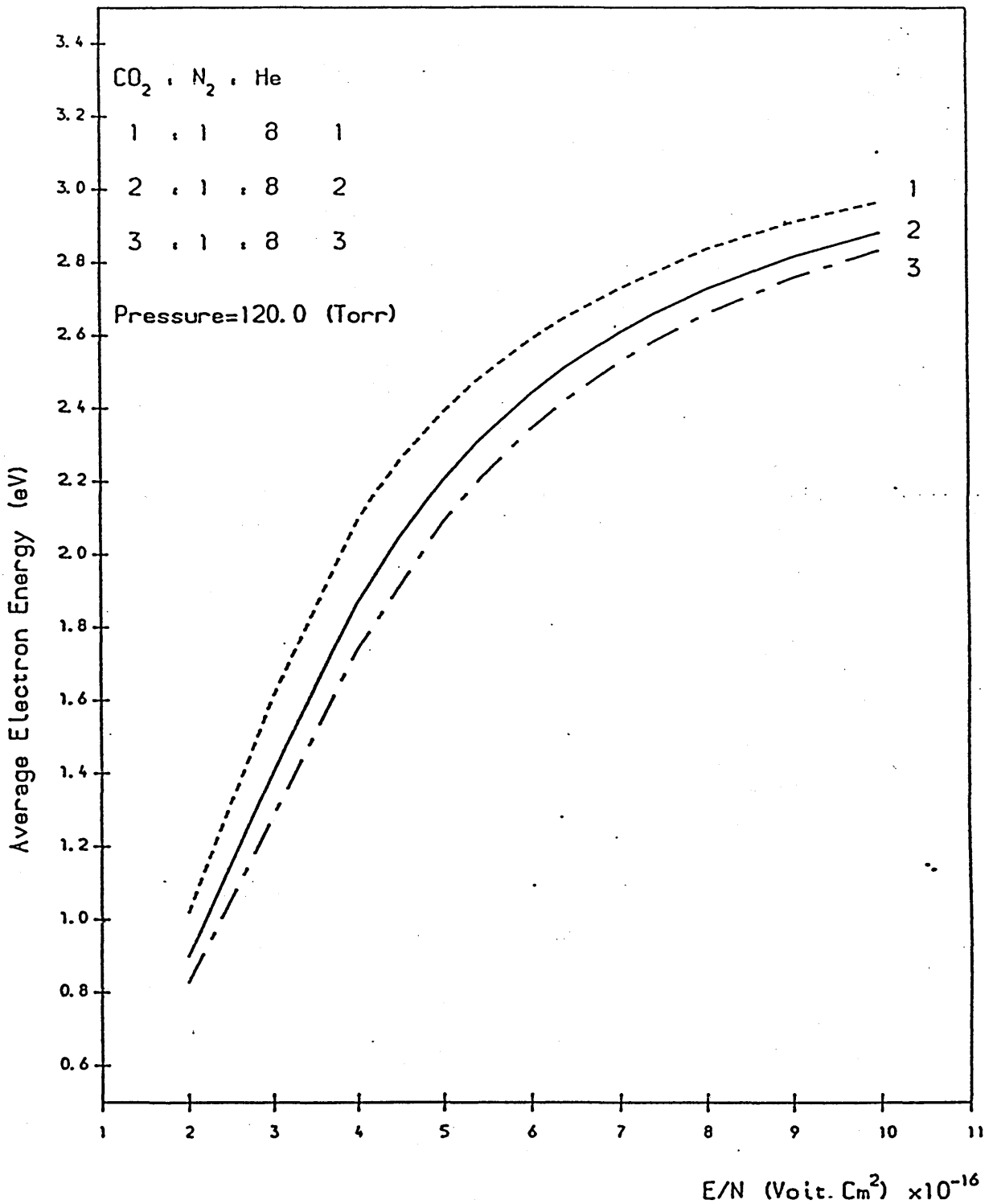

GRAPH OF AVERAGE ELECTRON ENERGY VERSUS E/N

GRAPH (2.12)

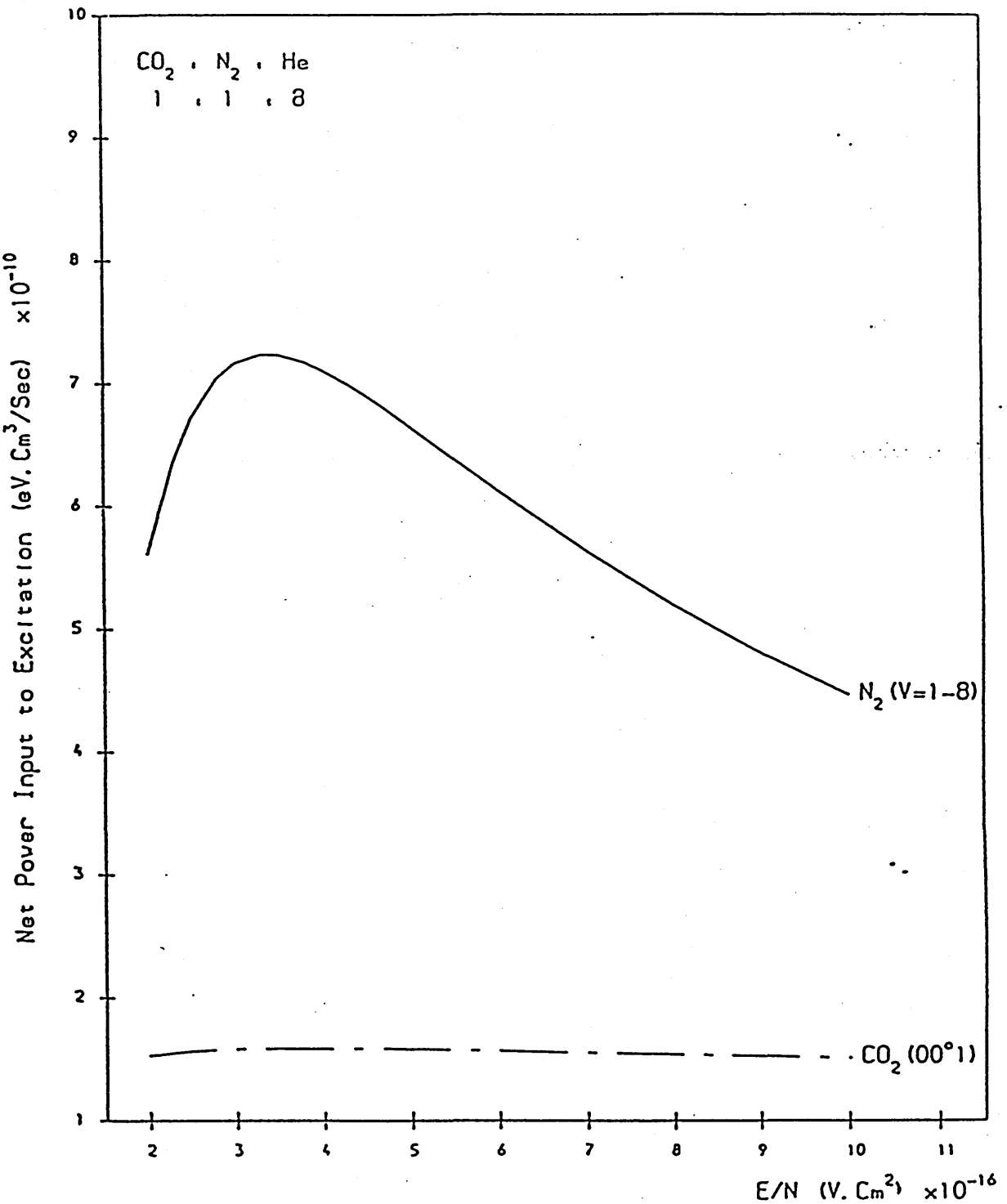

NET POWER INPUT TO EXCITATION VERSUS E/N

GRAPH (2.13)

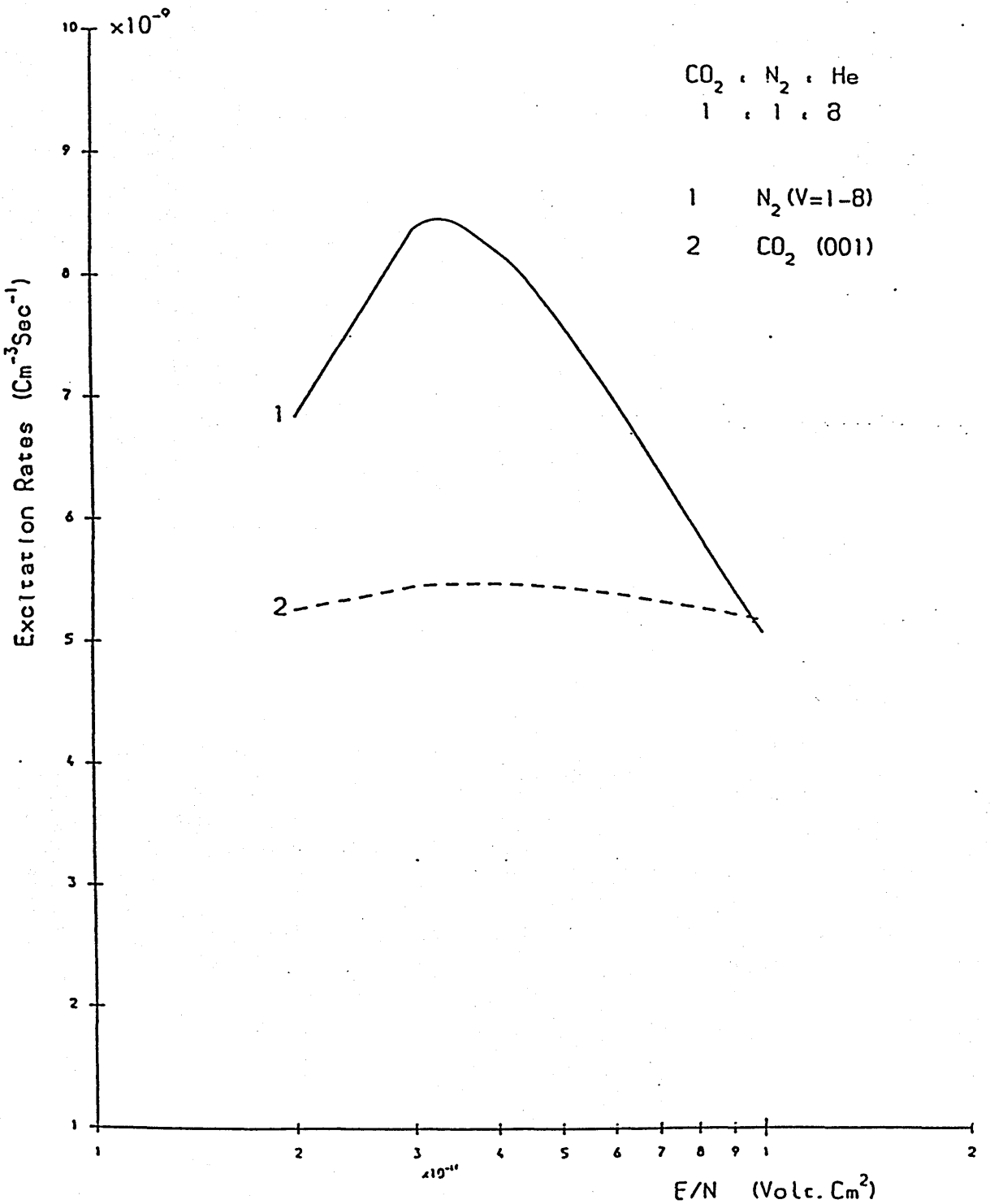

GRAPH OF EXCITATION RATES VERSUS E/N

GRAPH (2.14)

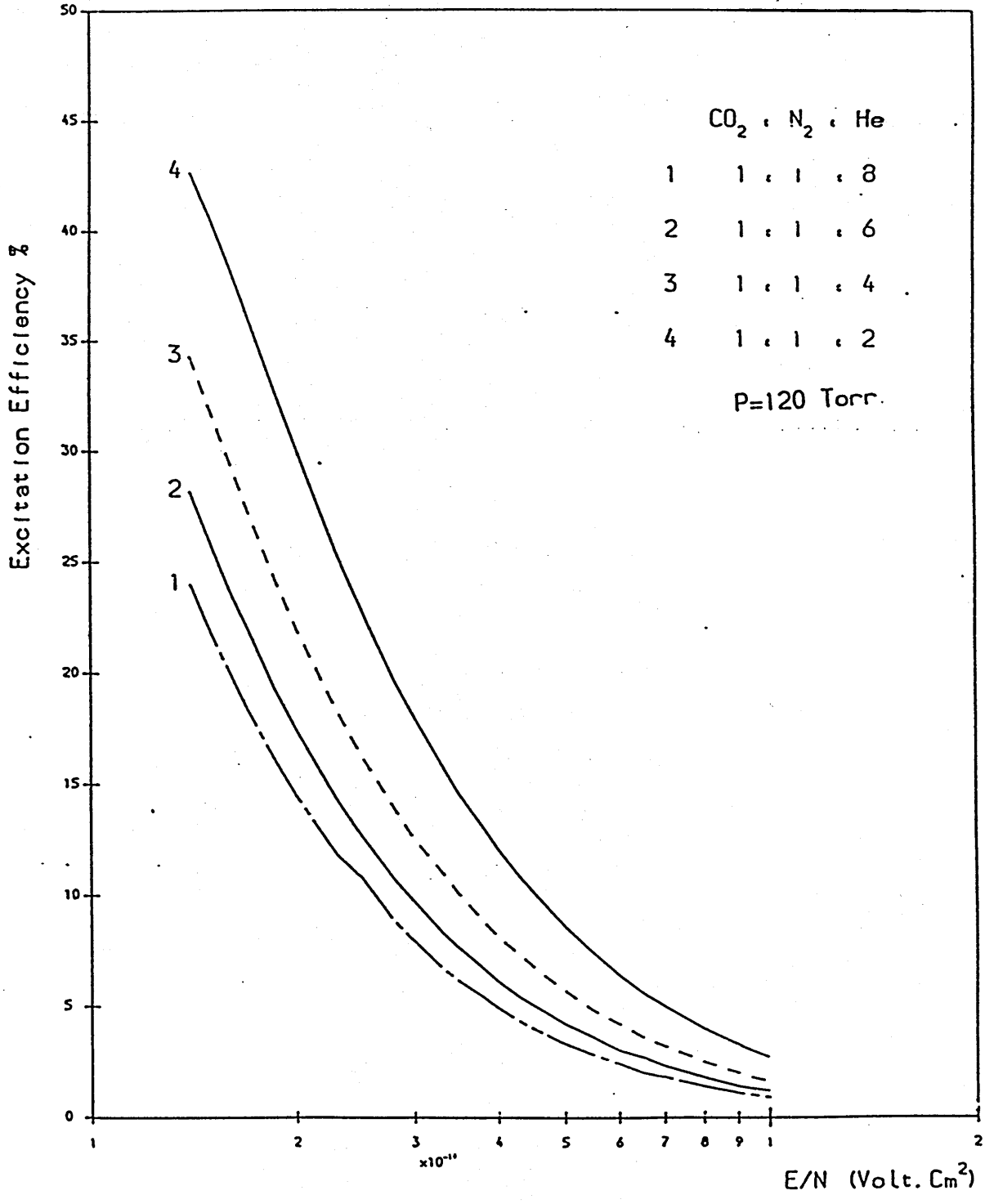

GRAPH OF EXCITATION EFFICIENCY VERSUS E/N OF CO2 (001) LEVEL

GRAPH (2.15)

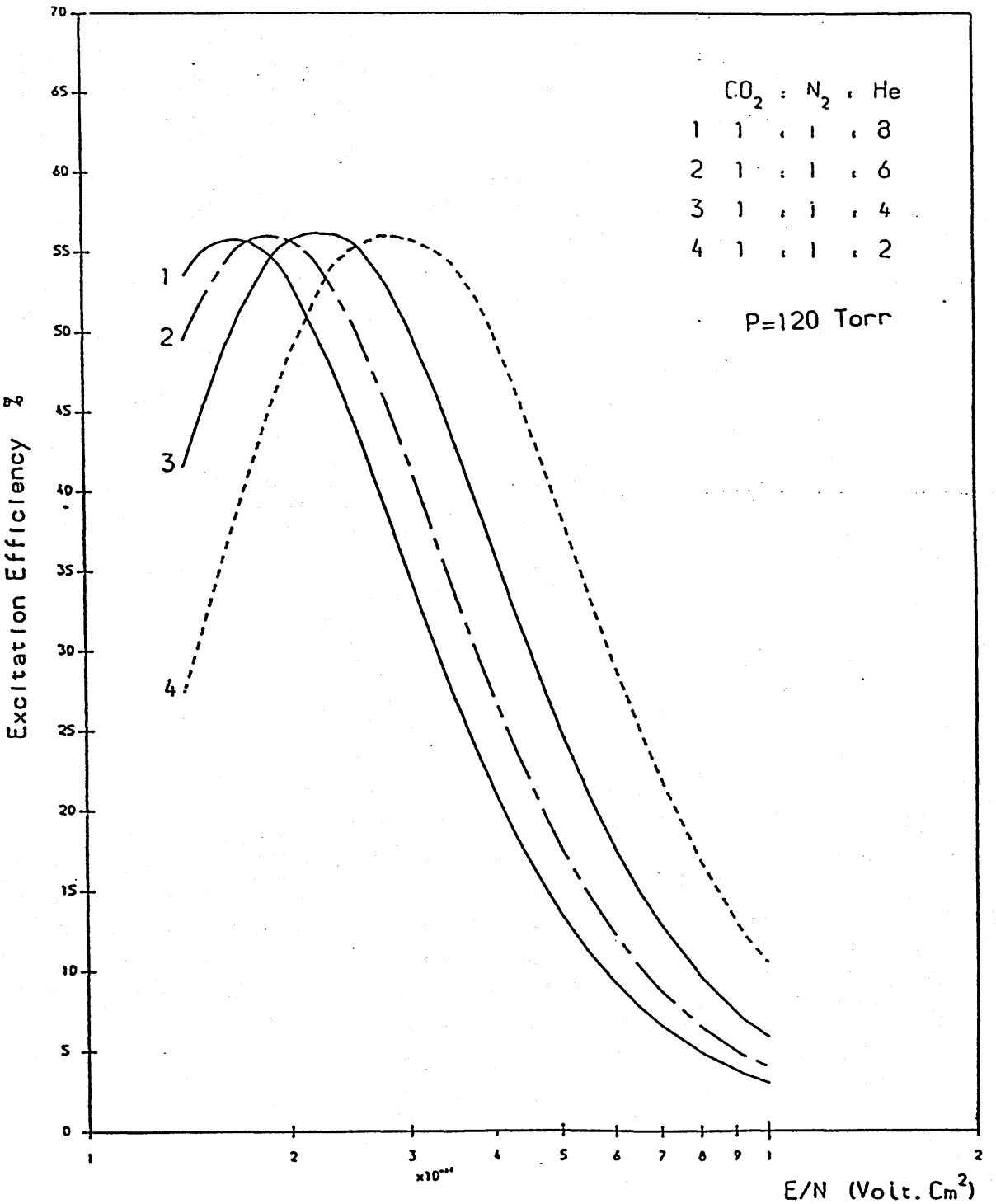

GRAPH OF EXCITATION EFFICIENCY VERSUS E/N OF N2 (V=1-8) LEVELS

GRAPH (2.16)

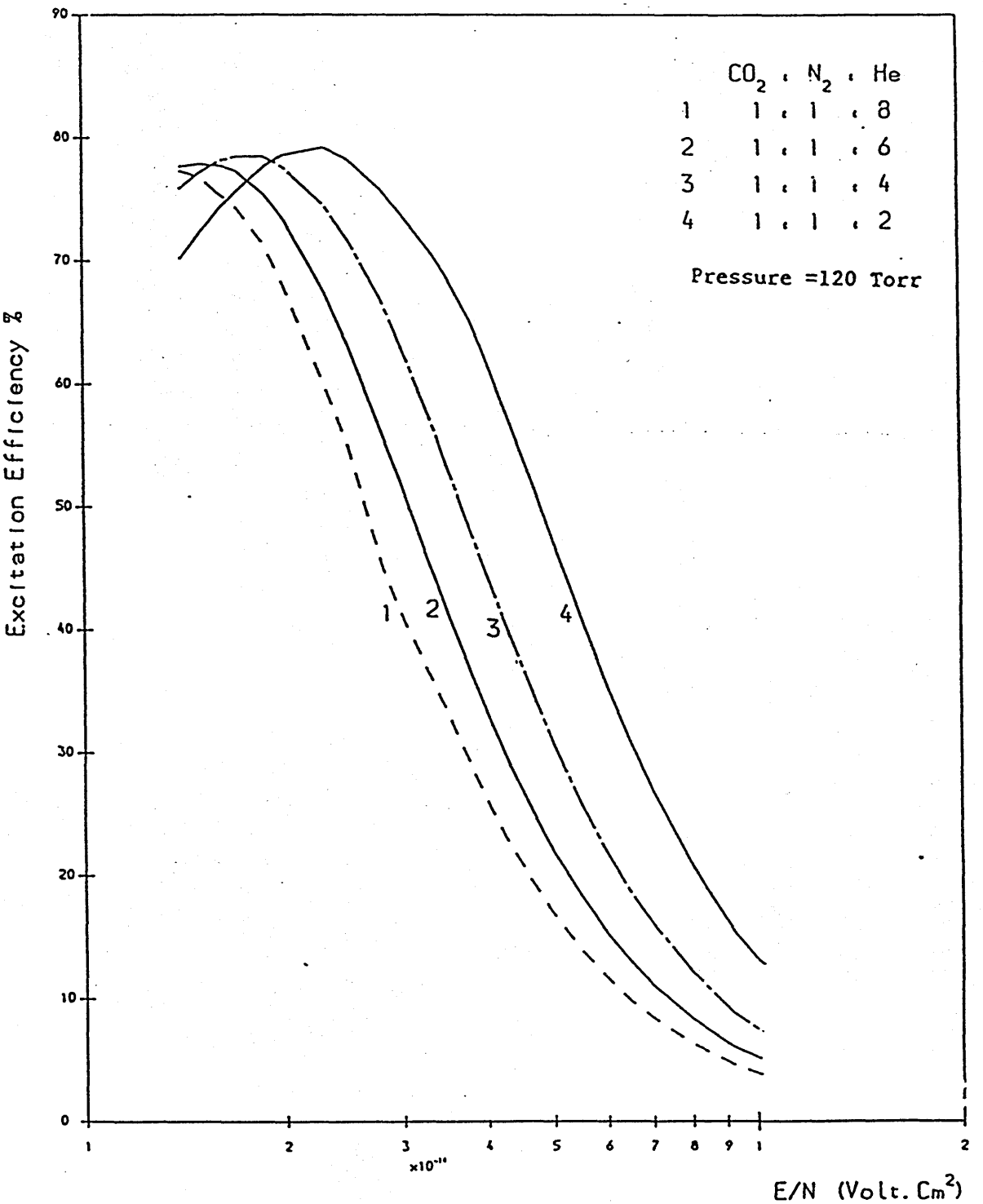

GRAPH OF EXCITATION EFFICIENCY VERSUS E/N OF N2 (V=1-8) + CO2 (001) LEVELS

GRAPH (2.17)

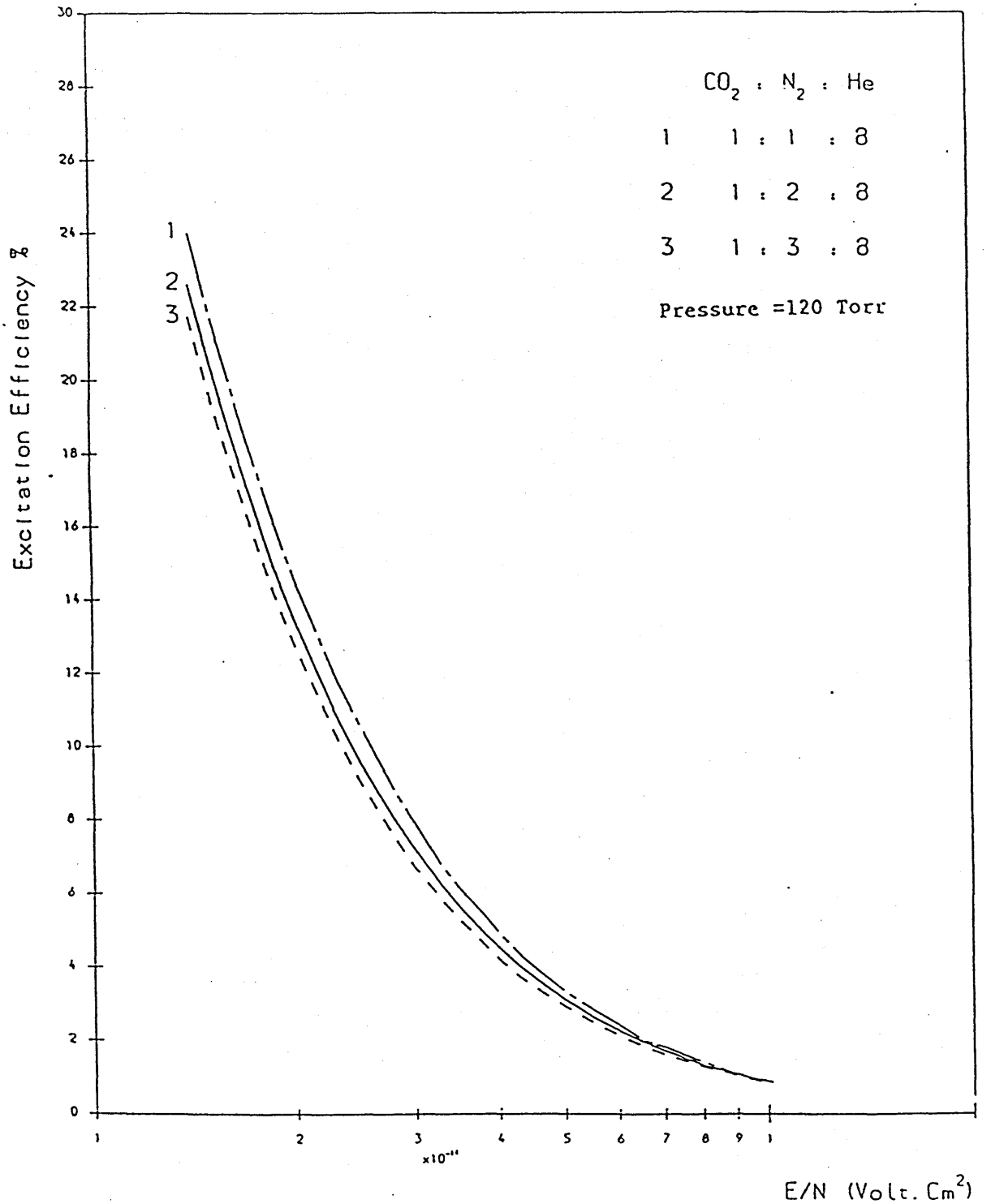

GRAPH OF EXCITATION EFFICIENCY VERSUS E/N OF CO2 (001) LEVEL

GRAPH (2.18)

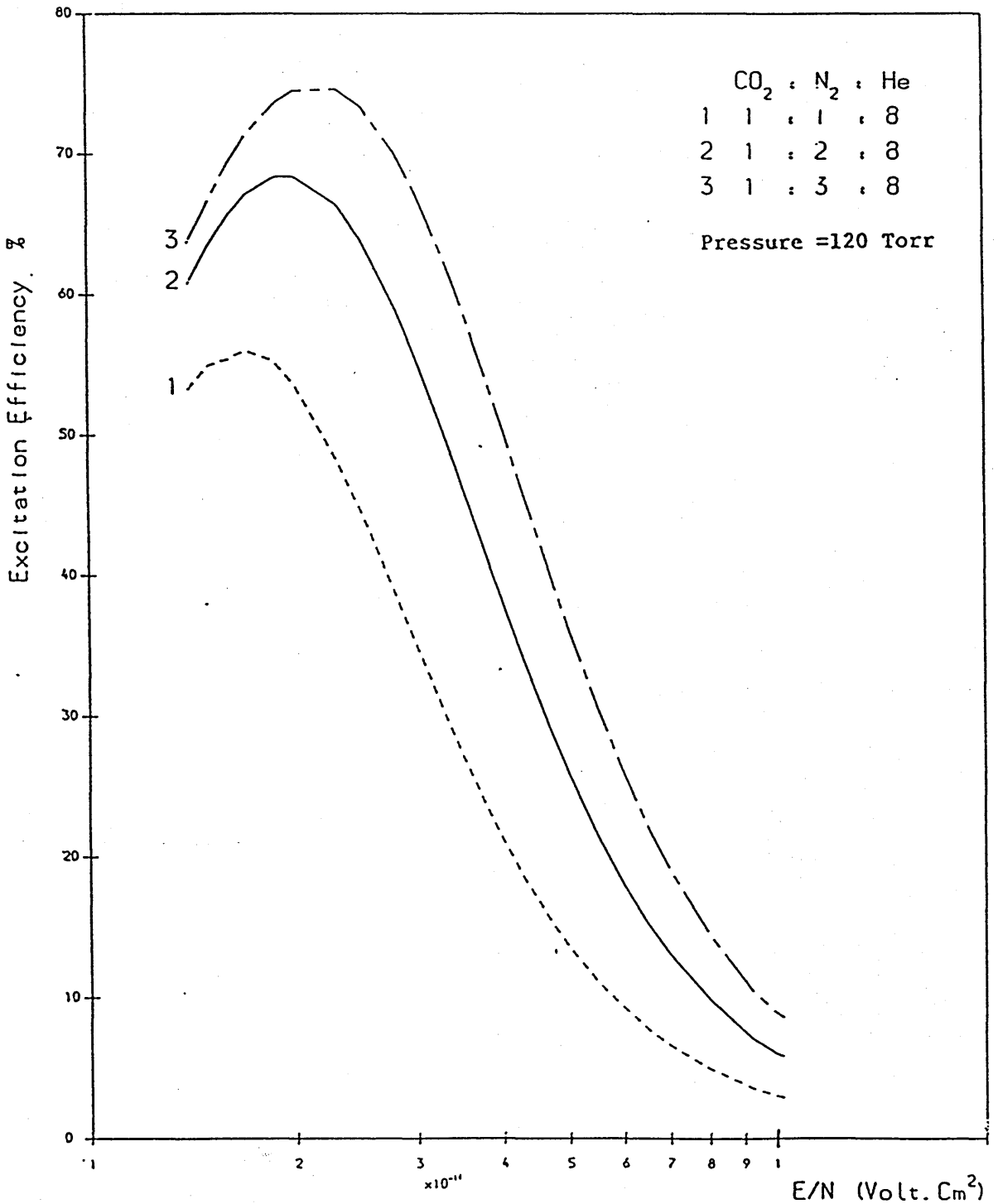

GRAPH OF EXCITATION EFFICIENCY VERSUS E/N OF N2 (V=1-8) LEVELS

GRAPH (2.19)

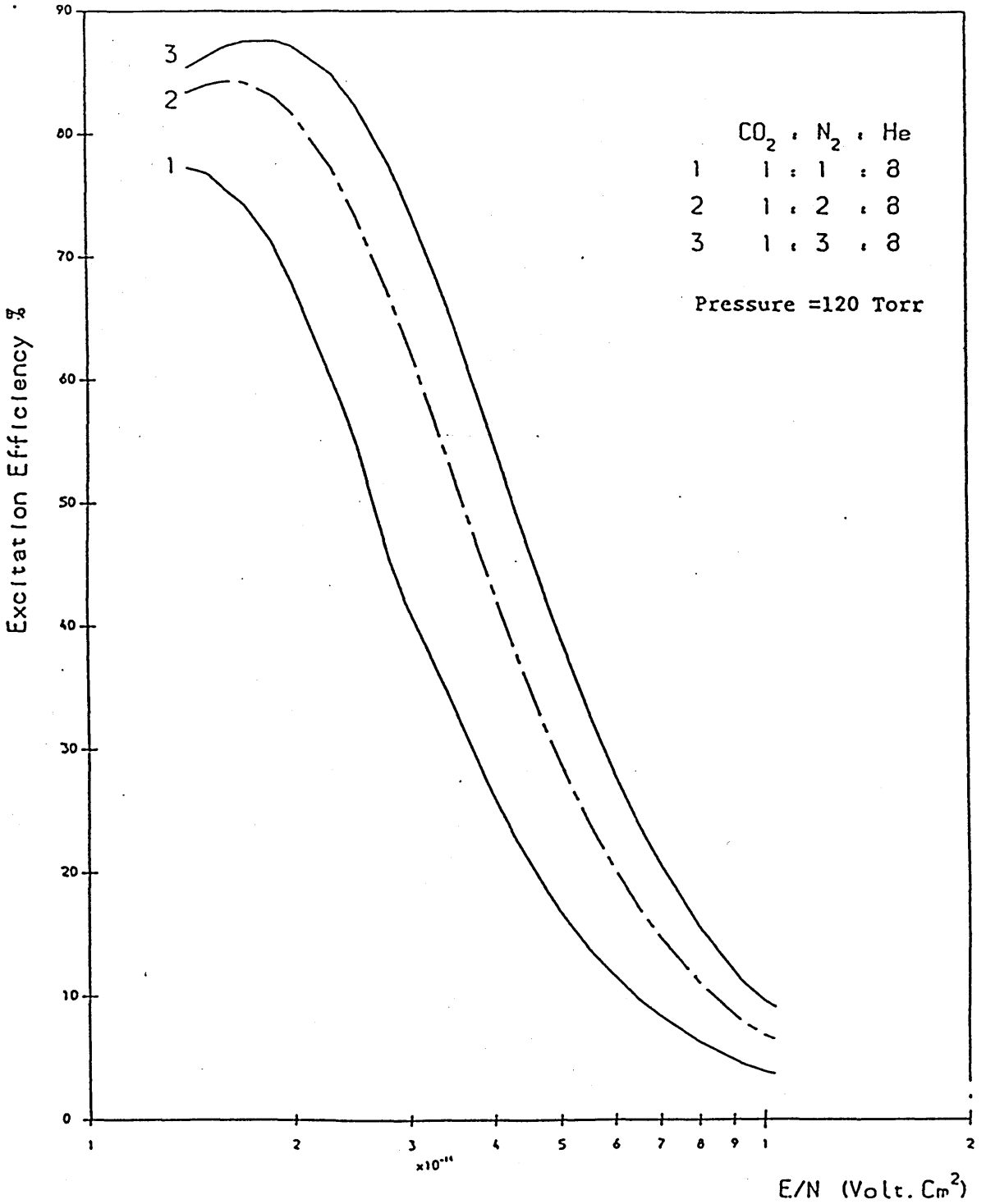

GRAPH OF EXCITATION EFFICIENCY VERSUS E/N OF N2 (V=1-8) + CO2 (001) LEVELS

GRAPH (2.20)

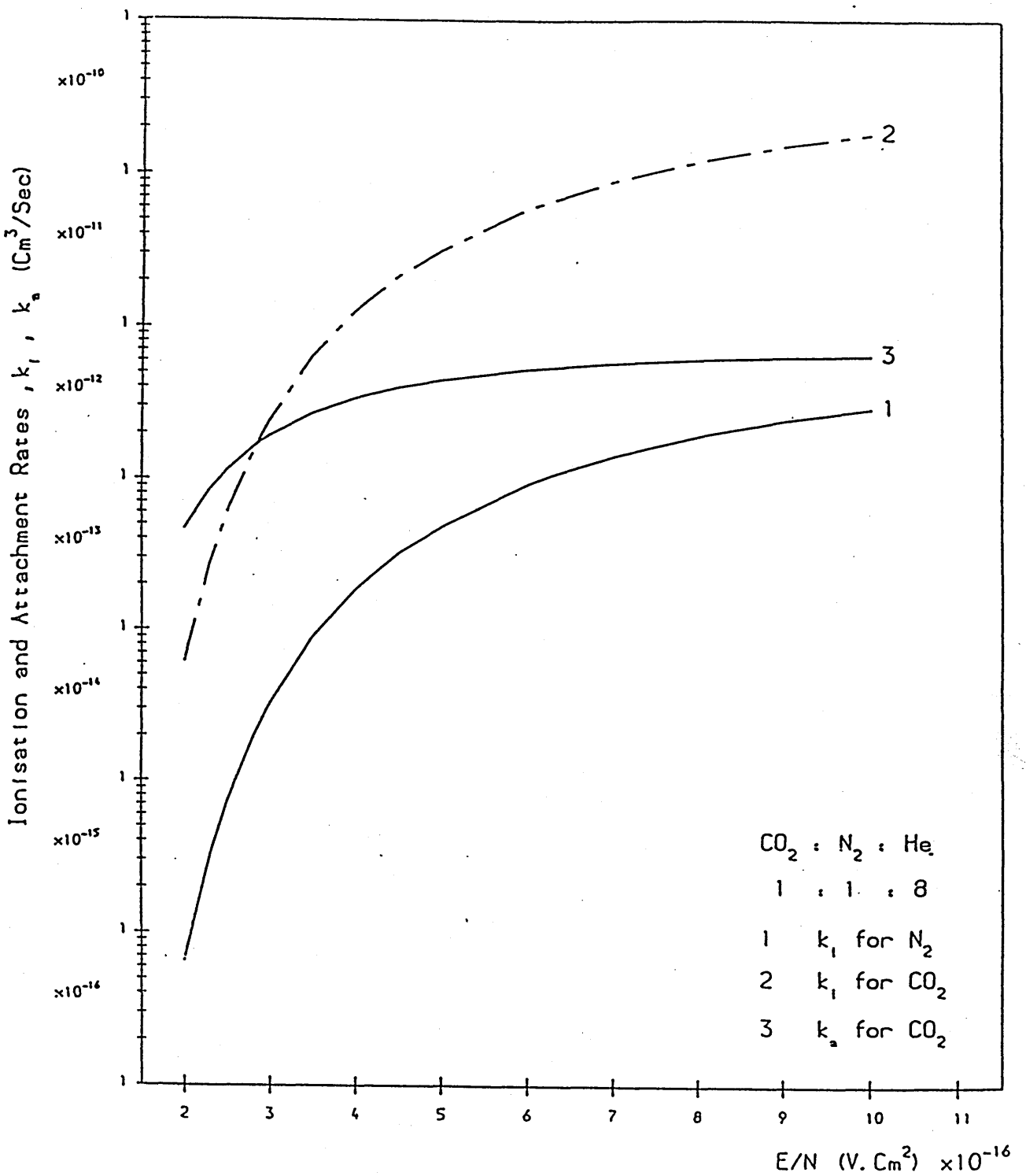

IONISATION AND ATTACHMENT RATES VERSUS E/N

GRAPH (2.21)

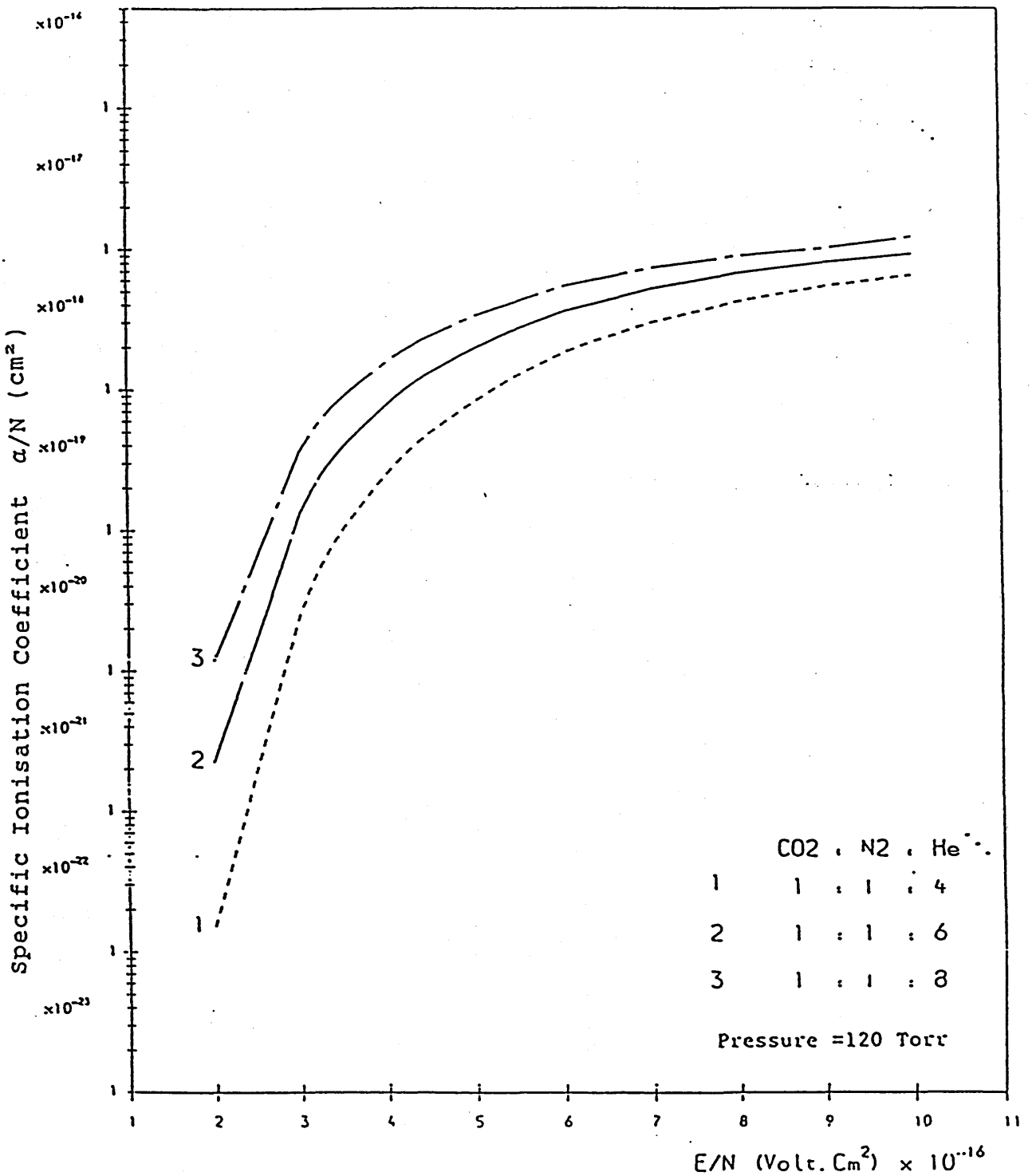

GRAPH OF SPECIFIC

IONISATION COEFFICIENT VERSUS E/N

GRAPH (2.22)

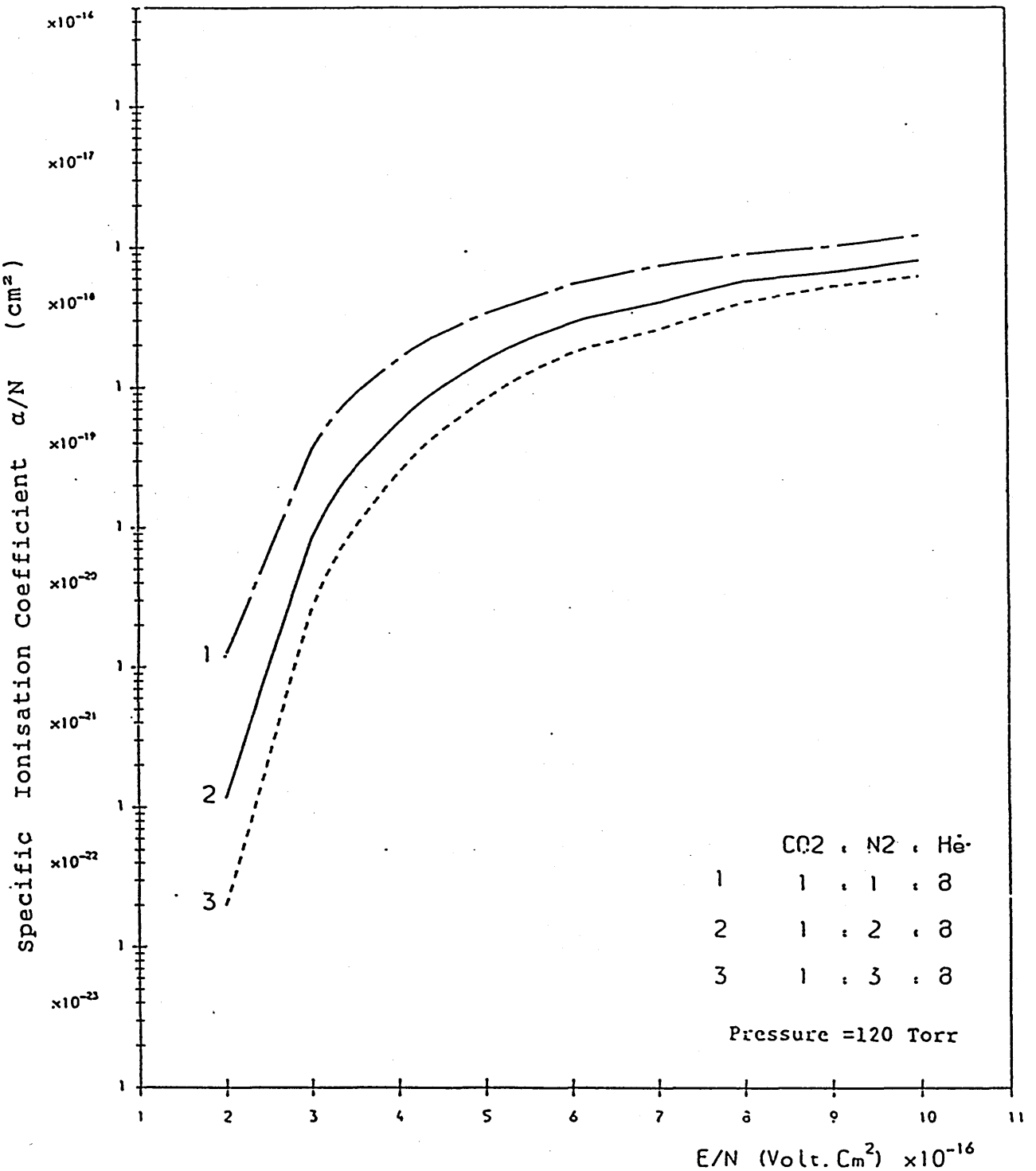

GRAPH OF SPECIFIC

IONISATION COEFFICIENT VERSUS E/N

GRAPH (2.23)

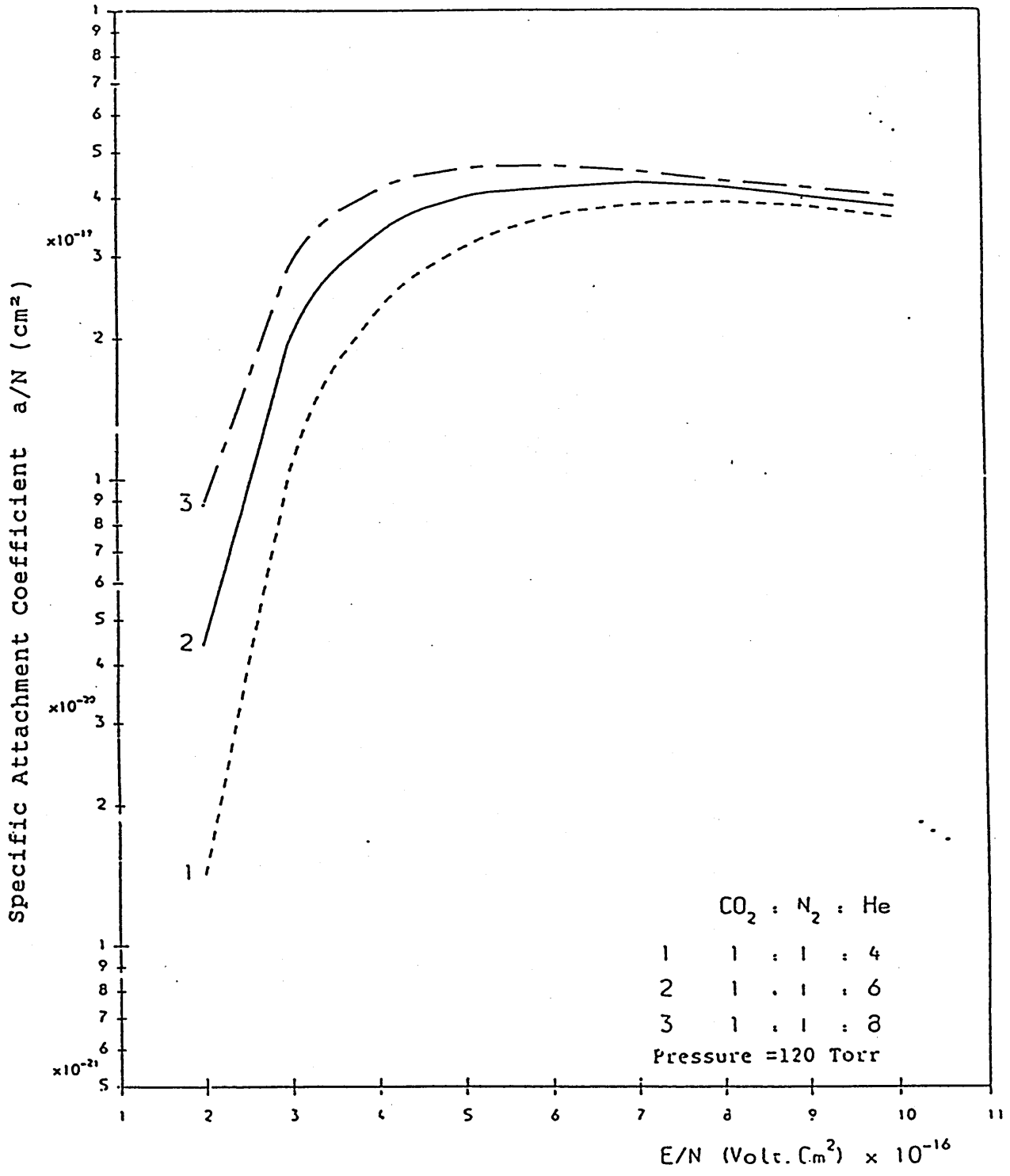

GRAPH OF SPECIFIC

ATTACHMENT COEFFICIENT VERSUS E/N

GRAPH (2.24)

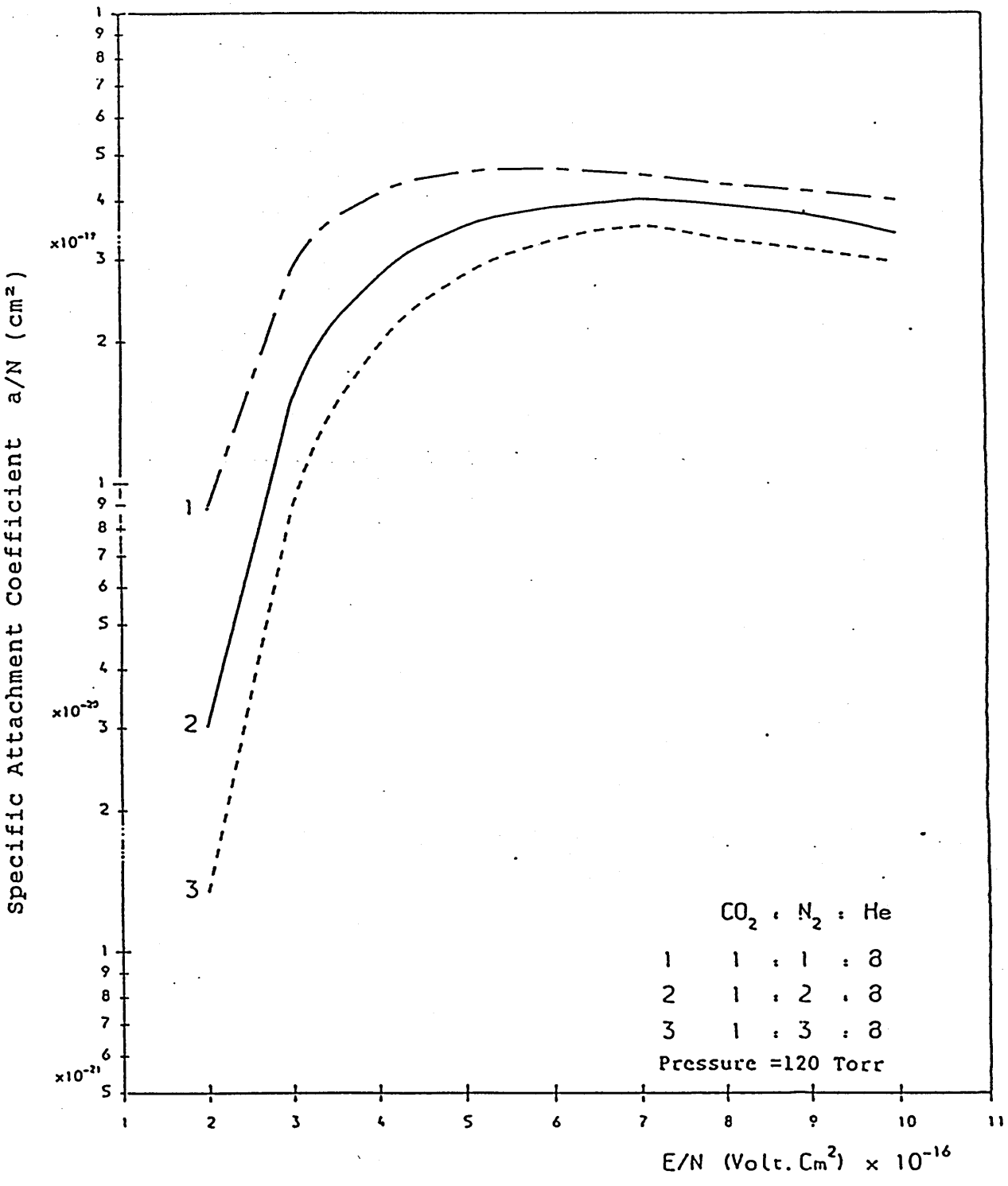

GRAPH OF SPECIFIC

ATTACHMENT COEFFICIENT VERSUS E/N

GRAPH (2.25)

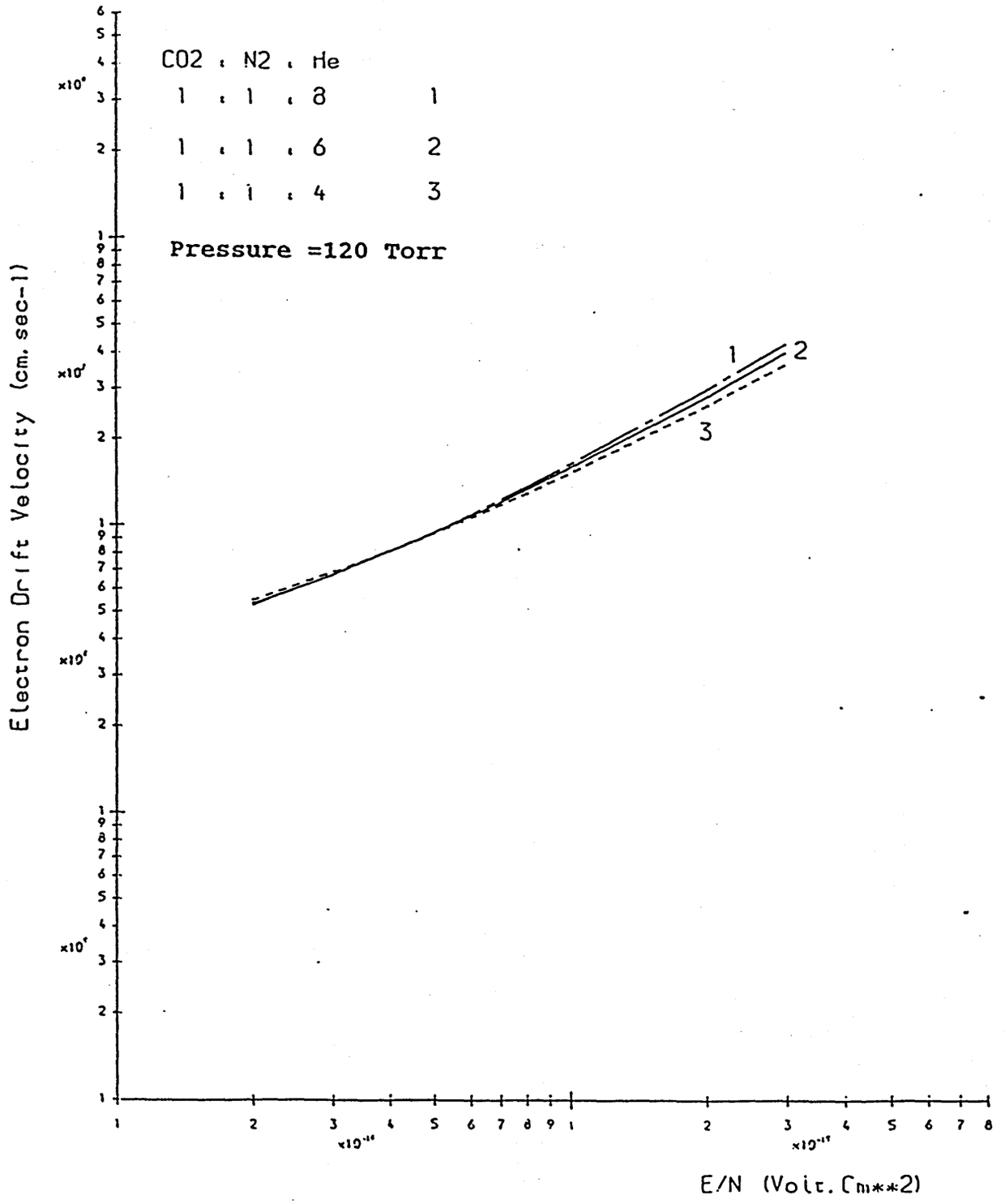

GRAPH OF ELECTRON DRIFT VELOCITY VERSUS E/N

GRAPH (2.26)

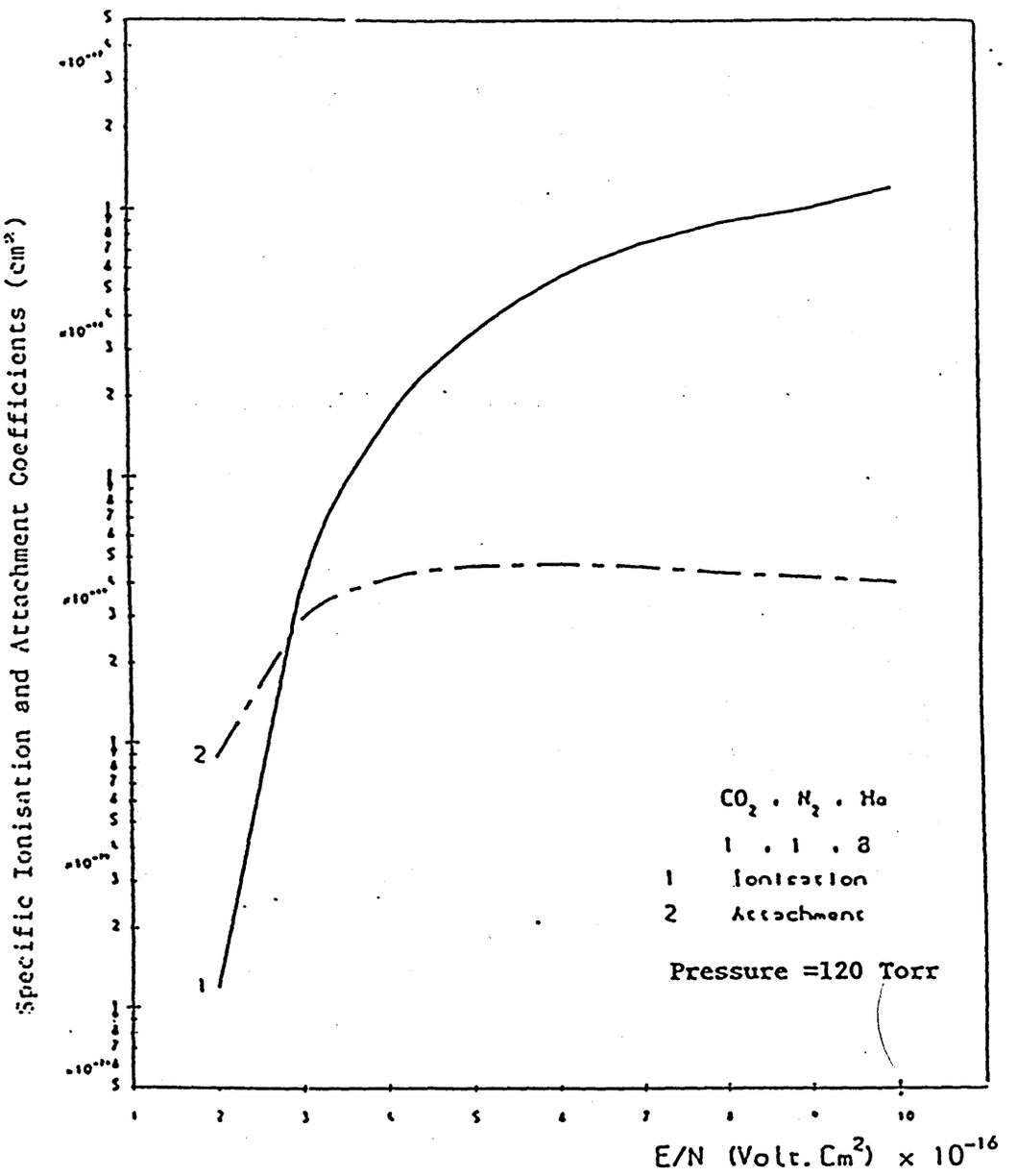

GRAPH OF SPECIFIC

IONISATION AND ATTACHMENT COEFFICIENTS VERSUS E/N

GRAPH (2.27)

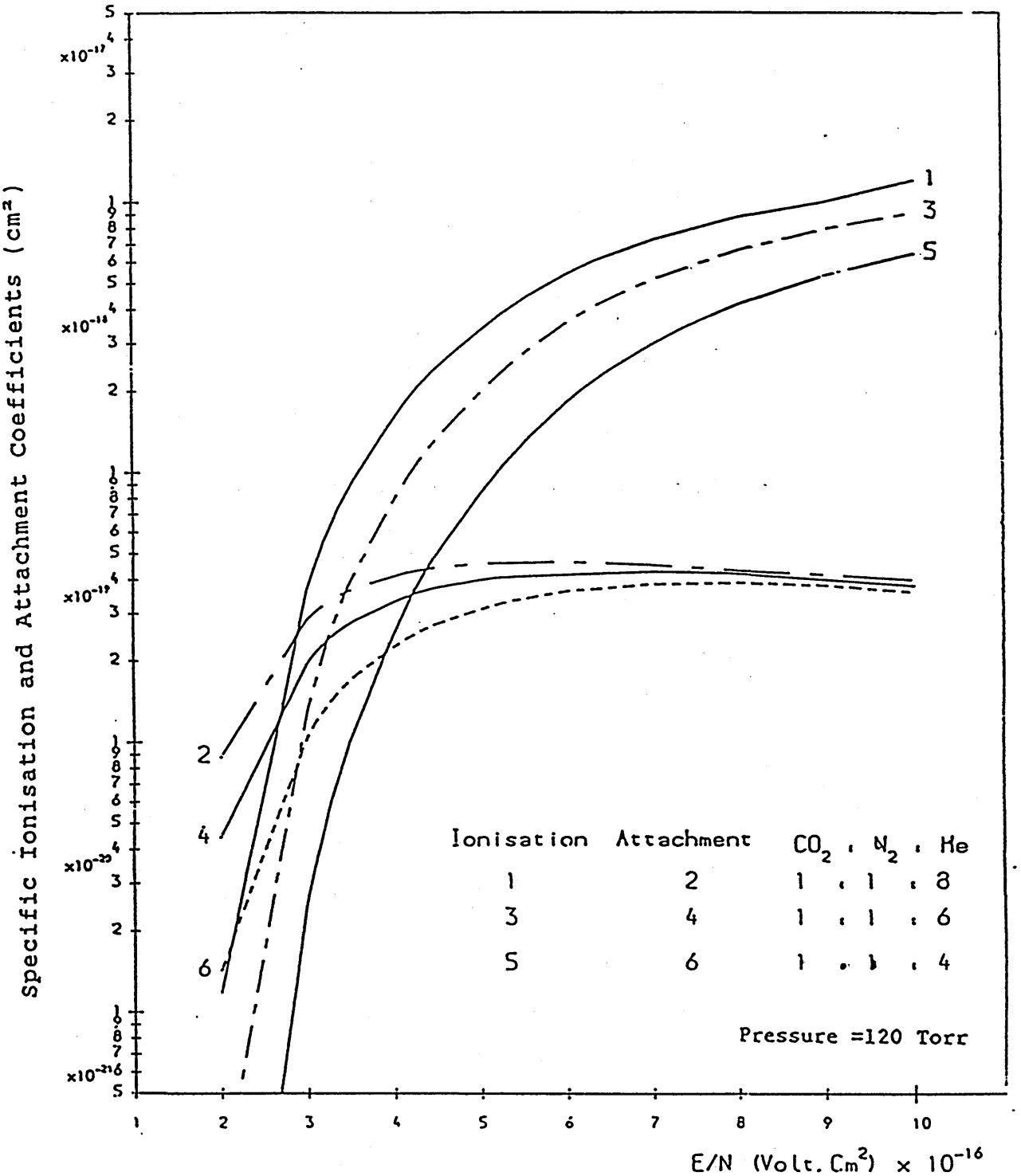

GRAPH OF SPECIFIC

IONISATION AND ATTACHMENT COEFFICIENTS VERSUS E/N

GRAPH (2.28)

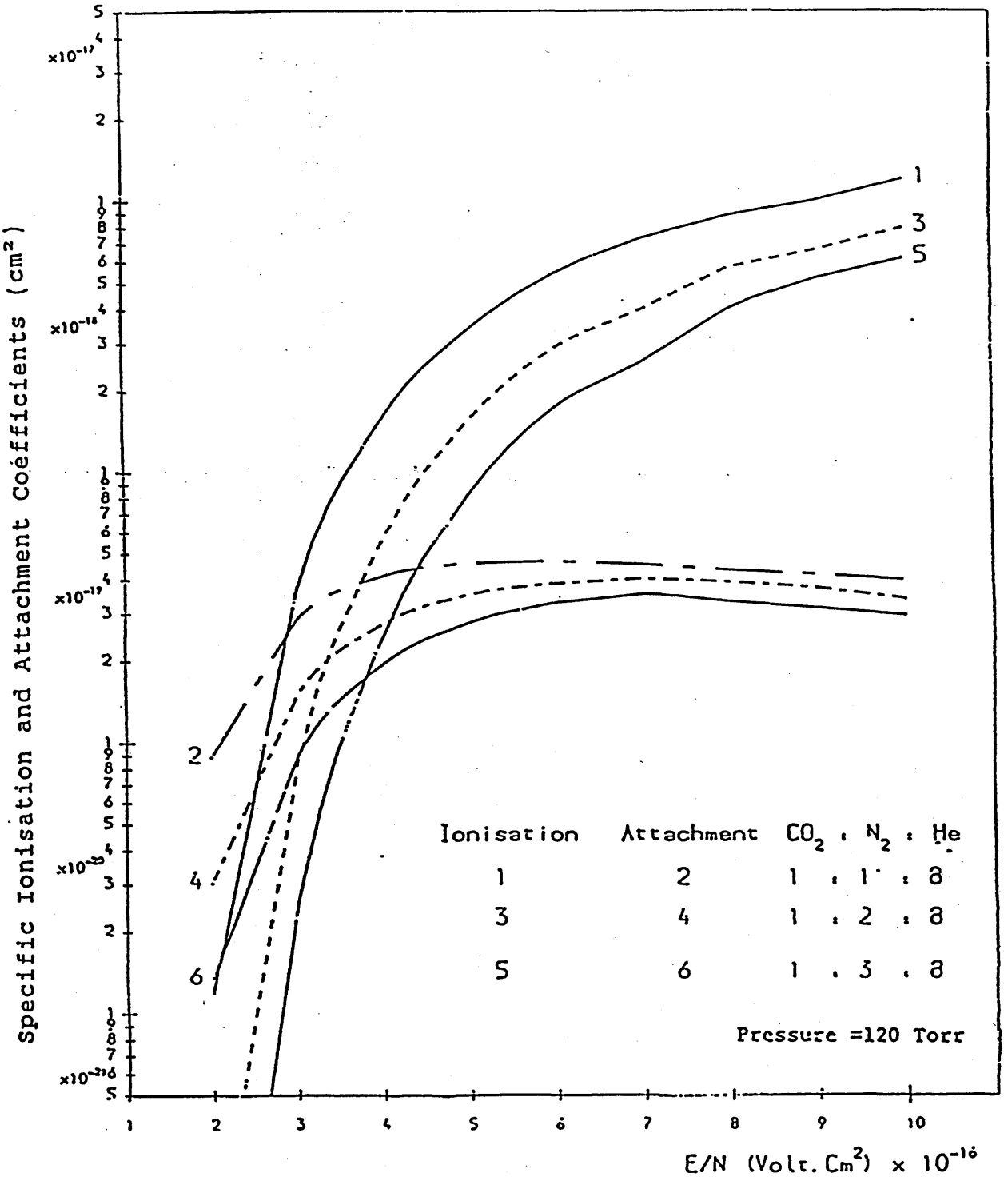

GRAPH OF SPECIFIC

IONISATION AND ATTACHMENT COEFFICIENTS VERSUS E/N

GRAPH (2.29)

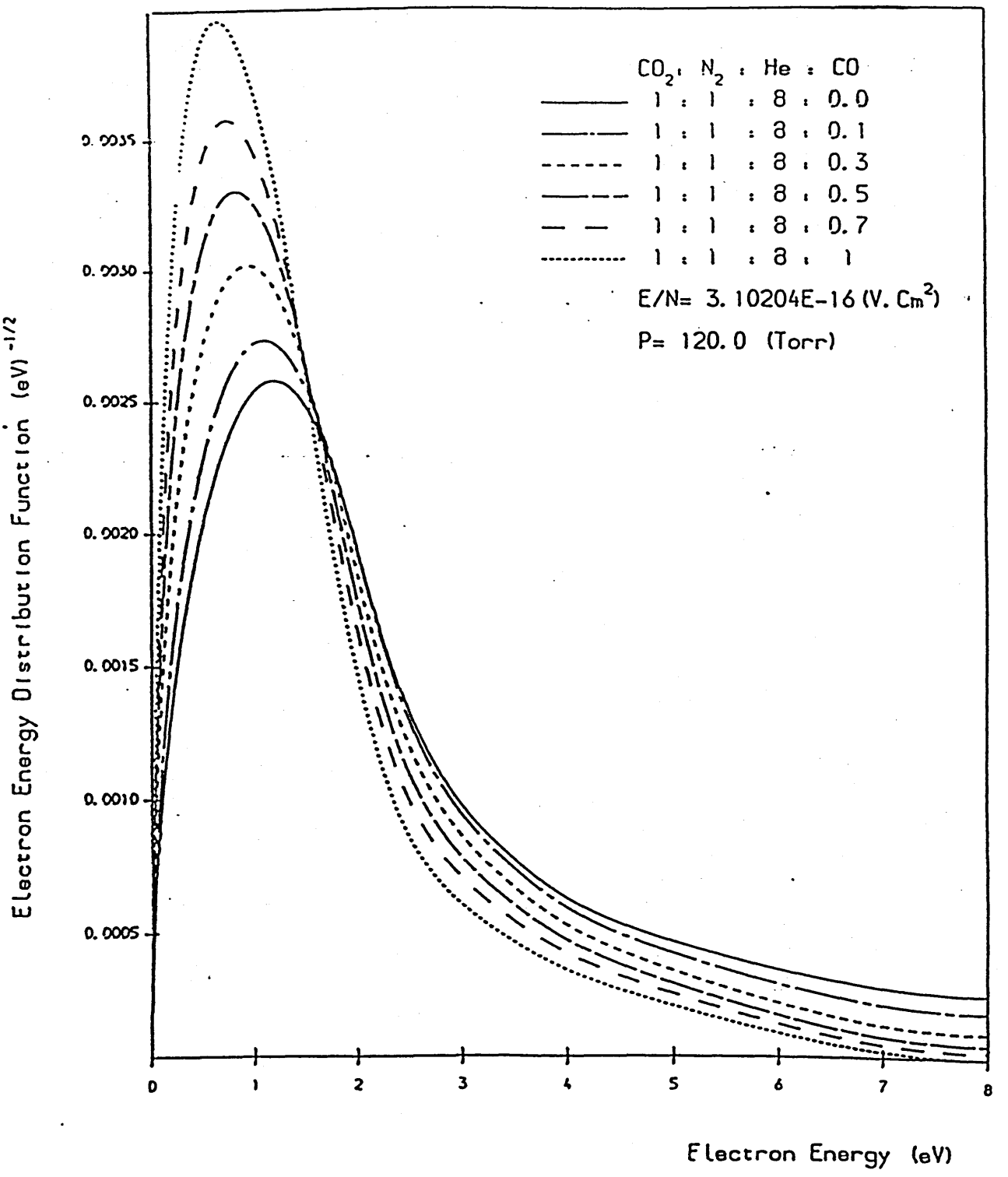

GRAPH OF ELECTRON ENERGY DISTRIBUTION FUNCTION

GRAPH (2.30)

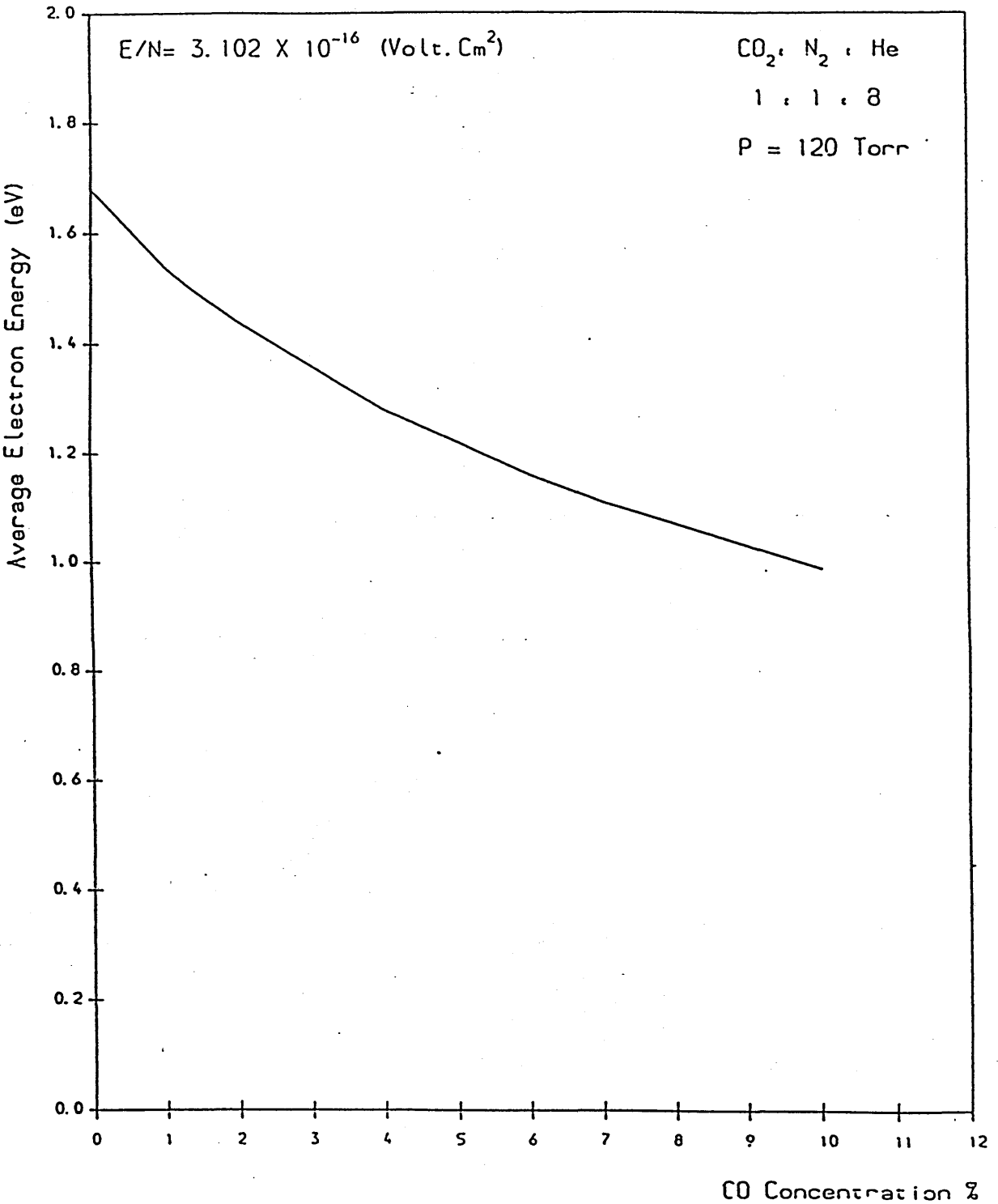

VARIATION OF AVERAGE ELECTRON ENERGY WITH ADDITION OF CO

GRAPH (2.31)

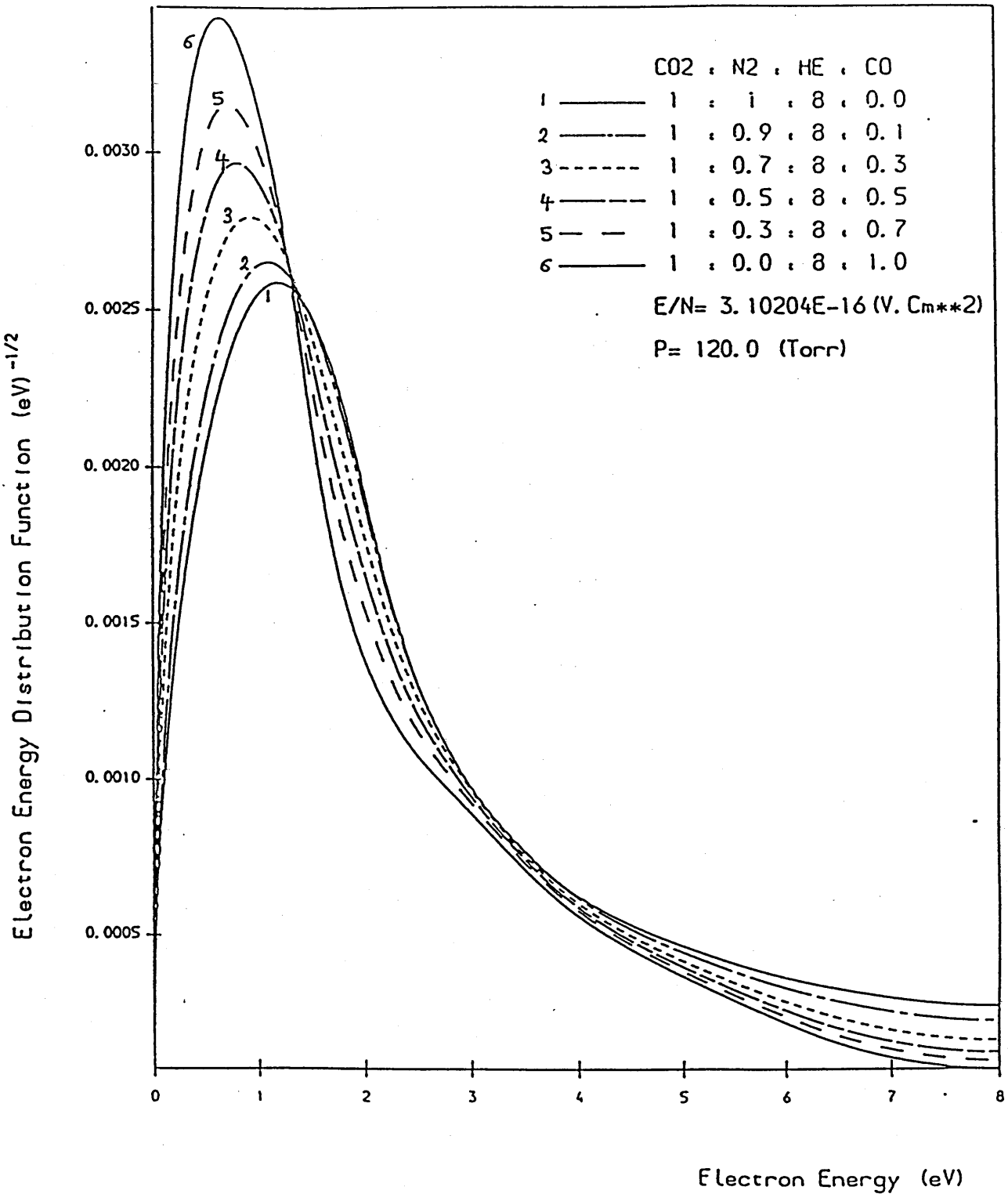

GRAPH OF ELECTRON ENERGY DISTRIBUTION FUNCTION

GRAPH (2.32)

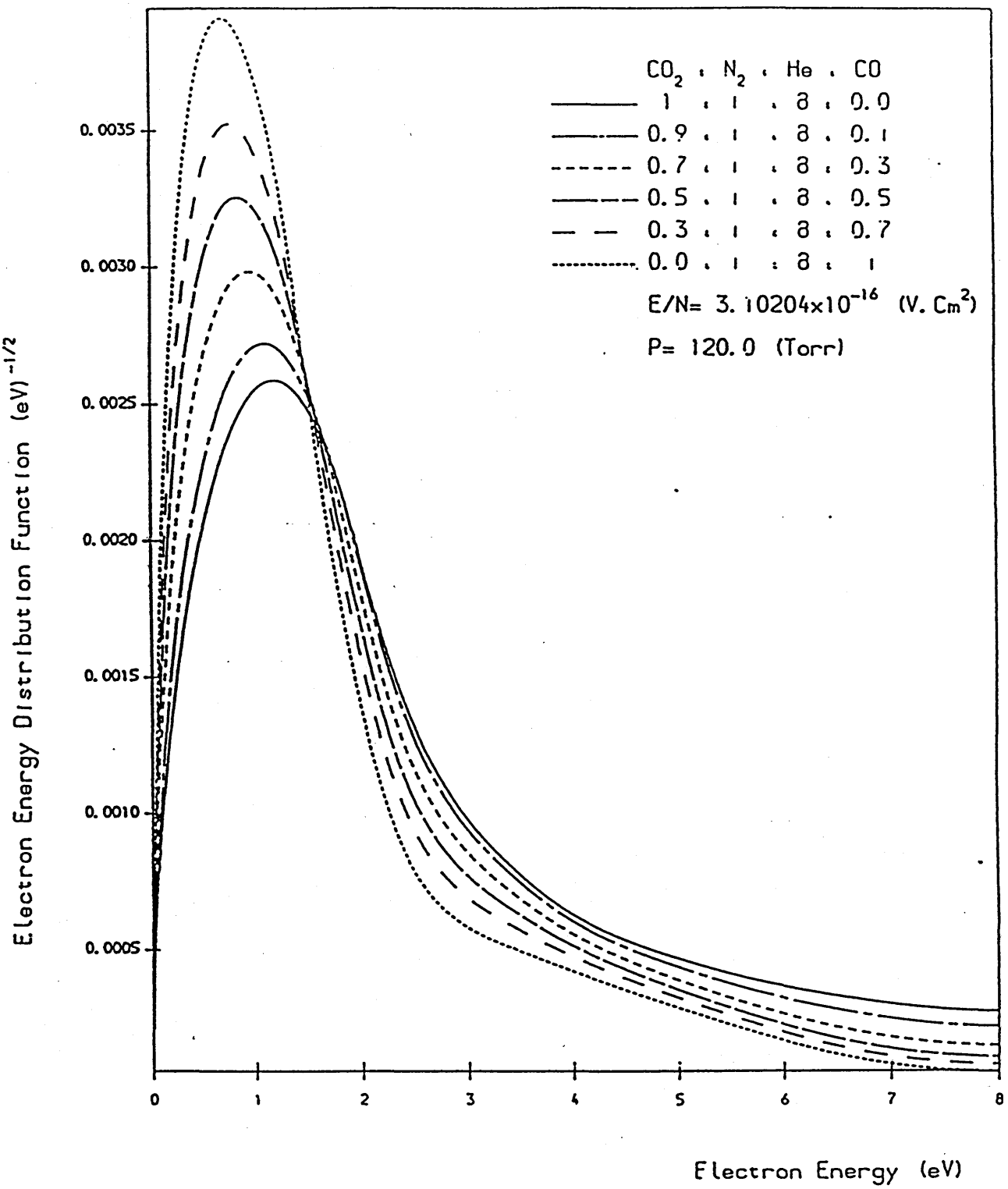

GRAPH OF ELECTRON ENERGY DISTRIBUTION FUNCTION

GRAPH (2.33)

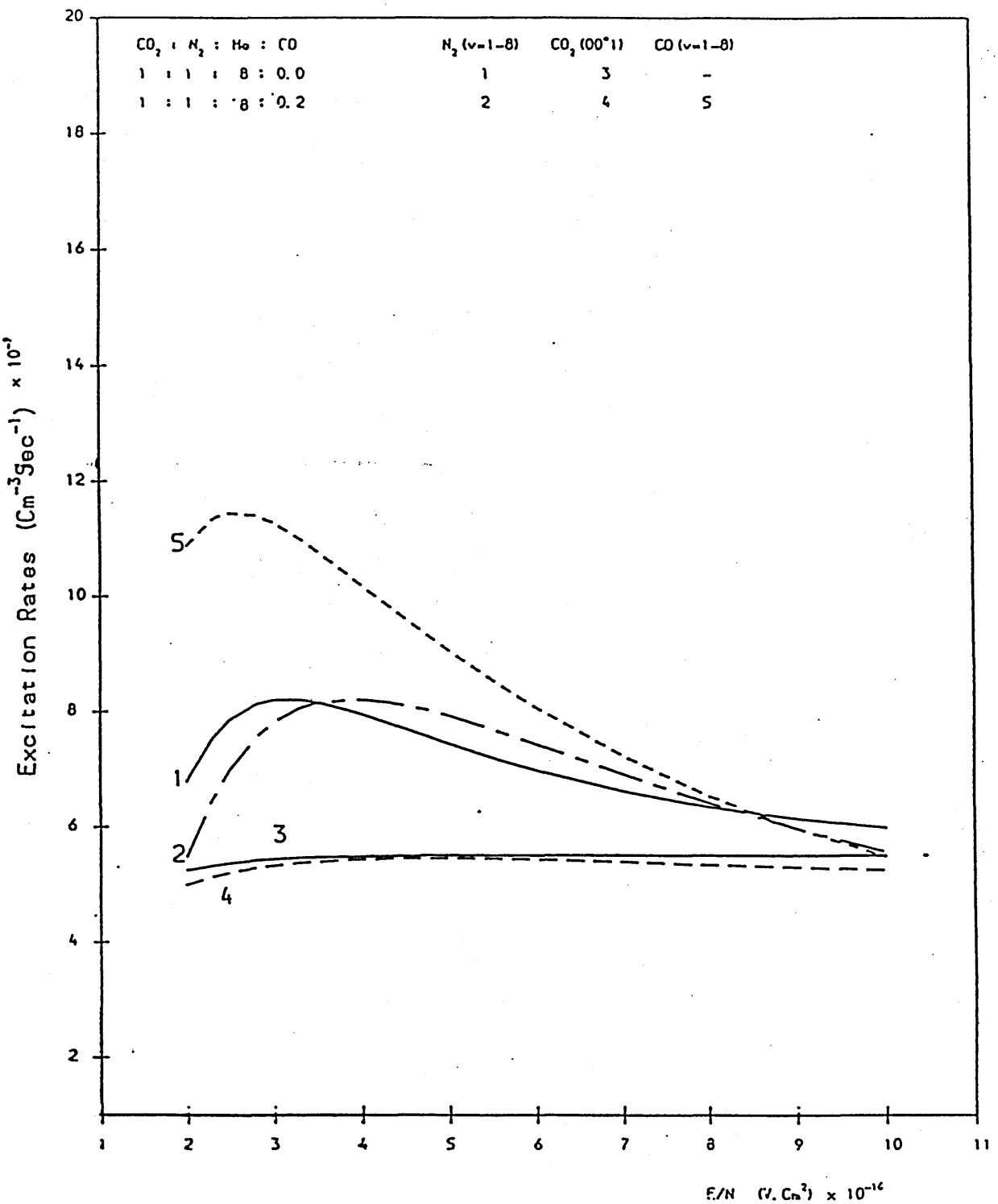

GRAPH OF EXCITATION RATES VERSUS E/N

GRAPH (2.34)

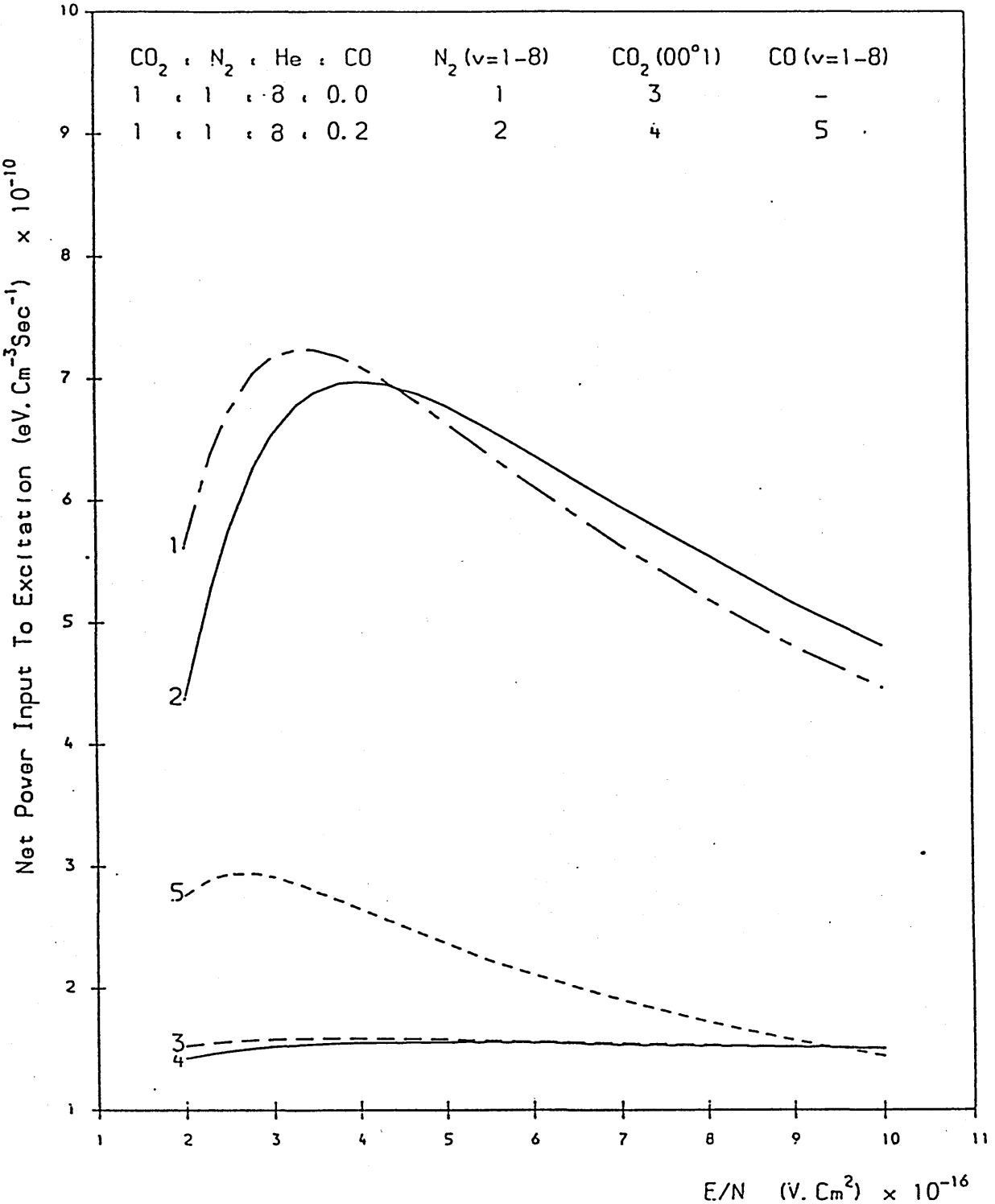

GRAPH OF NET POWER INPUT TO VIBRATIONAL EXCITATION VERSUS E/N

GRAPH (2.35)

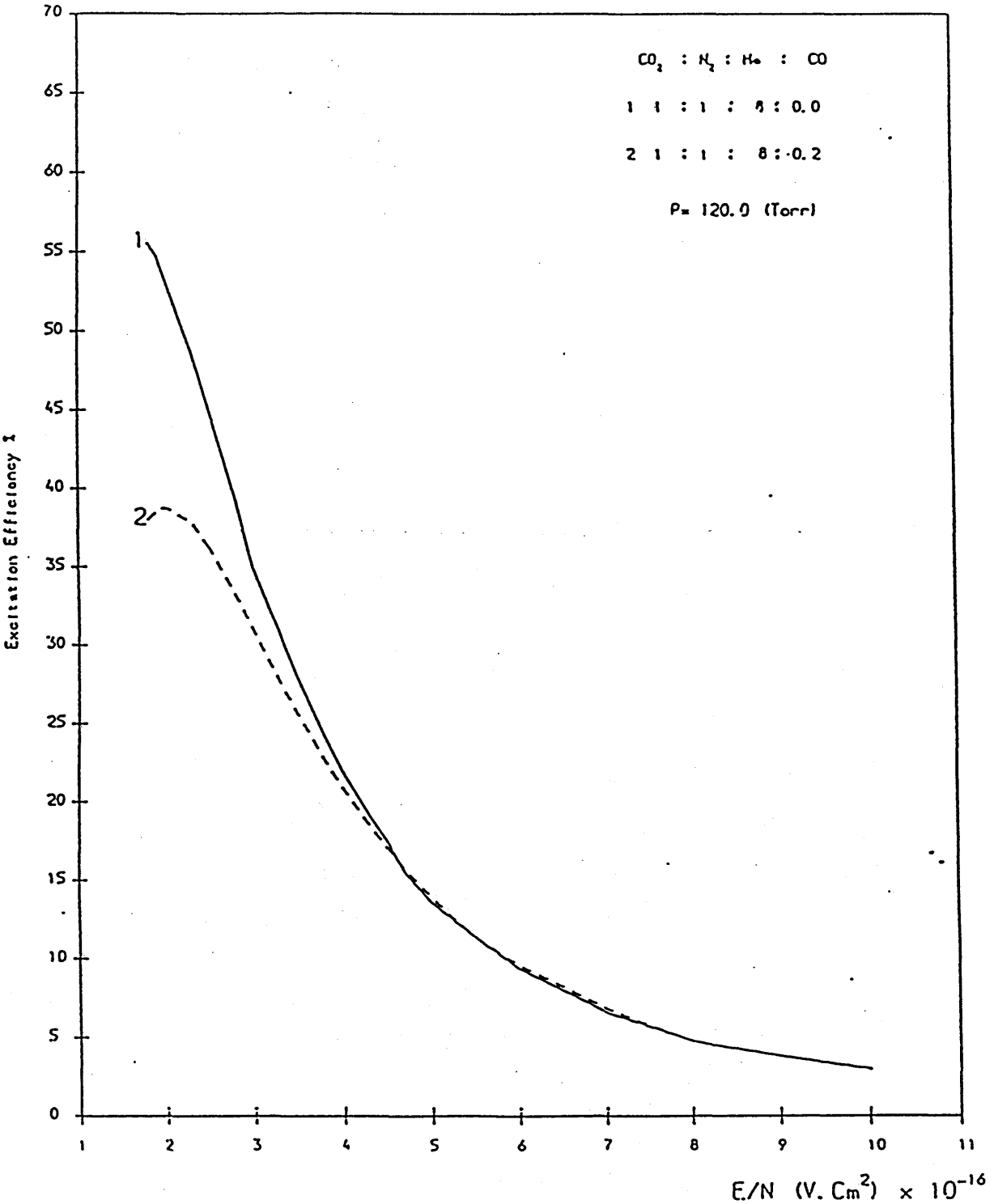

EXCITATION EFFICIENCY OF N_2 (v=1-8) LEVELS VERSUS E/N

GRAPH (2.36)

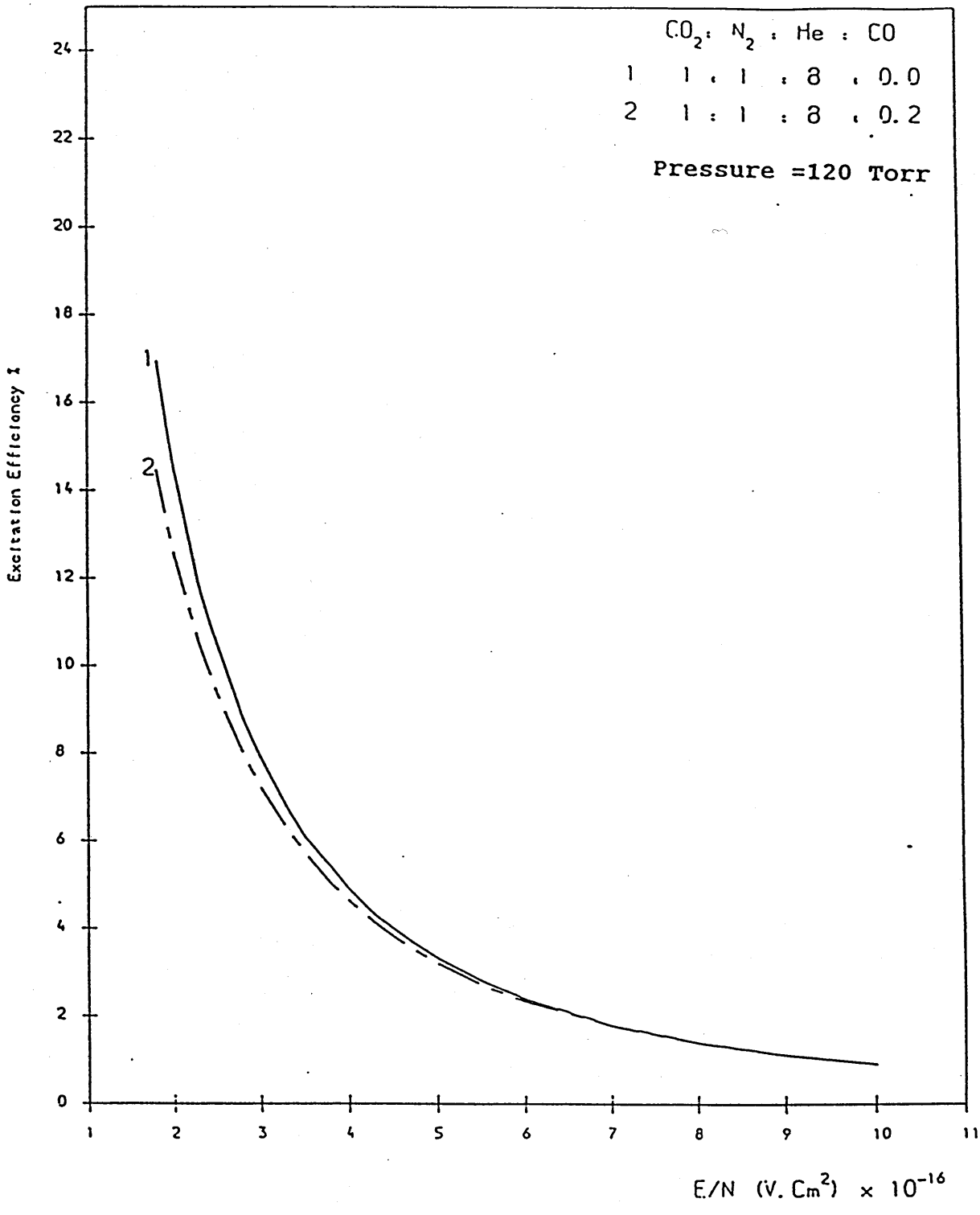

EXCITATION EFFICIENCY OF CO_2 (00°1) LEVEL VERSUS E/N

GRAPH (2.37)

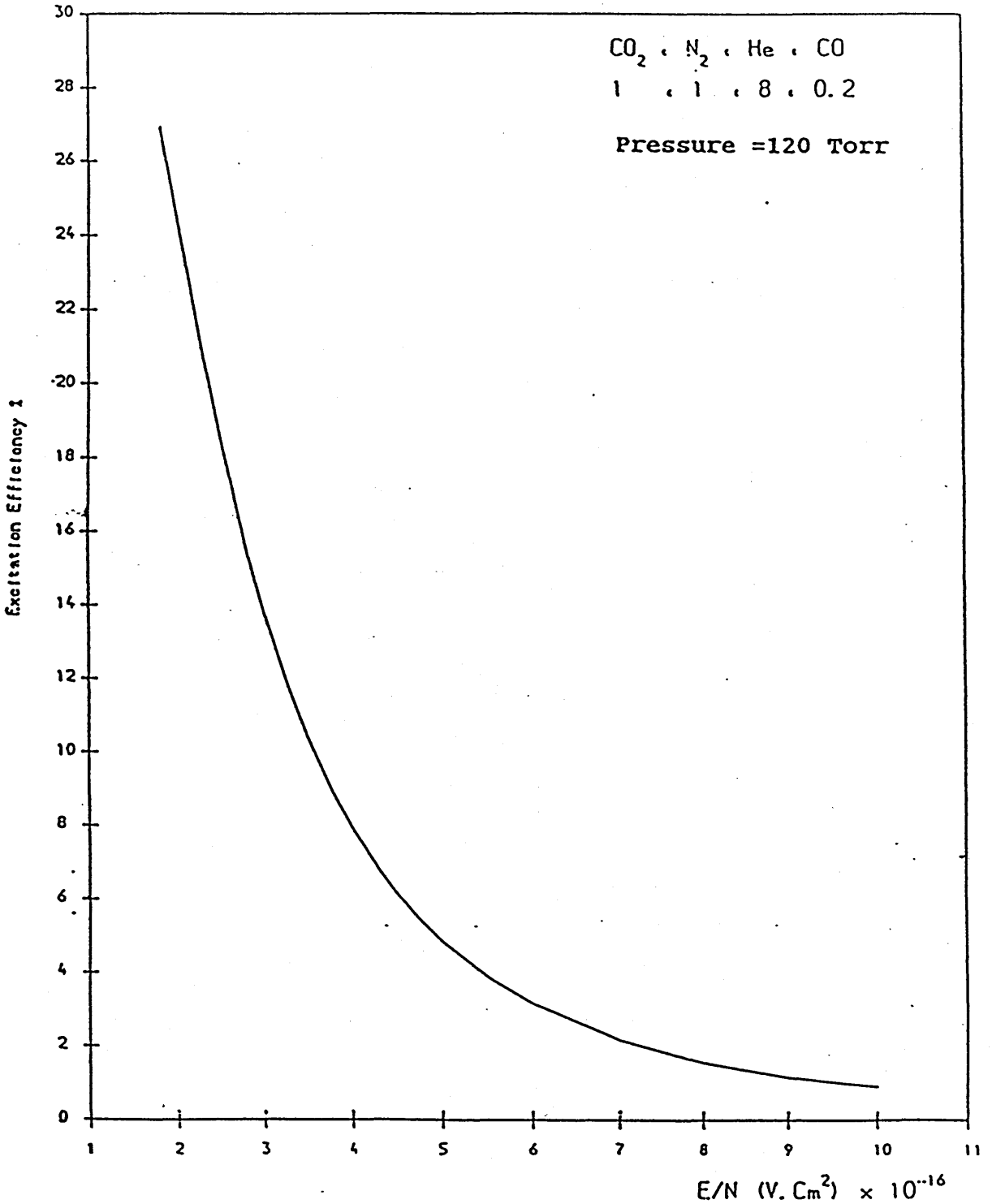

EXCITATION EFFICIENCY OF CO (v=1-8) LEVELS VERSUS E/N

GRAPH (2.38)

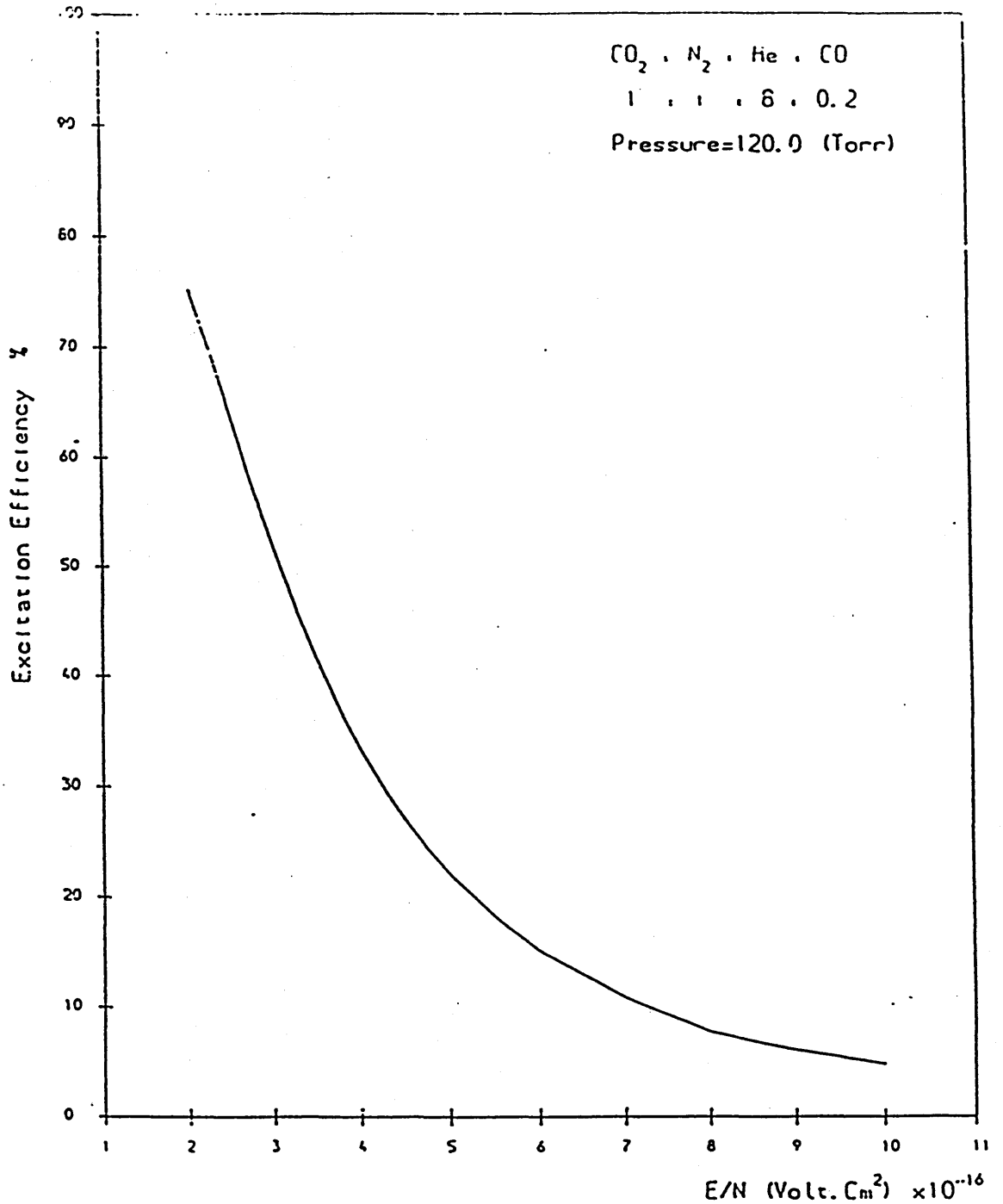

GRAPH OF EXCITATION EFFICIENCY OF

CO_2 (00°1) + N_2 (v=1-8) + CO (v=1-8) LEVELS VERSUS E/N

GRAPH (2.39)

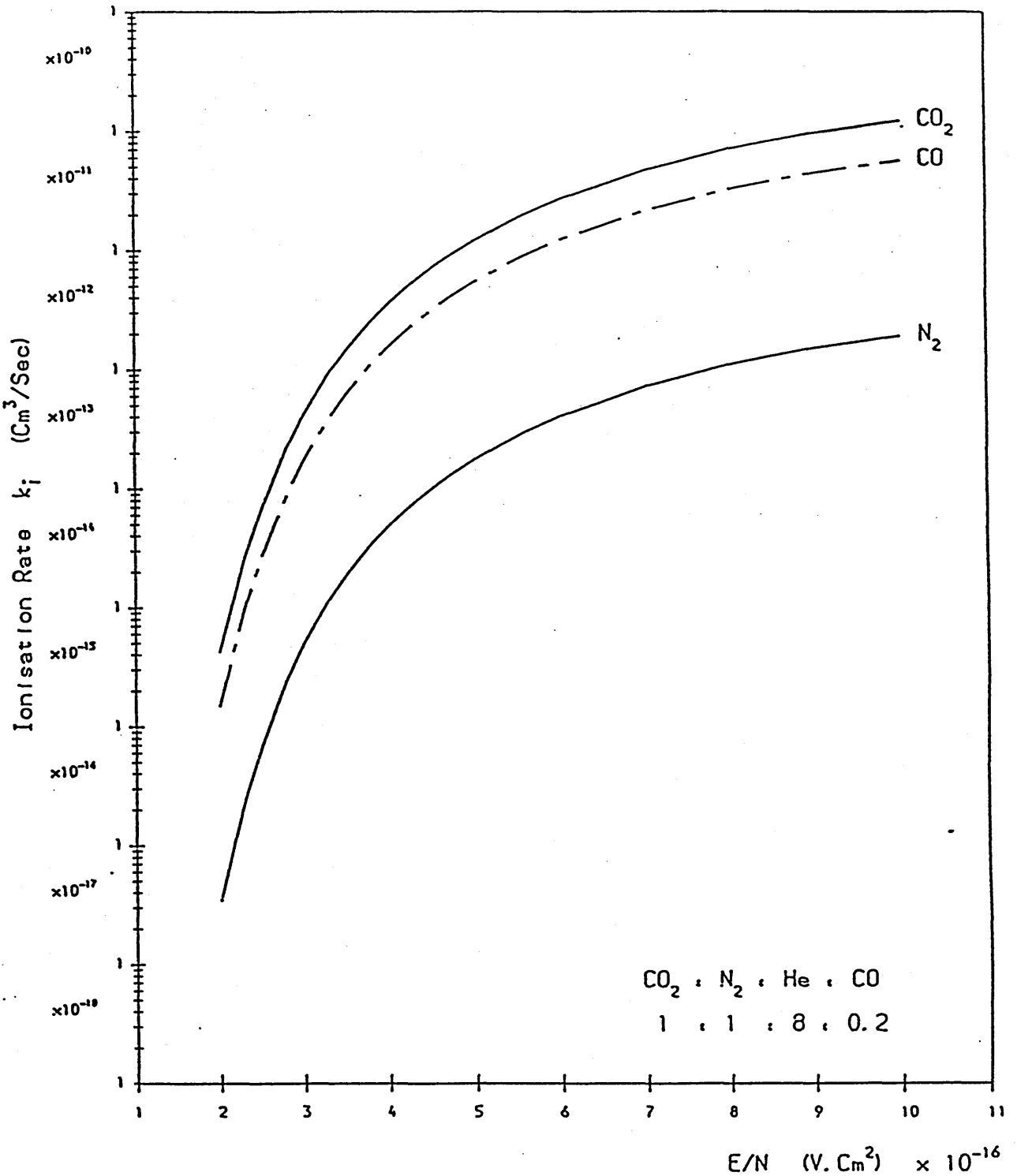

GRAPH OF IONISATION RATES VERSUS E/N

GRAPH (2.40)

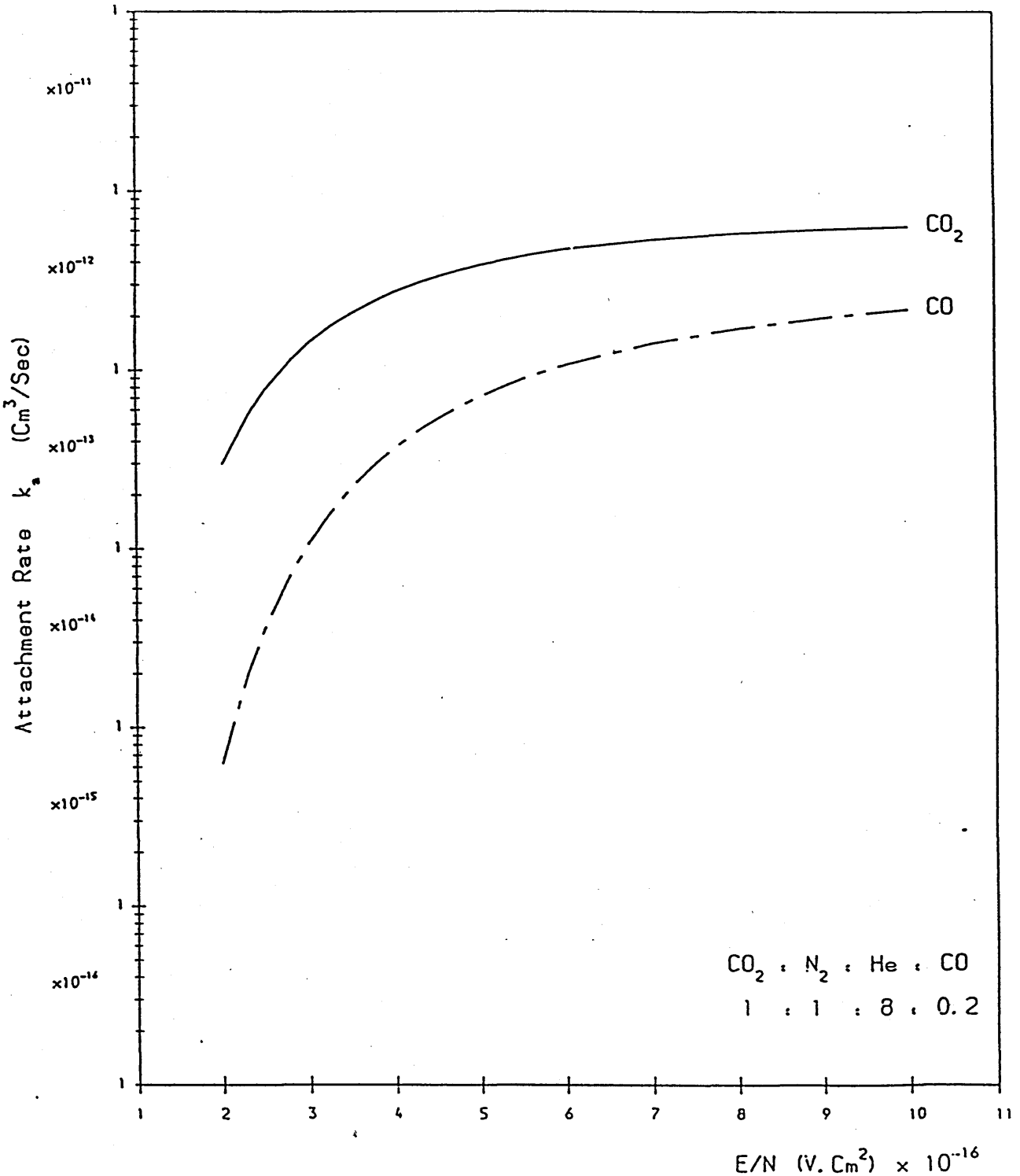

GRAPH OF ATTACHMENT RATES VERSUS E/N

GRAPH (2.41)

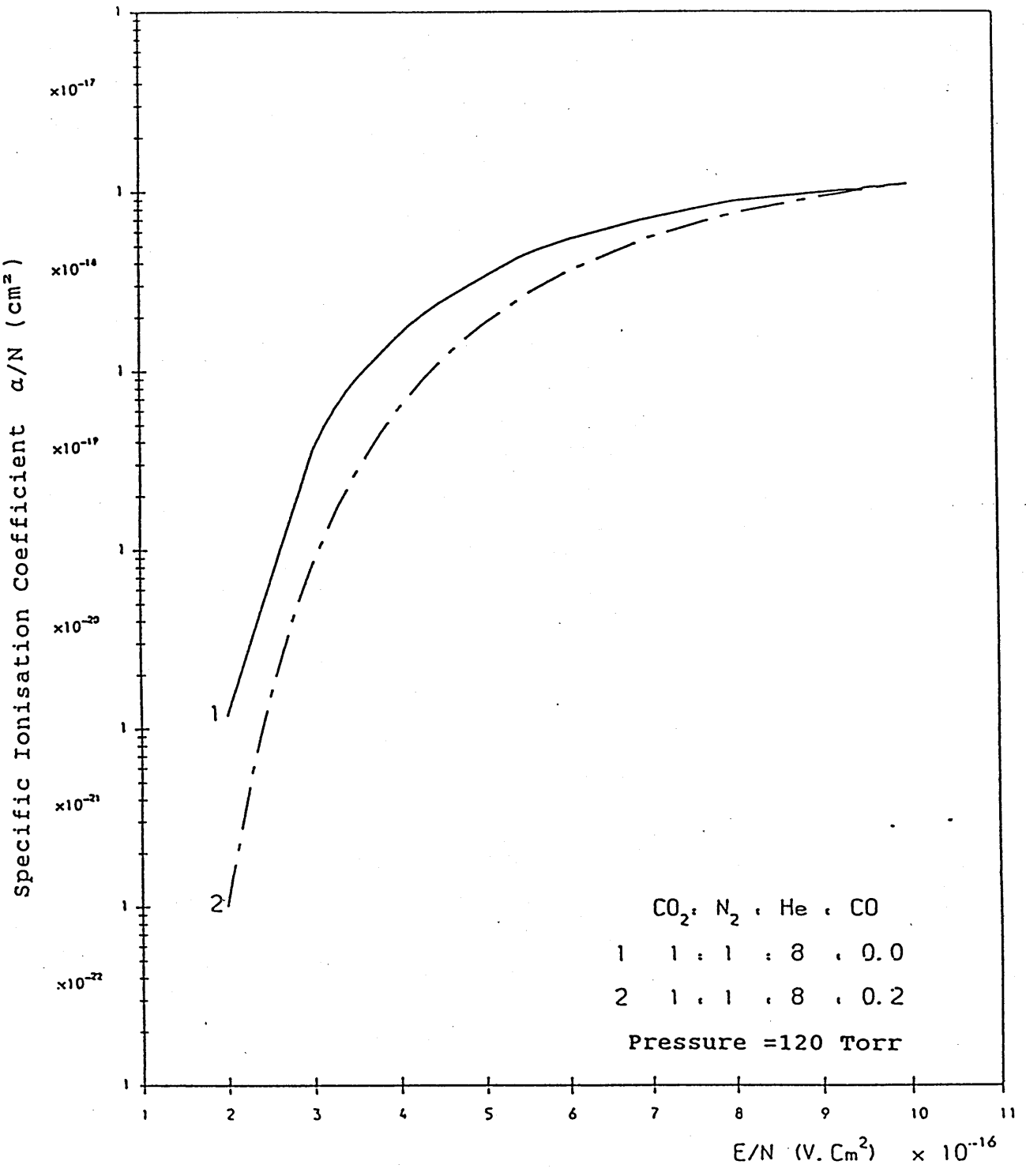

GRAPH OF SPECIFIC

IONISATION COEFFICIENT VERSUS E/N

GRAPH (2.42)

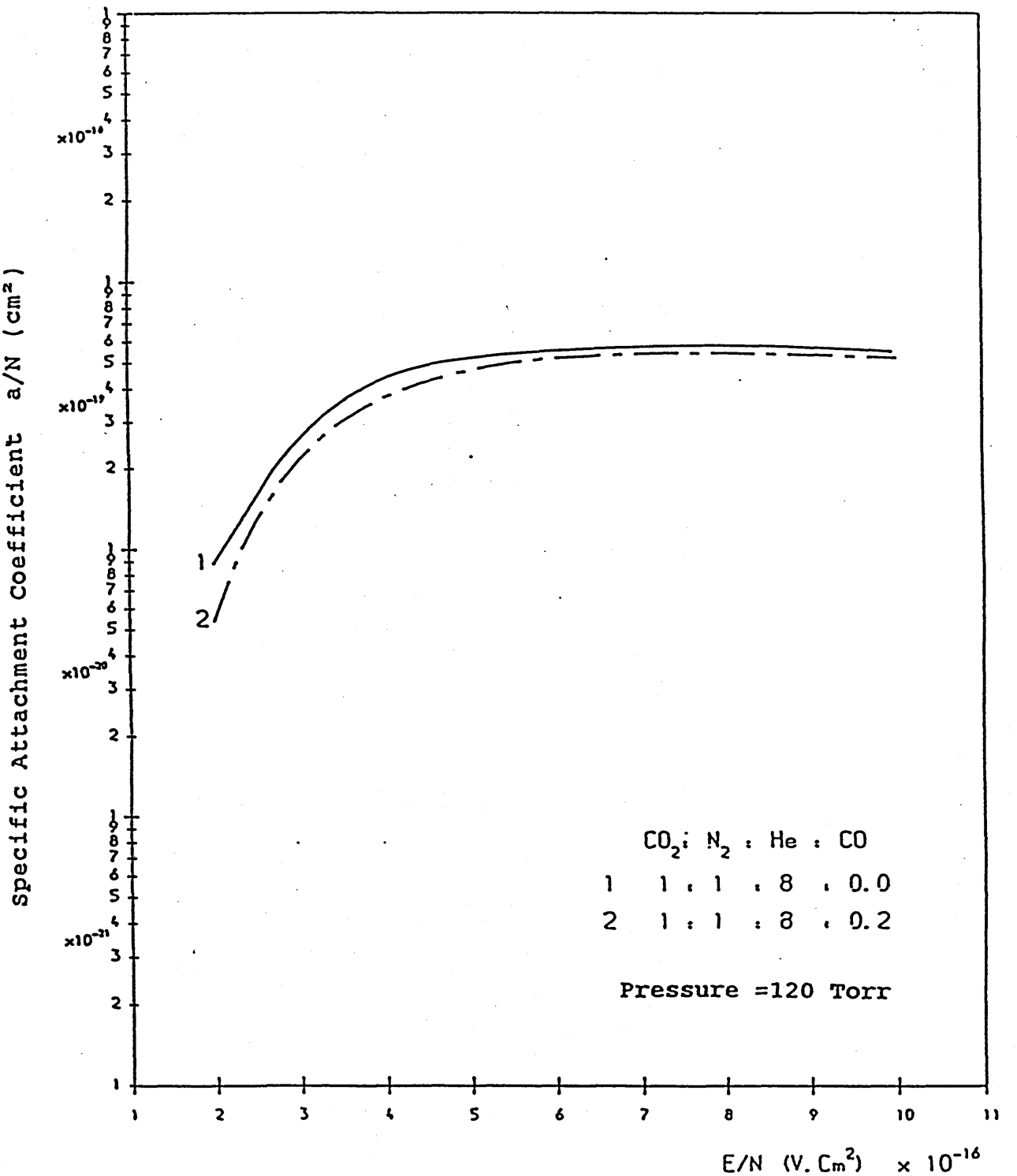

GRAPH OF SPECIFIC

ATTACHMENT COEFFICIENT VERSUS E/N

GRAPH (2.43)

CHAPTER THREE

THEORETICAL ANALYSIS OF PLASMA CHEMISTRY

3.1 Introduction:

The interaction between a flux of electrons and the particles of the gaseous fluid leads to a transfer of energy which is responsible for the creation of a plasma . In a laser cavity containing primary species CO_2,N_2,He,H_2, and CO low energy electrons interact with these species to form secondary species. Chemically active species are, usually, separated into three categories:

(1) species carying electrical charges (electrons,ions),

(2) excited molecules,

(3) neutral fragments of molecules (atoms, radicals) .

The modification of the molecular structure caused by means of changes in the internal energy preceeds the chemical reaction which often depends on an electron exchange. Chemical reactions involving electrons and ions rapidly become very complex,since ions polarize molecules and create molecular agregates (i.e clusters). On the other hand decomposition reactions lead to the formation of radicals and atoms from molecules.Furthermore, positive and negative ions can react with the electrons,or between themselves.Table (3.1) gives a list of different species within the plasma,[Smith and Thomson, 3.1],while Table(3.2) shows how long the list of elementary reactions can be,[Pace and Lacombe, 3.2].

The operating conditions for the CO_2 discharge are determined by a self-consistent balance of charged-particle production and loss, the laser performance is very sensitive to the relative number densities of the secondary species within the plasma. Hence serious attention has been paid by several workers to the plasma reaction kinetics to obtain detailed insight into the effects of the various processes and to permit performance optimisation. Theroretically, Nighan et al [3.3] predicted that negative ion densities play a significant role in the stability of molecular gas discharge lasers. Weigand and Nighan [3.4] have shown that in a CO_2 laser the dominant ion species is CO_3^- and its concentration may be greater than that of electrons, leading to plasma instability. Nighan and Weigand [3.5] have investigated the influence of negative ion processes on steady state properties in molecular gas discharges. They have shown that the existence of CO_2,CO,N_2, or O_2 molecules in the plasma can significantly influence the formation of negative ions. The loss of electrons by dissociative attachment,to form negative ions, will elevate the electron temperature to influence the excitation efficiency of the upper laser level. Pace and Lacomb[3.2] and Shields et al [3.6] have studied the negative ion processes occuring in a pulsed TEA CO_2 laser plasma. They have shown that the addition of small amount of H_2 and CO, to keep the oxygen concentration below 2 per cent, helps in reducing the CO_2 dissociation.Tannen et al[3.7] have carried out experimental investigations of species composition in a

low pressure CO_2 discharge laser.They have shown that presence of NO and NO_2 ,which easily form negative ions,can affect the performance of the laser, and NO^+ is the dominant positive ion. This is in agreement with Smith and Shields [3.8] who studied the positive ions in CO_2 laser discharges over the ranges(2-20 Torr). Recently,Ono and Teii [3.9] have studied both theoretically and experimentally the formation of negative ions and their effect on the electron temperature in CO_2 gas - mixture discharge plasmas , at pressures of 5-100 Torr. They found that the densities of dominant negative ions CO_3^- and O_2^- increase with increasing pressure ,while that of O^- decreases as the pressure increases, and all negative ion densities increase with increasing electron density. They also found , that with increasing amounts of CO, the electron temperature decreases as a result of the electron detachment processes involving CO molecules.

This chapter deals with theoretical analysis of plasma chemical phenomena occuring in CO_2 laser discharges.Emphasis is directed toward identification of principal reaction types of importance in such discharges.The time evolution of charged and neutral species in the discharge are predicted by a model of plasma chemical phenomena which considers over 300 reactions of the type indicated in Table (3.2)and follows the development of nearly 40 neutral and charged species. The model solves iteratively coupled rate equations describing the interaction kinetics for these species. The build-up of gaseous dissociation products of the CO_2-N_2-He

mixture and the effects of additive gases are investigated.

It was decided to investigate the development of the significant neutral and charged species during and up to 5 subsequent pulses as : at the maximum gas flow rate in the laser device constructed , this is the number of pulses experienced by a packet of gas as it preceedes through the discharge region . This computation requires about 6 hrs on the ICL 3980 to simulate the development of neutral and negative ion species , whereas it requires about 14 hrs to simulate the development of neutral , negative ion and positive ion species . Whilst it would be interesting to demonstrate the build-up of the dissociation products with and without gas additives during several thousand pulses , currently it is computationally unattainable.

NOMENCLATURE

E	applied electric field (volt/cm)
$f(u)$	electron energy distribution function ($eV^{-1/2}$)
$k_{ab,i\gamma}$	rate coefficient for two initial particle reactions $a+b \longrightarrow i+\gamma$ ($cm^3.sec^{-1}$)
$k_{abc,i\gamma}$	rate coefficient for three initial particle reactions $a+b+c \longrightarrow i+\gamma$ ($cm^6.sec^{-1}$)
n_e	electron number density (cm^{-3})
n^+	positive ion number density (cm^{-3})
n^-	negative ion number density (cm^{-3})
n_i	number density of species i (cm^{-3})
Q_{ij}	cross section for reaction $i \longrightarrow j$ (cm^2)
S_i	rate of production of species i from external source ($cm^{-3}.sec^{-1}$)
T_e	electron temperature (eV)
t	time (sec)
u	electron energy (eV)
V_d	electron drift velocity (cm/sec)
ν_i	frequency of loss of species i by processes other than reactions (sec^{-1})
ν_u	electron energy exchange collision frequency (sec^{-1})

3.3 PLASMA KINETIC PROCESSES:

3.3.1 Molecular dissociation:

The major problem arising with sealed rather than constant - gas - replacement lasers is associated with the dissociation of the CO_2 in the electrical discharge,which is typically 0.1-0.3 % per pulse. The dissociation of CO_2 is, mainly, by electron impact collisions, i.e :

$$e + CO_2 \xrightarrow{k_1} e + O + CO \qquad \text{.....(3.1)}$$

with a rate coefficient $k_1=1x10^{-9}$ cm^3/sec ,[Shields et al, 3.6].CO_2, also , dissociates by the dissociative attachment reaction:

$$e + CO_2 \xrightarrow{k_2} CO + O^- \qquad \text{..... (3.2)}$$

with a rate coefficient $k_2=5x10^{-13}$ cm^3/sec.

This loss of CO_2 is not in itself a major problem, but the dissociation product O_2 (formed by several subsequent reactions- Table 3.2) rapidly attaches to the preionisation electrons during the preionisation to main discharge delay period and also to the main discharge electrons; leading to discharge instability and arcing,[Smith and Norris ,3.10]. The oxygen released by this process also combines with the nitrogen to produce the various oxides ; leading to serious degradation of the laser operation ,[Tannen et al,3.7].

Since N_2 is dissociated at a considerably slower rate than CO_2 in a typical glow discharge,its dissociation is considered in general negligible , [Engel A. Von , 3.11].

The oxygen dissociates by the reaction:

$$e + O_2 \xrightarrow{k_3} O + O + e \qquad \text{.....(3.3)}$$

with a rate coefficient $k_3=1.9x10^{-12}$ cm^3/sec ,[Ono and Teii, 3.9],whereas the dissociation rate of hydrogen is about four orders greater than that of CO_2 , $k_{H2}=4x10^{-9}$ cm^3/sec , [Shields et al ,3.6] , and that of CO is equal to $3x10^{-14}$ cm^3/sec ,[Smith and Thomson ,3.1].

3.3.2 Electron-Molecule ionisation and attachment:

In a weakly ionised discharge, ionisation commonly proceeds by way of the single-step process[Nighan and Wiegand ,3.5], i.e. by electron impact collision such as:

$$e + CO_2 \xrightarrow{k_4} CO_2^+ + 2e \qquad \text{.....(3.4)}$$

which has a rate coefficient $k_4=5.1x10^{-15}$ cm^3/sec.

The electron impact ionisation of O_2 has a similar rate constant to that for CO_2. However,in such conditions when less than 1% O_2 is produced in the discharge,the direct production of O_2^+ by ionisation is not comparable with the charge exchange process:

$$CO_2^+ + O_2 \longrightarrow O_2^+ + CO_2 \qquad \text{.....(3.5)}$$

which has a rate coefficient of $1x10^{-10}$ cm^3/sec ,[Smith and Thomson ,3.1].

Elèctron impact ionisation of CO produces CO^+ ,but this ion is rapidly removed by the charge exchange reaction:

$$CO^+ + CO_2 \longrightarrow CO_2^+ + CO \qquad \text{.....(3.6)}$$

which has a rate coefficient of $1.1x10^{-9}$ cm^3/sec,[Smith and Thomson ,3.1].

Nitrogen has the lowest ionisation rate amongst the three gases (CO_2 ,N_2 ,CO),[Nighan and Wiegand ,3.5]. Figure (3.1) shows ionisation rate coefficients for some common

molecular species. The ionisation rate coefficients for the species indicated all have strong dependence on the electron temperature.

The attachment process takes place when an electron collides with a neutral gas atom or molecule and becomes attached to form a negative ion. This process depends on the energy of the electron and the nature of the gas. An electronegative gas(such as CO_2 ,CO and O_2) is an electron attaching gas in which long-lived negative ions are produced.Depending on the electron energy,the energy change of the system (i.e. the molecule and the colliding electron) must be balanced by either emission of a quantum or the molecule is dissociated ,[Engel A. Von ,3.11] . These two attachment processes are:

(1) radiative attachment, when an electron collides with a neutral molecule to form an excited negative ion which itself emits a photon hy on de-excitation to become a stable negative ion. For CO_2 molecule this is as follows:

$$e + CO_2 \longrightarrow CO_2^-{}_{ex} \longrightarrow CO_2^- + hy \quad .....(3.7)$$

(2) dissociative attachment,when an excited negative ion dissociates such as:

$$e + CO_2 \longrightarrow CO_2^-{}_{ex} \longrightarrow CO + O^- \quad .....(3.8)$$

The CO_2^- ion formed by electron attachment to a CO_2 molecule in vibrationally excited state of the bending mode (01^10) is likely to be more stable than the one formed by attachment to a linear molecule. Krishna Kumar and Venkatasubramanian [3.12] have shown that CO_2^- ions with a lifetime greater than 30 μsec were detected experimentally and could

significantally affect the ion chemistry of the discharge. Furthermore,Llewellyn-Jones [3.13] has shown that attachment can occur by the three-body process in which an excited ion is stabilised in collision with a slow neutral molecule which carries off excess energy,this can be represented as:

$$e + CO_2 \longrightarrow CO_2^{-}{}_{ex} \qquad \text{.....(3.9)}$$

$$CO_2^{-}{}_{ex} + CO_2 \longrightarrow CO_2^{-} + CO_2 \text{ (fast)} \qquad \text{.....(3.10)}$$

Dissociative attachment processes for different species such as CO_2,CO,O_2,H_2,and some oxides of nitrogen,with their rate coefficients are given by Shields et al [3.6] . The energy dependence of the rate coefficients for some species are shown in figure (3.2),[Nighan and Wiegand ,3.5]. It indicates that while certain of the attachment rate coefficients have strong dependence on the electron temperature,others do not. This is because of some oxides of nitrogen , have low energy thresholds for dissociative attachment, and large values of attachment cross sections.

3.3.3 Recombination Processes:

The particle species of molecules, atoms, positive and negative ions produced by reactions corresponding to the processes explained in previous sections are involved in a host of recombination reactions, which can be classified as follows:

(1) Neutral recombination,

(2) Electron-ion recombination, and

(3) Ion-ion recombination

Neutral recombination processes are relatively slow,e.g the reactions:

$$CO + O + M \xrightarrow{k_1} CO_2 + M \qquad \ldots\ldots\ldots\ldots(3.11)$$

$$O + O + M \xrightarrow{k_2} O_2 + M \qquad \ldots\ldots\ldots\ldots(3.12)$$

have rate coefficients $k_1=2x10^{-36}$ cm^6/sec and $k_2=3x10^{-33}$ cm^6/sec,[Ono and Teii ,3.9]. Much faster processes are those of dissociative recombination involving molecular positive ions. When the ion is approached by an electron,resonant capture giving an intermediate excited state,which breaks up and the recombination energy appears as kinetic energy of the system, such as:

$$O_2^+ + e \longrightarrow O_2^{**} \longrightarrow O\ (fast) + O\ (fast) \qquad \ldots.(3.13)$$

Dissociative recombination rates $\geq 10^{-7}$ cm^3/sec are commonly encountered. Much of the data for dissociative recombination is due to Biondi and his co-workers,[3.14]. Rate coefficients for N_2^+ and CO_2^+ recombination have been reported by Maier and Fessenden[3.15]. Recently,data for dissociative recombination of CO^+ is reported by Mitchell and Hus[3.16]. Since no large variation in values of rate constants for different species was found,a mean value of the recombination coefficient ($k=2x10^{-7}$ cm^3/sec) is commonly assumed. Positive ion-negative ion recombination is another fast process,which occurs widely for both atomic and molecular ions. As for electron-ion recombination processes, similar rate coefficients have been reported by several workers[Smith and Thomson ,3.1],[Nighan and Wiegand ,3.5].

Three-body recombination processes such as:

$$O^- + O^+ + N_2 \longrightarrow O_2 + N_2 \quad \text{.....(3.14)}$$

$$O^- + O^+ + O_2 \longrightarrow 2\ O_2 \quad \text{.....(3.15)}$$

are in general slow with rate coefficients in the range $1\text{-}2\times10^{-25}$ cm^6/sec, [Smith and Thomson ,3.1].

3.3.4 Detachment and Clustering Processes:

Negative ions produced by attachment processes can be destroyed by collisions with atomic and molecular species. Typical processes are:

(1) associative detachment reactions such as:

$$O^- + CO \longrightarrow CO_2 + e \quad \text{.....(3.16)}$$

$$O^- + O \longrightarrow O_2 + e \quad \text{.....(3.17)}$$

(2) collisional detachment reactions such as:

$$NO^- + M \longrightarrow NO + M + e \quad \text{.....(3.18)}$$

$$O_2^- + N_2 \longrightarrow O_2 + N_2 + e \quad \text{.....(3.19)}$$

Rate coefficients for different detachment processes have been reported by several workers[Nighan and Wiegand ,3.5],[Ono and Teii ,3.9],[Smith and Norris ,3.10].

At relatively high pressure , clustering of O^- with CO_2 molecules becomes faster than detachment reactions,[Shields et al ,3.6] ,thus the three body clustering reaction:

$$O^- + CO_2 + M \longrightarrow CO_3^- + M \quad \text{.....(3.20)}$$

can very rapidly convert the negative oxygen ion to more stable CO_3^- ion. This ion was found to be dominant and play a central role in the negative ion chemistry of CO_2 gas discharge plasmas,[Ono and Teii ,3.9].Other negative ion clustering processes are shown in Table(3.2).

3.4 THE BASIS OF THE MATHEMATICAL MODEL:

3.4.1 Chemical Reactions:

Within a plasma the chemical reactions which may take place,can be classified as:

- Neutral molecule reactions,
- Reactions involving electrons and/or negative ions,
- Reactions involving positive ions.

Detailed classification of these reactions with examples are given in Table(3.3).

3.4.2 Rate Equations and Rate Coefficients:

The time rates of change of the number densities of the various chemical species are described by a set of differential equations. For a species (i),the rate equation for the number density n_i (cm^{-3}),may be written as ,[Roberts ,3.17]:

$$dn_i/dt = S_i - \gamma_i n_i + \sum_{a,b} n_a n_b k_{ab,i\gamma} - \sum_{c} n_i n_c k_{ic,\gamma} + \sum_{a,b,c} n_a n_b n_c k_{abc,i\gamma} - \sum_{c,d} n_c n_d n_i k_{cdi,\gamma} \quad ....(3.21)$$

The first term from the right hand side represents the rate of production of species i from external source (i.e the inflow rate for gas-flow lasers). The second term accounts for loss of species i by processes other than reactions (i.e loss due to gas outflow rate). The third and fourth terms contribute for two initial particle reactions , such as ($a+b \longrightarrow i+\gamma$),while the fifth and sixth terms contribute for three initial particle reactions,such as ($a+b+c \longrightarrow i+\gamma$).

The effects of reactions involving collisions between molecules and the cavity walls are neglected in equation (3.21) . This has been shown [Ono and Teii , 3.9] to be a good approximation in large volume collision - dominated uniform plasma.

The source term S_i and the loss term (y_i n_i) in equation (3.21) will be zero for all primary species for a sealed-off laser,whereas for a gas-flow laser,S_i is given by:

$$S_i = R_i(dN/dt)_{in} \qquad \text{.....(3.22)}$$

and the loss frequency y_i is:

$$y_i = N^{-1}(dN/dt)_{out} \qquad \text{.....(3.23)}$$

where:

R_i is the fraction of primary species,

$(dN/dt)_{in}$ is the inflow rate in (cm^{-3}/sec) of primary species,

$(dN/dt)_{out}$ is the outflow rate in (cm^{-3}/sec) of both primary and secondary species.

For reactions in which electrons are initial particles, the corresponding rate coefficients are dependent on the effective electron temperature. The rate coefficient can be expressed as:

$$k=(2e/m)^{1/2} \int_0^\infty u\, f(u)\, Q_{ij}\, du. \qquad \text{.....(3.24)}$$

and the electron temperature is given by equation (2.8 -in Chapter 2).

The electron temperature is coupled to the electron density,[Smith and Thomson ,3.1],by the following equation:

$$d(3\, n_e\, k\, T_e/2)/dt = n_e\, E\, V_d - n_e\, y_u\, k\, T_e \qquad \text{.....(3.25)}$$

If the positive ions are dealt with collectivly,the charge neutrality equation is:

$$n^{+} = \sum_{i} n_i^{-} + n_e \qquad \text{.....(3.26)}$$

where the summation is over all negative ions; whereas if positive ions are dealt with individually, then the initial density of a positive ion n_i^{+},of the neutral particle i, is assumed proportional to the number density of the neutral particle and its rate of ionisation. The charge neutrality condition gives:

$$n_i^{+} = n_e \, k_i \, n_i \, / \, w \qquad \text{.....(3.27)}$$

where w is the normalisation factor:

$$w = \sum_{i} k_i \, n_i \qquad \text{.....(3.28)}$$

and the summation is over neutral particles.

For the laser cavity containing the primary species CO_2, N_2 , CO , H_2 , and He ,the variation with time of the number densities of the chemical species is described by a set of over 30 coupled differential equations involving over 300 reactions.Each primary, and each secondary species is described by an equation similar to equation(3.21).

A data base is created by utilizing a computer program [Roberts ,3.18] to contain all known rate information on chemical reactions within a given chemical system. The data base is designed to store three types of information:

(i) constant rate coefficients,

(ii) tables of rate coefficient versus the chemical name of a particle which does not change during the chemical reaction,e.g:

$$CO + O + He \longrightarrow CO_2 + He \qquad \text{.....(3.29)}$$

(iii) tables of rate coefficients versus effective electron temperature.

In a plasma of a given initial chemical content, all possible chemical reactions which may take place(as classified in 3.4.1) and for which rate information is stored in the data base, are generated by a computer program [Roberts ,3.19],which may be run to consider only neutral particle reactions, or neutral particle and negative ion reactions, or all possible reactions(i.e neutral particle, negative ion, and positive ion reactions). These chemical reactions with their rate coefficients are required for a further program [Roberts ,3.18] which is utilized to solve the differential equations numerically by stepwise integration using three alternative methods, Runge-Kutta method, a modified Hamming predictor-corrector method, and Gear's method which is based on a routine from the NAG library[3.20]. The Hamming and Gear methods have the advantage of an automatic adjustment to the time step in order to keep the local error within a given bound.

The electrical excitation for the model is provided in the form of a rectangular current pulse for time t=0 to t=10 μsec. The electron density and average energy are obtained from the predictions in Chapter 2.This being assumed to most closly approximate the actual pumping pulse . The gas temperature is assumed to be 300 °K and unchanged by the discharge. This has been shown to be good approximation for a pre-ionized TEA CO_2 laser,[Shields et al ,3.6].

3.5 NUMERICAL RESULTS AND DISCUSSION:

3.5.1 Negative ion predictions:

3.5.1.1 Formation of negative ions:

Graph (3.1) corresponds to the first current pulse where the gaseous decomposition products have not had a chance to accumulate significantly. It shows the computed development of the main negative ion species in a 1:1:8 mixture at 120 Torr during the discharge pulse.The main peak is found to be CO_3^- with other peaks involving CO_4^-,O_2^-,O^-.These results show that the principal source of negative ions in typical CO_2 laser gas mixtures is O^- produced by dissociative attachment of electrons to CO_2. This ion, then, very rapidly reacts with CO_2 molecules in a three body clustering process to form CO_3^- and subsequently O_2^- and CO_4^- by reactions 34 and 40 in Table (3.2). It can be seen from graph (3.1) that O^- reaches an approximate equilibrium value after about 30 nanosec.This is due to the loss of this ion by two and three body processes and by associative detachment processes. Graph (3.1),also , shows that CO_3^- reaches a maximum after about 3 μsec with a population of about 2.4×10^{11} cm^{-3} which gives a negative ion to electron concentration n^-/n_e of about 0.35. This is caused by the loss of this ion by three body recombination with positive ions [Shields et al ,3.6], and by negative ion-molecule reaction (i.e reaction 34 in Table 3.2).

Graph (3.2) shows the development of the main negative ion concentrations with time during and immediately subsequent to the discharge pulse. It can be seen that in the afterglow the total negative ion population decays by both recombination and detachment processes, but individual peaks may continue to increase in magnitude for a short time. This is because the ion-molecule processes produce the species faster than the ion-loss mechanisms can remove them.

The net increase in the loss of electrons due to attachment (i.e as negative ion concentrations increase) leads to a corresponding increase in the electron temperature so that ionisation can compensate for the additional losses. It can be seen from figure(3.2) that electron attachment rates for CO_2 ,O_2,and CO have strong electron temperature dependence, a condition necessary for dissociative attachment instability, [Beverly ,3.26]. The increase in negative ion density and the decrease in the electron density result in a decrease in the plasma conductivity. If the current density is constant, the local electric field is further increased which increases the attachment rates. A convective instability then ensues from the temporal amplification of the imbalance between charged particle production and loss processes.This results in local contractions of charged particles throughout the discharge which cause striations that finally develop into concentrated arcs.

3.5.1.2 Effects of gas impurities:

The exact plasma chemistry reactions involved depend on the purity of the gas mixture.Impurities such as O_2 and H_2O, in particular,are unavoidable in large devices and are introduced into the system as a result of the use of technical grade gases,through containment vessel outgassing, or from air leaks in the flow ducting (in the laser system built , this was found to be about 1 mbar/hour). Graph (3.3) shows the development with time of the main negative ion species in a 1:1:8 gas mixture at 120 Torr with an assumed impurity level of 500 ppm of water vapour which is a typical contaminant in commercial CO_2 laser mixtures. The H^- ion is mainly formed by dissociative attachment of H_2O (reaction 4 in Table 3.2) , and then OH^- is formed by two body processes (reactions 30 and 35). The total negative ion population is significantly increased by the addition of 1-5 % of H_2O , where H^- becomes the dominant ion as shown in graph (3.4).

Water vapour is known as a very fast collisional relaxant of the upper laser level with a rate constant of 4.2×10^4 $Torr^{-1}.sec^{-1}$ [Levine ,3.21]. Although H_2O is very effective in relaxing the 01^10 laser level and improvements in performance with H_2O additive has been reported with the sealed-off CO_2 lasers [Williams and Smith ,3.22] , the concentration of H_2O must be extremely small compared with other constituents and must be carefully controlled in order to obtain consistent results. Shields et al [3.6] have verified the assumption that H_2O leads to the discharge

arcing by passing the laser gases through a water-saturated alumina column before entering the laser. It has been found that for an arc-free discharge ,the H_2O content should be less than 1000 to 10000 ppm ; quantities above this level lead to arcing because of increasing electron attachment and negative ion effects [Smith et al ,3.23].

The oxygen rapidly attaches to the preionisation electrons during the preionisation to main discharge delay time. The initial electron density needed to ensure uniformity of main pulsed discharge is about 10^6 electrons/cm^3 [Smith et al 3.23]. In mixtures with moderate CO_2 content (10-20%) and with very efficient preionisation the established electron density is about 10^7 -10^8 electrons/cm^3 [Smith and Norris , 3.10],so it is only too easy for this to be reduced to $\approx 10^6$ and be insufficient to sustain the main discharge. Moreover, the main discharge electrons attach to O_2 molecules rapidly since its electron attachment rate is an order of magnitude higher than that of carbon dioxide (figure 3.2). As a result, the three-body attachment process(reaction 6 in Table 3.2) becomes significant in directly creating O_2^-, and later in the pulse CO_4^- is dominant , being formed by reaction 40. This is shown in graph (3.5) for a 1:1:8 gas mixture at 120 Torr with 2% added O_2. The total negative ion population is significantly increased, leading to discharge arcing. This trend is in agreement with the results of Pace and Lacombe[3.2] who have found that for a 1.5 : 1.5 : 7 gas mixture,discharge arcing had started to occur when the O_2 concentration reached about 2 percent , which was predicted

by their plasma model as a result of an order of magnitude increase in the negative ion concentration with addition of 2 percent oxygen.Furthermore , this additional electron loss mechanism caused by the presence of O_2 in the discharge slightly increases the E/N value of the discharge , which in turn affects the laser excitation rates and hence the output power . Smith et al [3.24] have found that with increasing amounts of added oxygen there is a slow decrease in the output power.

3.5.1.3 Effects of gas pressure:

Graphs (3.6 to 3.8) show the temporal evolution of the dominant negative ion concentrations ,i.e CO_3^-,CO_4^-,O_2^- and O^- as a function of pressure in a 1:1:8 gas mixture at three instants in times during the discharge pulse. At time t=300 nsec, graph (3.6) shows that the densities of CO_3^-,CO_4^-, and O_2^- increase with increasing pressure,whereas the density of O^- decreases as the pressure increases. This trend continues to occur at time t=3 μsec as shown in graph (3.7). At the end of the discharge pulse ,i.e at time t=10 μsec, the negative ion concentrations are shown by graph (3.8). It can be seen that the density of O_2^- tends to decrease with increasing pressure together with that of O^- ,while the densities of CO_3^- and CO_4^- continue to increase with increasing pressure. This can be explained as follows : dissociative attachment of electrons to CO_2 produce O^- which is then very rapidly consumed in a clustering reaction with

CO_2 molecules to form CO_3^- (reaction 39 in Table 3.2). At higher pressure this reaction becomes fast, [Shields et al , 3.6], with the result that O^- concentration decreases, while that of CO_3^- increases with increasing pressure.

Early in the pulse at time t=300 nsec, the concentration of O_2^- and CO_4^- increases with increasing pressure as a result of reactions 34 and 40.But later in the pulse reaction 40 which forms CO_4^- consumes more O_2^- than reaction 34 can produce,hence, CO_4^- density becomes greater than that of O_2^- (graph 3.1). Moreover,later in the pulse the concentration of oxygen atoms (being formed by dissociation processes : reactions 20 and 21) increases which, in turn, produces further mechanisms that destroy O_2^- (e.g reactions 13,31,and 32). With increasing pressure, there are more CO_2 molecules in the discharge,hence,more O atoms as shown in graph (3.9). This increases the concentration of CO_4^- and decreases that of O_2^- as shown in graph (3.8).

3.5.1.4. Effects of gas composition:

Discharge stability depends strongly on the gas composition which affects the electron temperature , hence the rate coefficients for ionisation and attachment processes . Graph (3.10) shows the development with time of the main negative ion species in a gas mixture with increasing helium content. Helium is found to be essential to stop the discharge developing in the arc mode [Smith et al ,3.24]. It can be seen from the graph that increasing helium content reduces negative ion concentrations. This can

be interpreted as follows : addition of helium to the gas mixture results in an increase in the average electron energy and an increase in the high energy tail of the electron energy distribution function (as discussed in chapter 2). The increasing electron energy together with the increasing number of high energy electrons both reduce dissociative attachment processes , which means a smaller O^- concentration ,as shown in graph (3.10), hence less negative ion population in the discharge since O^- represents the principal source of negative ion production in CO_2 laser gas mixtures. In addition ,there are more of the comparatively high energy ($\approx$ 7 eV) electrons which cause the dissociation of CO_2. The dissociation product CO produces a further mechanism to destroy negative ions in the gas discharge (e.g reaction 8 in Table 3.2). The net effect is such that the plasma conductivity increases,hence the discharge stability also increases .

The effect of increasing the propqrtion of N_2 in the gas mixture , on the development of negative ion species , is demonstrated in graphs(3.11 and 3.12).Although nitrogen does not form negative ions, oxides of nitrogen , specially NO_2 and N_2O are known to strongly attach electrons with attachment rates one to two orders of magnitude greater than carbon dioxide[Nighan and Wiegand ,3.5],[Rapp and Briglia ,3.25]. The low dissociation rate of nitrogen by direct electron impact leads to the assumption that different nitrogen oxides are mainly produced through the following mechanism: direct ionisation of nitrogen produces

N_2^+ ,which is followed by the dissociative recombination process:

$$N_2^+ + e \longrightarrow N + N \qquad \text{.....(3.30)}$$

which has a rate coefficient = 2.8 x 10^{-7} cm^3/sec . The resulting nitrogen atoms are then involved in a host of reactions to produce different neutral and charged species (see Table 3.3). Graph (3.11) shows that as the nitrogen content increases so too does the concentration of NO_2^- and NO_3^- , as a result of increasing concentration of secondary by-products NO_x and N_2O in the discharge. On the other hand graph (3.12) shows that the concentration of the main negative ion species fall off slowly with more nitrogen in the gas mixture. This is because that increasing proportion of nitrogen reduces the average electron energy (as discussed in chapter 2),which in turn significantly reduces ionisation rates for the main gas constituents, whereas the effect on attachment rates is relatively low, particularly for such species as NO_2 and N_2O (see figure 3.2). The net effect seems to be a slight decrease in the plasma conductivity, hence the E/N value necessary to sustain the discharge increases (see graph 2.28) ,which in turn affects the vibrational excitation rates, hence the output power. This trend is in agreement with the results of Smith et al [3.24] who found that the output power significantly decreases with the addition of less than 0.5 percent NO_2 or N_2O and these species encourage the discharge transition to arcing.

3.5.1.5 Effects of gas additives:

In a sealed-off CO_2 laser , dissociation products are found together with a small amount of H_2 which is disorbed from the laser walls and electrodes. The chemical reaction products of many discharge pulses may build up considerable concentrations of these species , which lead to changes in the operating characteristics of the discharge. Both CO and H_2 are known to be desirable additive gases in CO_2 lasers . This is because these gases

(i) rapidly depopulate the CO_2 (01^10) level,

(ii) reduce CO_2 dissociation rate,

(iii) combine with oxygen molecules formed by the discharge, thus reform CO_2 ,

In addition , CO reduces negative ion population , thus increases discharge stability.

To examine the effects of these gases on the development of negative ion species in the gas discharge , they are selectively added in different amounts to the gas mixtures. Graph (3.13) shows the effect of added CO on the main negative ion concentrations at time t=10 μsec in a 1:1:8 gas mixture at 120 Torr. The concentration of all negative ions decreases with increasing amount of added CO. This is explained by the detachment processes of negative ions by CO molecules as follows:

$$CO_3^- + CO \longrightarrow 2\,CO_2 + e \quad \ldots\ldots\ldots\ldots (3.31)$$

$$O^- + CO \longrightarrow CO_2 + e \quad \ldots\ldots\ldots\ldots (3.32)$$

These detachment processes reduce the electron temperature; as they release more low energy electrons. This in turn ,

reduces attachment rates for the main molecular species as shown in figure (3.2),therefore less negative ions are formed in the gas discharge. Graph (3.14) shows the variation with added CO of the electron temperature for a 1:1:8 gas mixture. As the proportion of CO increases, the electron temperature decreases due to the effects of detachment processes. This is in agreement with the experimental results of Ono and Teii [3.9]. However, if carbon monoxide is present in small proportion the CO_3^- ions are relatively stable and the electrons do not detach from the cluster in collisions with gas molecules. This is shown in graph (3.13) where the effect of small amounts (1-3%)of added CO on the dominant ion,CO_3^-,is relatively small. It has been shown that [Smith et al ,3.24] the negative ion population is small compared with the electron population only when the carbon monoxide concentration is the same or greater than the carbon dioxide concentration. On the other hand, with increasing amount of added CO ,the decrease in the electron energy is relatively large and so is the decrease in excitation efficiency of N_2 (as discussed in chapter 2). Moreover, with continued increase of CO concentration, the low level vibrational energy is transferred to higher levels in CO by V-V 'ladder climbing',[Basov ,3.27],where it is dissipated, primarily, by spontaneous radiation. This results in less energy transfer to the CO_2 (00°1) level from excited CO molecules. Thus, the output power is reduced.

The effect of added hydrogen on the main negative ion concentrations is shown in graph (3.15). Apart from the decrease in the concentration of CO_3^-,CO_4^-,O_2^- and O^- with addition of H_2 , the increasing concentration of OH^- and H^- is detrimental due to the negative ion build-up which causes discharge instability. Moreover,the dissociation of hydrogen produces H atoms (reaction 22 in Table 3.2) which, together with H_2, will react with other dissociation products such as O and OH to form considerable amounts of water vapour, which rapidly depopulates the upper laser level furthermore, it causes discharge arcing. It can be seen from graph (3.15) that when H_2 is added in considerable amounts ($\geq$ 2%) the concentration of H^- and OH^- slightly decrease. This can be explained as follows: with increasing amounts of added H_2 the concentration of dissociation products H and OH increases because of the large dissociation rate of H_2 (see section 3.3.1). The negative ions H^- and OH^- are then involved in several associative detachment processes with H and OH and other dissociation products (reactions 16-19 in Table 3.2) to form water vapour. For the operational envelope of this laser the predicted dissociation of H_2 is about 0.7 % per pulse so after about 150-450 pulses the H_2O concentration will be 1-3 %. However,if less than 1 % hydrogen is added to the gas mixture this will not cause a large increase in the negative ion population,thus an increase in output power can be obtained without arcing (taking advantage of (i) - (iii) page 135). This is in agreement with the experimental results of Smith et al [2.23].

3.5.2 Positive ion predictions:

3.5.2.1 Formation of positive ions:

The concentration of the neutral species in the cathode region of the discharge depends mainly on the composition of the gas mixture and on the reactions that occur in the positive column. Ions are produced in the cathode fall and negative glow regions by electron impact with neutral species. While moving towards the cathode under the influence of the cathode fall field,these ions collide with the intervening neutral species. These collisions serve to limit the energy that can be attained by the ions from the cathode fall field. In addition,under the strong field conditions encountered near the cathode,charge exchange is the main process in limiting the velocity of the ions in the field direction. However,the development of charge species in the positive column and the resulting plasma reaction kinetics are important since the positive column provides the stable laser excitation medium.

Graph (3.16) shows the computed development of the main positive ion species in a 1:1:8 gas mixture at 200 Torr during the discharge pulse . The main peaks are found to be CO_2^+ and O_2^+.Other peaks involving N_2^+,NO^+ and CO^+. CO_2^+ and N_2^+ are formed by electron impact ionisation of CO_2 and N_2 molecules.The ionisation rate coefficient for CO_2 is greater than that for N_2 (see figure 3.1) , hence more CO_2^+ ions are created in the discharge . Moreover , the formation of

this ion increases during the pulse, faster than N_2^+, due to its high rate coefficient ; later in the pulse the CO_2^+ peak begins to decrease as shown in graph (3.16). This is due to the fact that dissociation of CO_2 into CO and O also occur by electron impact and the concentration of molecular oxygen increases during the pulse. Thus,the charge exchange process

$$CO_2^+ + O_2 \longrightarrow CO_2 + O_2^+ \qquad \text{.....(3.33)}$$

becomes increasingly effective with more CO_2^+ being consumed. This also explains the increase in the O_2^+ , as time progresses, due to the increased abundance of O_2 produced by CO_2 dissociation. It should be noted that direct ionisation of O_2 by electron impact is not comparable with the charge exchange process (see 3.3.2).

The gradual increase in the CO^+ is similarly explained by the increased CO concentration produced in the discharge by dissociation of CO_2. However,this ion is rapidly removed by the charge exchange reaction

$$CO^+ + CO_2 \longrightarrow CO_2^+ + CO \qquad \text{.....(3.34)}$$

Since this loss rate is much faster than the corresponding ionisation rate producing CO^+ ,its concentration is very low (few ppm) as shown in graph (3.16). This is in agreement with the experimental results of Smith and Shields[3.8] who were unable to observe CO^+.

Direct ionisation of NO by electron impact accounts for the production of NO^+ , because its ionisation potential (9.25 eV) is low compared with CO_2 (13.3 eV). This gives NO an ionisation rate constant in a typical laser system nearly

an order of magnitude greater than that of CO_2 [Smith et al ,3.24](see figure 3.1).However,the charge exchange processes

$$CO_2^+ + NO \xrightarrow{k_1} NO^+ + CO_2 \quad \text{.....(3.35)}$$

$$O_2^+ + NO \xrightarrow{k_2} NO^+ + O_2 \quad \text{.....(3.36)}$$

which have rate coefficients $k_1 = 1x10^{-10}$ cm^3/sec and $k_2=7x10^{-10}$ cm^3/sec are also important in producing NO^+. This also explains the decrease in the CO_2^+ as shown in graph (3.16).

Graph (3.17) shows the development of the main positive ions during and subsequent to the discharge pulse. It can be seen that in the afterglow the population of all positive ions rapidly decay by both electron / positive - ion recombination and nagative-ion / positive-ion recombination. These recombination processes are in general fast, and being dissociative processes (see Table 3.3) , add further complexity to the evolution of subsequent pulses due to the presence of, not only the dissociation products O and CO , but also the oxides of nitrogen and other neutral species such as O_3 ,CO_3 and CO_4 . Moreover , the dissociative recombination of CO^+:

$$e + CO^+ \longrightarrow C + O \quad \text{.....(3.37)}$$

which has rate coefficient $=2x10^{-7}$ cm^3/sec produces carbon deposits much faster than the neutral dissociation of CO

$$e + CO \longrightarrow C + O \quad \text{.....(3.38)}$$

which has rate coefficient $=3x10^{-14}$ cm^3/sec.

3.5.2.2 Effects of gas pressure:

Graph (3.18) shows the variation with pressure of the main positive ion concentrations at time t=10 μsec in a 1:1:8 gas mixture. The concentration of CO_2^+ increases with increasing pressure due to the presence of more CO_2 molecules in the gas mixture. The concentration of N_2^+ is almost unchanged with increasing pressure. This seems to indicate that the ion loss rate is almost equal to the production rate and this can be explained as follows: with increasing pressure, there are more N_2 molecules in the discharge,hence, more N_2^+ being formed by direct electron impact ionisation. But this ion is rapidly removed from the discharge by recombination processes such as:

$$N_2^+ + e \longrightarrow N + N \qquad \text{.....(3.39)}$$

which has a rate coefficient =2.8×10^{-7} cm^3/sec. Moreover,N_2^+ is lost by several binary positive - ion molecule reactions with different species such as O,CO and O_2 (see Table 3.3c). These reactions have rate coefficients in the range 10^{-10} - 10^{-14} cm^3/sec. With increasing pressure , there are more of such species in the discharge ,hence ,the net effect is such that the production rate for N_2^+ is almost equal to the loss rate ,so the ion population is unaffected by increasing gas pressure.

It can be seen from graph (3.18) that the concentration of NO^+ increases with increasing pressure because of the increasing amount of NO produced in the gas discharge, so the charge exchange processes:

$$CO_2^+ + NO \longrightarrow NO^+ + CO_2 \quad \text{.....(3.40)}$$

$$O_2^+ + NO \longrightarrow NO^+ + O_2 \quad \text{.....(3.41)}$$

produce more NO^+ . The concentration of O_2^+ increases with increasing pressure as shown in graph (3.18) due to the charge exchange process:

$$CO_2^+ + O_2 \longrightarrow O_2^+ + CO_2 \quad \text{.....(3.42)}$$

since there are more CO_2^+ ions in the gas discharge and this process is much faster than direct ionisation of oxygen.

3.5.2.3 Effects of gas composition:

Graph (3.19) shows the variation of the main positive ion densities with helium content in the gas mixture at time t=10 μsec. As helium content increases, the concentration of all main positive ions increase. This is mainly because the addition of helium increases the electron energy and the high energy tail of the electron energy distribution function (as discussed in chapter 2) . Thus , the ion production rates for the main gas constituents are increased (see figure 3.1).

The effect of varying nitrogen proportion in the gas mixture on the development of positive ion species is shown in graph (3.20).With increasing nitrogen content the density of CO_2^+ decreases because of the decreasing ion production rate for CO_2 as a result of the decreasing electron energy . Thus, with less CO_2^+ in the discharge the density of O_2^+ decreases because,as discussed in 3.3.2,this ion is mainly

produced by the charge exchange process with CO_2^+. On the other hand,as nitrogen content in the gas mixture increases so too does the concentration of N_2^+ and thence NO^+ due to the presence of more nitrogen molecules in the discharge, hence more NO.The increasing density of NO^+ also explains the decrease in O_2^+ population since NO^+ is also produced by the charge exchange process involving NO and O_2^+. It can be seen from figure (3.1) that NO has the largest ionisation rate amongst other gases in the mixture and the decrease in the electron energy caused by addition of N_2 does not have large effect on this rate. Thus,the concentration of NO^+ increases due to the effects of these two production channels. The increased presence of NO^+ emphasizes the importance of minority species such as NO_2 and NO in the plasma, since these species also easily form negative ions,so their presence can affect the entire energy balance in the discharge [Tannen et al ,3.7]. Due to its low ionisation potential,Smith et al[3.24] suggested that NO may increase the preionisation ,so the E/N value necessary to sustain the discharge is reduced with addition of about 0.2% of NO. Moreover, they observed an increase in the output power with small amounts of added NO.

3.5.2.4 Effects of gas additives:

Graph (3.21) shows the development with time of the main positive ion species in a 1:1:8 gas mixture with 2% added O_2. The total positive ion population is significantly increased and O_2^+ becomes the dominant ion.This ion is formed by direct electron impact ionisation and charge exchange processes with CO_2^+. The charge exchange process consumes more CO_2^+ with the presence of more O_2 in the gas mixture, hence the population of CO_2^+ is less than that in a mixture without added O_2 . The gradual increase of NO^+ shown in the graph is mainly because of the charge exchange process

$$O_2^+ + NO \longrightarrow NO^+ + O_2 \qquad \text{.....(3.43)}$$

which can be understood as due to more NO molecules being produced in the discharge as time progresses, so charge exchange with O_2^+ becomes more favorable.Since NO^+ undergoes no ion - molecule reactions in the discharge [Smith and Shields ,3.8] it will be lost by electron and negative ion recombination processes.

As discussed in (3.5.1.2),the presence of O_2 in the gas mixture has a dramatic effect on the negative ion population in the discharge (graph 3.5) due to its large attachment rate, while its ionisation rate is similar to that of CO_2. Charge neutrality requires that the positive ion concentration balance the cumulative electron and negative ion densities. Therefore, when the negative ion density approaches the electron density, the corresponding rise in positive ion concentration results in an increase in recombination losses and the electron temperature rises

so that the ionisation rate can compensate for the additional losses. For this reason, the E/N value necessary to sustain the discharge increases with addition of O_2 to the gas mixture. This is in agreement with the experimental results of Smith et al[3.24] and Nagai et al [3.28].

The effect of added CO on the development of the main positive ions is shown in graph (3.22). As CO content in the gas mixture increases , the concentration of positive ion species decreases due to the decrease in the ionisation rates for the main gas constituents caused by the decrease in the electron energy (as discussed in chapter 2) . The initial increase in CO_2^+ observed in the graph is mainly because the sharp increase in CO^+ population due to the availability of more CO molecules ,which is then removed by the charge exchange process:

$$CO^+ + CO_2 \longrightarrow CO_2^+ + CO \qquad \text{.....(3.44)}$$

With increasing CO content (up to about 40 % of that of CO_2) the decrease in CO_2^+ population is caused by the decreasing ionisation rates.In addition, the dissociative recombination process:

$$e + CO^+ \longrightarrow C + O \qquad \text{.....(3.45)}$$

which produces more carbon deposits in the discharge . However, when the CO content is greater than 40 % of that of CO_2,the population of CO^+ again increases with increasing CO. This is thought to be as a result of the high content of CO molecules in the discharge , the ion production mechanism produces more CO^+ than the loss mechanisms can remove.

3.5.3 Neutral species predictions:

3.5.3.1 Development of neutral species:

Graph (3.23) shows the development of the dissociation products in a 1:1:8 gas mixture at 120 Torr. The density of CO and O_2 increases during the pulse as a result of the dissociation processes:

$$e + CO_2 \longrightarrow CO + O + e \qquad \text{.....(3.46)}$$

$$e + CO_2 \longrightarrow CO + O^- \qquad \text{.....(3.47)}$$

The resulting oxygen atoms are rapidly converted to molecular oxygen by three-body collision processes, thus O_2 concentration increases as more O atoms are produced. Discharge stability depends strongly on the gas composition, especially the amount of oxygen produced by dissociation of CO_2 . The Oxygen has a harmful effect on the discharge as discussed in previous sections.As higher output power can be obtained with increasing gas pressure it is essential to have a stringent oxygen control for a stable discharge. The large attachment rate for O_2 which exhibits a strong E/N dependence (see figure 3.2) reduces the discharge impedance. This introduces moving striations in the positive column which finally develop into arcing.

The atomic nitrogen is mainly produced by the mechanism shown in (3.5.1.4) due to the small dissociation rate of N_2. This species is the main source of the various nitrogen oxides, NO_x, which accumulate in the discharge - as shown in graph (3.24)- and have considerable effects on the discharge stability as discussed in sections (3.5.1 and 3.5.2).

Graph (3.25) shows the development of the dissociation products species during the pulse and a 90 μsec afterglow period.The concentration of O_2 continues to accumulate in the afterglow as a result of different recombination processes . The development of the dissociation products during 5 subsequent pulses with an interpulse gap of 90 μsec is shown in graph (2.26).In the present calculations,the dissociation of CO_2 is about 0.21% per pulse.

3.5.3.2 Effects of gas pressure:

The effects of varying gas pressure on the development of different neutral species are shown in graph (3.27). With increasing pressure the concentration of the main dissociation products CO and O_2 increases due to the presence of more carbon dioxide molecules in the gas discharge. This is in agreement with the experimental results of Willis et al [3.29] who show that the amount of carbon monoxide formed per pulse increases with increasing gas pressure up to 400 Torr, above which the decrease in CO yield is attributed to a reduced decomposition rate at low E/N which obtain at the higher pressures.

It can be seen from graph (3.27) that the concentration of nitrogen oxides increases with increasing pressure due to the presence of more nitrogen atoms and molecules in the gas discharge,together with more oxygen , as shown in the graph.

3.5.3.3 Effects of gas composition:

Graph (3.28) shows the effects of increasing the amount of helium in the gas mixture. The concentration of CO and O_2 produced in the discharge increases with increasing helium content. This is due to the fact that the addition of helium raises the average electron energy in the discharge and increases the high energy tail of the electron energy distribution function (as discussed in chapter 2) so there are more of the comparatively high energy ($\approx$ 7 eV) electrons which cause the dissociation of CO_2. It can be seen from the graph that with increasing amount of helium in the gas mixture,the concentration of NO increases due to the availability of more oxygen atoms and molecules in the discharge produced by CO_2 dissociation , whereas that of NO_2 decreases because the production mechanisms of NO consume more NO_2 molecules by the following reactions:

$$NO_2 + O \longrightarrow NO + O_2 \qquad \text{.....(3.48)}$$

$$NO_2 + N \longrightarrow NO + NO \qquad \text{.....(3.49)}$$

The effect of increasing nitrogen content in the gas mixture is shown in graph (3.29). The concentration of CO and O_2 decreases as the nitrogen content increases. This is because the addition of N_2 reduces both the average electron energy and the high energy part of the electron energy distribution function (as discussed in chapter 2),thus the dissociation of carbon dioxide is reduced.On the other hand, the concentration of NO and NO_2 increases with the amount of N_2 in the gas mixture because of the presence of more nitrogen atoms in the discharge as shown in the graph.

3.5.3.4 Effects of gas additives:

Graph (3.30) shows the effects of added carbon monoxide on the development of different neutral species in a 1:1:8 gas mixture at 120 Torr. The concentration of the species O and O_2 decreases with increasing CO content in the gas mixture. This is because of the decrease in the dissociation rate of CO_2 due to the decrease in the electron energy caused by the addition of CO. It can be seen from the graph that the oxygen concentration does not significantly decrease for higher initial CO contents.For low CO contents, more CO_2 is decomposed until an equilibrium is established. Whereas for high initial CO contents , the dissociation equilibrium is reduced so less CO_2 is decomposed to establish an equilibrium. This is in agreement with the results of Pace and Lacombe [3.2] and Shields et al [3.6].

Graph(3.30) also shows that as the CO content increases, the concentration of nitrogen oxides NO and NO_2 decreases as there is less oxygen in the discharge. In addition , a high content of CO in the laser gas mixture diminishes the degradation rate of the gas due to 'self-regeneration' reactions such as:

$$CO + N_2O \longrightarrow CO_2 + N_2 \qquad \text{.....(3.50)}$$

$$CO + NO_2 \longrightarrow CO_2 + NO \qquad \text{.....(3.51)}$$

The addition of CO also reduces the density of other neutral species such as O_3 and CO_3 as shown in graph (3.30).

The decrease in the density of different neutral species reduces the population of negative ion species in the discharge. This,with the decrease in the dissociation rate

of CO_2 ,increase both discharge stability and operation life for the laser. Basov et al [3.27] have shown that when CO is added to the gas mixture the laser gas degrades more slowly and subsequently operating times are increased.

Graph (3.31) shows the variation with added hydrogen of different neutral species concentrations in a 1:1:8 gas mixture at 120 Torr. The dissociation of CO_2 is reduced with the addition of H_2. Thus,the concentrations of CO and O_2 are decreased as shown in the graph . Moreover , several recombination processes also reduce the densities of CO and O_2. This can be explained as follows: the reactions

$$H + O_2 \longrightarrow OH + O \qquad \text{.....(3.52)}$$

$$H_2 + O \longrightarrow OH + H \qquad \text{.....(3.53)}$$

produce OH radicals which are then involved in the reaction:

$$OH + CO \longrightarrow CO_2 + H \qquad \text{.....(3.54)}$$

hence, in effect , CO and O_2 are recombined to form CO_2 and the hydrogen atoms are available to repeat the cycle.

It can also be seen from graph (3.31),that with addition of hydrogen, the concentrations of different neutral species in the discharge are decreased. On the other hand, with increasing amount of added H_2 , the concentration of water vapour in the discharge increases as shown in graph (3.31) .

This species, once present in considerable amounts (i.e >10000 ppm),promotes discharge arcing.In addition,it rapidly depopulates the upper laser level, thus reducing the output power. These harmful actions of water vapour have been observed by Nagai et al [3.28] and Smith et al [3.23]. However , Williams and Smith [3.22] have shown that the

presence of small amounts of H_2O control the carbon dioxide dissociation equilibrium by forming OH radicals which react with CO molecules to form CO_2.

3.6 CONCLUSIONS:

(1) Under the operating conditions of a CO_2 laser discharge, the important kinetic process is electron attachment since the formation of negative ions elevates the electron temperature in the discharge.This will affect the excitation processes of $CO_2(00°1)$ and $N_2(v=1-8)$ levels and strongly influences the discharge operation.

(2) In a CO_2:N_2:He gas mixture,the dominant negative ion is predicted to be CO_3^- and the total negative ion population density,under operational conditions ,is predicted to be less than the electron density depending on the gas mixture . Whereas,the dominant positive ion is CO_2^+ .

(3) The addition of O_2 to the gas mixture significantly increases the negative and positive ion populations, O_2^- and O_2^+ are the dominant ions.

(4) The presence of more than 1% H_2O significantly increases the negative ion population.

(5) Increasing gas pressure leads to an increase in the population of CO_3^- , CO_4^- , CO_2^+ , O_2^- and NO^- and a decrease in that of O^- .

(6) The discharge instability increases and arcing ensues under conditions when the negative ion population has been significantly increased.

(7) The presence of carbon monoxide reduces the electron temperature and the negative ion population due to detachment processes involving CO molecules with CO_3^- and O^- .

(8) The addition of more than 1% H_2 increases the negative ion population due to the formation of water vapour ,hence the formation of OH^- and H^- .

(9) The negative ion population decreases with increasing helium content in the gas mixture,whereas increasing nitrogen content increases the concentration of different nitrogen oxides. Thus , the negative ion population increases as these species easily form negative ions.

(10) The dissociation of CO_2 is predicted to be about 0.21% per pulse . The amount of CO and O_2 produced by CO_2 dissociation is greater in helium rich mixtures than in nitrogen rich mixtures.

(11) With increasing gas pressure,the amount of CO and O_2 formed per pulse increases . The concentration of nitrogen oxides also increases with pressure.

(12) The dissociation of CO_2 and subsequent formation of O_2 can effectively be controlled by the addition of CO and H_2, because CO reacts with OH radicals to form carbon dioxide. However, the amount of added H_2 should be < 1% in order to control the formation of water vapour due to dissociation of H_2 which is predicted to be about 0.7% per pulse.

REFERENCES

CHAPTER 3

3.1 Smith K and Thomson R M - 'Computer Modelling of Gas lasers'-Plenum Press,New York, 1978.

3.2 Pace P W and Lacombe M -'A sealed high-repetition rate TEA CO_2 laser'-IEEE J.QE, 14, 1978 (263) .

3.3 Nighan W L,Wiegand W J,and Haas R A-'Ionisation instability in CO_2 laser discharges '- Appl. Phys. Lett.,Vol 22,1973 (579) .

3.4 Wiegand W J and Nighan W L- 'Plasma chemistry of CO_2-N_2 -He discharges'- Appl.Phys.Lett.,Vol 22,1973(583).

3.5 Nighan W L and Wiegand W J-'Influence of negative -ion processes on steady-state properties and striations in molecular gas discharges '- Phys. Rev., A10,1974 (922) .

3.6 Shields H,Smith ALS,and Norris B- 'Negative ion effects in TEA CO_2 laser'-J.Phys.D: Appl.Phys.,9,1976(1587)

3.7 Tannen P D,Bletzinger P,and Garscadden A-'Species composition in the CO_2 discharge laser'- IEEE J.QE, 10, 1974 (7).

3.8 Smith ALS and Shields H-'Positive ion processes in the positive column of CO_2 laser electrical discharges' -J. Chem. Phys. ,Vol 67,1977 (1594) .

3.9 Ono S and Teii S-'Negative ion formations and their effects on the electron temperature in CO_2 -N_2 -He mixture gas discharges '-J.Phys. D: Appl. Phys.,17, 1984 (1999).

3.10 Smith ALS and Norris B- 'Limiting processes in sealed photoionisation TEA CO_2 lasers'-J.Phys.D:Appl.Phys. 11, 1978 (1949) .

3.11 Engel A. Von-'Ionized Gases'-Oxford University Press, 1965 (p215) .

3.12 Krishna Kumar S V and Venkatasubramanian V S-'CO_2^- ions in a low pressure glow discharge of carbon dioxide' -J.Chem.Phys.,Vol 79, 1983 (6423) .

3.13 Llewellyn-Jones F-'The development of theories of the electrical breakdown of gases'-in: Proceedings of a NATO Advanced Study on Electrical Breakdown and Discharges in Gases. Series B: Physics , Vol 89 a , Plenum Press, New York, 1983 (1).

3.14 Rees JA-'Basic processes of electrical discharges'-in: Proceedings of a NATO Advanced Study on Electrical Breakdown and Discharges in Gases.Series B:Physics, Vol 89 a , Plenum Press, New York, 1983 (73).

3.15 Maier H N and Fessnden R W-'Electron-ion recombination rate constants for some compounds of moderate complexity'-J.Chem.Phys.,Vol 62, 1975 (4790) .

3.16 Mitchell JBA and HUS H-'The dissociative recombination and excitation of CO^+'-J.Phys. B: Mol.Phys,Vol 18, 1985 (547).

3.17 Roberts S A-'Numerical Modeling of a Chemical Plasma'- Comput. Phys. Commun. ,Vol 18, 1979 (363) .

3.18 Roberts S A-'Numerical Modeling of a chemical Plasma'- Comput. Phys. Commun. ,Vol 18, 1979 (377).

3.19 Roberts S A-'Numerical Modeling of a Chemical Plasma'- Comput. Phys. Commun. ,Vol 18, 1979 (353).

3.20 NAG Library Manual, Numerical Algorithms GP,ICL 2980 System, 1984.

3.21 Levine A K- 'A series of advances in lasers' - Vol 3 , Chap 2, Marcel Dekker Inc., New York , 1971.

3.22 Williams G C R and Smith A L S - 'Plasma chemistry of RF discharges in CO_2 laser gas mixtures '- J. Phys. D: Appl. Phys. , 18 , 1985 (335).

3.23 Smith A L S ,Sephton J P and Scott G-'High-peak power extended lifetime sealed TEA CO_2 lasers'-J.Phys.E: Sci. Instrum., Vol 17, 1984 (590).

3.24 Smith A L S ,Bett T H and Browne P G- ' The effects of gas additives on TEA CO_2 lasers'- IEEE J.QE.,11, 1975 (335) .

3.25 Rapp D and Briglia D D - ' Total cross sections for ionisation and attachment in gases by electron impact. II Negative ion formation'- J. Chem. Phys. ,Vol 43 , 1965 (1480).

3.26 R E Beverly III - ' Ion aging effects on the dissociative-attachment instability in CO_2 lasers'- J. Opt. QE. , Vol 14 , 1982 (501).

3.27 Basov N.G ,Glotov E.P ,Danilychev V.A ,Kerimov O.M, Malysh M.M ,and Soroka A.M - ' High-power Electroionization CO_2 and CO Lasers for Industrial Applications '-IEEE J.QE.,21, 1985 (342).

3.28 Nagai H, Hishii M, Shibayama K, Nagai A and Akiba T- 'High-Pressure Sealed CW CO_2 Laser With High Efficiency'- IEEE J.QE.,18, 1982 (416).

3.29 Willis C,Sarjeant W J,and Wardlaw D M -' Initial rate of decomposition of CO_2 in volume discharges : An experimental study'- J. Appl. Phys. ,50,1979 (68).

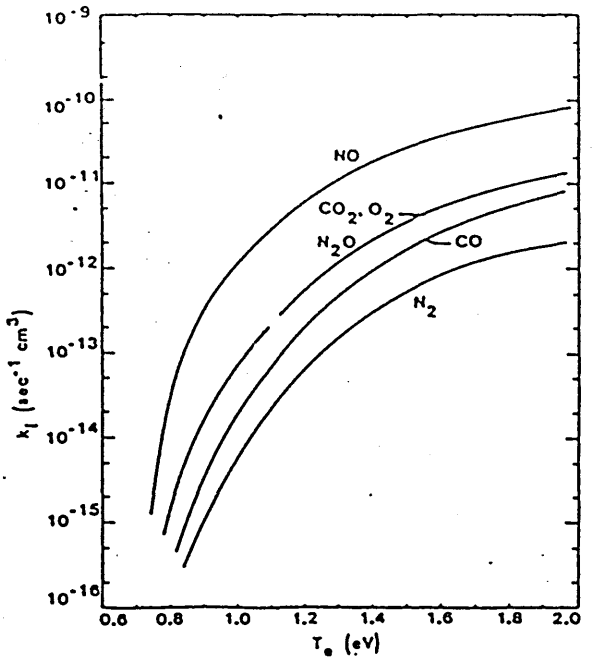

Ionisation rate coefficients [3.5]

FIGURE (3.1)

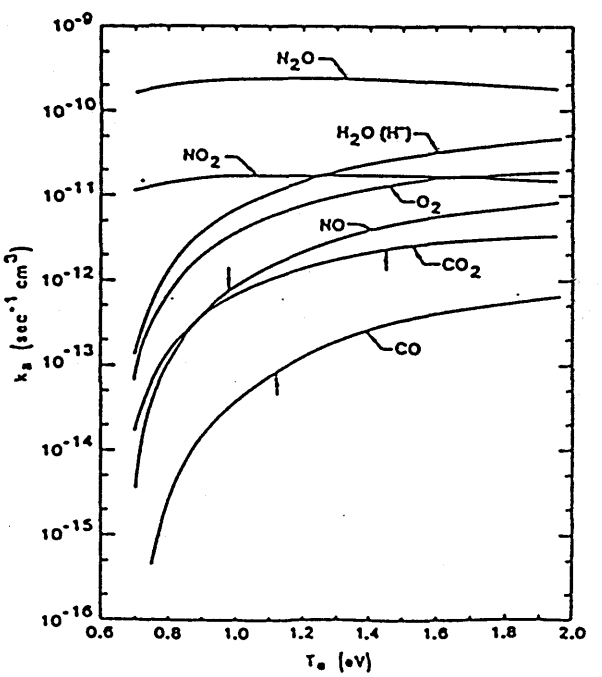

Attachment rate coefficients [3.5]

FIGURE (3.2)

TABLE (3.1)

LIST OF SPECIES WITHIN THE PLASMA (*)

Species number	Species	Species number	Species
1	e	31	O_2^+
2	CO_2	32	N_2^+
3	N_2	33	NO^+
4	He	34	O^+
5	H_2	35	N^+
6	CO	36	CO_2^+
7	O	37	He^+
8	O_2	38	CO^+
9	NO_2	39	C^+
10	O_3	40	OH^+
11	N_2O	41	N_2O^+
12	NO	42	H_2^+
13	N	43	H_3^+
14	H	44	HO_2^+
15	H_2O	45	He_2^+
16	NO_3	46	N_2OH^+
17	HO_2	47	H_2O^+
18	OH	48	H_3O^+
19	$O_2(^1\Delta_g)$	49	$O_2^+ \cdot N_2$
20	O^-	50	$NO^+ \cdot NO$
21	O_2^-	51	$NO^+ \cdot H_2O$
22	NO_2^-	52	$O_2^+ \cdot N_2O$
23	O_3^-	53	$O_2^+ \cdot H_2O$
24	H^-	54	$H_3O^+ \cdot OH$
25	NO^-	55	N_3^+
26	N_2O^-	56	NO_2^+
27	OH^-	57	O_4^+
28	NO_3^-	58	$NO_2^- \cdot H_2O$
29	CO_3^-	59	$CO_3^- \cdot H_2O$
30	CO_4^-	60	$O_2^- \cdot H_2O$

(*) Ref. [3.1]

TABLE (3.2)

ELECTRON ATTACHMENT AND DETACHMENT, NEGATIVE-ION-MOLECULE REACTIONS, NEUTRAL DISSOCIATION AND RECOMBINATION PROCESSES (*)

Number Reaction	Rate Constant (300 K)
Dissociation Attachment	
1. $e + CO_2 \longrightarrow CO + O^-$	5×10^{-13} cm$^3 \cdot$s^{-1}
2. $e + CO \longrightarrow C + O^-$	3×10^{-14} cm$^3 \cdot$s^{-1}
3. $e + O_2 \longrightarrow O + O^-$	3×10^{-12} cm$^3 \cdot$s^{-1}
4. $e + H_2O \longrightarrow H^- + OH$	5×10^{-12} cm$^3 \cdot$s^{-1}
5. $e + H_2 \longrightarrow H^- + H$	1×10^{-13} cm$^3 \cdot$s^{-1}
Three-Body Attachment	
6. $e + O_2 + M \longrightarrow O_2^- + M$	2×10^{-30} cm$^6 \cdot$s^{-1} ($M = O_2$)
	1×10^{-31} cm$^6 \cdot$s^{-1} ($M = N_2$)
	3×10^{-30} cm$^6 \cdot$s^{-1} ($M = CO_2$)
	2×10^{-30} cm$^6 \cdot$s^{-1} ($M =$ He)
7. $e + O + M \longrightarrow O^- + M$	1×10^{-31} cm$^6 \cdot$s^{-1} ($M = O_2$)
	1×10^{-31} cm$^6 \cdot$s^{-1} ($M = N_2$)
Associative Detachment	
8. $O^- + CO \longrightarrow CO_2 + e$	7×10^{-10} cm$^3 \cdot$s^{-1}
9. $O^- + O \longrightarrow O_2 + e$	2×10^{-10} cm$^3 \cdot$s^{-1}
10. $O^- + O_2(^1\Delta g) \longrightarrow O_3 + e$	1×10^{-10} cm$^3 \cdot$s^{-1}
11. $O^- + H_2 \longrightarrow H_2O + e$	8×10^{-10} cm$^3 \cdot$s^{-1}
12. $CO_3^- + CO \longrightarrow 2CO_2 + e$	5×10^{-13} cm$^3 \cdot$s^{-1}
13. $O_2^- + O \longrightarrow O_3 + e$	3×10^{-10} cm$^3 \cdot$s^{-1}
14. $O_2^- + O_2(^1\Delta g) \longrightarrow 2O_2 + e$	2×10^{-10} cm$^3 \cdot$s^{-1}
15. $O_2^- + H \longrightarrow HO_2 + e$	1×10^{-9} cm$^3 \cdot$s^{-1}
16. $H^- + H \longrightarrow H_2 + e$	1×10^{-9} cm$^3 \cdot$s^{-1}
17. $H^- + O_2 \longrightarrow HO_2 + e$	1×10^{-9} cm$^3 \cdot$s^{-1}
18. $OH^- + O \longrightarrow HO_2 + e$	2×10^{-10} cm$^3 \cdot$s^{-1}
19. $OH^- + H \longrightarrow H_2O + e$	1×10^{-9} cm$^3 \cdot$s^{-1}
Neutral Dissociation	
20. $e + CO_2 \longrightarrow CO + O + e$	0.5×10^{-9} cm$^3 \cdot$s^{-1}
21. $e + O_2 \longrightarrow O + O + e$	1×10^{-9} cm$^3 \cdot$s^{-1}
22. $e + H_2 \longrightarrow H + H + e$	4×10^{-9} cm$^3 \cdot$s^{-1}
23. $e + H_2O \longrightarrow H + OH + e$	2×10^{-9} cm$^3 \cdot$s^{-1}
Neutral Recombination	
24. $O + CO + M \longrightarrow CO_2 + M$	2×10^{-36} cm$^6 \cdot$s^{-1}
25. $O + O + M \longrightarrow O_2 + M$	3×10^{-33} cm$^6 \cdot$s^{-1}
26. $O + O_2 + M \longrightarrow O_3 + M$	5×10^{-34} cm$^6 \cdot$s^{-1}
27. $O + O_3 \longrightarrow O_2 + O_2$	9×10^{-15} cm$^3 \cdot$s^{-1}
28. $H + H + M \longrightarrow H_2 + M$	8.4×10^{-33} cm$^6 \cdot$s^{-1}
Negative-Ion-Molecule Two-Body Reactions	
29. $O^- + O_2(^1\Delta_g) \longrightarrow O_2^- + O$	1×10^{-9} cm$^3 \cdot$s^{-1}
30. $O^- + H_2 \longrightarrow OH^- + H$	3×10^{-11} cm$^3 \cdot$s^{-1}
31. $O_2^- + O \longrightarrow O_2 + O^-$	1×10^{-11} cm$^3 \cdot$s^{-1}
32. $O_2^- + O_3 \longrightarrow O_2 + O_3^-$	$.4 \times 10^{-10}$ cm$^3 \cdot$s^{-1}
33. $O_2^- + H \longrightarrow H^- + O_2$	2×10^{-9} cm$^3 \cdot$s^{-1}
34. $CO_3^- + O \longrightarrow O_2^- + CO_2$	8×10^{-11} cm$^3 \cdot$s^{-1}
35. $CO_3^- + H \longrightarrow OH^- + CO_2$	2×10^{-10} cm$^3 \cdot$s^{-1}
36. $CO_4^- + O \longrightarrow CO_3^- + O_2$	2×10^{-10} cm$^3 \cdot$s^{-1}
37. $CO_4^- + O_3 \longrightarrow O_3^- + CO_2 + O_2$	1×10^{-10} cm$^3 \cdot$s^{-1}

((CONTINUED ON NEXT PAGE))

TABLE (3.2) Cont.

38. $CO_4^- + H \longrightarrow CO_3^- + OH$	2×10^{-10} cm$^3 \cdot$s^{-1}
Negative-Ion-Molecule Three-Body Reactions	
39. $O^- + CO_2 + M \longrightarrow CO_3^- + M$	9×10^{-29} cm$^6 \cdot$s^{-1} ($M = CO_2$)
	2×10^{-28} cm$^6 \cdot$s^{-1} ($M = H_e$)
	3×10^{-28} cm$^6 \cdot$s^{-1} ($M = O_2$)
40. $O_2^- + CO_2 + M \longrightarrow CO_4^- + M$	1×10^{-29} cm$^6 \cdot$s^{-1} ($M = CO_2$)
	1×10^{-29} cm$^6 \cdot$s^{-1} ($M = O_2$)
	5×10^{-29} cm$^6 \cdot$s^{-1} ($M = O_2$)
Neutral Two-Body Reactions[b]	
41. $O + OH \longrightarrow O_2 + H$	3.3×10^{-11} cm$^3 \cdot$s^{-1}
42. $H_2 + O \longrightarrow H + OH$	1×10^{-14} cm$^3 \cdot$s^{-1}
43. $H + O_2 \longrightarrow O + OH$	1.2×10^{-15} cm$^3 \cdot$s^{-1}
44. $H + OH \longrightarrow H_2 + O$	3.5×10^{-17} cm$^3 \cdot$s^{-1}
45. $H_2 + OH \longrightarrow H_2O + H$	6.5×10^{-15} cm$^3 \cdot$s^{-1}
46. $H_2O + H \longrightarrow H_2 + OH$	2×10^{-25} cm$^3 \cdot$s^{-1}
47. $H_2O + O \longrightarrow OH + OH$	5×10^{-24} cm$^3 \cdot$s^{-1}
48. $OH + OH \longrightarrow H_2O + O$	2.4×10^{-13} cm$^3 \cdot$s^{-1}
49. $H + HO_2 \longrightarrow OH + OH$	1.7×10^{-11} cm$^3 \cdot$s^{-1}
50. $OH + OH \longrightarrow H + HO_2$	1×10^{-40} cm$^3 \cdot$s^{-1}
51. $H + HO_2 \longrightarrow H_2 + O_2$	1.3×10^{-11} cm$^3 \cdot$s^{-1}
52. $H_2 + O_2 \longrightarrow H + HO_2$	7×10^{-53} cm$^3 \cdot$s^{-1}
53. $H_2O_2 + OH \longrightarrow H_2O + HO_2$	8×10^{-13} cm$^3 \cdot$s^{-1}
54. $H_2O + HO_2 \longrightarrow H_2O_2 + OH$	6×10^{-35} cm$^3 \cdot$s^{-1}
55. $H_2O_2 + H \longrightarrow H_2 + HO_2$	5×10^{-15} cm$^3 \cdot$s^{-1}
56. $H_2 + HO_2 \longrightarrow H_2O_2 + H$	3×10^{-26} cm$^3 \cdot$s^{-1}
57. $HO_2 + CO \longrightarrow CO_2 + OH$	1.5×10^{-27} cm$^3 \cdot$s^{-1}
58. $O + CO \longrightarrow CO_2 + h\nu$	2×10^{-20} cm$^3 \cdot$s^{-1}
59. $OH + CO \longrightarrow CO_2 + H$	1.5×10^{-13} cm$^3 \cdot$s^{-1}
60. $O + HO_2 \longrightarrow OH + O_2$	9×10^{-12} cm$^3 \cdot$s^{-1}

[a] For a mean electron energy of 1 eV.
[b] Rates with a known temperature dependence have been quoted at 300 K.

(*) Ref. [3.2]

TABLE (3.3) (*)

3.3 A *Reactions Involving Electrons as Initial Particles*

Reaction	k^a ($cm^3\ sec^{-1}$)
$O+e \rightarrow O^- + h\nu$	1.3(−15)[b]
$O_2+e \rightarrow O_2^- + h\nu$	2.0(−19)
$NO_2+e \rightarrow NO_2^- + h\nu$	1.0(−17)
$O_3+e \rightarrow O_3^- + h\nu$	1.0(−17)
$O_3+e \rightarrow O^- + O_2$	3.0(−12)
$O_3+e \rightarrow O_2^- + O$	3.8(−22)
$O+e+O_2 \rightarrow O^- + O_2$	1.0(−31)
$O+e+N_2 \rightarrow O^- + N_2$	1.0(−31)
$O_2+e+O \rightarrow O_2^- + O$	1.89(−30)
$NO_2+e+O_2 \rightarrow NO_2^- + O_2$	3.0(−28)
$NO_2+e+N_2 \rightarrow NO_2^- + N_2$	8.0(−28)
$O_2+e+N_2 \rightarrow O_2^- + N_2$	1.0(−31)
$O_2^+ + e \rightarrow O+O$	2.2(−7)
$N_2^+ + e \rightarrow N+N$	2.8(−7)
$NO^+ + e \rightarrow N+O$	5.0(−7)
$O^+ + e+M \rightarrow O+M$	1.0(−26)
$O_2^+ + e+M \rightarrow O_2+M$	1.0(−26)
$N_2^+ + e+M \rightarrow N_2+M$	1.0(−26)
$NO^+ + e+M \rightarrow N+O+M$	1.0(−27)
$NO^+ + e+M \rightarrow NO+M$	1.0(−26)
$O^- + e \rightarrow O + h\nu$	3.5(−12)
$O_2^- + e \rightarrow O_2 + h\nu$	1.0(−12)
$N_2^- + e \rightarrow N_2 + h\nu$	1.0(−12)
$NO^- + e \rightarrow NO + h\nu$	1.0(−12)
$N^+ + e+M \rightarrow N+M$	1.0(−26)
$N^+ + e \rightarrow N + h\nu$	3.5(−12)
$CO_2^- + e \rightarrow CO+O$	6.0(−8)
$NO^- \cdot NO + e \rightarrow NO+NO$	1.7(−6)
$NO^- \cdot H_2O + e \rightarrow NO+H_2O$	1.0(−6)
$NO_2+He+e \rightarrow NO_2^- + He$	2.0(−11)[c]
$CO_2+e \rightarrow CO+O^-$	5.0(−13)
$CO+e \rightarrow C+O^-$	3.0(−14)
$O_2+e \rightarrow O+O^-$	3.0(−12)
$N_2O+e \rightarrow N_2+O^-$	2.0(−10)
$NO+e \rightarrow N+O^-$	1.0(−12)
$NO_2+e \rightarrow NO+O^-$	1.0(−11)

[a] k is expressed in $cm^6\ sec^{-1}$ for three initial particle reactions.
[b] Numbers in parentheses denote the power of 10.
[c] This is a saturated three-body process, expressed in $cm^3\ sec^{-1}$.

((CONTINUED ON NEXT PAGE))

3.3 B *Binary Negative-Ion Molecule Reactions*

Reaction	ΔE (eV)	k ($cm^3\ sec^{-1}$)
$H^- + H \rightarrow H_2 + e$	3.8	1.3(−9)[a]
$H^- + NO_2 \rightarrow NO_2^- + H$		2.9(−9)
$O^- + NO_2 \rightarrow NO_2^- + O$		1.1(−9)
$O_2^- + NO_2 \rightarrow NO_2^- + O_2$		1.9(−9)
$O^- + NO_2 \rightarrow O_2^- + NO$		1.0(−10)
$O^- + O_2 \rightarrow O_3^- + h\nu$		1.0(−17)
$O^- + O \rightarrow O_2 + e$	3.6	1.9(−10)
$O^- + O_2 \rightarrow O_3 + e$		5.0(−15)
$O^- + N \rightarrow NO + e$	5.1	2.6(−10)
$O^- + H_2 \rightarrow H_2O + e$	3.6	6.0(−10)
$O^- + NO \rightarrow NO_2 + e$	1.4	2.6(−10)
$O^- + CO \rightarrow CO_2 + e$	4.0	6.5(−10)
$O^- + N_2 \rightarrow N_2O + e$	0.2	2.0(−19)
$O^- + O_3 \rightarrow O_3^- + O$		5.3(−10)
$O^- + N_2O \rightarrow NO^- + NO$	>3.5	2.0(−10)
$\rightarrow N_2O^- + O$		2.0(−12)
$H^- + O_2 \rightarrow HO_2 + e$	0.3	1.5(−9)
$O_2^- + O_2 \rightarrow 2O_2 + e$		5.8(−19)
$O_2^- + O \rightarrow O_3 + e$	0.6	3.0(−10)
$O_2^- + N_2 \rightarrow O_2 + N_2 + e$		1.1(−19)
$O_2^- + N \rightarrow NO_2 + e$	4.1	4.0(−10)
$\rightarrow NO + O + e$	1.0	4.0(−10)
$O_2^- + O \rightarrow O_2 + O^-$		1.0(−11)
$O_2^- + O_3 \rightarrow O_3^- + O_2$		3.5(−10)
$O_2^- + NO \rightarrow NO_2^- + O$		<1.0(−12)
$O_2^- + NO_3 \rightarrow O_2 + NO_3^-$		5.0(−10)
$O_2^- + N_2O \rightarrow O_3^- + N_2$		~0.1(−10)
$OH^- + O \rightarrow HO_2 + e$	0.9	2.0(−10)
$OH^- + NO_2 \rightarrow NO_2^- + OH$		1.0(−9)
$OH^- + H \rightarrow H_2O + e$	3.2	1.0(−9)
$OH^- + N \rightarrow HNO + e$	2.4	<1.0(−11)
$CN^- + H \rightarrow HCN + e$	1.6	~8.0(−10)
$NO^- + O_2 \rightarrow O_2^- + NO$		9.0(−10)
$NH_2^- + NO_2 \rightarrow NO_2^- + NH_3$		1.0(−9)
$O_3^- + NO_3 \rightarrow O_3 + NO_3^-$		5.0(−10)
$O_3^- + CO_2 \rightarrow CO_3^- + O_2$		4.0(−10)
$O_3^- + NO \rightarrow NO_3^- + O$		1.0(−11)
$\rightarrow NO_2^- + O_2$		≪1.0(−11)
$O_3^- + O \rightarrow O_2^- + O_2$		1.0(−10)
$CO_3^- + O \rightarrow O_2^- + CO_2$		0.8(−10)
$CO_3^- + NO \rightarrow NO_2^- + CO_2$		9.0(−12)
$NO_2^- + O_3 \rightarrow NO_3^- + O_2$		1.8(−11)
$NO_3^- + NO \rightarrow NO_2^- + NO_2$		<1.0(−12)
$NO_2^- + NO_2 \rightarrow NO_3^- + NO$		4.0(−12)
$NO_2^- + NO_3 \rightarrow NO_2 + NO_3^-$		5.0(−10)
$O_4^- + NO \rightarrow NO_3^- + O_2$		2.5(−10)
$O_4^- + CO_2 \rightarrow CO_4^- + O_2$		4.3(−10)

((CONTINUED ON NEXT PAGE))

3.3 B *(continued)*

Reaction	ΔE (eV)	k (cm^3 sec^{-1})
$CO_4^- + NO \rightarrow NO_3^- + CO_2$		4.8(−11)
$O_4^- + O \rightarrow O_3^- + O_2$		4.0(−10)
$\rightarrow O^- + 2O_2$		<4.0(−10)
$CO_4^- + O \rightarrow CO_3^- + O_2$		1.5(−10)
$\rightarrow O_3^- + CO_2$		<1.5(−10)
$N_2O^- + O_2 \rightarrow O_3^- + N_2$		1.0(−9)
$O_2^- + O_2(^1\Delta) \rightarrow O_2 + e + O_2$		1.0(−9)
$O^- + O_2(^1\Delta) \rightarrow O_2^- + O$		1.0(−9)
$O^- + O_2(^1\Delta) \rightarrow O_3 + e$		1.0(−10)
$O^- + O_2(^1\Delta) \rightarrow O_2 + h\nu + O^-$		2.6(−4)
$CO_3^- + CO \rightarrow 2CO_2 + e$		5.0(−13)
$O_3^- + N_2 \rightarrow NO_2^- + NO$		<5.0(−14)
$O_3^- + NO_2 \rightarrow NO_2^- + O_3$		7.0(−11)
$O_3^- + NO_2 \rightarrow NO_3^- + O_2$		2.0(−11)
$CO_3^- + NO_2 \rightarrow NO_3^- + CO_2$		1.0(−10)

[a] Numbers in parentheses denote the power of 10.

3.3 C *Binary Positive Ion–Molecule Reactions*

Reaction	ΔE (eV)	k (cm^3 sec^{-1})
$He^+ + N_2 \rightarrow N^+ + N + He$	0.3	1.7(−9)[a]
$\rightarrow N_2^+ + He$	9.0	1.5(−9)
$He^+ + CO \rightarrow C^+ + O + He$	2.2	1.7(−9)
$He^+ + NO \rightarrow N^+ + O + He$	3.6	1.8(−9)
$He^+ + O_2 \rightarrow O^+ + O + He$	5.9	2.1(−9)
$He^+ + CO_2 \rightarrow O^+ + CO + He$	4.5	1.2(−9)
$\rightarrow CO^+ + O + He$	4.1	1.2(−9)
$C^+ + O_2 \rightarrow CO^+ + O$	3.27	1.0(−9)
$C^+ + CO_2 \rightarrow CO^+ + CO$	2.96	1.9(−9)
$C^+ + N_2O \rightarrow NO^+ + CN$	5.54	9.1(−10)
$N^+ + H_2 \rightarrow NH^+ + H$		7.0(−10)
$N^+ + N \rightarrow N_2^+ + h\nu$		3.0(−17)
$N^+ + CO \rightarrow CO^+ + N$	0.53	5.0(−10)
$N^+ + NO \rightarrow NO^+ + N$	5.30	8.0(−10)
$\rightarrow N_2^+ + O$		3.0(−12)
$\rightarrow O^+ + N_2$		1.0(−12)
$N^+ + O_2 \rightarrow O_2^+ + N$	2.47	4.5(−10)
$\rightarrow NO^+ + O$	6.70	5.0(−10)
$\rightarrow O^+ + NO$		1.0(−12)
$N^+ + CO_2 \rightarrow CO_2^+ + N$	0.75	1.3(−9)
$\rightarrow NO^+ + CO$	6.40	1.8(−11)
$N^+ + O \rightarrow N + O^+$		1.0(−12)
$\rightarrow NO^+ + h\nu$		1.0(−17)
$N^+ + N_2O \rightarrow NO^+ + N_2$		5.5(−10)
$O^+ + H_2 \rightarrow OH^+ + H$	0.30	2.0(−9)

((CONTINUED ON NEXT PAGE))

3.3 C *(continued)*

Reaction	ΔE (eV)	k (cm^3 sec^{-1})
$O^+ + N_2 \rightarrow NO^+ + N$	1.10	2.4(−12)
$O^+ + NO \rightarrow NO^+ + O$	4.36	2.4(−11)
$O^+ + O_2 \rightarrow O_2^+ + O$	1.50	2.0(−11)
$O^+ + CO_2 \rightarrow O_2^+ + O$	1.50	1.1(−9)
$O^+ + N_2O \rightarrow N_2O^+ + O$	0.7	4.0(−10)
$\rightarrow O_2^+ + N_2$	5.0	2.0(−11)
$H_2^+ + H_2 \rightarrow H_3^+ + H$		2.1(−9)
$H_2^+ + O_2 \rightarrow HO_2^+ + H$		6.9(−9)
$He_2^+ + N_2 \rightarrow N_2^+ + 2He$	6.7	1.3(−9)
$N_2^+ + H_2 \rightarrow N_2H^+ + H$		1.9(−9)
$N_2^+ + N \rightarrow N^+ + N_2$	1.04	1.0(−12)
$N_2^+ + O \rightarrow NO^+ + N$	3.05	2.5(−10)
$\rightarrow O^+ + N_2$	1.97	1.0(−12)
$N_2^+ + CO \rightarrow CO^+ + N_2$	1.6	7.0(−11)
$N_2^+ + O_2 \rightarrow O_2^+ + N_2$	3.5	1.1(−10)
$\rightarrow NO^+ + NO$	4.5	1.0(−17)
$N_2^+ + NO \rightarrow NO^+ + N_2$	6.3	4.9(−10)
$N_2^+ + CO_2 \rightarrow CO_2^+ + N_2$	1.75	9.0(−10)
$N_2^+ + N_2O \rightarrow NO^+ + N_2 + N$	1.8	4.0(−10)
$\rightarrow N_2O^+ + N_2$	2.6	5.0(−10)
$O_2^+ + N \rightarrow NO^+ + O$	4.0	1.8(−10)
$O_2^+ + NO \rightarrow NO^+ + O_2$	2.8	8.0(−10)
$O_2^+ + N_2 \rightarrow NO^+ + NO$		1.0(−16)
$CO^+ + H_2 \rightarrow COH^+ + H$		2.0(−9)
$CO^+ + O_2 \rightarrow O_2^+ + CO$	1.94	2.0(−10)
$CO^+ + CO_2 \rightarrow CO_2^+ + CO$	0.22	1.1(−9)
$H_3^+ + N_2 \rightarrow N_2H^+ + H_2$		1.0(−9)
$CO_2^+ + H_2 \rightarrow CO_2H^+ + H$		1.4(−9)
$CO_2^+ + O_2 \rightarrow O_2^+ + CO_2$	1.72	1.0(−10)
$CH_2^+ + H_2 \rightarrow CH_3^+ + H$		2.3(−10)
$N_2O^+ + H_2 \rightarrow N_2OH^+ + H$		4.0(−10)
$H_2O^+ + H_2O \rightarrow H_3O^+ + OH$		1.0(−9)
$O_2^+ \cdot N_2 + O_2 \rightarrow O_4^+ + N_2$		≥5(−11)
$O_4^+ + N_2O \rightarrow O_2^+ \cdot N_2O + O_2$		2.5(−10)
$O_2^+ \cdot N_2O + H_2O \rightarrow O_2^+ \cdot H_2O + N_2O$		≥1.0(−10)
$O_4^+ + H_2O \rightarrow O_2^+ \cdot H_2O + O_2$		1.2(−9)
$O_2^+ \cdot H_2O + H_2O \rightarrow H_3O^+ + OH + O_2$		3(−10)
$\rightarrow H_3O^+ \cdot OH + O_2$		1(−9)
$He_2^+ + NO \rightarrow NO^+ + 2He$		1.3(−9)
$He_2^+ + O_2 \rightarrow O_2^+ + 2He$		1.1(−9)
$He_2^+ + CO \rightarrow CO^+ + 2He$		1.4(−9)
$O^+ + O \rightarrow O_2^+ + h\nu$		1.0(−17)
$O^+ + NO \rightarrow O_2^+ + N$		3.0(−12)
$O^+ + N \rightarrow NO^+ + h\nu$		1.0(−18)
$O_2^+ + NO_2 \rightarrow NO^+ + O_3$		1.0(−11)

[a] Numbers in parentheses denote the power of 10.

((CONTINUED ON NEXT PAGE))

3.3 D *Three-Molecule Reactions*

Reaction	k ($cm^6 sec^{-1}$)
$He^+ + 2He \rightarrow He_2^+ + He$	8.7(−32)*
$N_2^+ + 2N_2 \rightarrow N_4^+ + N_2$	7.2(−29)
$CO_2^+ + 2CO_2 \rightarrow C_2O_4^+ + CO_2$	3.0(−28)
$O^- + 2O_2 \rightarrow O_3^- + O_2$	8.6(−31)
$O^- + 2CO_2 \rightarrow CO^- + CO_2$	8.0(−29)
$O_2^- + 2CO_2 \rightarrow CO_4^- + CO_2$	9.0(−30)
$O_2^- + CO_2 + O_2 \rightarrow C_2O_4^- + O_2$	2.0(−29)
$H^+ + 2H_2 \rightarrow H_3^+ + H_2$	3.2(−29)
$N^+ + 2N_2 \rightarrow N_3^+ + N_2$	1.8(−29)
$O^- + CO_2 + He \rightarrow CO_3^- + He$	1.5(−28)
$N_2^+ + N_2 + He \rightarrow N_4^+ + He$	1.9(−29)
$N^+ + N_2 + He \rightarrow N_3^+ + He$	8.6(−30)
$O_2^+ + O_2 + He \rightarrow O_4^+ + He$	3.1(−29)
$O^+ + N_2 + He \rightarrow N_2O^+ + He$	5.4(−29)
$NO^+ + 2NO \rightarrow NO^+ \cdot NO + NO$	5.0(−30)
$O_2^+ + 2O_2 \rightarrow O_4^+ + O_2$	2.8(−30)
$O_2^- + 2O_2 \rightarrow O_4^- + O_2$	3.0(−31)
$O^- + O^+ + N \rightarrow O_2 + N$	2.0(−25)
$O^- + O^+ + N_2 \rightarrow O_2 + N_2$	2.0(−25)
$O^- + O^+ + O_2 \rightarrow 2O_2$	2.0(−25)
$O^- + O^+ + O \rightarrow O_2 + O$	2.0(−25)
$O_2^- + O^+ + M^b \rightarrow O_3 + M$	2.0(−25)
$O^- + O_2^+ + M \rightarrow O_3 + M$	2.0(−25)
$O_2^- + O_2^+ + M \rightarrow 2O_2 + M$	2.0(−25)
$O^- + N_2^+ + M \rightarrow N_2O + M$	2.0(−25)
$O_2^- + N_2^+ + M \rightarrow O_2 + N_2 + M$	2.0(−25)
$O^- + NO^+ + M \rightarrow NO_2 + M$	2.0(−25)
$O_2^- + NO^+ + M \rightarrow O_2 + NO + M$	2.0(−25)
$O^+ + O + M \rightarrow O_2^+ + M$	1.0(−29)
$O^+ + N + M \rightarrow NO^+ + M$	1.0(−29)
$O^- + NO + M \rightarrow NO_2^- + M$	1.0(−29)
$O_2^- + N + M \rightarrow NO_2^- + M$	1.0(−29)
$O_2^- + O_2 + N_2 \rightarrow NO_2^- + NO_2$	5.8(−42)
$O + O + O_2 \rightarrow O_2 + O_2$	3.0(−33)
$O + O + O \rightarrow O_2 + O$	3.0(−33)
$O + O + N_2 \rightarrow O_2 + N_2$	3.0(−33)
$O + O_2 + O_2 \rightarrow O_3 + O_2$	5.5(−34)
$O + O_2 + N_2 \rightarrow O_3 + N_2$	5.5(−34)
$O + O_2 + O \rightarrow O_3 + O$	5.5(−34)
$N + O + M \rightarrow NO + M$	1.1(−32)
$O + N_2 + M \rightarrow N_2O + M$	1.4(−45)
$O + NO + O_2 \rightarrow NO_2 + O_2$	1.0(−31)
$O + NO + N_2 \rightarrow NO_2 + N_2$	1.0(−31)
$N + N + M \rightarrow N_2 + M$	5.0(−33)
$N + NO + M \rightarrow N_2O + M$	3.6(−36)
$NO + O_2 + NO \rightarrow NO_2 + NO_2$	1.6(−46)
$N^+ + O + M \rightarrow NO^+ + M$	1.0(−29)

((CONTINUED ON NEXT PAGE))

3.3 D *(continued)*

Reaction	k ($cm^6\ sec^{-1}$)
$N^+ + N + M \rightarrow N_2^+ + M$	1.0(−29)
$NO^+ + H_2O + M \rightarrow NO^+ \cdot H_2O + M$	2.0(−28)
$NO^+ + NO + M \rightarrow NO^+ \cdot NO + M$	4.0(−30)
$NO_2^- + H_2O + M \rightarrow NO_2^- \cdot H_2O + M$	1.0(−28)
$O^- + CO_2 + O_2 \rightarrow CO_3^- + O_2$	3.1(−28)
$CO_3^- + H_2O + M \rightarrow CO_3^- \cdot H_2O + M$	1.0(−28)
$O_2^- + H_2O + M \rightarrow O_2^- \cdot H_2O + M$	2.2(−28)
$H + O_2 + M \rightarrow HO_2 + M$	3.7(−32)
$O + 2NO \rightarrow NO_2 + NO$	1.5(−31)
$O + NO + He \rightarrow NO_2 + He$	6.7(−32)
$O + O_2 + CO \rightarrow O_3 + CO$	6.7(−34)
$O + 2CO \rightarrow CO_2 + CO$	3.2(−32)
$O + CO + N_2 \rightarrow CO_2 + N_2$	2.2(−36)
$O + CO + CO_2 \rightarrow 2CO_2$	6.2(−36)
$H + H + M \rightarrow H_2 + M$	8.4(−33)

[a] Numbers in parentheses denote the power of 10.
[b] Symbol M represents spectator particle for energy/momentum conservation.

3.3 E *Rates with Temperature Dependence Known Explicitly*

Reaction	n[a]	E/R[a] (°K)	A[a] ($cm^6\ mole^{-2}\ sec^{-1}$)	Temperature range (°K)
$N + N + N_2 \rightarrow N_2 + N_2$	0	−500	3.0(14)[b]	200–600
$O + N + N_2 \rightarrow NO + N_2$	−0.5	0	6.4(16)	200–400
$NO + NO + O_2 \rightarrow NO_2 + NO_2$	0	−530	1.2(9)	273–660
$NO_2 + NO + O_2 \rightarrow NO_2 + NO_3$	0	−400	2.9(7)	300–500
$O + NO + O_2 \rightarrow NO_2 + O_2$	0	−940	1.1(15)	200–500
$O_2 + H + He \rightarrow HO_2 + He$	0	−500	1.5(15)	300–2000
$O + CO + M^c \rightarrow CO_2 + M(CO)$	0	2184	2.4(15)	250–500
$O + O + M \rightarrow O_2 + M(Ar)$	0	900	1.9(13)	190–4000

[a] See Eq. (6.12).
[b] Numbers in parentheses denote the power of 10.
[c] Symbol M represents spectator particle for energy/momentum conservation.

3.3 F *Binary Positive-Ion–Negative-Ion Reactions*

Reaction	k ($cm^3\ sec^{-1}$)
$O^- + O^+ \rightarrow O + O$	2.0(−7)[a]
$O_2^- + O^+ \rightarrow O_2 + O$	2.0(−7)
$NO_2^- + O^+ \rightarrow NO_2 + O$	2.0(−7)
$O_3^- + O^+ \rightarrow O_3 + O$	2.0(−7)
$O^- + O_2^+ \rightarrow O + O_2$	2.0(−7)
$O_2^- + O_2^+ \rightarrow O_2 + O_2$	2.0(−7)

((CONTINUED ON NEXT PAGE))

3.3 F *(continued)*

Reaction	k ($cm^3\ sec^{-1}$)
$NO_2^- + O_2^+ \rightarrow NO_2 + O_2$	2.0(−7)
$O_3^- + O_2^+ \rightarrow O_3 + O_2$	2.0(−7)
$O^- + N_2^+ \rightarrow O + N_2$	2.0(−7)
$O_2^- + N_2^+ \rightarrow O_2 + N_2$	2.0(−7)
$NO_2^- + N_2^+ \rightarrow NO_2 + N_2$	2.0(−7)
$O_3^- + NO_2^+ \rightarrow O_3 + NO_2$	2.0(−7)
$O_2^- + NO^+ \rightarrow O_2 + NO$	2.0(−7)
$O^- + NO^+ \rightarrow O + NO$	2.0(−7)
$NO_2^- + NO^+ \rightarrow NO_2 + NO$	2.0(−7)
$O_3^- + NO^+ \rightarrow O_3 + NO$	2.0(−7)
$NO_3^- + NO^+ \rightarrow NO_3 + N + O$	1.0(−7)
$O_2^- + NO^+ \cdot NO \rightarrow O_2 + NO + NO$	1.0(−7)
$O_3^- + NO^+ \cdot NO \rightarrow O_3 + NO + NO$	1.0(−7)
$NO_2^- + NO^+ \cdot NO \rightarrow NO_2 + NO + NO$	1.0(−7)
$NO_3^- + NO^+ \cdot NO \rightarrow NO_3 + NO + NO$	1.0(−7)
$O_2^- + NO^+ \cdot H_2O \rightarrow O_2 + NO + H_2O$	1.0(−7)
$O_3^- + NO^+ \cdot H_2O \rightarrow O_3 + NO + H_2O$	1.0(−7)
$NO_2^- + NO^+ \cdot H_2O \rightarrow NO_2 + NO + H_2O$	1.0(−7)
$O_2^- + NO^+ \rightarrow O_2 + N + O$	1.0(−7)
$NO_3^- + NO^+ \cdot H_2O \rightarrow NO_3 + NO + H_2O$	1.0(−7)
$O_2^- + O_2^+ \rightarrow O_2 + O + O$	1.0(−7)
$O_3^- + O_2^+ \rightarrow O_3 + O + O$	1.0(−7)
$NO_2^- + O_2^+ \rightarrow NO_2 + O + O$	1.0(−7)
$NO_3^- + O_2^+ \rightarrow NO_3 + O + O$	1.0(−7)
$NO_3^- + NO^+ \rightarrow NO_3 + NO$	2.0(−7)
$O_2^- + N_2^+ \rightarrow O_2 + N + N$	1.0(−7)
$NO_2^- + N_2^+ \rightarrow NO_2 + N + N$	1.0(−7)
$O_3^- + N_2^+ \rightarrow O_3 + N + N$	1.0(−7)
$NO_2^- + NO^+ \rightarrow NO_2 + N + O$	1.0(−7)
$O_3^- + NO^+ \rightarrow O_3 + N + O$	1.0(−7)
$N^+ + O^- \rightarrow N + O$	2.0(−7)
$O_2^- + O_2^+ \rightarrow O_2 + O_2(^1\Delta)$	1.0(−8)
$NO_2^- \cdot H_2O + NO^+ \rightarrow NO_2 + H_2O + NO$	1.0(−7)
$NO_2^- \cdot H_2O^+ O_2^+ \rightarrow NO_2 + H_2O + O_2$	1.0(−7)
$NO_2^- \cdot H_2O + NO^+ \cdot H_2O \rightarrow NO_2 + 2H_2O + NO$	1.0(−7)
$NO_2^- \cdot H_2O + NO^+ \cdot NO \rightarrow NO_2 + H_2O + 2NO$	1.0(−7)

[a] The numbers in parentheses denote the power of 10.

3.3 G *Binary Neutral Molecule Collisions*

Reaction	k ($cm^3\ sec^{-1}$)
$N + O \rightarrow NO + h\nu$	2.0(−17)[a]
$O + NO \rightarrow NO_2 + h\nu$	6.2(−17)
$N + N \rightarrow N_2 + h\nu$	1.0(−17)
$O + N_2 \rightarrow NO + N$	3.2(−65)

((CONTINUED ON NEXT PAGE))

3.3 G (*continued*)

Reaction	k ($cm^3\ sec^{-1}$)
$O+NO \rightarrow O_2+N$	6.7(−41)
$O+NO_2 \rightarrow NO+O_2$	4.5(−12)
$O+N_2O \rightarrow NO+NO$	8.1(−31)
$O+N_2O \rightarrow O_2+N_2$	2.7(−31)
$O+O_3 \rightarrow O_2+O_2$	9.4(−15)
$N+O_2 \rightarrow NO+O$	8.6(−17)
$N+NO \rightarrow N_2+O$	2.2(−11)
$N+NO_2 \rightarrow N_2+O_2$	1.5(−11)
$N+NO_2 \rightarrow NO+NO$	3.0(−12)
$N+NO_2 \rightarrow N_2O+O$	1.5(−13)
$NO+O_3 \rightarrow NO_2+O_2$	1.3(−14)
$NO_2+O_3 \rightarrow NO_3+O_2$	7.0(−17)
$O_3+O_2(^1\Delta) \rightarrow O+O_2+O_2$	1.9(−15)
$O_2(^1\Delta)+M^a \rightarrow O_2+M$	1.0(−19)
$O_2(^1\Delta)+N \rightarrow NO+O$	3.0(−12)
$H+O_2 \rightarrow OH+O$	3.0(−22)
$O+H_2 \rightarrow OH+H$	>9.0(−18)
$O+HO_2 \rightarrow OH+O_2$	9.0(−12)
$OH+CO \rightarrow CO_2+H$	1.8(−13)
$O+OH \rightarrow O_2+H$	3.6(−11)
$H_2+OH \rightarrow H_2O+H$	7.0(−15)
$OH+OH \rightarrow H_2O+O$	2.4(−13)
$H+OH \rightarrow H_2+O$	3.1(−17)

[a] Symbol M represents spectator particle for energy/momentum conservation.

(*) REF. [3.1]

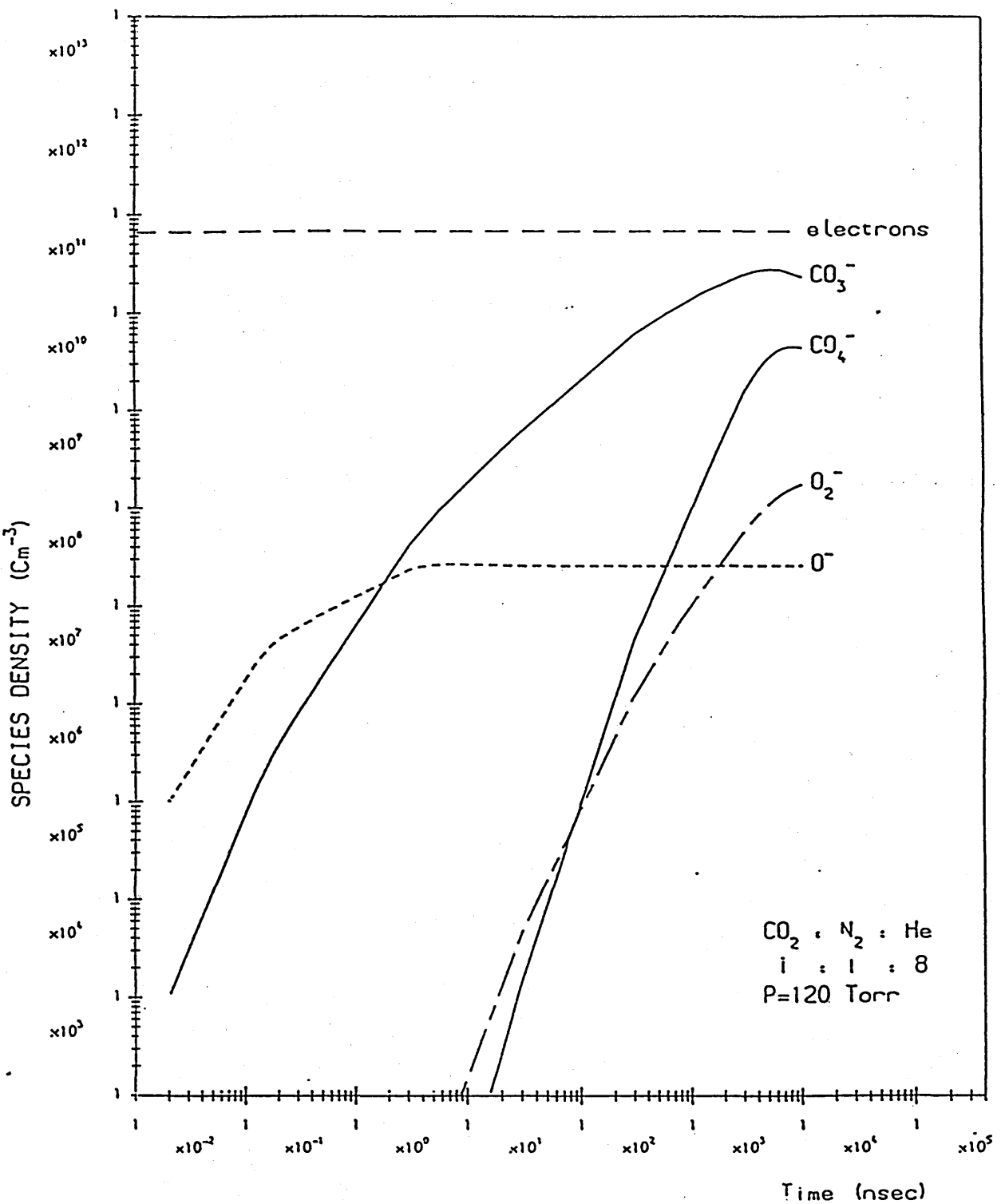

VARIATION WITH TIME OF THE MAIN NEGATIVE ION CONCENTRATIONS

GRAPH (3.1)

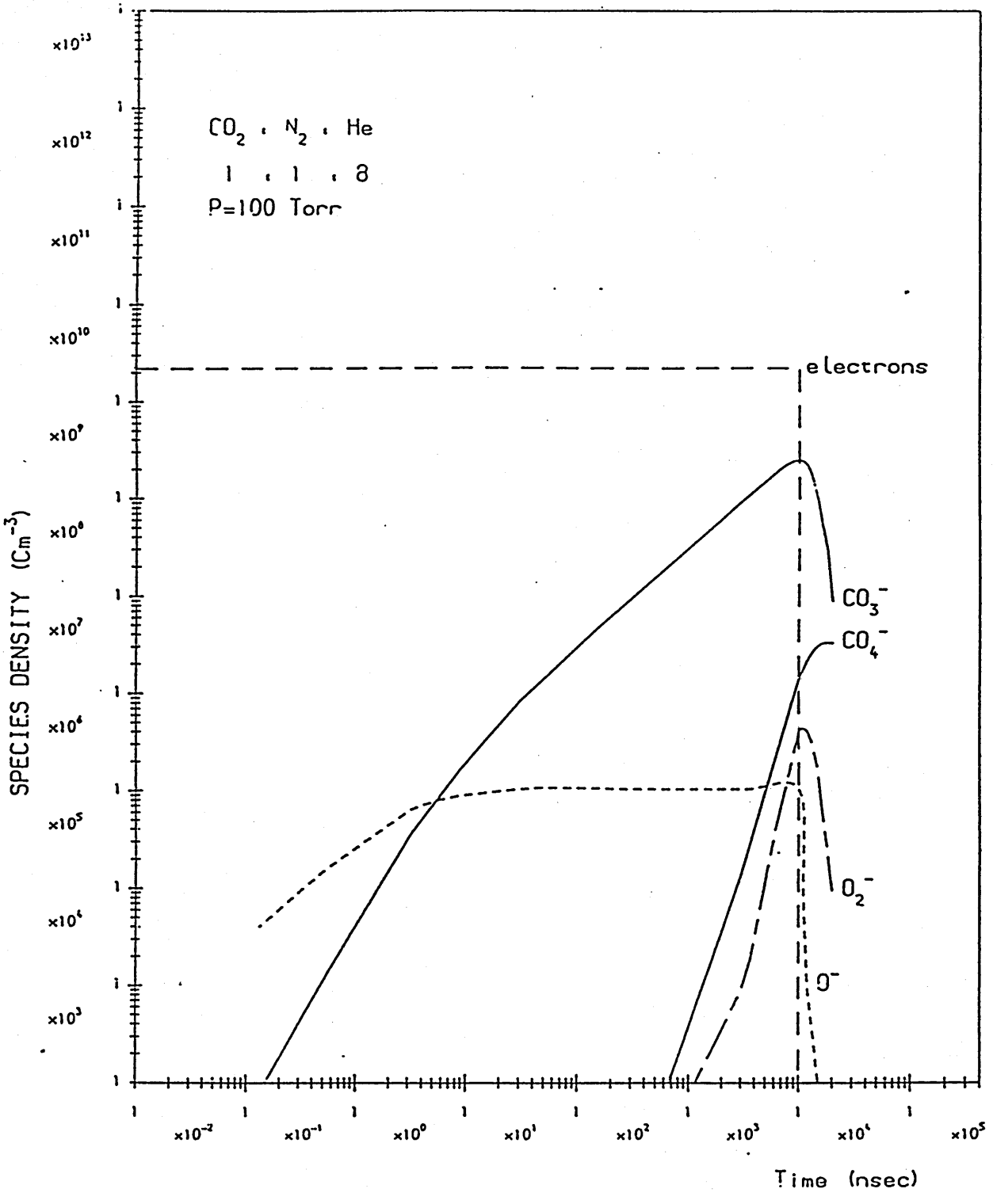

VARIATION WITH TIME OF THE MAIN NEGATIVE ION CONCENTRATIONS

GRAPH (3.2)

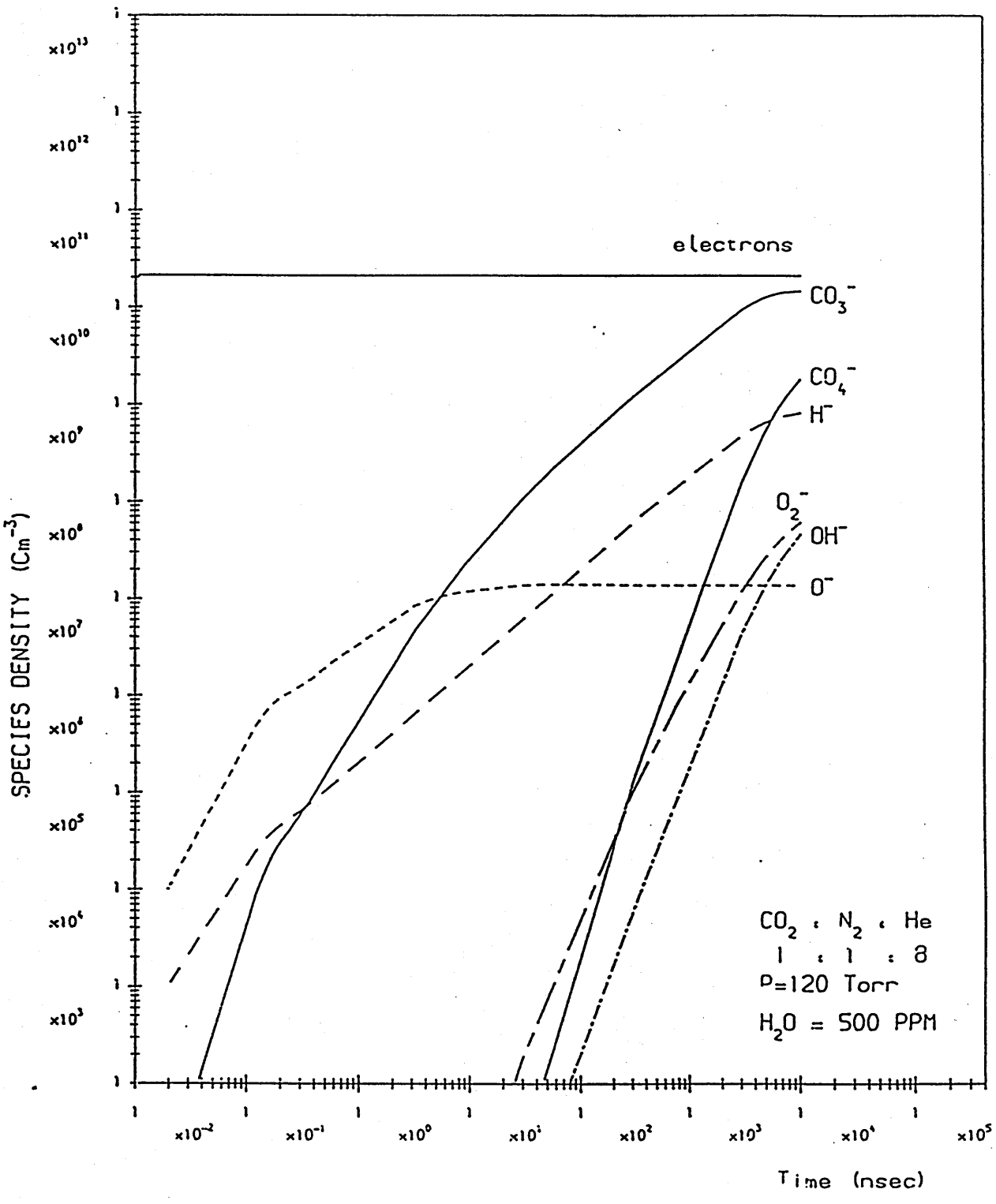

VARIATION WITH TIME OF THE MAIN NEGATIVE ION CONCENTRATIONS WITH ADDED H_2O

GRAPH (3.3)

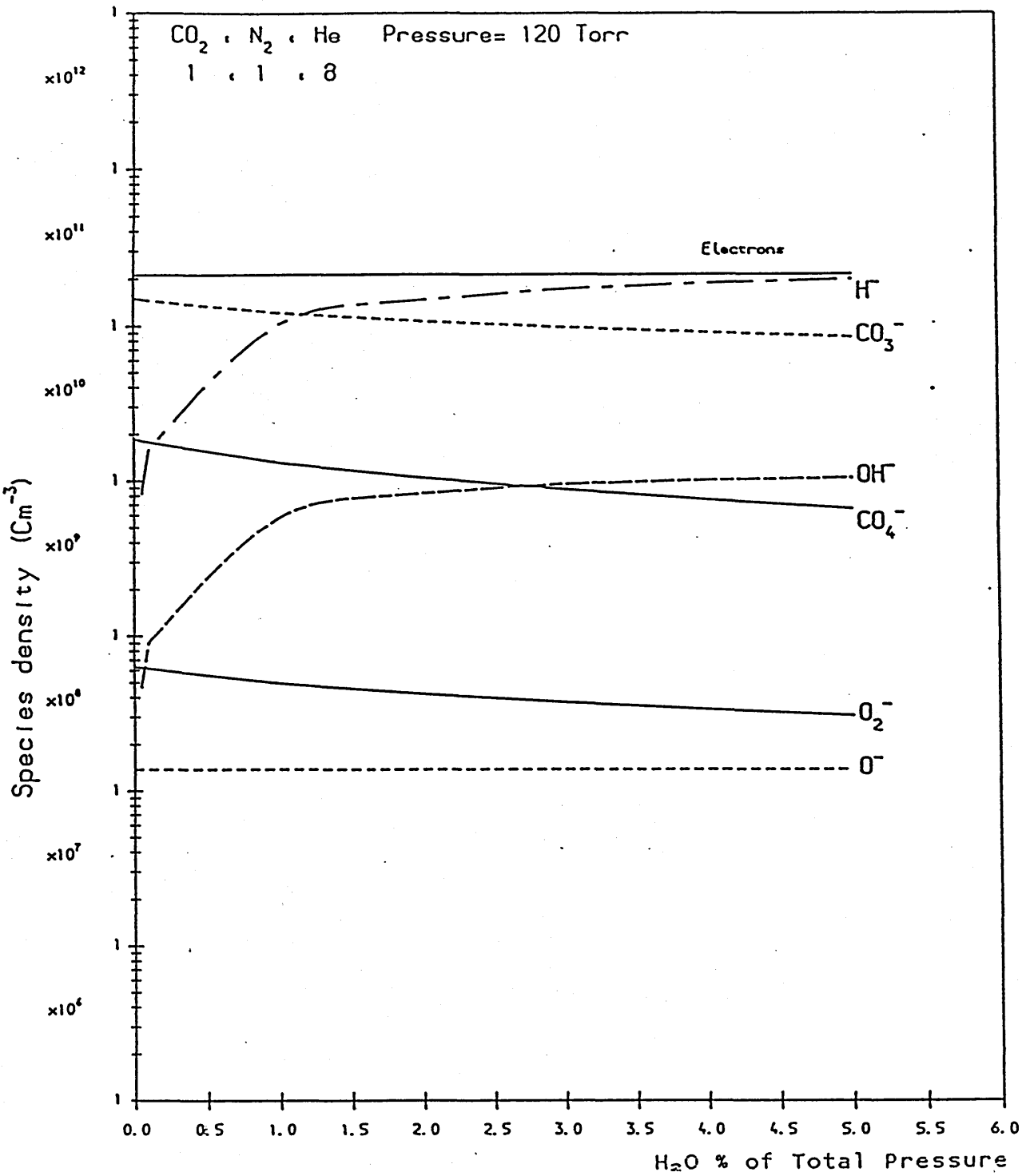

VARIATION WITH ADDED H_2O OF THE MAIN NEGATIVE ION CONCENTRATIONS AT TIME = 10 μ SEC

GRAPH (3.4)

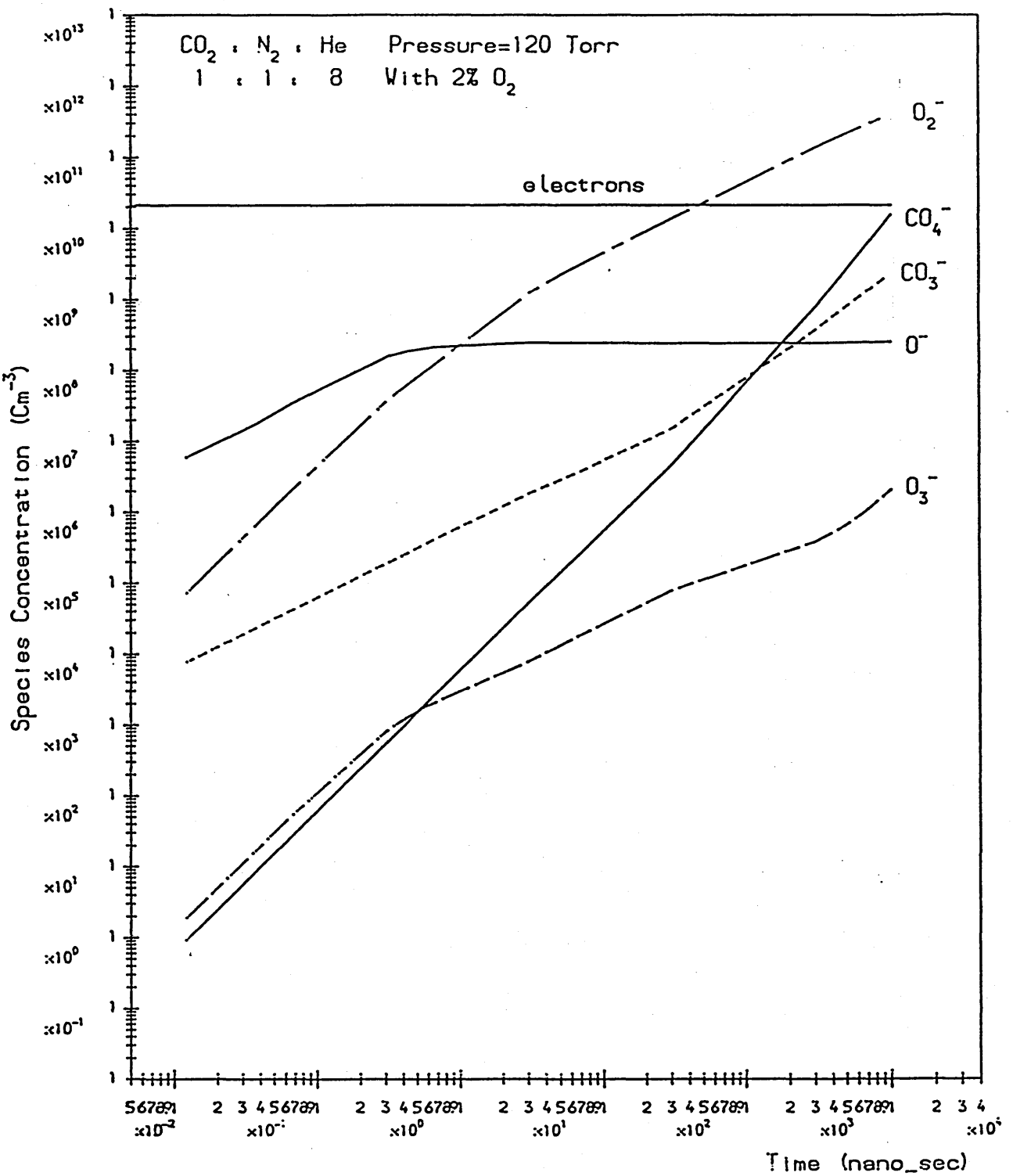

VARIATION WITH TIME OF THE MAIN NEGATIVE ION CONCENTRATIONS WITH ADDED OXYGEN

GRAPH (3.5)

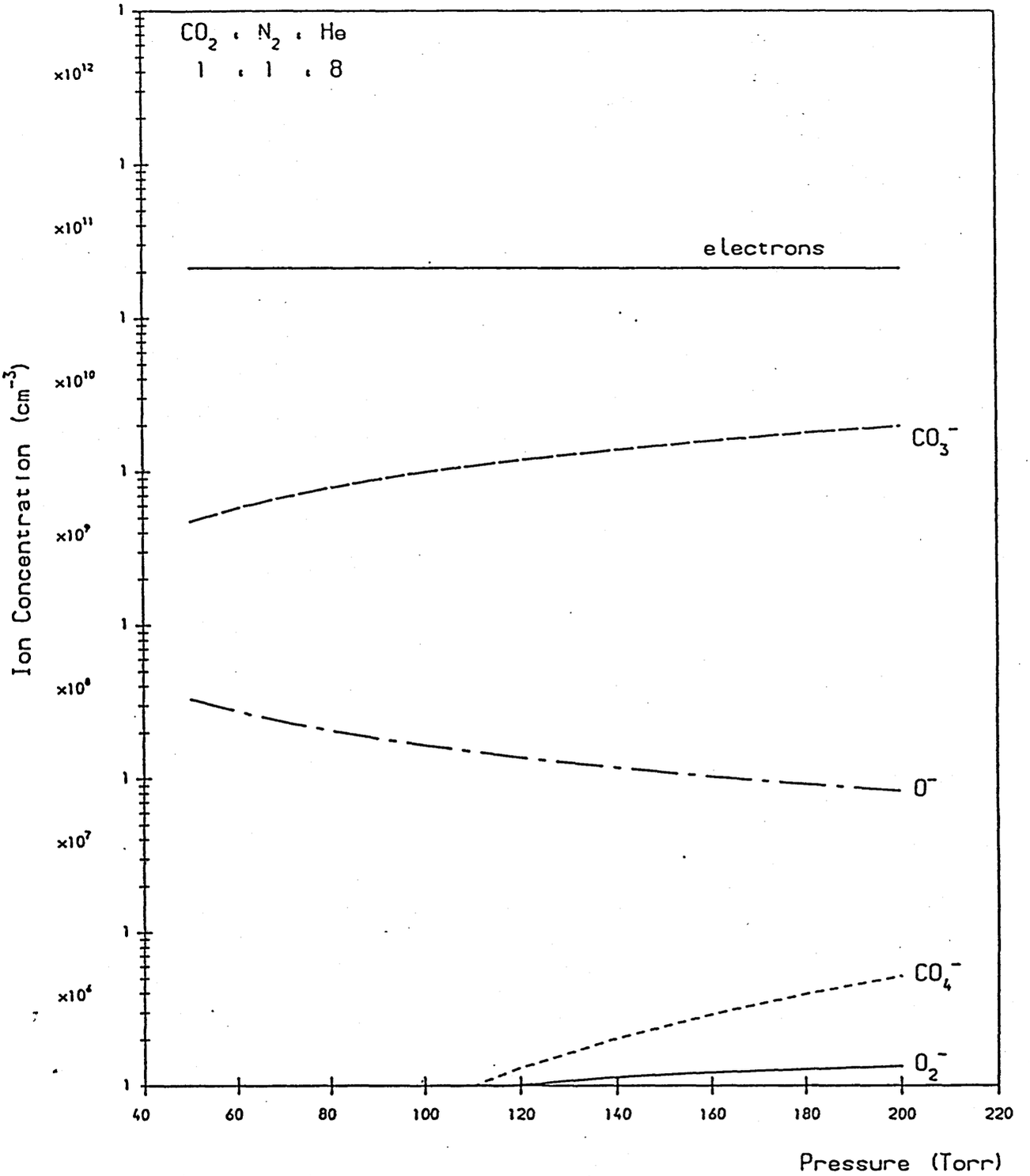

VARIATION WITH PRESSURE OF THE MAIN NEGATIVE ION CONCENTRATIONS AT TIME=300 NANO SEC

GRAPH (3.6)

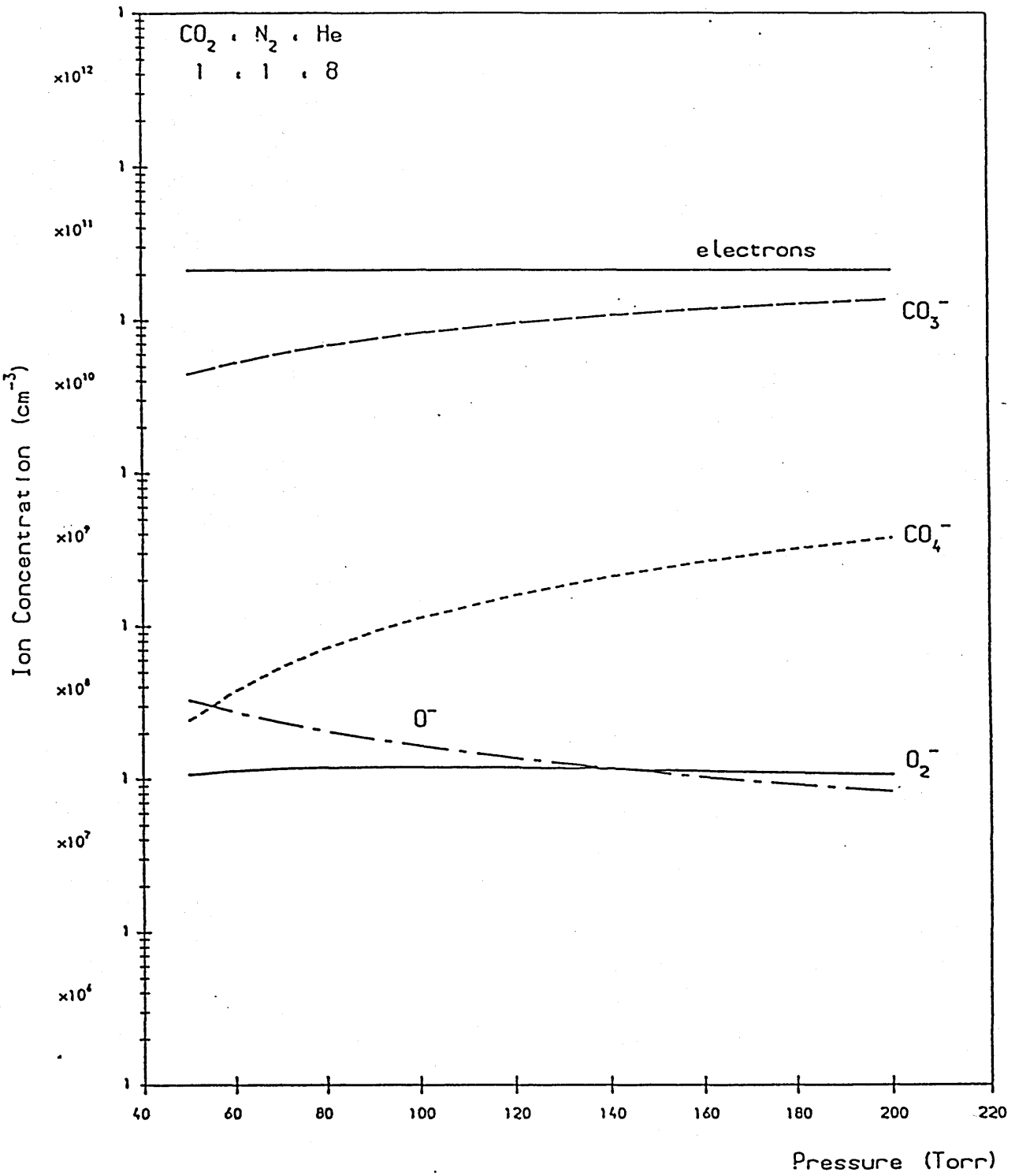

VARIATION WITH PRESSURE OF THE MAIN NEGATIVE ION CONCENTRATIONS AT TIME=3 μSEC

GRAPH (3.7)

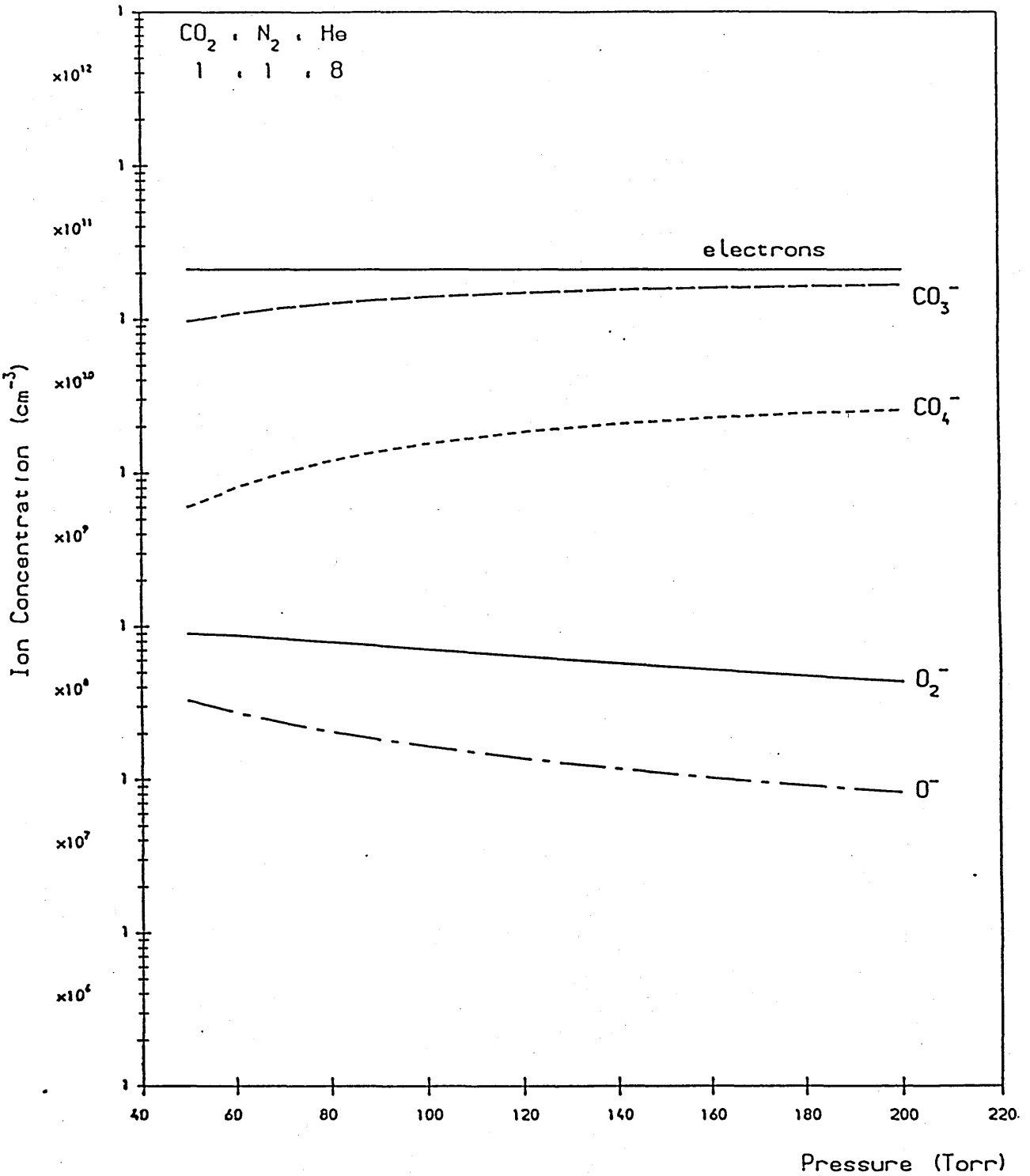

VARIATION WITH PRESSURE OF THE MAIN NEGATIVE ION CONCENTRATIONS AT TIME=10 μSEC

GRAPH (3.8)

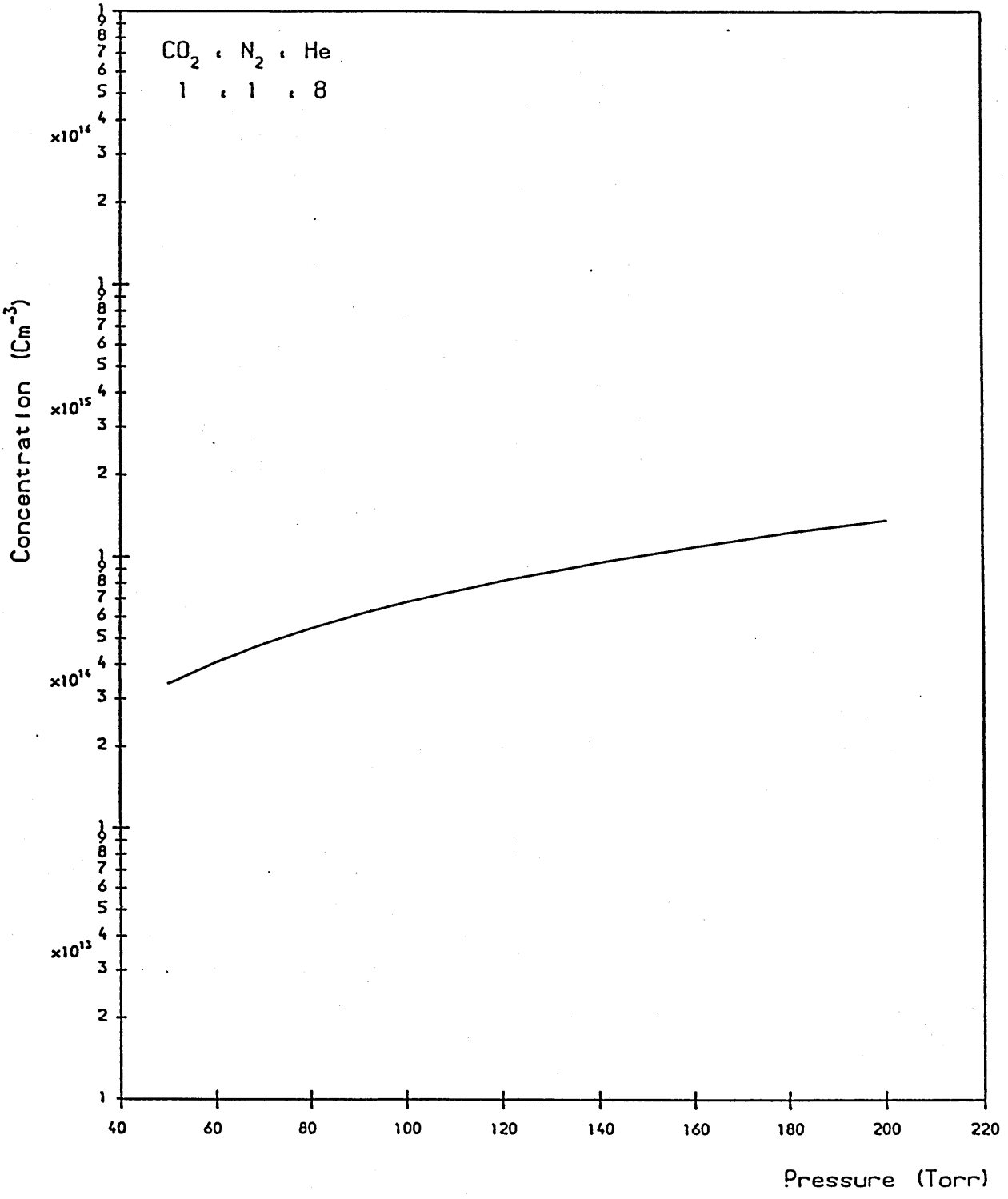

VARIATION WITH PRESSURE OF O CONCENTRATION AT TIME = 10 μSEC

GRAPH (3.9)

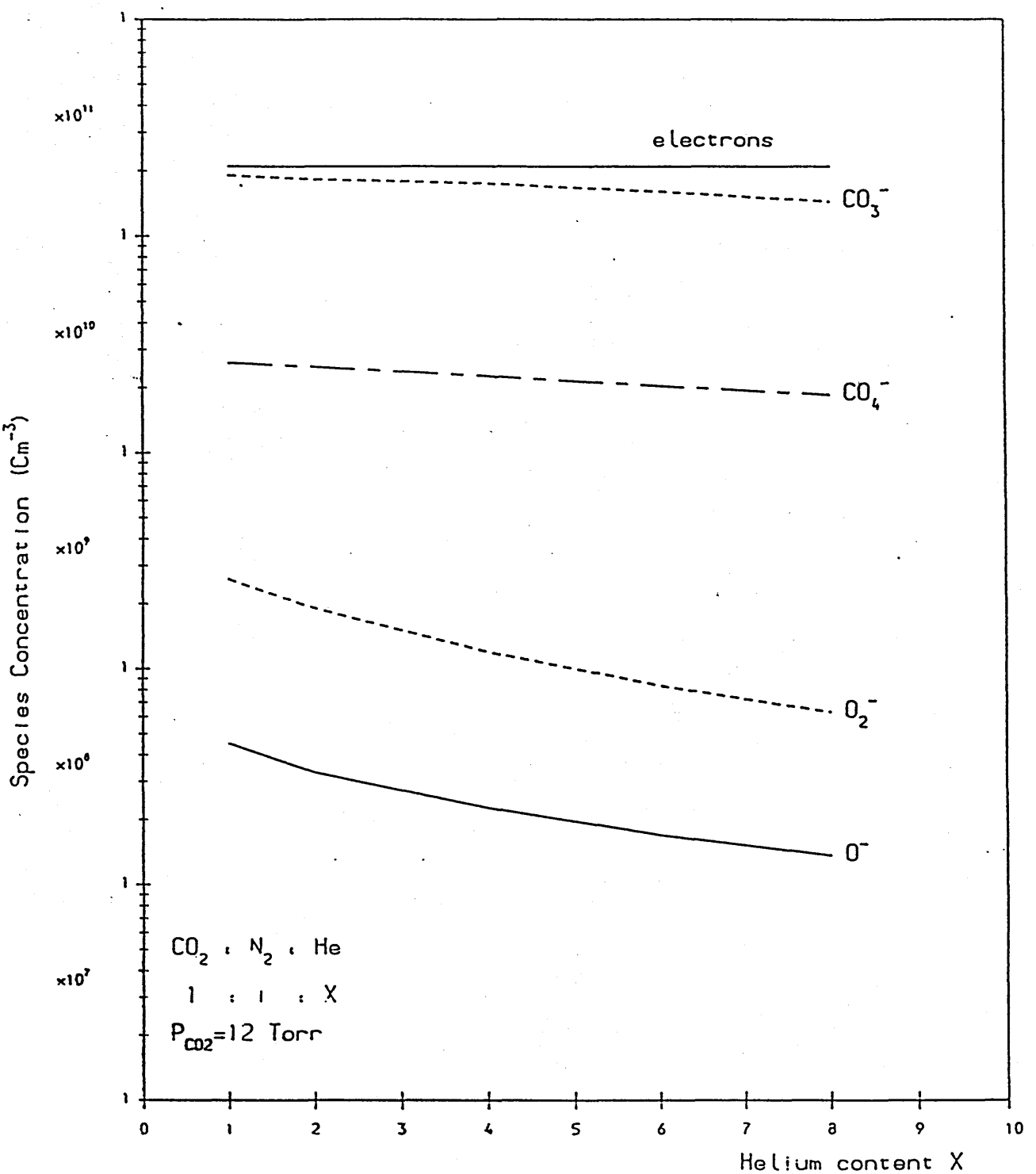

VARIATION WITH HELIUM CONTENT OF THE MAIN NEGATIVE ION SPECIES AT TIME t=10 μ SEC

GRAPH (3.10)

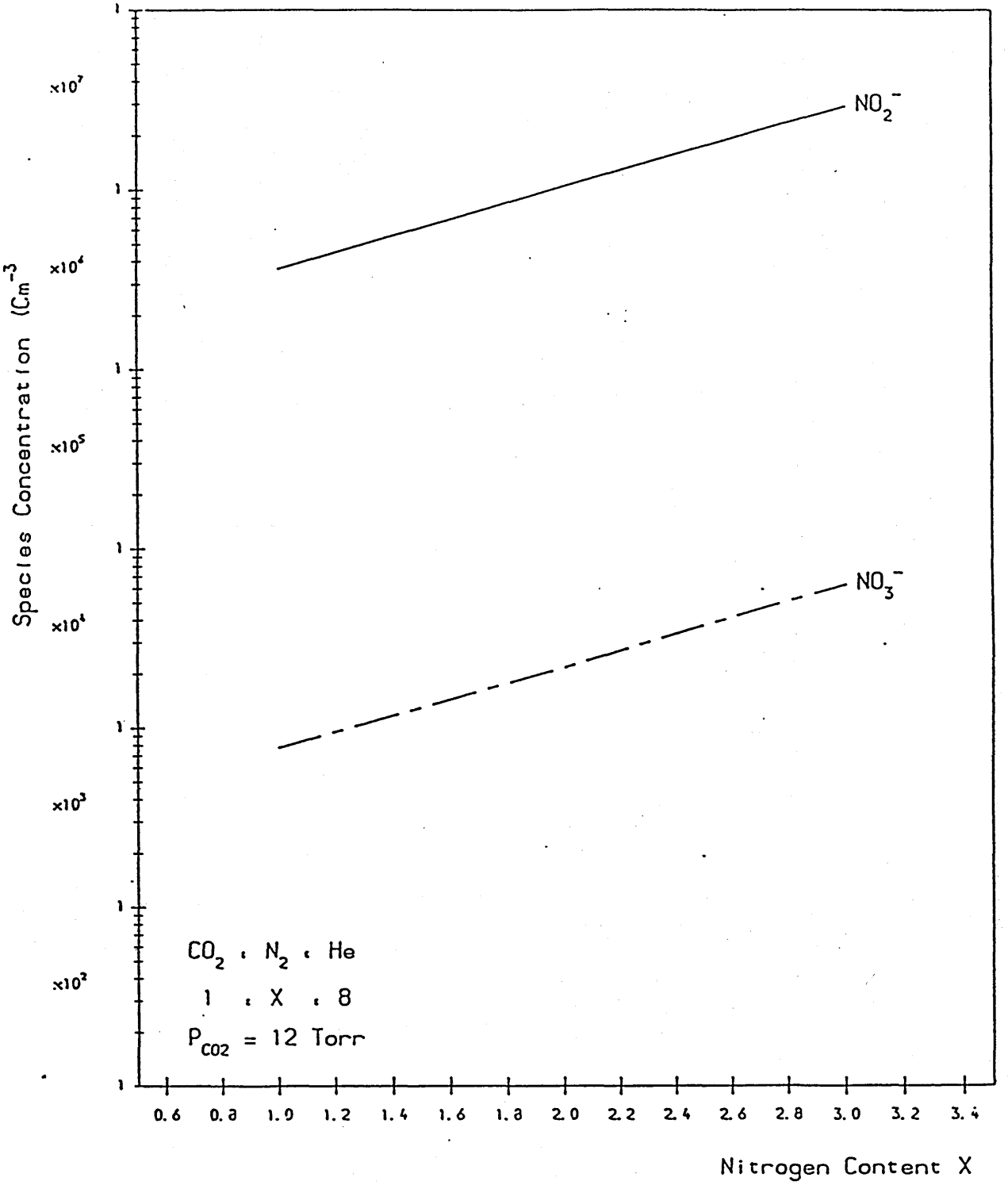

VARIATION WTIH NITROGEN CONTENT OF THE MAIN NITROGEN OXIDES NEGATIVE IONS AT t=10 μSEC

GRAPH (3.11)

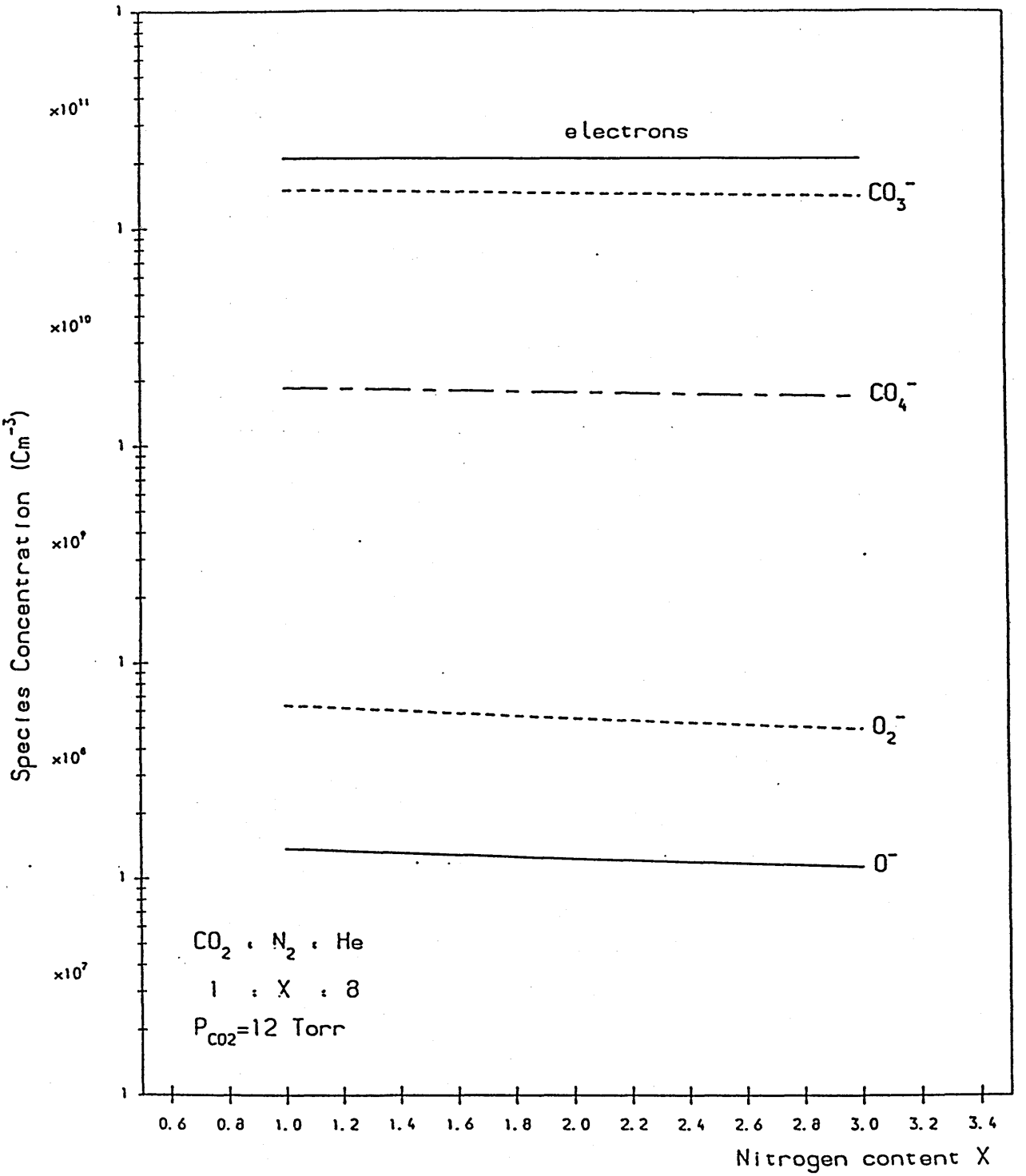

VARIATION WITH NITROGEN CONTENT OF THE MAIN NEGATIVE ION SPECIES AT TIME t=10 μ SEC

GRAPH (3.12)

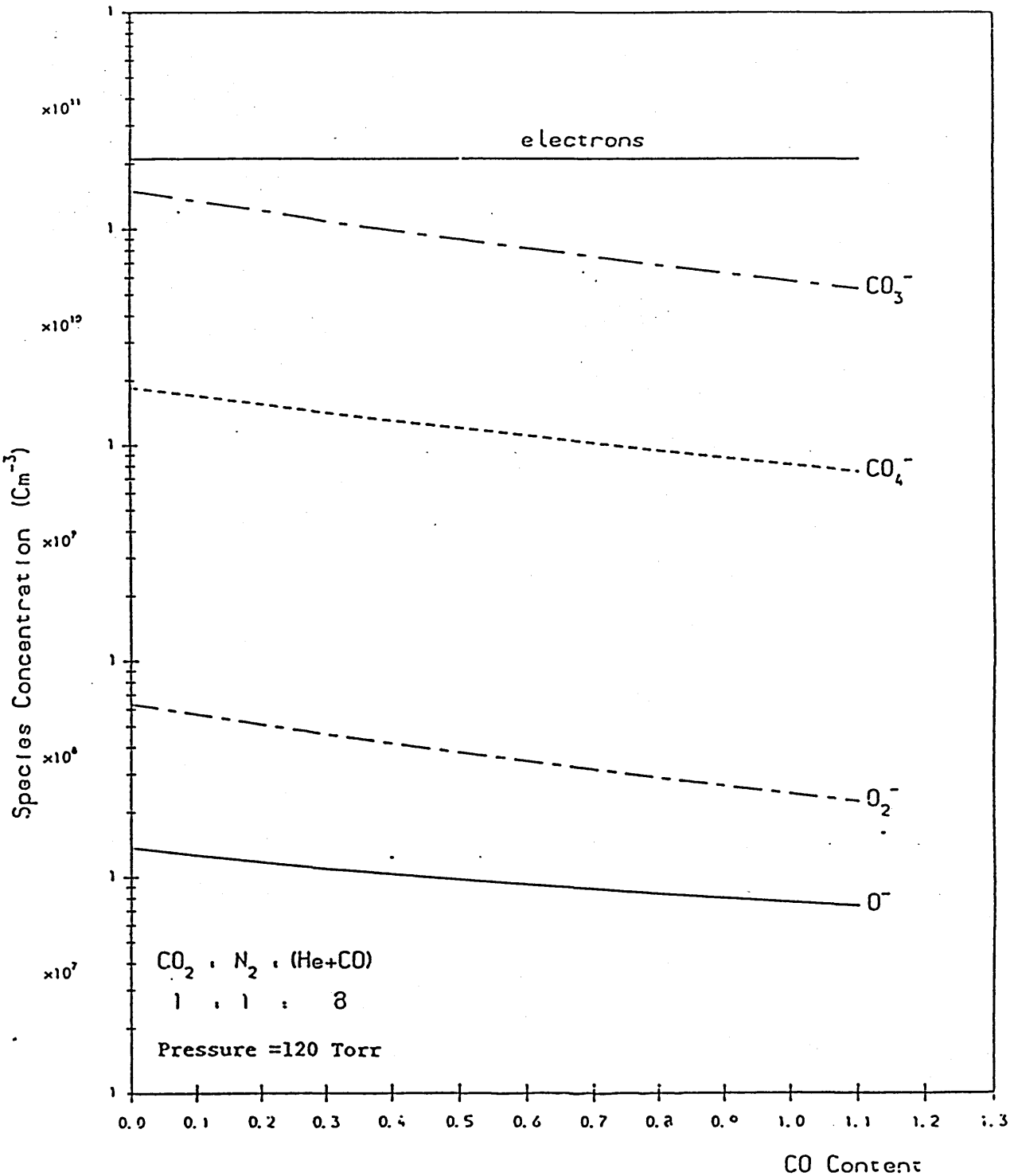

VARIATION WITH ADDED CO OF THE MAIN NEGATIVE ION CONCENTRATIONS AT t=10 μSEC

GRAPH (3.13)

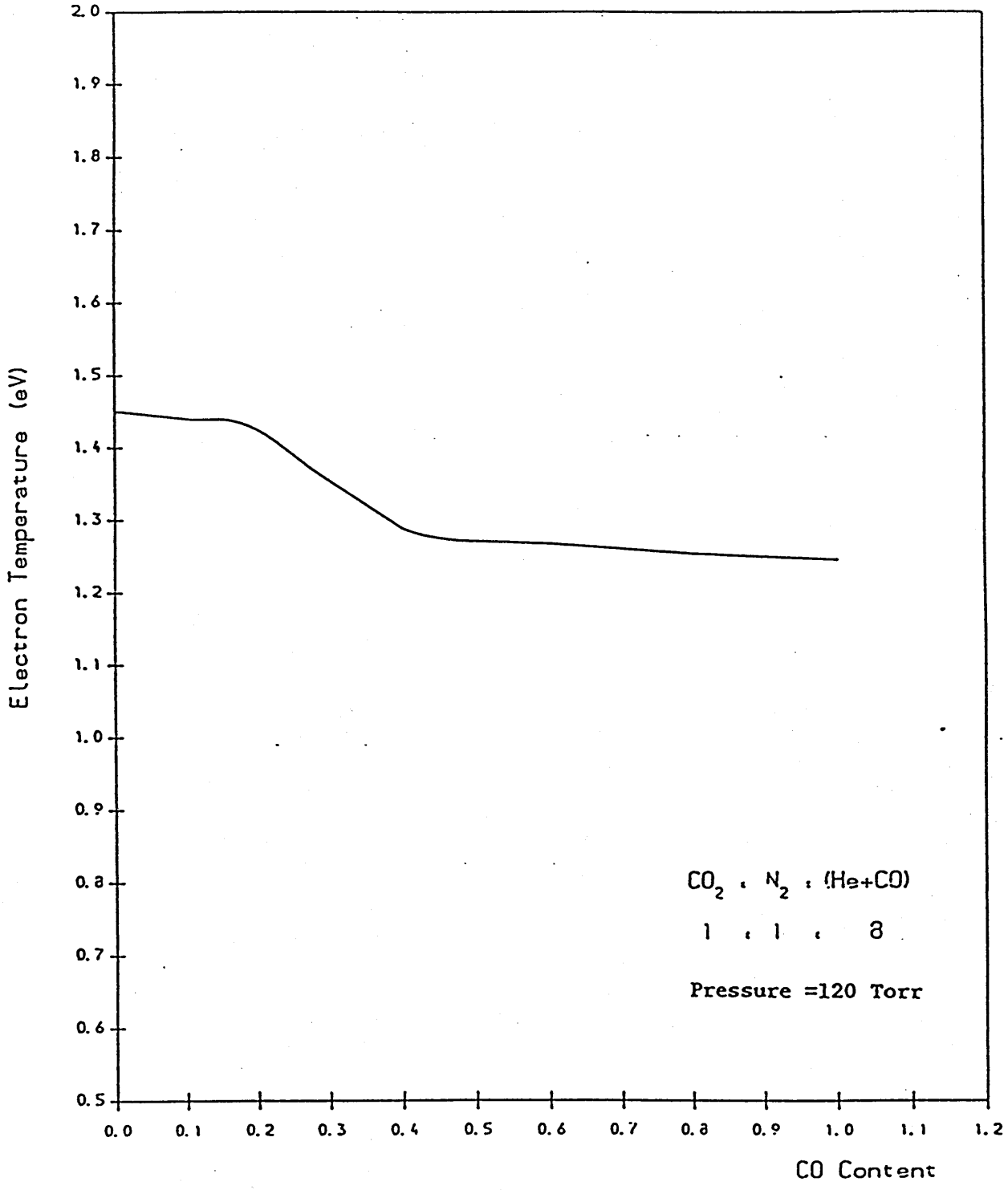

VARIATION WITH ADDED CO OF THE ELECTRON TEMPERATURE

GRAPH (3.14)

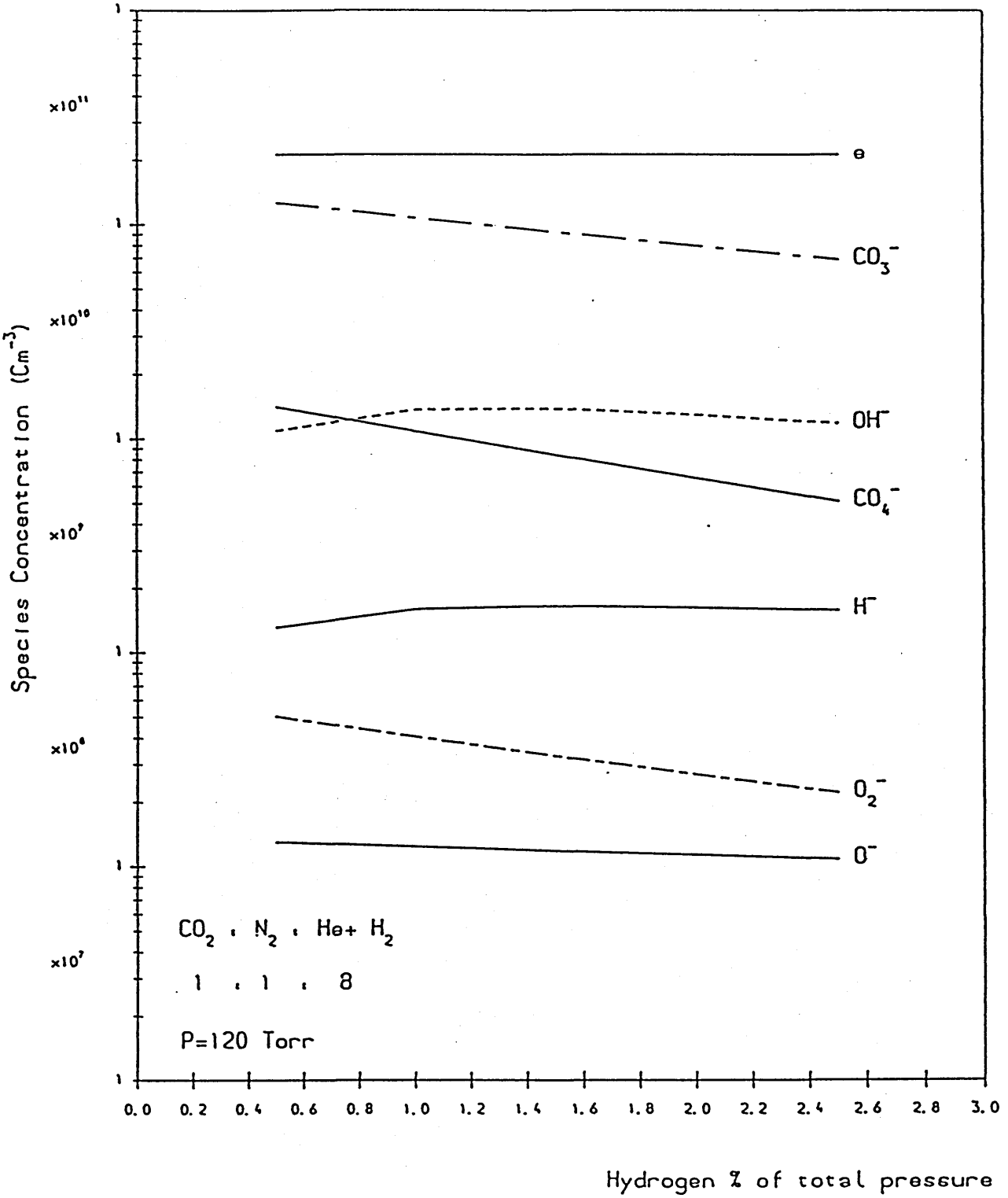

VARIATION WITH ADDED HYDROGEN OF THE MAIN NEGATIVE ION SPECIES AT TIME t=10 μsec

GRAPH (3.15)

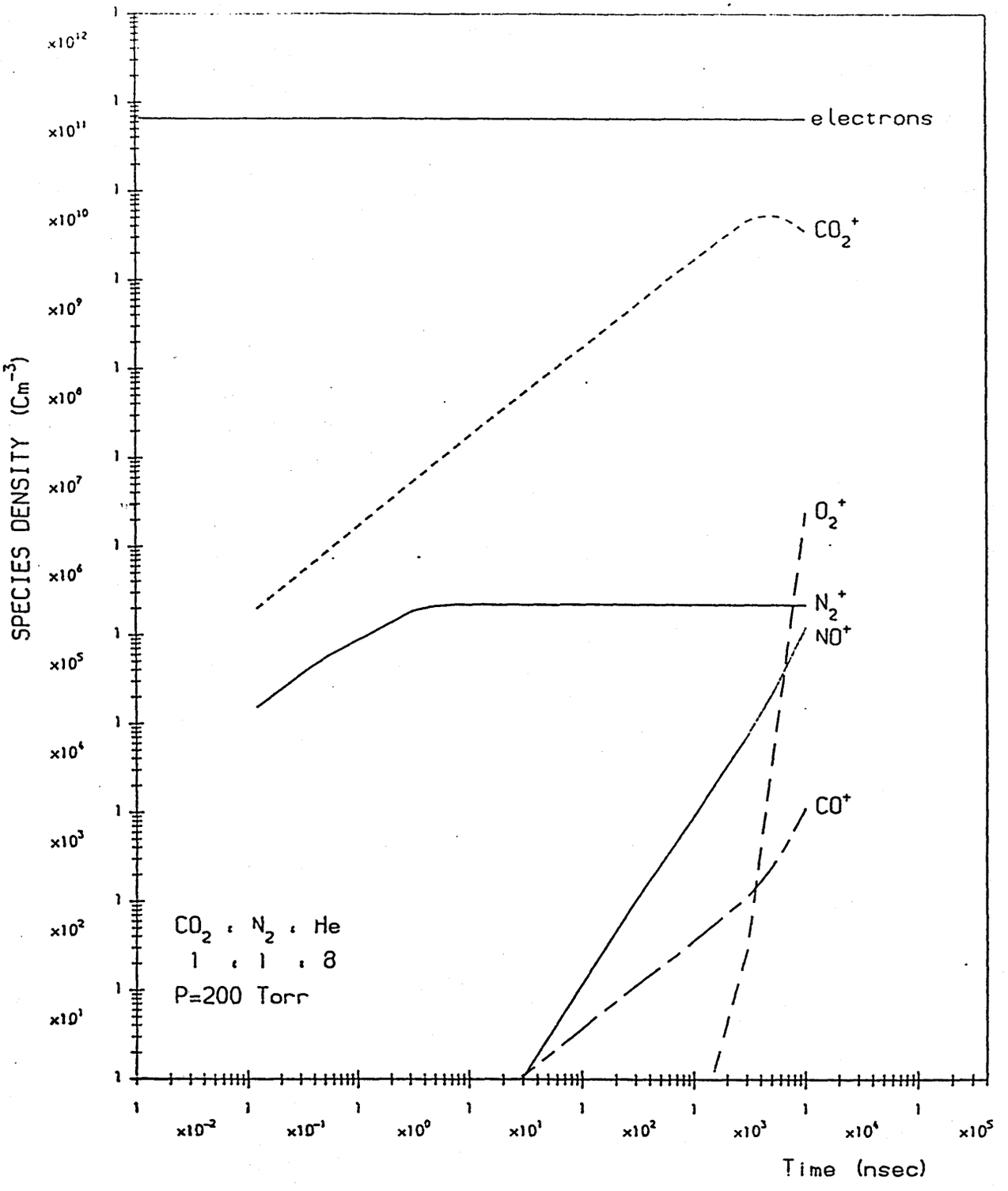

VARIATION WITH TIME OF THE MAIN POSITIVE ION CONCENTRATIONS

GRAPH (3.16)

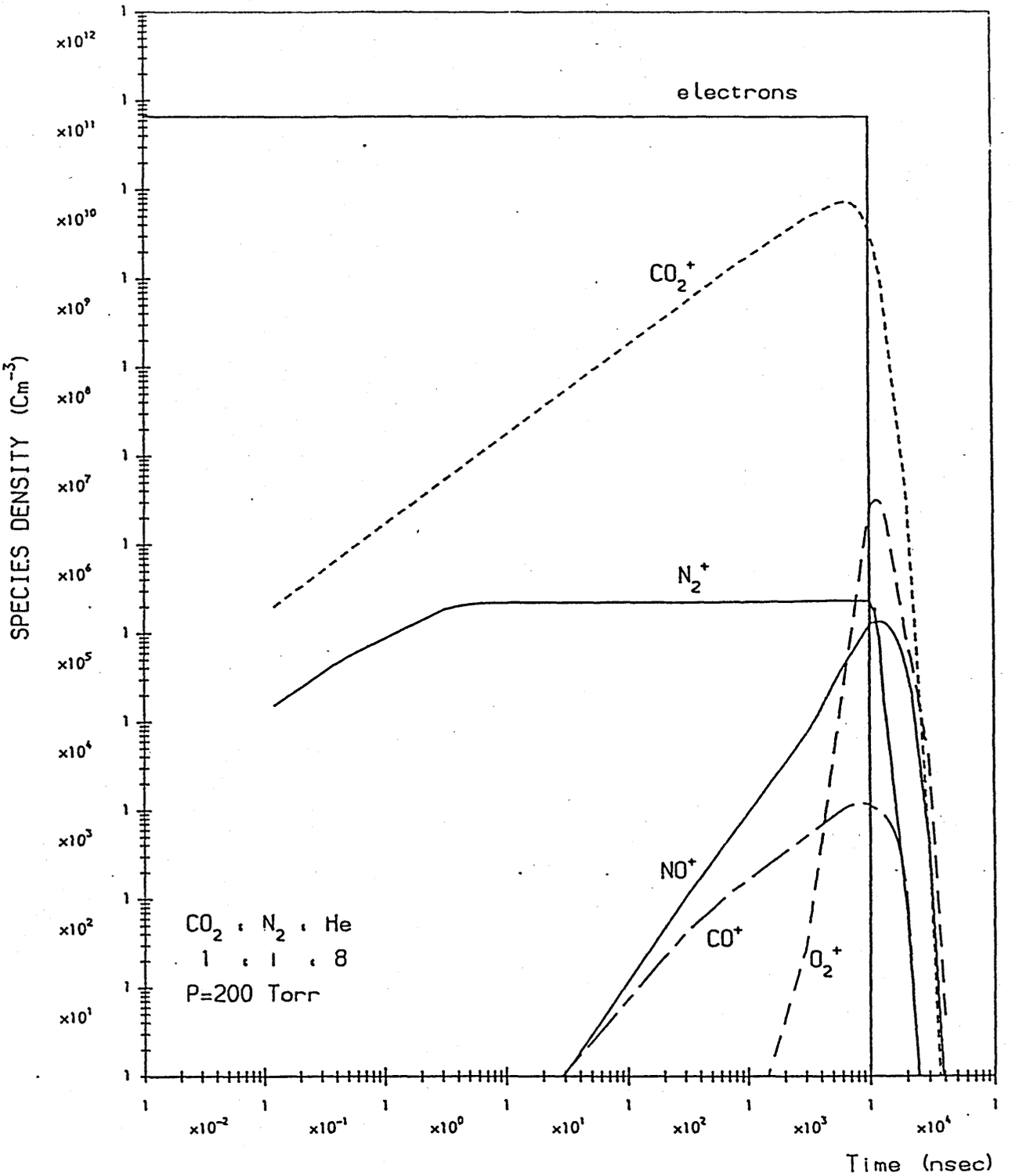

VARIATION WITH TIME OF THE MAIN POSITIVE ION CONCENTRATIONS

GRAPH (3.17)

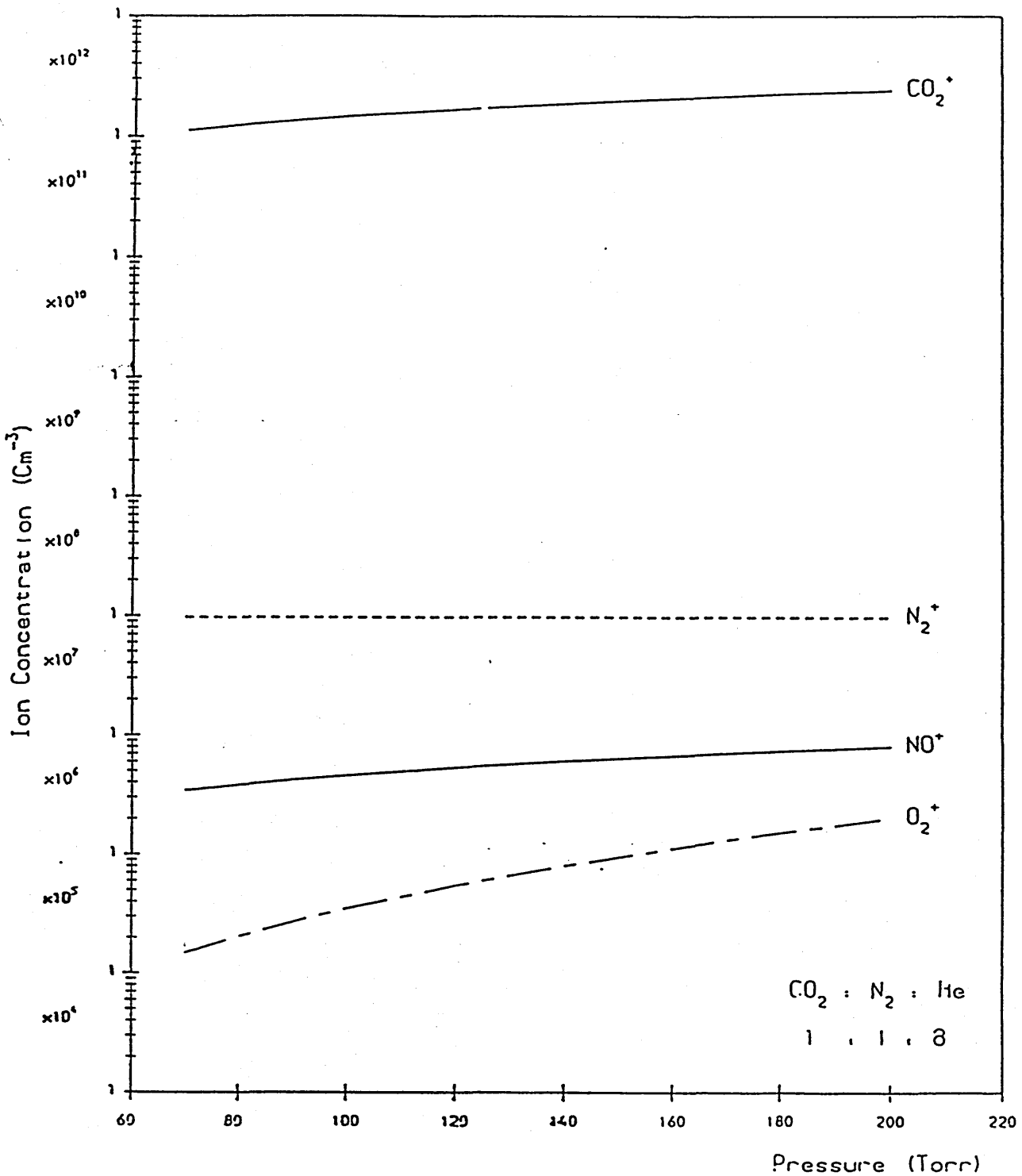

VARIATION WITH PRESSURE OF THE MAIN POSITIVE ION CONCENTRATIONS AT $\tau = 10$ μ SEC

GRAPH (3.18)

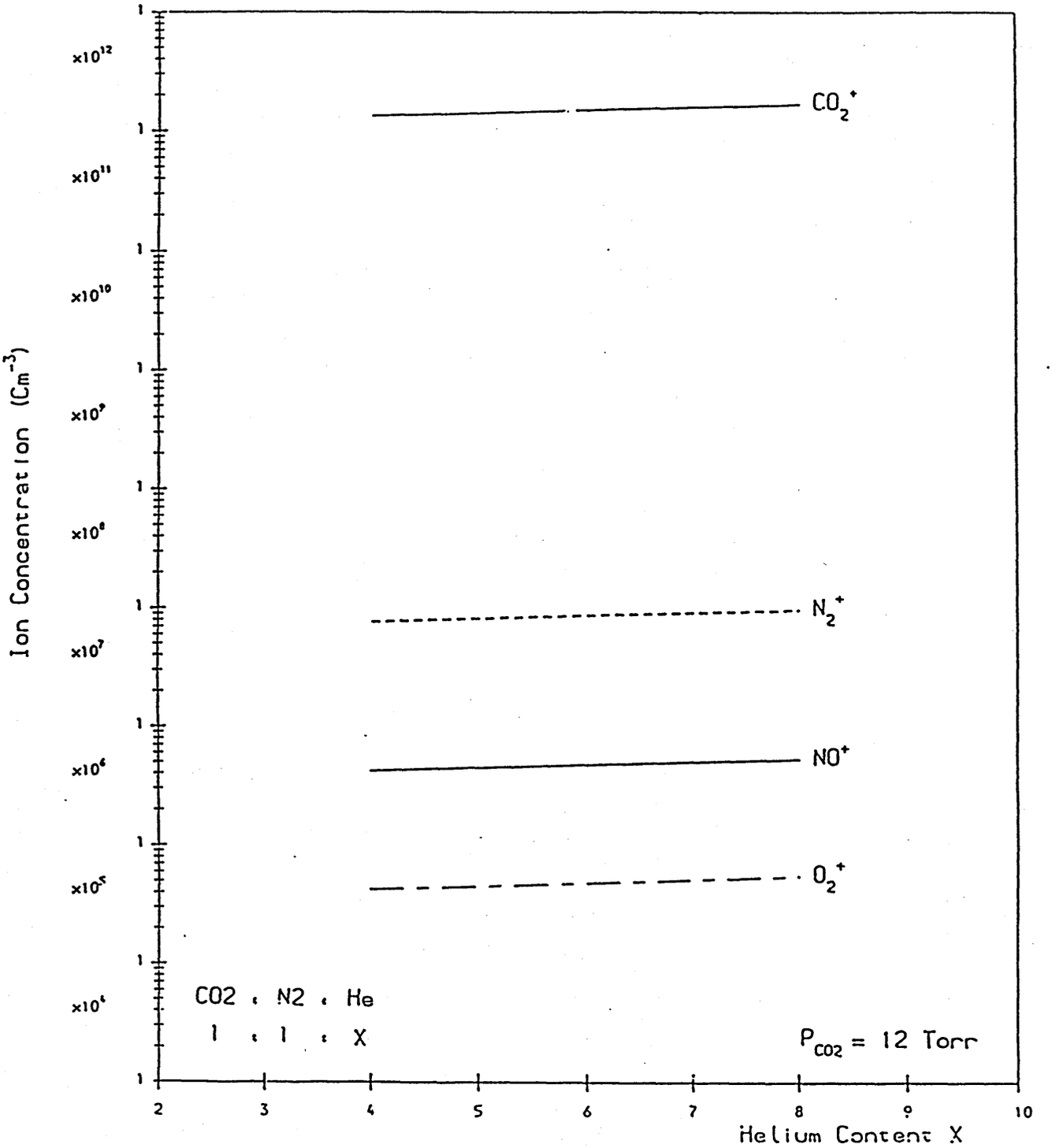

VARIATION WITH HELIUM CONTENT OF THE MAIN POSITIVE ION CONCENTRATIONS AT t=10 μ SEC

GRAPH (3.19)

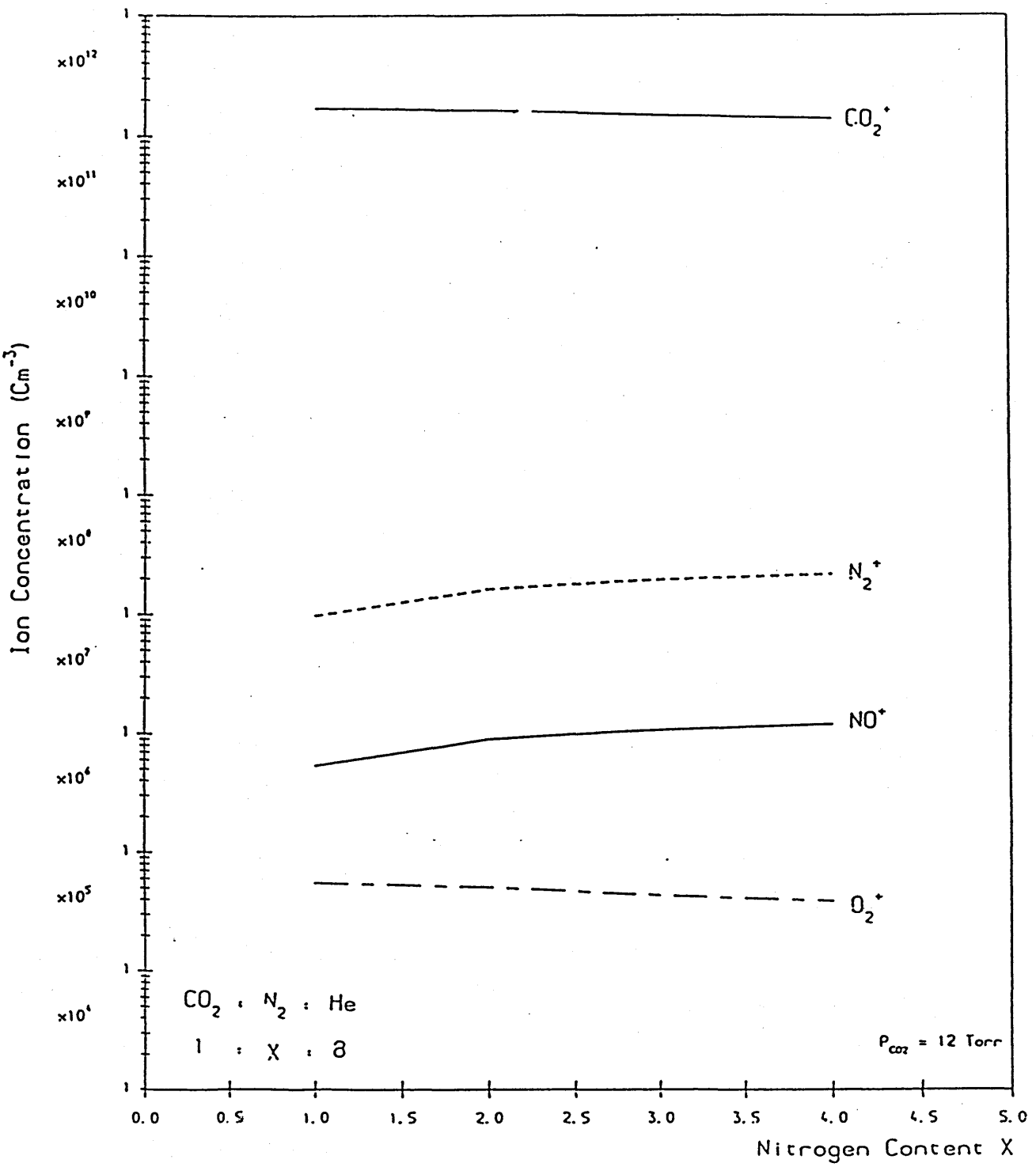

VARIATION WITH NITROGEN CONTENT OF THE MAIN POSITIVE ION CONCENTRATIONS AT $t = 10\ \mu$SEC

GRAPH (3.20)

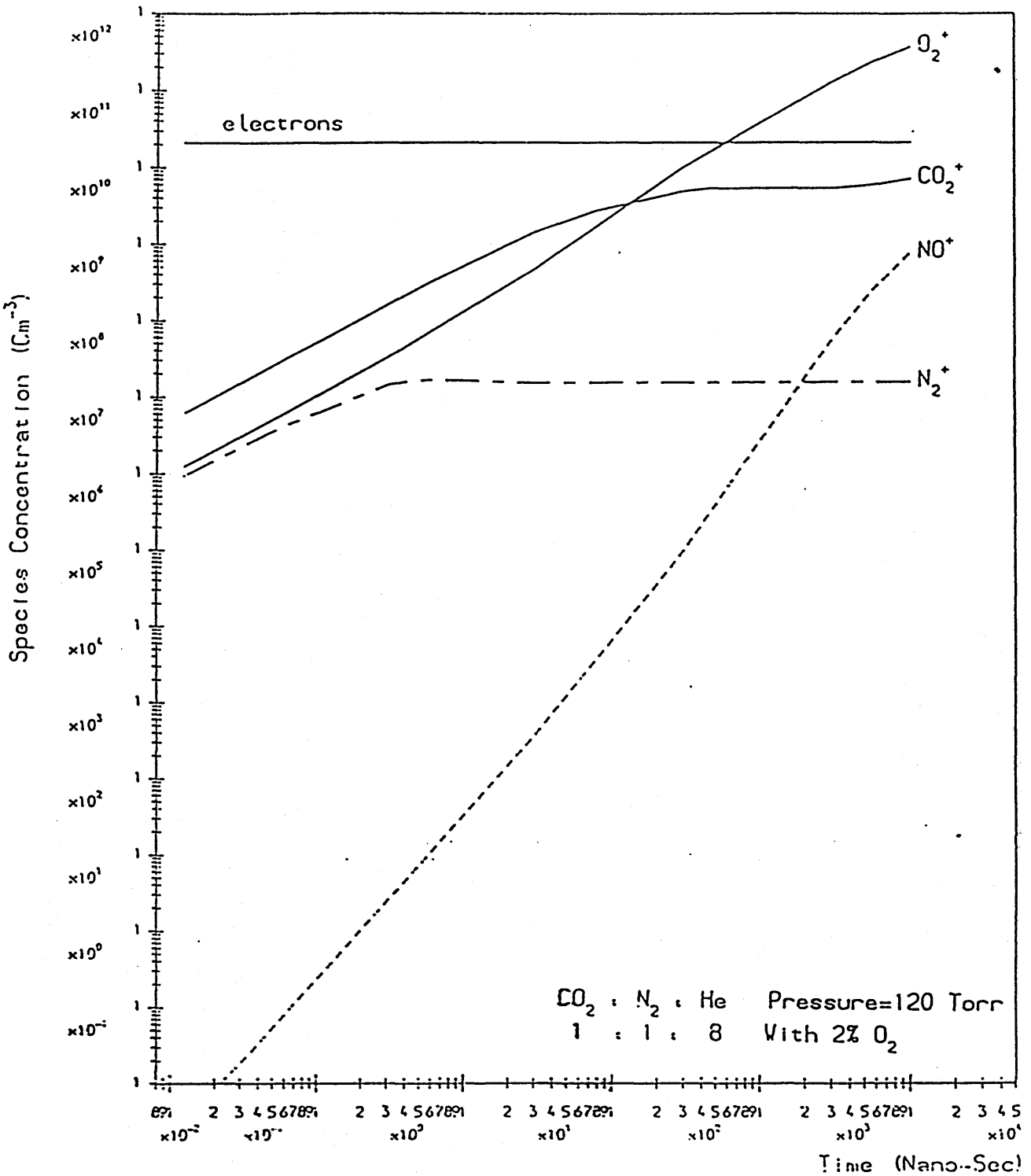

VARIATION WITH TIME OF THE MAIN POSITIVE ION CONCENTRATIONS WITH ADDED OXYGEN GRAPH (3.21)

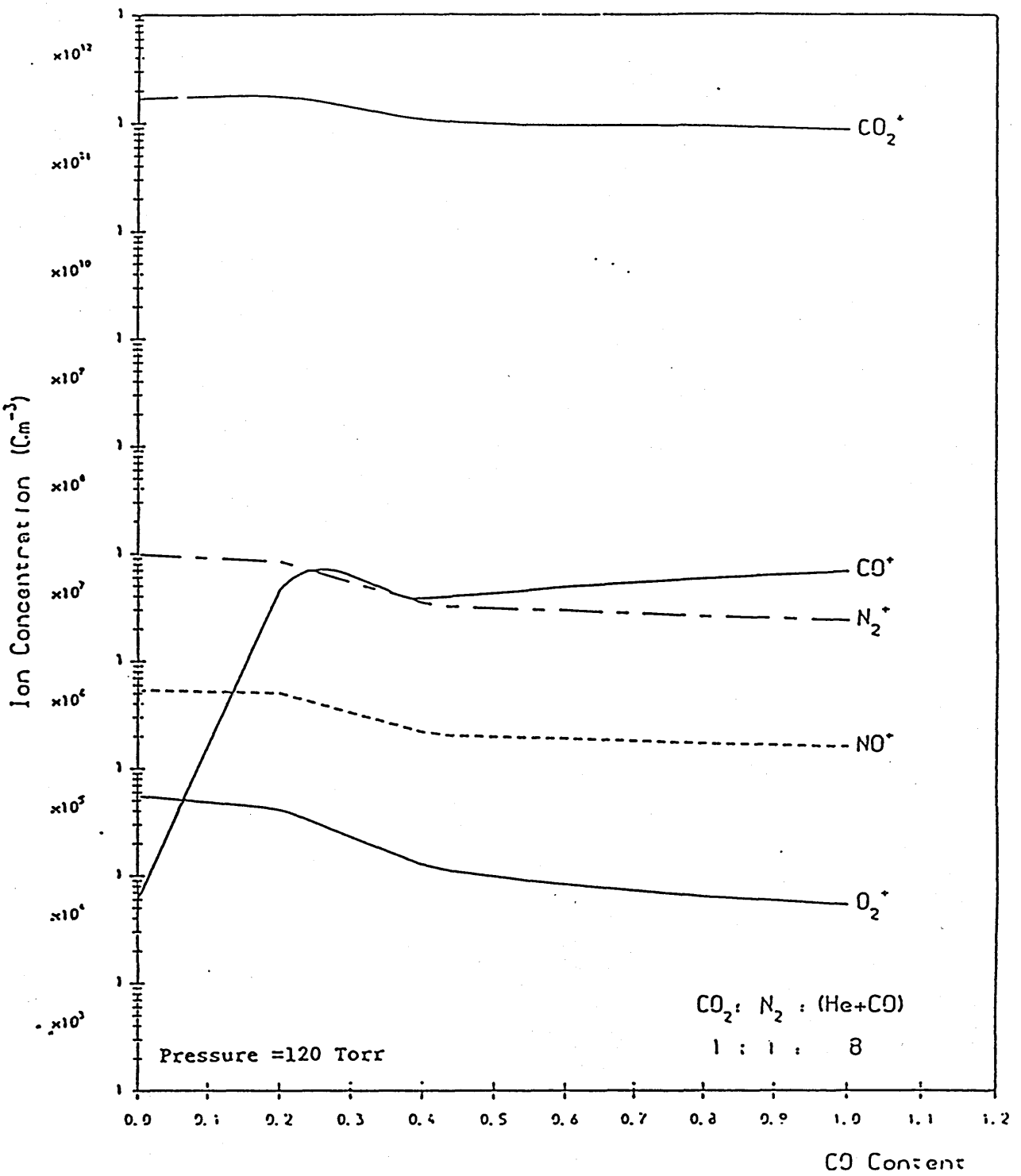

VARIATION WITH ADDED CO OF POSITIVE ION CONCENTRATIONS AT t=10 μSEC

GRAPH (3.22)

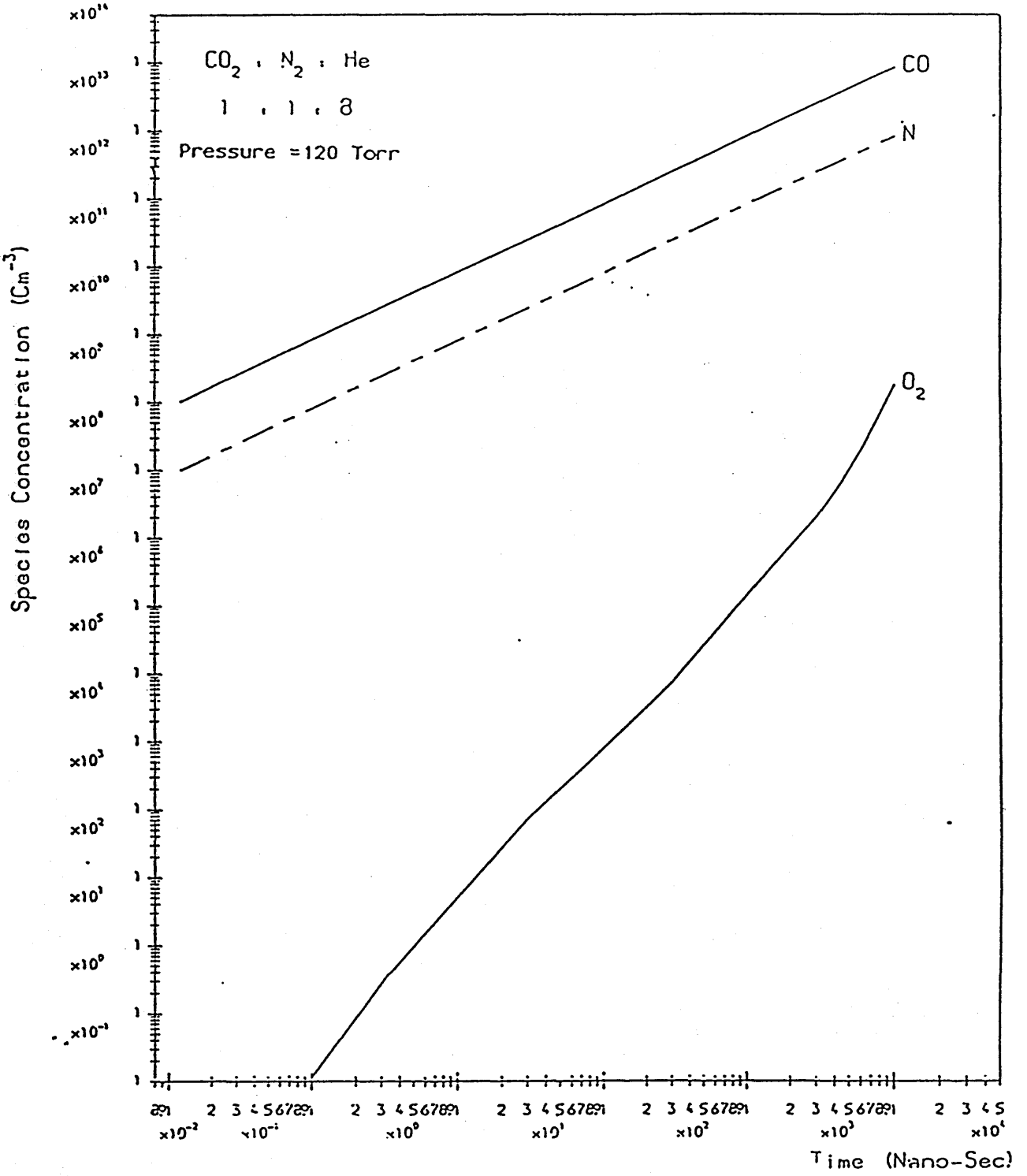

VARIATION WITH TIME
OF THE MAIN DISSOCIATION PRODUCTS

GRAPH (3.23)

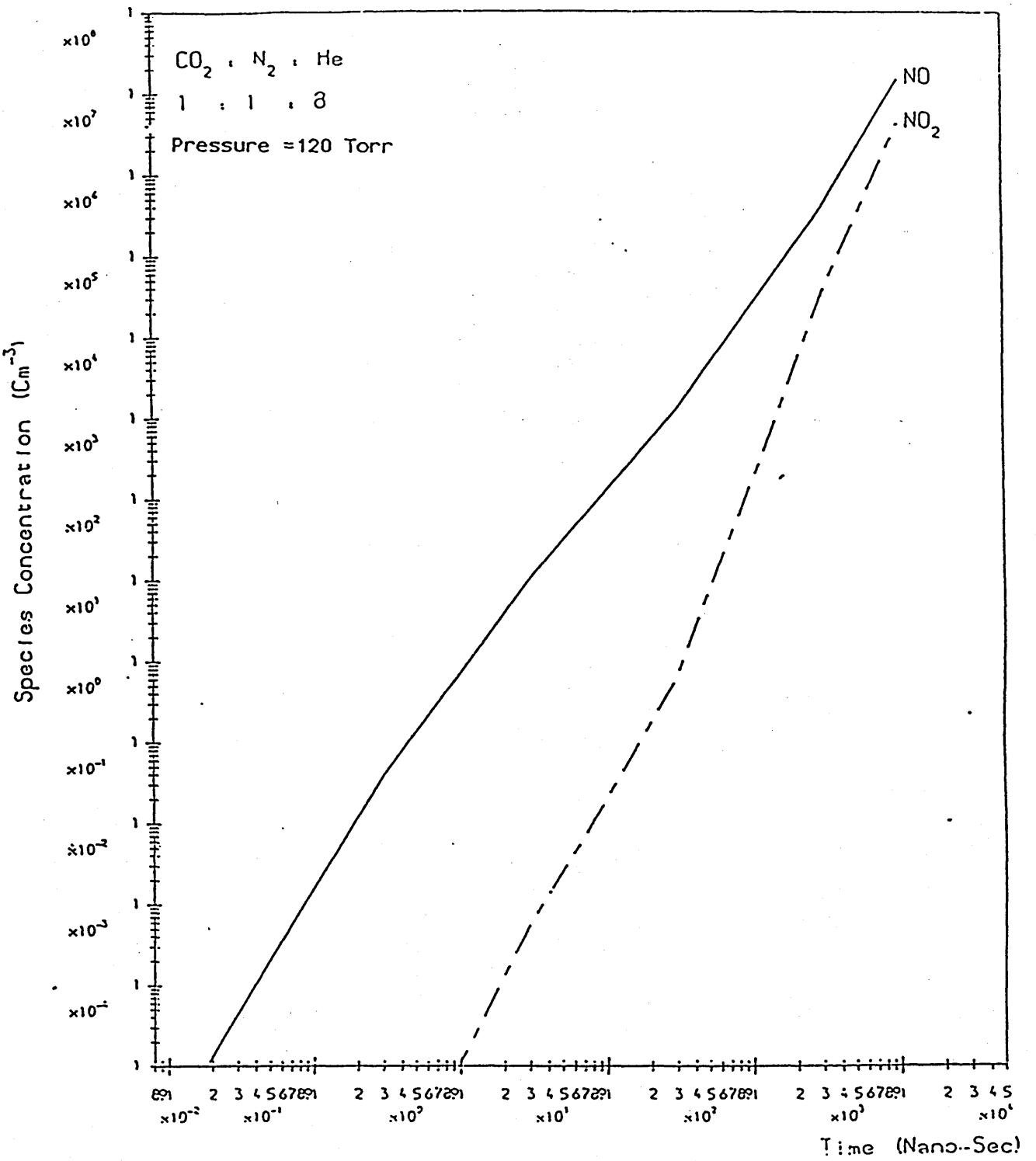

VARIATION WITH TIME OF NITROGEN OXIDES

GRAPH (3.24)

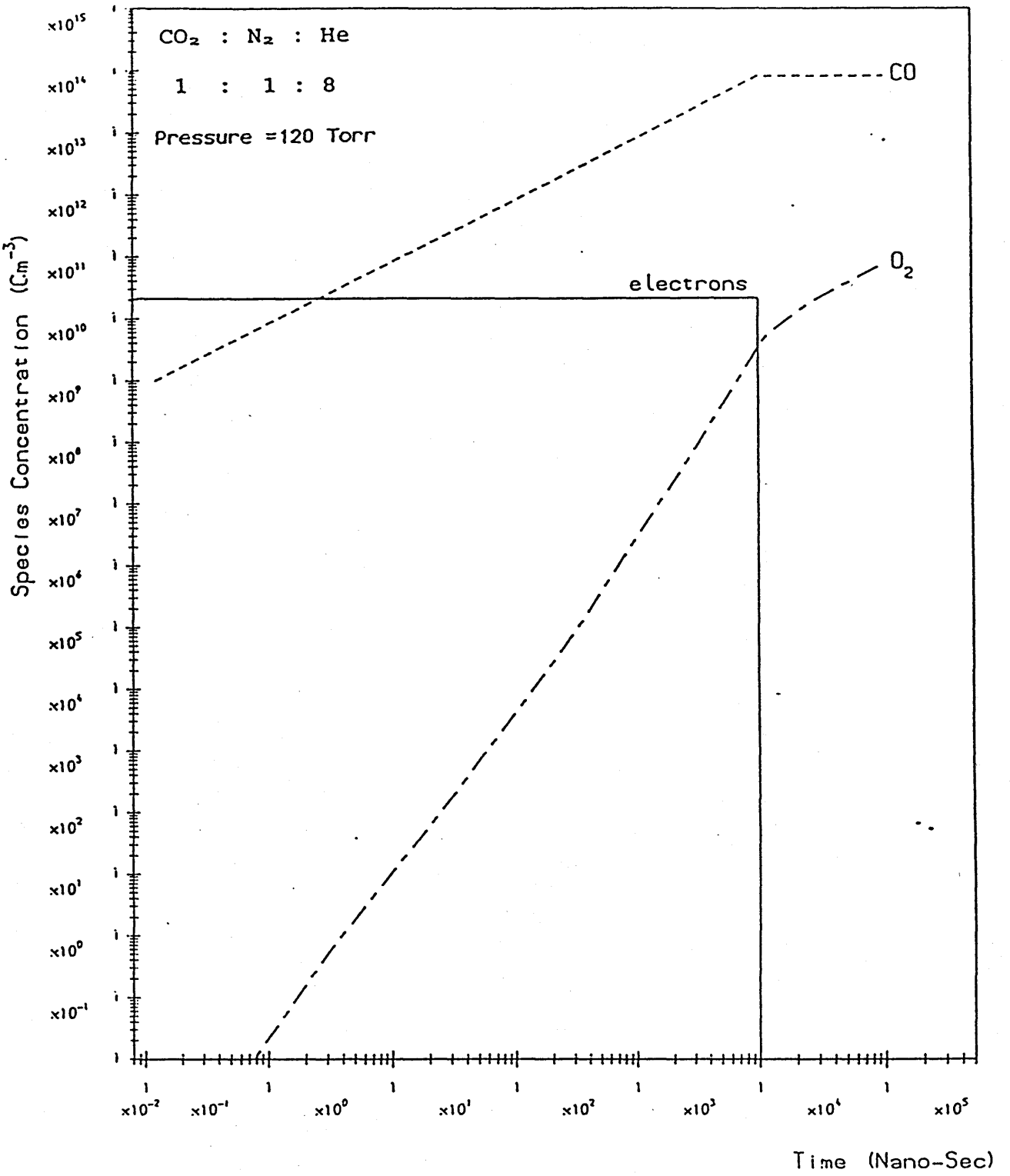

VARIATION WITH TIME
OF THE MAIN DISSOCIATION PRODUCTS
GRAPH (3.25)

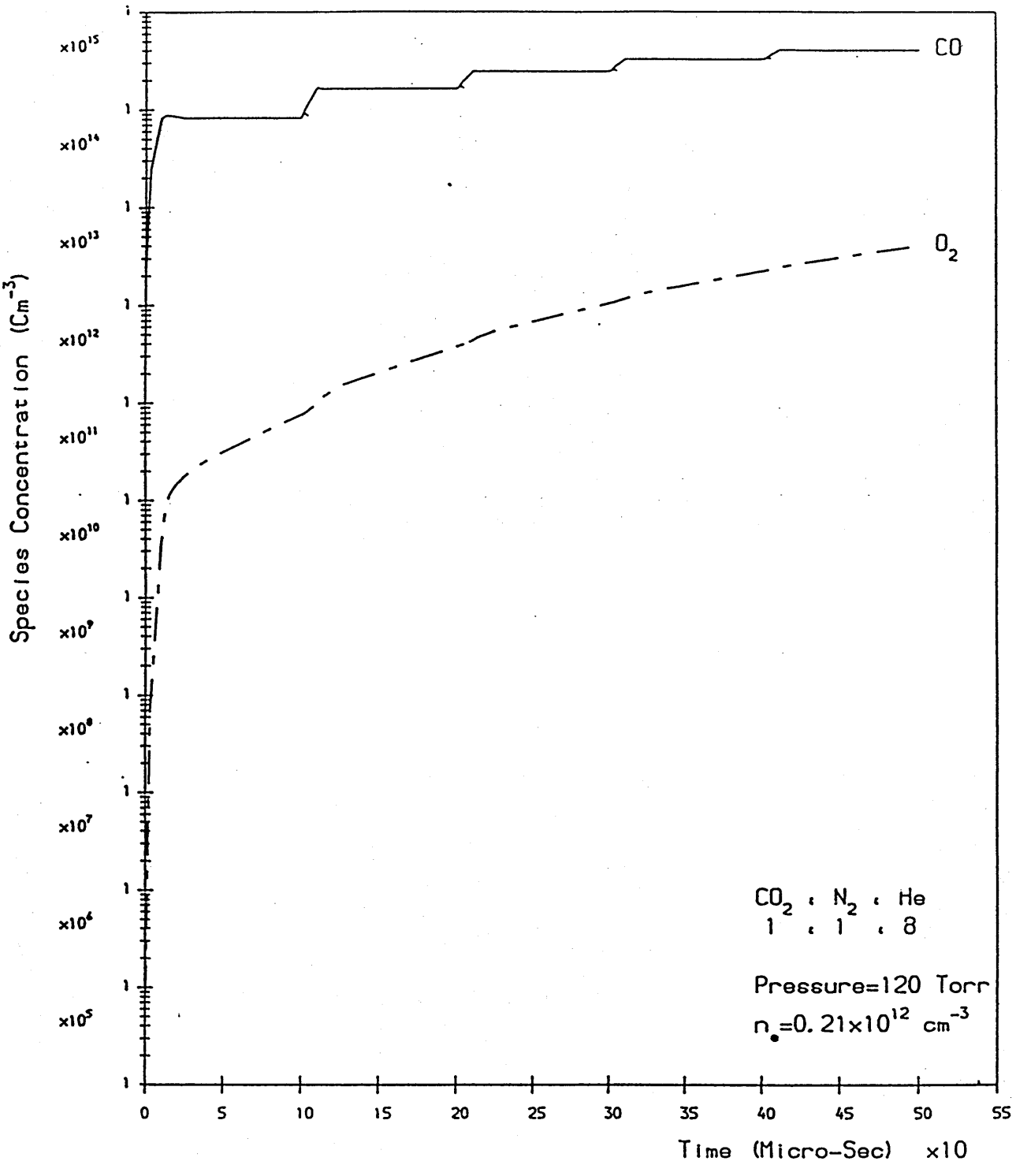

DEVELOPMENT OF THE MAIN DISSOCIATION PRODUCTS DURING 5 PULSES

GRAPH (3.26)

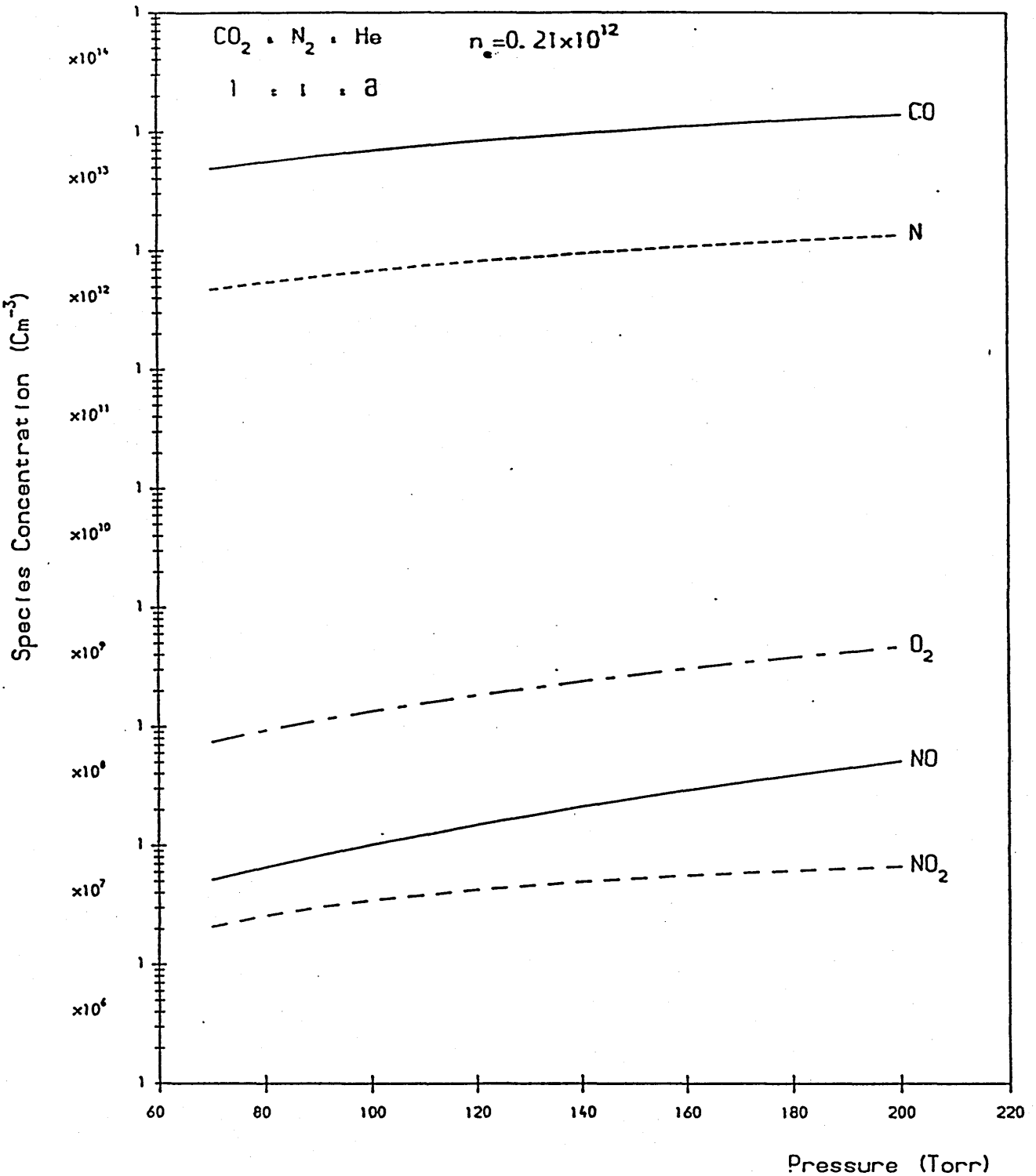

VARIATION WITH PRESSURE OF NEUTRAL SPECIES CONCENTRATIONS AT t=10 μ SEC

GRAPH (3.27)

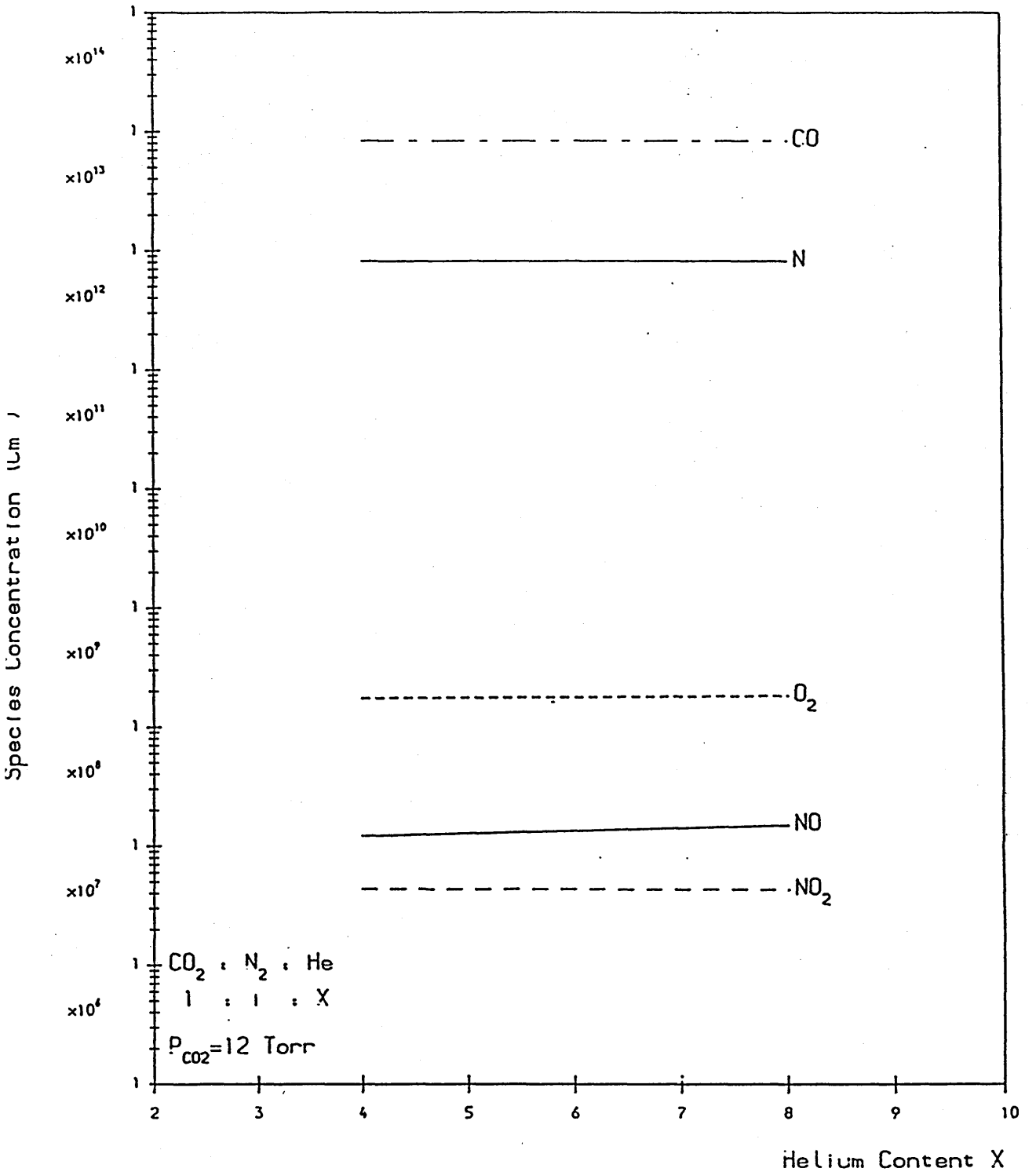

VARIATION WITH HELIUM CONTENT OF
NEUTRAL SPECIES CONCENTRATIONS AT t=10 μ SEC

GRAPH (3, 28)

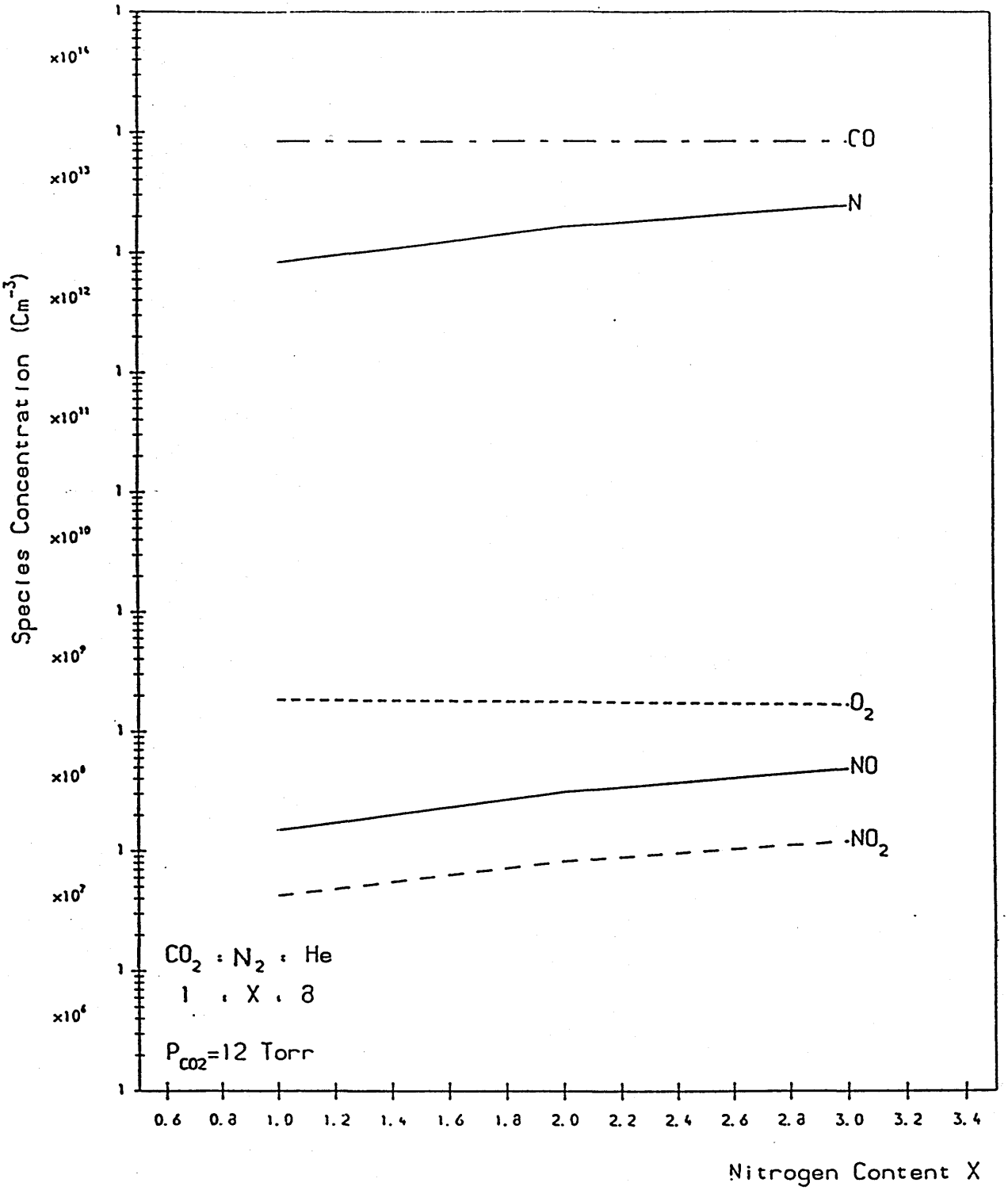

VARIATION WITH NITROGEN CONTENT OF

NEUTRAL SPECIES CONCENTRATIONS AT t=10 μSEC

GRAPH (3.29)

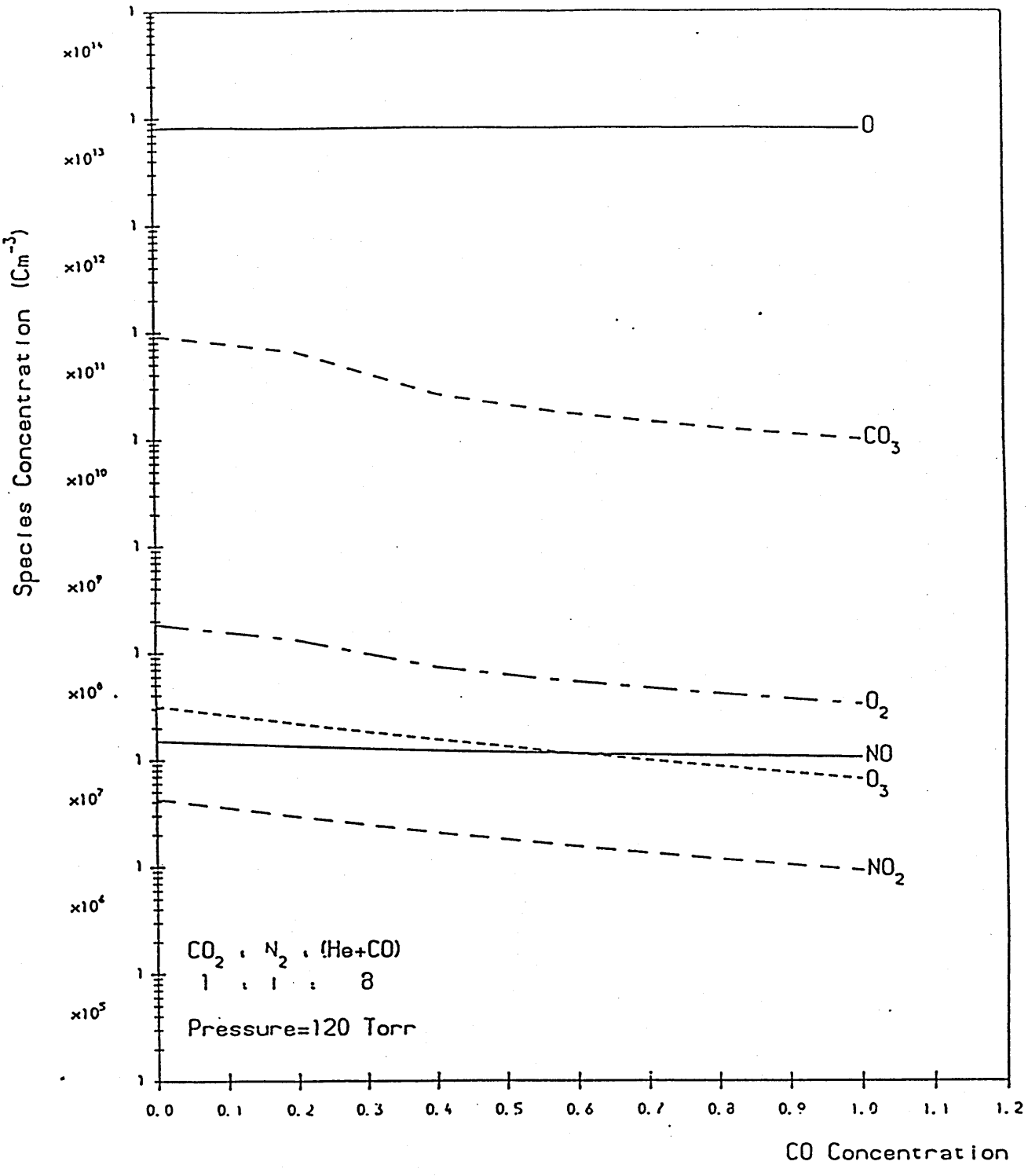

VARIATION WITH ADDED CO OF NEUTRAL SPECIES CONCENTRATIONS AT t=10 μ SEC

GRAPH (3.30)

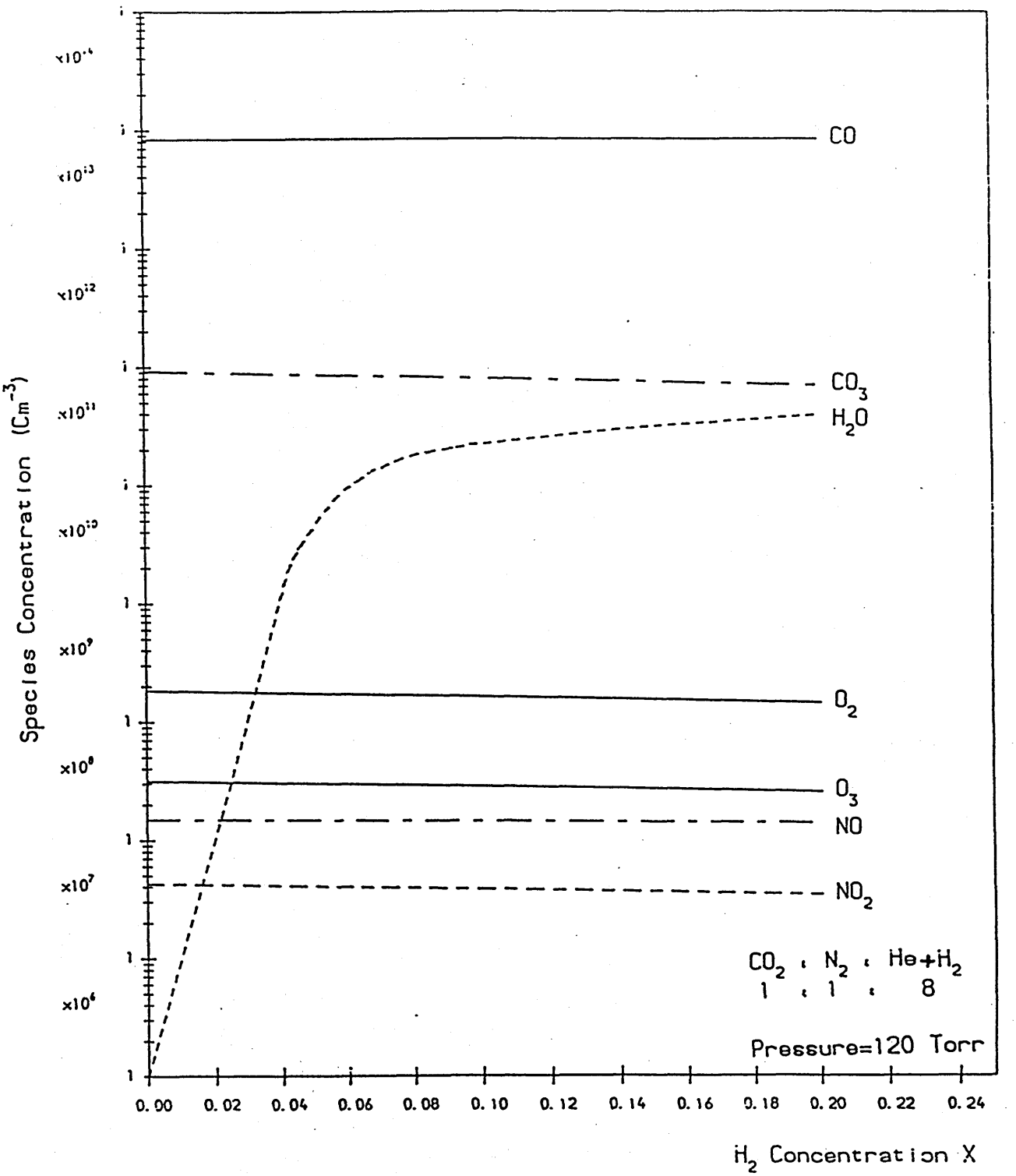

VARIATION WITH ADDED H_2 OF THE NEUTRAL SPECIES CONCENTRATIONS AT $t=10\ \mu$SEC

GRAPH (3.31)

CHAPTER FOUR

THEORETICAL INVESTIGATION OF A HIGH PRF CO_2 LASER KINETICS

4.1 INTRODUCTION:

A multi-kilowatt, transverse discharge, high pulse repetition frequency (p.r.f), CO_2 laser is currently under development, being prompted by an increasing demand for the expansion of materials processing applications . The system will be operable at prf's variable up to 10 kHz , giving an output suitable for a broad range of process requirements.A kinetic model has been developed that assists in understanding the relationship between the laser output characteristics to the many interdependent design parameters. This model represents an extension of the 'six energy level' model reported by Chatwin and Scott [4.1] and subsequently developed by Byabagambi et al [4.2]. The extension is to allow for the presence of CO in the laser cavity. CO may be introduced intentionally or produced by dissociation of CO_2. Electrons excite the CO molecules into their first excited state , v=1. The resulting CO will then be available to transfer energy in Vibration-Vibration collisions to both N_2 and CO_2 since the quantum $h\nu_{CO2} \approx h\nu_{N2} \approx h\nu_{CO}$. Moreover, CO is effective for the deactivation of the lower laser level. Figure (4.1) shows schematically the set of processes that results in the 'eight energy level' model which is necessary to describe the CO_2 : N_2 : He : CO system.

4.2 NOMENCLATURE :

A	Effective area of the smallest cavity mirror for reflection (cm^2).
c	Speed of light (2.997927×10^{10} cm/sec).
C_p	Specific heat at constant pressure (J/kg.°K).
C_v	Specific heat at constant volume (J/kg.°K).
E	Energy (J).
F	Fraction of input power coupled into excitation.
g	Gain (cm^{-1}).
g_i	Degeneracy of energy level i .
G	Fraction of photons spontaneously radiated into a small angular aperture.
H	Laser cavity hight (cm).
IP	Electrical input power ($watt/cm^3$).
I_p	Photon density (cm^{-3}).
k	Boltzmann constant (1.38026×10^{-23} J/°K).
k_e	Equilibrium constant between level 02^20 and 01^10.
K_{15}	Transfer rate constant between levels 1 and 5 (sec^{-1}).
K_{51}	Transfer rate constant between levels 5 and 1 (sec^{-1}).
K_{17}	Transfer rate constant between levels 1 and 7 (sec^{-1}).
K_{71}	Transfer rate constant between levels 7 and 1 (sec^{-1}).
K_{75}	Transfer rate constant between levels 7 and 5 (sec^{-1}).

K_{132} Transfer rate constant between levels 1 and 32 (sec^{-1}).

K_{2131} Transfer rate constant between levels 21 and 31 (sec^{-1}).

K_{2231} Transfer rate constant between levels 22 and 31 (sec^{-1}).

K_{320} Transfer rate constant between levels 32 and 0 (sec^{-1}).

K_{sp} Spontaneous emission rate (sec^{-1}).

L Laser cavity length (cm).

m Mass of gas mixture (kg).

$\dot{m}$ Mixture gas mass flow rate (kg/sec).

n Population density of excited states (cm^{-3}).

P Gas pressure (Torr).

Q Power density ($watt/m^3$).

R_F Front mirror reflectivity.

T Gas temperature (°K).

T_o Photon decay time (sec).

U Average electron energy (J).

α Rate of direct excitation of CO_2 (sec^{-1}).

η Rate of direct de-excitation of CO_2 (sec^{-1}).

γ Rate of direct excitation of N_2 (sec^{-1}).

β Rate of direct de-excitation of N_2 (sec^{-1}).

μ_1 Rate of direct excitation of CO (sec^{-1}).

μ_2 Rate of direct de-excitation of CO (sec^{-1}).

λ Wavelength of the output power (cm).

σ Absorption cross-section (cm^2).

4.3 THE BASIS OF THE MATHEMATICAL MODEL :

4.3.1 General:

As diatomic molecules, N_2 and CO each have one vibrational mode. CO_2 is a linear triatomic molecule and has three vibrational modes; a symmetric stretch mode, an asymmetric stretch mode, and a doubly degenerate bending mode. The energy content of any mode is called the vibrational mode energy of that mode, E_v, and is given, per unit volume, by

$$E_v = [Nh\nu/\{\exp(h\nu/kT_v)-1\}] \quad \text{.....(4.1)}$$

The vibrational temperature of the mode, T_v, is equal to the ambient gas temperature, T, when the gas is at equilibrium. Figure (4.1) shows schematically the physical processes considered by the model. The dashed lines refer to the excitation of the vibrational modes resulting from inelastic electron-molecule collisions. The dotted lines represent the relaxation of vibrationally excited molecules to the ground state. The chain lines refer to the de-excitation processes of the vibrational modes. The continuous lines represent vibrational energy exchange between modes. The wavy line represents the laser action, the stimulated emission and absorption of radiation which takes place between particular rotational levels of the asymmetric, $CO_2(00^o1)$ and symmetric, $CO_2(10^o0)$, states. The intensity of this emission depends upon the degree of population inversion between these states, as well as being affected by spontaneous emission and cavity losses.

4.3.2 Assumptions :

The kinetic rate equations can be derived by introducing the following approximations:

(i) In each vibrational mode group designation, local Boltzmann equilibrium is assumed. This allows the use of the Boltzmann equation for the evaluation of both vibrational and rotational energy level molecular populations.

(ii) Stimulated emission ocurrs only for transitions in the $00^{0}1 \longrightarrow 10^{0}0$ band (i.e P20).

(iii) The cavity dimensions and flow velocities are such that boundary layer development and diffusion processes can be neglected.

(iv) Direct excitation and de-excitation of the lower laser levels have been neglected because, from theoretical calculations,these have been found to be very small (chapter 2). In addition, the experimental resulsts of Siemsen et al [4.3] show that the populations of the lower laser level are always small compared to the upper laser level populations in CO_2:N_2:He discharges.

4.3.3 Stimulated emission :

In a laser cavity with two mirrors (one at each end) , the light emitted spontaneously at various points in the laser medium normal to the end mirrors and within the resonant mode of the cavity is amplified through stimulated emission. The rate of change of photon population density within the laser cavity can be written as:

$$dI_p/dt = -I_p/T_o + I_p c g + n_1 K_{sp} G \quad \ldots\ldots\ldots\ldots (4.2)$$

where T_o is the photon decay time which is defined as the average time a photon remains inside the laser cavity before being lost through the laser output window. The photon decay time is related to the cavity length and the reflectivity of the output mirror and can be written as:

$$T_o = -2L/c \ln(R_r) \quad \text{.....(4.3)}$$

where R_r is the front mirror reflectivity. The back mirror is fully reflecting. The third term on the right hand side in equation (4.2) represents the spontaneous emission where the rate constant (K_{sp}) is the inverse radiative lifetime of the lasing transition and the quantity (G) indicates the fraction of photons being spontaneously radiated into a small angular aperture defined by the resonator. Assuming monochromatic radiation,Byabagambi [4.5] gives the following expression for G:

$$G = \lambda^2/A \quad \text{.....(4.4)}$$

where λ is the wavelength of the output radiation and A is the reflectivity area of the smallest cavity mirror. This term is important for initiating stimulated emission but becomes insignificant once stimulated emission takes off.

4.3.4 Kinetic Rate Equations :

Expressions may be derived describing the time rate of change of the populations of the vibrational states due to the processes described in section (4.3.1). These five equations together with the equations for the cavity radaition field intensity and the gas-kinetic temperature are the seven coupled differential ordinary equations which comprise the model , i.e :

$$dn_1/dt = \alpha n_o - \eta n_1 + K_{51}n_5 - K_{15}n_1 - K_{ep}n_1$$
$$- K_{132}\{n_1 - (n_1/n_{32})_e n_{32}\}$$
$$- I_p cg + K_{71}n_7 - K_{17}n_1 \quad \ldots\ldots\ldots\ldots (4.5)$$

$$dn_2/dt = K_{ep}n_1 + I_p cg - K_{2131}\{n_{21} - (n_{21}/n_{31})_e n_{31}\}$$
$$- K_{2231}\{n_{22} - (n_{22}/n_{31})_e n_{32}\} \quad \ldots\ldots\ldots\ldots (4.6)$$

$$dn_3/dt = \{2K_{2131}/(1+k_e)\}\{n_{21} - (n_{21}/n_{31})_e n_{31}\}$$
$$+ \{2K_{2231}/(1+k_e)\}\{n_{22} - (n_{22}/n_{31})_e n_{31}\}$$
$$+ K_{132}\{n_1 - (n_{22}/n_{32})_e n_{32}\}$$
$$- K_{320}\{n_{32} - (n_{32}/n_o)_e n_o\} \quad \ldots\ldots\ldots\ldots (4.7)$$

$$dn_5/dt = \gamma n_4 - \beta n_5 - K_{51}n_5 + K_{15}n_1 + K_{75}n_7 \quad \ldots\ldots (4.8)$$

$$dn_7/dt = \mu_1 n_6 - \mu_2 n_7 - K_{71}n_7 + K_{17}n_1 - K_{75}n_7 \quad \ldots\ldots (4.9)$$

$$dI_p/dt = I_p cg - I_p/T_o + K_{ep}n_1 G \quad \ldots\ldots\ldots\ldots (4.10)$$

$$dT_e/dt = (2/mc_v)dQ/dt - \{(2\dot{m}c_p/mc_v)(T_e - T_1)\} \quad \ldots\ldots (4.11)$$

Rate constants (K) are given in Appendix (4.I).

4.3.5 Electrical Excitation :

Direct excitation of CO_2, N_2, and CO ground state molecules occurs by electron impact through inelastic collision processes. The excitation rates α , γ ,and μ_1 are calculated by considering the fraction of the power input,F, coupled into excitation of $CO_2(00°1)$,$N_2(v=1)$,and $CO(v=1)$ levels respectively. These rates can be written as follows:

$$\alpha = F_{co2}\ IP\ /E_{oo1}\ n_o \qquad \text{.....(4.12)}$$

$$\gamma = F_{N2}\ IP\ /E_{v-1}\ n_4 \qquad \text{.....(4.13)}$$

$$\mu = F_{co}\ IP\ /E_{v-1}\ n_6 \qquad \text{.....(4.14)}$$

The values of F_{co2}, F_{N2} and F_{co} were obtained from the predictions in chapter 2. The reverse process can also take place,where excited molecules lose energy to the electrons and the electrons gain an equal amount of kinetic energy.The rates of these processes depend upon the electron energy distribution in the discharge and can be written as follows:

$$\eta = \alpha \exp(E_i/U) \qquad \text{.....(4.15)}$$

$$\beta = \gamma \exp(E_i/U) \qquad \text{.....(4.16)}$$

$$\mu_2 = \mu_1 \exp(E_i/U) \qquad \text{.....(4.17)}$$

where E_i is the energy of level i and U is the average electron energy in the discharge. Values of U were obtained from the predictions in chapter 2.

4.3.6 <u>Gain</u> :

The relationship between small signal gain and population inversion has been derived by many authors (e.g Reid and Siemsen[4.6],Siemsen et al[4.3],Brimacombe and Reid [4.7], and Sato and Miura[4.8]). The gain (g) is related to the population inversion density by:

$$g=\sigma\{n_u - (g_u/g_1)n_1\} \qquad \text{.....(4.18)}$$

where n_u and n_1 are the population densities of the upper and lower laser levels,g_u and g_1 are the level degeneracies, σ is the absorption coefficient.Referring to figure (4.1),it has been shown by Chatwin [4.4] that the population of the lower laser level may be partitioned such that:

$$n_{1oo} = 0.408\ n_{21} \qquad \text{.....(4.19)}$$

The energy level degeneracies ,g_u and g_l , may be droped by neglecting the unit change in rotational quantum number, hence equation (4.34) can be written as:

$$g = \sigma (n_1 - 0.408\, n_{21}) \qquad \ldots\ldots\ldots\ldots\ldots\ldots (4.20)$$

The small signal gain in CO_2 laser systems depends strongly upon the pressure-broadened widths of the translational rotational lines in the 10 μm band.The absorption coefficient (σ) is that of high pressure (P>10 Torr) collision-broadening where the intensity distribution function describing the line shape is Lorentzian. Hoffman [4.9] gives an approximate value of σ=718/nT (cm^2) which does not take into account the substantial line broadening effects of helium. Measurements of the pressure-broadened linewidth in TE CO_2 discharges made by Brimacombe and Reid [4.10] show that these effects are very important where collisions with He are dominant in the discharge. Chatwin [4.4] gives an expression for the absorption coefficient which is extended herein to include the effects of carbon monoxide (see Appendix 4.II). Thus, the following expression is used:

$$\sigma = 692.5/T\ [\ n_{co2} + 1.063\, n_{N2} + 1.484\, n_{He} + 1.1238\, n_{co}] \qquad \ldots\ldots\ldots\ldots (4.21)$$

4.4 INITIAL AND BOUNDARY CONDITIONS :

A unique solution to equations(4.5 to 4.11) exists for each set of initial and boundary conditions. This system of seven,first-order ordinary differential equations is solved numerically using Merson's version of the Runge-Kutta method [4.11] for two successive 10 μsec electrical input pulses with an interpulse gap of 90 μsec giving a p.r.f of

10 kHz. The current and voltage profiles of these input pulses, as shown in figure (4.2), are based on experimental measurements. The following initial and boundary conditions are sufficient to solve the rate equations:

(i) in thermodynamic equilibrium ,the population densities n_i and n_j of the two vibrational energy levels E_i and E_j can be written as:

$$n_i/n_j = (g_i/g_j) \exp\{-(E_i - E_j)/kT\} \quad .....(4.22)$$

(ii) at low pressure,the total population density per unit volume can be evaluated according to the equation of state for an ideal gas,i.e

$$n_t = P/kT \quad .....(4.23)$$

(iii) the initial gas temperature is taken as ambient and at cavity entrance the temperature is constant due to a continuous flow of the gas, i.e

$$dT_i/dt = 0 \quad .....(4.24)$$

(iv) the initial value of the photon density is taken as that due to spontaneous emission and is given by:

$$I_p = n_i G \quad .....(4.25)$$

4.5 DEFINITION OF LASER PULSE PARAMETERS:

Figure (4.3) shows the laser pulse parameters used in the analysis of the output power. These are as follows:

(i) **Delay Time:**

This is defined as the difference in time between the start of the current input pulse and the start of the laser output pulse. It is assumed that the laser output pulse starts when the output poweris

7.0 w/cc . This value was chosen because when multiplied by the cavity volume it gives the minimum power necessary for material processing applications [Khahra, 4.12].

(ii) **Pulse Duration:**

This is the time taken , after the delay time , for the pulse power to fall to 7.0 w/cc.

(iii) **Dimensionless Spike Power:**

This indicates the maximum power of each pulse , made dimensionless by dividing it by the maximum input power.

(iv) **Dimensionless Flat Pulse Power:**

This is the mean flat pulse power, made dimensionless by dividing it by the maximum input power.

(v) **Efficiency:**

The useful efficiency (η_{us}) for each pulse is based on the pulse duration, i.e, when the power output is high enough for material processing. Whereas , the overall efficiency (η_{ov}) is taken over the period of 120 µsec.

4.6 THEORETICAL INVESTIGATION:

The following cases are considered herein:

(i) gas mixtures without carbon monoxide addition,

(ii) gas mixtures with CO addition as a substitute for helium, and

(iii) gas mixtures with CO addition as a substitute for nitrogen.

Tables (4.1),(4.2) and (4.3) detail the precise mixtures investigated where CO was added in amounts up to 100% of the CO_2 content. The peak power was held constant at 230 w/cc since this value is experimentally achievable for all the gas mixtures considered. It was decided to do a detailed analysis using the 1:3:4 mixture. This mixture gave greatly improved laser parameters for the second pulse and therefore subsequent pulses [Bybagambi , 4.5].

4.7 RESULTS AND DISCUSSION ; CASE ONE - GAS MIXTURES WITH NO CARBON MONOXIDE ADDITION:

4.7.1 Effects of Helium :

It can be seen from Table (4.1) that addition of helium results in a decreased average electron energy. In addition, helium enrichment up to a partial pressure of 81 Torr of the mixture increases the CO_2 and N_2 excitation efficiencies , hence increasing the direct excitation and de-excitation rates. Moreover , helium reduces the stimulated emission cross-section due to collision line broadening ,this can be inferred from equation (4.21) where the helium term has the dominant coefficient.

4.7.1.1 Excitation of the upper laser level (n_4) :

The increase in the direct excitation rate caused by the addition of helium results in an increased population inversion gradient which when combined with the increased delay time results in large upper laser level populations as shown by the spikes in graphs (4.1) to (4.3). When direct excitation starts the net rate of resonant energy transfer is insignificant , however , once the upper laser level collapses , the net rate becomes substantial. This explains the oscillatory nature of graphs (4.1) to (4.3) and that of the output which is greater for helium rich mixtures as shown in graphs (4.13) to (4.15).

After direct excitation cut off, the population of the upper laser level falls off more steadily for mixtures with high helium contents due to the fast depopulation of this level directly to the 01^10 level by helium (see figure 4.1).

4.7.1.2 Excitation of the upper nitrogen level (n_5) :

The improvement in excitation efficiency produced by helium addition results in a greater direct excitation rate.This gives an increased population inversion which when combined with the increased delay time results in an increased upper nitrogen population as shown in graph (4.4). When direct excitation is cut off, the upper nitrogen level decays exponentially via its resonant interaction with carbon dioxide.

4.7.1.3 Effects of Stimulated Emission on Delay Time and Spike Power:

Stimulated emission is a function of population inversion and stimulated emission cross-section.With increasing helium the increasing population inversion gradient and the decreasing cross-section both result in reduced gain as shown in graphs (4.7) to (4.9) . This reduction in stimulated emission which is combined with an increased direct excitation rate significantly increases the time required for stimulated emission to overcome direct excitation. Hence,the delay time increases as shown in graph (4.16). However , the second pulse delay time is smaller due to residual gain and power left by the previous excitation pulse. Because of its useful effect on subsequent pulses, a high value of interpulse gain is of interest. Increasing helium content of the gas mixture reduces the gain after direct excitation, hence reduces the effect of residual gain on subsequent pulses.

For helium rich mixtures in which the gain is reduced the population of the upper laser level has more time (greater delay time) to increase to large values before being overwhelmed by stimulated emission , therefore a large spike develops, see graph (4.13). Hence, the dimensionless maximum power increases in the same manner as the delay time curve , see graph (4.17).

4.7.1.4 Gas Mixture Temperature:

One of the important effects of helium is to reduce the gas temperature due to its high thermal capacity(mc_p) so the depletion rate of the upper laser level population by collisions is decreased. Another important role played by helium is to increase the relaxation rate of the lower laser level through CO_2-He collisions, this yields a larger population inversion and therefore more energy can be dumped in the gas mixture. Therefore increasing amounts of helium decrease the maximum mixture temperature, see graph (4.18).

It can be seen from graphs (4.10) to (4.12) that the maximum temperature is well below 600°K , which is the maximum allowed in the laser cavity [DeMaria , 4.13].

4.7.1.5 Pulse Duration and Mean Power:

Graphs (4.13) to (4.15) show the output power for two successive electrical pumping pulses. Because the time taken to establish a significant population inversion is shorter than the cavity field intensity build-up time, the initial output occurs in the form of a narrow spike which increases in mixtures with high helium content and the output pulse shows a highly oscillatory behaviour which is not useful for machining applications. The pulse duration is determined by the relaxation times of the excited molecules.With high pressures and increased helium content these times become shorter, thus the pulse length decreases. However, the initial increase in the pulse duration shown by graph (4.19) is due to the effect of the long power pulse tail in

mixtures with low helium content, see graph (4.13).This effect can be explained as follows: when a small amount of helium is added to the gas mixture, the wasted power in the long tail is released sooner within the main output pulse so that no more energy is left in the pulse tail for increasing He to have a positive effect. Graph (4.20) shows that the mean power for the second pulse increases with increasing helium, while that of the first pulse tends to decrease , especially for nitrogen rich mixtures where, as can be seen from graphs (4.14) and (4.15), the delay time increases with no significant change in the pulse tail profile.

4.7.1.6 Efficiencies:

Graphs (4.21) and (4.22) show the variation with helium content of efficiencies.The increase in efficiency is caused by several factors:

(i) increasing helium content , up to a certain value as shown in Table (4.1) , results in an increased excitation efficiency of the upper CO_2 and N_2 levels, hence more of the input electrical energy is effectively absorbed so the output power is improved.

(ii) the reduction in the gas mixture temperature helps to empty the lower laser level and therefore maintain the population inversion. Hence improves the efficiency.

(iii) helium atoms cause a rapid depopulation of the lower laser level by collisional relaxation process (as discussed in chapter 2).This increases the population inversion and hence increases efficiency.

However, graph (4.21) shows that the efficiency tends to decrease after a certain value of added helium. This is mainly due to the decrease in the excitation efficiencies (as shown in Table 4.1) and the increase in the relaxation rate K_{132}. As the helium content becomes significant, the amount of excited molecules deactivated to the 32 level (see figure 4.1) increases significantly and therefore leads to a decrease in efficiency. Graph (4.22) shows that the useful efficiency for the second pulse is increased, especially for mixtures with high amounts of nitrogen. This is because the upper nitrogen level is left populated from the previous pulse and because of a finite positive gain and output power at the beginning of the second pulse.

4.7.2 Effects of Nitrogen:

As the total pressure of CO_2 and N_2 was held constant at 27 Torr, therefore as the partial pressure of nitrogen was increased the partial pressure of carbon dioxide was correspondingly decreased. Thus, the population inversion is small due to the small population of the upper and lower laser levels. As shown in chapter 2, the nitrogen electron excitation cross-sections are larger than those of CO_2. Thus, with increasing N_2 content more nitrogen molecules are excited to their upper vibrational level , hence more energy is transferred to the CO_2 (00°1) level through the resonant transfer process. This leads to a more efficient coupling of the electrical energy into the discharge.

4.7.2.1 Excitation of the Upper Laser Level (n_1):

Graphs (4.1) to (4.3) show that as the nitrogen content increases the population of the upper laser level decreases due to the decreased ground level population and decreased excitation rate constants. For reduced population of the upper laser level resonant energy transfer is decreased and therefore the oscillations in the output pulse are reduced as shown in graphs (4.13) to (4.15).

After direct excitation cut off, the population of the upper laser level falls off more slowly in mixtures with more nitrogen due to the continuous supply of energy from the $N_2(v=1)$ level as shown in graph (4.3).

4.7.2.2 Excitation of the Upper Nitrogen Level (n_4):

For increased nitrogen the population of the upper N_2 level increases very rapidly as shown in graphs (4.5) and (4.6). This is because of the increased ground level population and increased excitation efficiency.

After direct excitation cut off, the population of the N_2 (v=1) level falls off to a value determined by both the $CO_2(00°1)$ level population and pressure ratio of CO_2 and N_2. Thus, increasing the nitrogen content relative to CO_2 leaves more N_2 molecules trapped in the upper level (v=1) which are not used for exciting CO_2 molecules within the duration of the pulse. The final population at excitation cut off is , therefore , greater for mixtures with more nitrogen as shown by comparison of graphs (4.5) and (4.6).

4.7.2.3 Effects of Stimulated Emission on Delay Time and Spike Power:

Due to the reduction of CO_2 partial pressure as nitrogen content increases, the population of the lower laser level is decreased. This allows a very rapid population inversion, hence a rapid build-up of stimulated emission which gives a reduced delay time and spike hight as shown in graphs (4.16) and (4.17). It can be seen from graphs (4.5) and (4.6) that increasing N_2 produces a long tail in the output pulse so there is sufficient power and gain at the start of the second pulse to reduce the spike hight and delay time.

During the interpulse period , the continuous supply of vibrational energy from the $N_2(v=1)$ level to the upper laser level produces almost a constant gain, especially for high nitrogen content. This is shown in graph (4.9).

4.7.2.4 Gas Mixture Temperature:

Because thermal properties of nitrogen are not very much different from those of carbon dioxide and as the total pressure of these gases was held constant, an increase in the nitrogen content has no significant effect on the temperature as shown in graph (4.18).

4.7.2.5 Pulse Duration and Mean Power:

Graph (4.19) shows that increased nitrogen leads to a longer pulse duration and the difference between the pulse duration of the first and second pulses increases with increasing nitrogen.This is due to the 'spreading effect' of nitrogen on the output pulse profile where the energy is

released over a longer period. Thus, at the start of the second pulse, the residual energy is sufficient to increase the pulse duration. Moreover , this results in a decreased mean power as nitrogen content increases, see graph (4.20).

4.7.2.6 Efficiencies:

Graph (4.21) shows that increasing nitrogen improves the laser efficiency due to the increased excitation efficiency. While graph (4.22) indicates the useful effect of increasing nitrogen on the efficiency of the second pulse since increased N_2 leaves more energy in the output pulse tail.

4.7.3 Effects of Cavity Length:

4.7.3.1 Pulse delay time, peak and mean power:

Increased cavity length means that on average the residence time of a photon within the resonator is increased,hence, a fast build-up of the photon flux occurs. This reduces the delay time and the maximum power as shown in graphs (4.23) and (4.24). In addition,with the increased cavity length the energy left in the first pulse tail increases and therfore decreases the delay time and peak power for the second pulse. This effect is observed up to a cavity length of 300 cm whereafter the pulse delay time and peak power remain constant.The pulse energy is released over a longer time period, hence it increases the pulse length as shown in graph (4.25) and leads to a decreasing mean pulse power as shown in graph (4.26).

4.7.3.2 Efficiencies:

Since the energy output per pulse is increased as the cavity length increases,both overall and useful efficiencies are increased as shown in graphs (4.27) and (4.28).

4.7.4 Effects of Front Mirror Reflectivity:

Graphs (4.29) to (4.34) indicate that increasing the front mirror reflectivity reduces delay time and spike height, increases pulse duration and efficiency. These effects are similar to those of increasing the cavity length (i.e increasing photon residence time). If the output mirror reflection is too high the intensity of radiation on the internal face of the output mirror would be so great as to damage the mirror surface, a compromised value of 0.85 is recommended.

4.8 RESULTS AND DISCUSSION ; CASE TWO - GAS MIXTURES WITH CO ADDITION AS A SUBSTITUTE FOR HELIUM:

It can be seen from Table (4.2) that the addition of CO reduces the average electron energy and this reduction becomes considerable as the CO content increases owing to large cross-sections for CO (as discussed in chapter 2).This has more effect on the N_2 excitation efficiency than on that of CO_2 as shown in the Table. The CO excitation efficiency increases with increased CO due to the presence of more CO molecules and the decreased average electron energy.

4.8.1 Excitation of the Upper Laser Level (n_1):

Since the excitation efficiency of the upper laser level is slightly reduced with the addition of CO and as the CO_2 partial pressure is held constant , no significant change in the upper laser level population is observed . See graphs (4.35) to (4.37). After direct excitation cut off, the upper laser level is replenished by a continuous supply of energy from both N_2(v=1) and CO (v=1) through resonant energy transfer processes (see figure 4.1).Increasing CO means that more resonant energy is transferred. This leads to a relatively constant value of the upper laser level population as shown in graph (4.35) .

4.8.2 Excitation of the Upper Nitrogen Level (n_5):

The decrease in the N_2 excitation efficiency produced by CO addition considerably decreases the N_2 direct excitation rate. This results in a decreased upper nitrogen level population as shown in graphs (4.38) to (4.40).

After direct excitation cessation, the exponential decay of the upper nitrogen level was observed to be almost unaffected by the addition of CO since the rate of energy transfer from CO (v=1) to N_2 is relatively small (K_{75}=490 $sec^{-1}.Torr^{-1}$ at 300°K,[Smith and Thomson, A4.I.2]).

4.8.3 Excitation of the upper CO level (n_7):

The upper CO level is populated very rapidly due to the increased ground level population and increased excitation efficiency.This is shown in graphs (4.41) to (4.43) . After direct excitation cut off, the upper CO level decays exponentially via its resonant interaction with CO_2.

4.8.4 Effects of Stimulated Emission on Delay Time and Spike Power:

The dominant features of CO addition to the gas mixture are:

(i) effective relaxation of the CO_2 (01^10) level where the rate constant for CO is about 8 times that of He (see Appendix A.2.II).

(ii) effective relaxation of the lower laser level, where CO has a comparable rate constant to He.

(iii) reduction in stimulated emission cross-section, see equation (4.21) where CO has a significant coefficient.

(iv) resonance transfer of energy from CO (v=1) level to CO_2 (00^o1).

When CO is added in amounts up to 50% of CO_2 , the CO_2 vibrational population is increased due to (iv) and the reduction in stimulated emission cross-section is relatively small as the coefficient applied to He is not substantially greater than that for CO. This, combined with (i) and (ii) allows a rapid population inversion and gives an increased gain as shown in graphs (4.44) to (4.46). The resulting stimulated emission is very rapid to build up and quickly overturns direct excitation giving a reduced delay time, see graphs (4.47 to 4.49). The main effect of CO shows up on the second pulse where it produces a long output tail so that at the start of the second pulse there is enough power and gain to reduce the delay time and spike height. These results are shown in graphs (4.50) and (4.51).

With a considerable amount of added CO ($CO:CO_2$ =1:1),the decrease in direct excitation rates of N_2 and CO_2 and the decrease in helium content both give a reduced population inversion. Hence,the resulting gain is slightly reduced, see graph (4.44).Reduced stimulated emission increases the delay time, especially for the first pulse,whereas the increase in the second pulse delay time is smaller due to the interpulse gain, see graph (4.50) .

4.8.5 Gas Mixture Temperature:

One of the beneficial effects of CO is that electrons below 1 eV can excite the vibrational levels of CO whilst they are ineffective in exciting N_2.Hence the addition of CO makes the coupling of the electrical energy into the discharge more efficient. It also reduces the low energy electron pumping of the lower CO_2 levels.These effects are greater than that due to the reduction in the heat capacity (mc_p) caused by CO substitution for He. This reduces the gas temperature as shown in graphs (4.52) to (4.55) . The vibrational energy left in CO is not instantly transformed into heat but remains in the gas for a long time [Basov et al , 4.14] . After direct excitation cut off, the stored energy in CO dissipates by collisional heating during the interpulse period. This is shown in graph (4.52) .

4.8.6 Pulse Duration and Mean Power:

Graph (4.56) shows that increased CO leads to a longer pulse duration due to the effect of CO on the output pulse profile where energy is released over a longer time period. This means that at the start of the second pulse , there is sufficient residual energy to suppress the gain switched spike, hence decreasing delay time and further increasing pulse length. In addition , as the CO content increases the corresponding decrease in helium content increases the pulse duration due to the decrease in the relaxation rate of the upper laser level.The mean power increases as the CO content is increased up to 50% of CO_2 as illustrated in graph (4.57) . With a continued increase in the CO content the mean power decreases , especially for helium rich mixtures due to the decreasing excitation efficiencies for CO_2 and N_2 . However, for a low helium mixture the mean power continues to increase with increasing CO ,graph (4.57), due to the increased pulse power and duration, as shown in graphs (4.47) and (4.56) .

4.8.7 Efficiencies:

Due to the improvement in the excitation efficiencies, CO improves the laser efficiency. Graphs (4.58) and (4.59) show this improvement in both the overall efficiency and the useful efficiency. The beneficial effect on the efficiency of the second pulse shown in graph (4.59) is due to the energy left in the pulse tail. However, in a helium rich gas mixture both efficiencies drop off when a considerable amount of CO is added (CO: CO_2 =1:1). This is due to the decreased mean power as can be seen from grpah (4.57) .

4.9 RESULTS AND DISCUSSION ; CASE THREE - GAS MIXTURES WITH CO ADDITION AS A SUBSTITUTE FOR NITROGEN :

It can be seen from Table (4.3) that when CO is added in amounts up to 50 % of the nitrogen content the average electron energy decreases and the excitation efficiency of CO_2 increases while that of N_2 decreases. When CO replaces all the N_2 in the gas mixture the operating value of E/N of the discharge and the average electron energy both slightly increase. The excitation efficiency of CO_2 decreases whereas that of CO increases due to the increased CO content.

4.9.1 Excitation of the Upper Laser Level (n_1):

Since the excitation efficiency of the upper laser level is increased with the addition of CO the population of the upper laser level increases as shown in graphs (4.60) and (4.61). However , when CO replaces all the nitrogen (graph 4.60) or substitutes for 50 % of the N_2 (graph 4.61) the population of the upper laser level decreases due to the decrease in the excitation efficiency of CO_2.

After direct excitation cut off , the upper laser level is replenished by a continuous supply of energy from both the N_2 (v=1) and CO (v=1) levels through resonant energy transfer processes.However,the transfer rate between CO(v=1) and CO_2 is less than that between N_2 (v=1) and CO_2 (see Appendix A4.I) therefore the energy supply during the interpulse period is reduced when CO replaces all the N_2.

4.9.2 Excitation of the Upper Nitrogen Level (n_5):

Graphs (4.62) and (4.63) show that the population of the upper nitrogen level decreases with the addition of CO due to the two-fold effect of decreased ground level population and decreased rate constant for direct excitation of N_2.

4.9.3 Excitation of the Upper CO level (n_7):

The population of the upper CO level increases with the increasing CO content as shown in graphs (4.64) and (4.65) due to the increased ground level population and increased excitation efficiency. After direct excitation cut off, the upper CO level decays exponentially via its resonant interaction with carbon dioxide. It can be seen from graphs (4.64) and (4.65) that this decay is relatively slow as compared with that of the upper nitrogen level (see graphs 4.62 and 4.63). This is due to the fact that the transfer rate between N_2(v=1) and CO_2 is more rapid than that between CO (v=1) and CO_2 (see Appendix A4.I).

4.9.4 Effects of Stimulated Emission on Pulse Delay Time and Spike Power:

Due to the effects of added CO (discussed in 4.8.4) an increase in the CO content up to 50% of the initial nitrogen content increases the population of the upper laser level and allows a rapid population inversion. This gives an increased gain as shown in graphs (4.66) and (4.67). The resulting stimulated emission rapidly build up and overturns direct excitation , giving a reduced delay time.

This is shown in graphs (4.68) and (4.69). This effect shows up on the second pulse, where CO produces a long output tail so at the start of the second pulse there is sufficient power and gain to reduce the delay time,see graph (4.70).

With increasing amounts of added CO, the decrease in the direct excitation rate of CO_2 decreases the population inversion . This , together with the reduction in stimulated emission cross section (see equation 4.21) reduces the gain as shown in graph (4.66).Reduced stimulated emission greatly increases the time required for stimulated emission to overcome direct excitation , this results in a greater delay time. Graph (4.70) shows this clearly.The second pulse delay time is smaller because of the residual gain and power left by the previous pulse.

It can be seen from grpahs (4.68) and (4.69) that when CO is substituted for 50 % of the nitrogen,very large spikes develop. This is because of the great population inversion magnitude left when the upper laser level collapses due to stimulated emission action.However , when CO is substituted for all the nitrogen , the resulting stimulated emission is relatively small. Hence, as shown in graph (4.68), a smaller spike is developed and the output pulse profile is highly oscillatory with a reduced mean power. This is due to both the de-stablising effect of resonant energy transfer between CO (v=1) to CO_2 and the reduced direct excitation rate for CO_2.

4.9.5 Gas Mixture Temperature:

For the same total pressure of N_2 and CO and a given input energy , an increase in the CO content relative to the N_2 hardly affects the maximum temperature because the thermal properties of CO are not much different from those of N_2. This is shown in graphs (4.72) and (4.73).

4.9.6 Pulse Duration and Mean Power:

Graph (4.74) shows the pulse duration variation with CO. It can be seen that increased CO initially leads to a higher pulse length for both the first and second pulses. This is due to the effect of CO on the output pulse profile as the energy is released over a longer time period , see graph (4.69). With increasing amounts of added CO,the pulse length decreases due to the increased delay time (as already discussed in section 4.9.4).

When CO is substituted for N_2 ,the increase in the pulse duration is smaller than that when CO is substituted for He (see graphs 4.56 and 4.74). This is due to the fact that He has more influence on the relaxation times of the excited molecules than nitrogen.The mean power for the nitrogen rich mixture shows an initial increase due to the increase in the excitation efficiencies for CO_2 and CO, see Table (4.3).This is shown in graph (4.75). With increasing amounts of added CO , the mean power decreases due to the spreading effect of CO on the output pulse profile and the decreased excitation efficiency of CO_2 and N_2. Graph (4.75) shows the significant decrease in the mean power when CO replaces all the N_2. This is in full agreement with the results of Basov et al [4.14].

4.9.7 Efficiencies:

Graphs (4.76) and (4.77) show the improvement in both the overall efficiency and the useful efficiency with the addition of small amounts of CO due to the improvement in the excitation efficiency of CO_2. However, with increasing CO, both efficiencies decrease due to the decreased population of $CO_2(00°1)$ and the increased relaxation rate K_{132}.

4.10 CONCLUSIONS :

This chapter is aimed at identifying optimum parameters for controlling laser output characteristics for materials processing applications. The simulations were carried out to investigate the effects of CO on the laser output pulses . Previous chapters show that CO has significant effects on both the electron energy distribution function and the negative - ion processes in the discharge. Moreover, the experimental results of Siemsen et al [4.3] show that the experimental gain is substantially lower than the theoretical predictions due to dissociation which becomes significant at high discharge currents.The present results show that CO has a substantial effect on the laser output and some of these effects could be used for improving the laser output.

These results lead to the following conclusions:

(1) Increasing helium in the gas mixture reduces the gas temperature and gives high powers over small time periods. Maximum powers and delay times are high.This is unsuitable for materials processing because of excessive plasma production.

(2) Increasing He reduces the gain after direct excitation cut off , this reduces the beneficial effect of the residual gain on subsequent pulses.

(3) Helium enrichment, up to a certain limit, improves the laser efficiency. Continued increase in the He content reduces the laser efficiency due to decreased excitation efficiencies and an increased relaxation rate of the upper laser level.

(4) Increasing nitrogen produces a long output pulse tail. This suppresses the gain switched spike for the second pulse , hence decreasing delay time and maximum power. Moreover, increasing N_2 improves the laser efficiency due to improvement in the excitation efficiency.

(5) Increasing the cavity length,up to 300 cm, decreases the delay time and maximum power , increases the laser efficiency due to increased pulse length and energy left in the pulse tail.

(6) The effects of increasing the front mirror reflectivity are similar to those of increasing the cavity length . However, due to physical problems of overheating and mirror damage a value of 0.85 has been chosen.

(7) When CO is substituted for helium (up to 50% of CO_2),the delay time decreases and the output pulse has a long tail. This increases the pulse duration and the mean power. With increasing CO in helium rich mixtures ,the delay time increases due to the decreased population inversion. Thus the mean power is decreased. Whereas in mixtures with low helium content the mean power

increases with increasing CO due to the increased pulse duration and pulse power.

(8) CO substitution for helium improves the laser efficiency due to its effects on the output pulse profile . The improvement increases in mixtures with low initial He content due to the beneficial effects of CO on the gas temperature and relaxation rates of the excited levels.

(9) When CO is substituted for up to 50 % of the N_2, the delay time is reduced , especially for the second pulse due to the energy left in the previous pulse tail. The resulting maximum power increases due to great magnitude of population inversion left when stimulated emission overturns direct excitation . The laser efficiency increases due to increased excitation efficiency.

(10) When CO is substituted for all of the N_2, the output pulse has high oscillation and the mean power is greatly reduced due to the de-stablising effect of resonant energy transfer between CO (v=1) and CO_2. This, together with the decrease in both the overall efficiency and useful efficiency clearly make this mixture unattractive for a high power CO_2 laser.

(11) In general the second pulse is enhanced due to residual gain from the previous pulse.

(12) The following mixture is recommended if all arguments of temperature and second pulse profile are taken account of:

P_{CO2}	:	P_{N2}	:	P_{He}	:	P_{CO}	Torr
13.5	:	20.25	:	81	:	6.75	

REFERENCES

CHAPTER FOUR

4.1 Chatwin C R and Scott B F -'High PRF Nitrogen-Carbon dioxide laser for continuous manufacturing process in metals'-1 Int. Conf.on Lasers in Manufacturing, Brighton, U.K ,1983.

4.2 Byabagambi C A ,Chatwin C R,and Scott B F -' Prediction of output power from high pulse repitition frequency CO_2 lasers for use in manufacturing processes'-3 Int. Conf. on Optical and Optoelectronics, Applied Science and Engineering, Innsbruck, April 1986.

4.3 Siemsen J K ,Reid J,and Dang C - ' New Techniques for Determining Vibrational Temperatures, Dissociation, and Gain Limitations in CW CO_2 Lasers '-IEEE J.QE , 16, 1980(668).

4.4 Chatwin C R - ' Thermodynamics of pulsed CO_2 laser for machining metals'-Ph.D Thesis, University of Birmingham, 1980.

4.5 Byabagambi C A -' Surface Heating in Metals Irradiated by Fast I.R. Laser Pulses ' - Ph.D Thesis , University of Glasgow, 1987.

4.6 Reid J and Siemsen J K-'Gain of High-Pressure CO_2 lasers' - IEEE J.QE. , 14 , 1978 (217).

4.7 Brimacombe R K and Reid J - ' Measurements of Anomalous Gain Coefficients in Transversely Excited CO_2 Lasers'- IEEE J.QE. , 19 , 1983 (1674).

4.8 Sato H and Miura Y -'Line Shape Parameter Analysis of Individual Vibrational-Rotational Transitions in a CO_2 Laser Amplifier '- IEEE J.QE., 19 ,1983 (410).

4.9 Hoffman A L and Vlases G C -' A Simplified Model For Predicting Gain,Saturation, and Pulse Length For Gas Dynamic Lasers ' - IEEE J.QE., 8 , 1972 (46).

4.10 Brimacombe R K and Reid J -'Accurate Measurements of Pressure-Broadened Linewidths in a Transversely Excited CO_2 Discharge '-IEEE J.QE.,19,1983 (1668).

4.11 Hall G and Watt J M - ' Modern Numerical Methods for Ordinary Differential Equations '- Clarendon Press, Oxford,1976.

4.12 Khahra JS - Ph.D Theses , University of Birmingham , 1976.

4.13 DeMaria A J -'Review of CW High-Power CO_2 Lasers'- Proc. IEEE , Vol. 61 , No 6 , 1973 (731) .

4.14 Basov N G , Glotov E P ,Danilychev V A , Kerimov O M , Malysh M M ,and Soroka A M - ' High - power Electroionization CO_2 and CO Lasers For Industrial Applications '- IEEE J. QE. , 21 , 1985 (342).

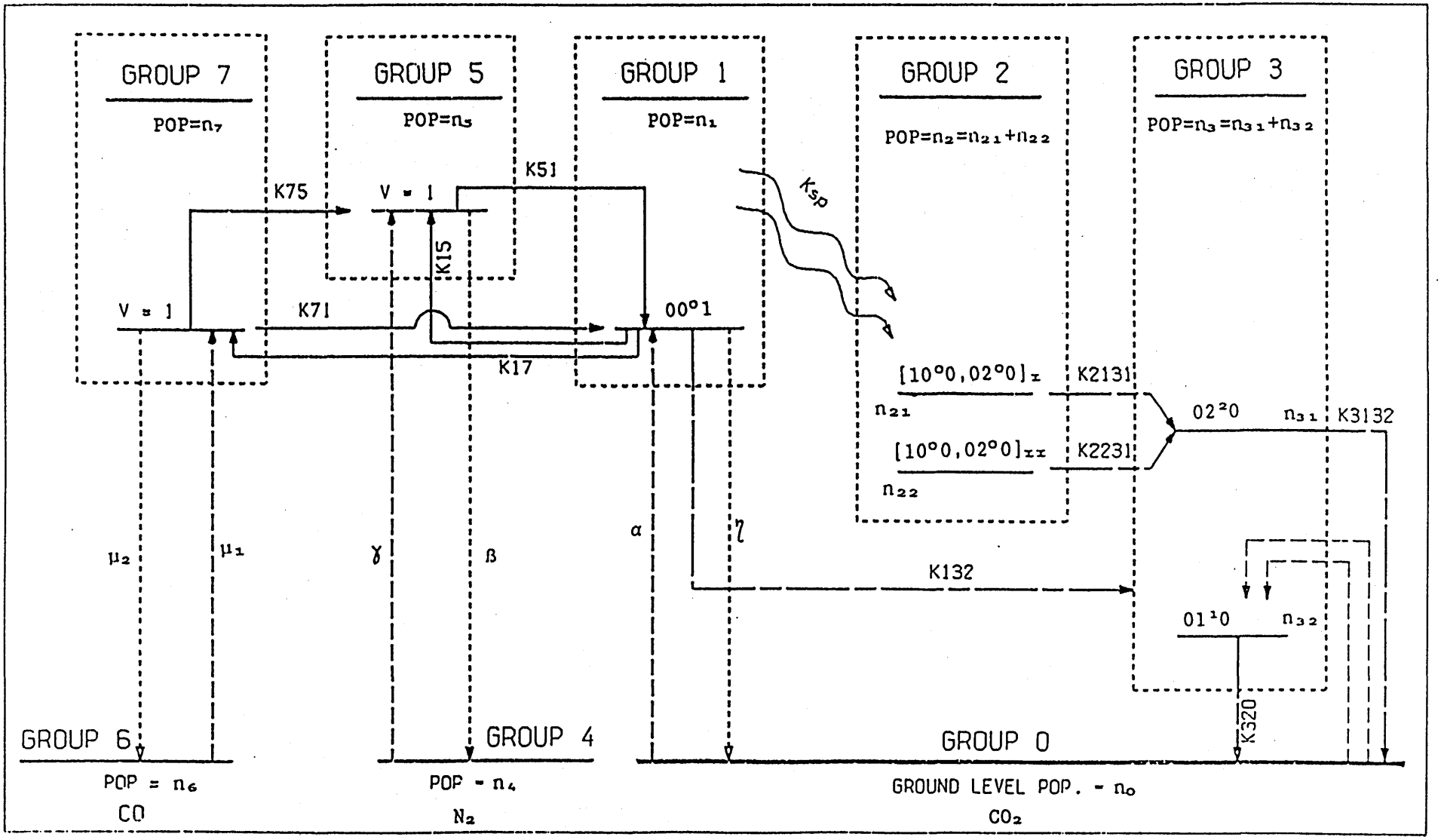

Energy Level Diagram for CO_2, N_2, and CO

FIGURE (4.1)

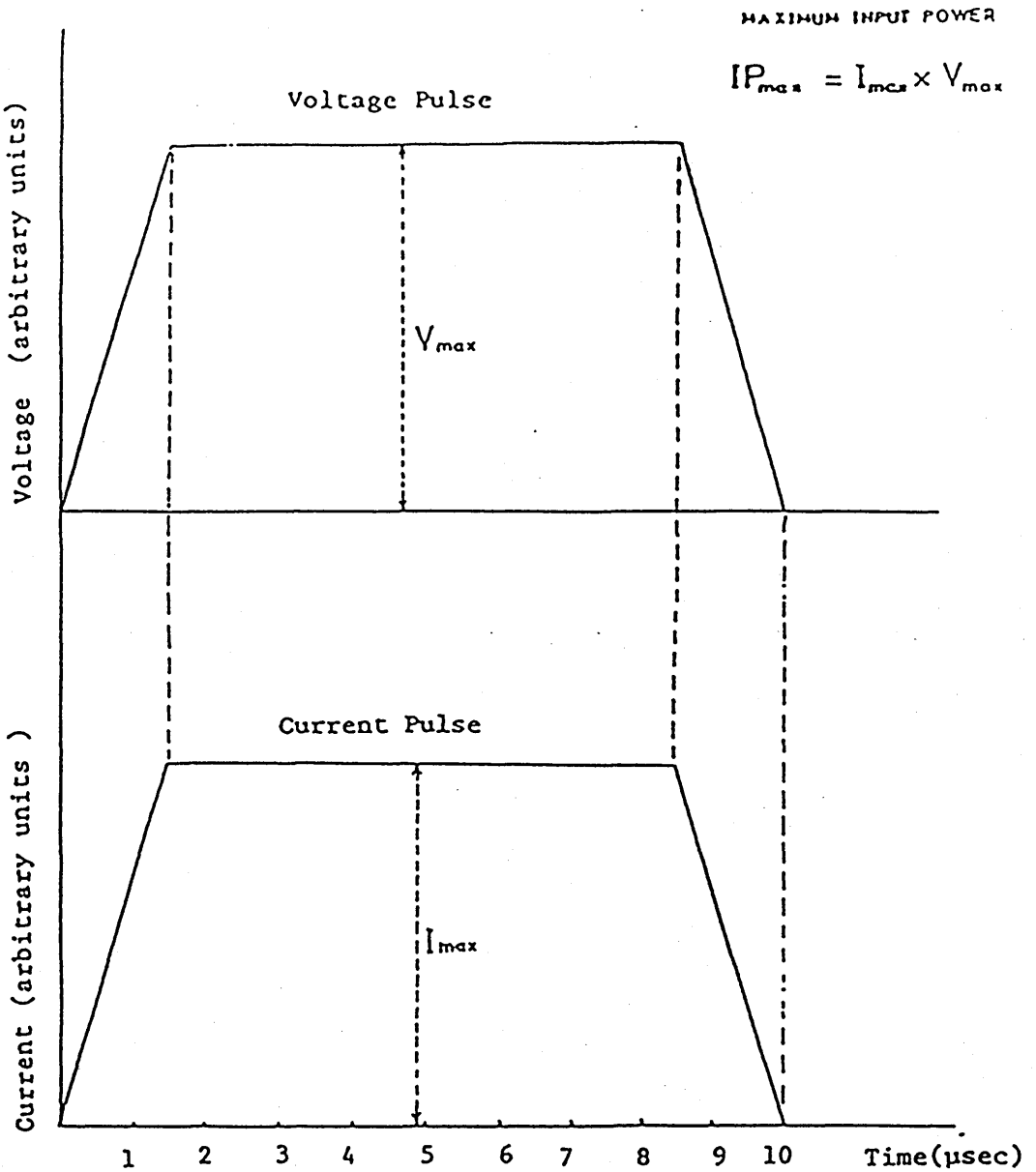

VOLTAGE AND CURRENT PULSE SHAPES USED FOR THEORETICAL CALCULATION OF LASER OUTPUT

FIGURE (4.2)

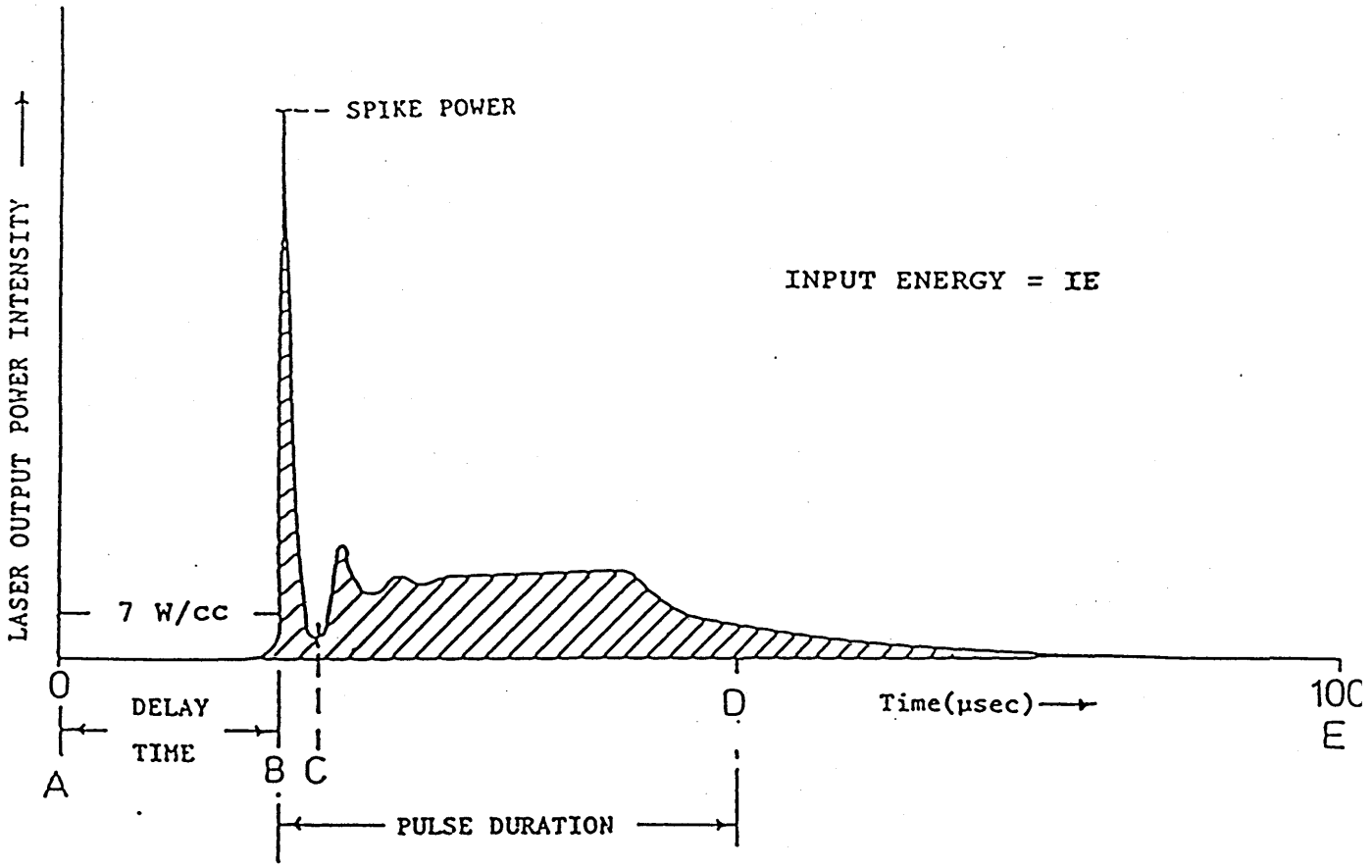

(i) PULSE ENERGY (PE) =INTEGRATE BETWEEN B AND D .

(ii) TOTAL OUTPUT ENERGY (TOE) =INTEGRATE BETWEEN B AND E .

(iii) FLAT PULSE POWER (FPP) =INTEGRATE BETWEEN C AND D AND DIVIDE BY TIME (C-D) .

(iv) USEFUL EFFICIENCY , η_{us} = (PE/IE) x 100 % .

(V) OVERALL EFFICIENCY , η_{oy} = (TOE/IE) x 100 % .

PULSE PARAMETERS

FIGURE (4.3)

TABLE (4. 1)

GAS DISCHARGE EXPERIMENTAL DATA

Mixture	Total Pressure $P_{CO2}+P_{N2}$=27 Torr	E/N x 10^{-16} Volt. cm^2	U eV	Excit. Eff. F_{N2}	Excit. Eff. F_{CO2}	E Volt/cm	I Amps
1:1:0	27	8. 757	1. 627	0. 3556	0. 0765	762. 21	141. 9451
1:1:2	54	5. 224	1. 577	0. 3635	0. 0803	909. 36	118. 9759
1:1:4	81	3. 989	1. 558	0. 3645	0. 0816	1041. 66	103. 8649
1:1:6	108	3. 291	1. 528	0. 3711	0. 0838	1145. 88	94. 4182
1:1:8	135	2. 894	1. 529	0. 3680	0. 0835	1259. 55	85. 8973
1:2:0	27	8. 521	1. 437	0. 4742	0. 0563	742. 23	145. 7661
1:2:2	45	5. 828	1. 434	0. 4745	0. 0568	845. 55	127. 9545
1:2:4	63	4. 606	1. 427	0. 4748	0. 0574	935. 55	115. 6453
1:2:6	81	3. 902	1. 424	0. 4741	0. 0576	1018. 98	106. 1767
1:2:8	99	3. 502	1. 45	0. 4616	0. 0560	1117. 71	96. 7979
1:3:0	27	8. 384	1. 348	0. 5321	0. 0442	729. 81	148. 2468
1:3:2	40. 5	6. 204	1. 357	0. 5327	0. 0446	810. 00	133. 5703
1:3:4	54	5. 041	1. 355	0. 5330	0. 0450	877. 50	123. 2957
1:3:6	67. 5	4. 358	1. 365	0. 5274	0. 0445	948. 37	114. 0820
1:3:8	81	3. 927	1. 388	0. 5160	0. 0434	1025. 36	105. 5161

TABLE (4.2)

GAS DISCHARGE EXPERIMENTAL DATA

Mixture CO_2 : N_2 : He : CO	P_{total} (P_{CO2}=13.5) (Torr)	E/N $\times 10^{-16}$ Volt.cm^2	U (eV)	Excit. Eff. F_{N2}	F_{CO2}	F_{CO}	E (Volt/cm)	I (Amps)
1 : 1 : 8.00 : 0.00	135	2.8941	1.529	0.3680	0.0835	0.00	1259.5	85.8973
1 : 1 : 7.78 : 0.22	135	2.7218	1.283	0.3896	0.0911	0.0897	1184.5	91.3368
1 : 1 : 7.50 : 0.50	135	2.9034	1.240	0.3610	0.0863	0.1771	1263.6	85.6226
1 : 1 : 7.22 : 0.78	135	2.9904	1.185	0.3280	0.0795	0.2528	1301.4	83.1329
1 : 1 : 7.00 : 1.00	135	3.2604	1.220	0.3030	0.0781	0.2877	1418.9	76.2478
1 : 1 : 6.00 : 0.00	108	3.2911	1.528	0.3711	0.0838	0.00	1145.8	94.4182
1 : 1 : 5.78 : 0.22	108	3.2015	1.317	0.3783	0.0872	0.0915	1114.5	97.0715
1 : 1 : 5.50 : 0.50	108	3.3112	1.238	0.3484	0.0830	0.1784	1152.3	93.8813
1 : 1 : 5.22 : 0.78	108	3.4794	1.202	0.3154	0.0773	0.2479	1210.7	89.3646
1 : 1 : 5.00 : 1.00	108	3.6078	1.174	0.2920	0.0763	0.2722	1256.1	86.1373
1 : 1 : 4.00 : 0.00	81	3.9891	1.558	0.3645	0.0816	0.00	1041.6	103.8649
1 : 1 : 3.78 : 0.22	81	3.8965	1.348	0.3729	0.0848	0.0868	1017.5	106.3357
1 : 1 : 3.50 : 0.50	81	4.0636	1.260	0.3415	0.0802	0.1754	1061.1	101.9624
1 : 1 : 3.22 : 0.78	81	4.2451	1.212	0.3113	0.0760	0.2485	1108.5	97.6040
1 : 1 : 3.00 : 1.00	81	4.5459	1.090	0.2821	0.0734	0.2585	1187.1	91.1449

TABLE (4.3)

GAS DISCHARGE EXPERIMENTAL DATA

Mixture	P_{total} (P_{CO2}=13.5) (Torr)	E/N x 10^{-16} Volt.cm^2	U (eV)	Excit. Eff.			E (Volt/cm)	I (Amps)
CO_2 : N_2 : He : CO				F_{N2}	F_{CO2}	F_{CO}		
1 : 1.00 : 6 : 0.00	108	3.2911	1.588	0.3711	0.0838	0.00	1145.8	94.4182
1 : 0.50 : 6 : 0.50	108	3.0406	1.346	0.2209	0.0951	0.2116	1058.6	102.2025
1 : 0.00 : 6 : 1.00	108	3.1355	1.412	0.00	0.0928	0.4067	1091.6	99.1091
1 : 2.00 : 6 : 0.00	121.5	3.9021	1.427	0.4748	0.0574	0.00	1528.5	70.7845
1 : 1.50 : 6 : 0.50	121.5	3.4222	1.201	0.4216	0.0708	0.1515	1340.4	80.7162
1 : 1.00 : 6 : 1.00	121.5	3.4965	1.225	0.2817	0.0687	0.2869	1369.5	79.00

POPULATION OF UPPER LASER LEVEL VERSUS TIME

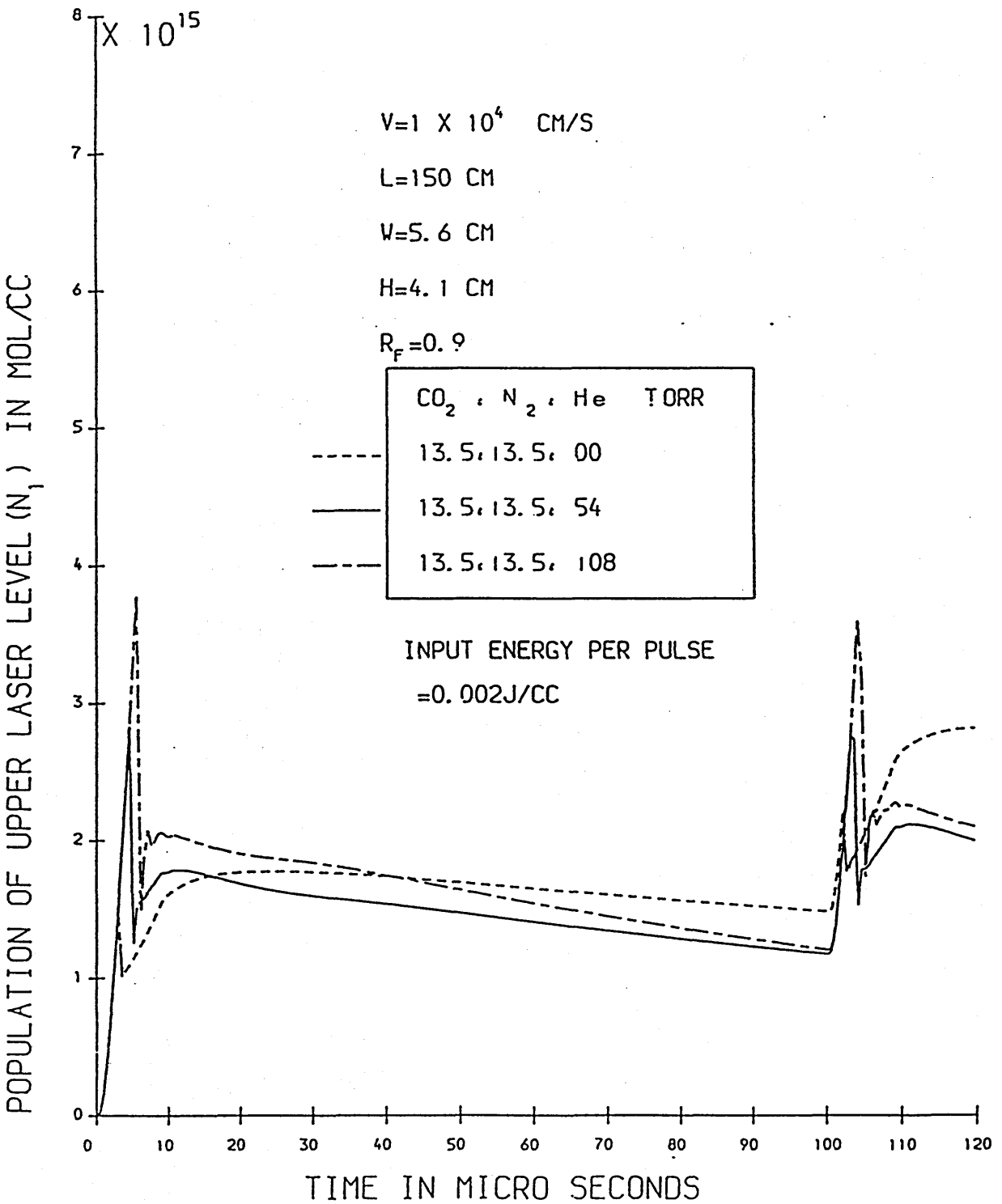

GRAPH (4.1)

POPULATION OF UPPER LASER LEVEL VERSUS TIME

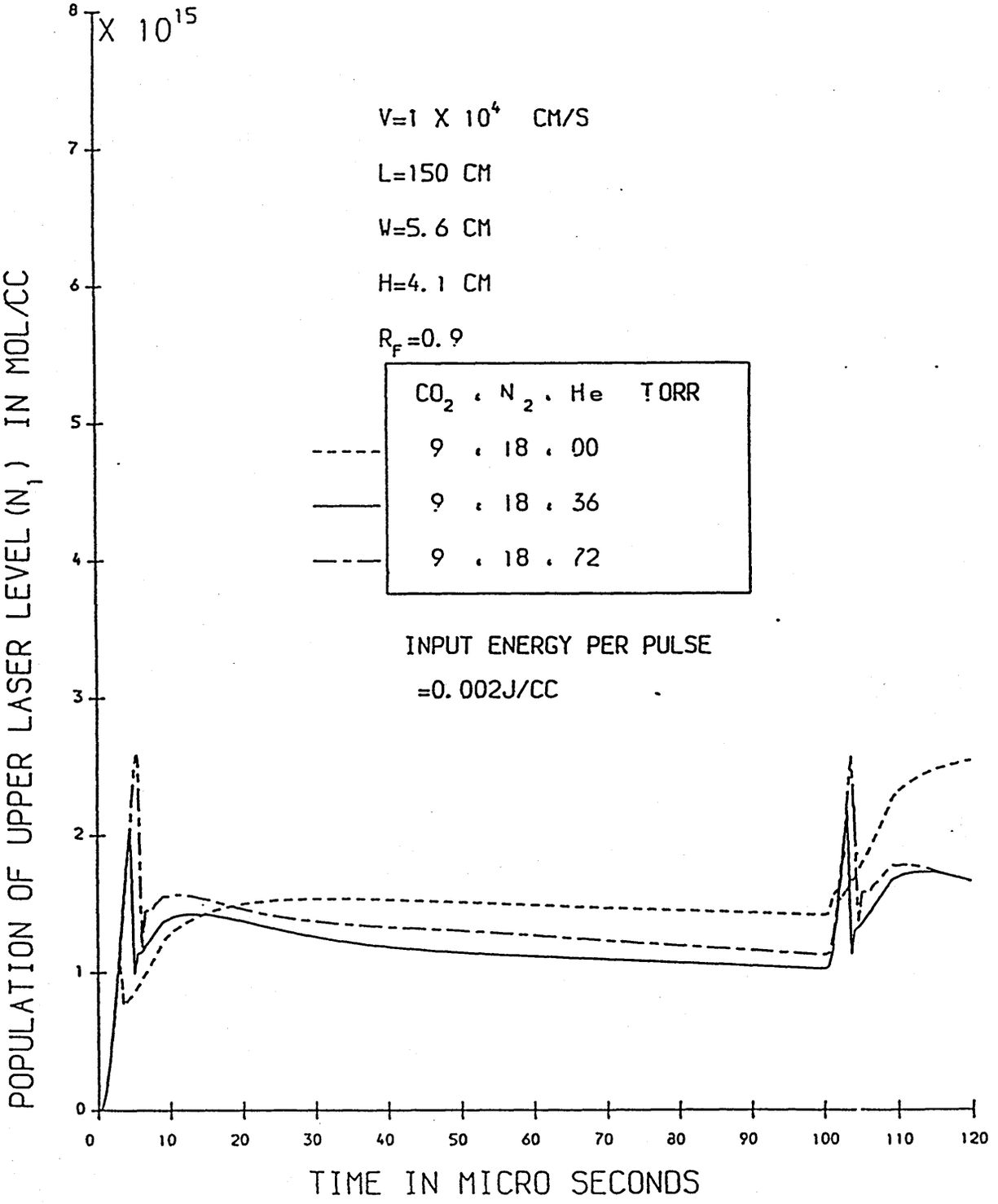

GRAPH (4.2)

POPULATION OF UPPER LASER LEVEL VERSUS TIME

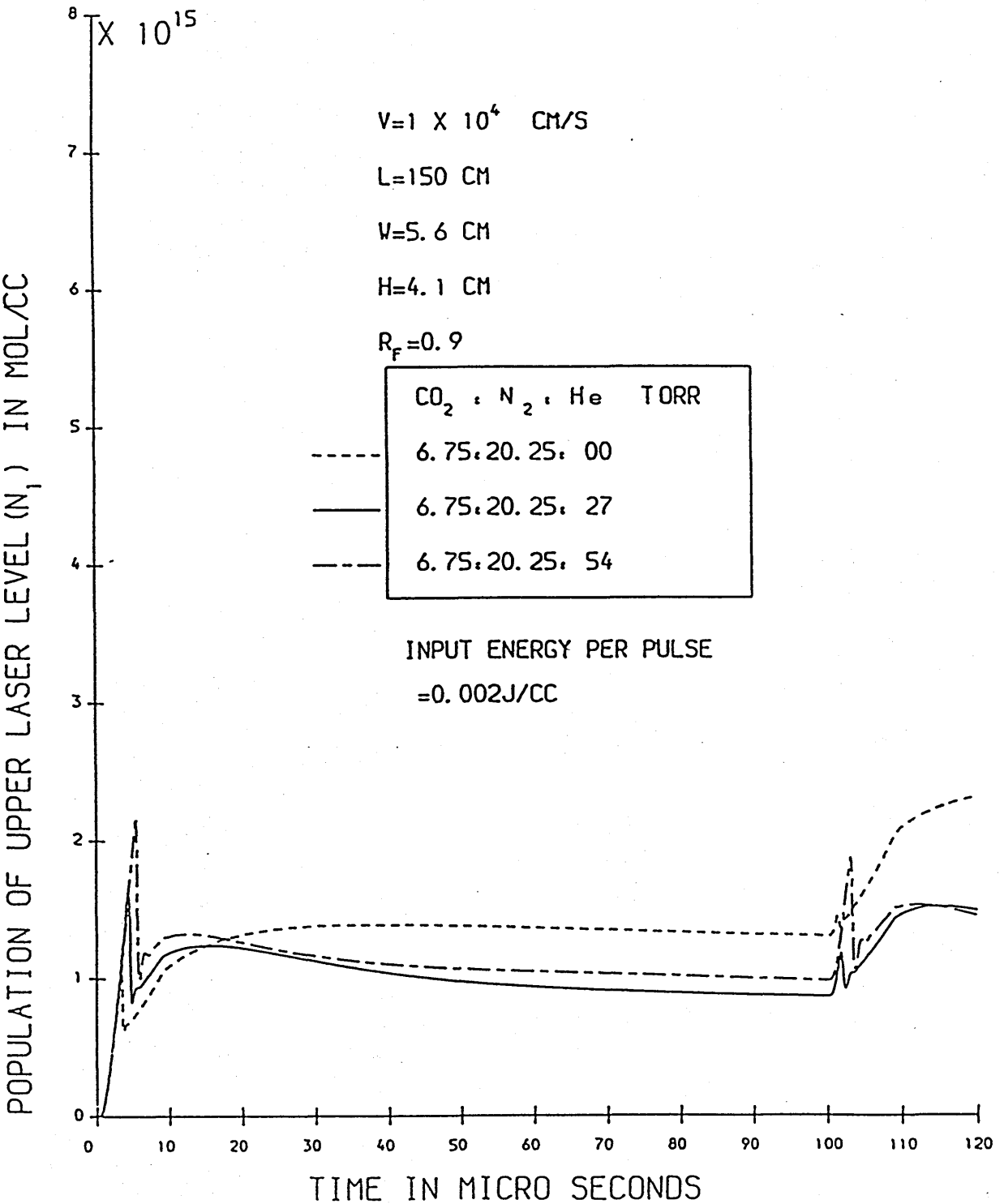

GRAPH (4.3)

POPULATION OF UPPER NITROGEN LEVEL VERSUS TIME

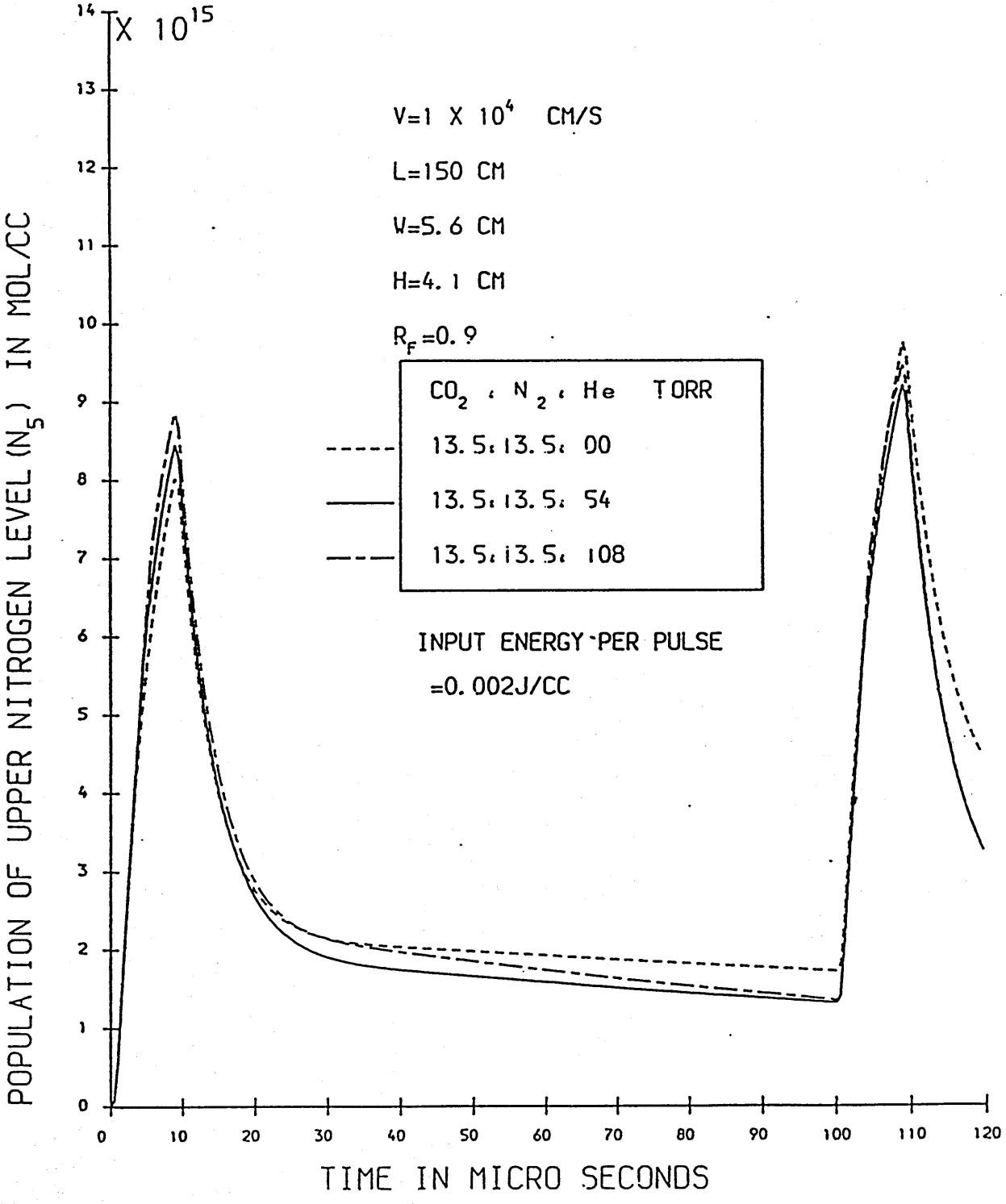

GRAPH (4.4)

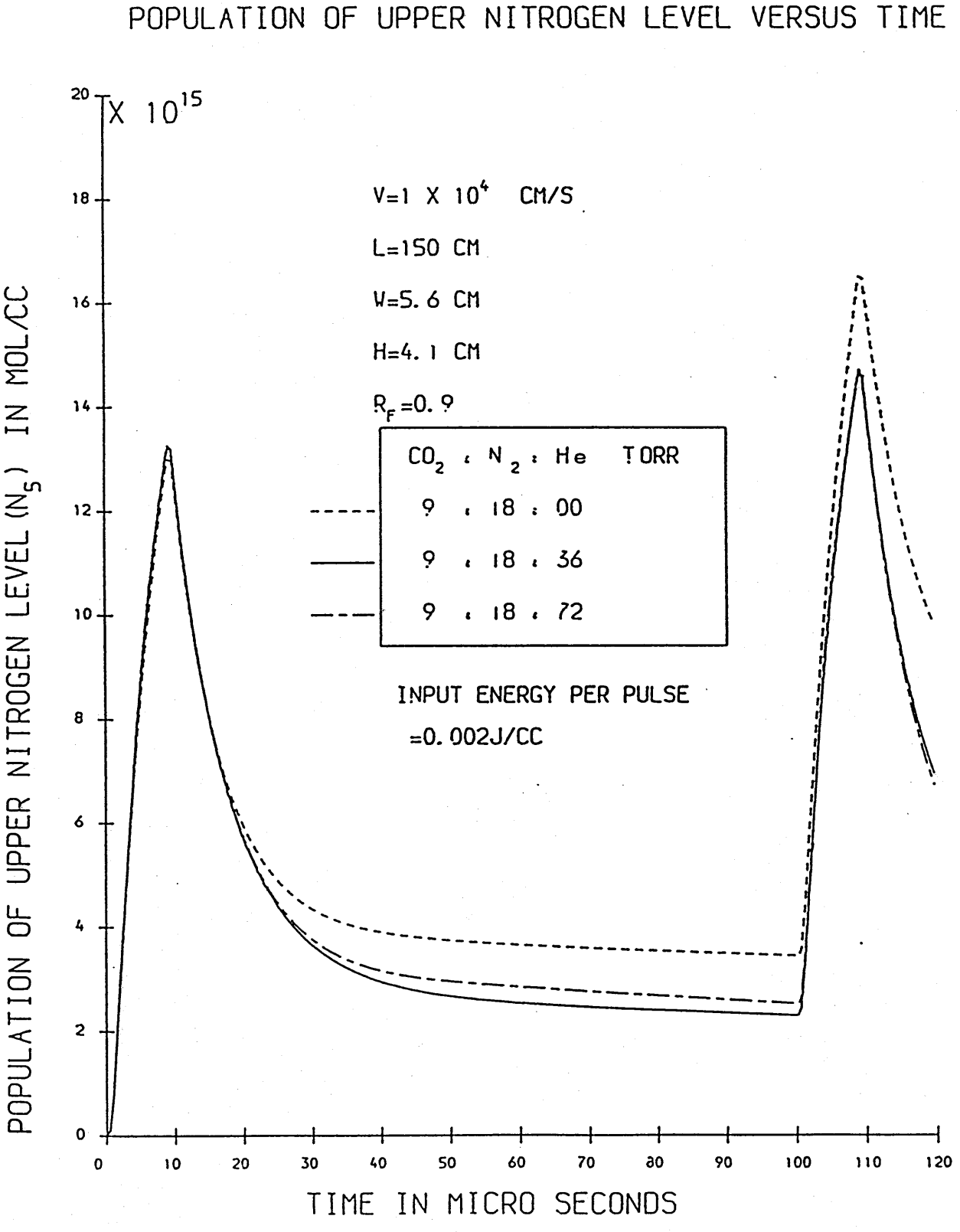
POPULATION OF UPPER NITROGEN LEVEL VERSUS TIME
X 10^15
V=1 X 10^4 CM/S
L=150 CM
W=5.6 CM
H=4.1 CM
R_F=0.9
CO2 : N2 : He TORR
9 : 18 : 00
9 : 18 : 36
9 : 18 : 72
INPUT ENERGY PER PULSE
=0.002J/CC
POPULATION OF UPPER NITROGEN LEVEL (N5) IN MOL/CC
TIME IN MICRO SECONDS
0
2
4
6
8
10
12
14
16
18
20
0
10
20
30
40
50
60
70
80
90
100
110
120

GRAPH (4.5)

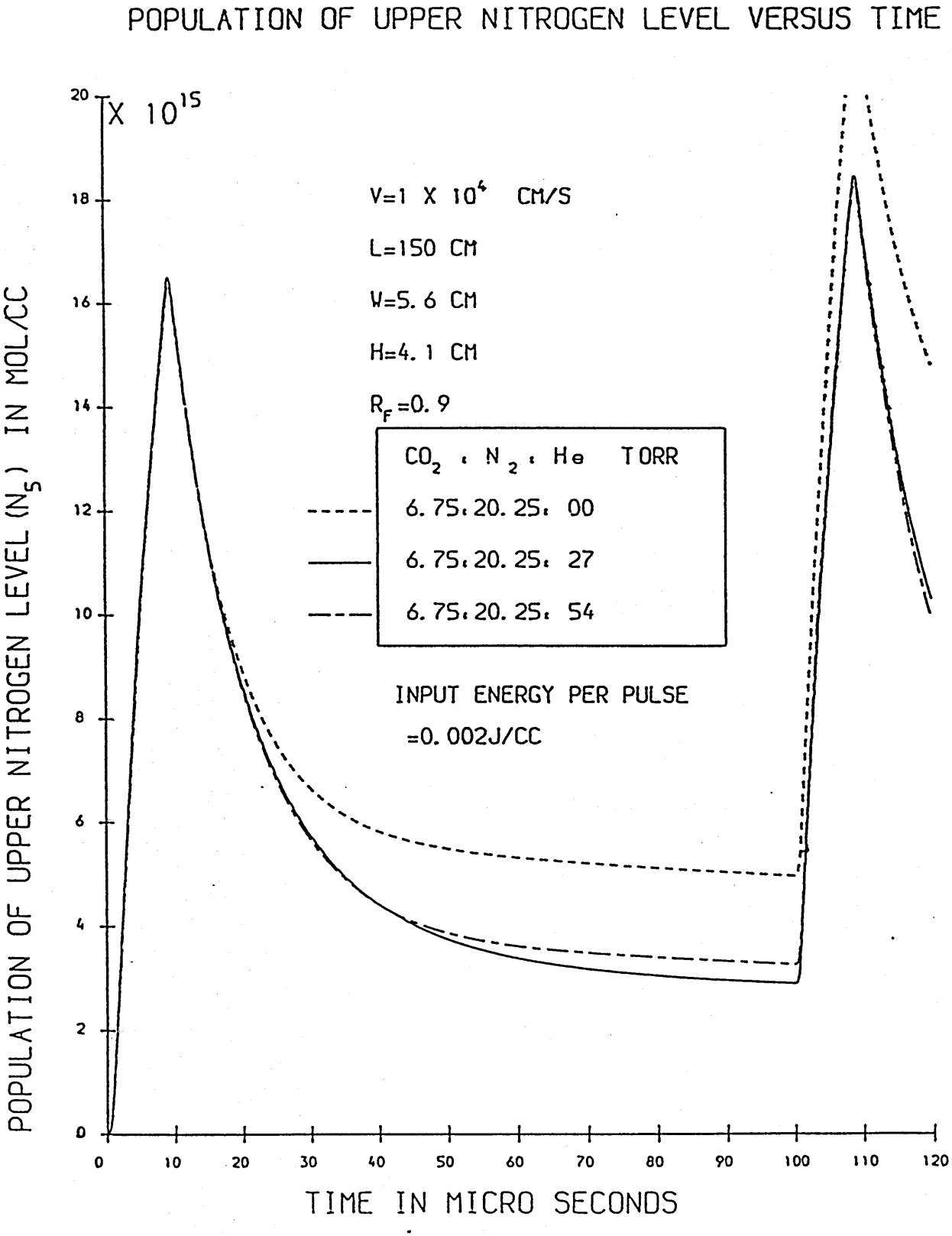
POPULATION OF UPPER NITROGEN LEVEL VERSUS TIME
X 10^15
V=1 X 10^4 CM/S
L=150 CM
W=5.6 CM
H=4.1 CM
R_F=0.9
CO2 : N2 : He TORR
6.75: 20.25: 00
6.75: 20.25: 27
6.75: 20.25: 54
INPUT ENERGY PER PULSE
=0.002J/CC
POPULATION OF UPPER NITROGEN LEVEL (N5) IN MOL/CC
TIME IN MICRO SECONDS
0
2
4
6
8
10
12
14
16
18
20
0
10
20
30
40
50
60
70
80
90
100
110
120

GRAPH (4.6)

GAIN VERSUS TIME

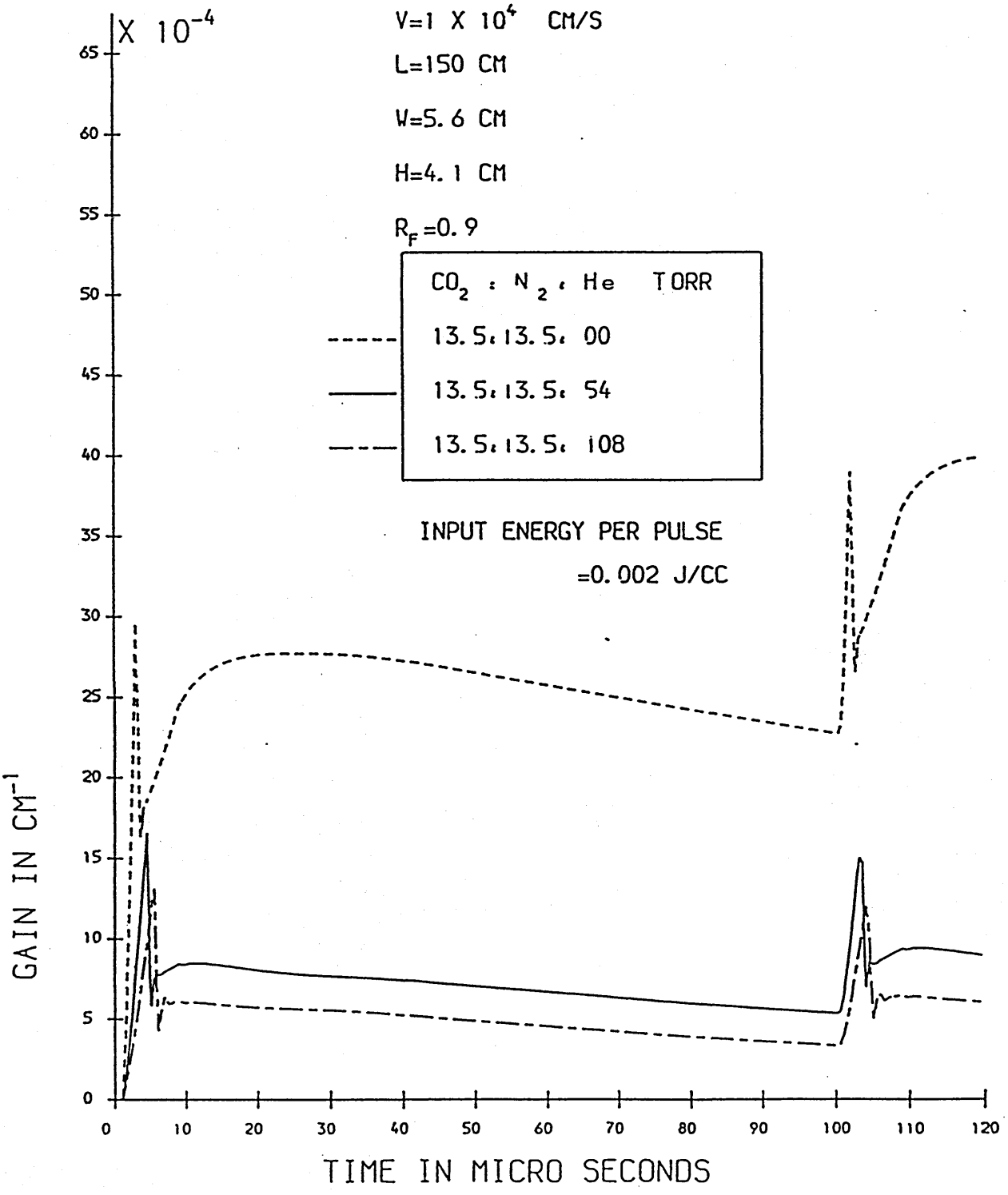

GRAPH (4.7)

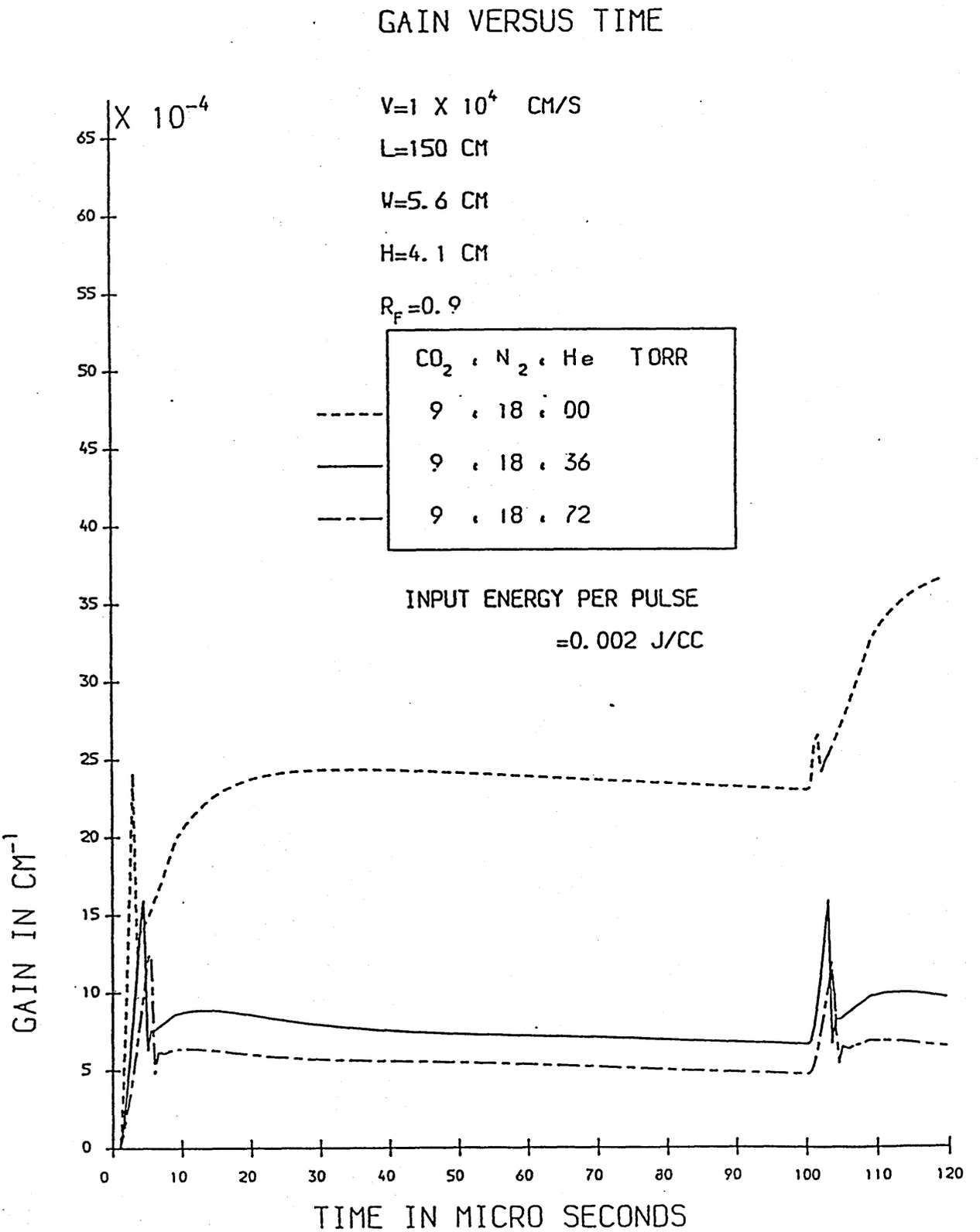
GAIN VERSUS TIME
X 10^-4
V=1 X 10^4 CM/S
L=150 CM
W=5.6 CM
H=4.1 CM
R_F=0.9
CO2 : N2 : He TORR
9 : 18 : 00
9 : 18 : 36
9 : 18 : 72
INPUT ENERGY PER PULSE
=0.002 J/CC
GAIN IN CM^-1
TIME IN MICRO SECONDS
0
5
10
15
20
25
30
35
40
45
50
55
60
65
0
10
20
30
40
50
60
70
80
90
100
110
120

GRAPH (4.8)

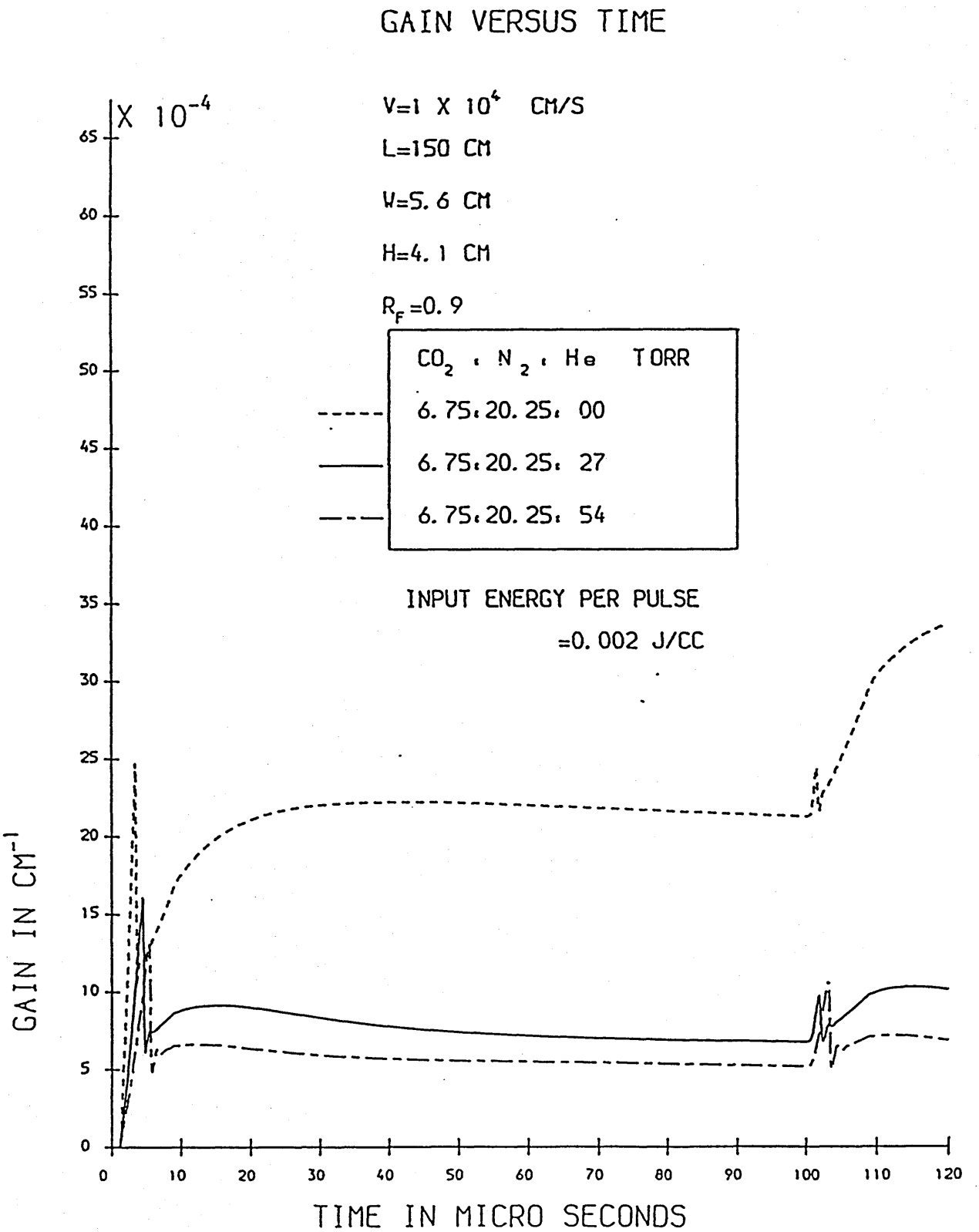
GAIN VERSUS TIME
X 10^{-4}
V=1 X 10^4 CM/S
L=150 CM
W=5.6 CM
H=4.1 CM
R_F=0.9
CO_2 : N_2 : He TORR
6.75: 20.25: 00
6.75: 20.25: 27
6.75: 20.25: 54
INPUT ENERGY PER PULSE
=0.002 J/CC
GAIN IN CM^{-1}
TIME IN MICRO SECONDS
0
5
10
15
20
25
30
35
40
45
50
55
60
65
0
10
20
30
40
50
60
70
80
90
100
110
120

GRAPH (4.9)

TEMPERATURE OF LASER GASES VERSUS TIME

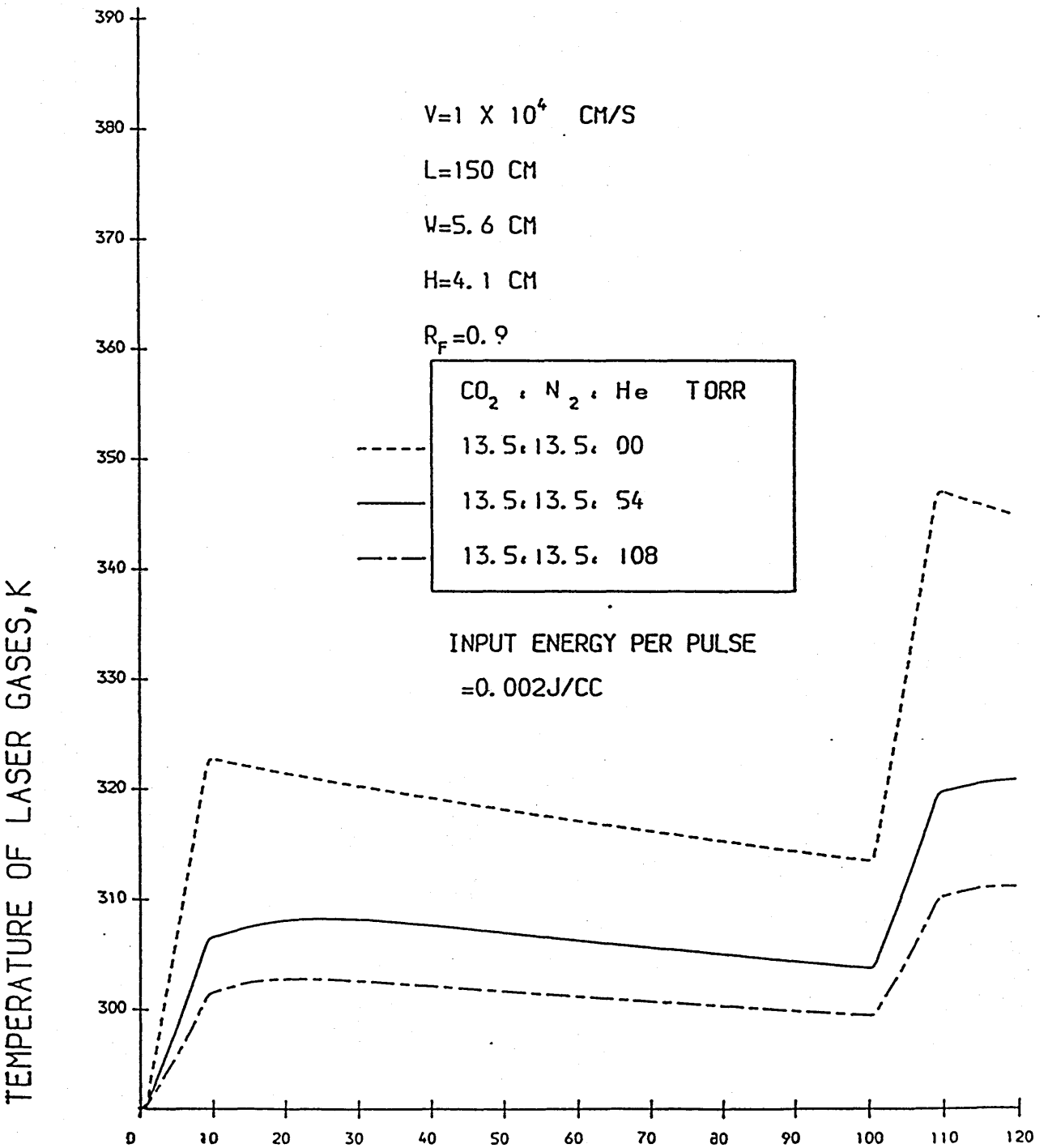

GRAPH (4.10)

TEMPERATURE OF LASER GASES VERSUS TIME

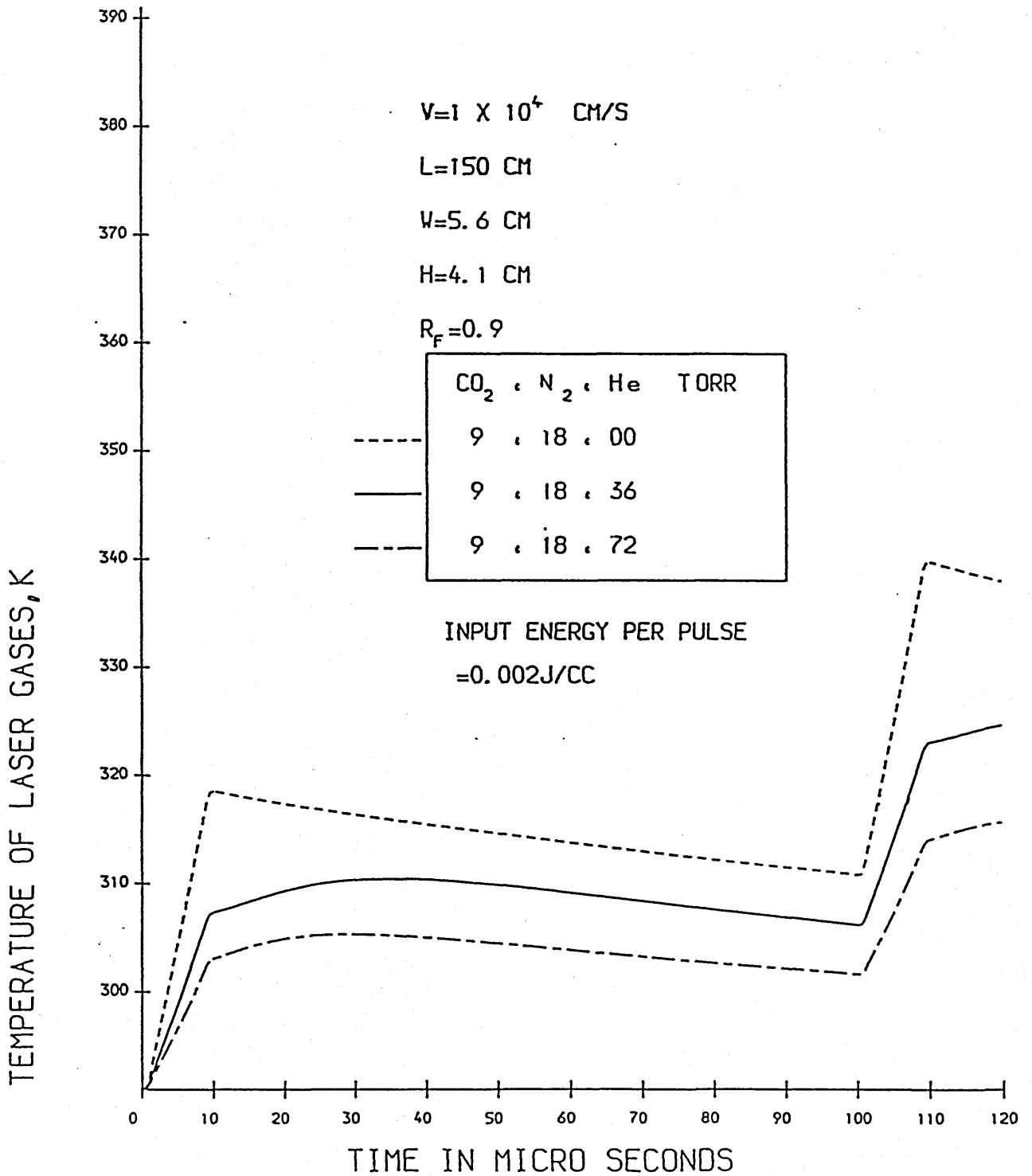

GRAPH (4.11)

TEMPERATURE OF LASER GASES VERSUS TIME

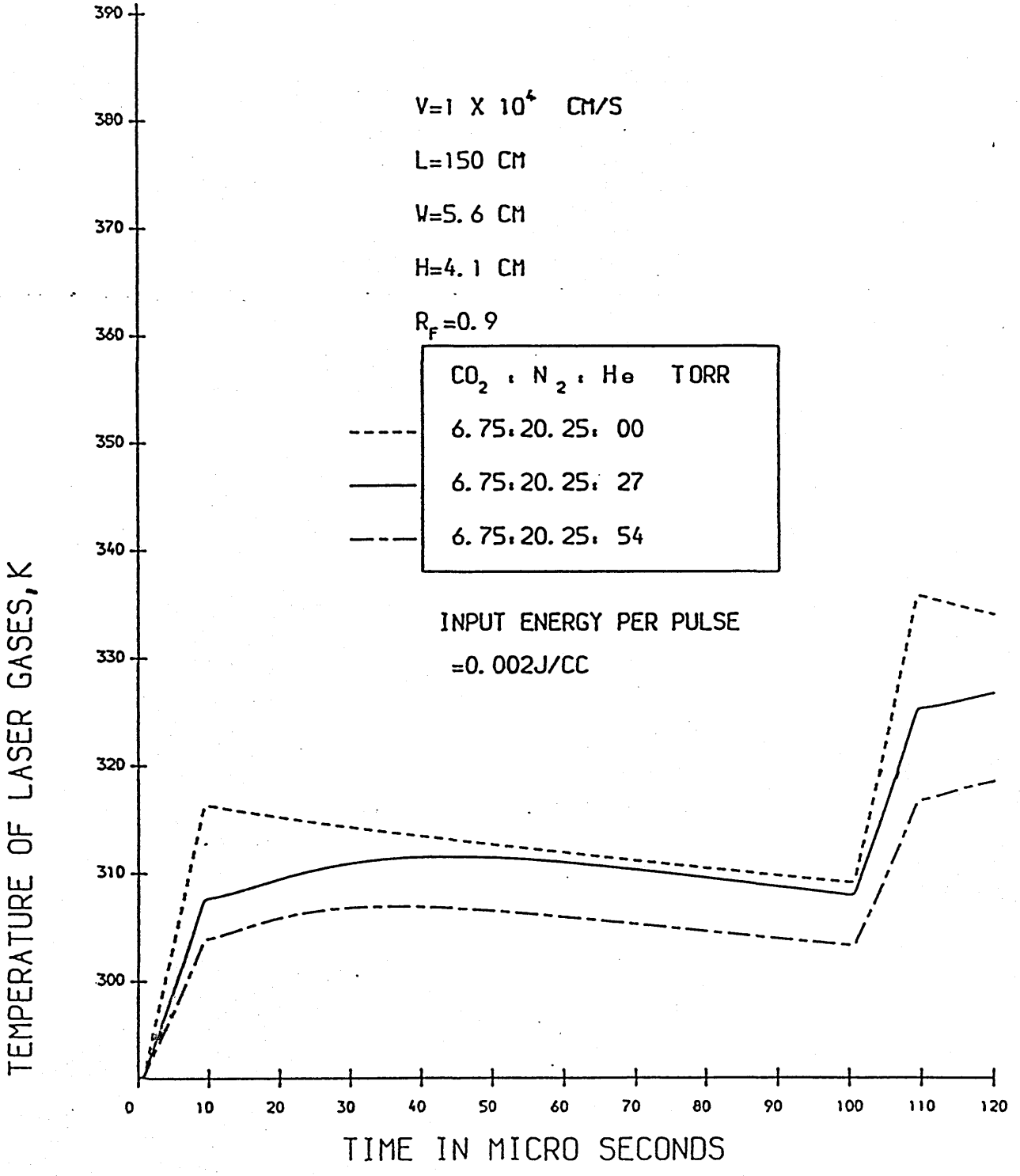

GRAPH (4.12)

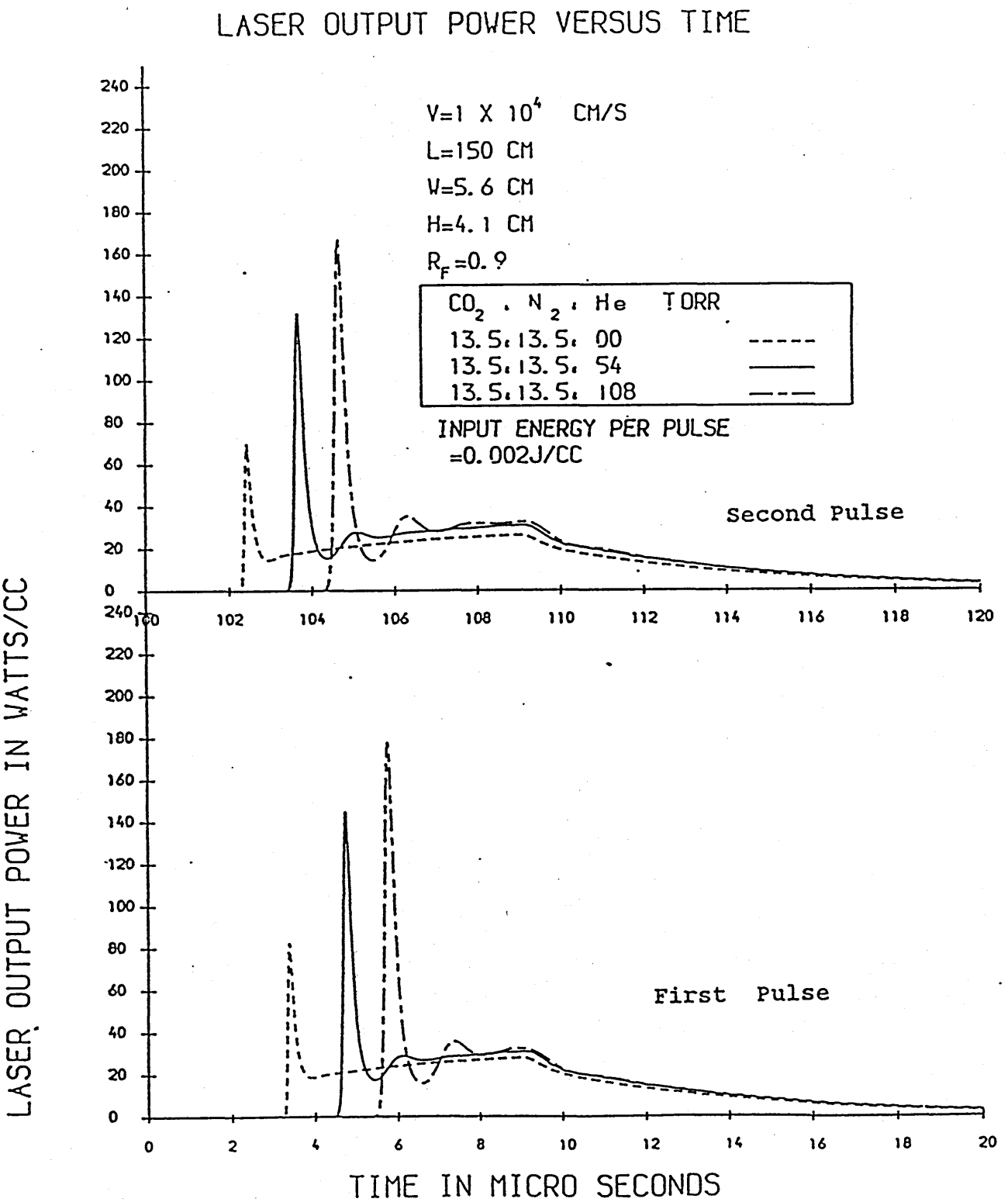
LASER OUTPUT POWER VERSUS TIME
V=1 X 10⁴ CM/S
L=150 CM
W=5.6 CM
H=4.1 CM
R_F=0.9
CO₂ , N₂ , He TORR
13.5, 13.5, 00
13.5, 13.5, 54
13.5, 13.5, 108
INPUT ENERGY PER PULSE
=0.002J/CC
Second Pulse
First Pulse
LASER OUTPUT POWER IN WATTS/CC
TIME IN MICRO SECONDS

GRAPH (4. 13)

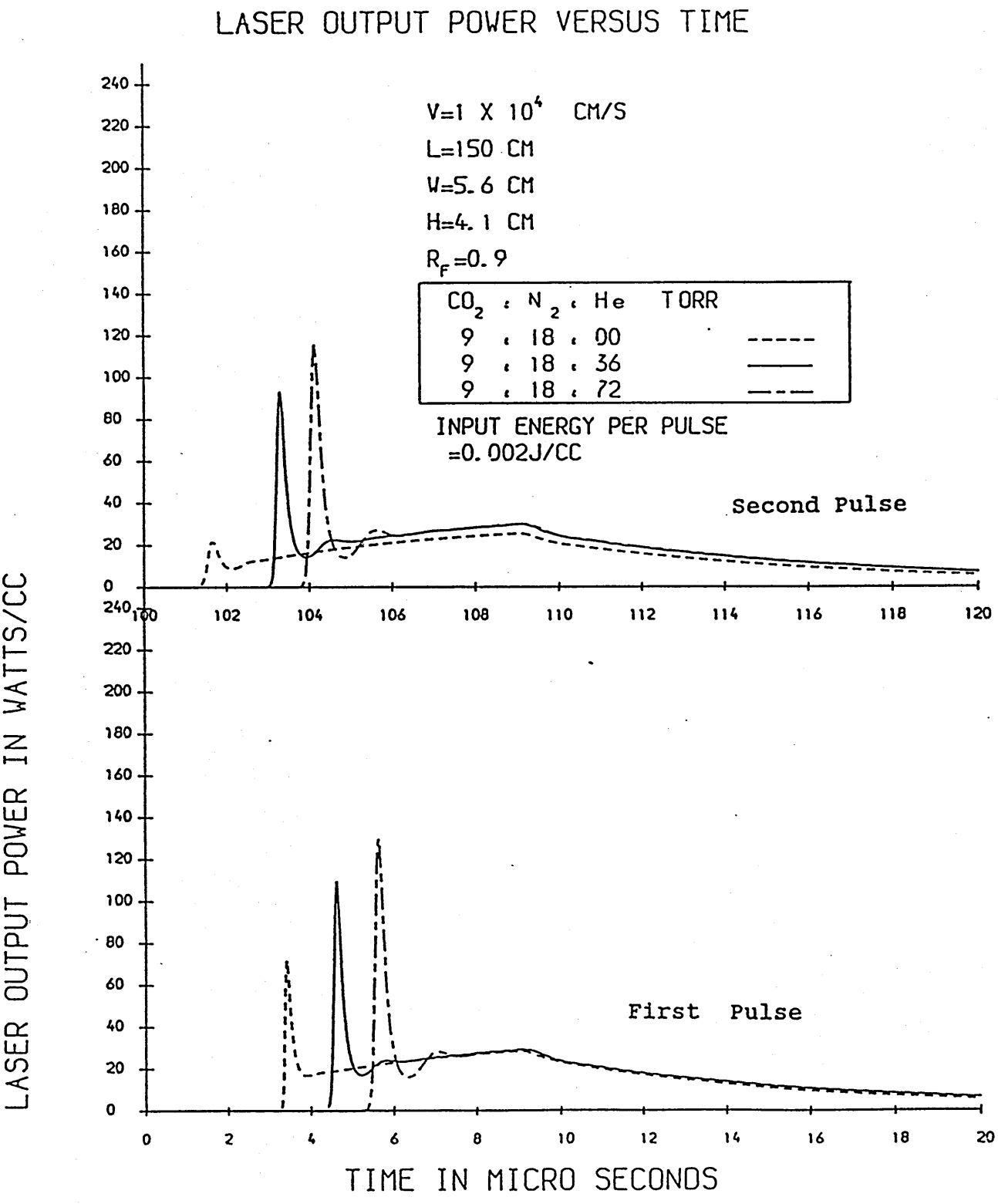
LASER OUTPUT POWER VERSUS TIME
V=1 X 10^4 CM/S
L=150 CM
W=5.6 CM
H=4.1 CM
R_F=0.9
CO2 : N2 : He TORR
9 : 18 : 00
9 : 18 : 36
9 : 18 : 72
INPUT ENERGY PER PULSE
=0.002J/CC
Second Pulse
First Pulse
LASER OUTPUT POWER IN WATTS/CC
TIME IN MICRO SECONDS

GRAPH (4.14)

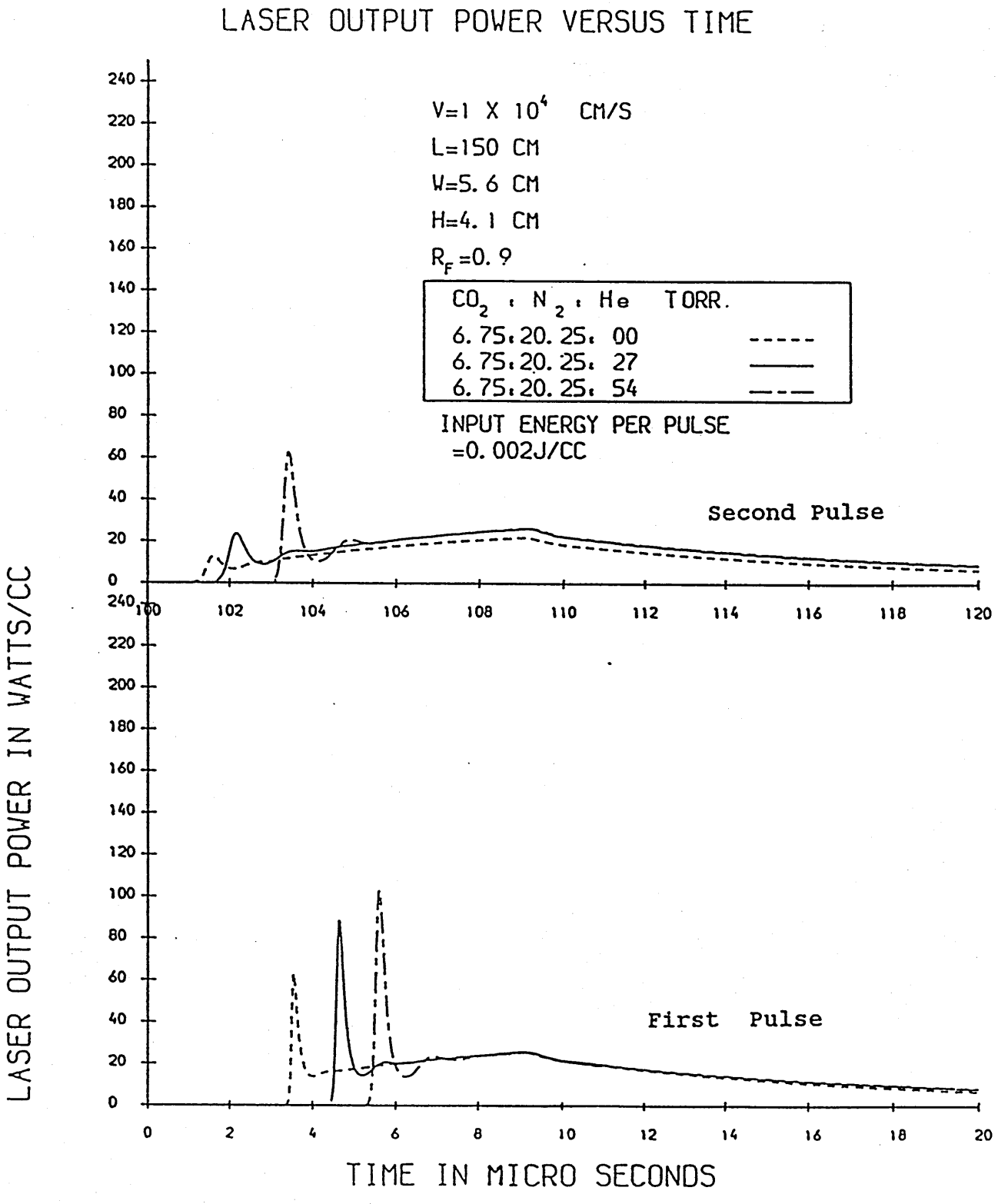
LASER OUTPUT POWER VERSUS TIME
V=1 X 10^4 CM/S
L=150 CM
W=5.6 CM
H=4.1 CM
R_F=0.9
CO2 : N2 : He TORR.
6.75:20.25: 00
6.75:20.25: 27
6.75:20.25: 54
INPUT ENERGY PER PULSE
=0.002J/CC
Second Pulse
First Pulse
LASER OUTPUT POWER IN WATTS/CC
TIME IN MICRO SECONDS

GRAPH (4.15)

PULSE DELAY TIME VERSUS HELIUM CONTENT

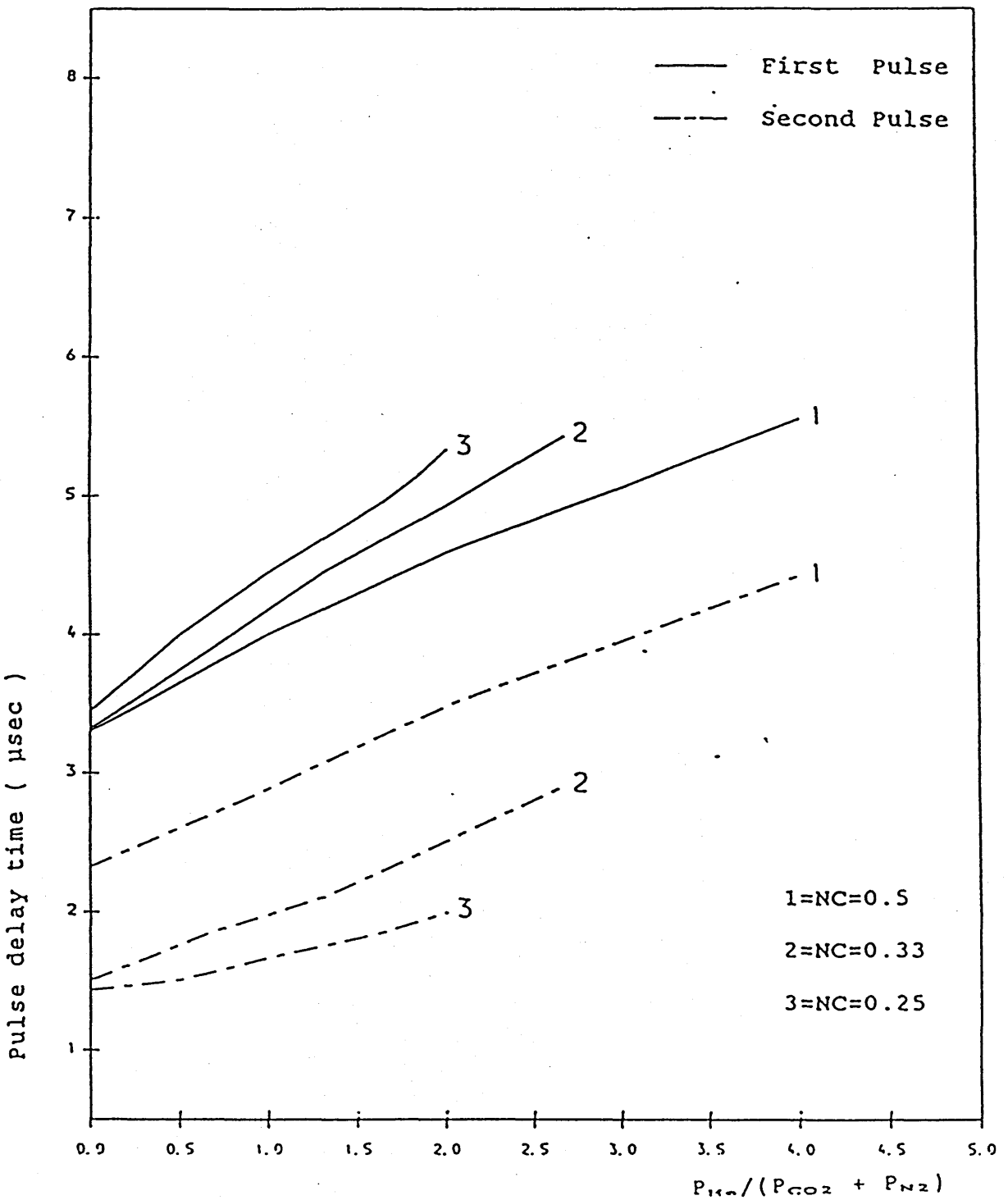

GRAPH (4.16)

MAXIMUM POWER VERSUS HELIUM CONTENT

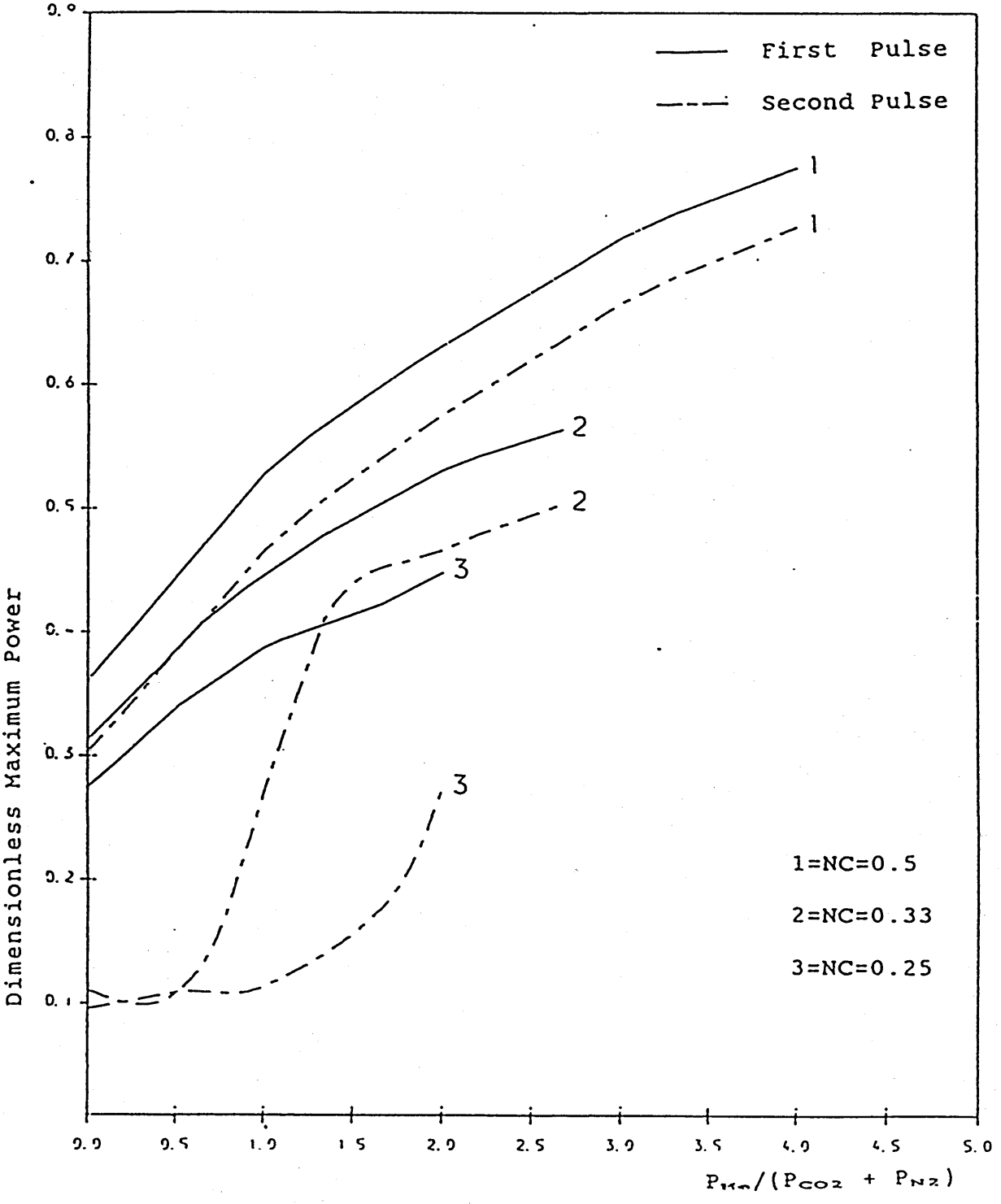

GRAPH (4.17)

MAXIMUM GAS TEMPERATURE VERSUS HELIUM CONTENT

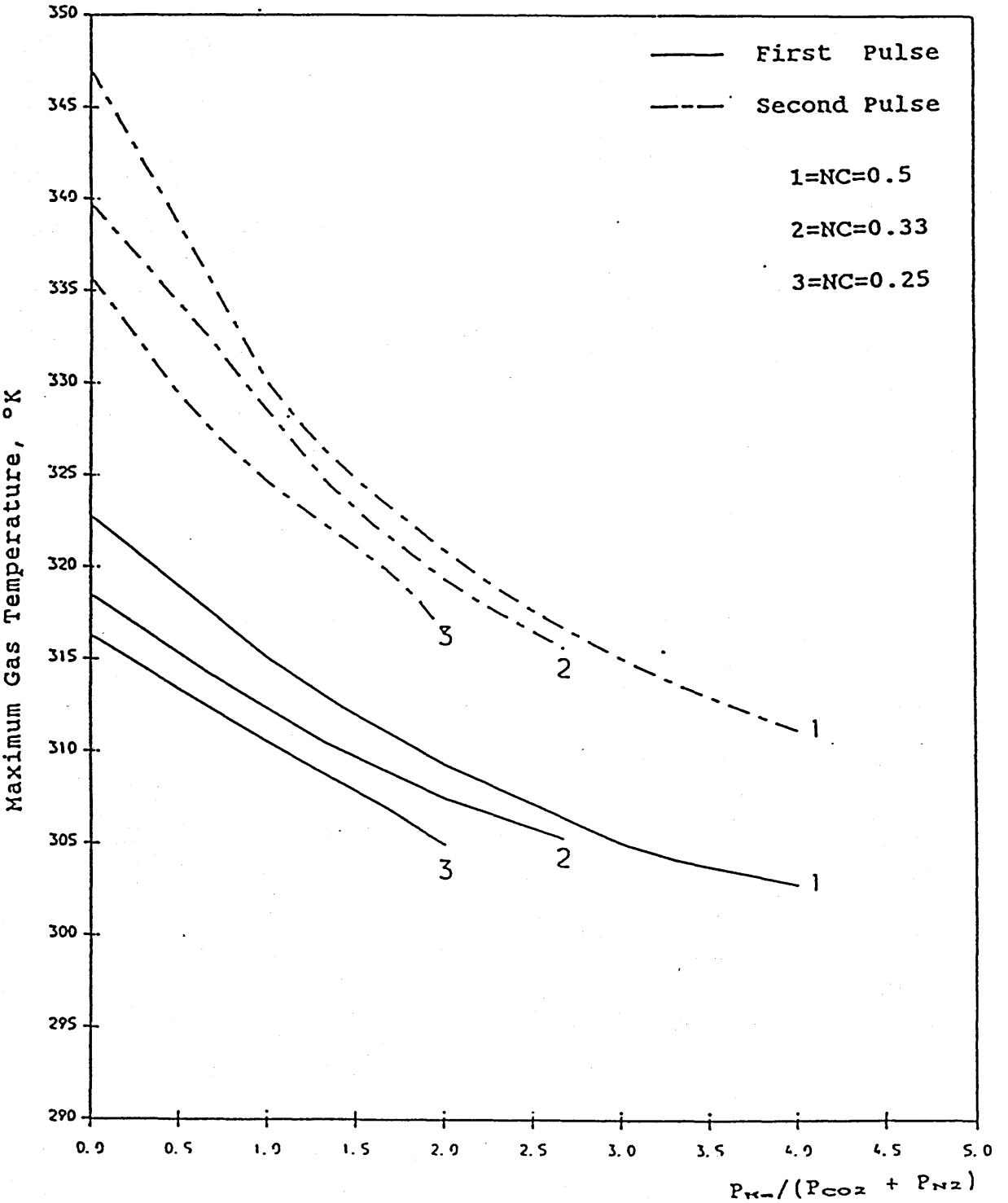

GRAPH (4.18)

PULSE DURATION VERSUS HELIUM CONTENT

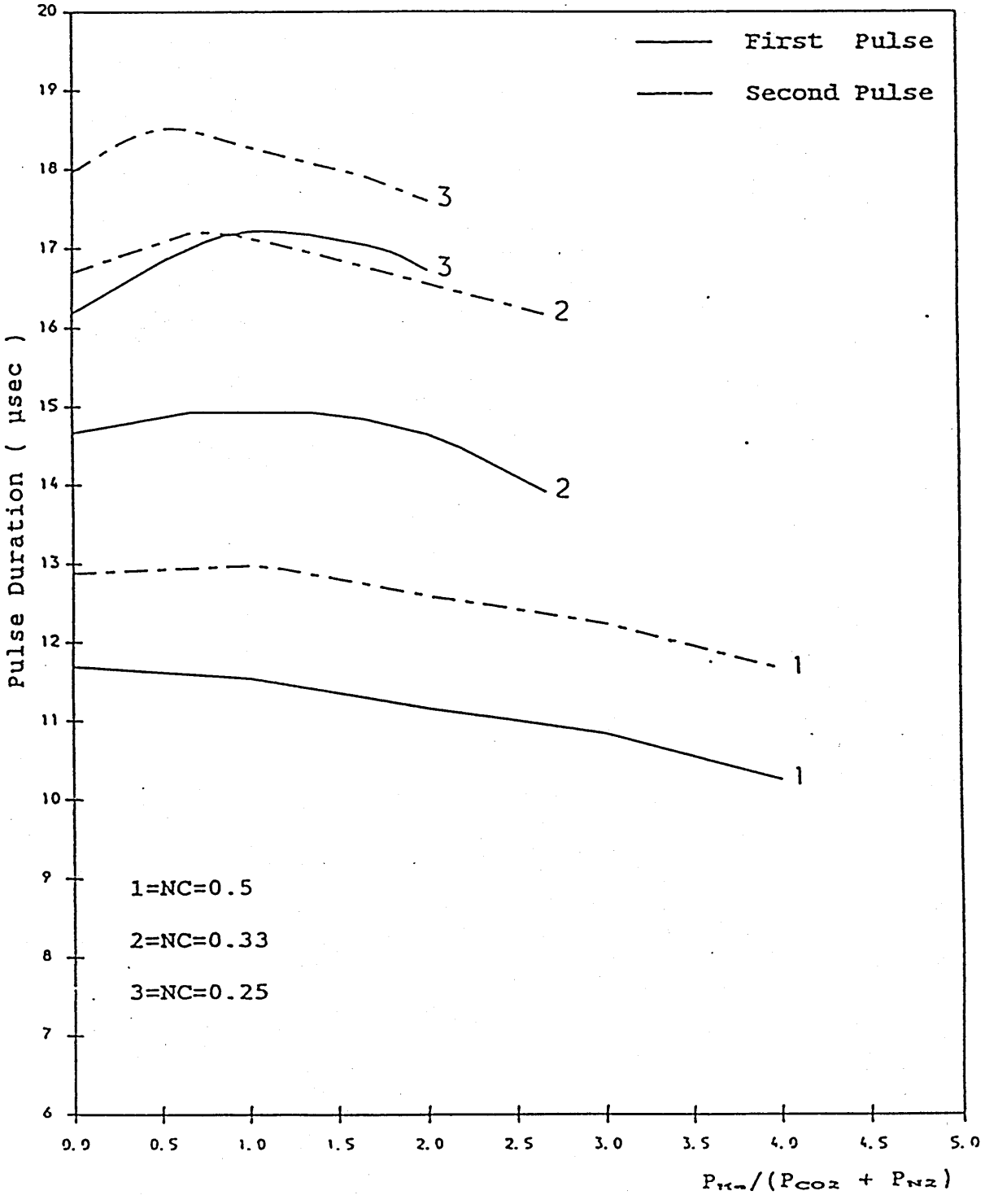

GRAPH (4.19)

AVERAGE POWER VERSUS HELIUM CONTENT

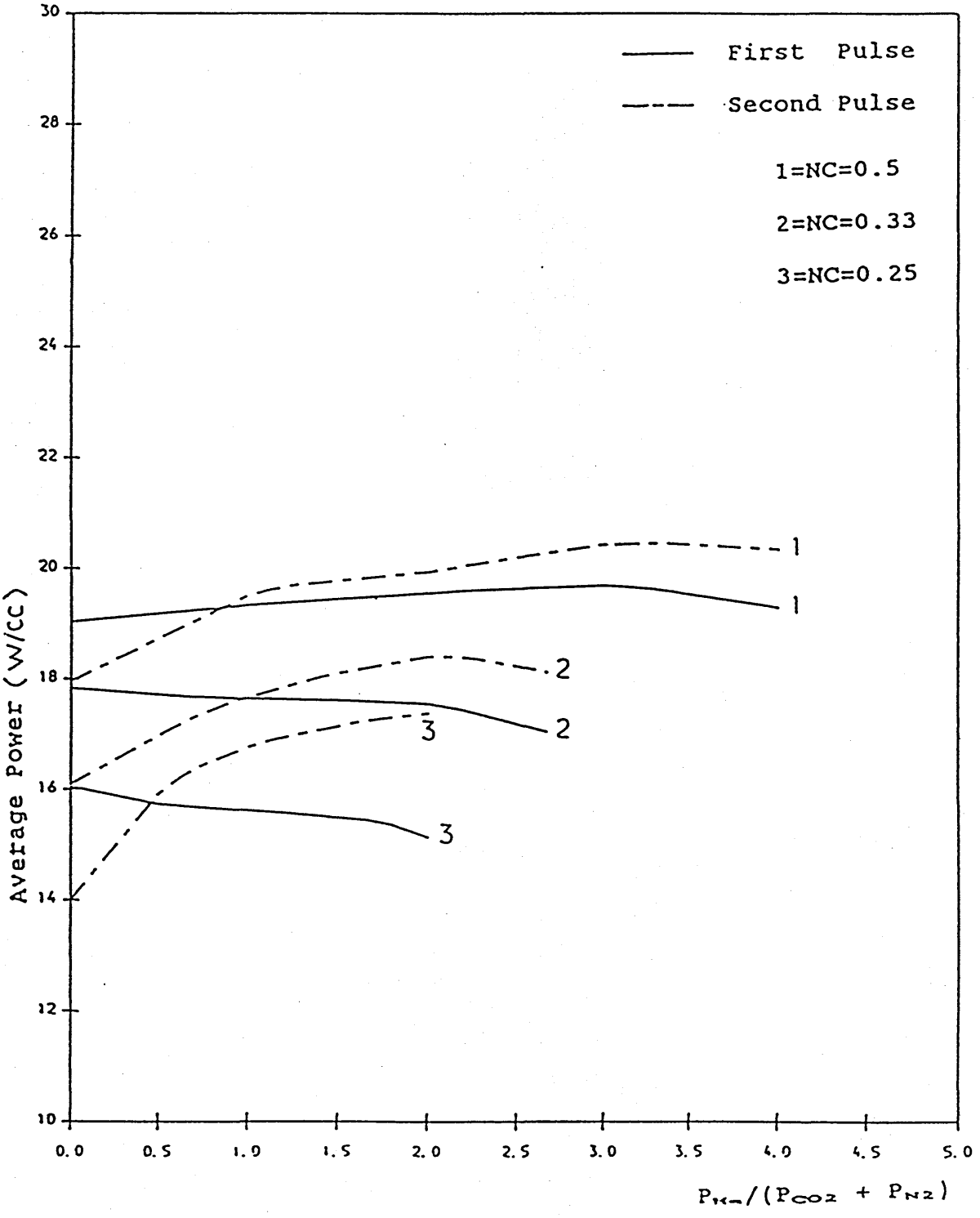

GRAPH (4.20)

OVERALL EFFICIENCY VERSUS HELIUM CONTENT

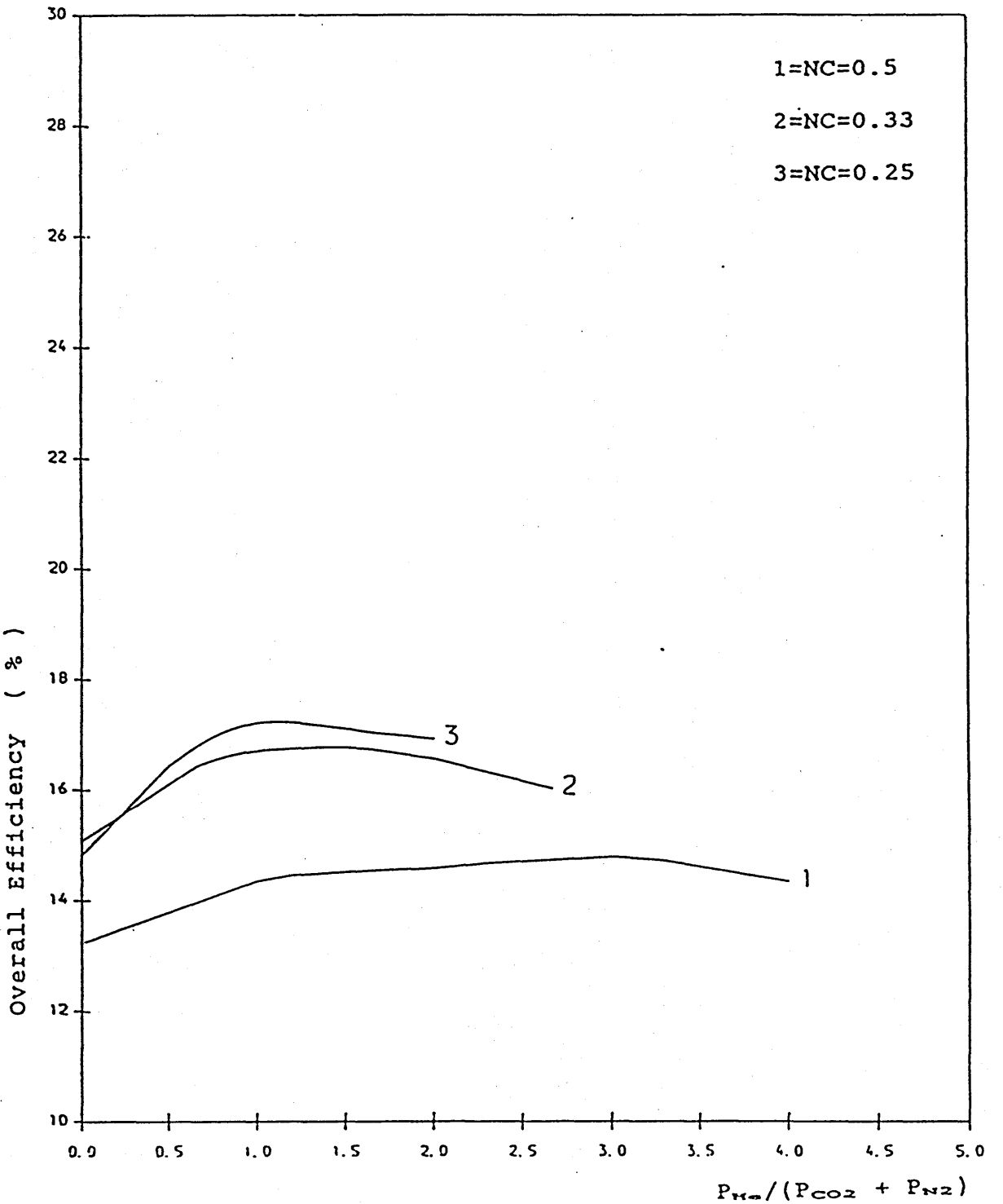

graph (4.21)

EFFECTIVE EFFICIENCY VERSUS HELIUM CONTENT

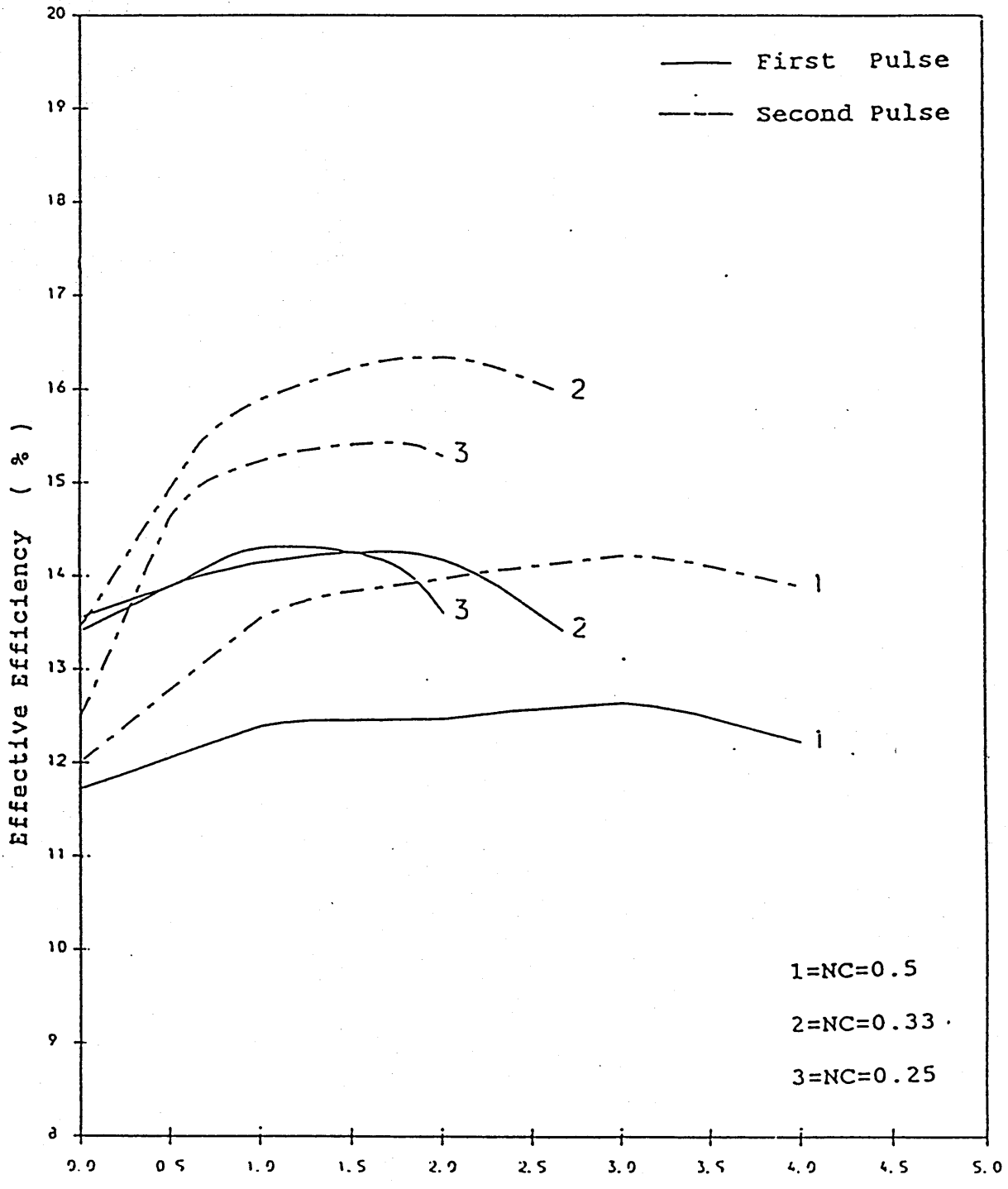

GRAPH (4.22)

PULSE DELAY TIME VERSUS CAVITY LENGTH

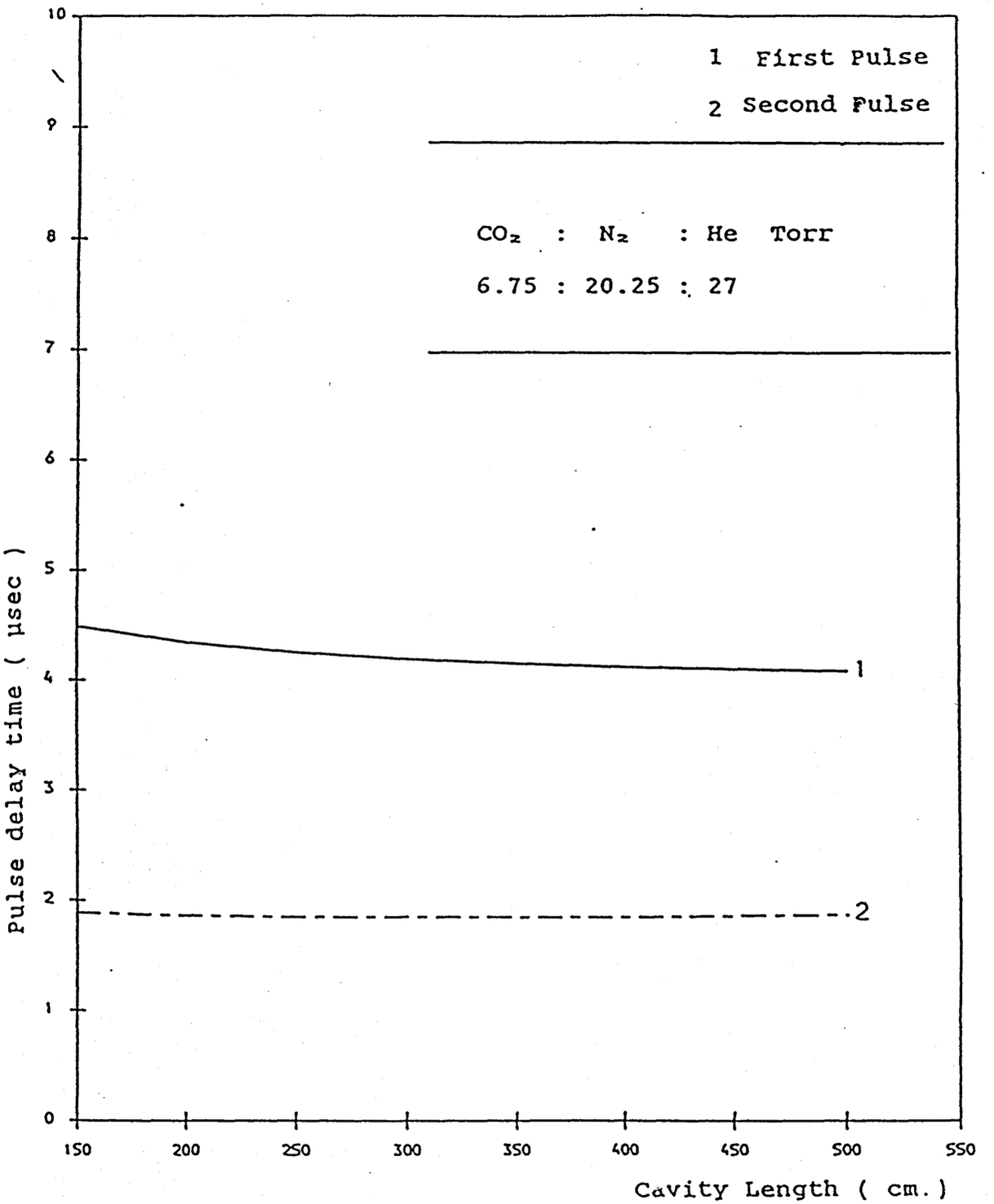

GRAPH (4.23)

MAXIMUM POWER VERSUS CAVITY LENGTH

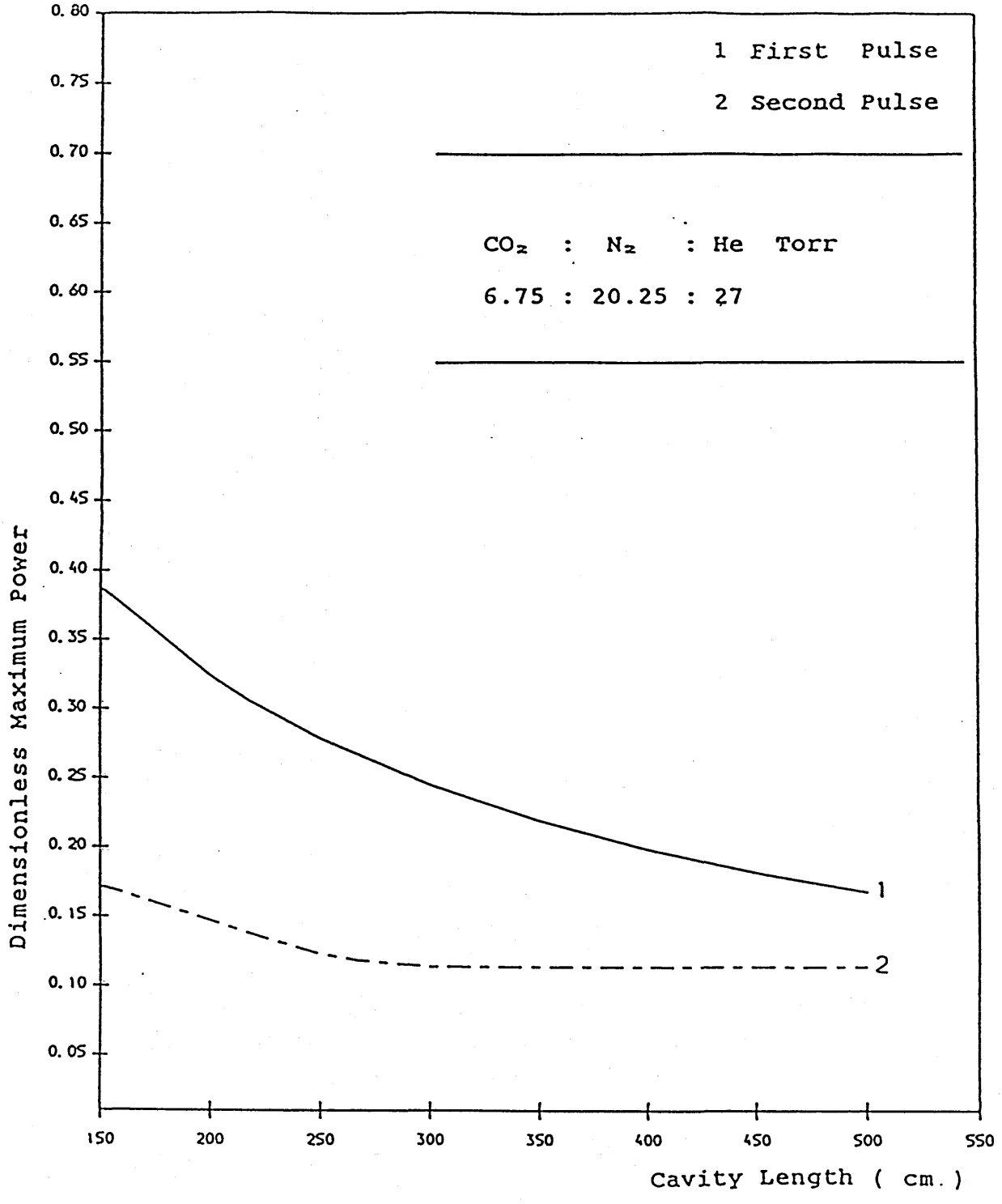

GRAPH(4.24)

PULSE DURATION VERSUS CAVITY LENGTH

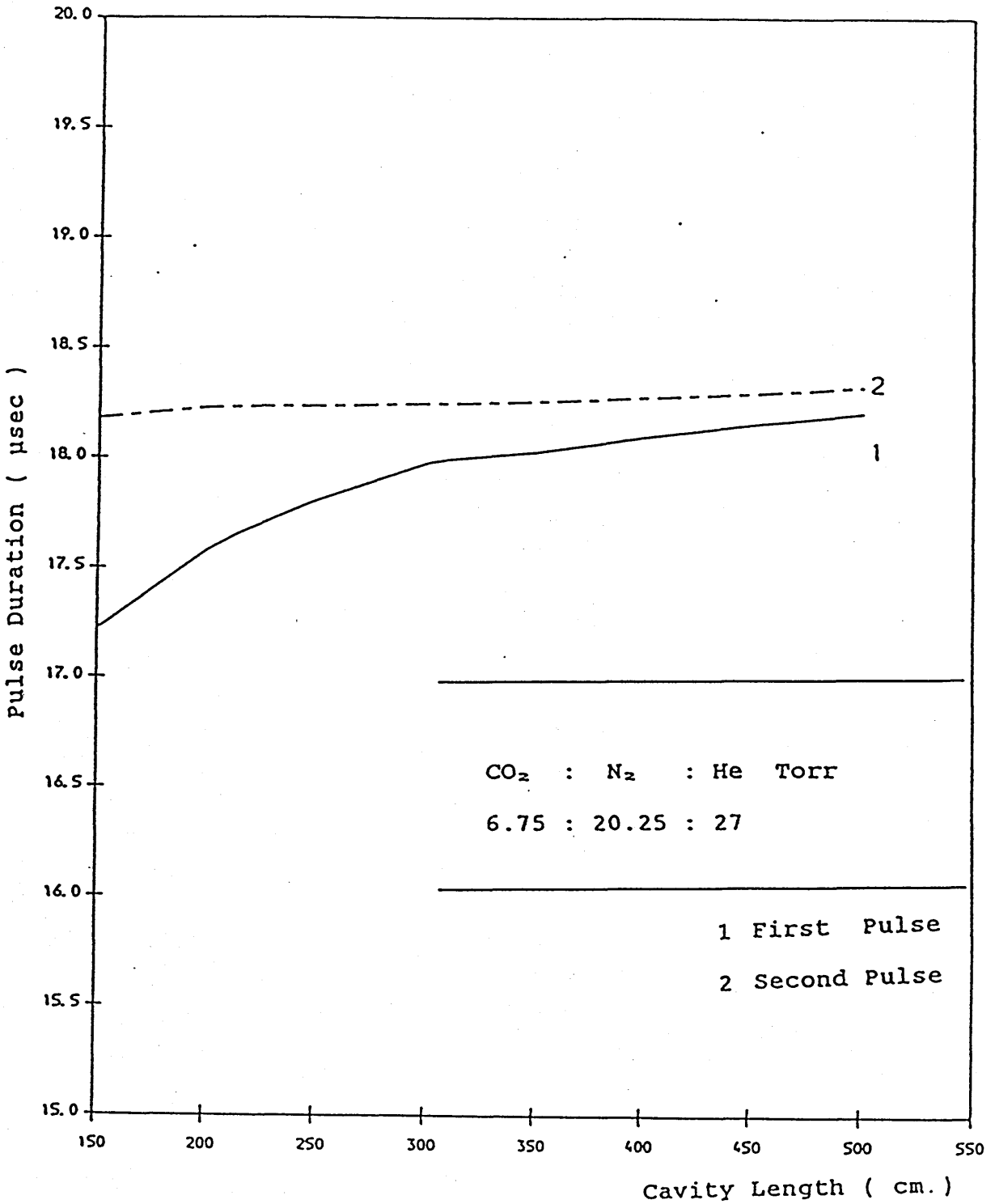

GRAPH (4.25)

AVERAGE POWER VERSUS CAVITY LENGTH

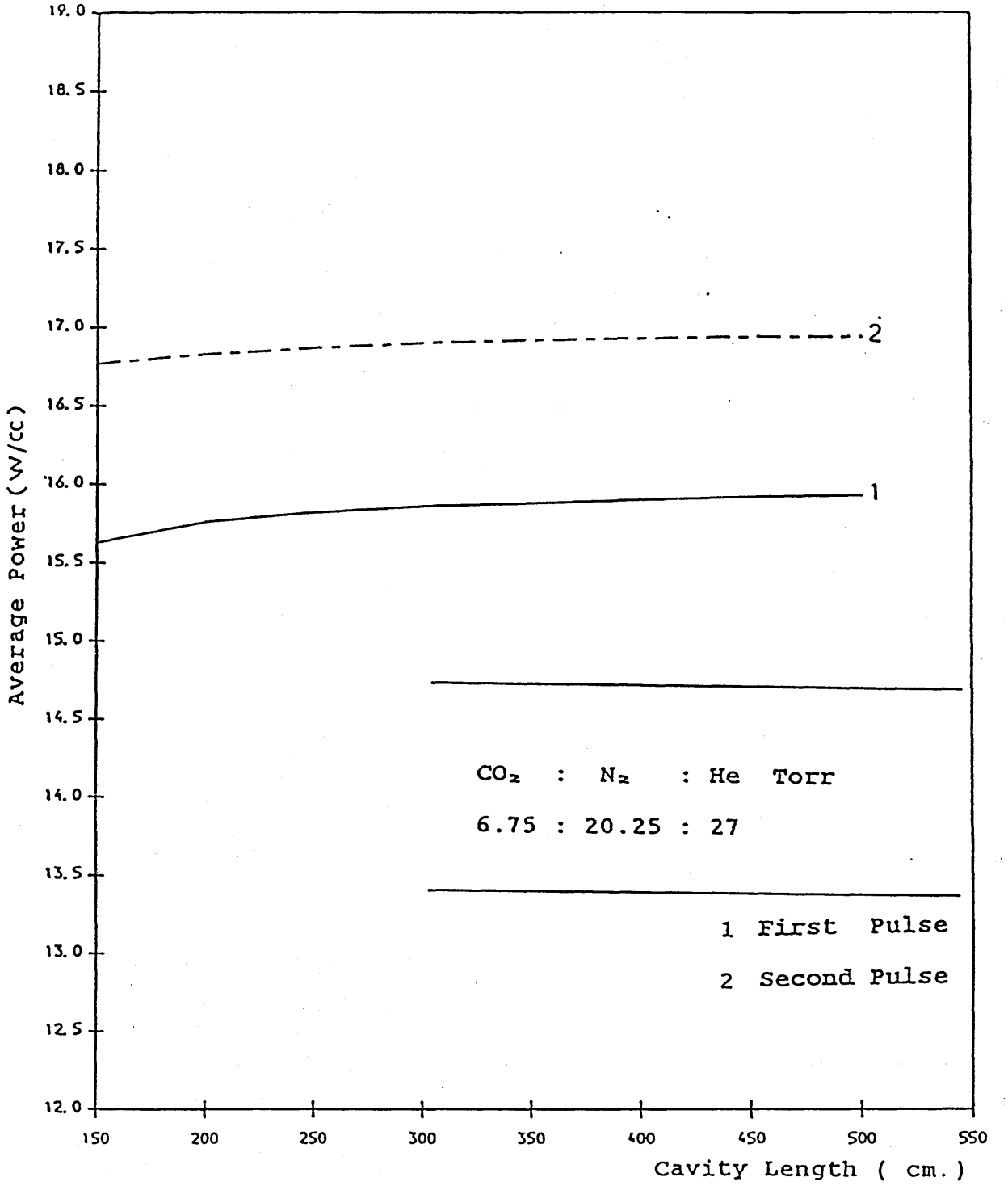

GRAPH (4.26)

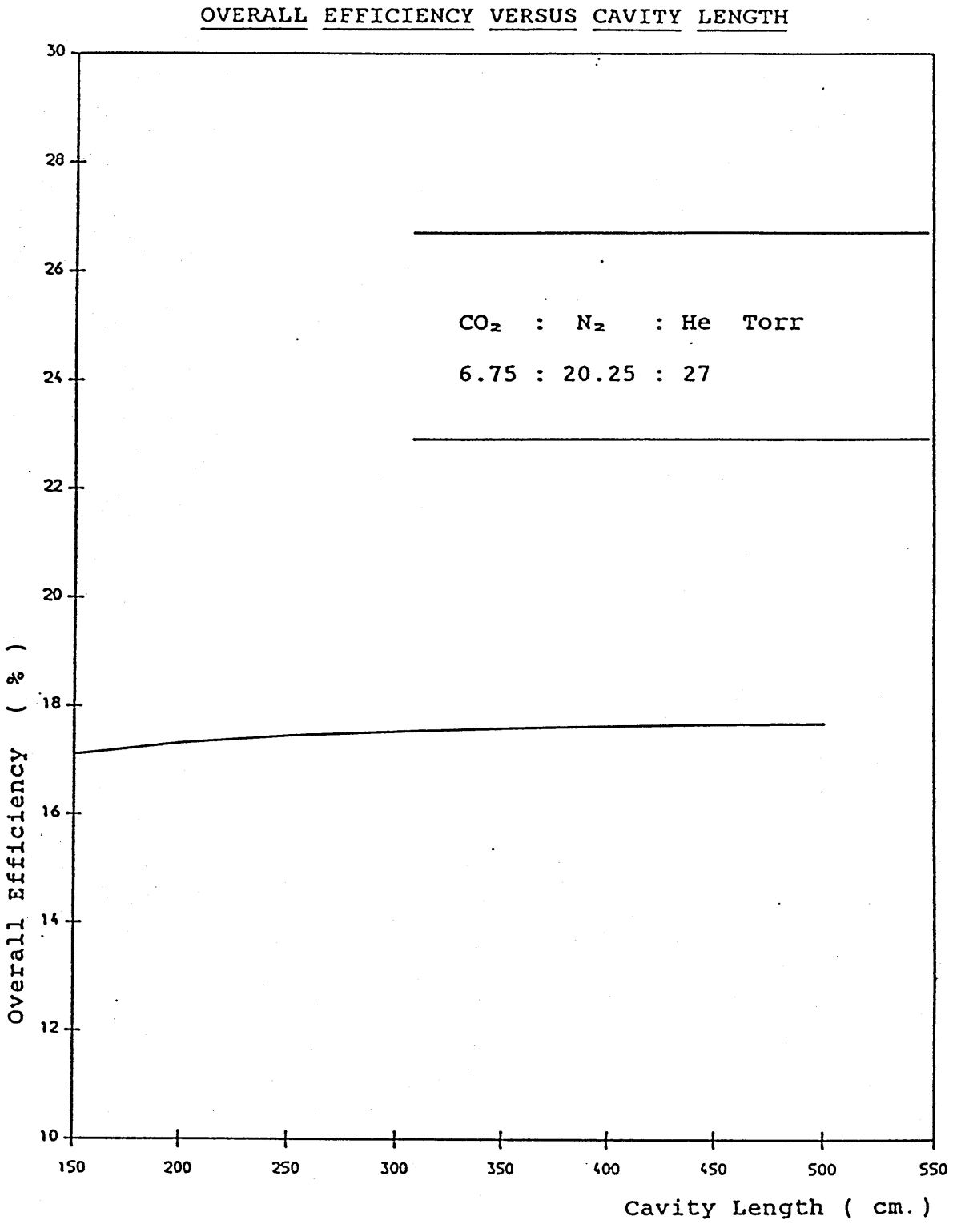
OVERALL EFFICIENCY VERSUS CAVITY LENGTH
CO2 : N2 : He Torr
6.75 : 20.25 : 27
Overall Efficiency (%)
Cavity Length (cm.)
30
28
26
24
22
20
18
16
14
12
10
150
200
250
300
350
400
450
500
550

GRAPH (4.27)

EFFECTIVE EFFICIENCY VERSUS CAVITY LENGTH

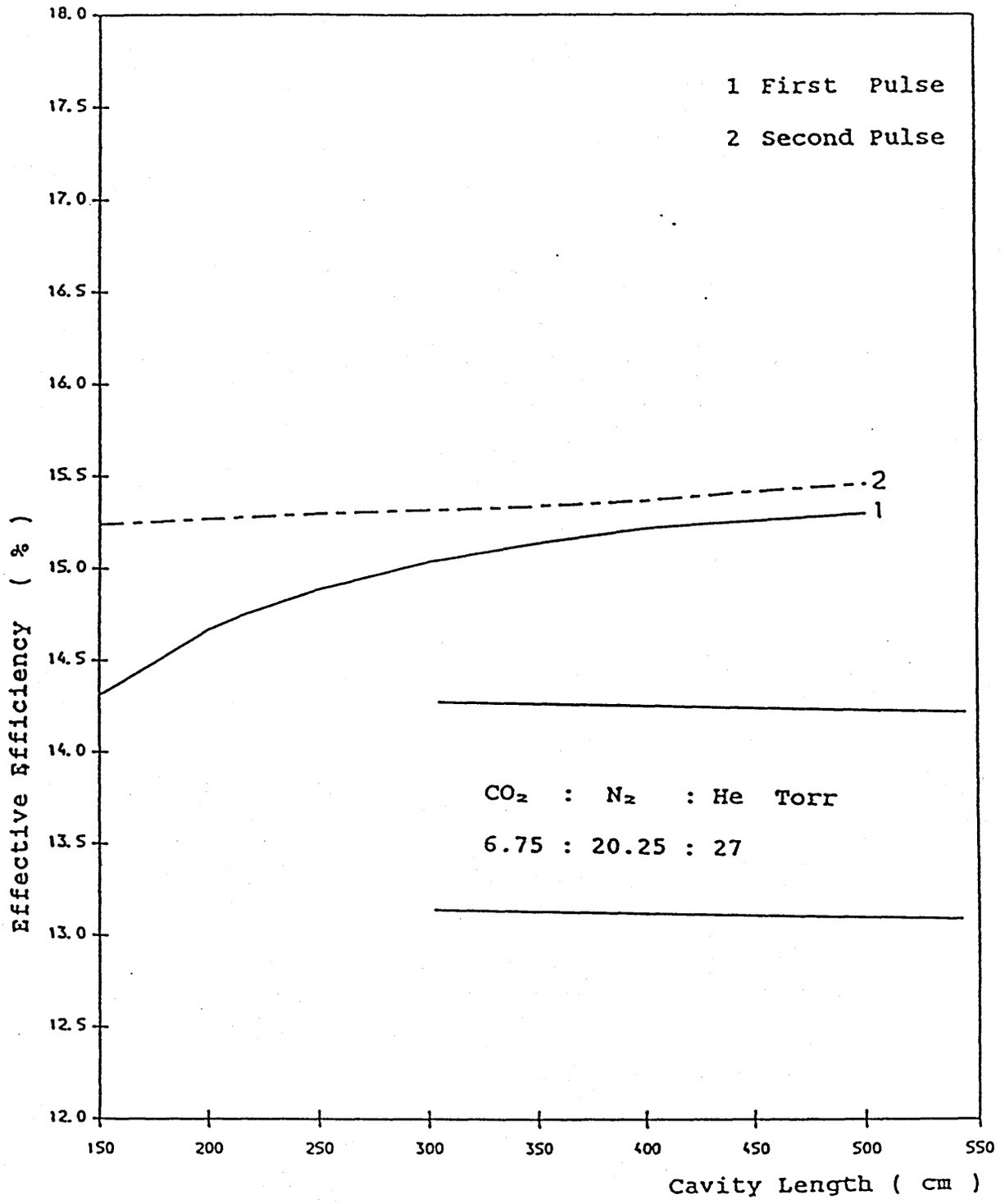

GRAPH (4.28)

PULSE DELAY TIME VERSUS MIRROR REFLECTIVITY

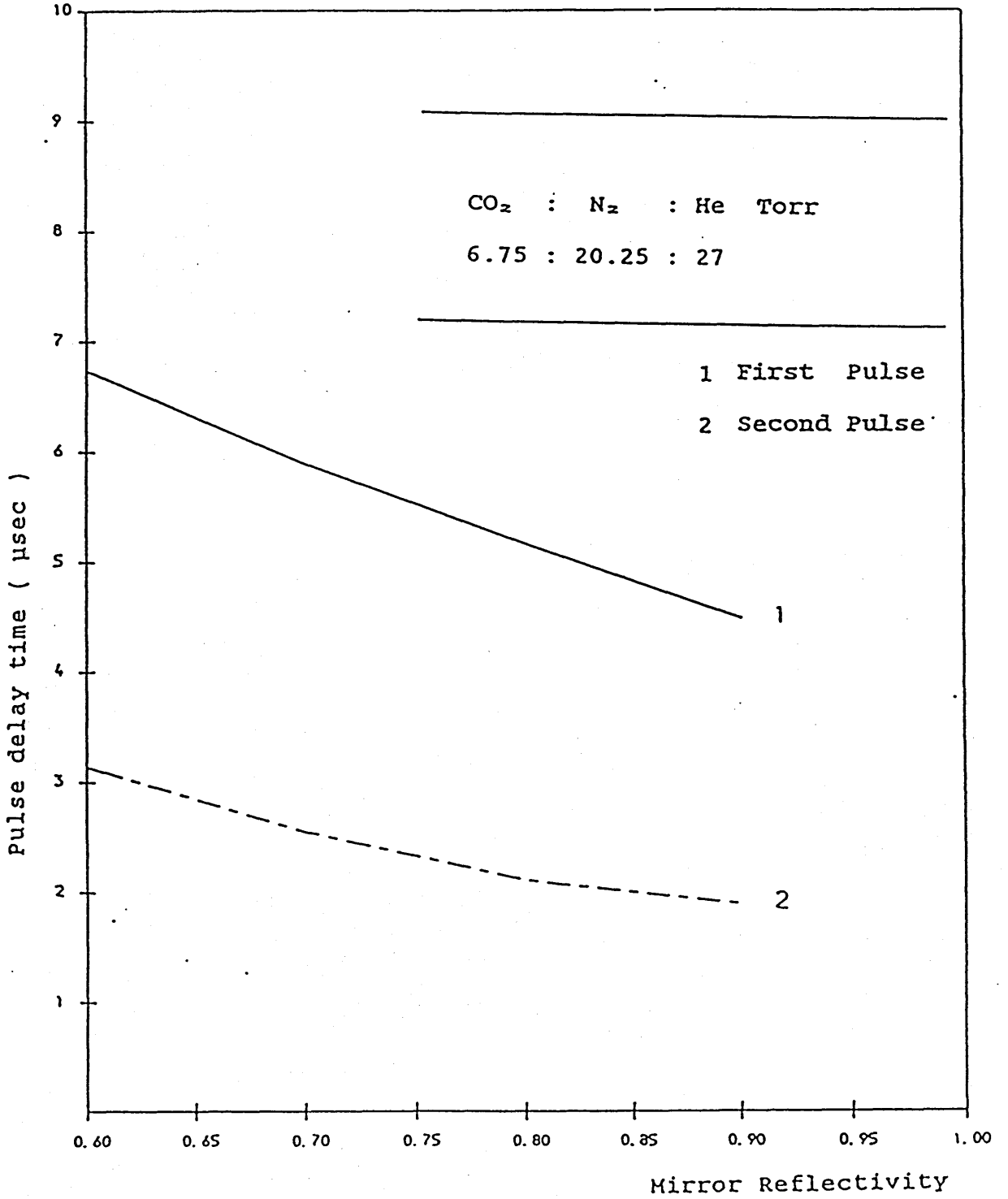

GRAPH (4.29)

MAXIMUM POWER VERSUS MIRROR REFLECTIVITY

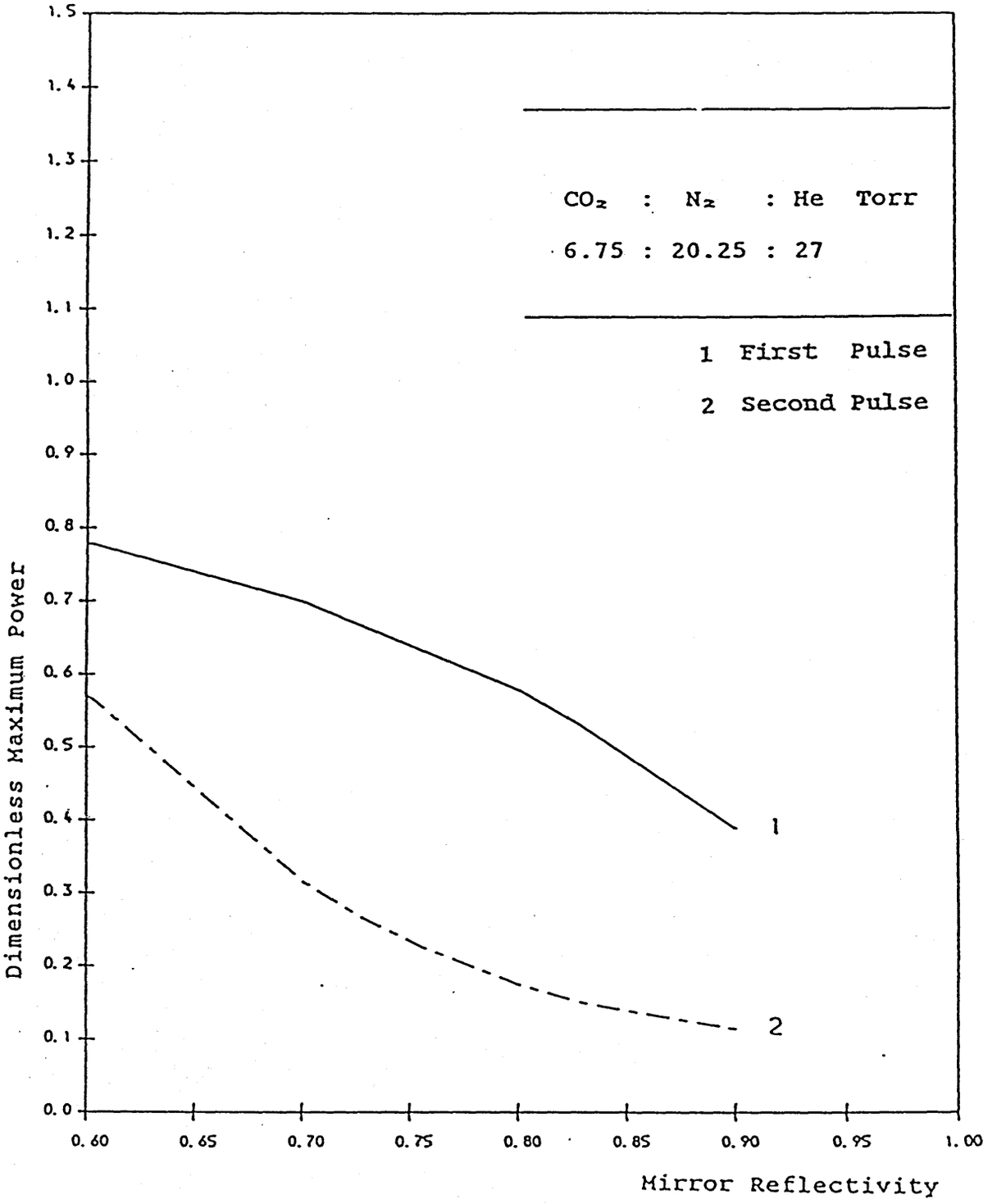

GRAPH (4.30)

PULSE DURATION VERSUS MIRROR REFLECTIVITY

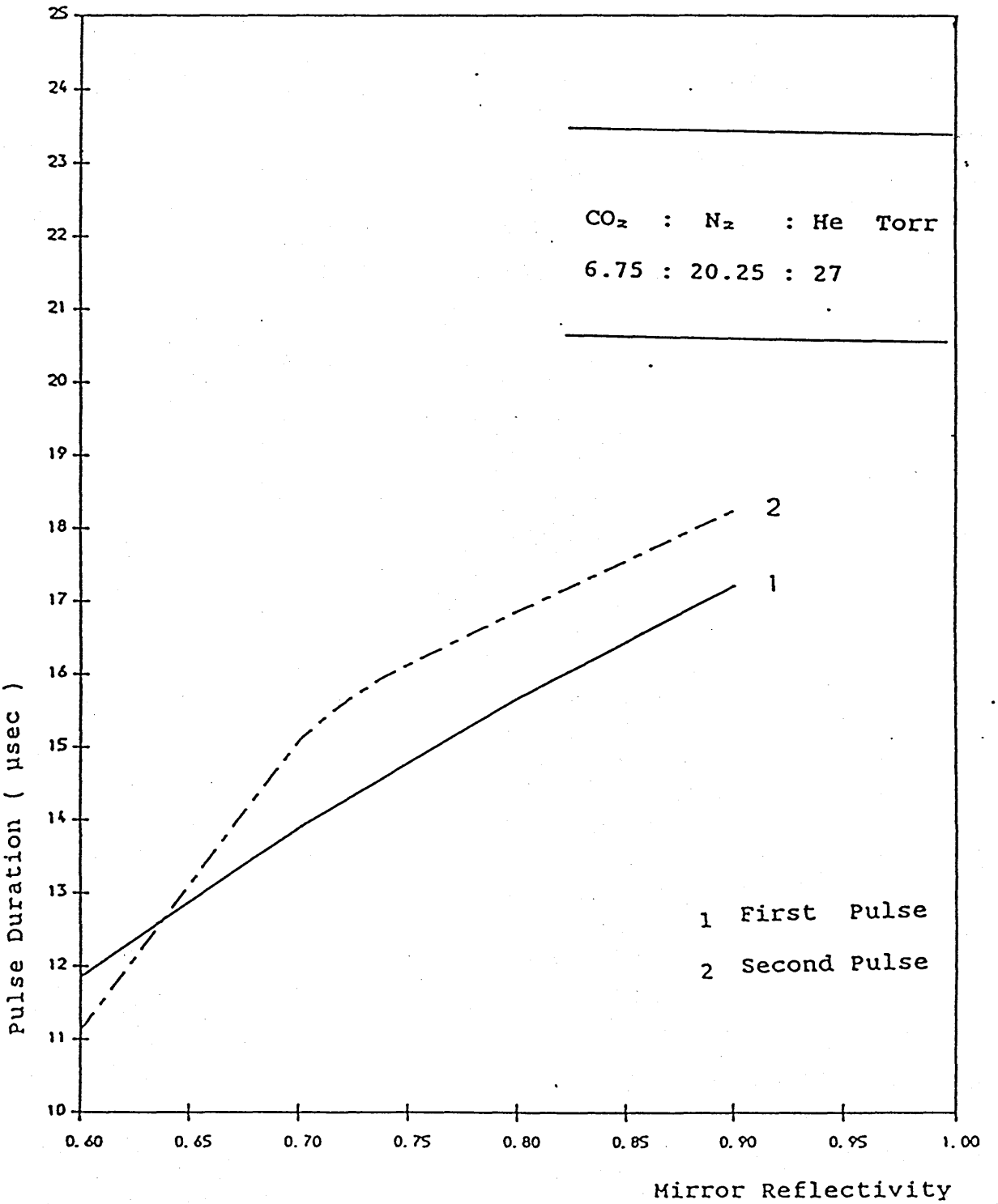

GRAPH (4.31)

AVERAGE POWER VERSUS MIRROR REFLECTIVITY

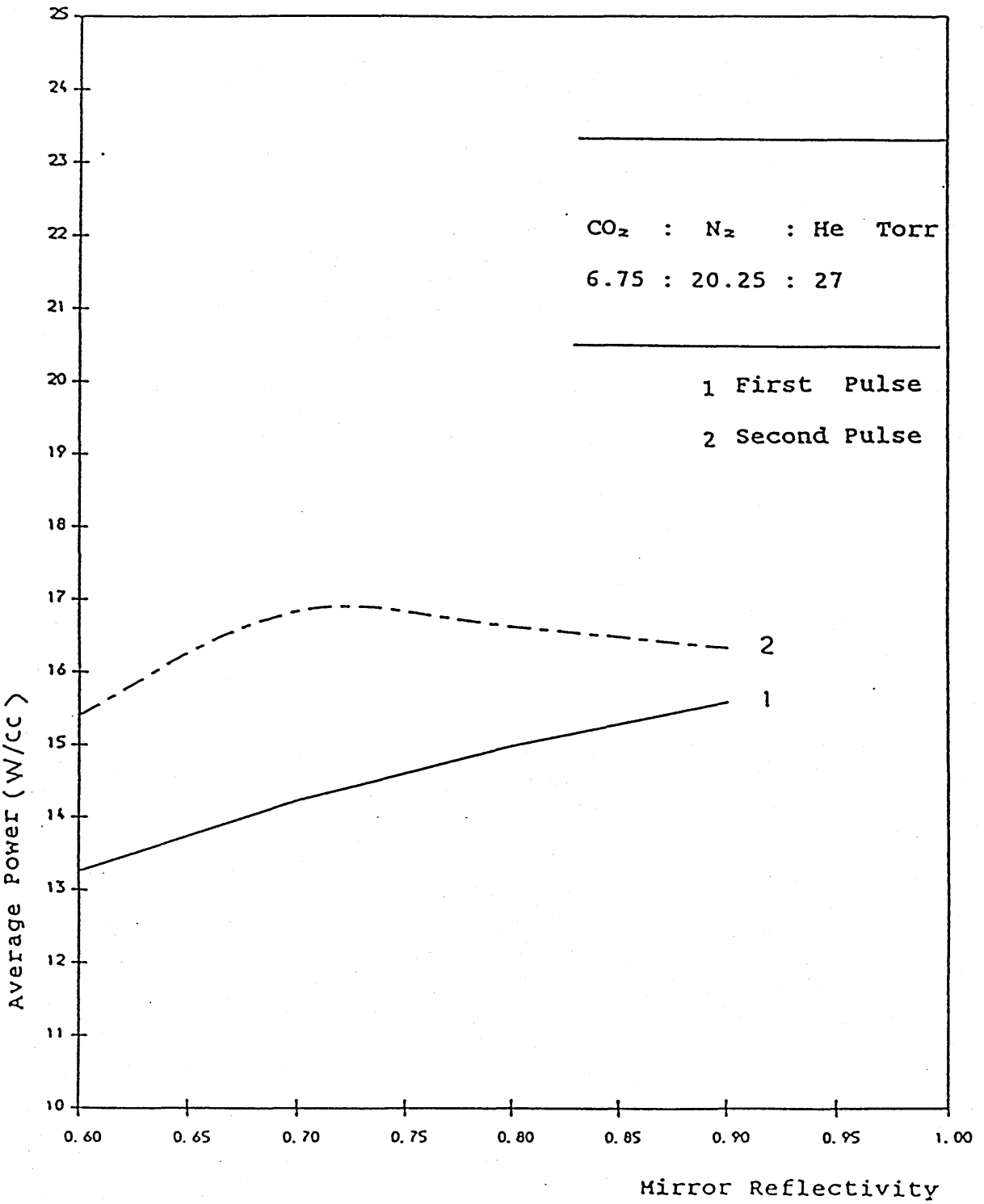

GRAPH (4.32)

OVERALL EFFICIENCY VERSUS MIRROR REFLECTIVITY

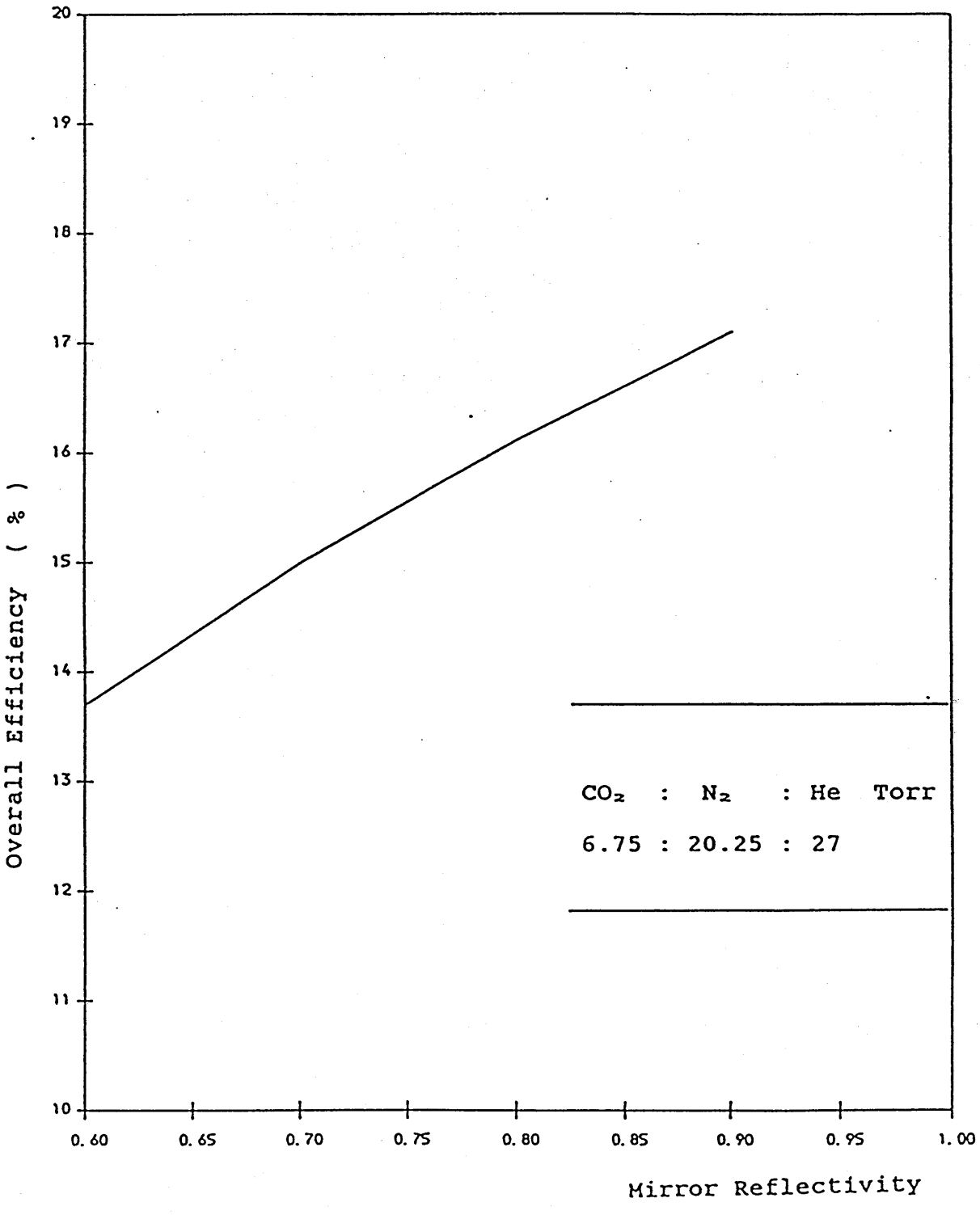

GRAPH (4.33)

EFFECTIVE EFFICIENCY VERSUS MIRROR REFLECTIVITY

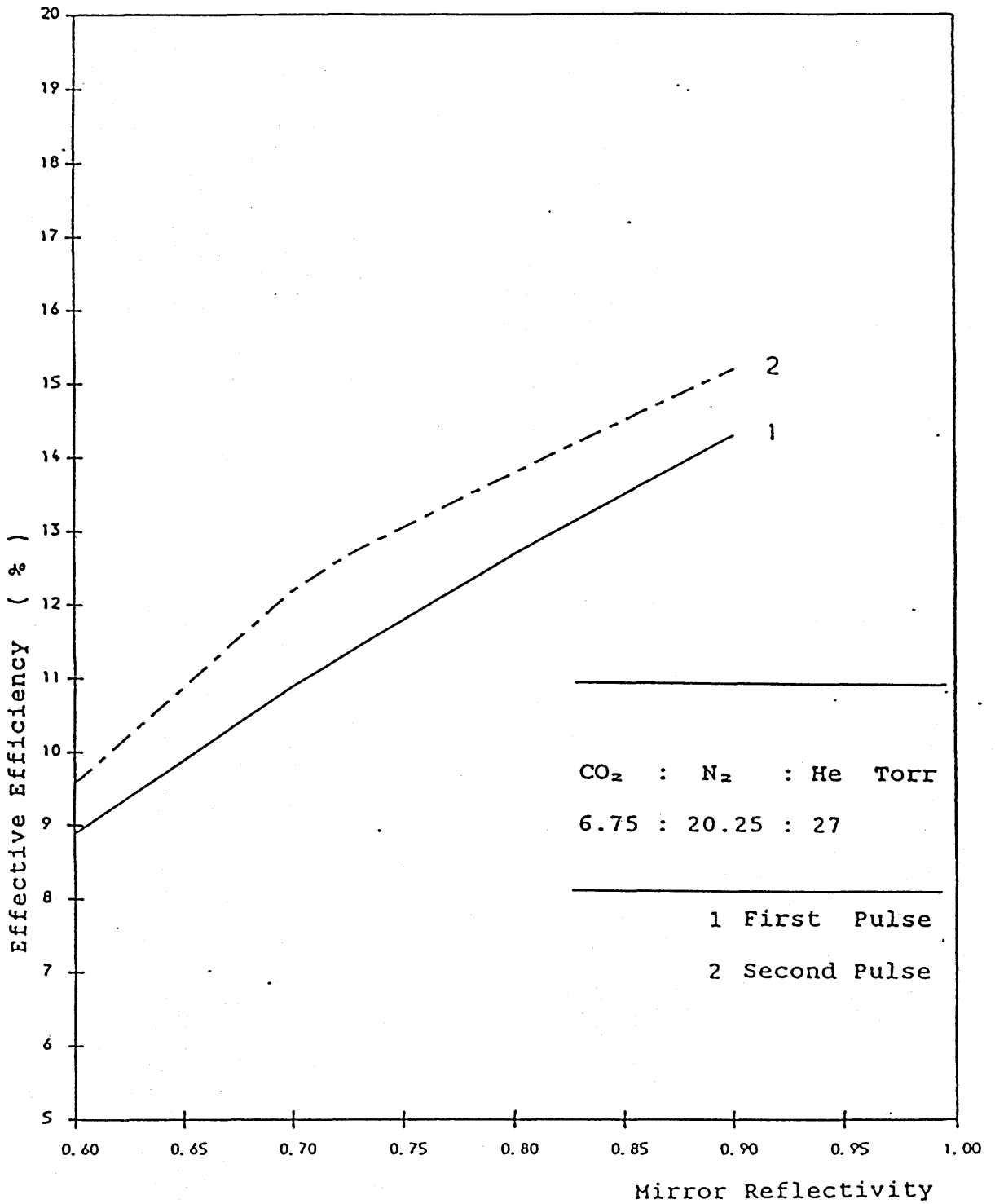

GRAPH (4.34)

POPULATION OF UPPER LASER LEVEL VERSUS TIME

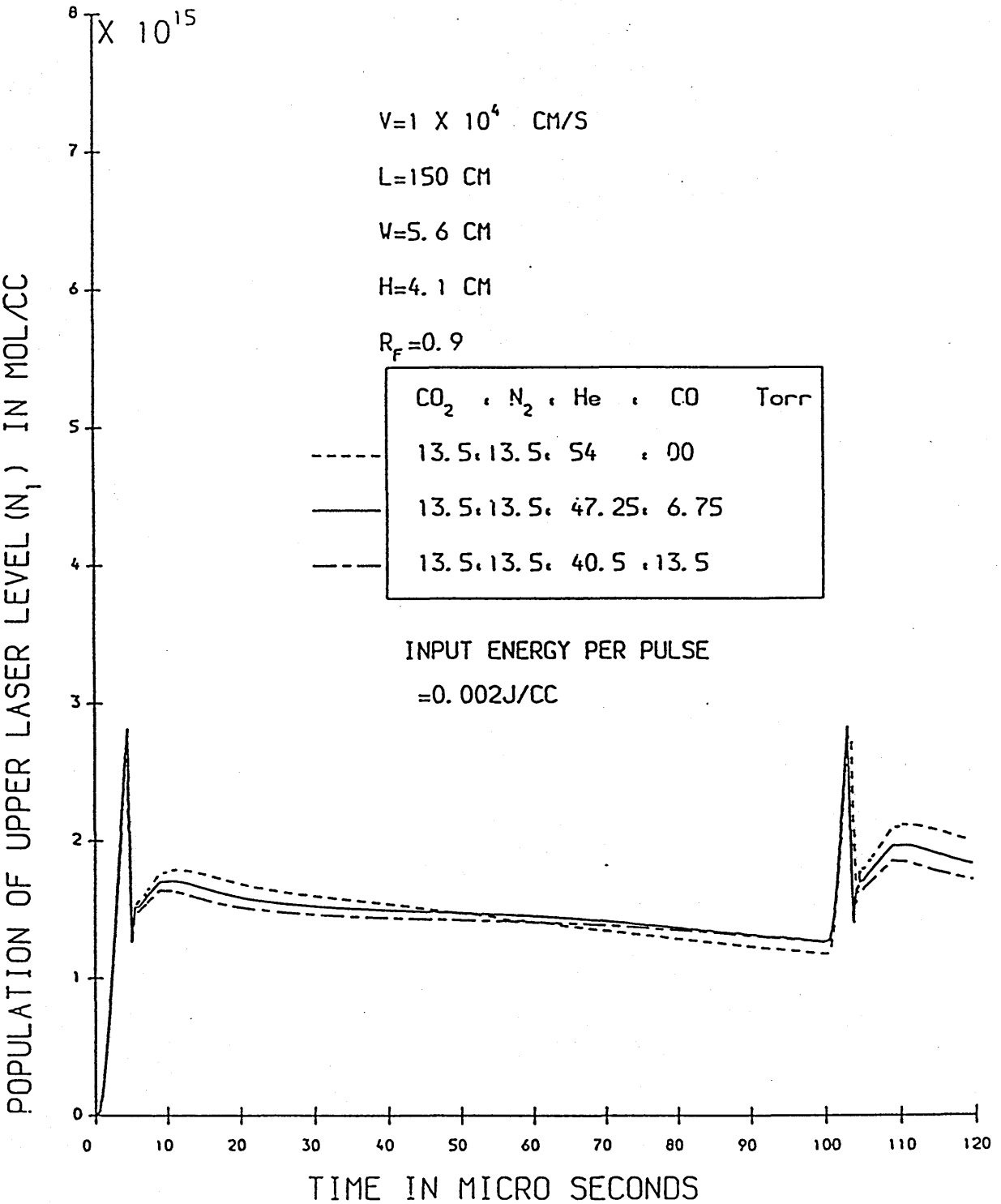

GRAPH (4.35)

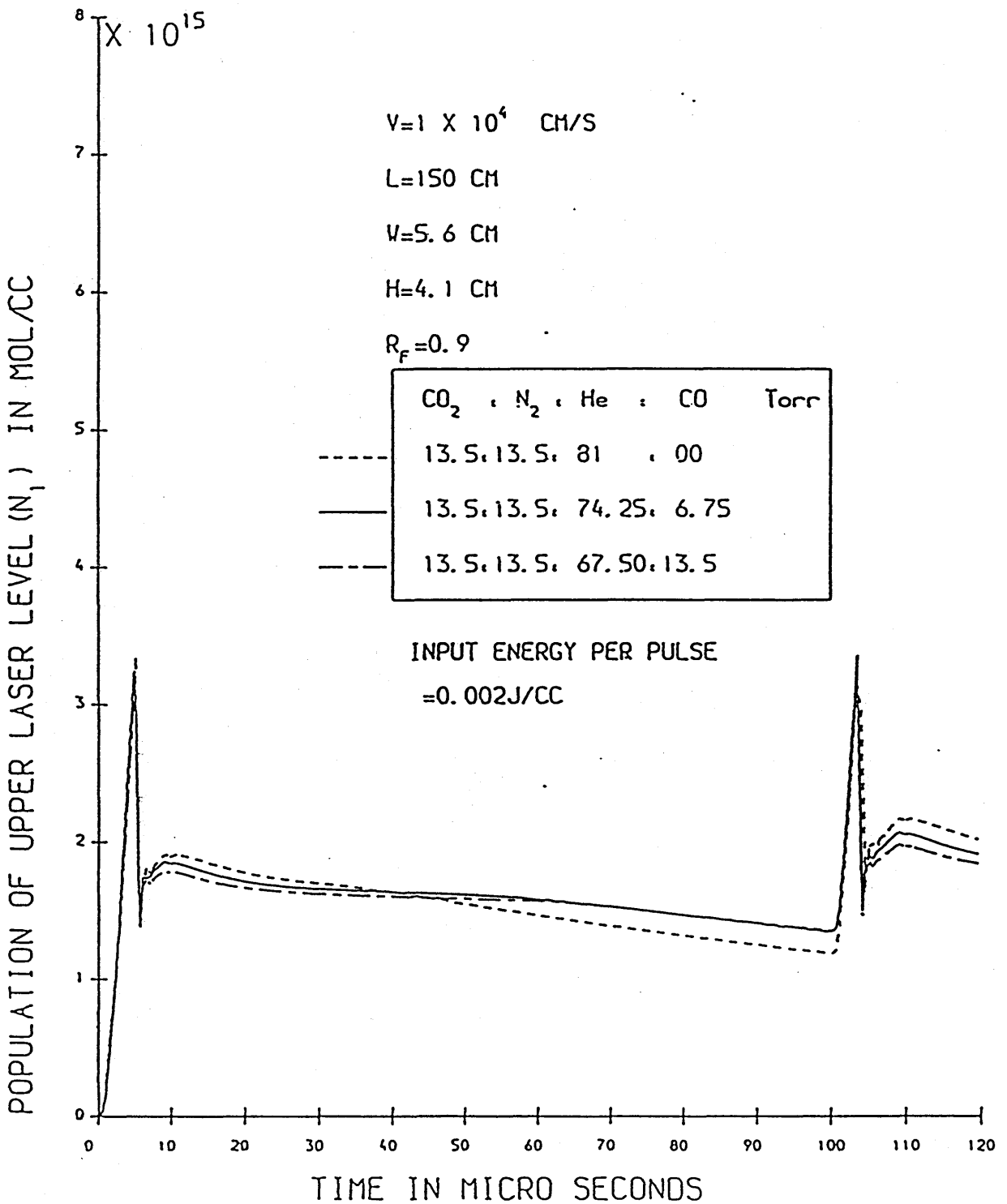
POPULATION OF UPPER LASER LEVEL VERSUS TIME
X 10^15
V=1 X 10^4 CM/S
L=150 CM
W=5.6 CM
H=4.1 CM
R_F=0.9
CO2 : N2 : He : CO Torr
13.5 : 13.5 : 81 : 00
13.5 : 13.5 : 74.25 : 6.75
13.5 : 13.5 : 67.50 : 13.5
INPUT ENERGY PER PULSE
=0.002J/CC
POPULATION OF UPPER LASER LEVEL (N1) IN MOL/CC
TIME IN MICRO SECONDS
0
1
2
3
4
5
6
7
8
0
10
20
30
40
50
60
70
80
90
100
110
120

GRAPH (4.36)

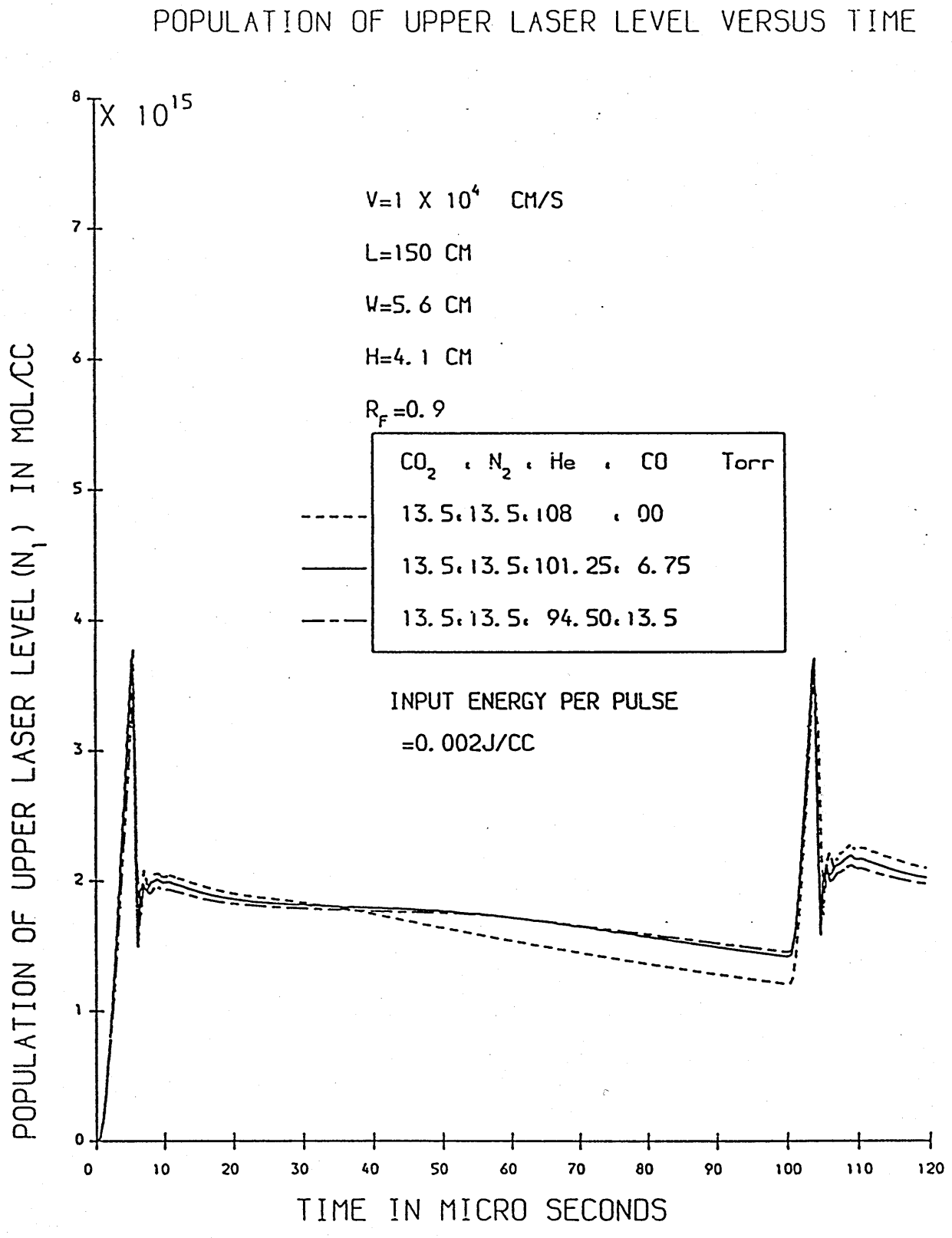
POPULATION OF UPPER LASER LEVEL VERSUS TIME
X 10^15
V=1 X 10^4 CM/S
L=150 CM
W=5.6 CM
H=4.1 CM
R_F=0.9
CO2 : N2 : He : CO Torr
13.5 : 13.5 : 108 : 00
13.5 : 13.5 : 101.25 : 6.75
13.5 : 13.5 : 94.50 : 13.5
INPUT ENERGY PER PULSE
=0.002J/CC
POPULATION OF UPPER LASER LEVEL (N1) IN MOL/CC
TIME IN MICRO SECONDS
0
1
2
3
4
5
6
7
8
0
10
20
30
40
50
60
70
80
90
100
110
120

GRAPH (4.37)

POPULATION OF UPPER NITROGEN LEVEL VERSUS TIME

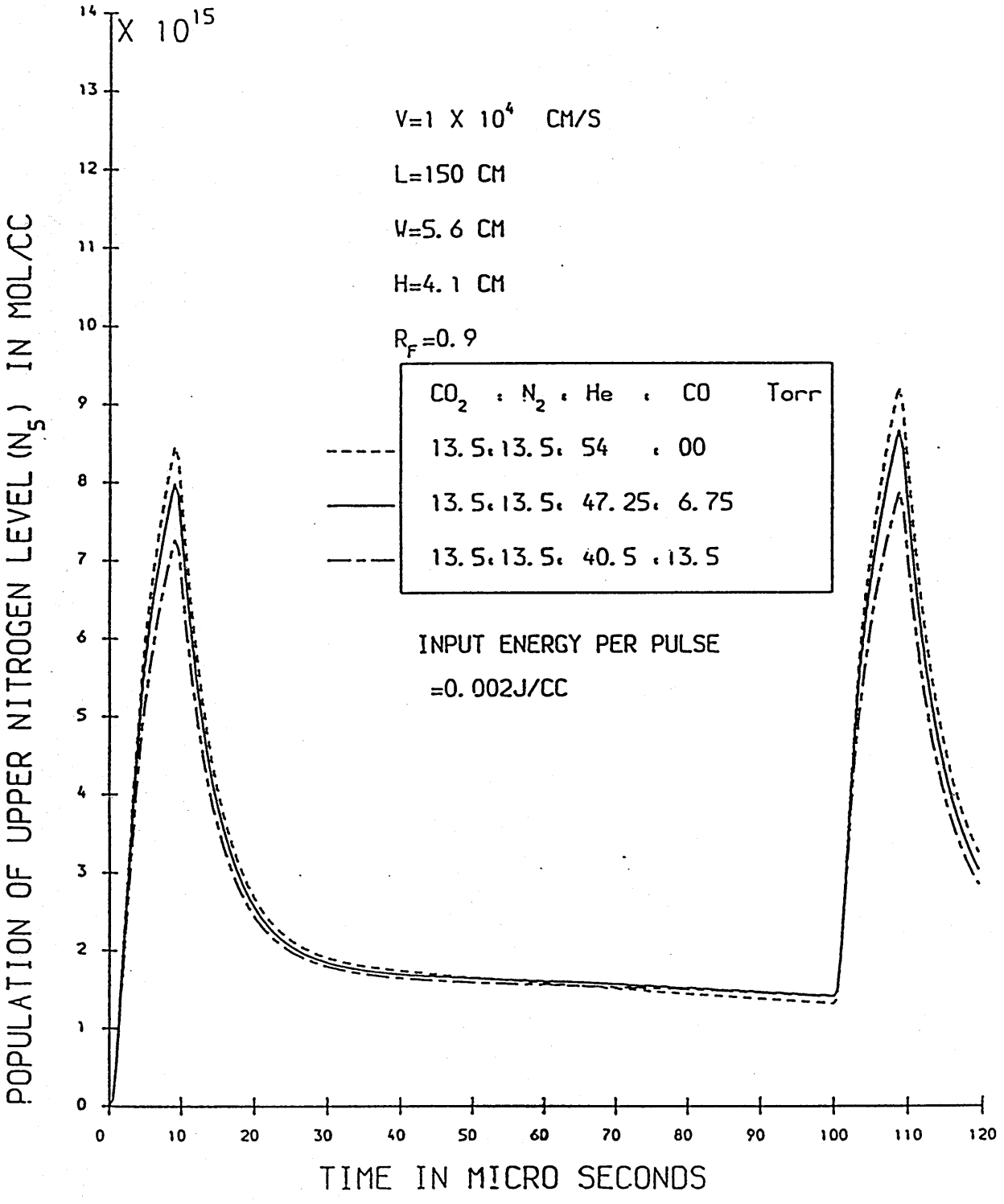

GRAPH (4.38)

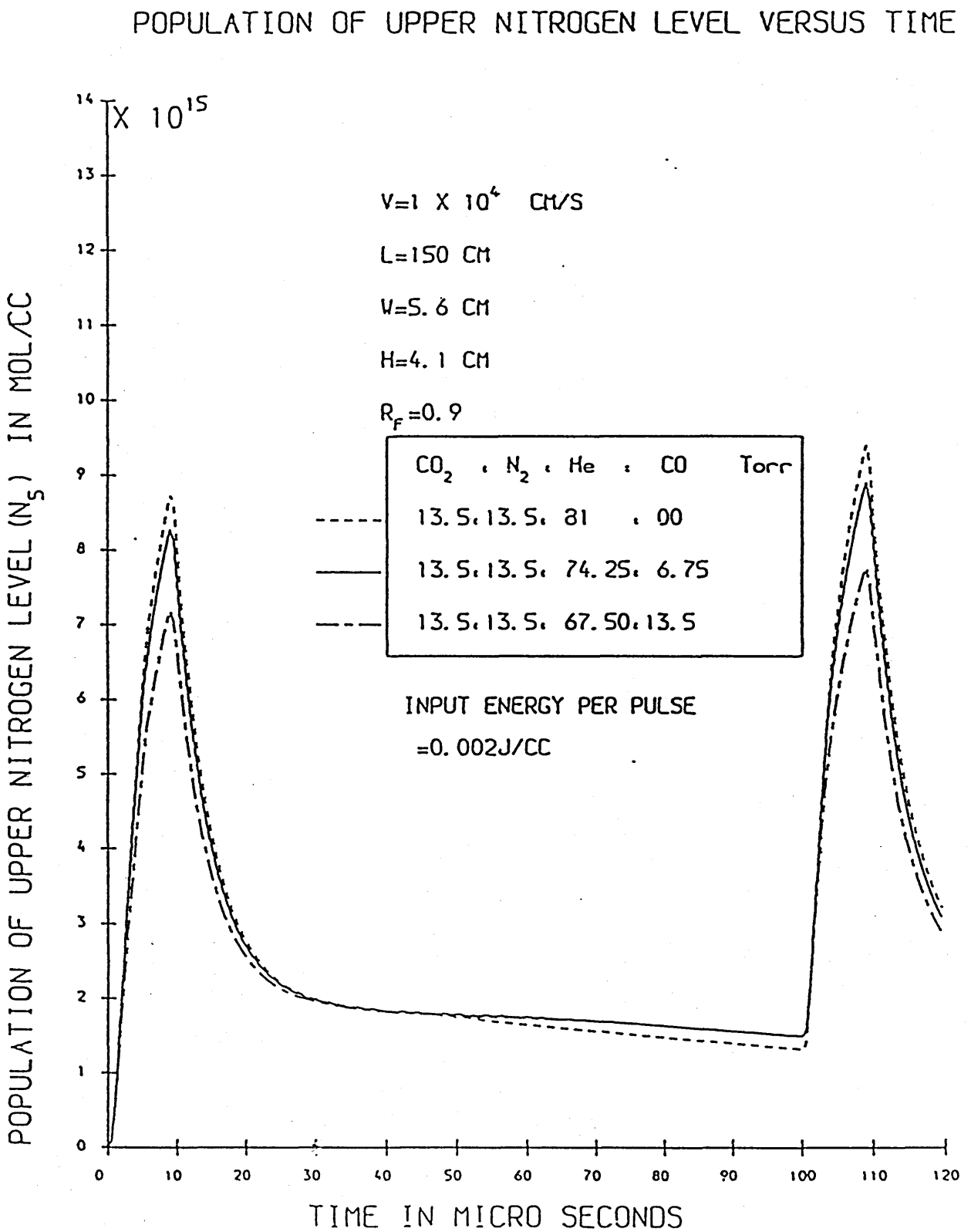
POPULATION OF UPPER NITROGEN LEVEL VERSUS TIME
X 10^15
V=1 X 10^4 CM/S
L=150 CM
W=5.6 CM
H=4.1 CM
R_F=0.9
CO2 : N2 : He : CO Torr
13.5 : 13.5 : 81 : 00
13.5 : 13.5 : 74.25 : 6.75
13.5 : 13.5 : 67.50 : 13.5
INPUT ENERGY PER PULSE
=0.002J/CC
POPULATION OF UPPER NITROGEN LEVEL (N5) IN MOL/CC
TIME IN MICRO SECONDS
0 10 20 30 40 50 60 70 80 90 100 110 120
0 1 2 3 4 5 6 7 8 9 10 11 12 13 14

GRAPH (4.39)

POPULATION OF UPPER NITROGEN LEVEL VERSUS TIME

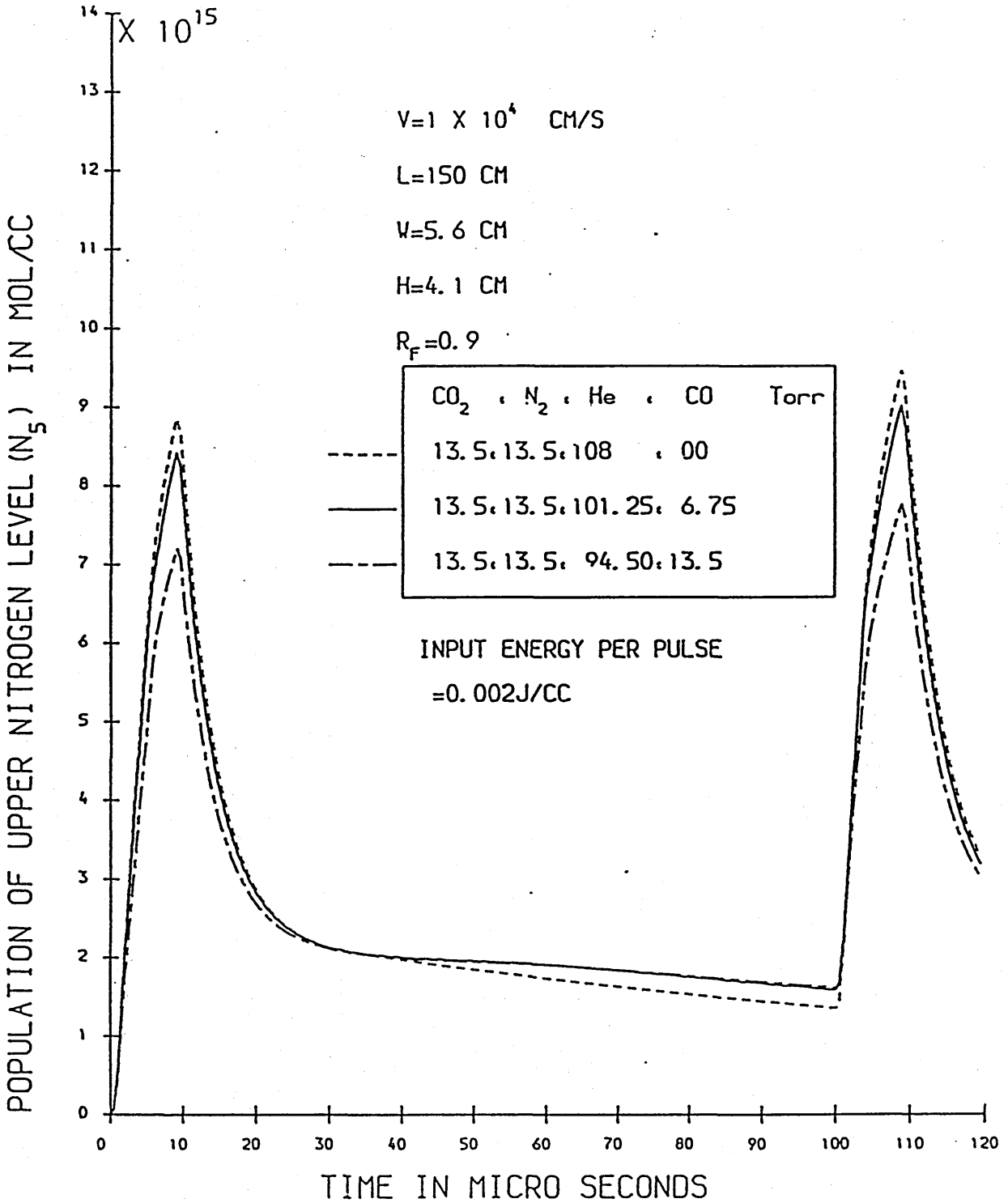

GRAPH (4.40)

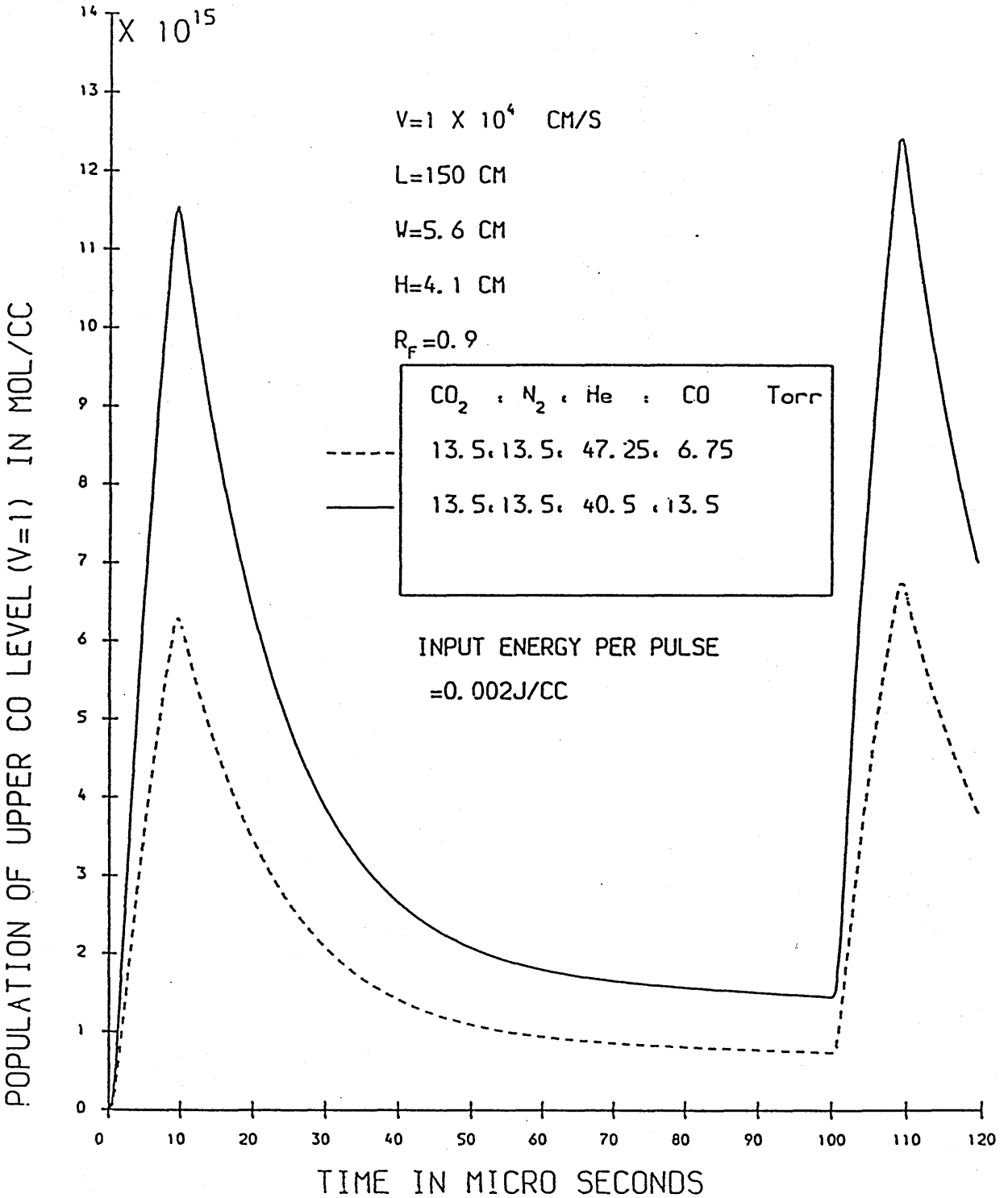
POPULATION OF UPPER CO LEVEL VERSUS TIME
X 10^15
V=1 X 10^4 CM/S
L=150 CM
W=5.6 CM
H=4.1 CM
R_F=0.9
CO2 : N2 : He : CO Torr
13.5 : 13.5 : 47.25 : 6.75
13.5 : 13.5 : 40.5 : 13.5
INPUT ENERGY PER PULSE
=0.002J/CC
POPULATION OF UPPER CO LEVEL (V=1) IN MOL/CC
TIME IN MICRO SECONDS
0 10 20 30 40 50 60 70 80 90 100 110 120
0 1 2 3 4 5 6 7 8 9 10 11 12 13 14

GRAPH (4.41)

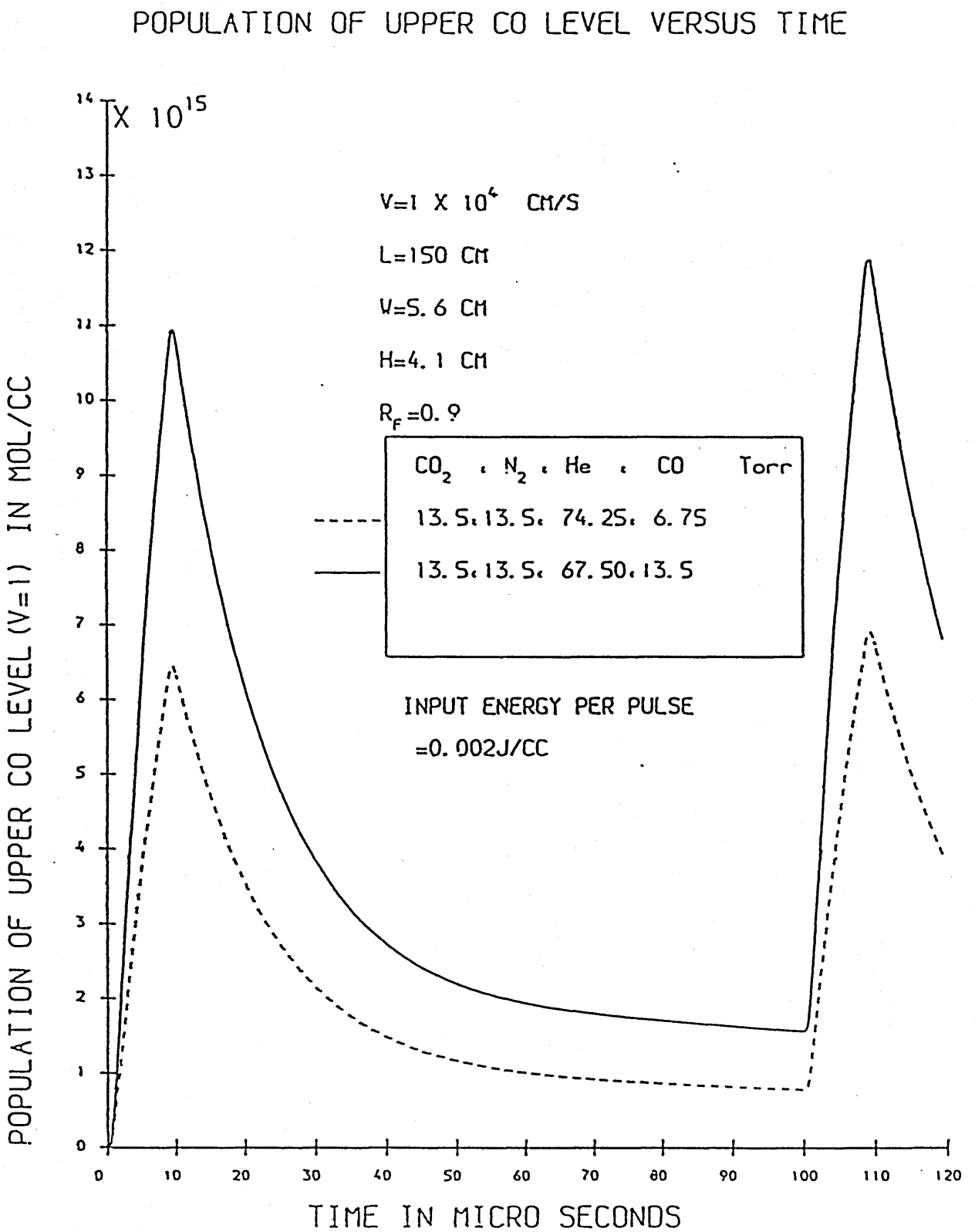
POPULATION OF UPPER CO LEVEL VERSUS TIME
X 10^15
POPULATION OF UPPER CO LEVEL (V=1) IN MOL/CC
V=1 X 10^4 CM/S
L=150 CM
W=5.6 CM
H=4.1 CM
R_F=0.9
CO2 : N2 : He : CO Torr
13.5 : 13.5 : 74.25 : 6.75
13.5 : 13.5 : 67.50 : 13.5
INPUT ENERGY PER PULSE
=0.002J/CC
0 1 2 3 4 5 6 7 8 9 10 11 12 13 14
0 10 20 30 40 50 60 70 80 90 100 110 120
TIME IN MICRO SECONDS

GRAPH (4.42)

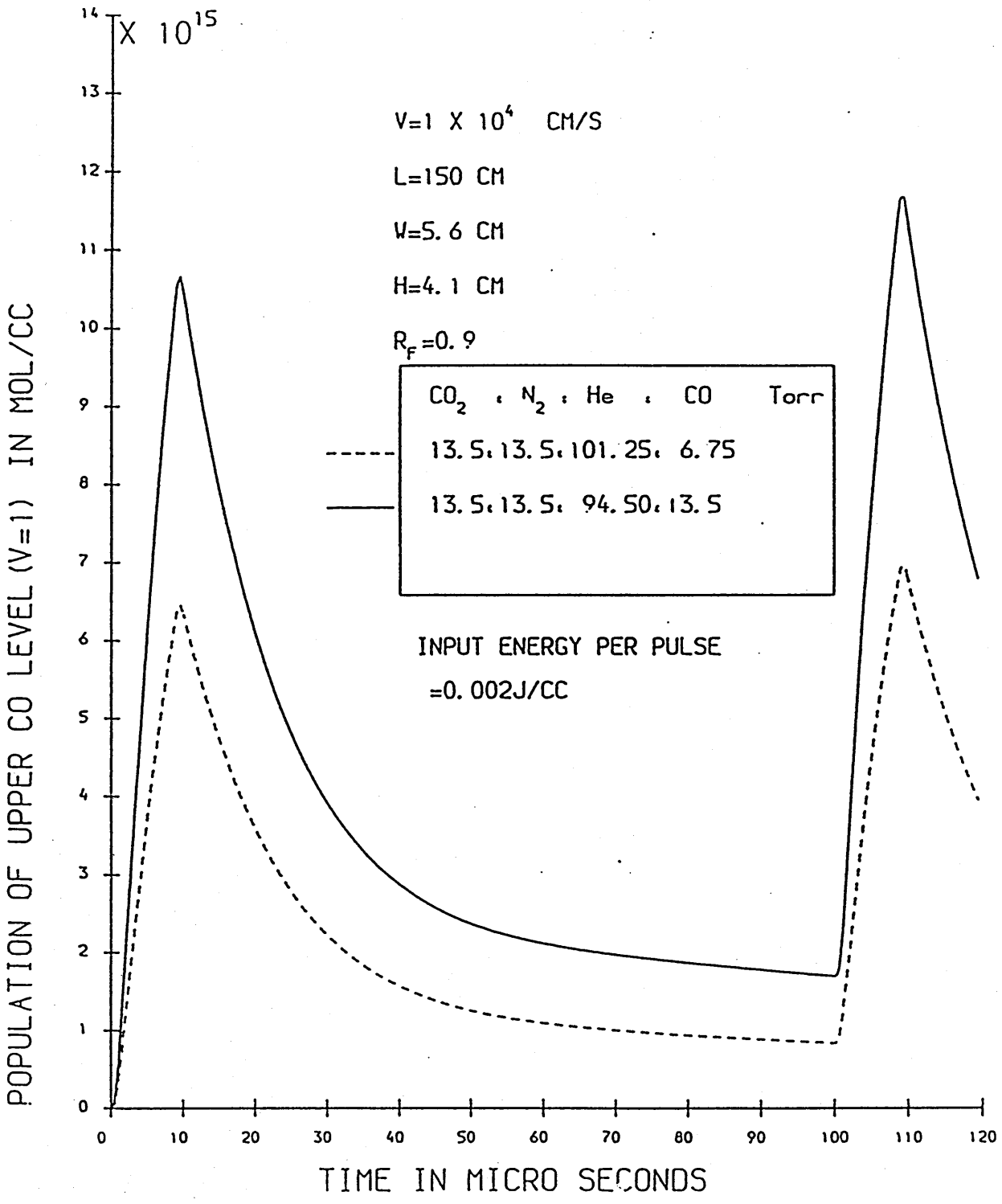
POPULATION OF UPPER CO LEVEL VERSUS TIME
X 10^15
V=1 X 10^4 CM/S
L=150 CM
W=5.6 CM
H=4.1 CM
R_F=0.9
CO2 : N2 : He : CO Torr
13.5 : 13.5 : 101.25 : 6.75
13.5 : 13.5 : 94.50 : 13.5
INPUT ENERGY PER PULSE
=0.002J/CC
POPULATION OF UPPER CO LEVEL (V=1) IN MOL/CC
TIME IN MICRO SECONDS
0 10 20 30 40 50 60 70 80 90 100 110 120
0 1 2 3 4 5 6 7 8 9 10 11 12 13 14

GRAPH (4.43)

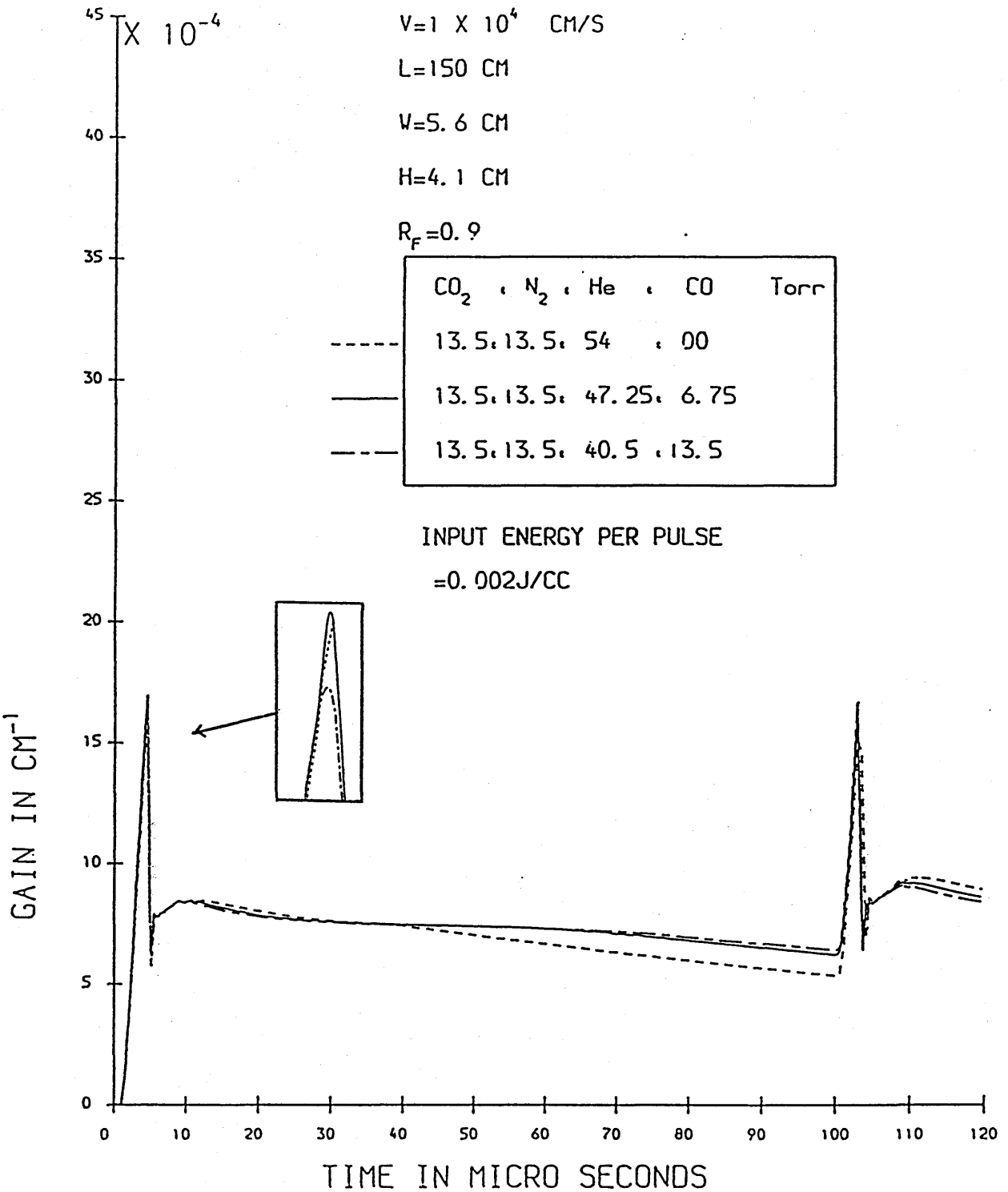
GAIN VERSUS TIME
X 10^-4
V=1 X 10^4 CM/S
L=150 CM
W=5.6 CM
H=4.1 CM
R_F=0.9
CO2 : N2 : He : CO Torr
13.5 : 13.5 : 54 : 00
13.5 : 13.5 : 47.25 : 6.75
13.5 : 13.5 : 40.5 : 13.5
INPUT ENERGY PER PULSE
=0.002J/CC
GAIN IN CM^-1
TIME IN MICRO SECONDS
0
5
10
15
20
25
30
35
40
45
0
10
20
30
40
50
60
70
80
90
100
110
120

GRAPH (4.44)

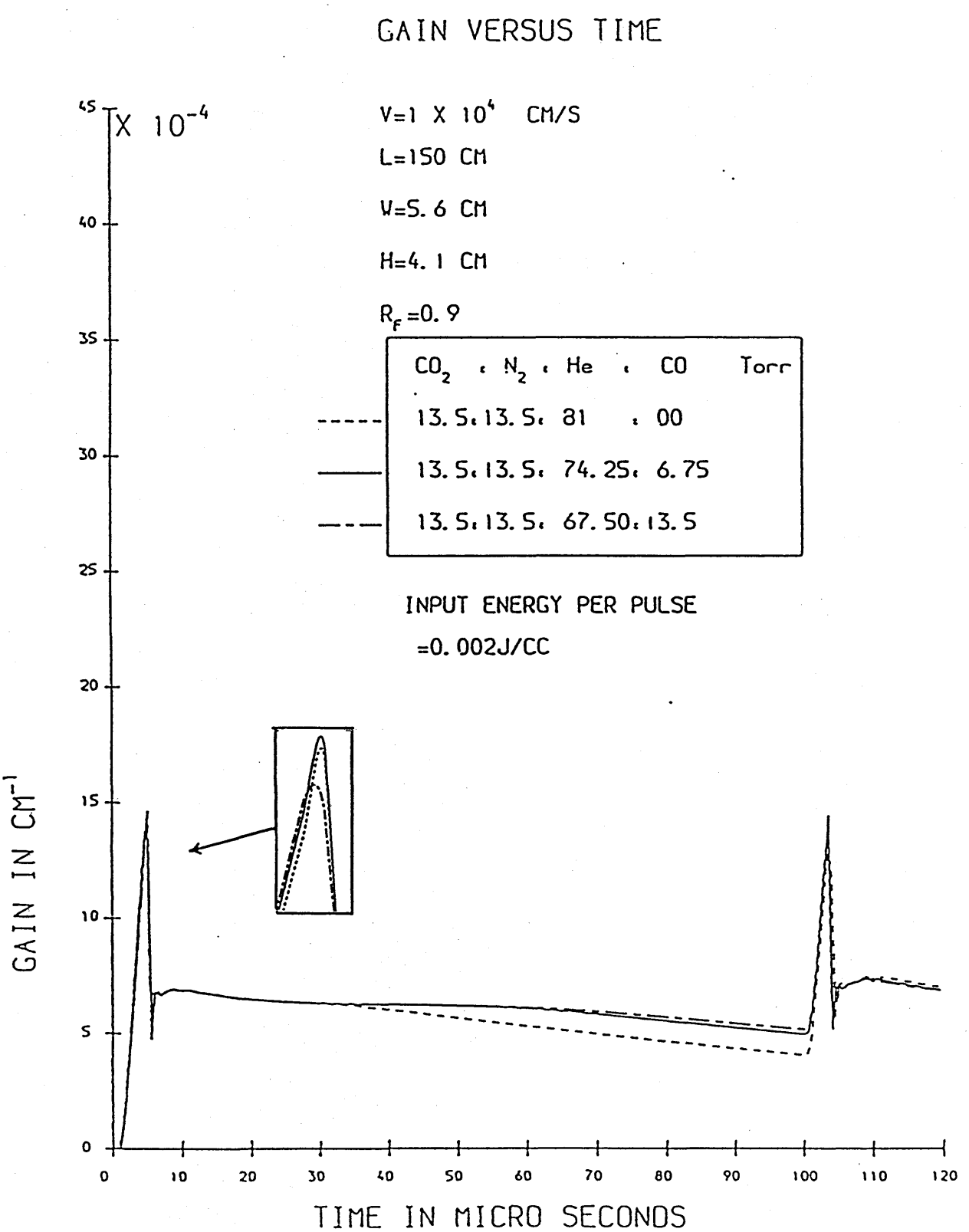
GAIN VERSUS TIME
X 10^-4
V=1 X 10^4 CM/S
L=150 CM
W=5.6 CM
H=4.1 CM
R_F=0.9
CO2 : N2 : He : CO Torr
13.5 : 13.5 : 81 : 00
13.5 : 13.5 : 74.25 : 6.75
13.5 : 13.5 : 67.50 : 13.5
INPUT ENERGY PER PULSE
=0.002J/CC
GAIN IN CM^-1
TIME IN MICRO SECONDS
0
5
10
15
20
25
30
35
40
45
0
10
20
30
40
50
60
70
80
90
100
110
120

GRAPH (4.45)

GAIN VERSUS TIME

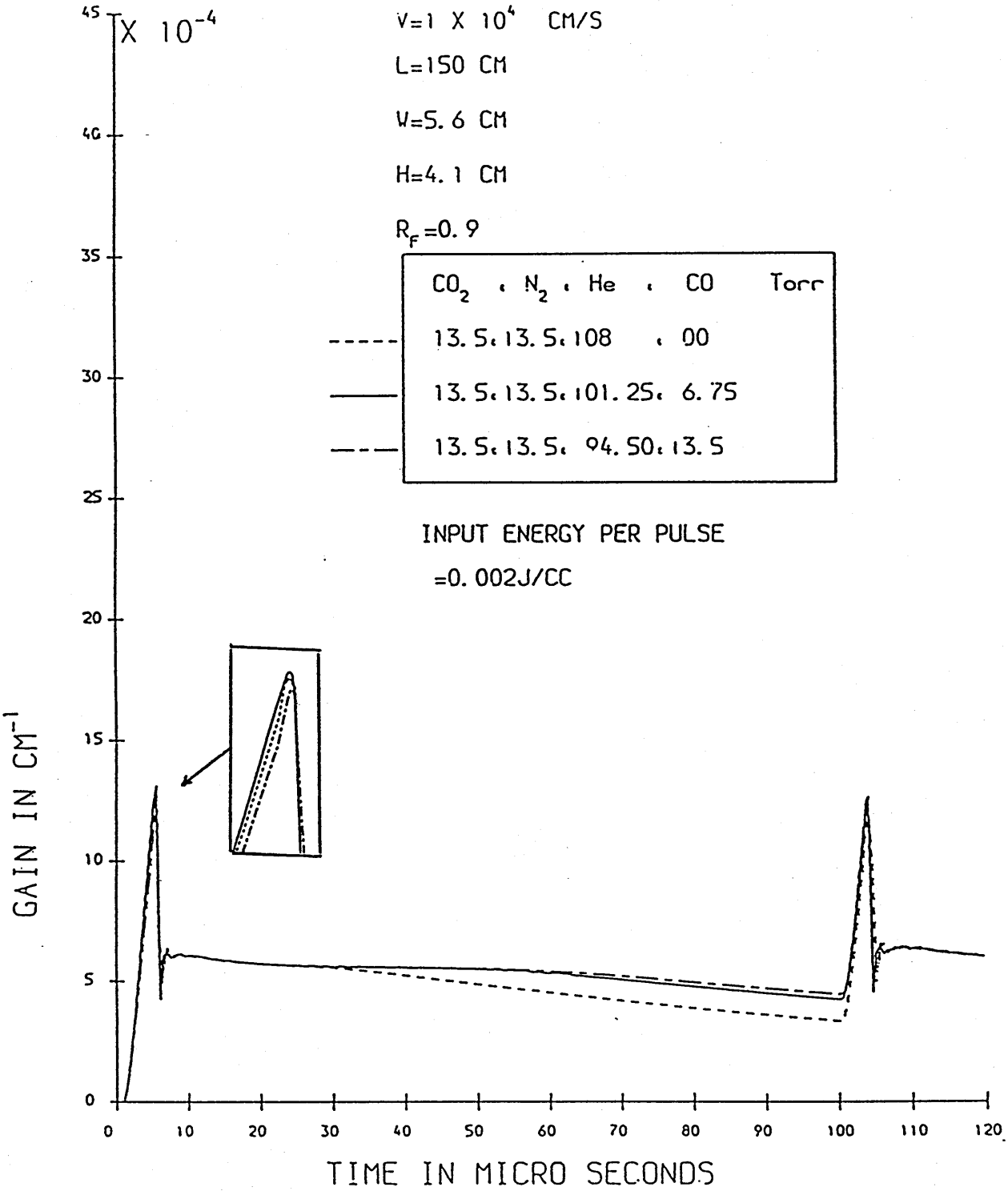

GRAPH (4.46)

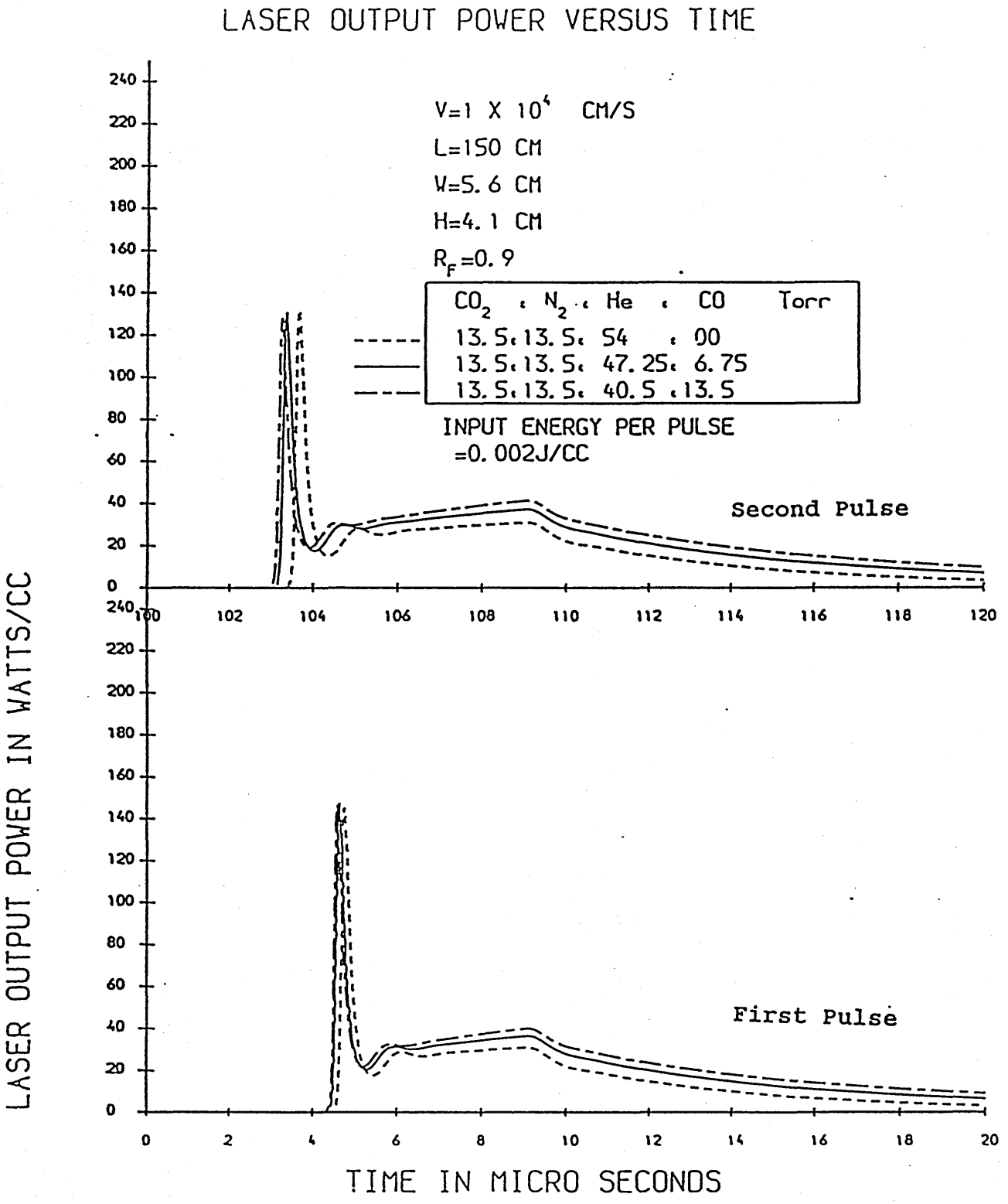
LASER OUTPUT POWER VERSUS TIME
V=1 X 10⁴ CM/S
L=150 CM
W=5.6 CM
H=4.1 CM
R_F=0.9
CO2 : N2 : He : CO Torr
13.5 : 13.5 : 54 : 00
13.5 : 13.5 : 47.25 : 6.75
13.5 : 13.5 : 40.5 : 13.5
INPUT ENERGY PER PULSE
=0.002J/CC
Second Pulse
First Pulse
LASER OUTPUT POWER IN WATTS/CC
TIME IN MICRO SECONDS

GRAPH (4.47)

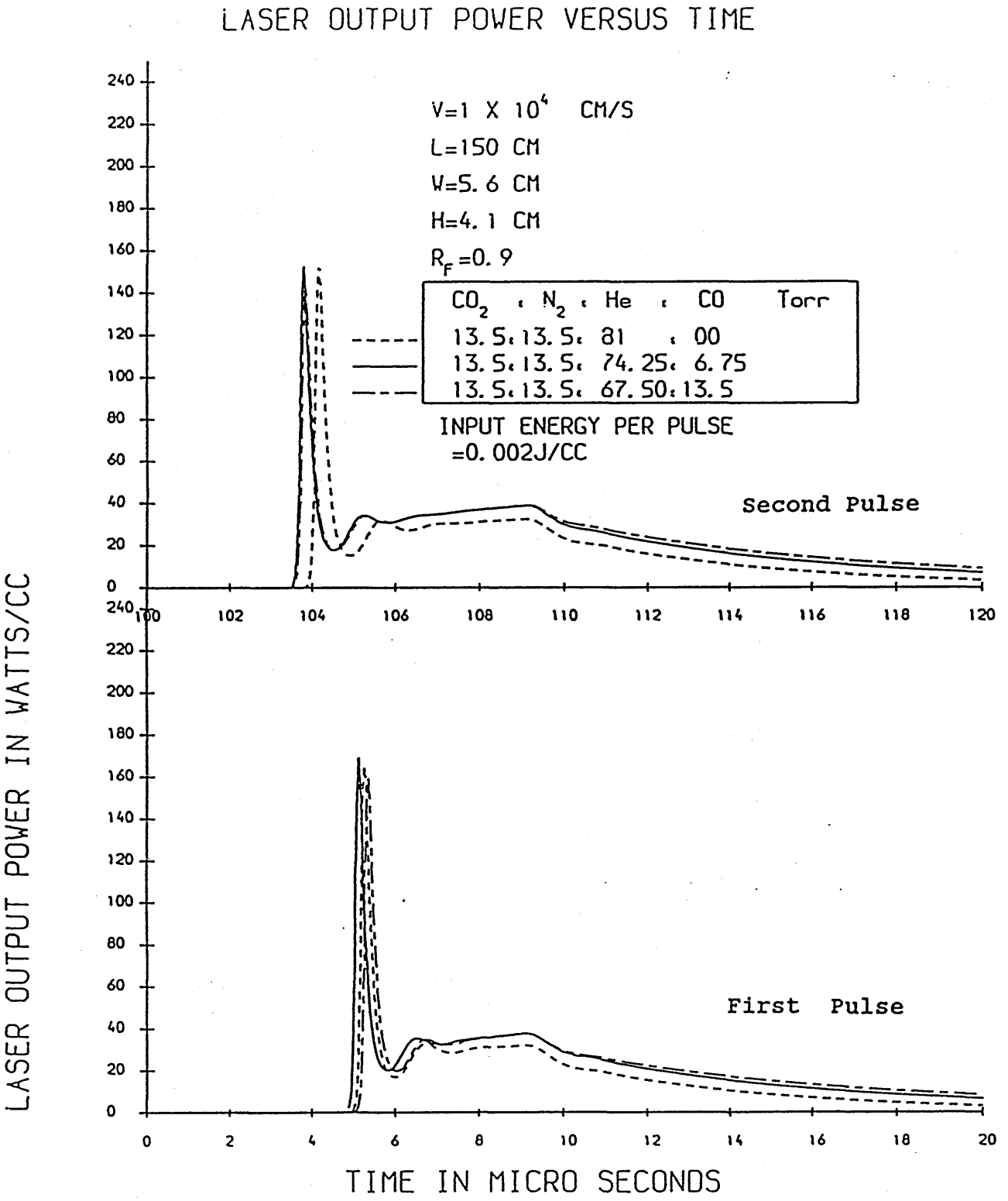
LASER OUTPUT POWER VERSUS TIME
V=1 X 10^4 CM/S
L=150 CM
W=5.6 CM
H=4.1 CM
R_F=0.9
CO2 : N2 : He : CO Torr
13.5 : 13.5 : 81 : 00
13.5 : 13.5 : 74.25 : 6.75
13.5 : 13.5 : 67.50 : 13.5
INPUT ENERGY PER PULSE
=0.002J/CC
Second Pulse
First Pulse
LASER OUTPUT POWER IN WATTS/CC
TIME IN MICRO SECONDS

GRAPH (4.48)

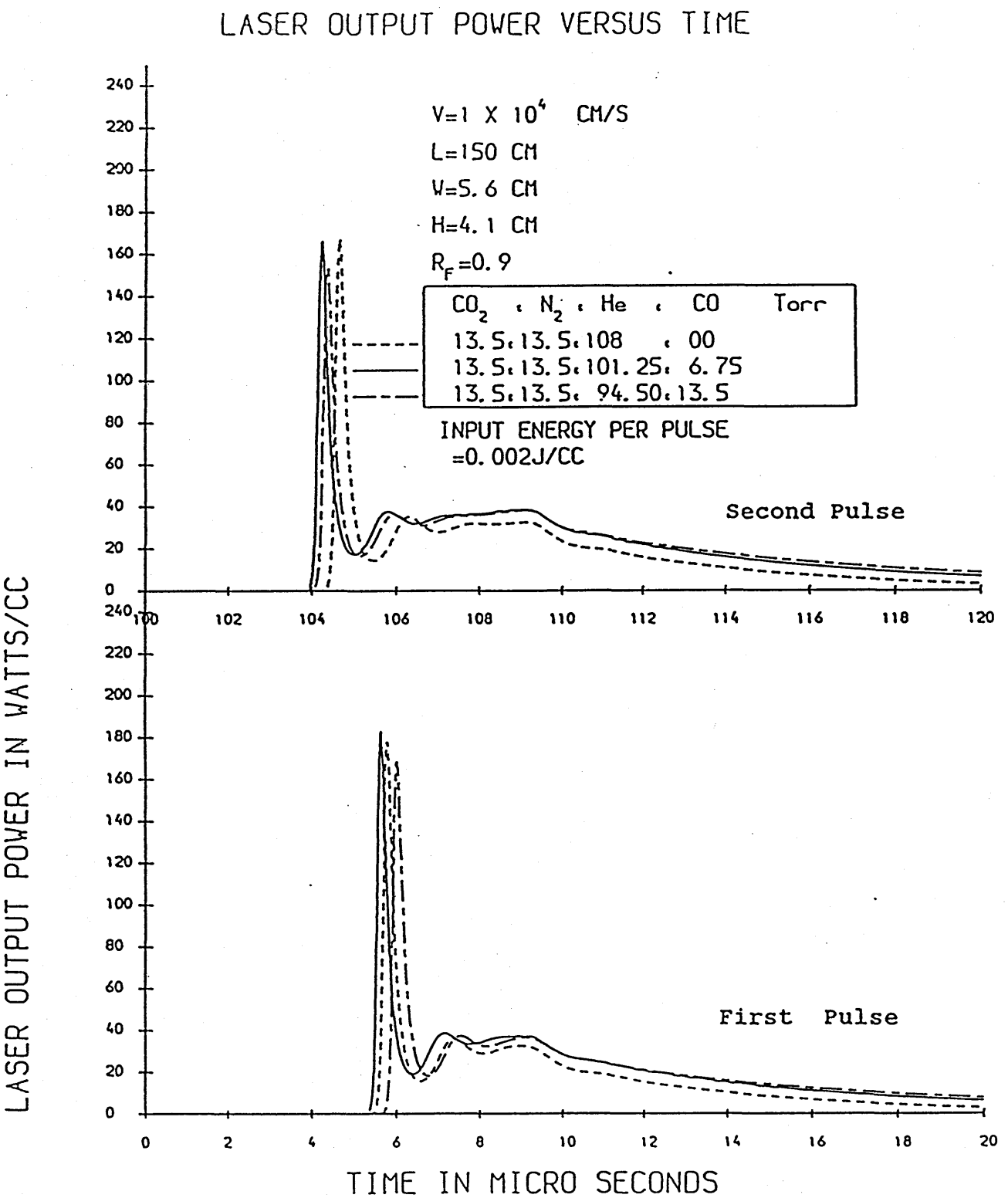
LASER OUTPUT POWER VERSUS TIME
V=1 X 10^4 CM/S
L=150 CM
W=5.6 CM
H=4.1 CM
R_F=0.9
CO2 : N2 : He : CO Torr
13.5 : 13.5 : 108 : 00
13.5 : 13.5 : 101.25 : 6.75
13.5 : 13.5 : 94.50 : 13.5
INPUT ENERGY PER PULSE
=0.002J/CC
Second Pulse
First Pulse
LASER OUTPUT POWER IN WATTS/CC
TIME IN MICRO SECONDS

GRAPH (4.49)

PULSE DELAY TIME VERSUS CO CONTENT

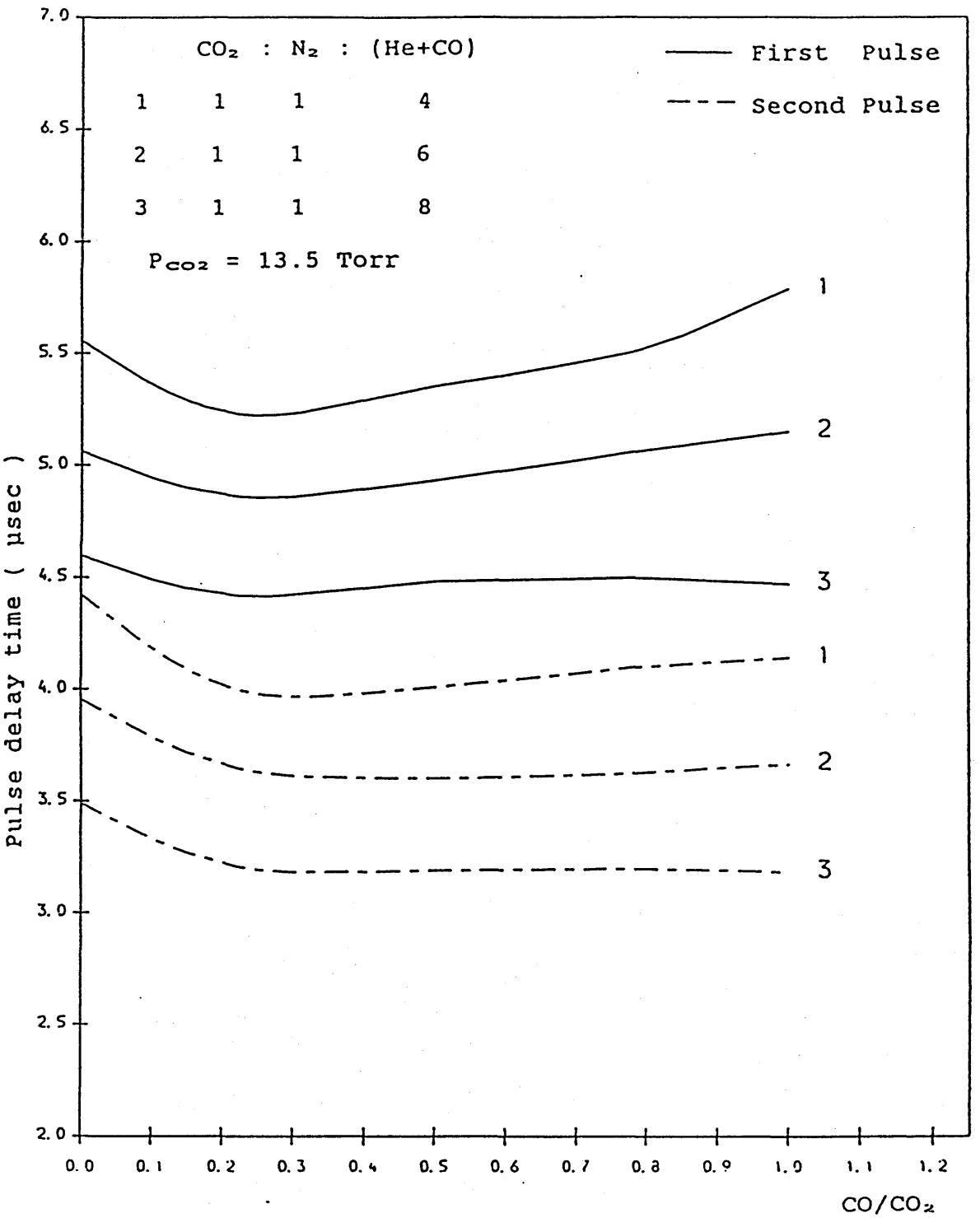

GRAPH (4.50)

MAXIMUM POWER VERSUS CO CONTENT

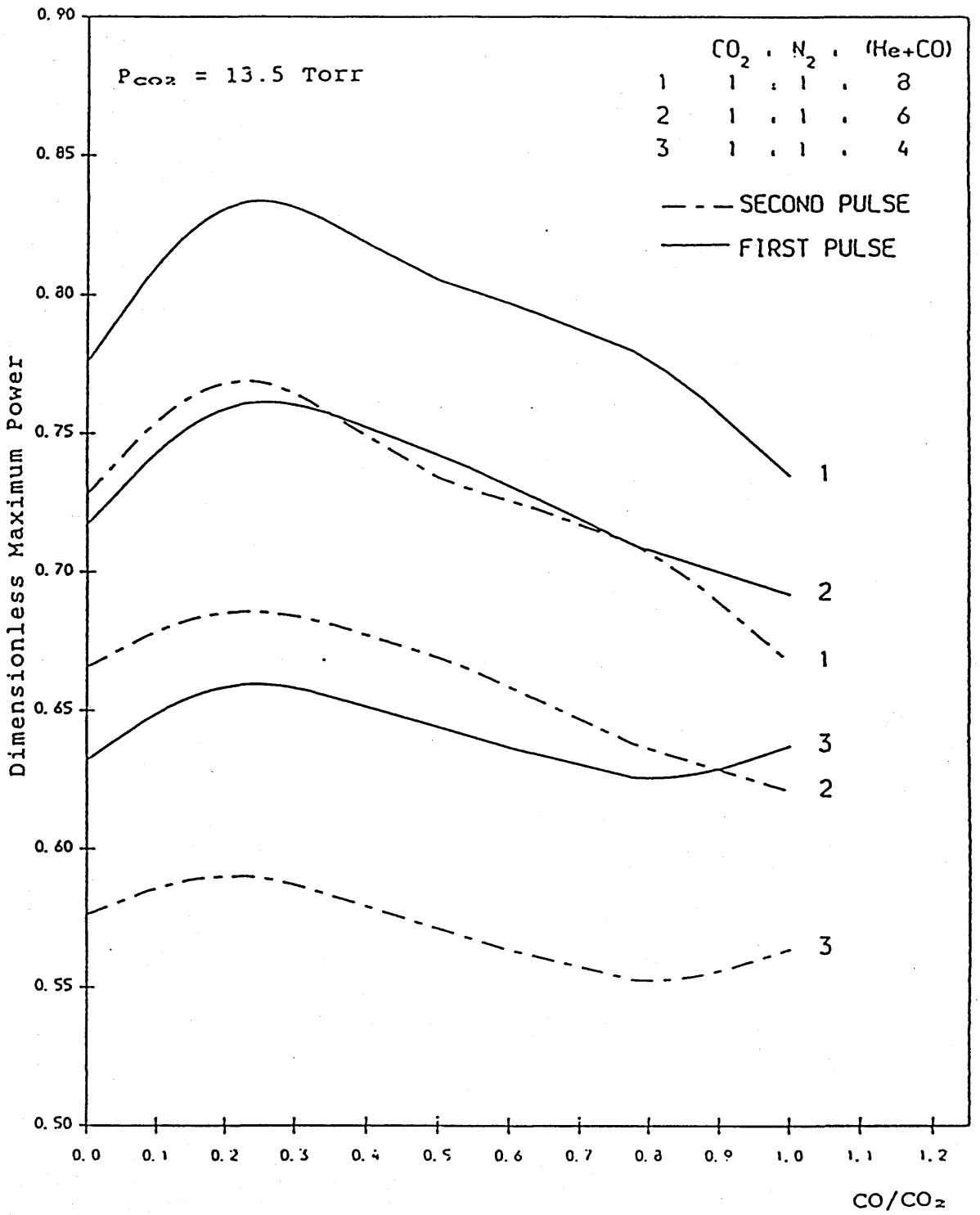

GRAPH (4.51)

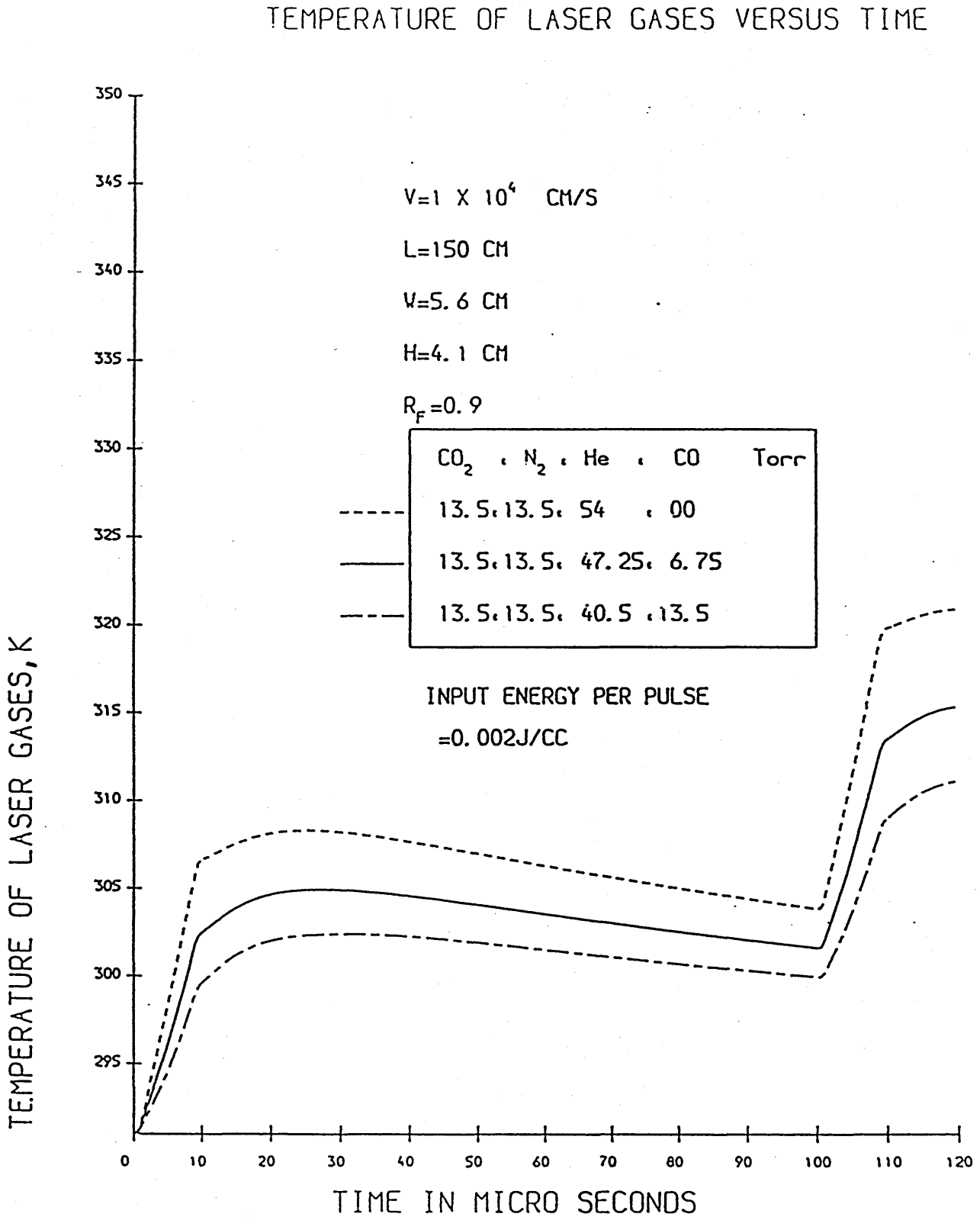
TEMPERATURE OF LASER GASES VERSUS TIME
V=1 X 10^4 CM/S
L=150 CM
W=5.6 CM
H=4.1 CM
R_F=0.9
CO2 : N2 : He : CO Torr
13.5 : 13.5 : 54 : 00
13.5 : 13.5 : 47.25 : 6.75
13.5 : 13.5 : 40.5 : 13.5
INPUT ENERGY PER PULSE
=0.002J/CC
TEMPERATURE OF LASER GASES, K
350
345
340
335
330
325
320
315
310
305
300
295
0
10
20
30
40
50
60
70
80
90
100
110
120
TIME IN MICRO SECONDS

GRAPH (4.52)

TEMPERATURE OF LASER GASES VERSUS TIME

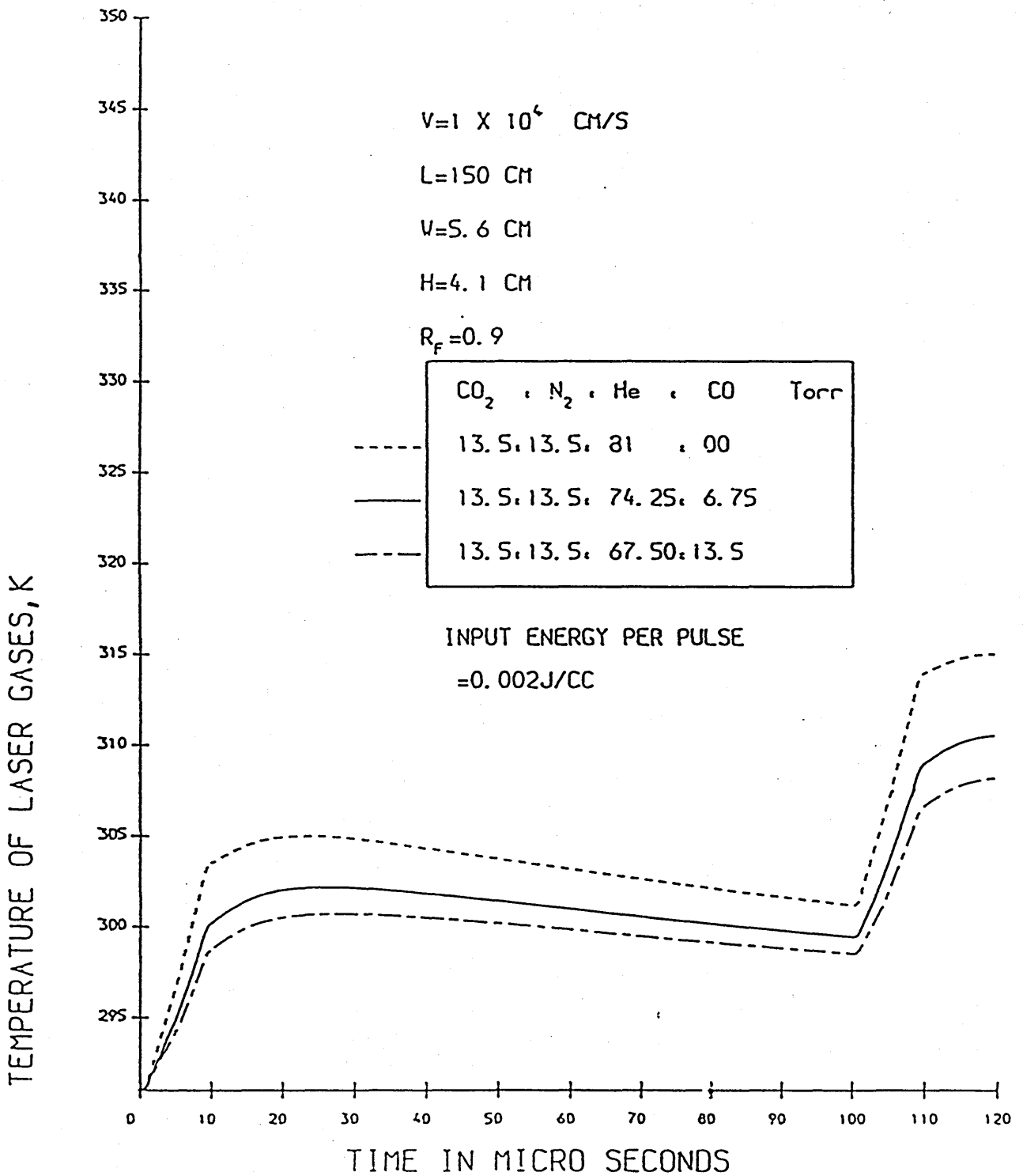

GRAPH (4.53)

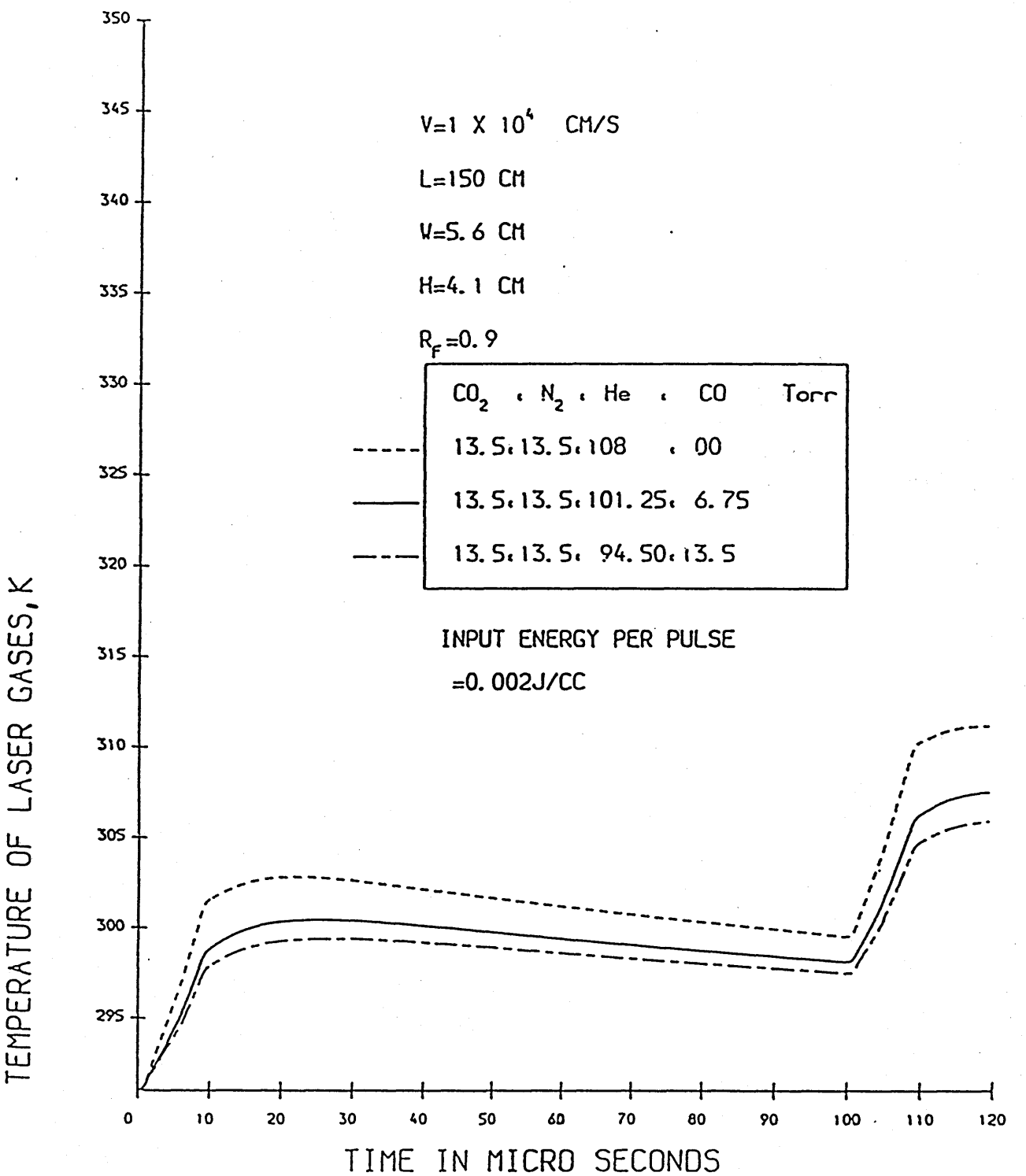
TEMPERATURE OF LASER GASES VERSUS TIME
V=1 X 10⁴ CM/S
L=150 CM
W=5.6 CM
H=4.1 CM
R_F=0.9
CO2 : N2 : He : CO Torr
13.5 : 13.5 : 108 : 00
13.5 : 13.5 : 101.25 : 6.75
13.5 : 13.5 : 94.50 : 13.5
INPUT ENERGY PER PULSE
=0.002J/CC
TEMPERATURE OF LASER GASES, K
350
345
340
335
330
325
320
315
310
305
300
295
0
10
20
30
40
50
60
70
80
90
100
110
120
TIME IN MICRO SECONDS

GRAPH (4.54)

MAXIMUM GAS TEMPERATURE VERSUS CO CONTENT

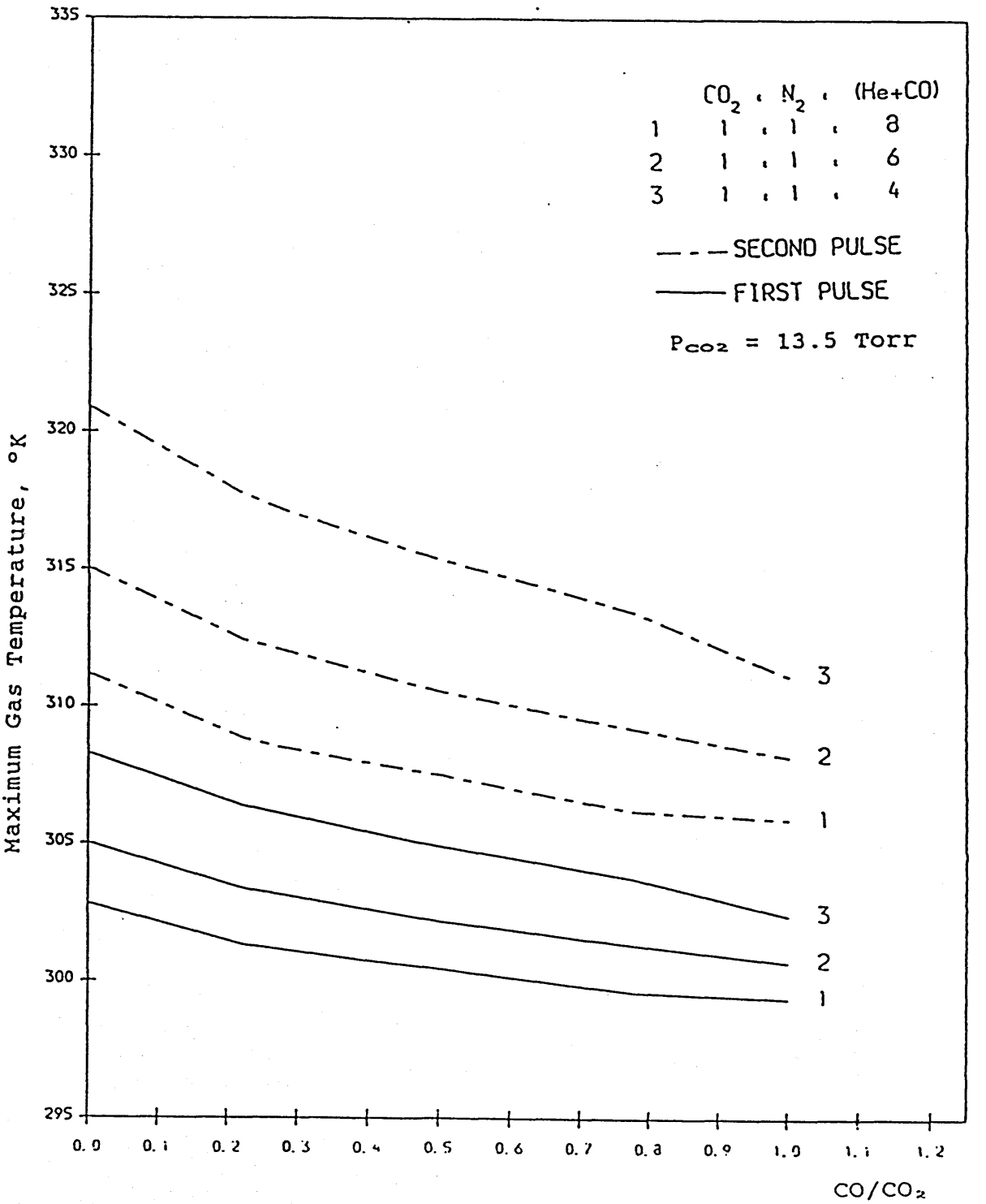

GRAPH (4.55)

PULSE DURATION VERSUS CO CONTENT

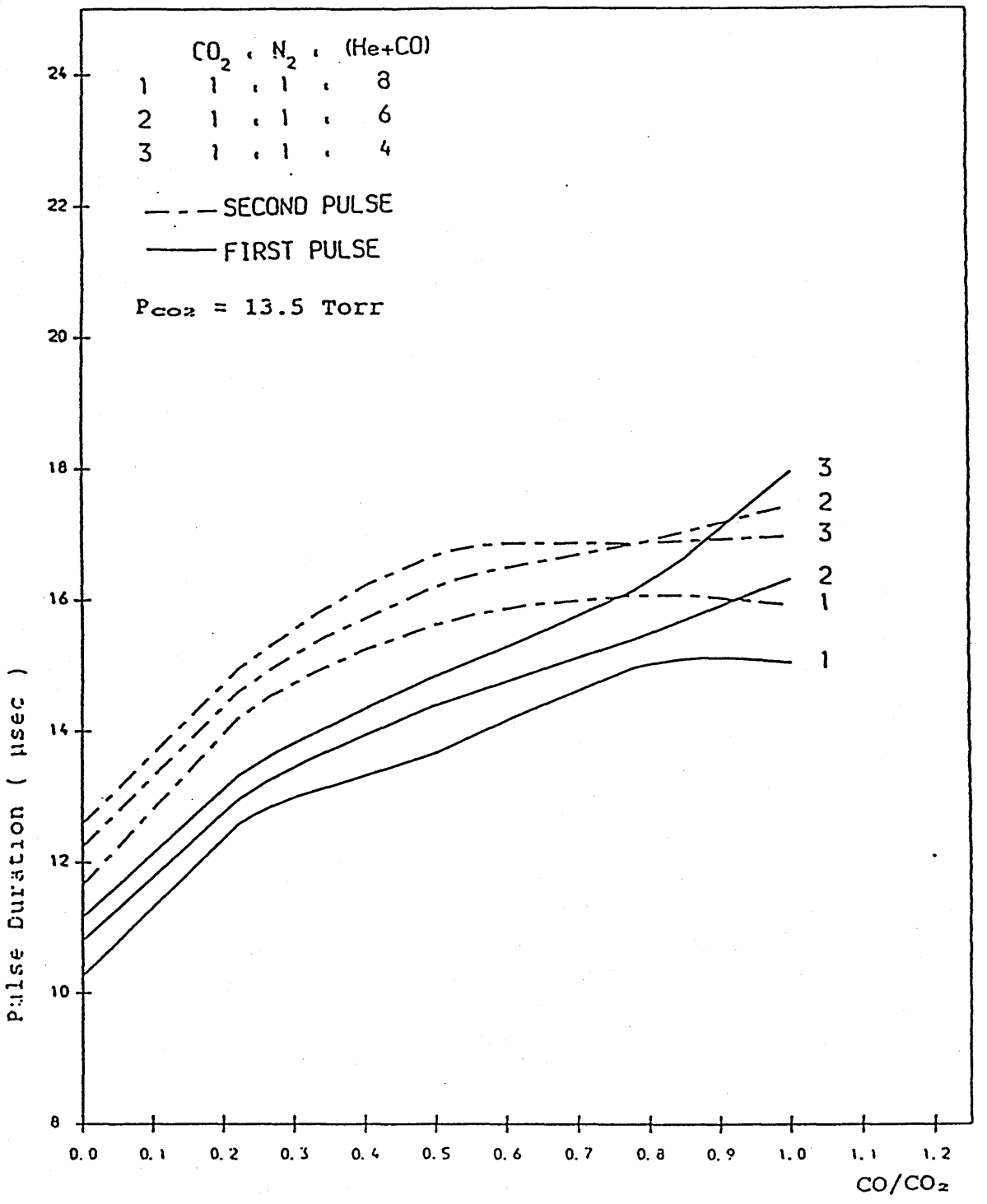

GRAPH (4.56)

AVERAGE POWER VERSUS CO CONTENT

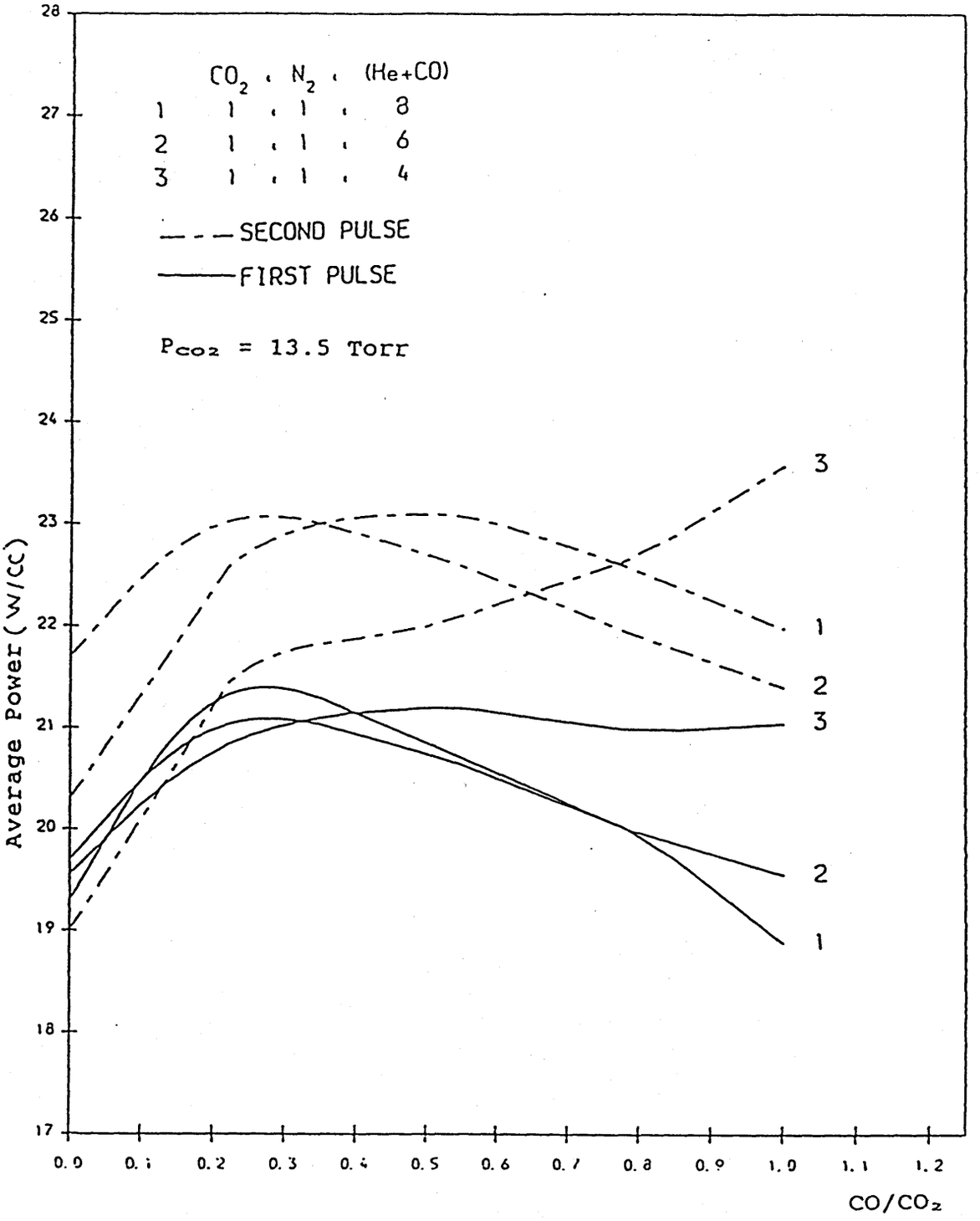

GRAPH (4.57)

OVERALL EFFICIENCY VERSUS CO CONTENT

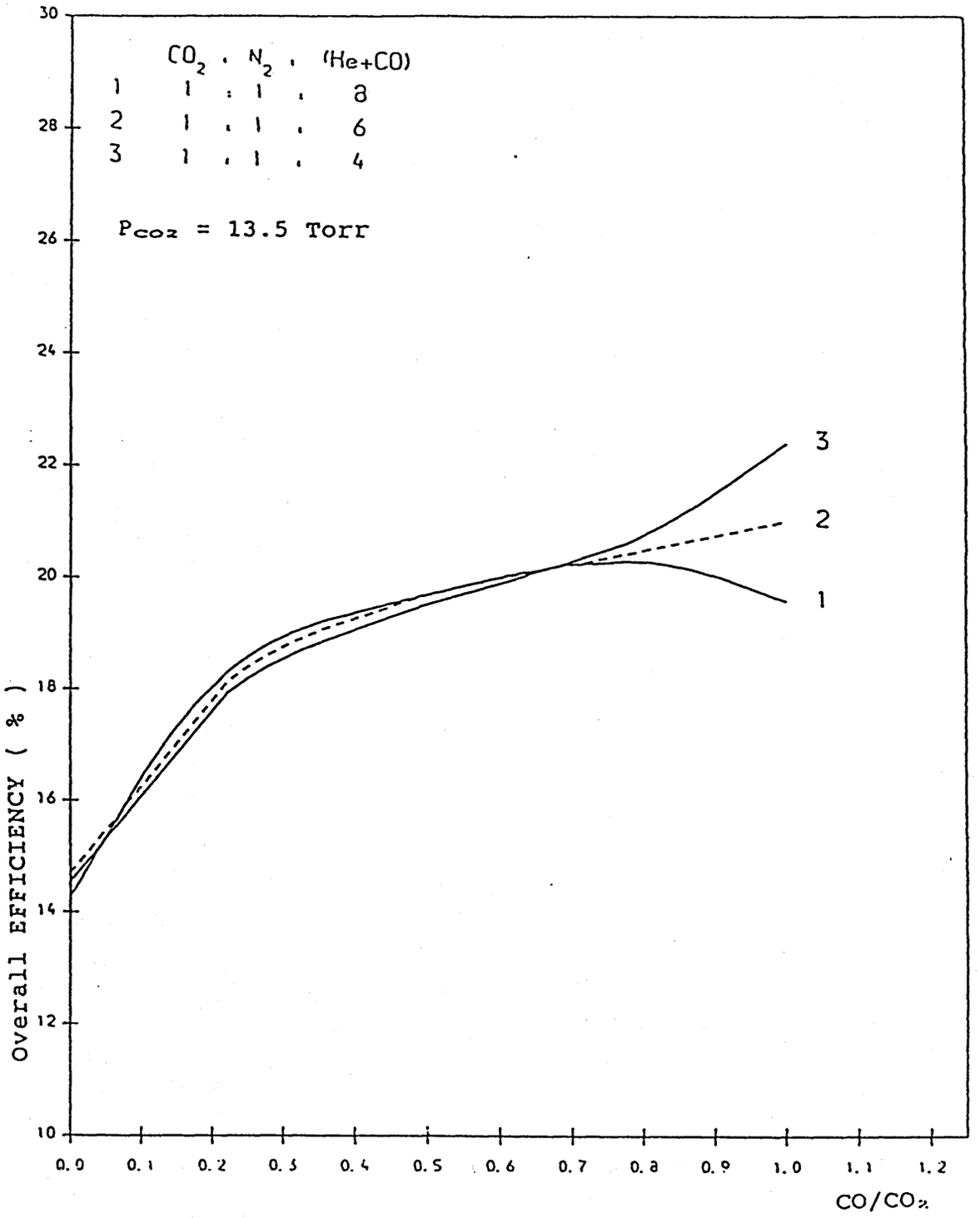

GRAPH (4.58)

EFFECTIVE EFFICIENCY VERSUS CO CONTENT

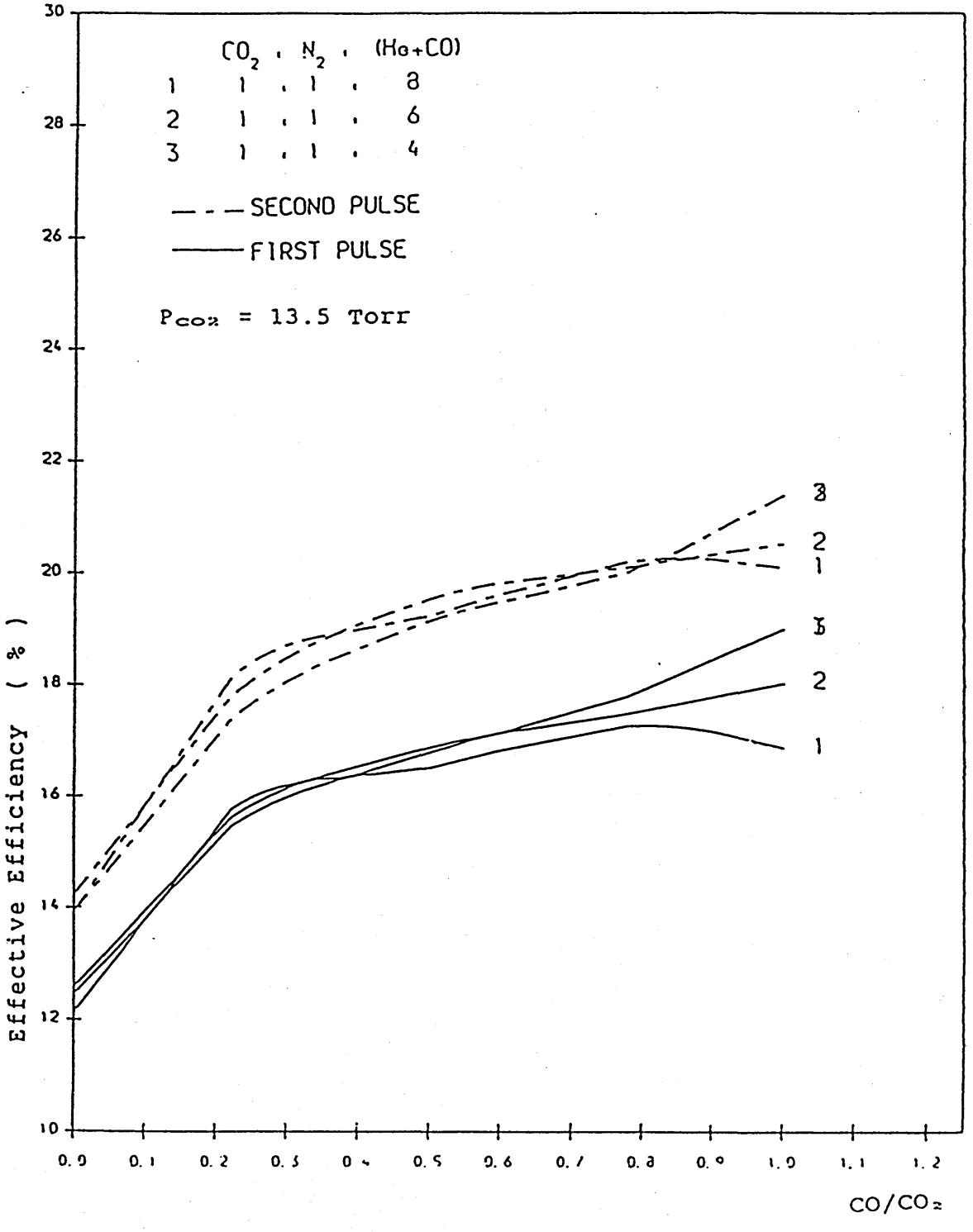

GRAPH (4.59)

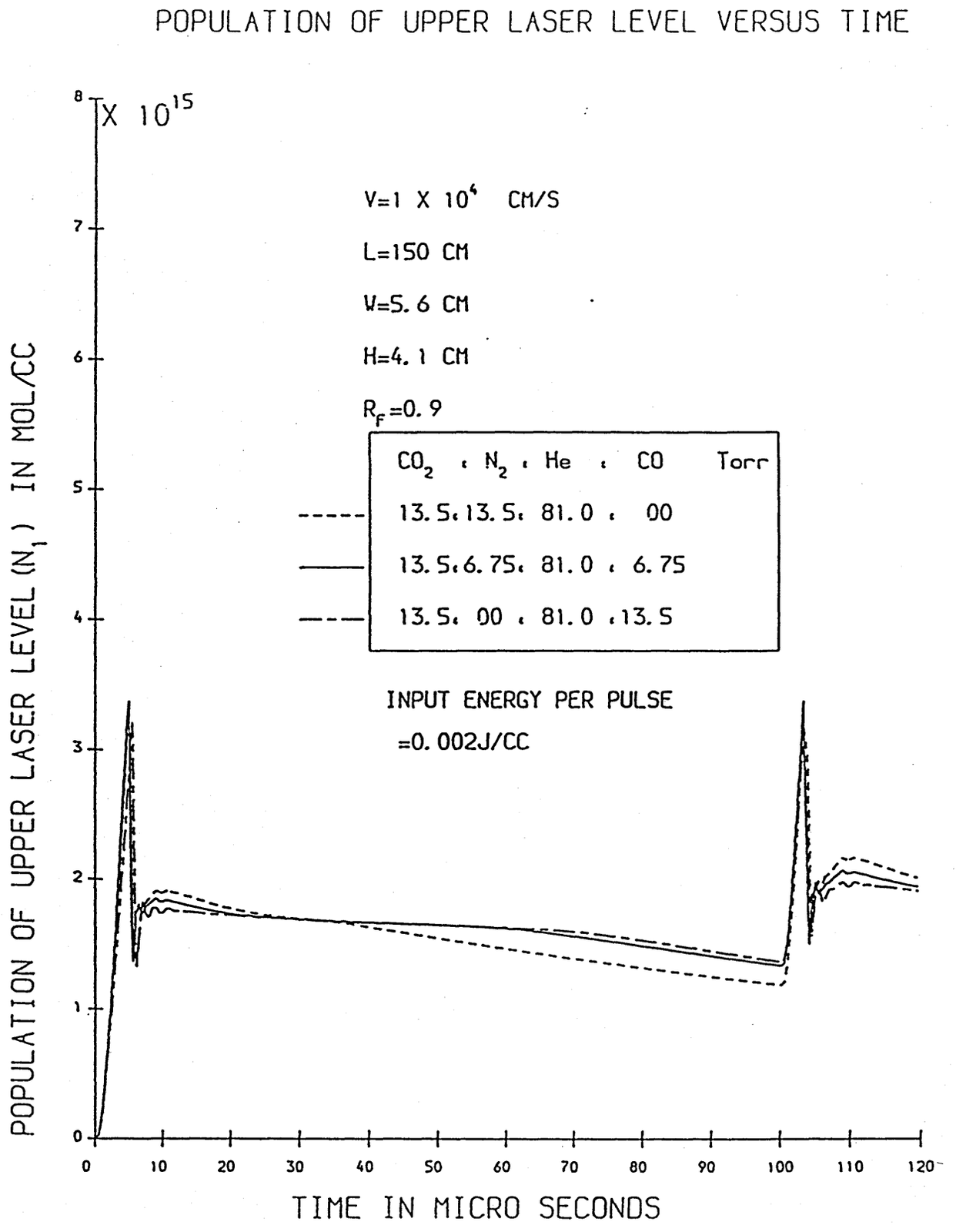
POPULATION OF UPPER LASER LEVEL VERSUS TIME
X 10^15
V=1 X 10^4 CM/S
L=150 CM
W=5.6 CM
H=4.1 CM
R_F=0.9
CO2 : N2 : He : CO Torr
13.5 : 13.5 : 81.0 : 00
13.5 : 6.75 : 81.0 : 6.75
13.5 : 00 : 81.0 : 13.5
INPUT ENERGY PER PULSE
=0.002J/CC
POPULATION OF UPPER LASER LEVEL (N1) IN MOL/CC
0
1
2
3
4
5
6
7
8
0
10
20
30
40
50
60
70
80
90
100
110
120
TIME IN MICRO SECONDS

GRAPH (4.60)

POPULATION OF UPPER LASER LEVEL VERSUS TIME

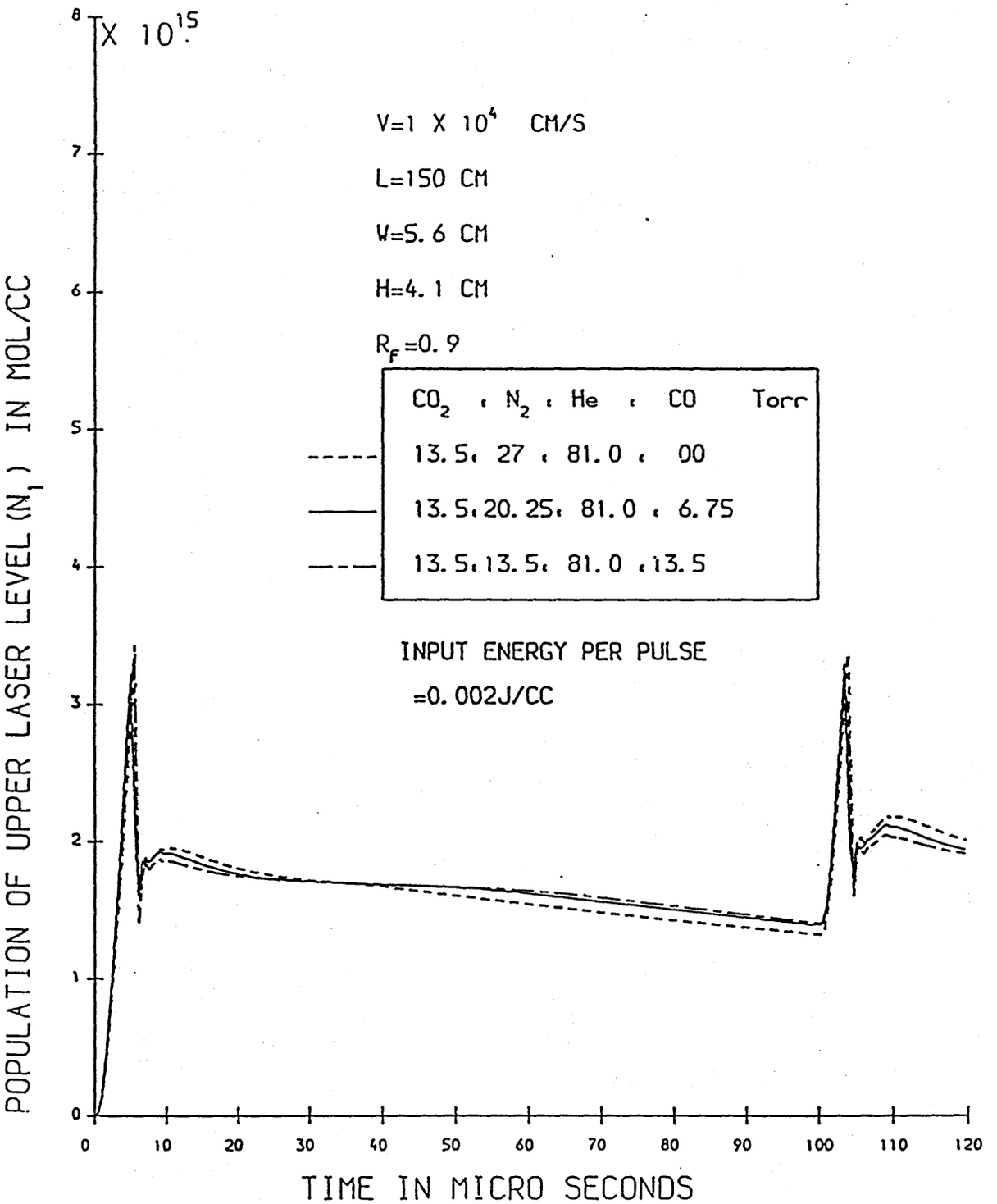

GRAPH (4.61)

POPULATION OF UPPER NITROGEN LEVEL VERSUS TIME

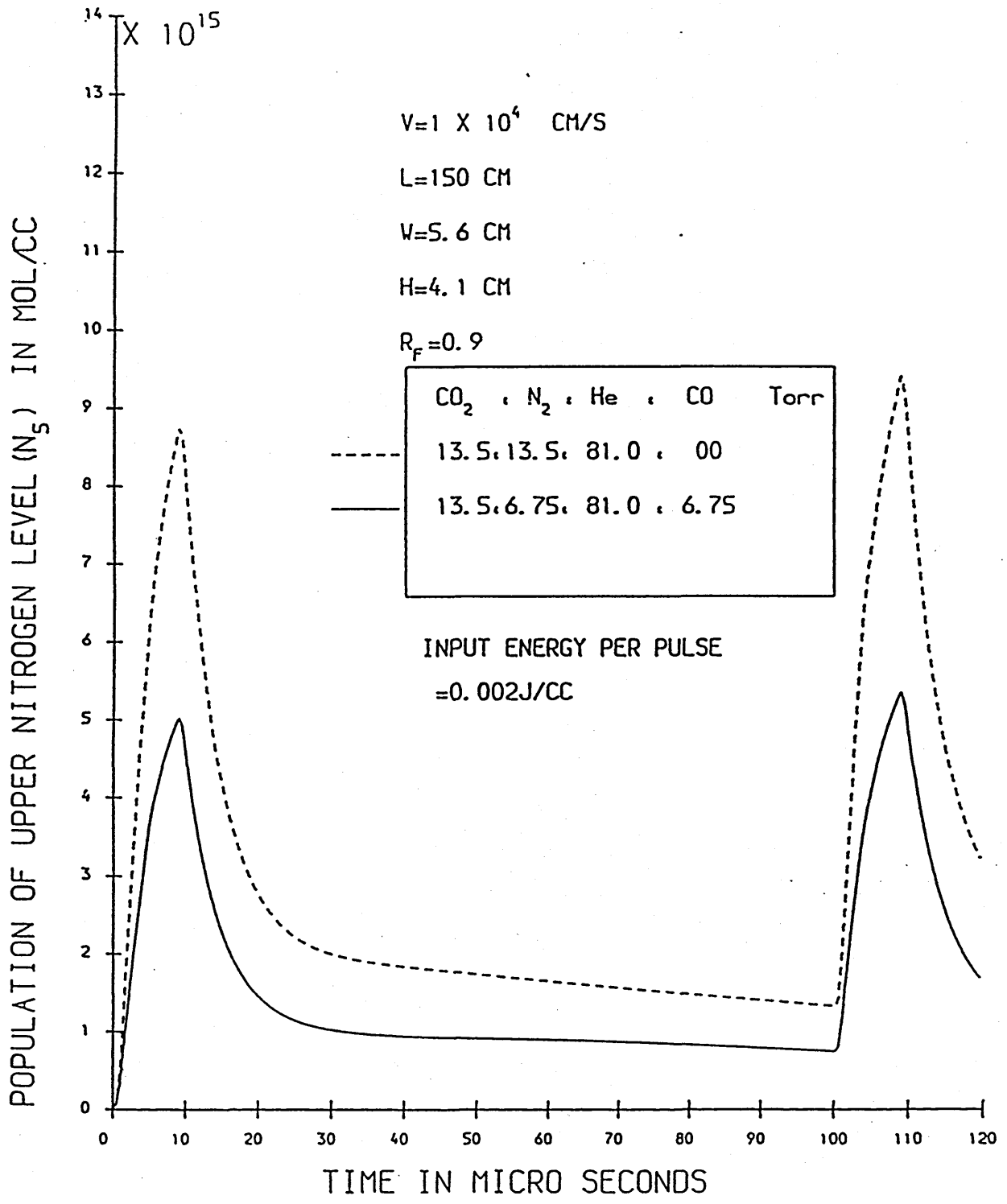

GRAPH (4.62)

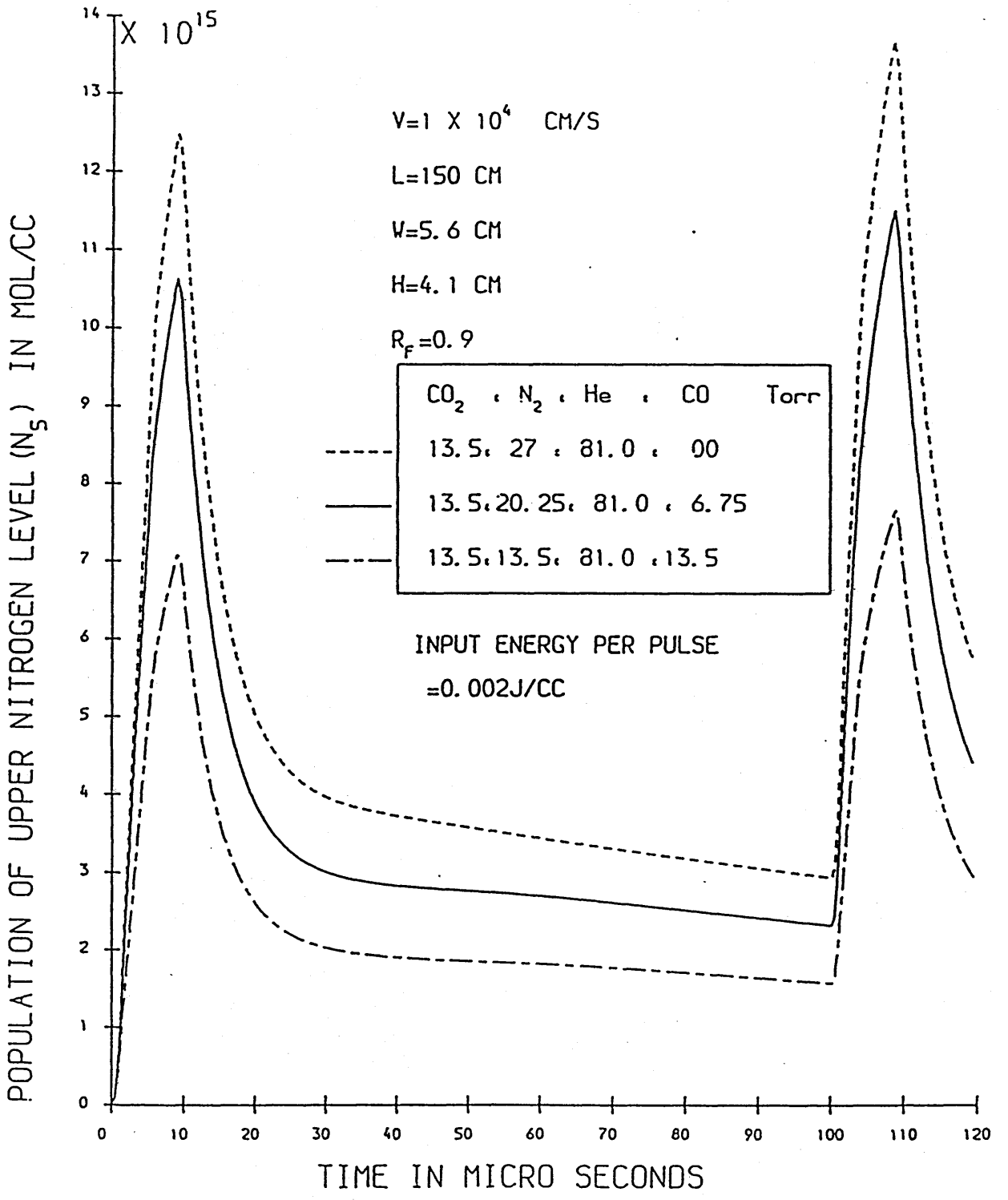
POPULATION OF UPPER NITROGEN LEVEL VERSUS TIME
X 10^15
POPULATION OF UPPER NITROGEN LEVEL (N_5) IN MOL/CC
V=1 X 10^4 CM/S
L=150 CM
W=5.6 CM
H=4.1 CM
R_F=0.9
CO_2 : N_2 : He : CO Torr
13.5: 27 : 81.0 : 00
13.5:20.25: 81.0 : 6.75
13.5:13.5: 81.0 :13.5
INPUT ENERGY PER PULSE
=0.002J/CC
0 1 2 3 4 5 6 7 8 9 10 11 12 13 14
0 10 20 30 40 50 60 70 80 90 100 110 120
TIME IN MICRO SECONDS

GRAPH (4.63)

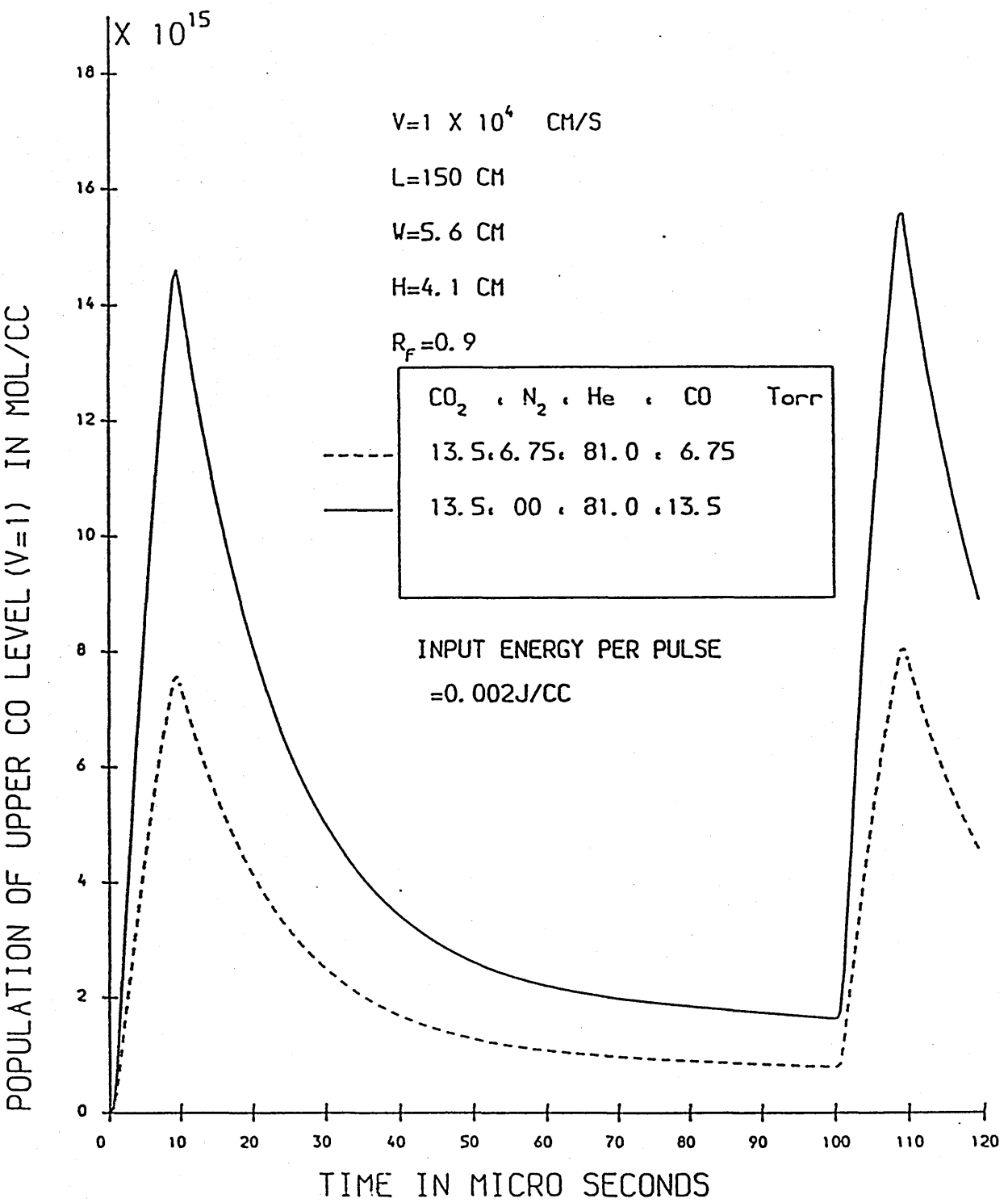
POPULATION OF UPPER CO LEVEL VERSUS TIME
X 10^15
V=1 X 10^4 CM/S
L=150 CM
W=5.6 CM
H=4.1 CM
R_F=0.9
CO2 : N2 : He : CO Torr
13.5:6.75: 81.0 : 6.75
13.5: 00 : 81.0 :13.5
INPUT ENERGY PER PULSE
=0.002J/CC
POPULATION OF UPPER CO LEVEL (V=1) IN MOL/CC
0
2
4
6
8
10
12
14
16
18
0
10
20
30
40
50
60
70
80
90
100
110
120
TIME IN MICRO SECONDS

GRAPH (4.64)

POPULATION OF UPPER CO LEVEL VERSUS TIME

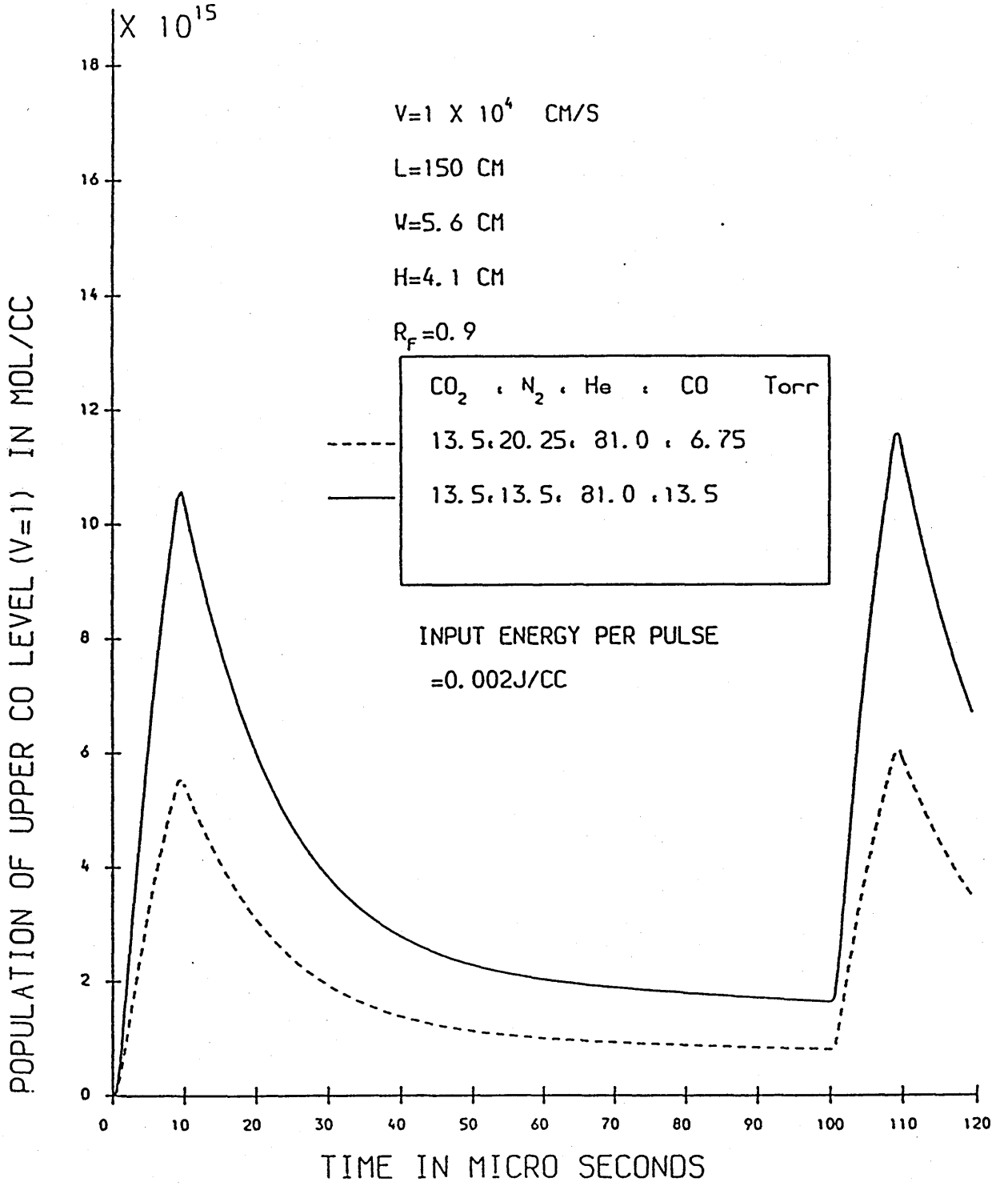

GRAPH (4.65)

GAIN VERSUS TIME

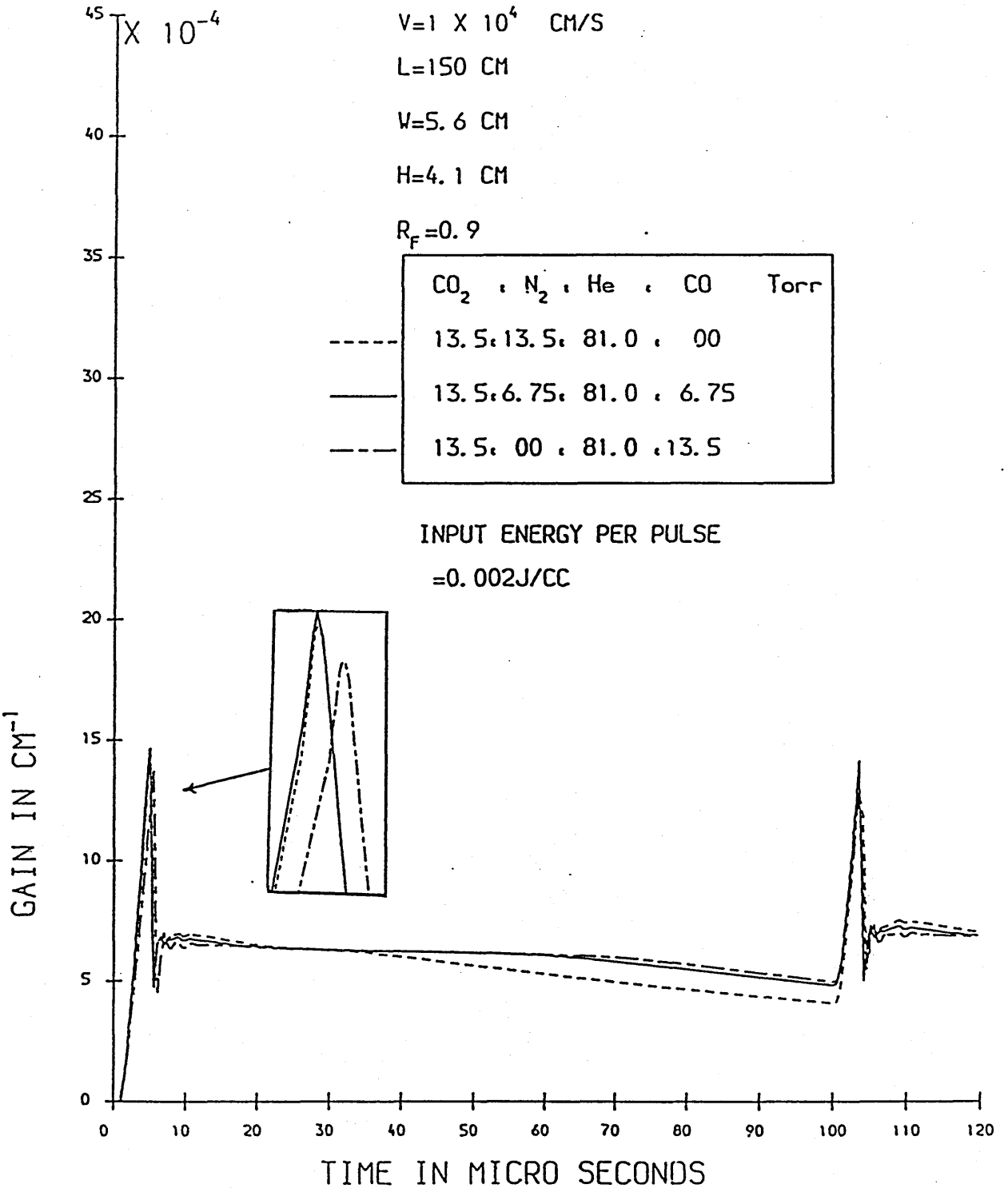

GRAPH (4.66)

GAIN VERSUS TIME

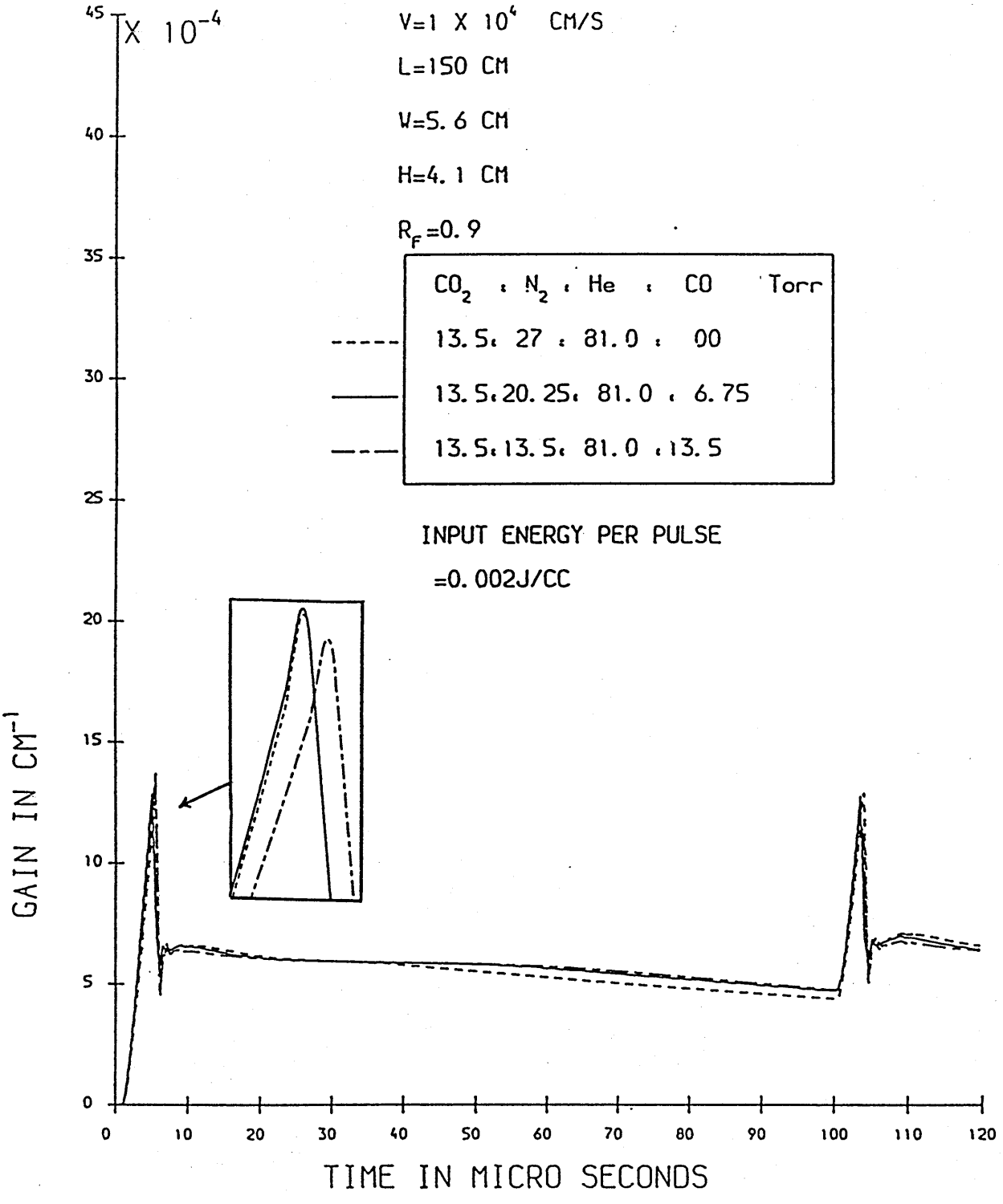

GRAPH (4.67)

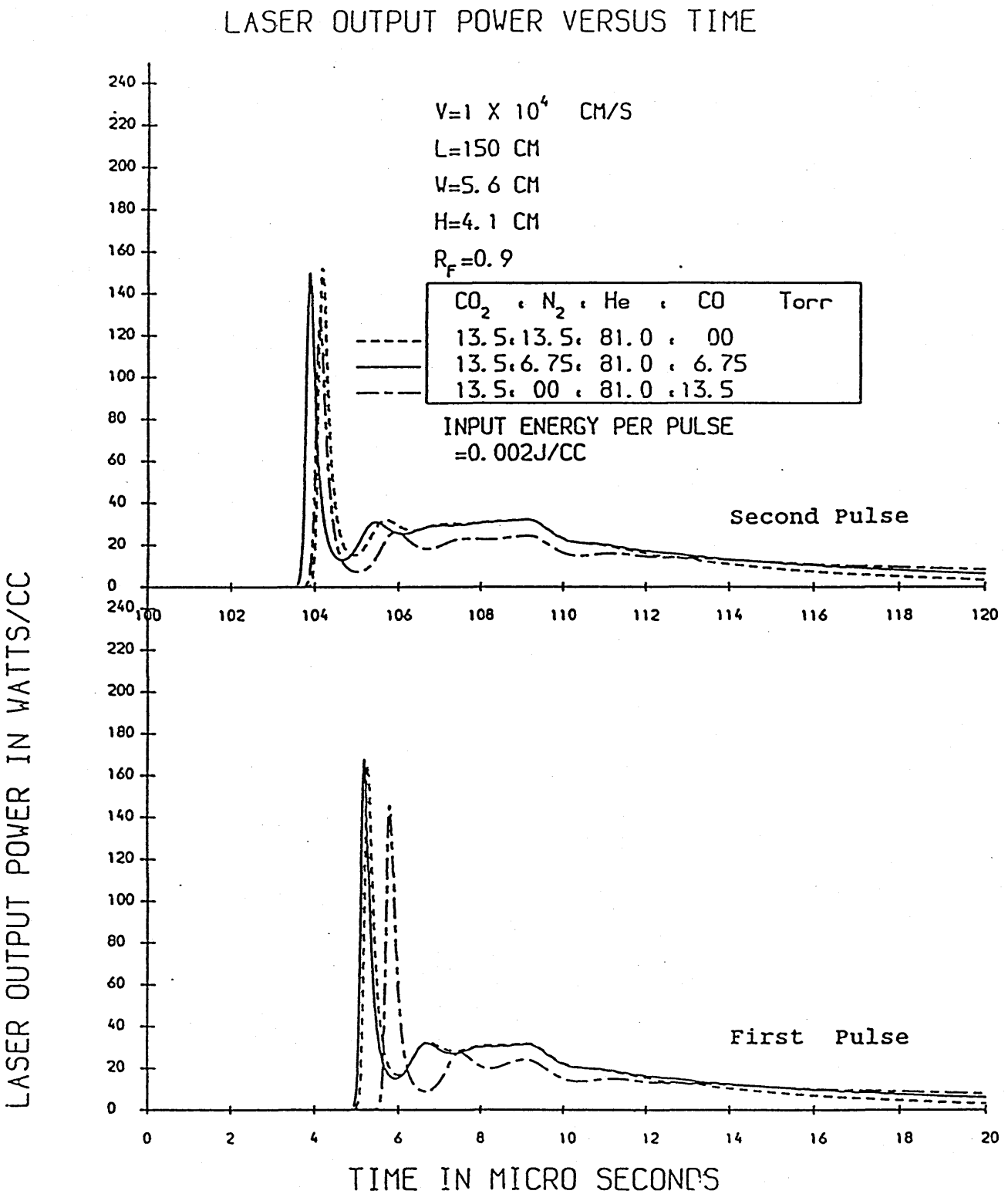
LASER OUTPUT POWER VERSUS TIME
V=1 X 10^4 CM/S
L=150 CM
W=5.6 CM
H=4.1 CM
R_F=0.9
CO2 : N2 : He : CO Torr
13.5 : 13.5 : 81.0 : 00
13.5 : 6.75 : 81.0 : 6.75
13.5 : 00 : 81.0 : 13.5
INPUT ENERGY PER PULSE
=0.002J/CC
Second Pulse
First Pulse
LASER OUTPUT POWER IN WATTS/CC
TIME IN MICRO SECONDS

GRAPH (4.68)

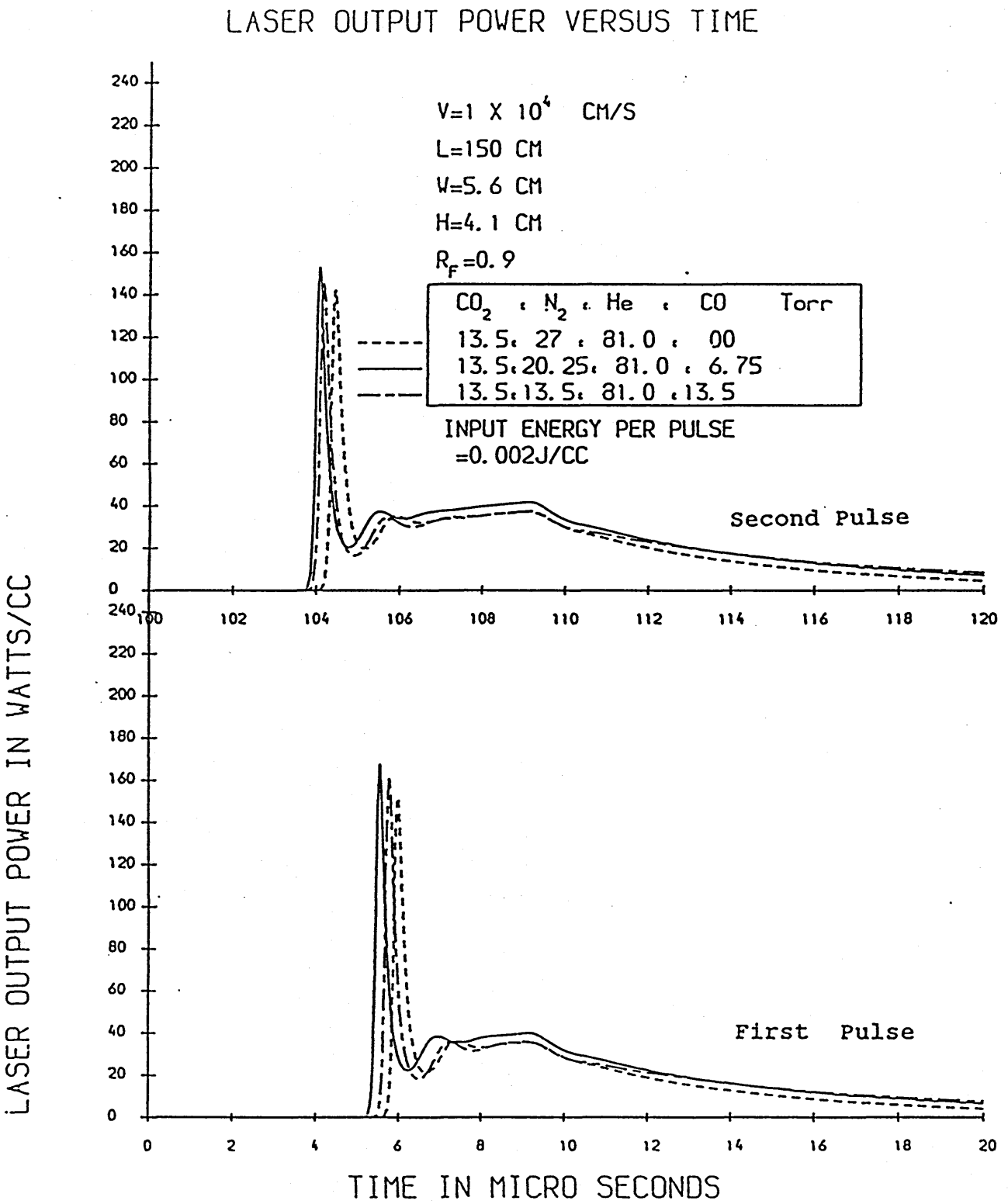
LASER OUTPUT POWER VERSUS TIME
V=1 X 10^4 CM/S
L=150 CM
W=5.6 CM
H=4.1 CM
R_F=0.9
CO2 : N2 : He : CO Torr
13.5: 27 : 81.0 : 00
13.5:20.25: 81.0 : 6.75
13.5:13.5: 81.0 :13.5
INPUT ENERGY PER PULSE
=0.002J/CC
Second Pulse
First Pulse
LASER OUTPUT POWER IN WATTS/CC
TIME IN MICRO SECONDS

GRAPH (4.69)

PULSE DELAY TIME VERSUS CO CONTENT

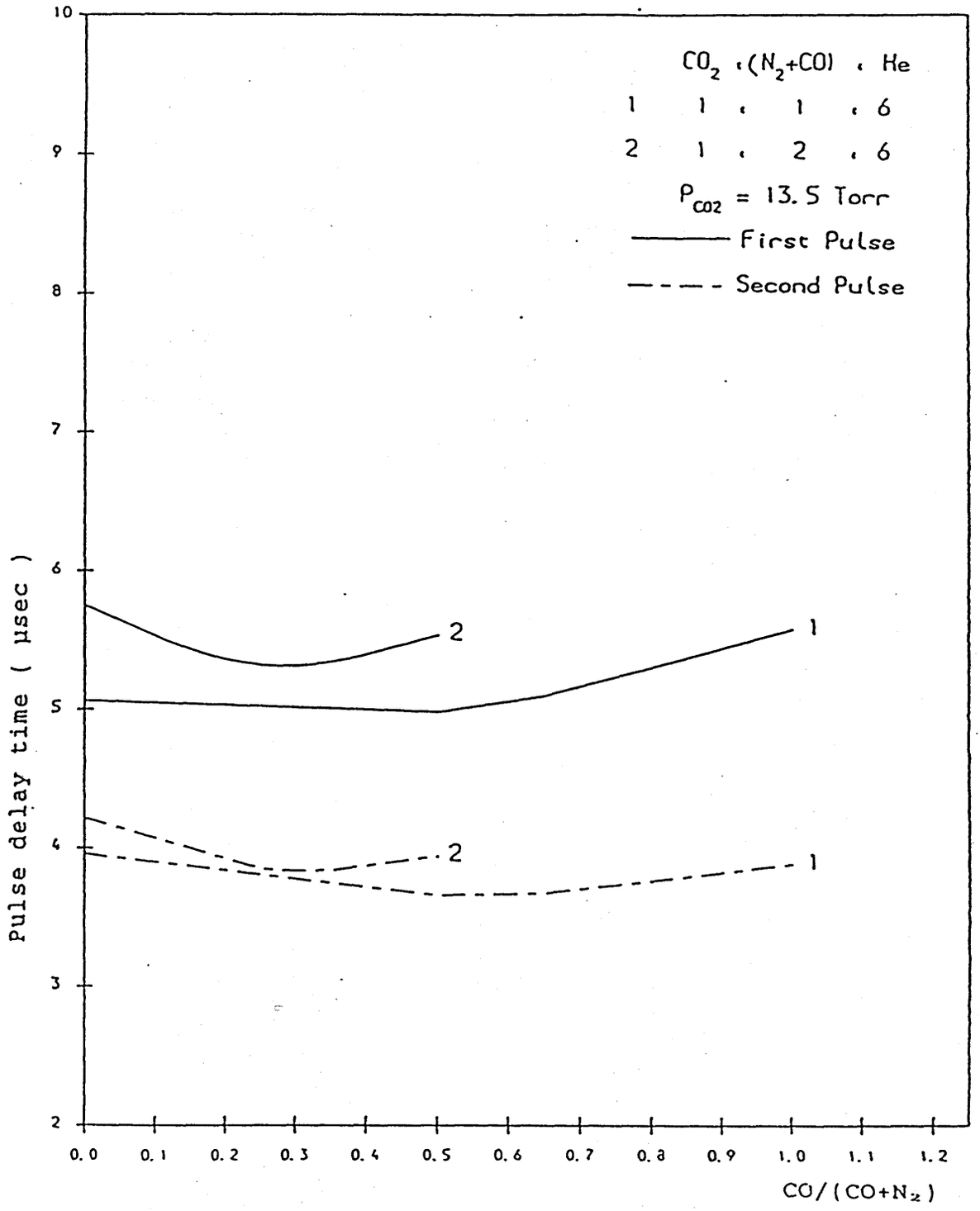

GRAPH (4.70)

MAXIMUM POWER VERSUS CO CONTENT

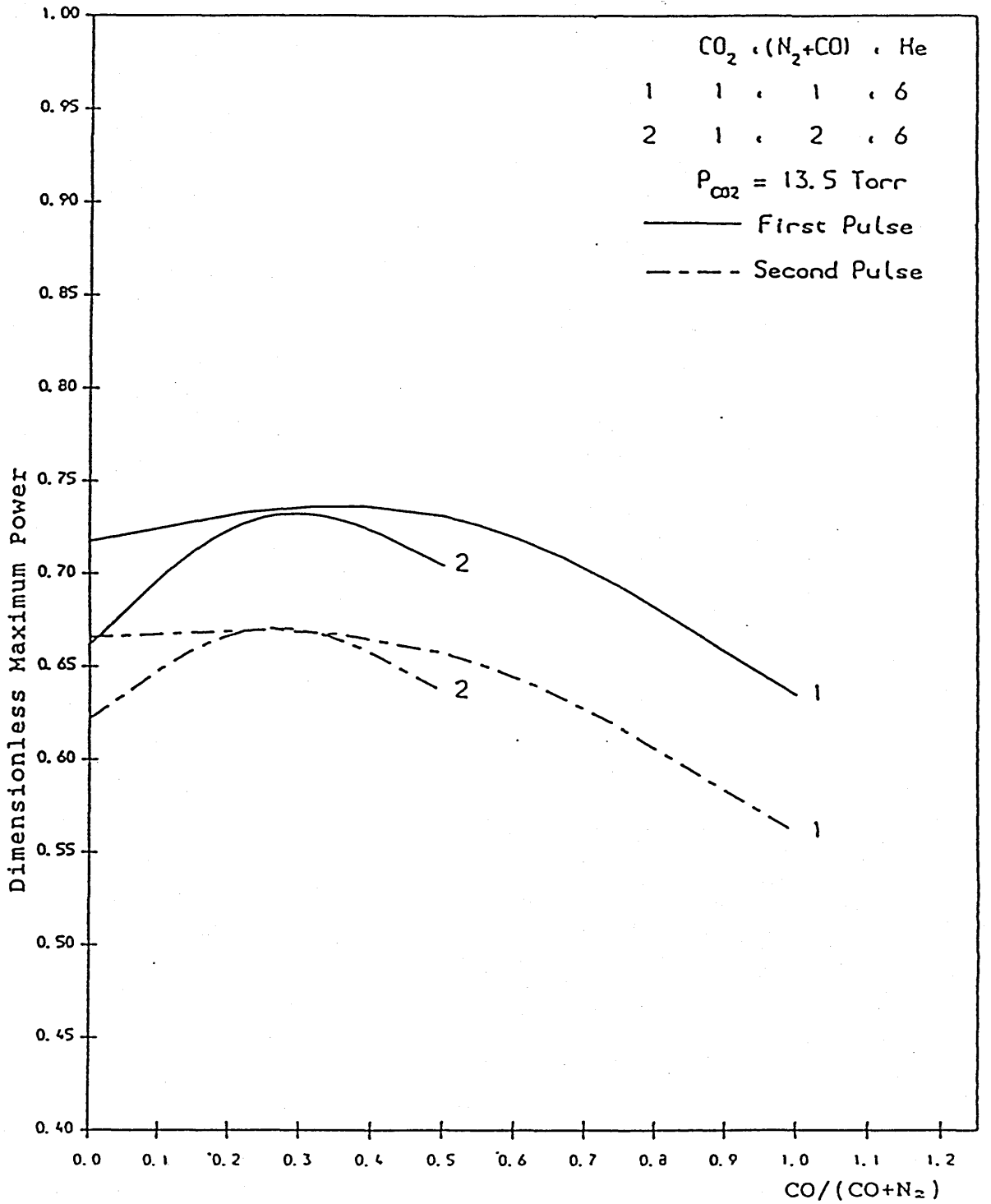

GRAPH (4.71)

TEMPERATURE OF LASER GASES VERSUS TIME

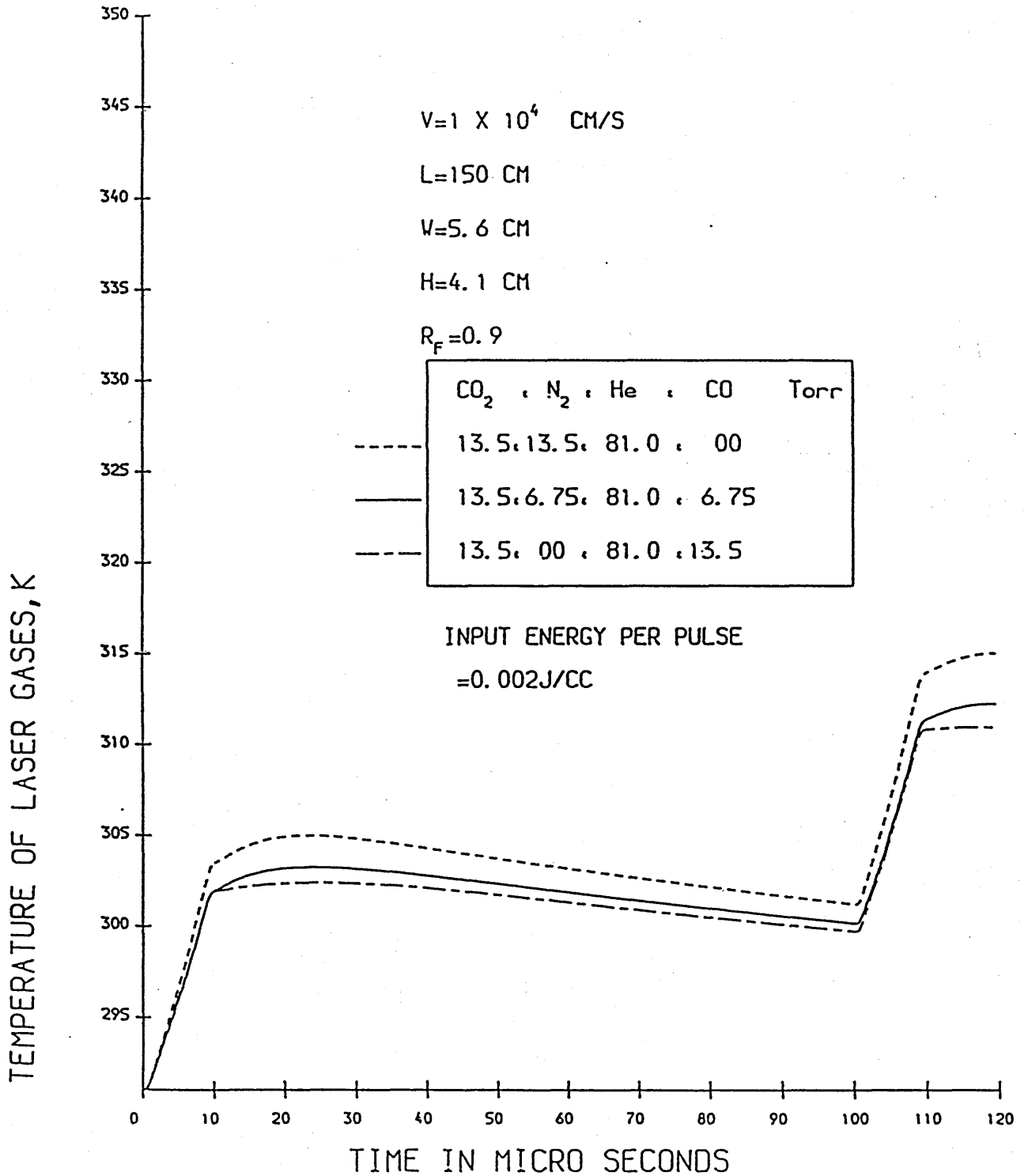

GRAPH (4.72)

TEMPERATURE OF LASER GASES VERSUS TIME

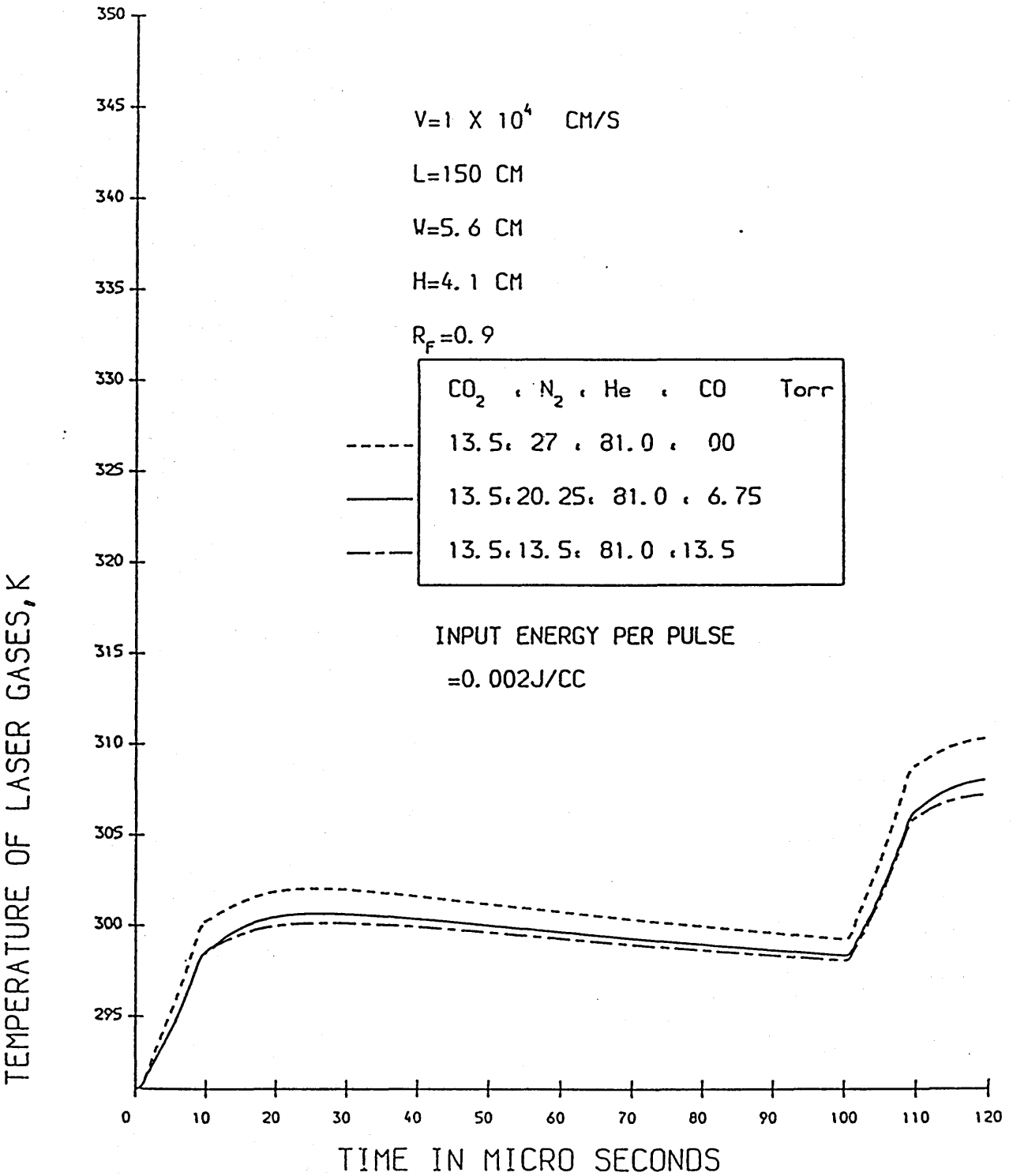

GRAPH (4.73)

PULSE DURATION VERSUS CO CONTENT

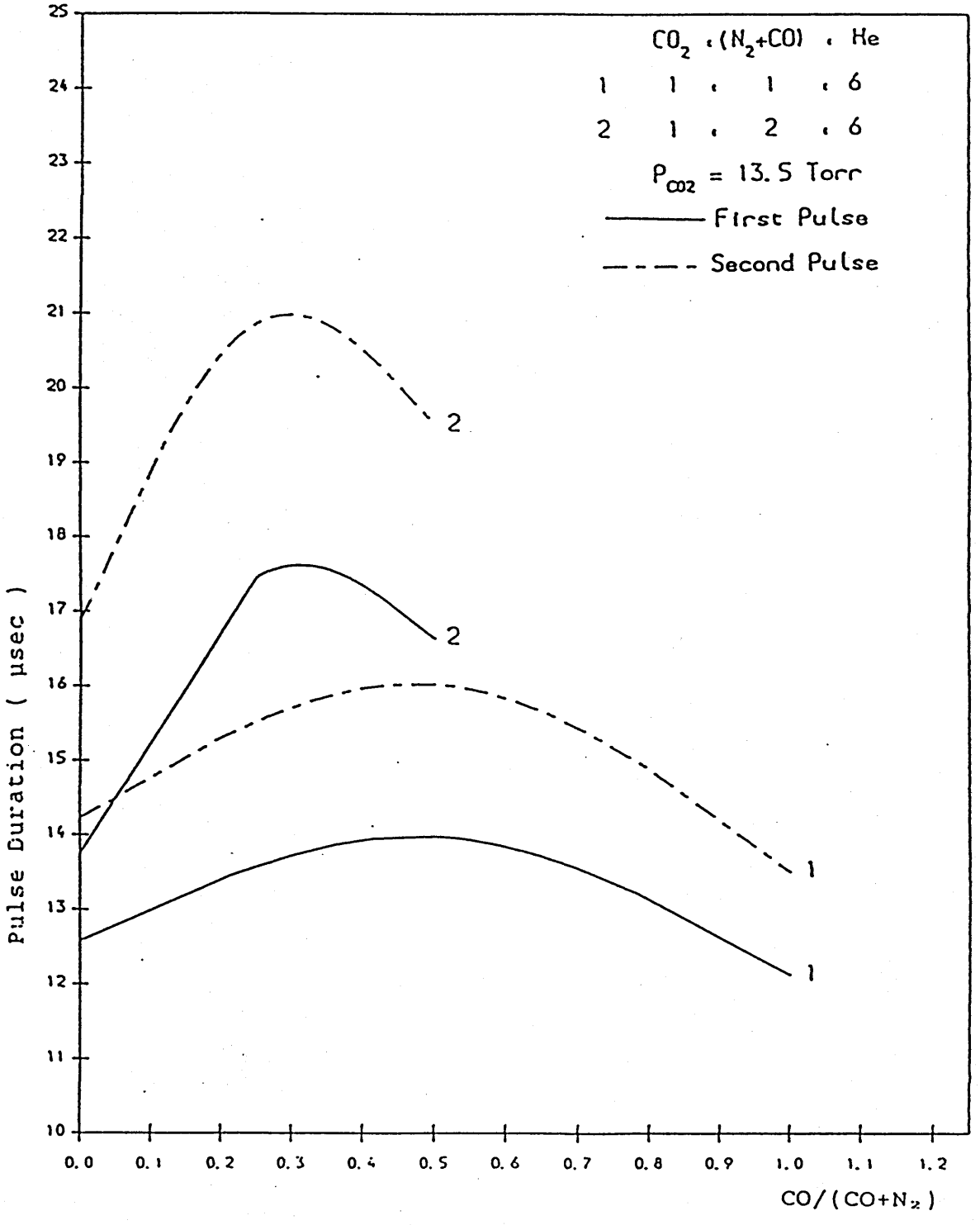

GRAPH (4.74)

AVERAGE POWER VERSUS CO CONTENT

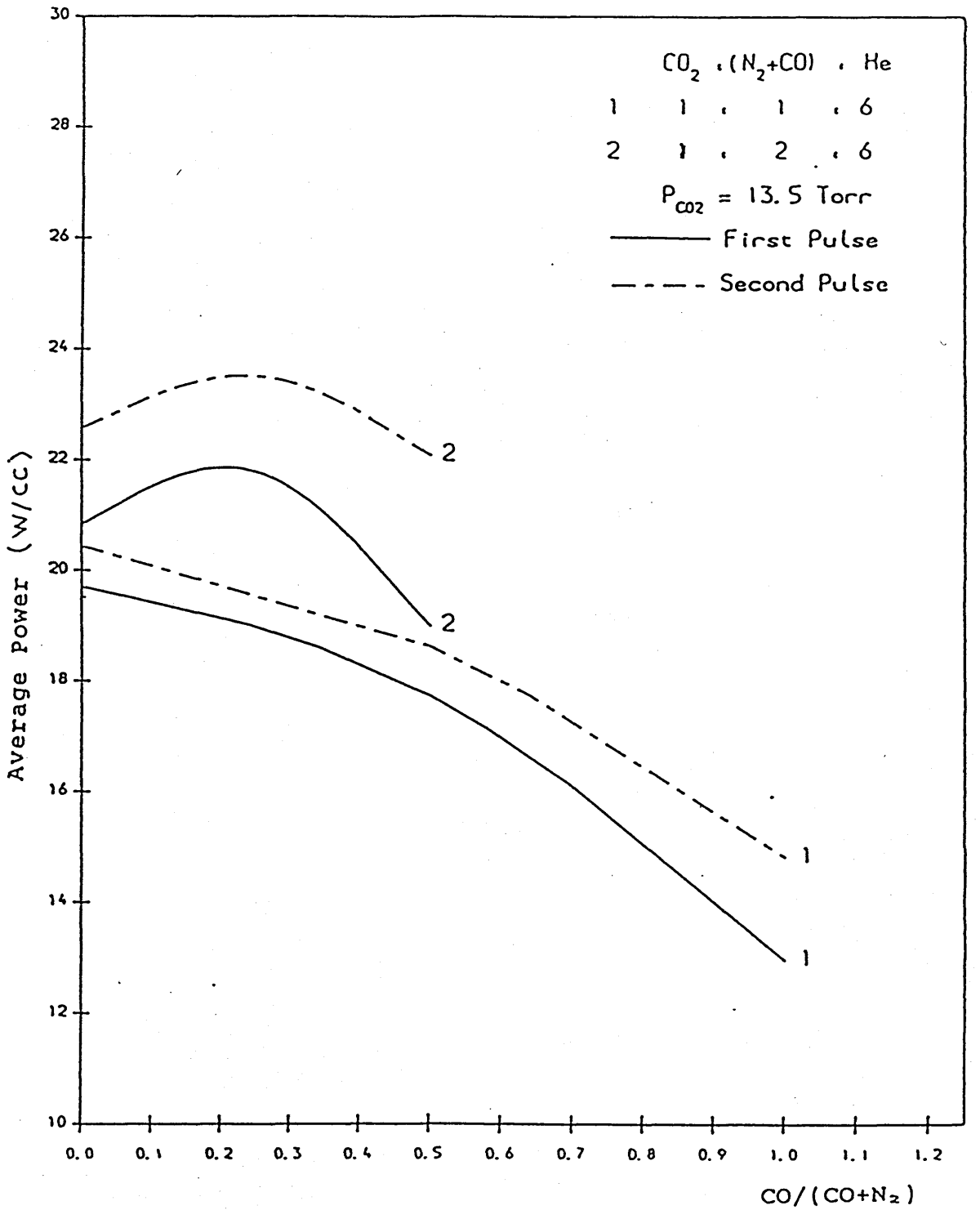

GRAPH (4.75)

OVERALL EFFICIENCY VERSUS CO CONTENT

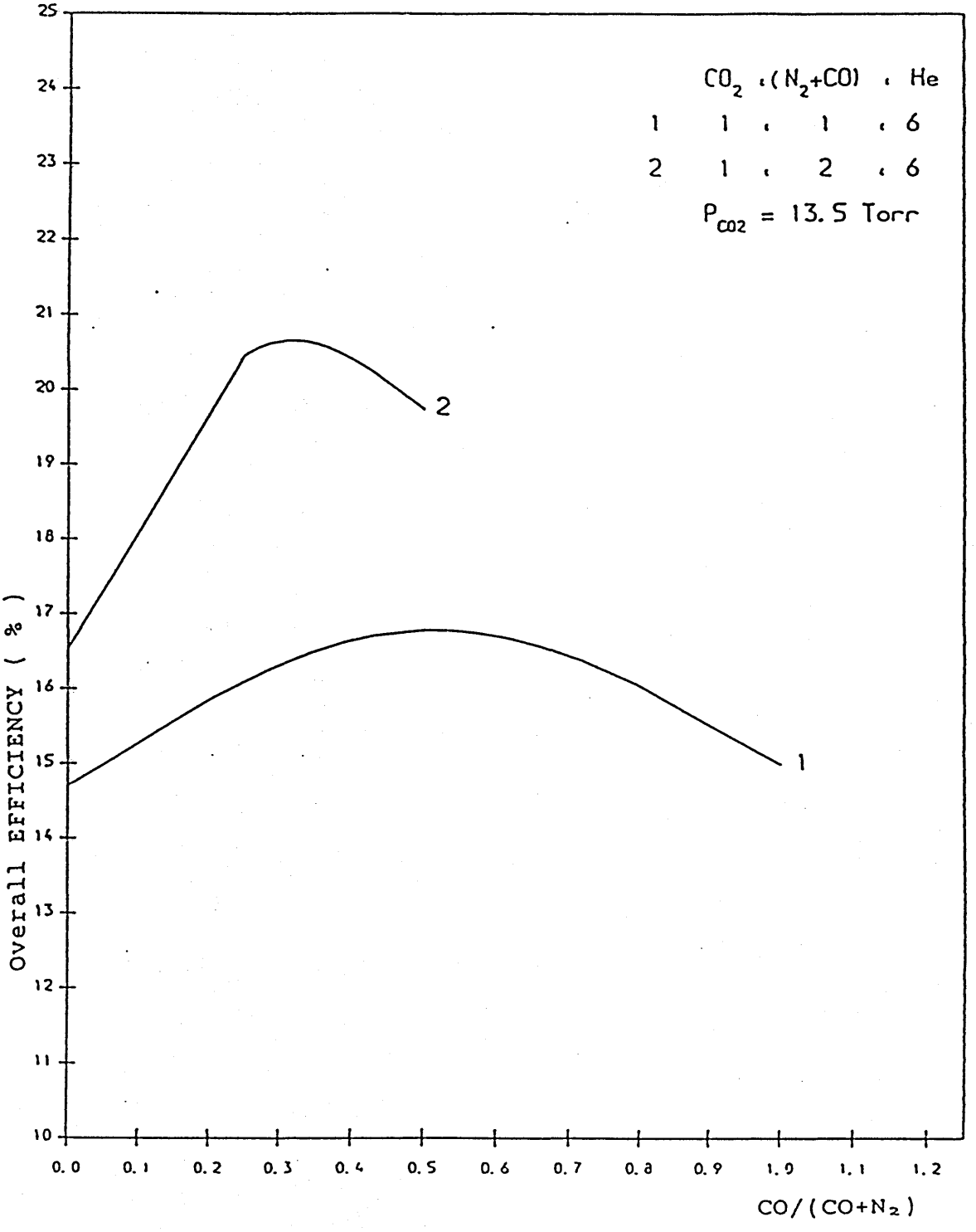

GRAPH (4.76)

EFFECTIVE EFFICIENCY VERSUS CO CONTENT

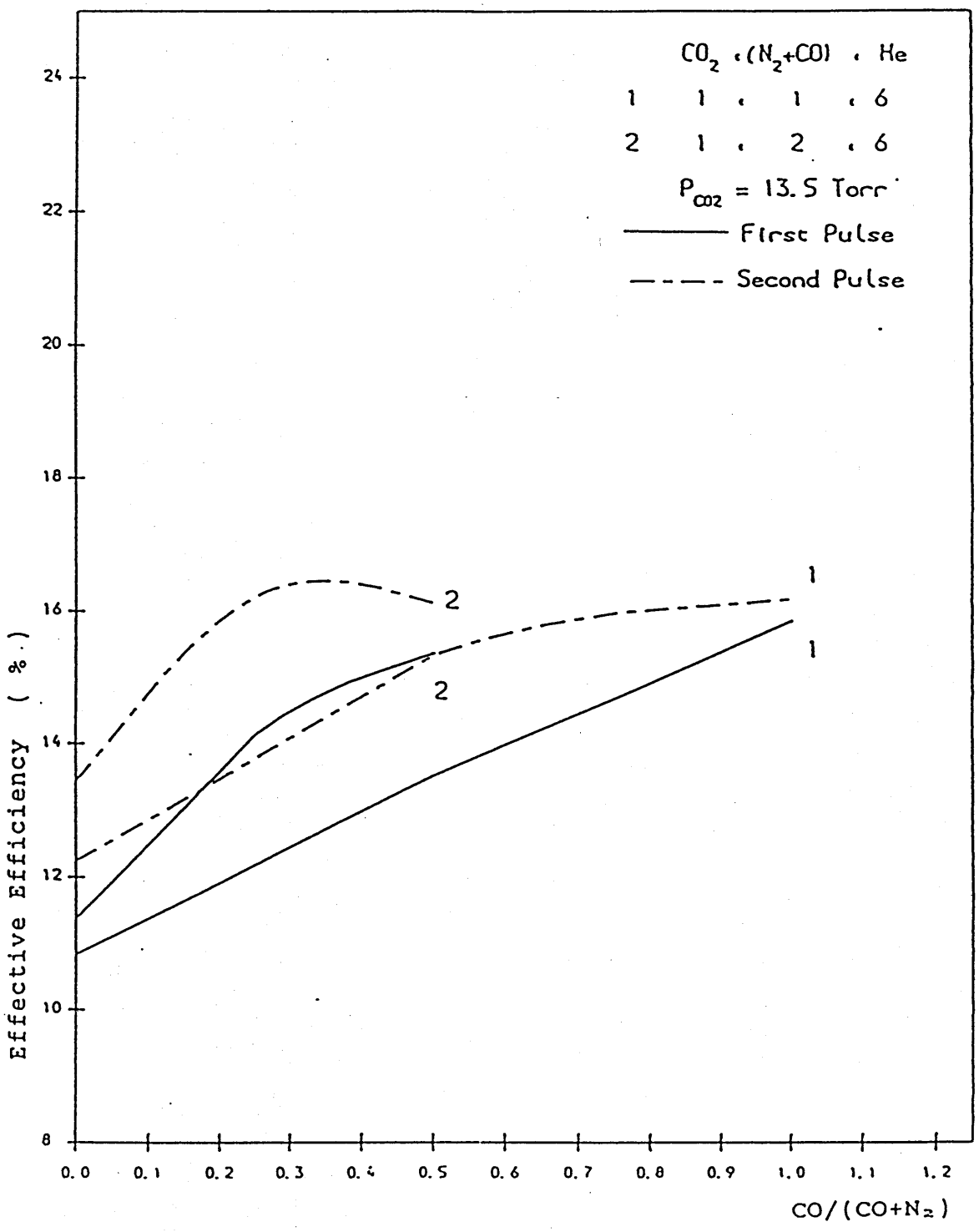

GRAPH (4.77)

CHAPTER FIVE

EXPERIMENTAL INVESTIGATION OF THE GAS DISCHARGE OPERATION

5.1 INTRODUCTION :

Since the invention of the CO_2 laser , there has been a renewed interest in electrical discharges. The population inversion between the vibrational states of CO_2 can be produced by electrons generated by a self-sustained electrical discharge in a CO_2- N_2- He gas mixture.To achieve a high power and efficient laser,the following conditions are to be satisfied, [DeMaria , 5.1]:

(i) the gas temperature should remain below about 600° K, since otherwise the lower laser level is filled and the population inversion destroyed.

(ii) the electron energy should be around 1 eV in order to obtain high excitation efficiency for the $CO_2(00°1)$ and $N_2(v=1-8)$ levels.

To produce a high power laser, a considerable electrical energy should be introduced into the discharge, whilst satisfying conditions i and ii. An effective configuration which achieves this is to combine the electrical discharge with gas flow in a transverse-discharge configuration. This configuration has many advantages over the conventional cylindrical-discharge arrangement,[Freiberg and Clark, 5.2]. Since the gas-flow paths are substantially shorter in the discharge , more uniform gas flow can be maintained and hot gases can be efficiently extracted from the volume of the active medium. To satisfy condition (ii),the electron energy

should be around 1 eV , it is also necessary to maintain a stable glow discharge, however, when the gas pressure or the discharge current are increased ,the glow discharge becomes unstable and collapses into arclike filaments or streamers [Yamabi et al , 5.3]. The instability of the glow discharge is accompanied by a substantial drop in the electron energy, well below the required 1 eV , which results in the destruction of the population inversion and lasing.

One of the main reasons for discharge instability is believed to be thermal effects . The main mechanism seems to be the following : a local uneven heating decreases the gas density which increases the electron energy , electron density , and electrical conductivity . Hence , the local current density increases and so does the Ohmic heating , which further raises the temperature , thus causing instability , [Nighan and Wiegand ,5.4] . Since discharge instability is caused by uneven heating of the gas , it is normal to assume that if the Ohmic heating could be made more uniform by the gas flow configuration , the glow-to-arc transition of the discharge could be postponed.

The CO_2 laser device currently under construction mainly comprises of the following sections ,(shown in figure 5.1) :

- Power Supply ,
- Pulse Forming Network ,
- Triggering Circuit ,
- Electrode Cavity ,
- Gas recirculating system , and
- Resonator .

The first three sections have been designed and built by McDonald [5.5] following the work of Khahra [5.6] and Spall [5.7]. The electrode cavity and the gas recirculating system have been designed and built by Chatwin [5.8] , who also designed the resonator. Figure (5.2) shows a 3D view of the laser system.

The time for which a stable discharge can be sustained before arcing occurs is affected by many factors including : electrode profile, material and surface finish , gas mixture and gas pressure, dissociation,and pre-ionisation triggering technique used. In this chapter the discharge operation and characteristics are investigated. The experimental work studies the relationship between voltage , current , gas mixture and pressure to obtain the best glow discharge. The effects of CO substitution for He and N_2 on the discharge operating characteristics are also investigated.

5.2 THE GAS DISCHARGE SYSTEM :

5.2.1 General :

In view of the requirements and possibilities of developing a laser system for metal machining processes, a transverse arrangement of the discharge with respect to both the gas flow and the resonator, as shown in figure (5.3),was adopted.This configuration allows a short discharge length and a large discharge volume. It also allows high working pressures,hence, high output power can be achieved. However,in transverse discharge systems it is very difficult to achieve a homogeneous glow discharge over a sufficiently large surface area of the electrodes because the discharge

has a tendency , especially at pressures above 20 Torr, to develop into distinct local arcs. The discharge voltage rapidly collapses when an arc forms and laser pumping ends abruptly. Moreover, arcing can damage system components. A brief description of the discharge system is given here, while a more detailed analysis of the system is given by McDonald [5.5].

5.2.2 **'Volumetric-Discharge' System** :

To obtain a uniform glow discharge in a large volume of the gas, the 'volumetric-discharge' technique is found to be more useful than the 'pin-electrode' technique,[Khahra,5.6]. The 'volumetric-discharge' technique mainly consists of two steps. First, the pre-ionisation of the gas by a small discharge and second , the main discharge throughout the volume. The electrode structure used (shown in figure 5.4) consists of solid uniform cathode and anode with glass covered trigger wires running transverse to the cathode - in the same direction as the gas flow-this architecture reduces their interference with the gas flow so uniformity of the discharge is improved. As the discharge produced must be free from edge effects , the electrode edges have a sufficiently smooth radius to prevent localised arcs developing. This is especially important at the corners where the three radii meet.The electrodes are each of 100 cm length ,7.4 cm width and made of brass due to its excellent thermal properties and ease of machining, [Khahra, 5.6]. The electrode separation is 4.1 cm ,the electrode gap uniformity is within 1% giving a quite uniform discharge.

5.3 EXPERIMENTAL WORK ON THE GAS DISCHARGE:

In a self-sustained glow discharge , the voltage-current (V-I) characteristics control the excitation efficiency of $CO_2(00^0 1)$ and $N_2(V=1-8)$ levels.Whereas,the product of voltage and current indicates the power fed into the discharge. Such discharges in a typical CO_2 laser are found to operate at a characteristic quasi-steady electric field -to- gas density ratio, E/N,in each gas mixture, [Denes and Lowke ,5.9]. It is, therefore ,important to study the relationship between current ,voltage ,gas mixture and pressure in the discharge.

5.3.1 Effects of current on voltage :

The discharge voltage and current were measured for various gas mixtures and total pressures. Figure (5.5) shows typical current and voltage pulse shapes for a 1:1:8 gas mixture at 120 Torr measured by a LeCroy 9400 oscilloscope . The results obtained for several gas mixtures are shown in graph (5.1). It can be seen that in each gas mixture the discharge stabilizes at a certain value of E/N which is independent of the discharge current .

5.3.2 Effects of gas pressure on voltage:

Graph (5.2) shows the results obtained for some of gas mixtures.It shows that the E/N value remains almost constant for all the pressures of every gas mixture. However, for low gas pressures (less than 50 Torr) there is a slight increase in the E/N value due to the effects of the cathode fall voltage which becomes significant at low gas pressures.

5.3.3 Effects of gas mixture on voltage:

From the observed relationship between discharge voltage ,current, and total gas pressure, it is clear that E/N is constant for any gas mixture. Thus,in a self- sustained glow discharge the excitation efficiency is a property of the gas mixture. Hence, it is important to investigate different gas mixtures to obtain the most efficient excitation.

In graph (5.3) the measured values of E/N are plotted against (CO_2/(CO_2+N_2)) pressure in helium free mixtures, and graph (5.4) shows measured values of E/N in various mixture of CO_2 ,N_2 , and He. The behaviour shown in these graphs is similar to that in the work of Khahra [5.6]. It can be seen from graph (5.3) that in helium free mixtures the E/N value necessary to sustain the discharge increases as the nitrogen proportion decreases. This is due to the fact that addition of nitrogen reduces the electron energy in the discharge, hence reducing both the ionisation and attachment rates (as discussed in chapter 2) and alters the intersection point of the specific ionisation and attachment coefficients curves (see graphs 2.28 and 2.29). Thus ,the operating value of E/N for the discharge is reduced (see Table 2.3). On the other hand, the discharge can be sustained at a lower value of E/N with increasing helium content in the gas mixture as shown in graph (5.4),but with increasing nitrogen content the E/N value increases too. This is because the addition of helium increases the electron energy, the ionisation and attachment rates of the gas constituents and therefore shifts E/N to a lower value. Whereas, the addition of nitrogen reduces the

electron energy and the ionisation and attachment rates ,the value of E/N increases (as discussed in chapter 2).

The measured values of E/N for self-sustained discharges in several gas mixtures are listed in Table (5.1). These are in excellent agreement ,within 1-4 %, with the theoretically computed values of E/N (shown in Table (2.3)). In addition there is good agreement between the present results and the results of Khahra [5.6] and Denes and Lowke [5.9] , the discrepancy may be due to gas impurity or some air leak in the system and the precision of the instrumentation used.

5.4 EXCITATION EFFICIENCIES AT EXPERIMENTALLY DETERMINED VALUES OF (E/N) :

Actual excitation efficiencies for the CO_2 (00°1) and N_2(v=1-8) levels in several gas mixtures are shown in graphs (5.5) to (5.8). These are determined by the intersection of experimentally determined values of E/N (as shown in Table 5.1) and the predicted excitation efficiencies as shown in graphs (2.15) to (2.20) in chapter two.

For increased nitrogen in helium free mixtures , the excitation efficiency of N_2 (v=1-8) shows a significant increase as shown in graph (5.5).This is due to the presence of more nitrogen in the gas mixture and the decrease in the operating value of E/N which brings it nearer to the optimum value for best excitation. On the other hand,the excitation efficiency of the CO_2(00°1) level increases as the carbon dioxide content is increased.Although an increase in the CO_2 content slightly increases the value of E/N (1-4 %) , the

effect on the excitation efficiency of the $CO_2(00^o1)$ level is insignificant as this hardly affects the cross - sections for CO_2.The addition of helium to the gas mixture leads to a substantial decrease in the operating value of E/N since it has no vibrational excitation in the region of electron energies of interest (as discussed in chapter 2). The effect of helium enrichment of three different (CO_2:N_2) ratio (γ_1) gas mixtures is shown in graphs (5.6) to (5.8).It can be seen that the excitation efficiencies show a maxima at a certain value of ε_1=0.3-0.75 (ε_1= He/(He+CO_2+N_2)) depending upon the CO_2:N_2 ratio.

5.5 IONISATION AND ATTACHMENT COEFFICIENTS AT EXPERIMENTALLY DETERMINED VALUES OF (E/N):

Graphs (5.9) and (5.10) show the variation of the specific ionisation and attachment coefficients with helium content in several gas mixtures . These coefficients are calculated at the experimentally determined values of E/N . It can be seen from these graphs that both (α/N) and (a/N) increase with increasing helium in the gas mixture . This is due to the fact that helium enrichment increases the average electron energy,thus increasing the ionisation and attachment rates (as discussed in chapter 2). On the other hand, as the nitrogen content increases both (α/N) and (a/N) decrease due to the decreased electron energy.

The experimentally evaluated (α/N) are slightly greater than those of (a/N) ,(within 5%). Referring to graphs (2.28) and (2.29) in chapter 2 , this indicates a slightly higher

value of E/N than that corresponding to the intersection point of (α/N) and (a/N) curves in the graphs. This is due to gas impurity or air leaks into the system which have a significant effect on the balance of charged particles in the discharge (as discussed in chapter 3). Moreover, these were found to alter the operating value of E/N, [Denes and Lowke, 5.9].

The variation with helium content of the electron drift velocity is shown in graph (5.11). As the helium content is increased , the electron drift velocity decreases due to the substantial decrease in the operating value of E/N caused by helium enrichment. The drift velocity also decreases with increasing N_2 due to the decreased mean electron energy.

5.6 EFFECTS OF THE ADDITION OF CARBON MONOXIDE :

With the addition of CO the discharge colour changes from voilet to light blue due to the emission of the visible ($B^1\Sigma^+ \longrightarrow A^1\Pi$) Angstrom system of the CO molecule associated with the excited electronic state, [Schinca et al, 5.10], [Osgood et al, 5.11]. This emission dominates the discharge spectra where the intensity of the violet band of the transition ($B^2\Sigma_u^+ \longrightarrow X^2\Sigma_g^+$) of the molecular nitrogen ion is decreased because the addition of CO reduces the average electron energy and the high energy electrons in the discharge and therefore reduces the ionisation rates (as discussed in chapter 2). The discharge has a great number of fine filaments and the appearance of these filaments becomes less noticeable as the CO content increases. This is in good

agreement with the influence of CO on negative-ion processes discussed in chapter 3 . Figure (5.6) shows the current and voltage pulses in a (CO_2:N_2:He:CO = 1:1.5:6:0.5) gas mixture at 108 Torr.The variation of the operating value of E/N with added CO for some of gas mixtures is shown in graphs (5.12) to (5.14). The initial decrease in the values of E/N is due to modification of the discharge impedance caused by changes in the electron density with small amounts of added CO. This is shown in graph (5.15). The discharge impedance is

$$R = V_G / I_G$$

where V_G and I_G are ,respectively,the quasi-steady discharge voltage and current.

It can be seen that when CO is substituted for helium , the decrease in E/N is less than that when CO is substituted for N_2. This is due to the fact that helium has a dominant role in determining the electron energy distribution function (as discussed in chapter 2),thus with the substitution of CO for helium , the decrease in the average electron energy is more significant than that with the substitution of CO for nitrogen as shown in the table below :

Gas Mixture CO_2 : N_2 : He : CO	Average Electron Energy (eV)
1.0 : 1.0 : 6.0 : 0.0	1.53
1.0 : 1.0 : 5.5 : 0.5	1.23
1.0 : 0.5 : 6.0 : 0.5	1.35

With continued increases of CO concentrations the corresponding decrease in the helium content raises the operating value of E/N as shown in graphs (5.12) and (5.13). This is due to the significant decrease in the average electron energy as shown in the following table :

Gas Mixture CO_2 : N_2 : He : CO	Average Electron Energy (eV)
1.0 : 1.0 : 6.0 : 0.0	1.53
1.0 : 1.0 : 5.0 : 1.0	1.17
1.0 : 0.0 : 6.0 : 1.0	1.41

However,when CO is substituted for all of the nitrogen , the decrease in the average electron energy is relatively small due to the comparable vibrational excitation cross - sections for CO_2 and N_2 (see Appendix 2.III). This high content of CO has a significant influence on the negative - ion processes (as discussed in chapter 3). In addition, this shifts the E/N value of the discharge to a lower value as shown in graph (5.14).The measured values of E/N for a self-sustained discharge in several gas mixtures with CO addition are listed in Tables (5.2) and (5.3).

5.7 EXCITATION EFFICIENCIES:

Graphs (5.16) to (5.21) show the excitation efficiencies for the $CO_2(00°1)$, $N_2(v=1-8)$ and $CO(v=1-8)$ levels in several gas mixtures determined at the experimental values of E/N.In gas mixtures where CO is substituted for He, it can be seen

that the addition of CO in amounts up to 2.5 % of the total pressure (CO/CO_2 =0.25) improves the excitation efficiencies for N_2 and CO_2 as shown in graphs (5.16) and (5.17). This is because of the slight decrease in both the average electron energy and the operating value of E/N (as already discussed in section 5.7) which brings it nearer to the optimum value for best excitation. With a continued increase in the CO content, both excitation efficiencies of CO_2 and N_2 decrease because of the significant decrease in the average electron energy which has more effect on the excitation efficiency of N_2(v=1-8) , see graph (5.17) , due to the sharp fall of the N_2 excitation cross sections (see figure 2.3 in chapter 2).

Graph (5.18) shows that the excitation efficiency of CO increases with increasing CO due to two effects. Firstly the presence of more CO molecules and secondly the broad cross sections for CO (see Appendix 2.III).

Graph (5.19) shows the sharp decrease in the N_2 (v=1-8) excitation efficiency when CO is substituted for N_2. This is simply due to the decreased N_2 and the decreased excitation cross sections for nitrogen. The variation of the excitation efficiency of CO_2(00°1) with CO substitution for nitrogen is shown in graph (5.20). The initial increase shown in the graph is due to the decrease in both the average electron energy and the operating value of E/N.With increasing CO the excitation efficiency of CO_2(00°1) slightly decreases due to the increase in E/N (see graph 5.14).Graph (5.21) shows that the excitation efficiency of CO increases with increasing CO due to the presence of more CO molecules.

5.8 IONISATION AND ATTACHMENT COEFFICIENTS :

Graphs (5.22) to (5.25) show the variation of the specific ionisation and attachment coefficients with CO content in several gas mixtures. It can be seen that the specific ionisation and attachment coefficients decrease due to the decrease in the average electron energy which reduces both the ionisation and attachment rates (as discussed in chapter 2). However, when CO is substituted for N_2 , graphs (5.24) and (5.25) ,the decrease in the specific ionisation and attachment coefficients is smaller than that when CO is substituted for He due to the relatively small decrease in the average electron energy (as discussed in section 5.7).

5.9 CONCLUSIONS:

(1) The measured values of E/N for self-sustained discharges in several gas mixtures show an excellent agreement with the calculated values based on a simple balance of electron production and attachment rates.Thus,attachment is the dominant electron loss process in the discharge.

(2) The addition of small amounts of CO as a substitute for helium or nitrogen decreases the operating E/N value of the discharge due to the modification of the discharge impedance caused by changes in the electron density.

(3) Increasing amounts of added CO raise the operating E/N value due to the significant decrease in the average electron energy and therefore in the ionisation and attachment rates which leads to an increase in the discharge impedance.

REFERENCES

CHAPTER FIVE

5.1 DeMaria A J - ' Review of CW High-Power CO_2 Lasers '- Proc. IEEE , Vol 61 , No 6 , 1973 (731).

5.2 Freiberg R J and Clark P O - 'CO_2 Transverse-Discharge Lasers ' IEEE J. QE. , 6 , 1970 (105).

5.3 Yamabi C , Matsushita T , Sato S , and Horii K - 'Parametric Studies of UV Preionzation in TEA CO_2 Lasers'- J. Appl. Phys. , 51 , 1980 (898).

5.4 Nighan W L and Wiegand W J - ' Causes of arcing in CW CO_2 convection laser discharges '- Appl. Phys. Lett. , 25 , 1974 (633).

5.5 Mcdonald D - Ph.D Thesis , University of Glasgow , (to be submitted).

5.6 Khahra J S -'Optimisation of the output characteristics of a pulsed CO_2 laser for processing of materials' - Ph.D Thesis , University of Birmingham , 1976.

5.7 Spall R - 'Pulsed Power Supply for an Unstable Resonator and mode simulation in unstable resonators ' - Ph.D Thesis , University of Birmingham , 1979.

5.8 Chatwin C R - ' Thermodynamics of Pulsed CO_2 laser for machining metals ' - Ph.D Thesis , University of Birmingham , 1980.

5.9 Denes L J and Lowke J J - ' V-I characteristics of pulsed CO_2 laser discharges ' - Appl. Phys. Lett., 23 , 1973 (130).

5.10 Schinca D ,Scaffardi L,and Tocho J O -' Population mechanisms in visible carbon monoxide pulsed lasers'- Appl. Opt. , Vol 25, 1986 (102) .

5.11 Osgood Jr. R M , Eppers Jr. W C ,and Nichols E R - 'An Investigation of the High-Power CO Laser' IEEE J. Q.E. , Vol 6 , 1970 (145) .

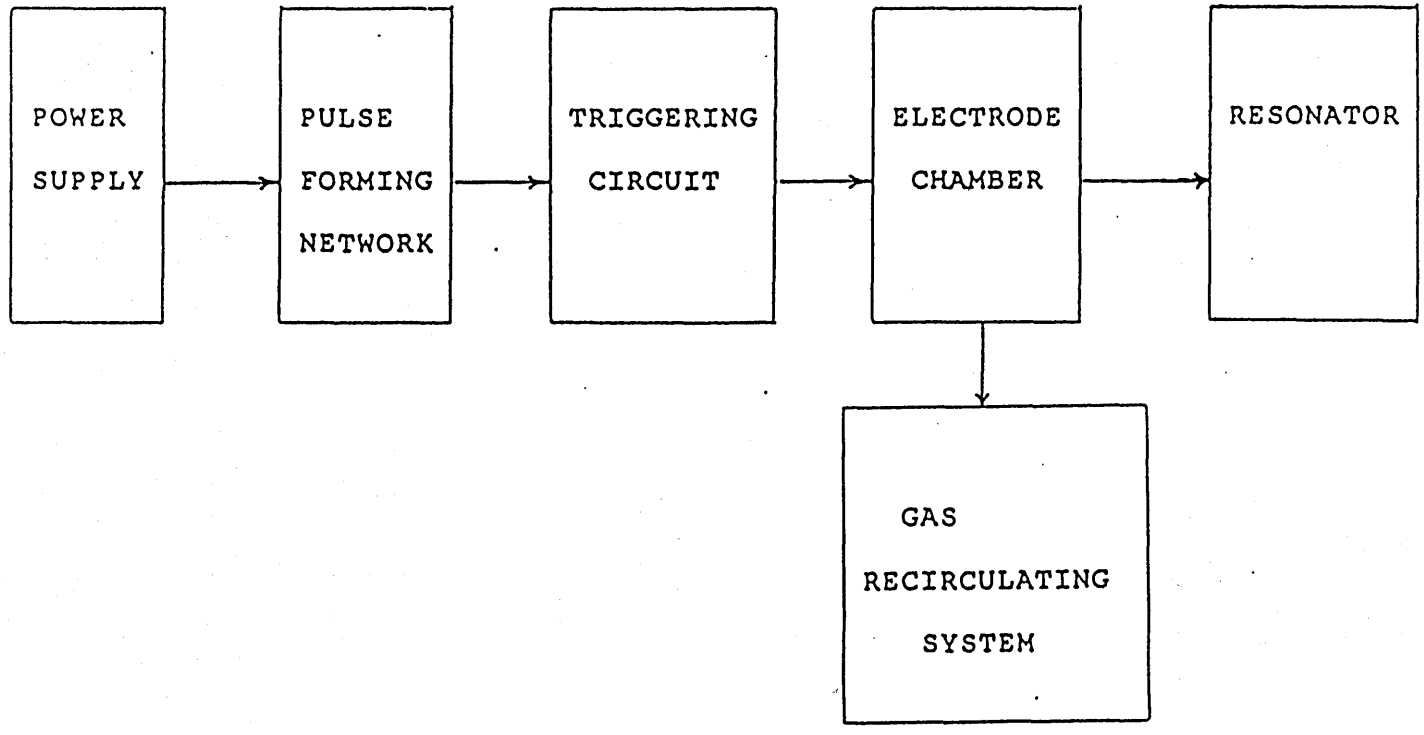

BLOCK DIAGRAM OF THE CO_2 LASER SYSTEM

FIGURE (5.1)

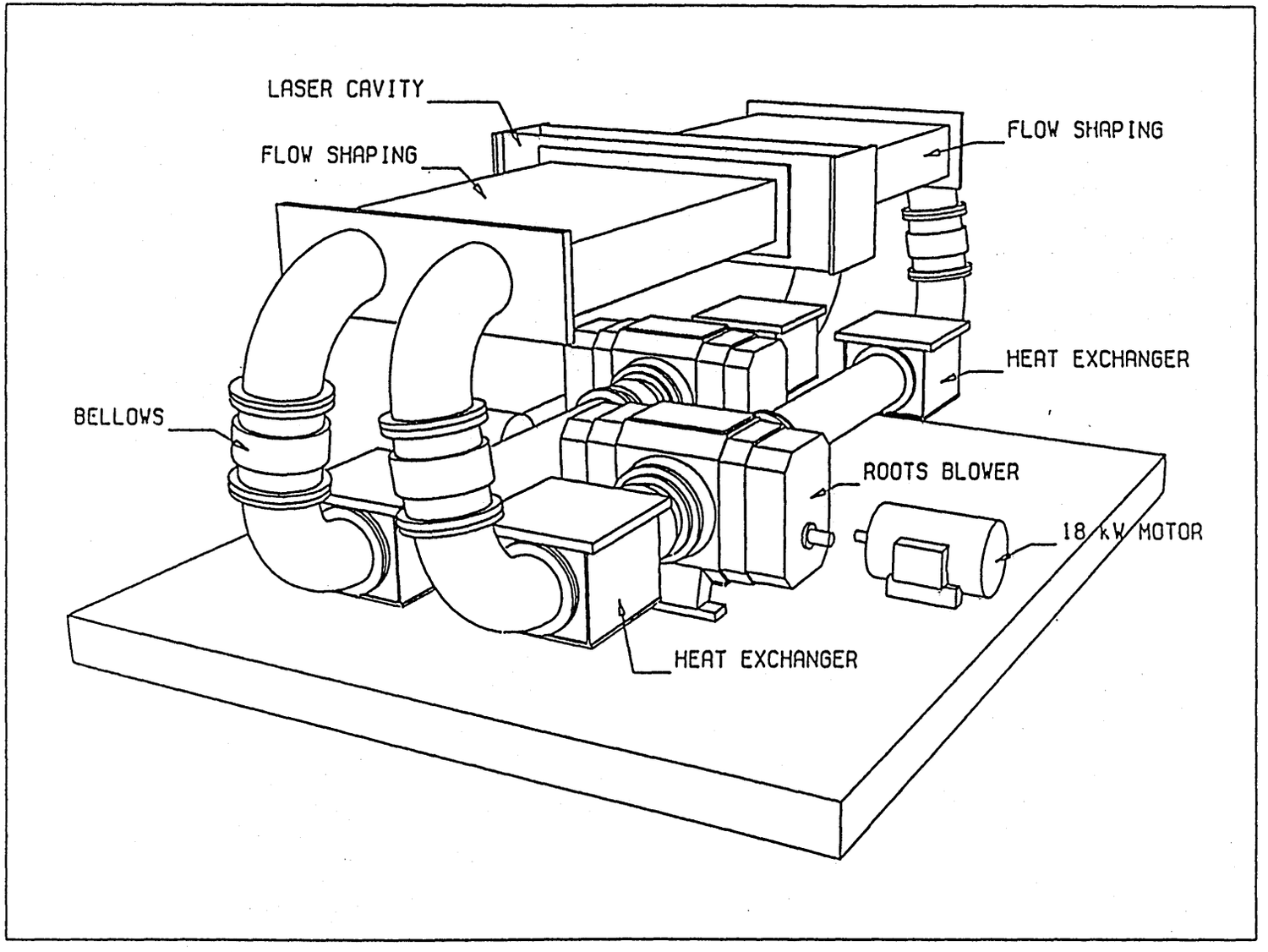

3D VIEW OF THE LASER SYSTEM

FIGURE (5.2)

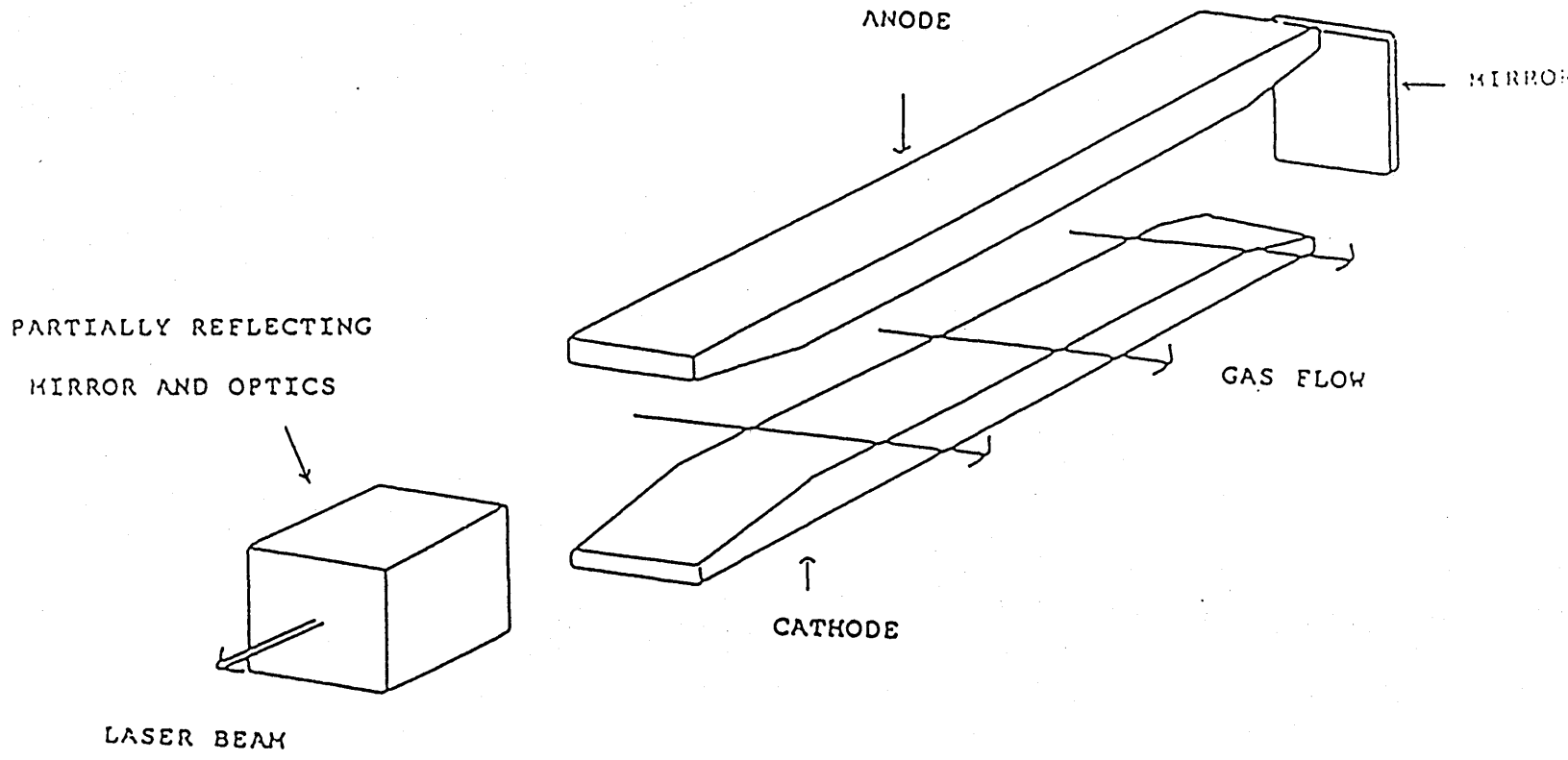

SCHEMATIC DIAGRAM

OF A TRANSVERSE DISCHARGE ARRANGEMENT

FIGURE (5.3)

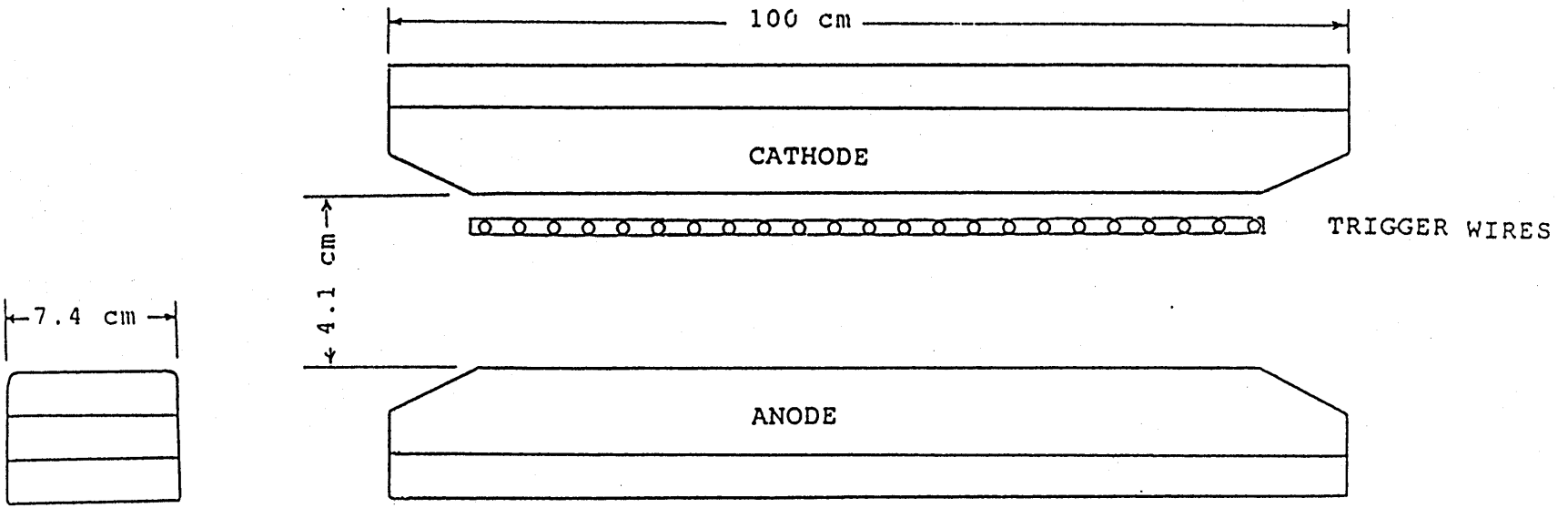

ELECTRODE STRUCTURE

FIGURE (5.4)

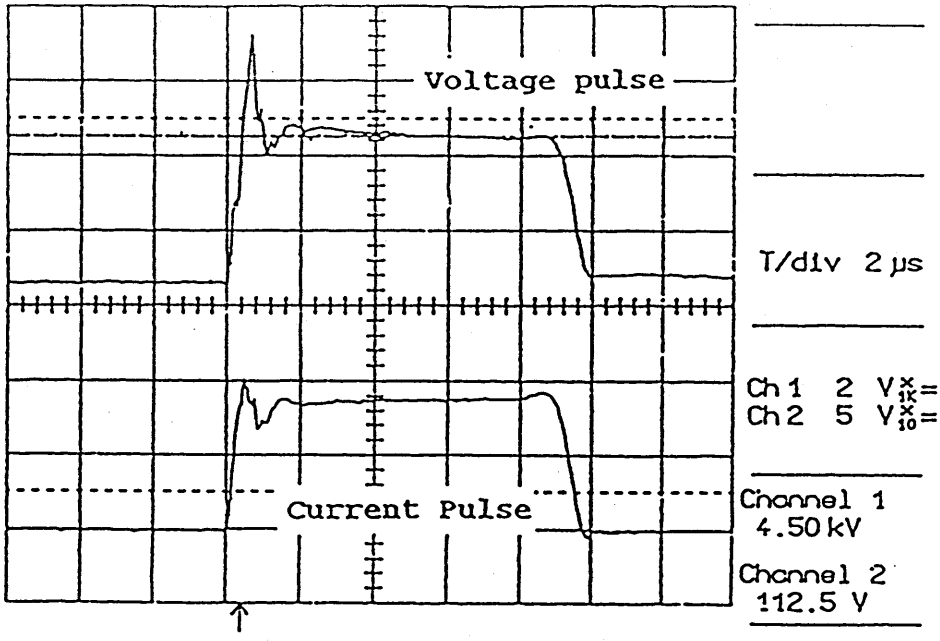

VOLTAGE AND CURRENT PULSES

FOR A (1:1:8) GAS MIXTURE AT 120 TORR

FIGURE (5.5)

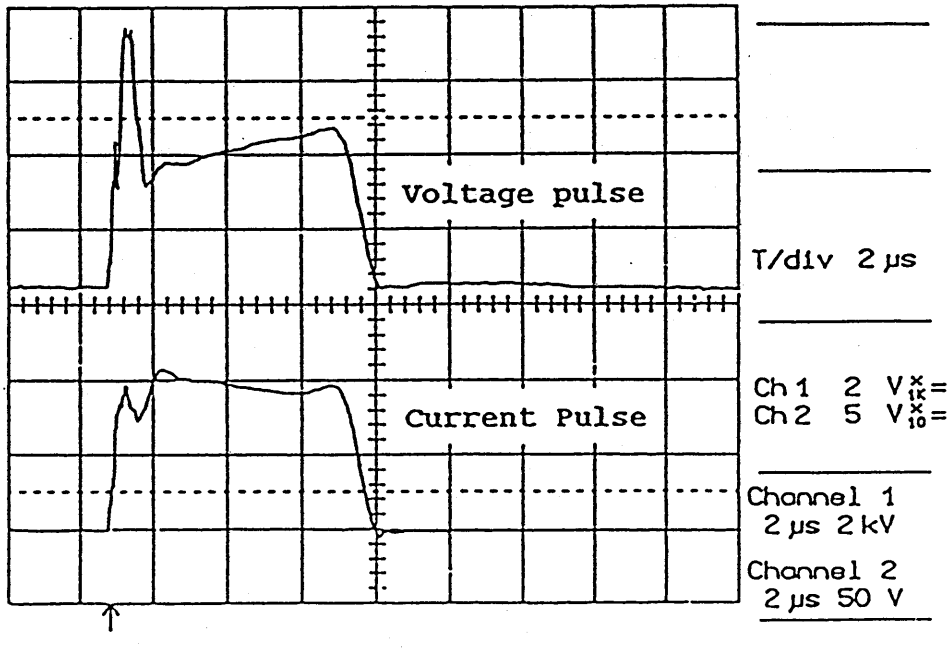

VOLTAGE AND CURRENT PULSES

FOR A (1:1.5:6:0.5) GAS MIXTURE AT 108 TORR

FIGURE (5.6)

TABLE (5.1)

MEASURED VALUES OF E/N

Mixture CO_2 : N_2 : He	E/N x 10^{-16} (volt.cm^2)
1 : 1 : 0	8.7571
1 : 1 : 1	6.3933
1 : 1 : 2	5.2238
1 : 1 : 4	3.9892
1 : 1 : 6	3.2912
1 : 1 : 8	2.8942
1 : 2 : 0	8.5213
1 : 2 : 1	6.8121
1 : 2 : 2	5.8287
1 : 2 : 4	4.6065
1 : 2 : 6	3.9023
1 : 2 : 8	3.5022
1 : 3 : 0	8.3848
1 : 3 : 1	7.0851
1 : 3 : 2	6.2041
1 : 3 : 4	5.0408
1 : 3 : 6	4.3583
1 : 3 : 8	3.9272

TABLE (5.2)

MEASURED VALUES OF E/N

Gas Mixture	E/N x 10^{-16}
CO_2 : N_2 : He : CO	(volt.cm^2)
1 : 1 : 8.00 : 0.00	2.894
1 : 1 : 7.78 : 0.22	2.722
1 : 1 : 7.50 : 0.50	2.903
1 : 1 : 7.22 : 0.78	2.991
1 : 1 : 7.00 : 1.00	3.261
1 : 1 : 6.00 : 0.00	3.291
1 : 1 : 5.78 : 0.22	3.201
1 : 1 : 5.50 : 0.50	3.311
1 : 1 : 5.22 : 0.78	3.479
1 : 1 : 5.00 : 1.00	3.607
1 : 1 : 4.00 : 0.00	3.989
1 : 1 : 3.78 : 0.22	3.896
1 : 1 : 3.50 : 0.50	4.063
1 : 1 : 3.22 : 0.78	4.245
1 : 1 : 3.00 : 1.00	4.545
1 : 2 : 6.00 : 0.00	3.902
1 : 2 : 5.78 : 0.22	3.632
1 : 2 : 5.50 : 0.50	3.782
1 : 2 : 5.22 : 0.78	4.287

TABLE (5.3)

MEASURED VALUES OF E/N

Gas Mixture CO_2 : N_2 : He : CO	E/N x 10^{-16} (volt.cm^2)
1 : 1.0 : 6 : 0.0	3.291
1 : 0.5 : 6 : 0.5	3.041
1 : 0.0 : 6 : 1.0	3.135
1 : 2.0 : 6 : 0.0	3.902
1 : 1.5 : 6 : 0.5	3.422
1 : 1.0 : 6 : 1.0	3.496

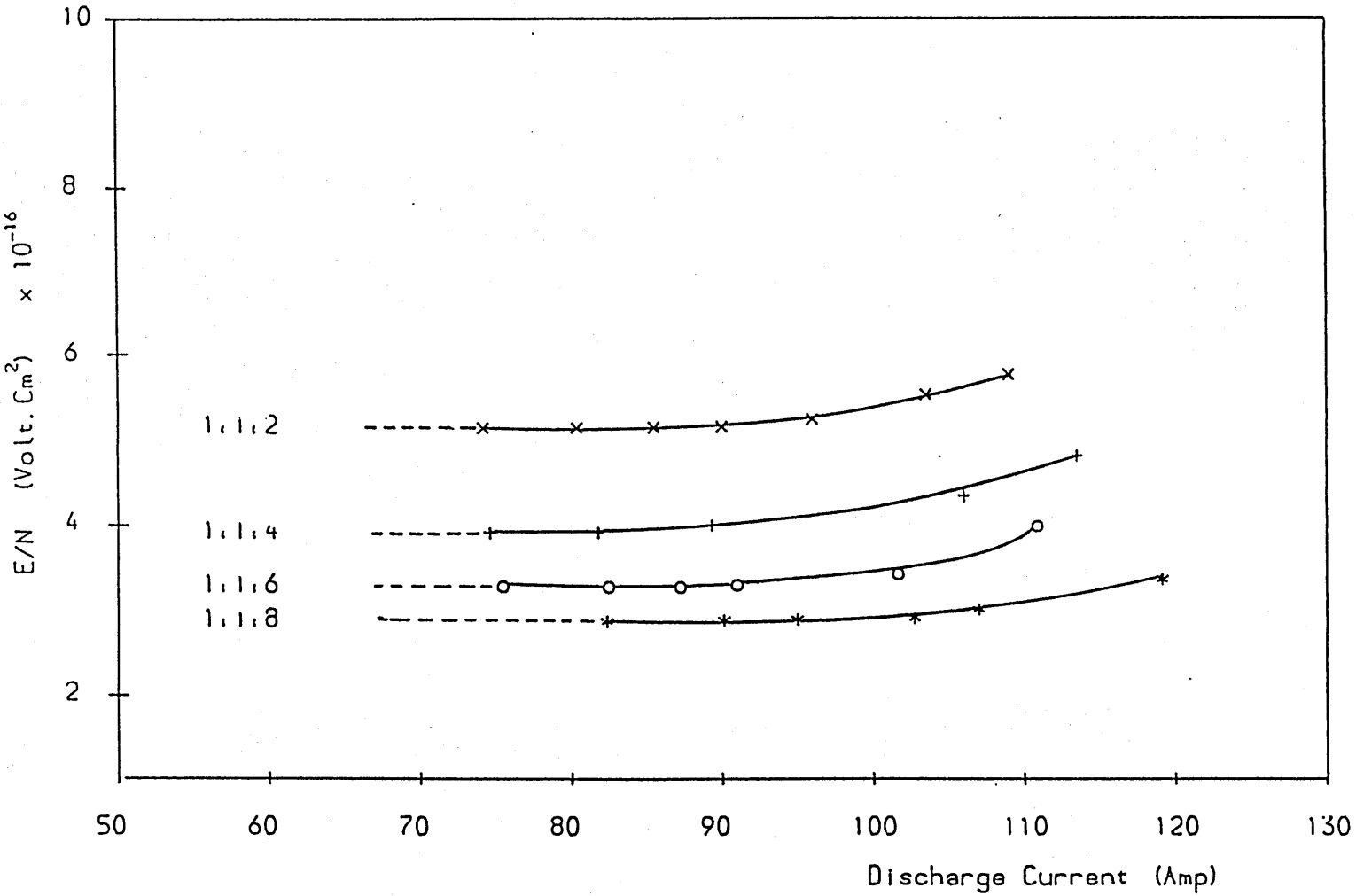

GRAPH OF (E/N) VERSUS DISCHARGE CURRENT

GRAPH (5.1)

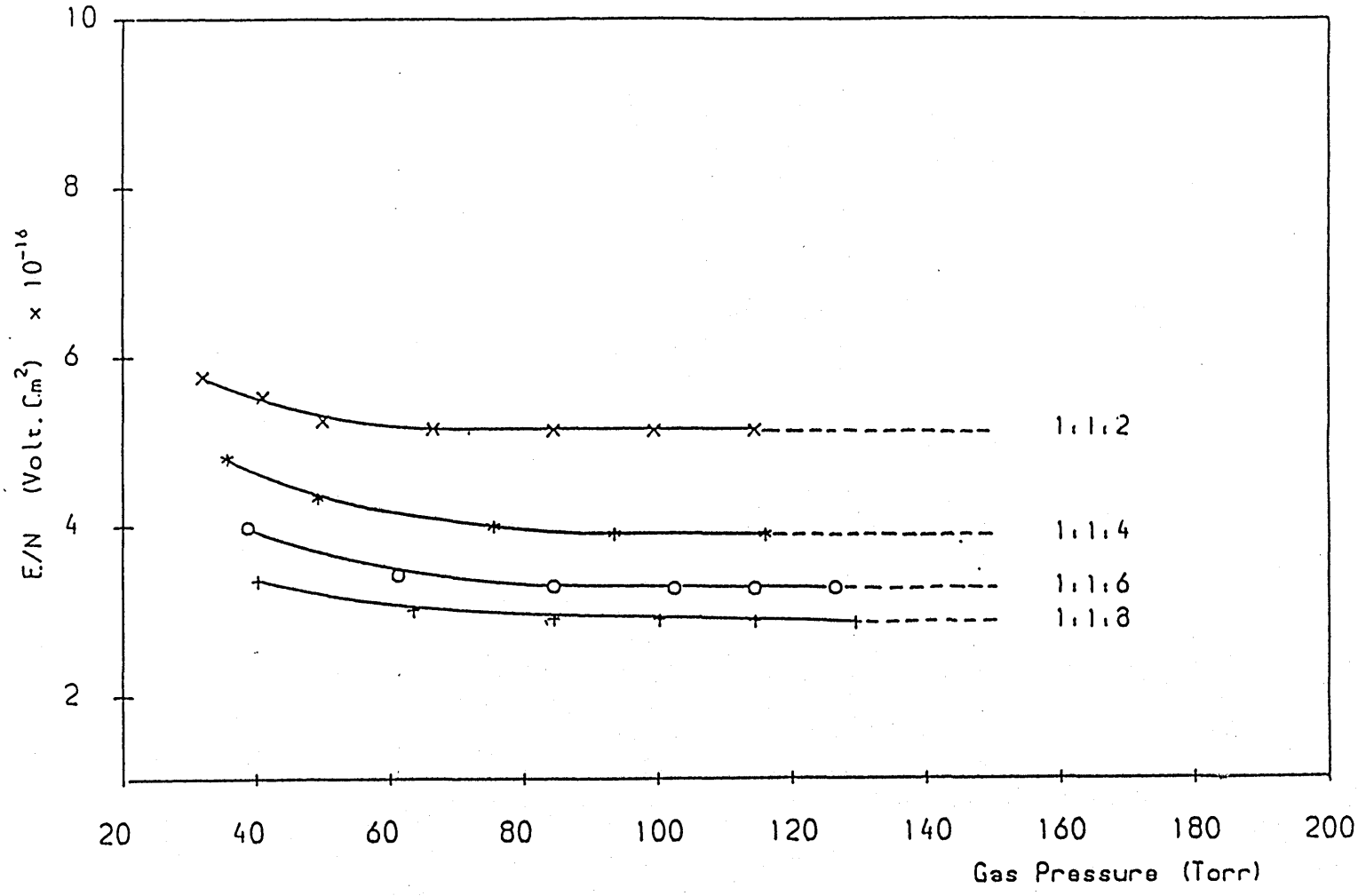

GRAPH OF (E/N) VERSUS GAS PRESSURE

GRAPH (5. 2)

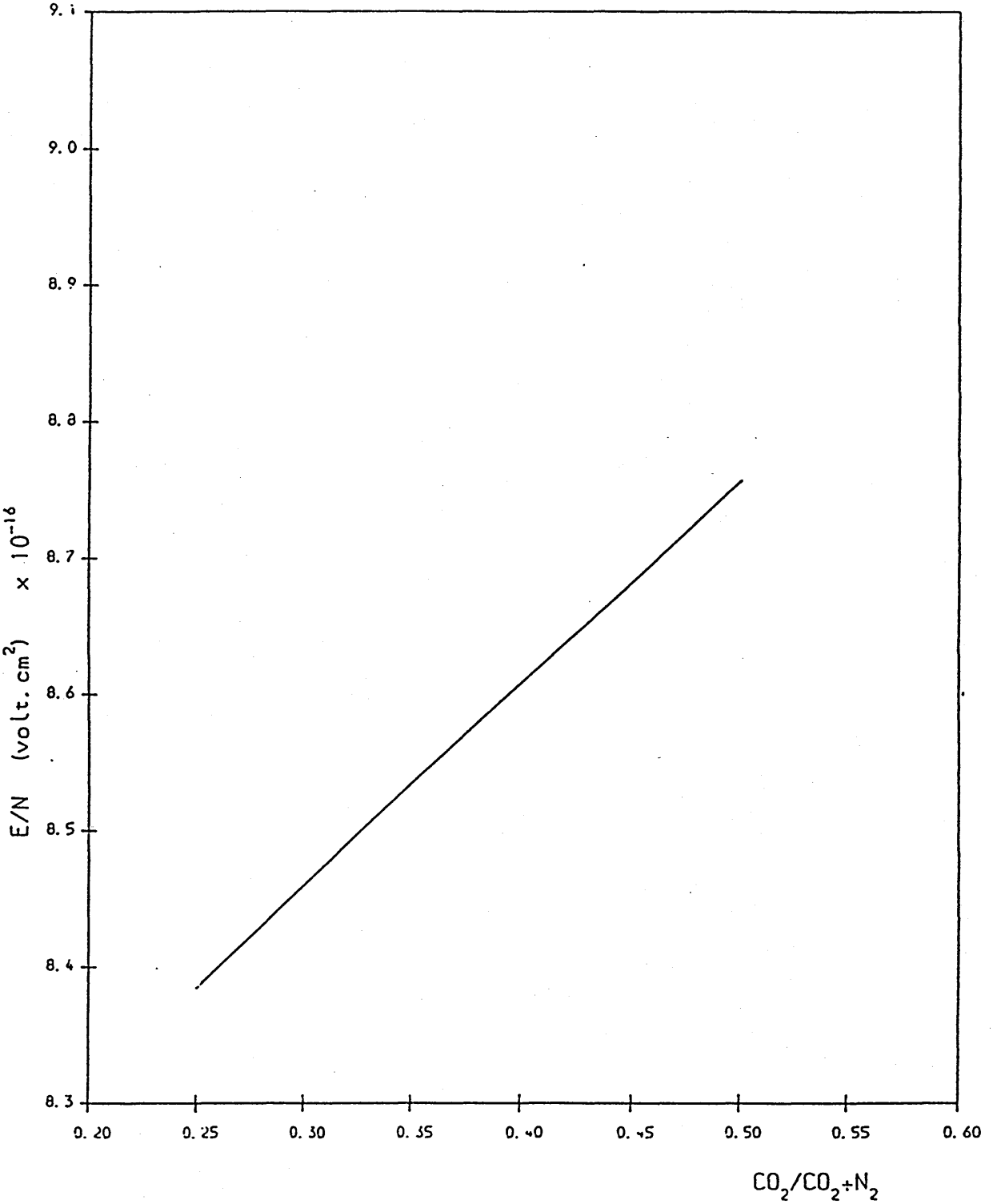

GRAPH OF E/N VERSUS CO_2 CONTENT

GRAPH (5.3)

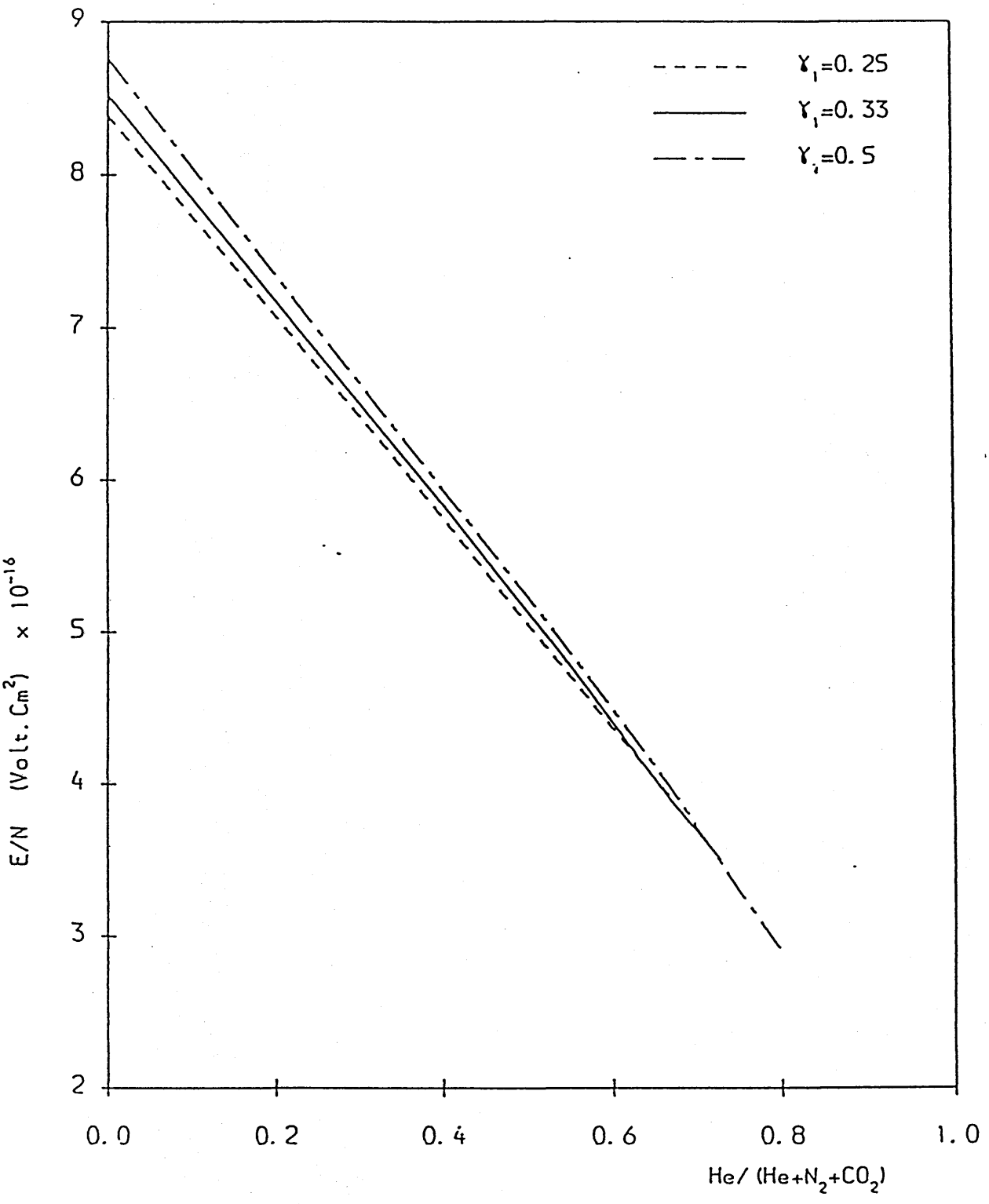

GRAPH OF E/N VERSUS He CONTENT

GRAPH (5.4)

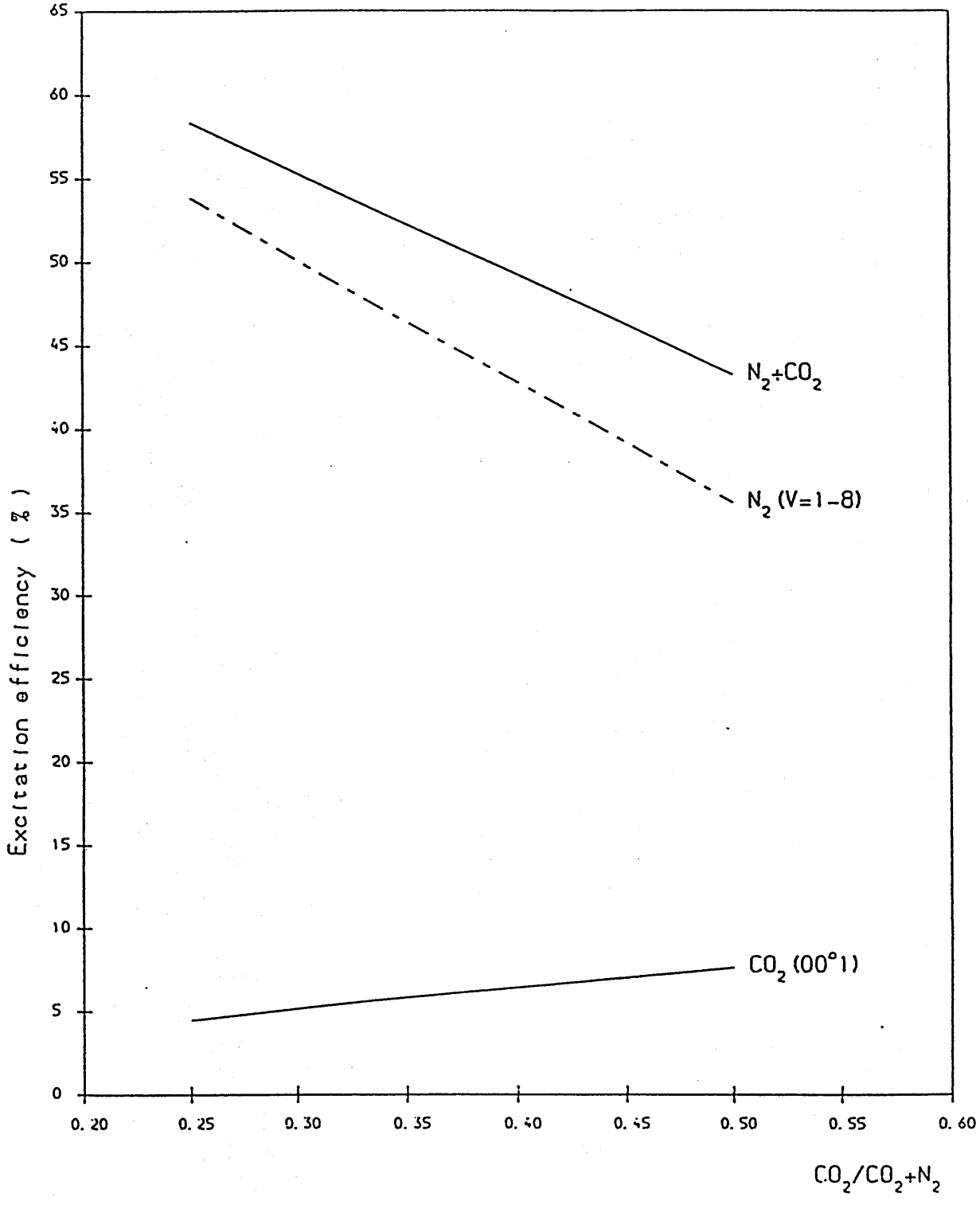

GRAPH OF EXCITATION EFFICIENCY VERSUS CO_2 CONTENT

GRAPH (5.5)

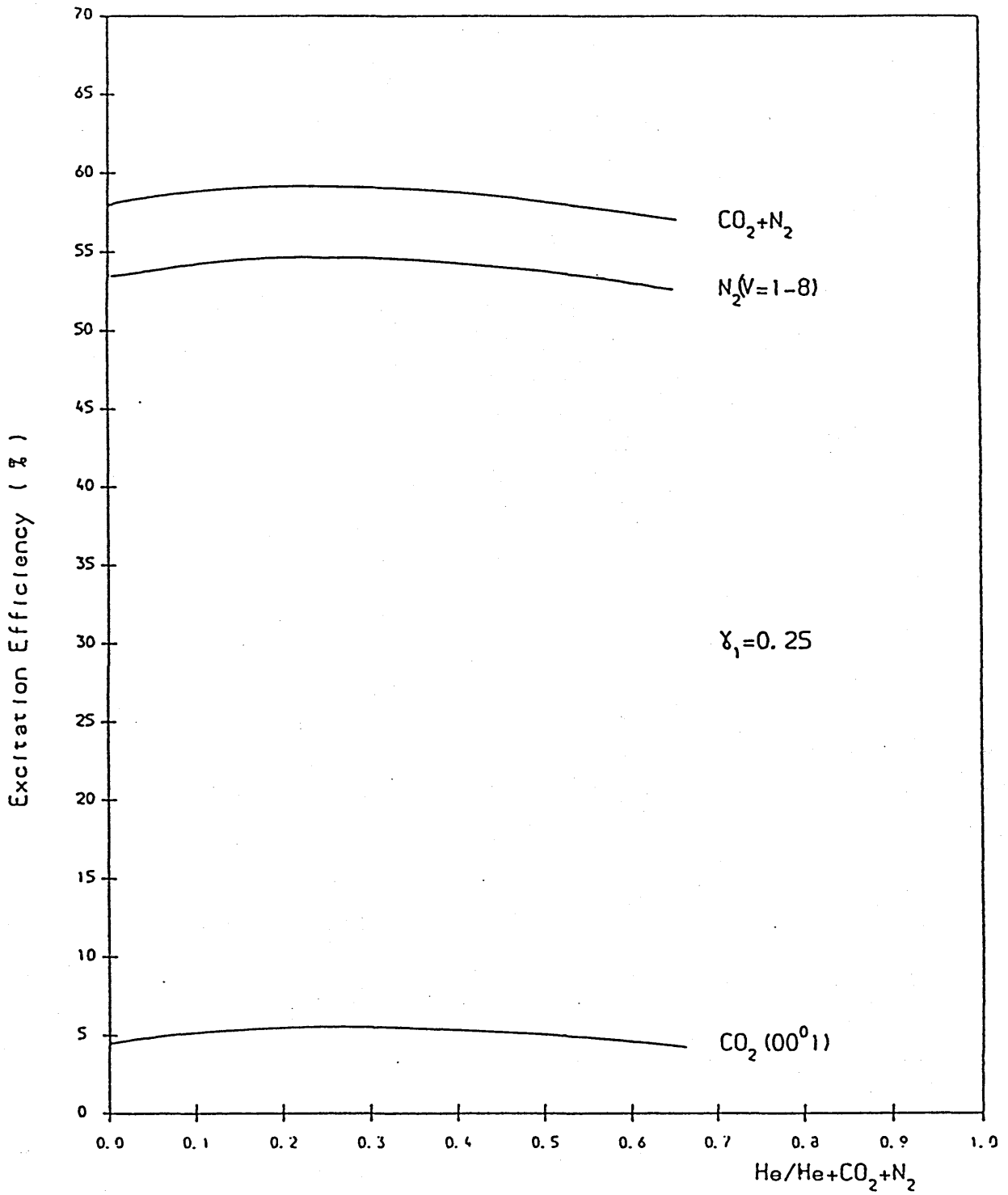

GRAPH OF

EXCITATION EFFICIENCY VERSUS He CONTENT

GRAPH (5.6)

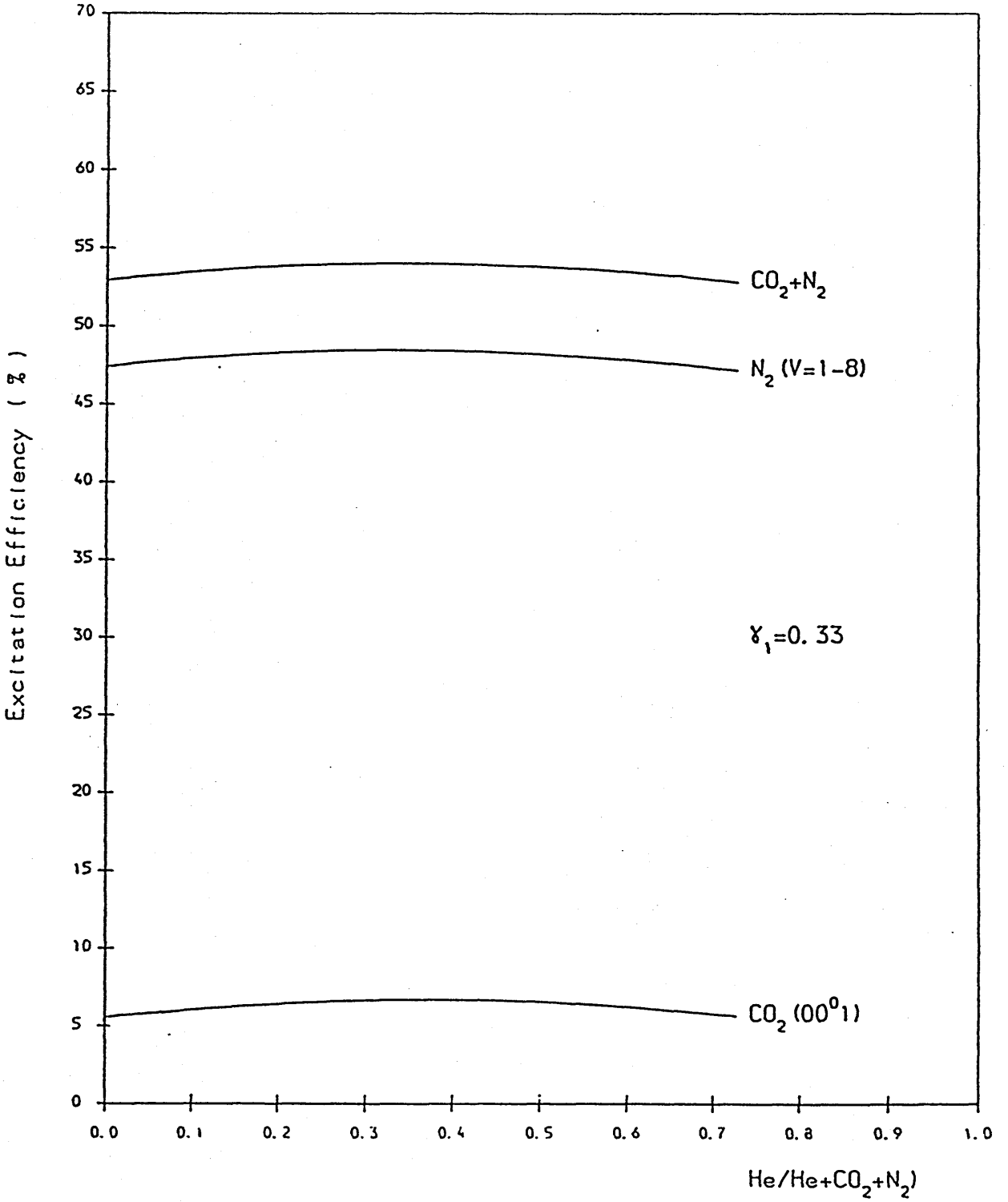

GRAPH OF

EXCITATION EFFICIENCY VERSUS He CONTENT

GRAPH (5.7)

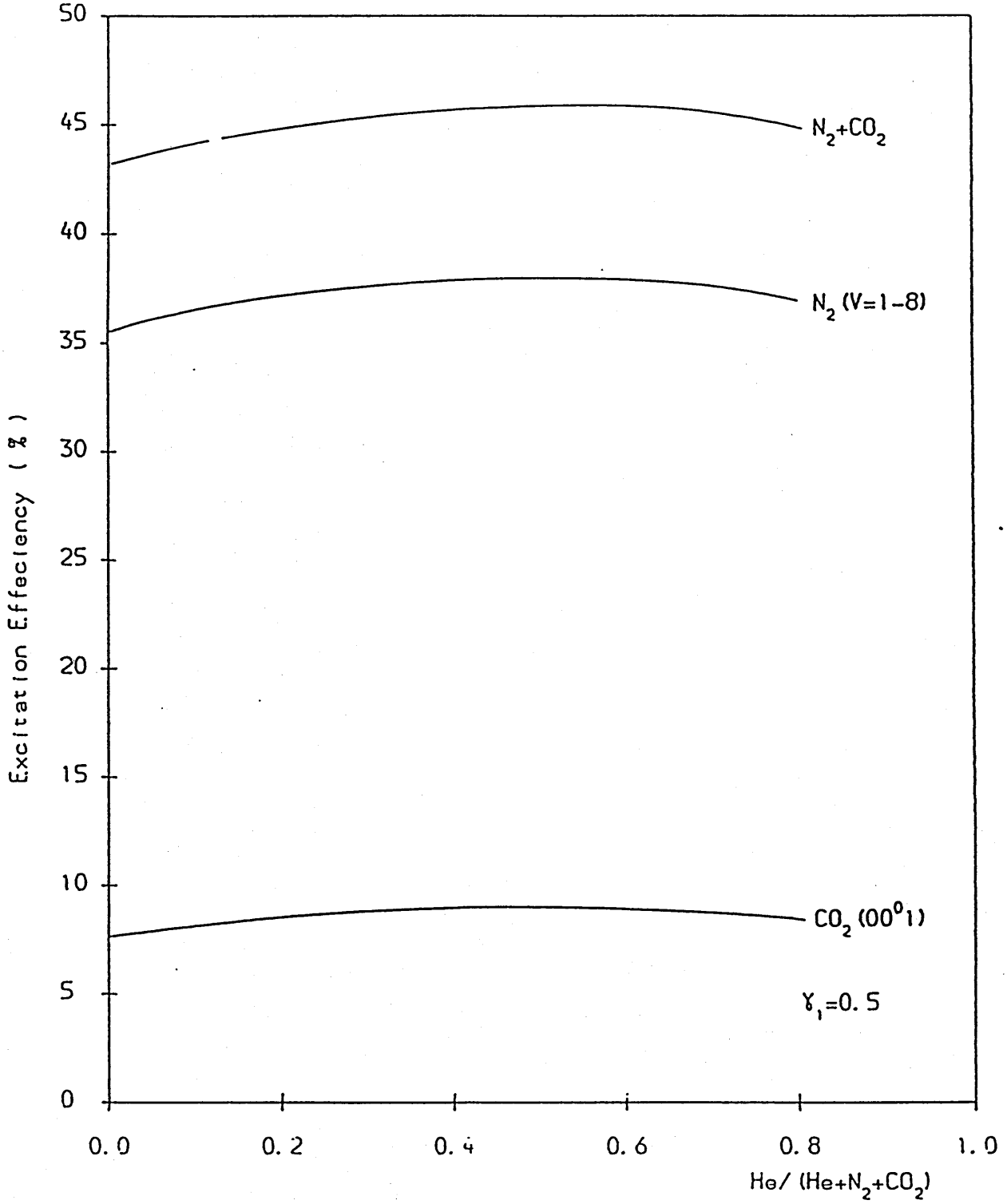

GRAPH OF

EXCITATION EFFICIENCY VERSUS He CONTENT

GRAPH (5.8)

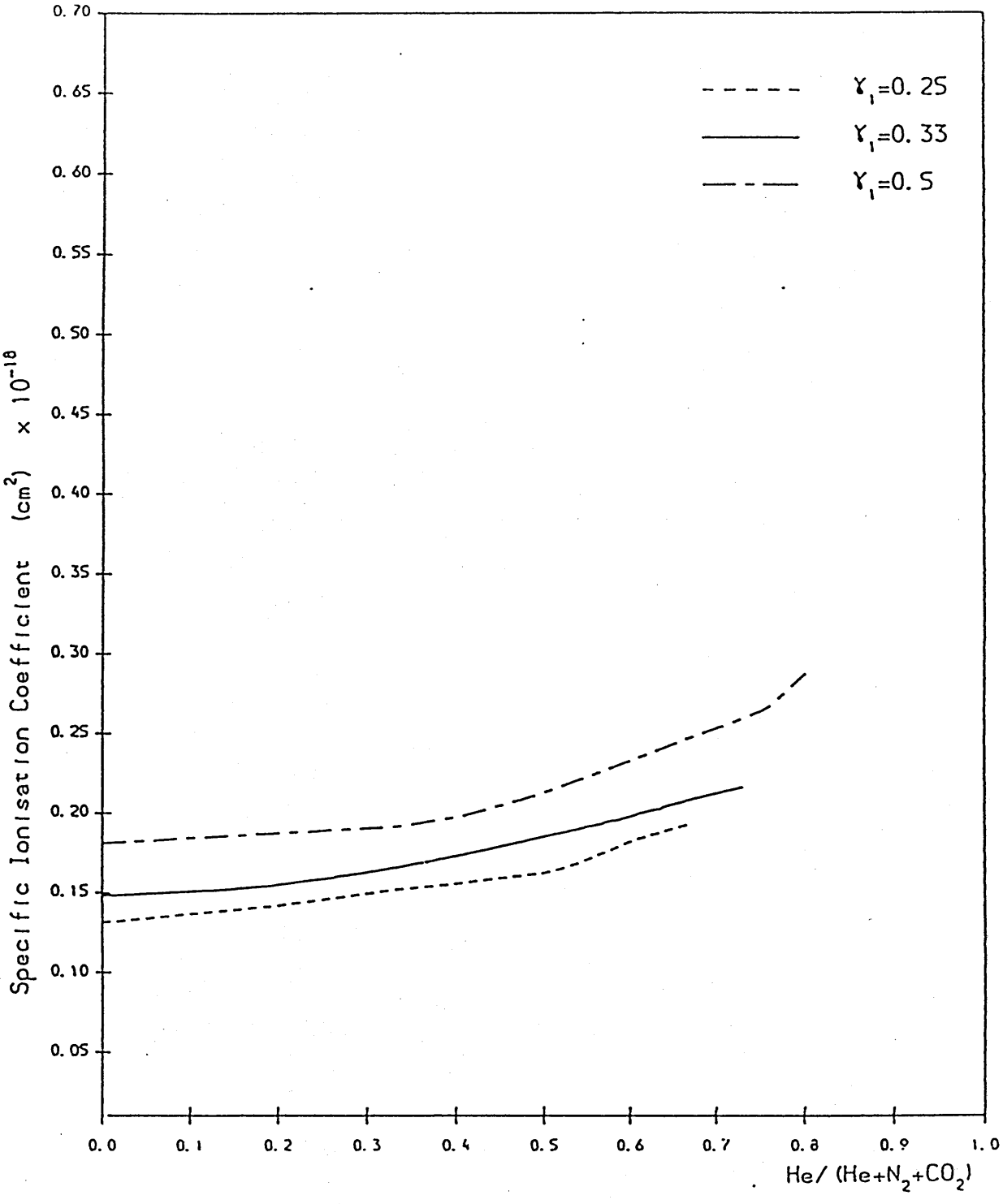

GRAPH OF SPECIFIC

IONISATION COEFFICIENT VERSUS HELIUM CONTENT

GRAPH (5.9)

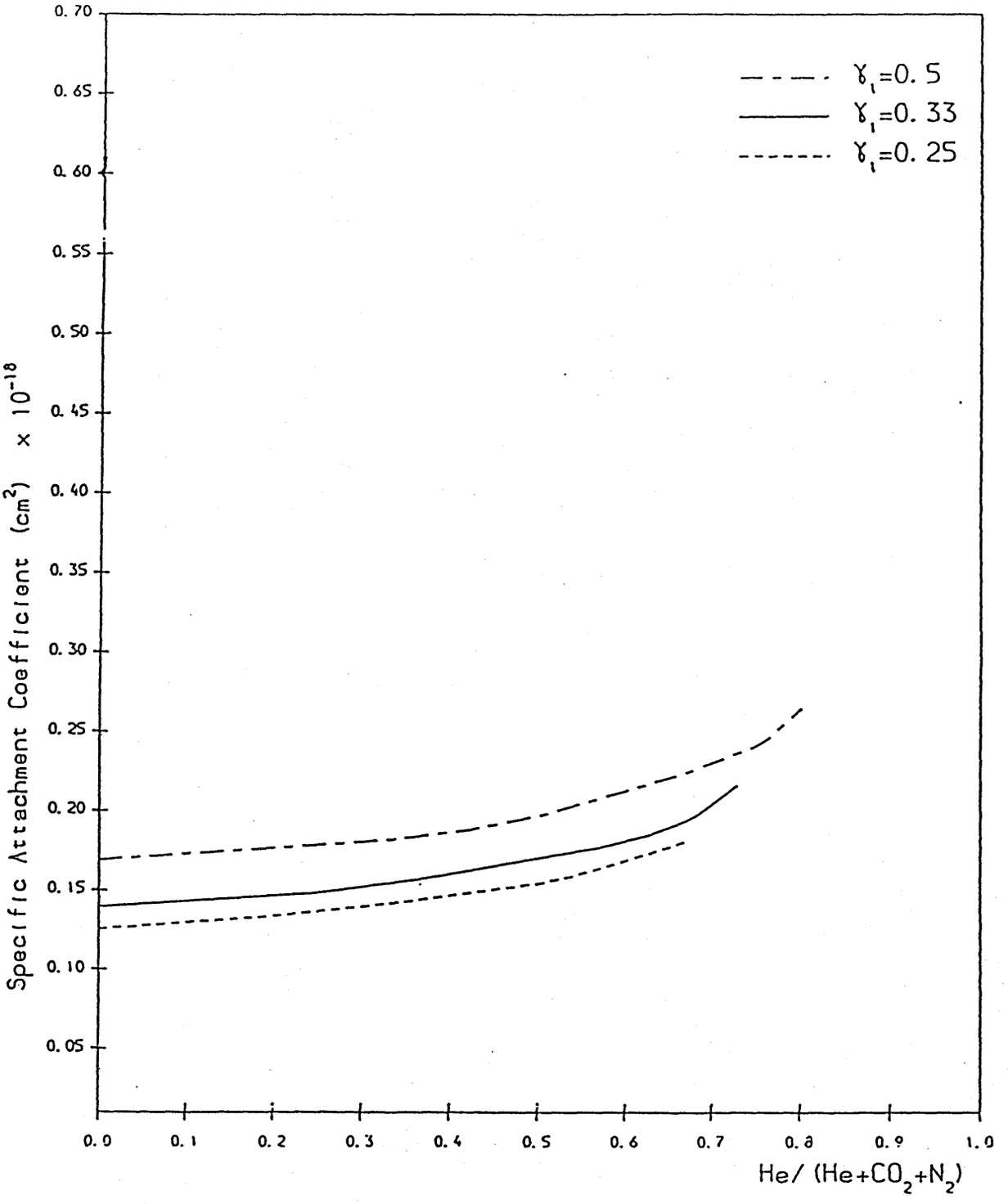

GRAPH OF SPECIFIC ATTACHMENT

COEFFICIENT VERSUS HELIUM CONTENT

GRAPH (5.10)

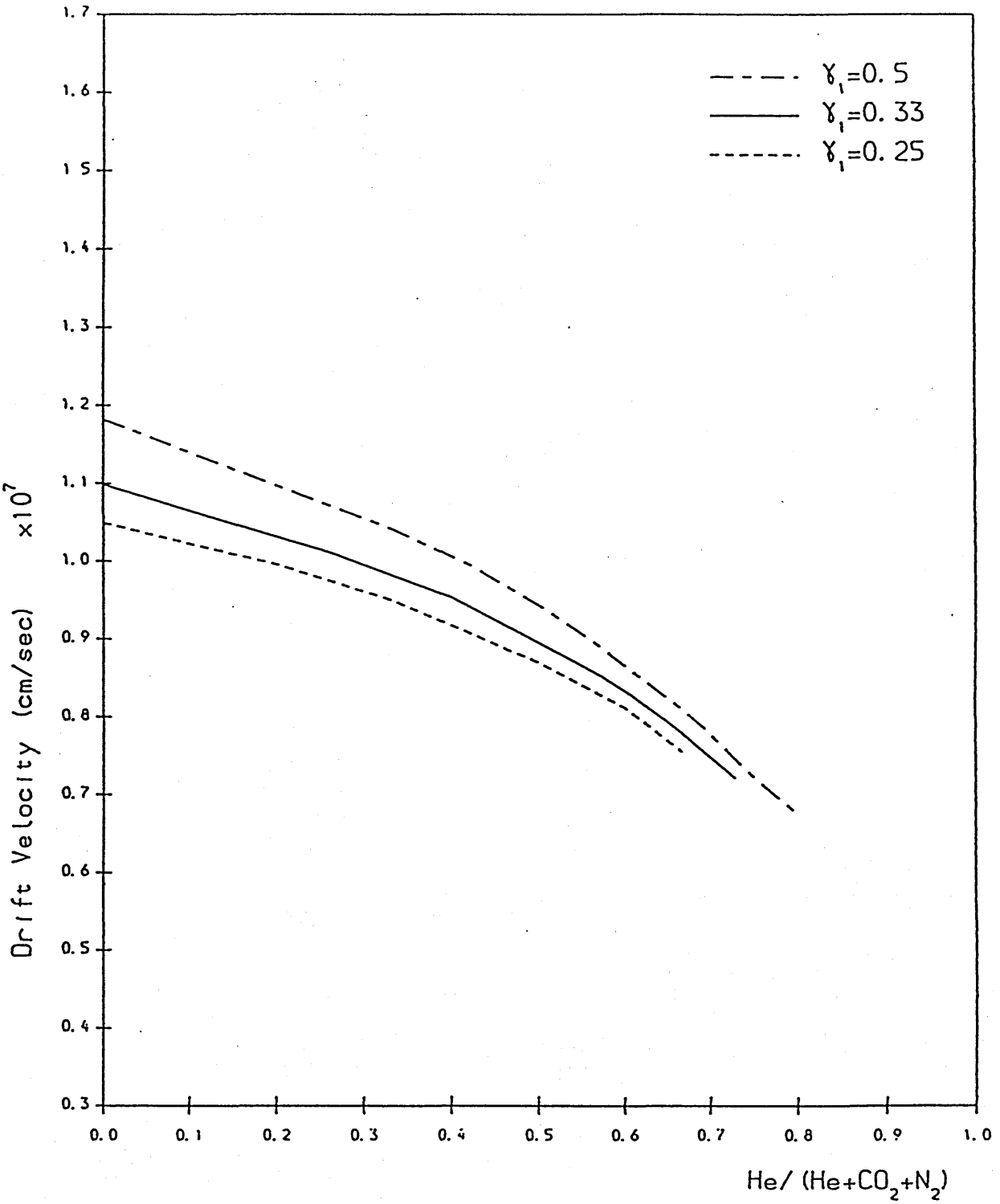

GRAPH OF

ELECTRON DRIFT VELOCITY VERSUS HELIUM CONTENT

GRAPH (5.11)

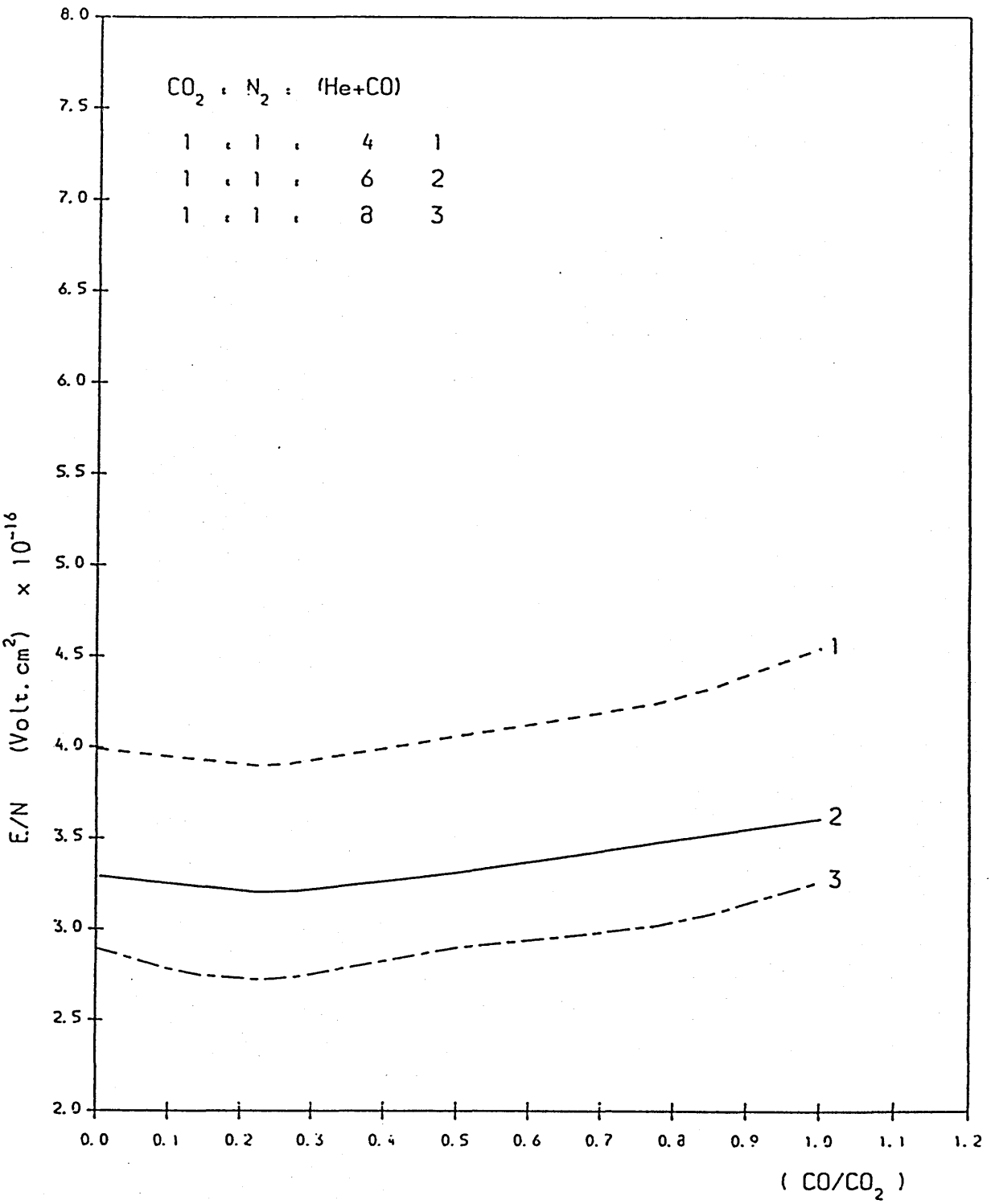

GRAPH OF E/N VERSUS CO CONTENT

GRAPH (5.12)

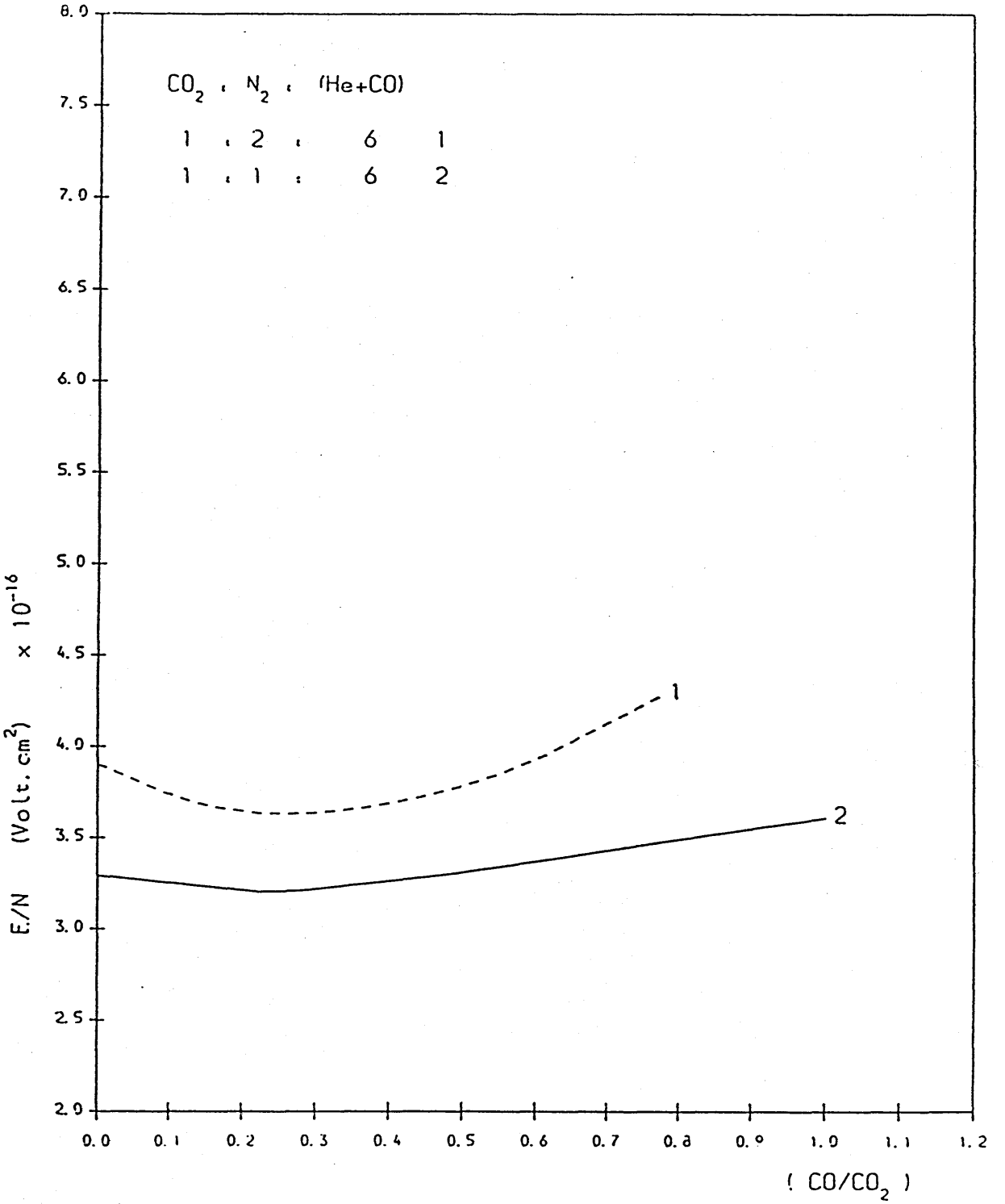

GRAPH OF E/N VERSUS CO CONTENT

GRAPH (5.13)

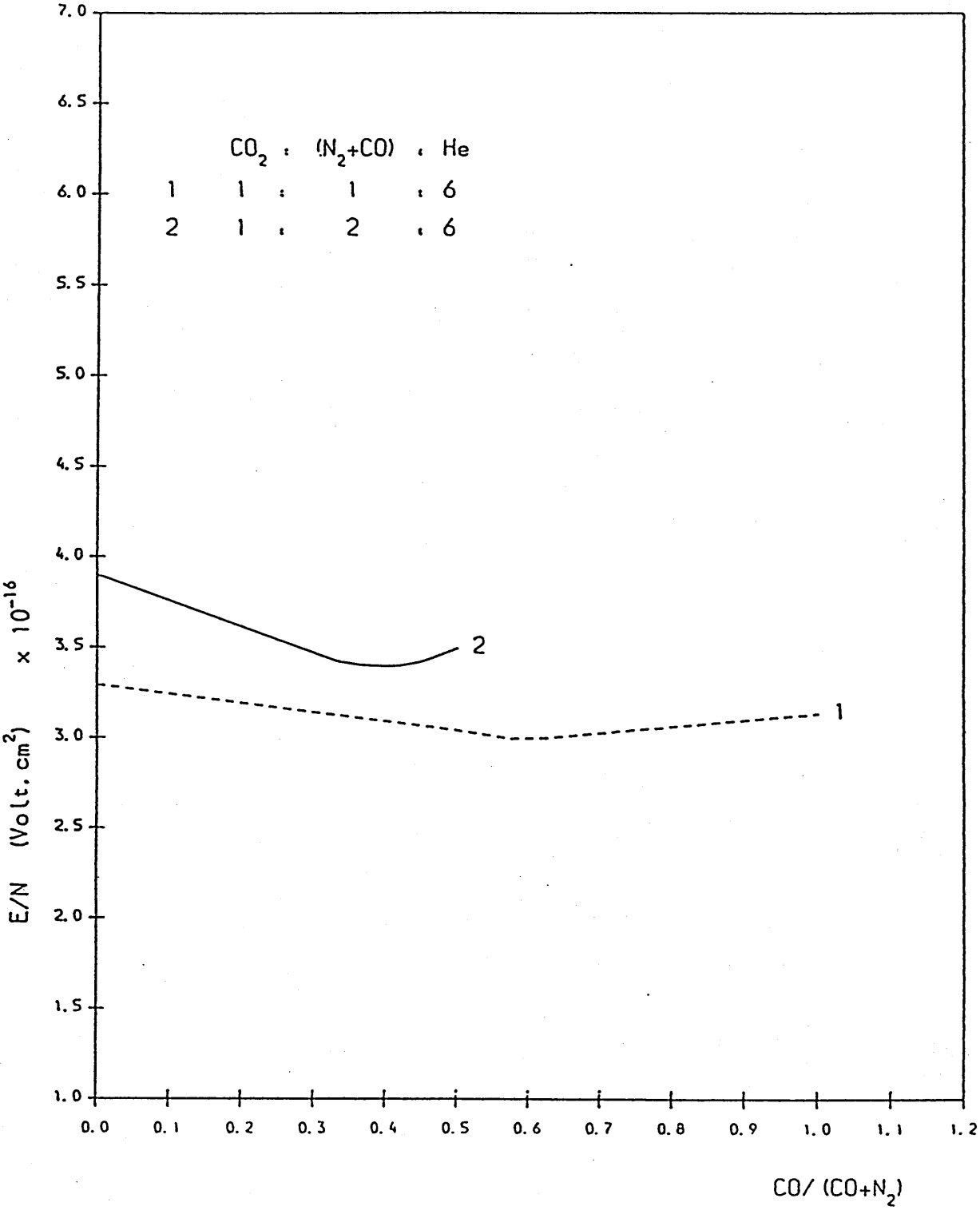

GRAPH OF E/N VERSUS CO CONTENT

GRAPH (5.14)

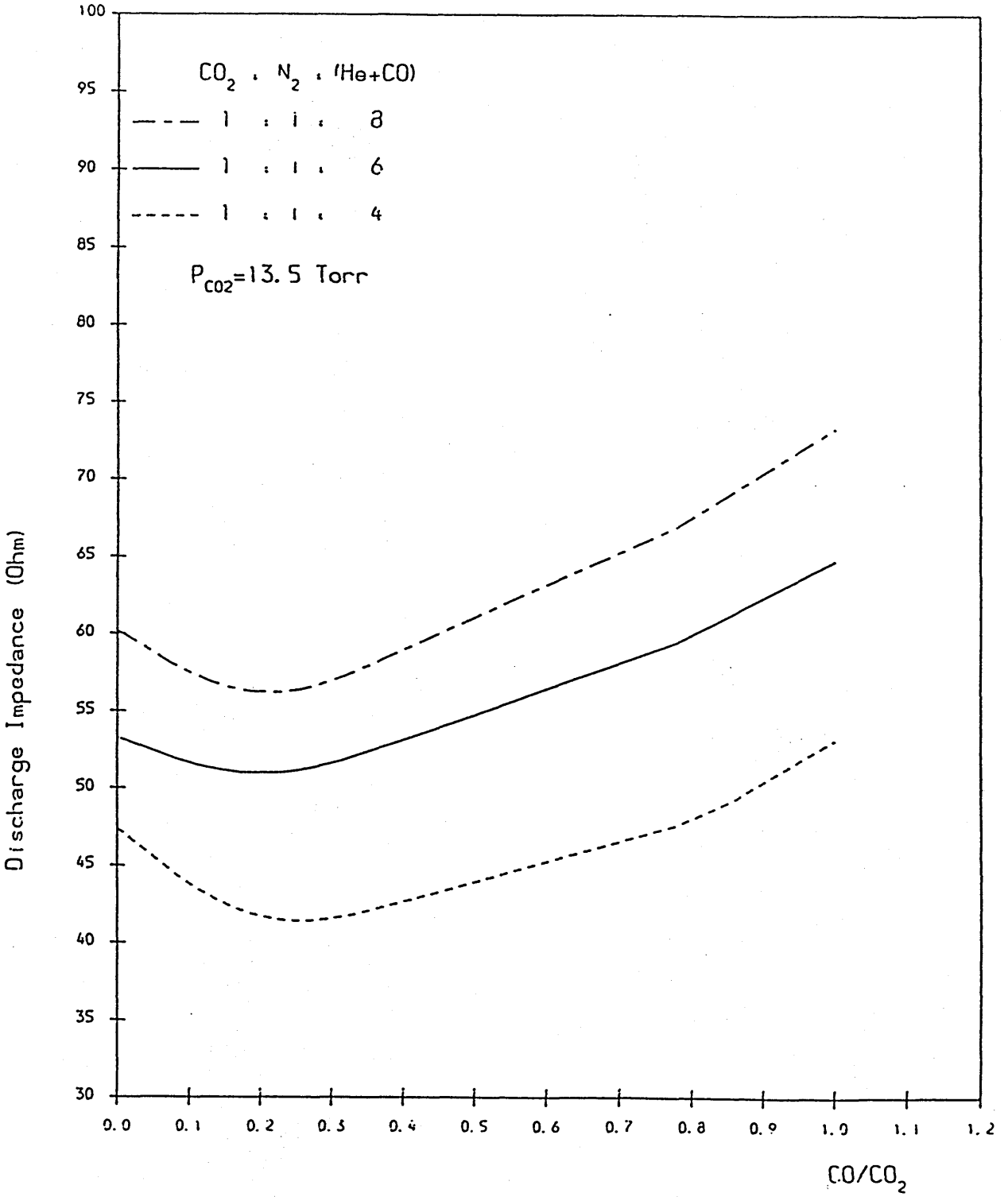

VARIATION OF DISCHARGE IMPEDANCE WITH CO CONTENT

GRAPH (5.15)

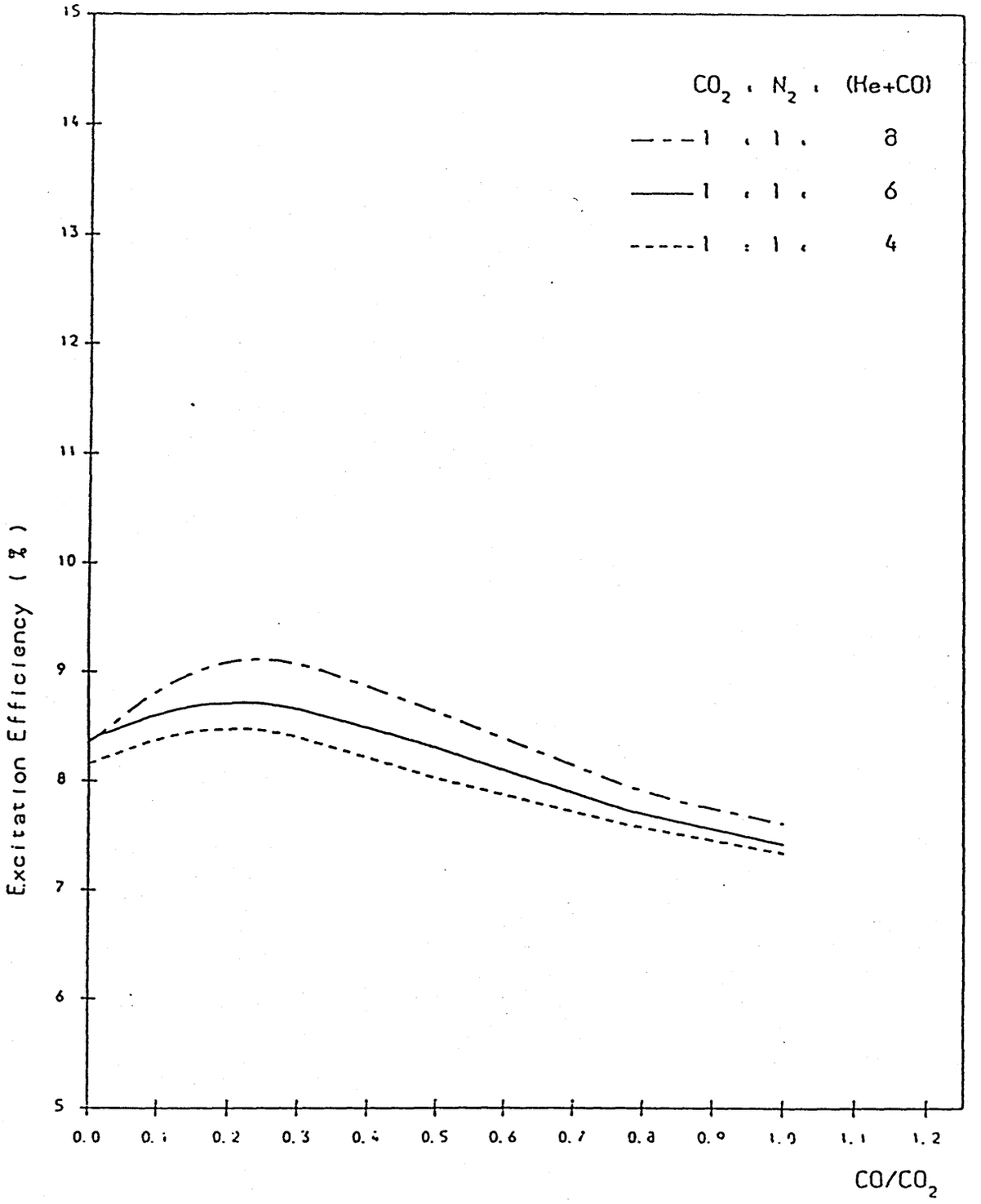

EXCITATION EFFICIENCY OF CO_2 (00°1) VERSUS CO CONTENT

GRAPH (5.16)

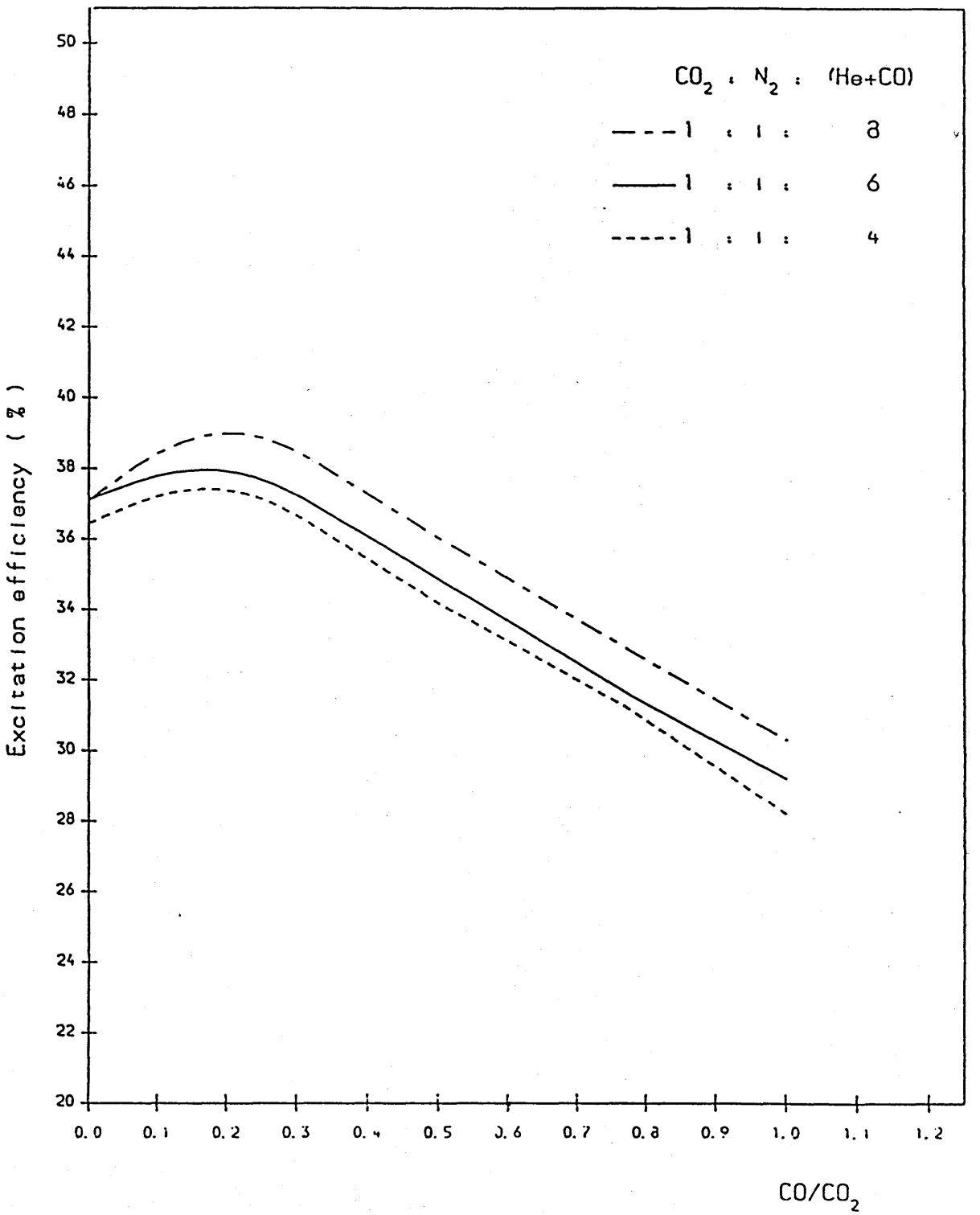

EXCITATION EFFICIENCY OF N_2 (V=1-8) VERSUS CO CONTENT

GRAPH (5.17)

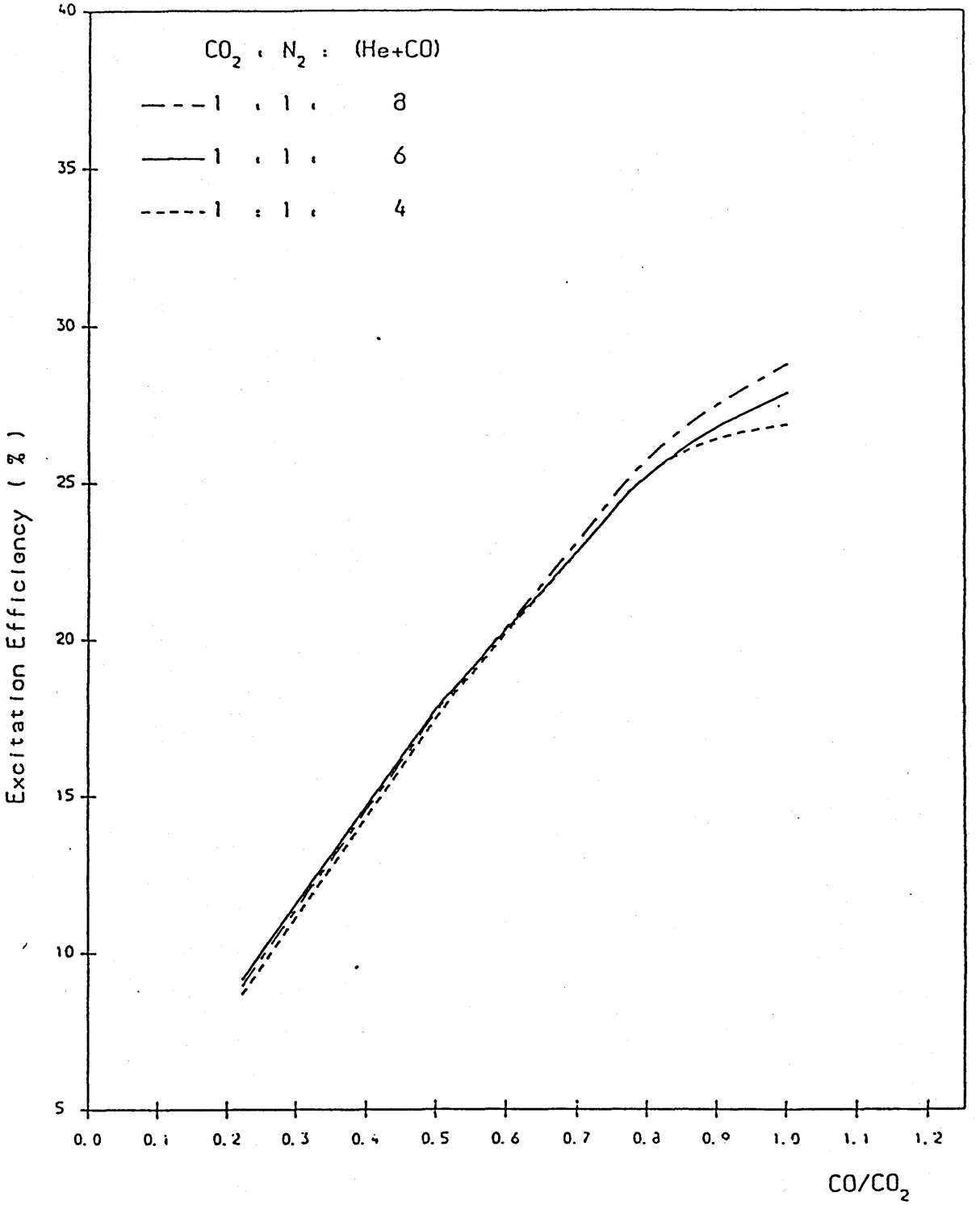

EXCITATION EFFICIENCY OF CO (V=1-8) VERSUS CO CONTENT

GRAPH (5.18)

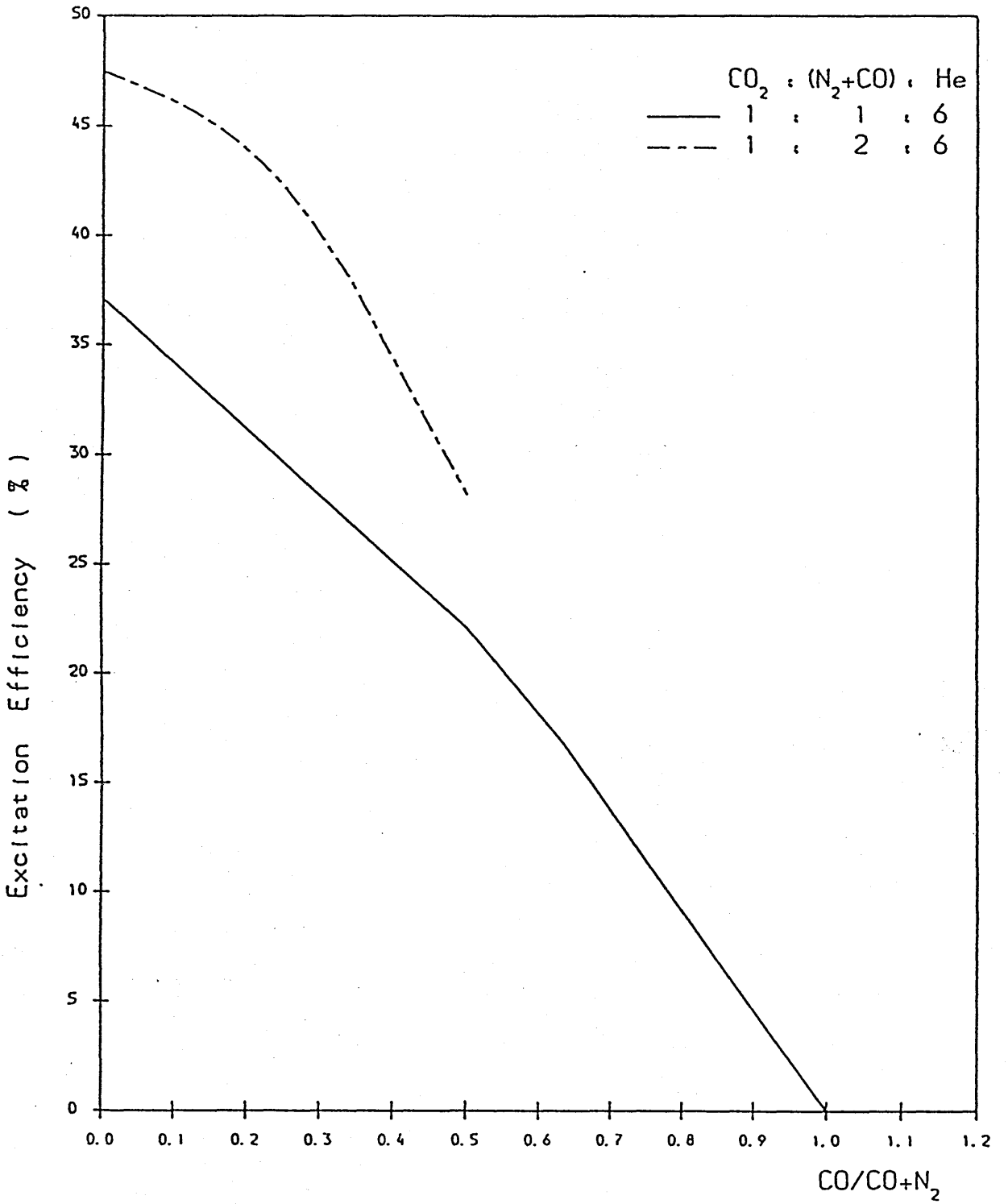

GRAPH OF EXCITATION

EFFICIENCY OF N_2 (V=1-8) VERSUS CO CONTENT

GRAPH (5.19)

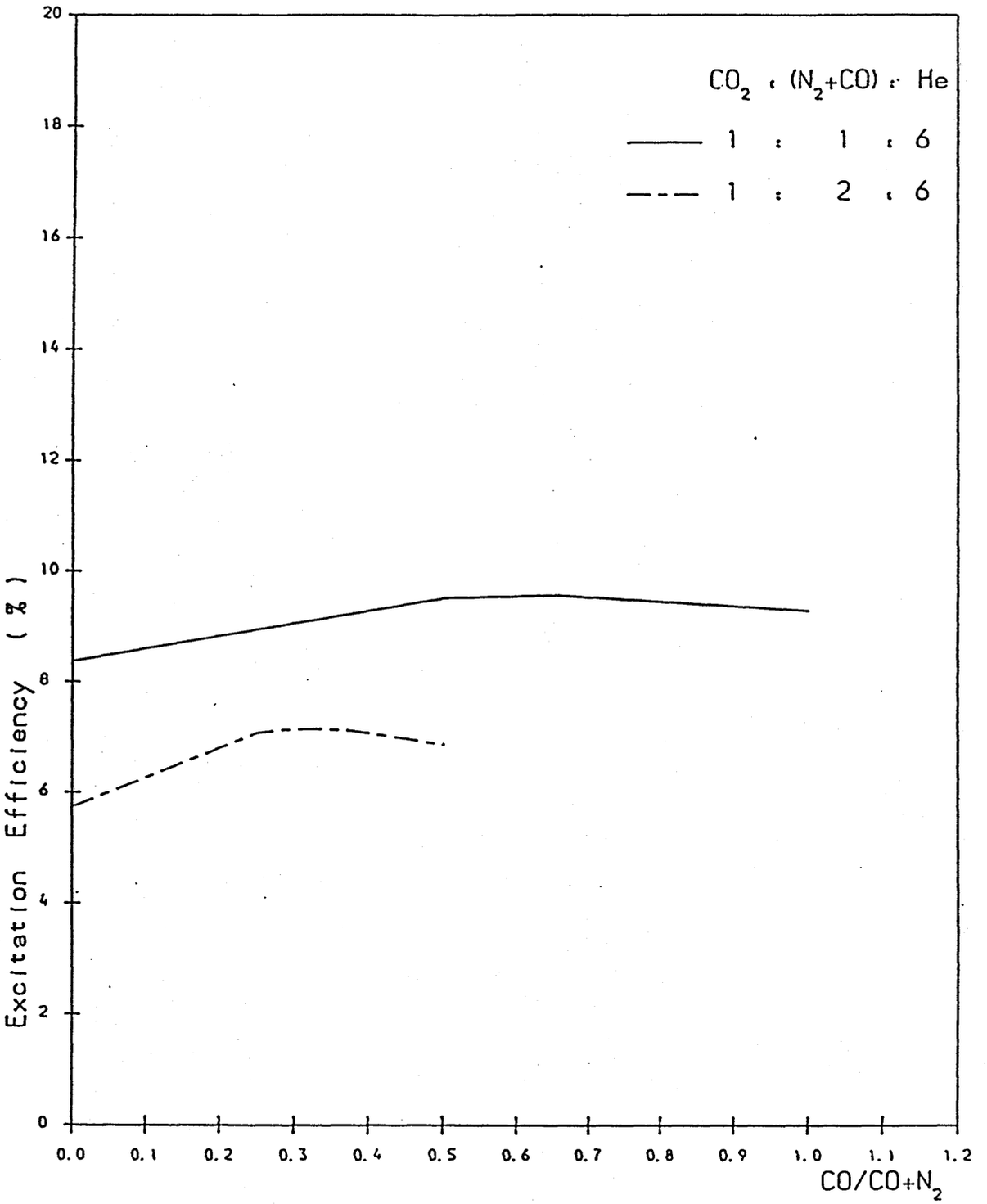

GRAPH OF EXCITATION

EFFICIENCY OF CO_2 ($00^0 1$) VERSUS CO CONTENT

GRAPH (5.20)

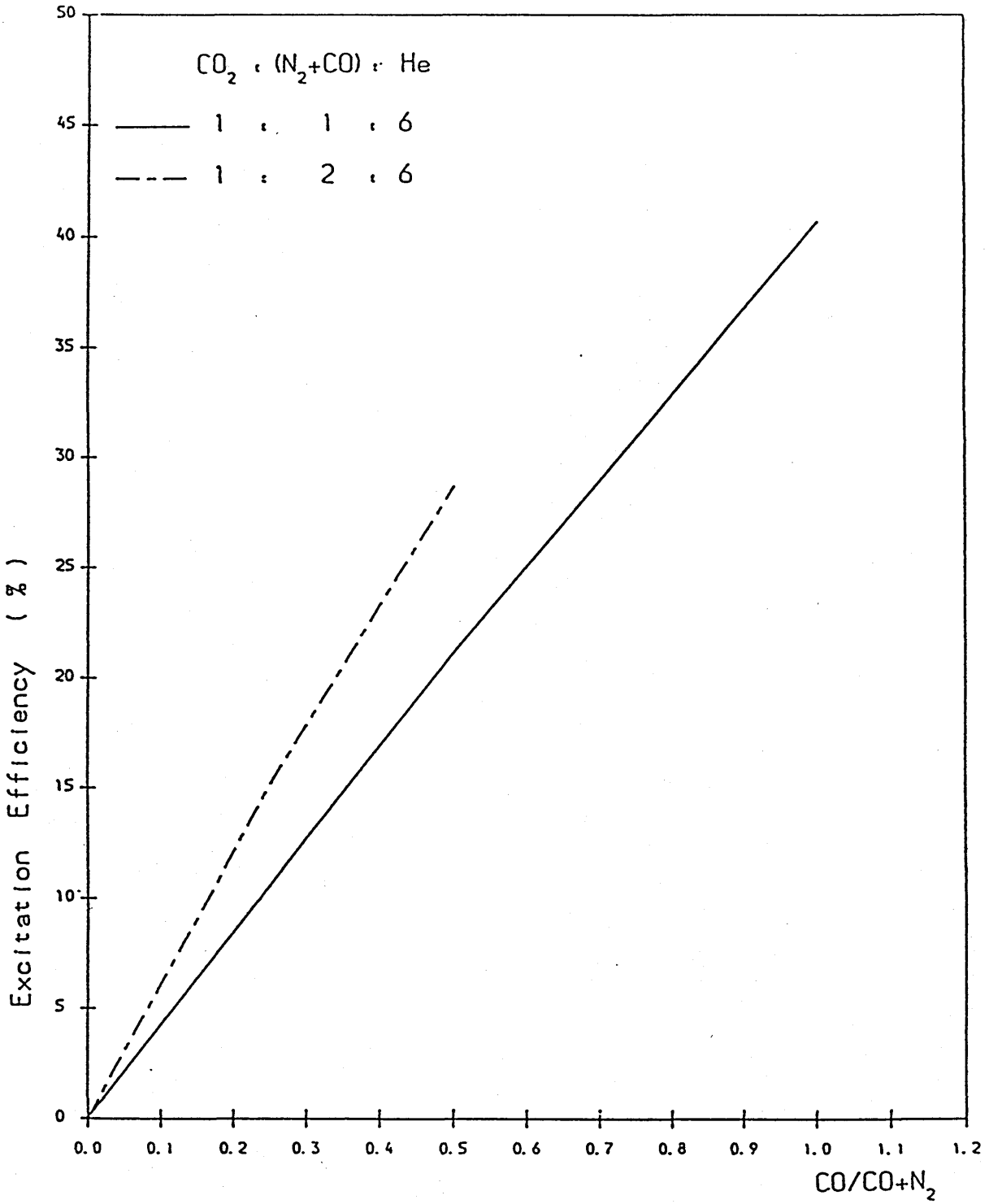

GRAPH OF

EXCITATION EFFICIENCY OF CO (V=1-8) VERSUS CO CONTENT

GRAPH (5.21)

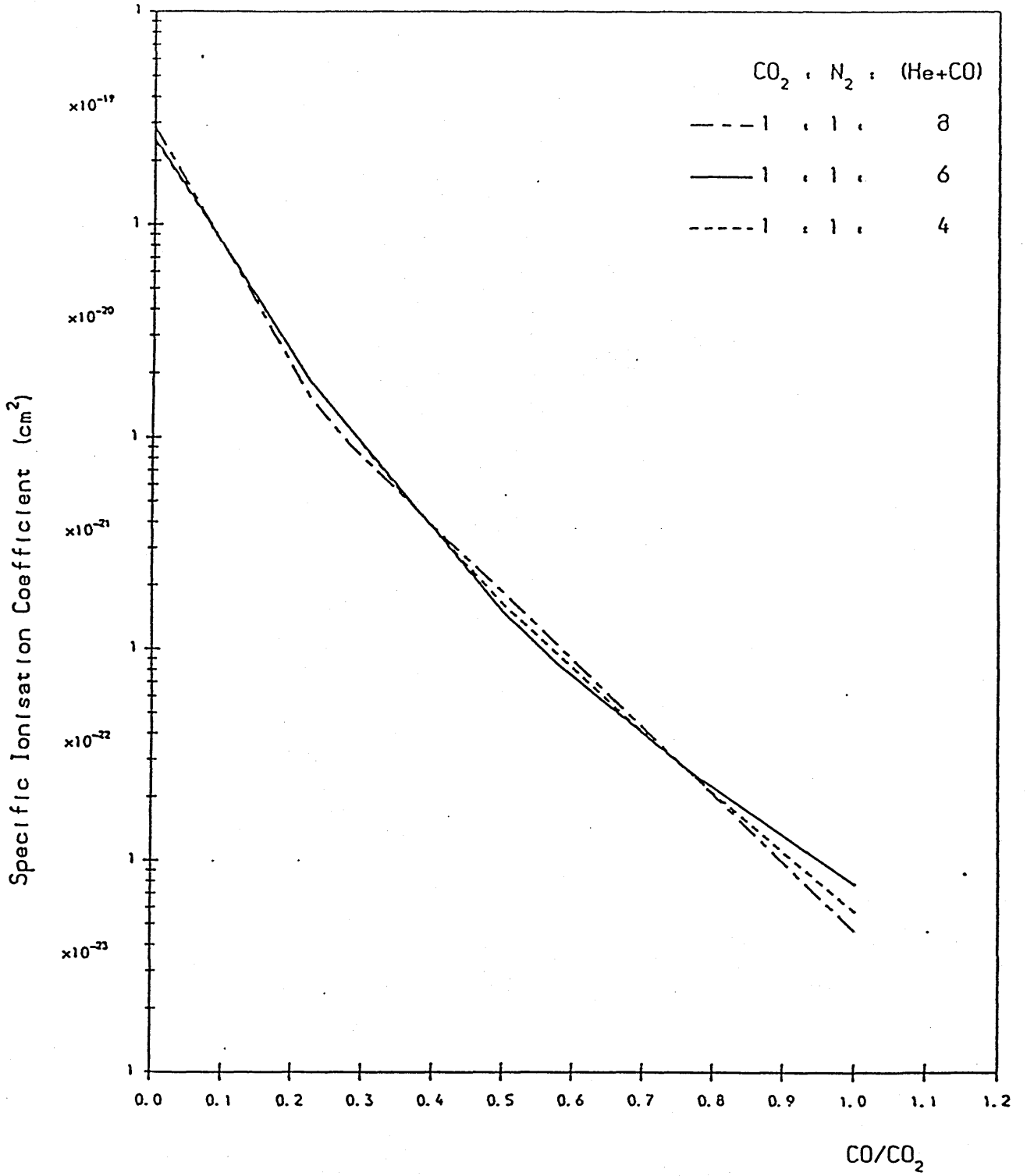

SPECIFIC IONISATION COEFFICIENT VERSUS CO CONTENT

GRAPH (5.22)

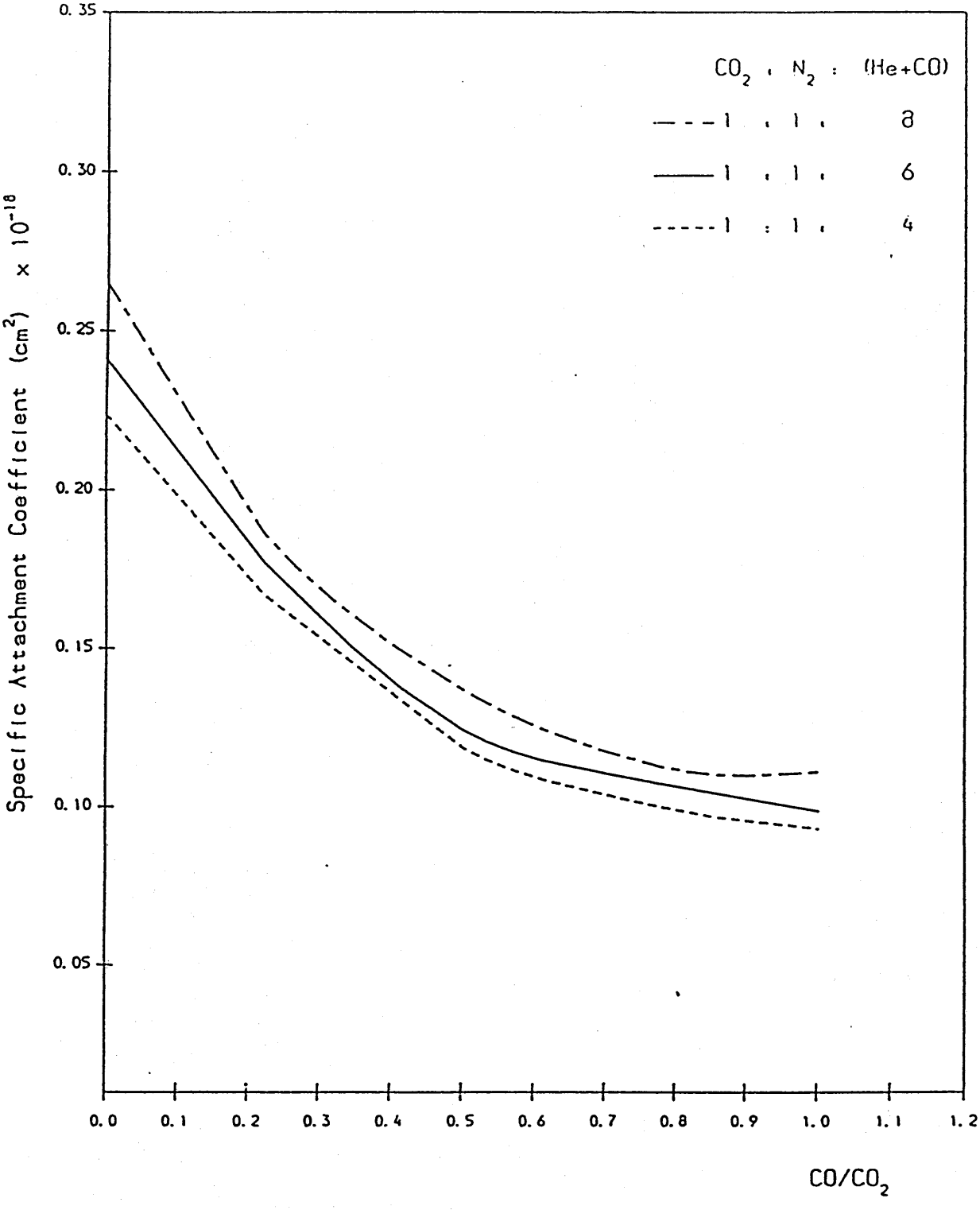

SPECIFIC ATTACHMENT COEFFICIENT VERSUS CO CONTENT

GRAPH (5.23)

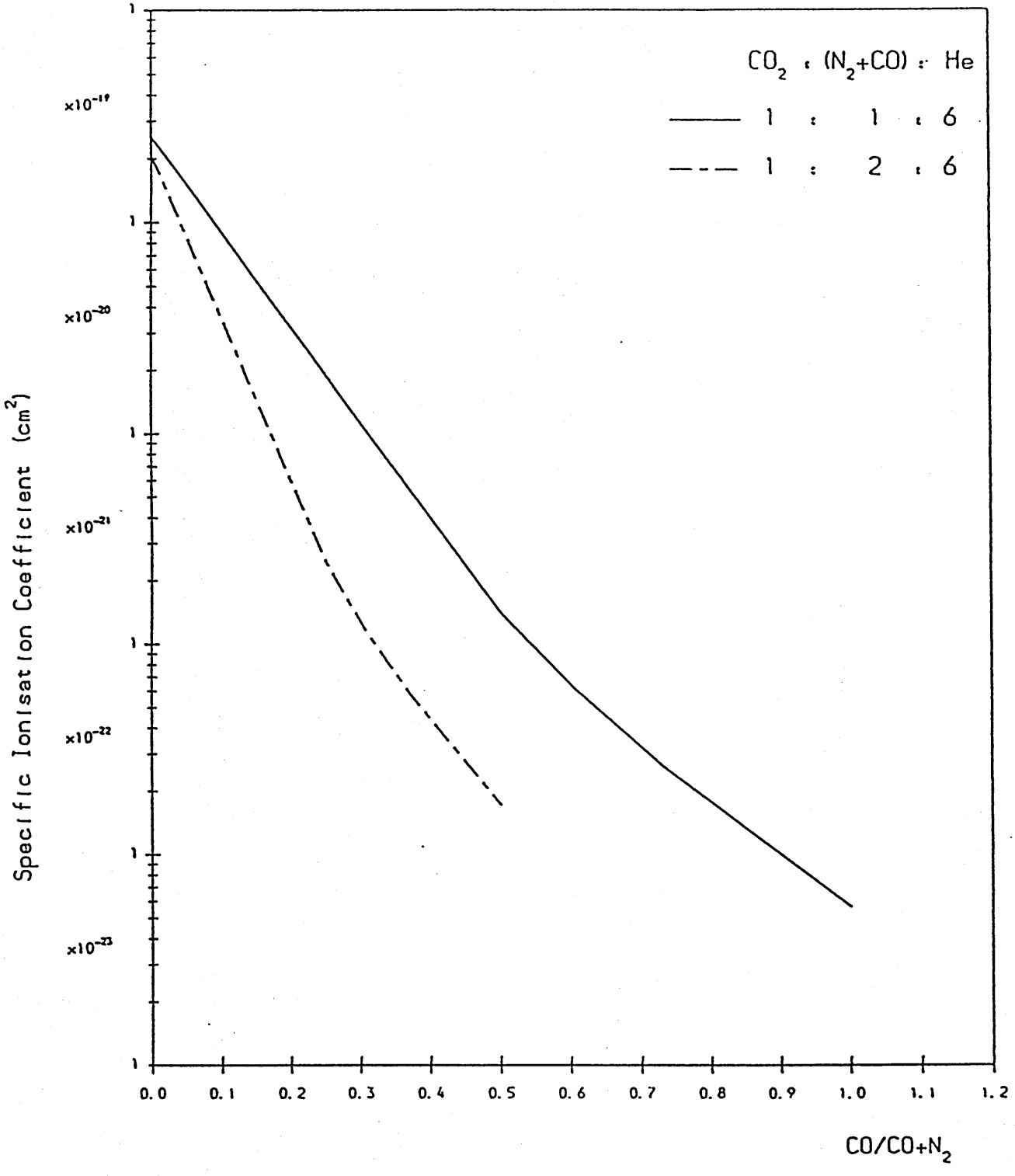

SPECIFIC IONISATION COEFFICIENT VERSUS CO CONTENT

GRAPH (5.24)

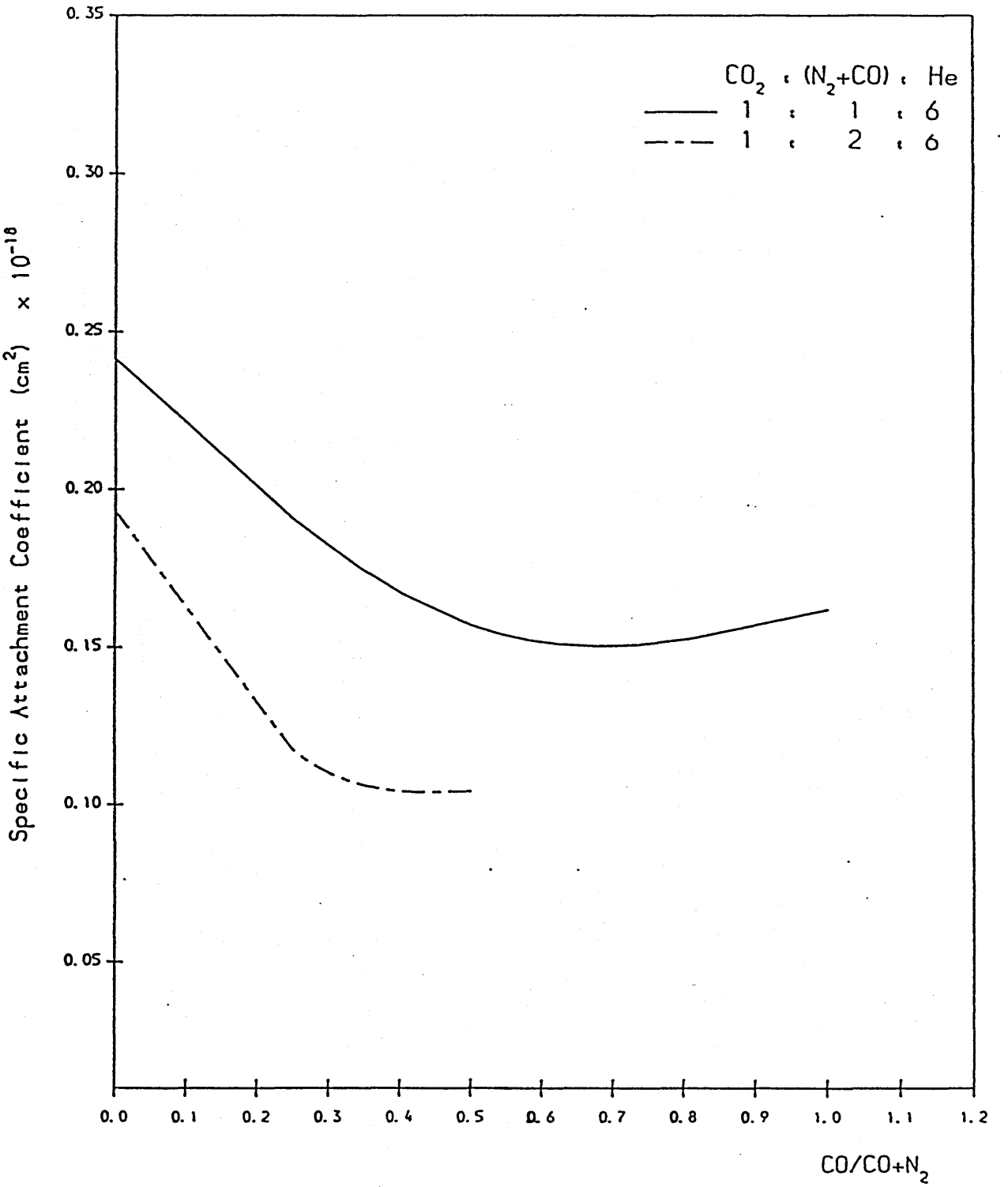

SPECIFIC ATTACHMENT COEFFICIENT VERSUS CO CONTENT

GRAPH (5.25)

CHAPTER SIX

GENERAL CONCLUSIONS AND SUGGESTIONS FOR FUTURE WORK

6.1 GENERAL CONCLUSIONS:

Improvement in CO_2 laser design has made it all the more necessary to understand the glow discharge behaviour so that more efficient,higher-power-output laser systems can be created. Simulations have been carried out in chapter 2 to predict the electron swarm parameters and the fractional energy transfer by electrons to the vibrational levels of CO_2 and N_2 in gas mixtures with various concentration ratios of CO_2,N_2,and He for a wide range of (E/N). The calculations are based on the determination of the electron energy distribution function (EEDF) obtained by solving the Boltzmann transport equation. Consequently, it is apparent that the accuracy of these predictions depends,in particular, on the accuracy of the experimental data used to infer the cross-sections of the component gases, as well as on the accuracy of the theory used for swarm parameter analysis (Appendix 2.IV). However, the experimental determination (chapter 5) of the operating characteristics of the discharge, particularly the parameter E/N, has shown an excellent agreement between the predicted and measured values of this parameter (within 1-4%),therefore proving the soundness of the theoretical results.

The theoretical predictions have shown that for values of $E/N \geq 2\times10^{-16}$ volt.cm^2 superelastic collisions can be neglected as their effects on the (EEDF) are insignificant

compared with other inelastic collisions. Helium has been shown to play a dominant role in determining the (EEDF). Increasing the proportion of helium in the gas mixture leads to an increase in the average electron energy and in the ionisation and attachment coefficients for a given E/N. Thus, the E/N value for maximum excitation efficiency and the operating value of E/N for the discharge are reduced. On the other hand, the theoretical predictions have shown that increasing the proportion of nitrogen in the gas mixture results in a reduced average electron energy and decreased ionisation and attachment coefficients. Therefore the E/N for maximum excitation efficiency and the operating value of E/N for the discharge are both increased. The results obtained have shown that the laser excitation efficiency is increased with increasing ratio of nitrogen to carbon dioxide. Thus, more electrical energy is coupled into the discharge instead of being lost in the excitation of bending and stretching modes of CO_2. This is a beneficial factor which is shown to improve the laser output power (chapter 4). The effects of the addition of carbon monoxide to the gas mixture on the (EEDF) has been examined. This allows prediction of the discharge parameters and transport coefficients with the effects of dissociation and therefore provides the necessary data for simulation of the laser output parameters. It has been shown that with the addition of CO the average electron energy and the ionisation and attachment coefficients are reduced. Consequently, both the E/N for maximum excitation efficiency and the operating

value of E/N for the discharge are increased.

For laser performance optimisation it is necessary to obtain a detailed insight into the effects of various plasma kinetic processes. Theoretical analysis of plasma chemical phenomena occuring in the discharge has been carried out (chapter 3). The results obtained have shown that under the operating conditions of the CO_2 discharge, electron attachment is the important kinetic process since the formation of negative ions elevates the electron temperature which affects the excitation processes and therefore strongly influences the discharge operation. The dissociation of CO_2 is predicted to be 0.21 % per pulse. Moreover, helium enrichment of the gas mixture is found to increase dissociation because of the increase in the average electron energy. Dissociation products, particularly oxygen, are found to increase appreciably with increasing pressure. Oxygen is found to be the most harmful species from the discharge stability point of view as it forms negative ions easily and therefore significantly influences both the pre-ionisation and main discharge formation. In laser systems,air leaks and the use of technical grade gases make mixture contamination inevitable. In the laser system built air leaks were measured to be 1 mbar/hr. The predictions have shown that H_2O has a deleterous effect on the charged particle balance in the discharge; 1% H_2O is sufficient to produce a significant increase in the negative ion population and subsequent increase in the discharge instability. It has been shown that the dissociation of CO_2

and subsequent formation of O_2 can effectively be controlled by the addition of CO and H_2, because CO reacts with OH to form CO_2. However, the results obtained have shown that addition of more than 1% H_2 has a harmful effect because the dissociation of H_2, which is predicted to be 0.7% per pulse, leads to the formation of water vapour.

Investigations of laser output parameters have been carried out (Chapter 4). A theoretical model has been developed in order to predict the laser output and hence facilitates the optimization of designs and controls for matching output characteristics to the workpiece requirements. The results obtained have shown that the pulse profile, power intensity and spike height can be controlled by the gas mixture, partial and total pressures, cavity length and the output mirror reflectivity. It has been shown that the effect of CO on the laser output parameters are very important. The extent of this effect has been examined in several gas mixtures where CO was added intentionally as a substitute for both helium and nitrogen. The theoretical predictions have shown that addition of small amounts of CO to the gas mixture improves the laser performance due to its effect on the population and relaxation processes of excited states and on the gas temperature. Experimental verification of theoretical predictions have just started.

Experimental investigations of the gas discharge operation have been carried out (chapter 5). It has been shown that the operating value of E/N for a glow discharge is strongly dependent on the gas mixture. This is an

indication for the need to examine the extent of gas impurity effects. Excellent agreement has been found between the theoretically predicted and the experimentally evaluated discharge parameters. The extent of the effects of CO on the discharge operating characteristics has been examined and the beneficial effects of the addition of small amounts of CO has been verified. The results obtained have shown that large amounts of added CO have a harmful effect on the operating characteristics of the discharge ; verifying the theoretical predictions from both the simulation of the discharge parameters and the simulation of the laser output parameters.

6.2 SUGGESTIONS FOR FUTURE WORK:

The simulation of the gas discharge can be extended to analyse the discharge initiation process and to predict the 'V-I' characteristics of the discharge. This can be dealt with by a model which considers the space charge effects on the electric field. The electron energy distribution function would have to be evaluated at each time and distance step since the electric field is nonuniform throughout the electrode gap. This model would allow the incorporation of actual excitation pulses in both : simulation of the discharge plasma chemistry,and prediction of the laser output parameters. The major draw-back with this full simulation of the laser system is the very large computing time required. However, a model for simulation of discharge initiation is under development.

Although the present work gives a detailed insight into the mechanisms occuring within the discharge,the complexity of these mechanisms still makes it necessary to examine the scale of discharge instability and its relationship to various operating parameters in order to minimise the adverse effects. Thermal instability and the effects of O_2 and H_2O on the EEDF,electron transport parameters and plasma parameters would have to be considered. Their influence on the operating characteristics can be predicted and verified experimentally using a hetrogeneous catalyst (Pt-Rh coated alumina spheres and/or SnO_2-Pd catalyst). Furthermore, the effects of O_2 and H_2O must be included in the rate equations that govern the molecular kinetic processes in the laser gas mixture. However,the necessary data on the rate constants of energy transfer processes involving these species with N_2 and CO_2 is not fully available in the literature.

Experimental work is needed to verify the theoretical predictions of the CO_2 dissociation products by using spectroscopic technique or mass spectrometric analysis. Furthermore, the effects of dissociation products on the laser output parameters need to be experimentally examined.

APPENDIX 2.I

ELEMENTARY PROCESSES IN CO_2 LASERS

A2.I.1 Excitation processes :

In thermal equilibrium , the population of different energy levels in the gas is controlled by Boltzmann's distribution.The molecules are excited by collision processes within the gas discharge causing the population to depart from equilibrium. The dominant processes which cause the population of the low lying vibrational energy levels are:

(1) collisions of the first kind.

(2) collisions of the second kind.

(3) resonance trapping.

(1) Collisions of the first kind:

This is the important process by which molecules in the gas discharge get excited.It involves inelastic collisions between moving electrons and ground state molecules.When an electron with kinetic energy equal to or greater than the potential energy of an excited state of the gas molecule, collides with the molecule, it looses kinetic energy equal to the potential energy of the molecule's excited state and leaves the molecule in an excited state.This can be represented by:

$$e\ (fast) + molecule \longrightarrow excited\ molecule + e\ (slow)$$

This process is responsible for direct excitation of N_2 and CO_2 molecules,which can be written as:

$$N_2(v=0) + e \text{ (fast)} \longrightarrow N_2(v=1) + e \text{ (slow)}$$

$$CO_2(00°0) + e \text{ (fast)} \longrightarrow CO_2(00°1) + e \text{ (slow)}$$

The reverse process can also occur, when the excited molecule looses energy to the electron and the electron gains en equal amount of kinetic energy.This is referred to as a superelastic collision and can be represented by:

excited molecule + electron $\longrightarrow$ fast electron + molecule

The rates of these processes depend on the collision cross sections of a particular transition and on electron energy distribution in the gas discharge.

(2) Collisions of the second kind:

In these processes an excited molecule collides with a molecule in the ground state, hence energy is transformed from the excited molecule to the ground state one.This can be represented by:

excited molecule A + molecule B

$\longrightarrow$ excited molecule B + molecule A

These collisions are very important in CO_2 lasers where a large proportion of the excitation of the upper laser level takes place via collisions between ground state CO_2 molecules and excited N_2 molecules as:

$$N_2(v=1) + CO_2(00°0) \longrightarrow CO_2(00°1) + N_2(v=0) - 18 \text{ cm}^{-1}$$

The rate of this process is 1.9×10^4 $Torr^{-1}.sec^{-1}$. at 300°K.

(3) Resonance trapping:

In this process of excitation an excited molecule releases a quantum of energy (light) which is absorbed by another molecule leaving it in an excited state.

A2.I.2 Emission and Absorption Processes:

When the gas molecule in the lower laser energy level is exposed to radiation, it will absorb a photon and be excited to the upper laser level.This process is reffered to as stimulated absorption and shown in figure (A2.I.1 a).

Very soon after being excited to the higher energy level the molecule will emit a photon and return to the lower level.The emission process can occur in two distinct ways, it can be stimulated or it can occur entirely spontaneously as illustrated in figures (A2.I.1 b and A2.I.1 c).

There are two very important points concerning stimulated emission upon which the properties of the laser light depend.Firstly the photon produced by stimulated emission has the same energy as the stimulating photon and hence the associated light waves must have the same frequency.Secondly the light waves associated with the two photons travel in the same direction are in phase and have the same state of polarization.This means that if a molecule is stimulated to emit light energy the wave representing the stimulated photon adds to the incident wave constructively , thereby increasing its amplitude.In the laser medium ,as the

number of molecules in higher energy levels of the transition are far greater than the lower levels , there are more molecules available for stimulated emission than there are available for absorption .Therefore, stimulated emission is observed as a dominant process.

In spontaneous emission the molecules emit in an entirely random way such that there is no phase or directional relationship between the waves. The light emitted spontaneously at various points in the laser medium is amplified through stimulated emission.Since frequency, phase and direction are preserved in a stimulated emission process,light initially emitted normal to the end mirrors (one at each end of the laser cavity) and within the resonant modes of the system, increases in intensity.Once the gain in one pass between the mirrors is more than the losses ,the intensity in the mode begins to build up until the optical field is strong enough to compete with the spontaneous decay for other molecules whose centre frequencies are within the natural width of the mode.Thus,as the gain in the medium is made to compensate for the loss, molecules within the characteristic frequency range switch from random spontaneous emission to a forced stimulated emission in a particular resonant mode of the system,i.e. in a particular direction and at a particular frequency, i.e laser action takes place.

A2.I.3 The Vibrational Energy Levels in CO_2 :

The CO_2 molecule has three different vibrational levels of importance for laser action , as shown in figure (2.1), these are: the symmetric mode (1388.3 cm^{-1}) , the doubly degenerate bending mode (667.3 cm^{-1}) vibrating in the plane of the paper and perpendicular to it, and the asymmetric mode (2349.3 cm^{-1}).

The vibrational levels are normally designated by three numbers representing the number of vibrational quanta of each mode associated with the levels and written in the order $\nu 1, \nu 2$ and $\nu 3$.

As well as vibrating , the whole molecule can rotate about its centre of mass.The fundamental rotational energy quanta are much smaller than the vibrational quanta and as a result the vibrational energy levels are split into a number of closely spaced rotational sub-levels. Figure (A2.I.2) shows the energy-level diagram of CO_2 and N_2.

Figure (A2.I.3) shows the scheme of lower vibrational levels of the electronic ground state of CO_2 molecule and the population distribution among the rotational levels belonging to each vibrational level, as shown in reference [2.21].The figure also illustrates the energy kT_{gas} of the thermal motion of molecules, and the position of the first vibrational level of the nitrogen molecule.

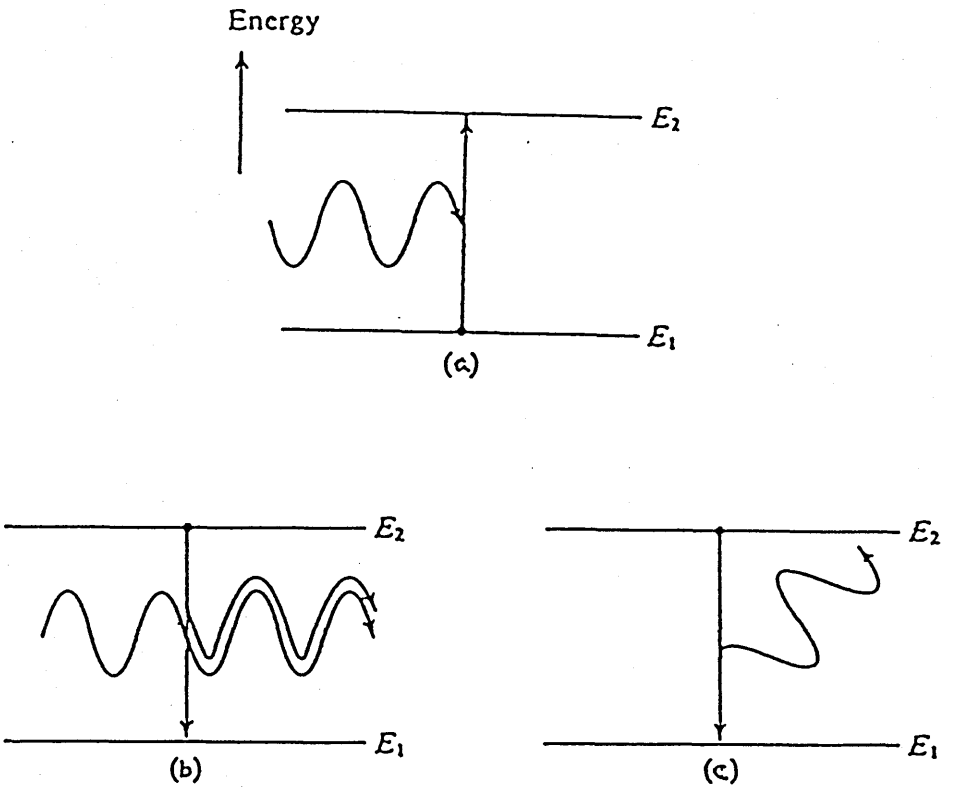

Energy-level Diagram

(a) stimulated absorption (b) stimulated emission (c) spontaneous emission .The black dot indicates the energy state of the molecule before the absorption or emission event

FIGURE (A2.I.1)

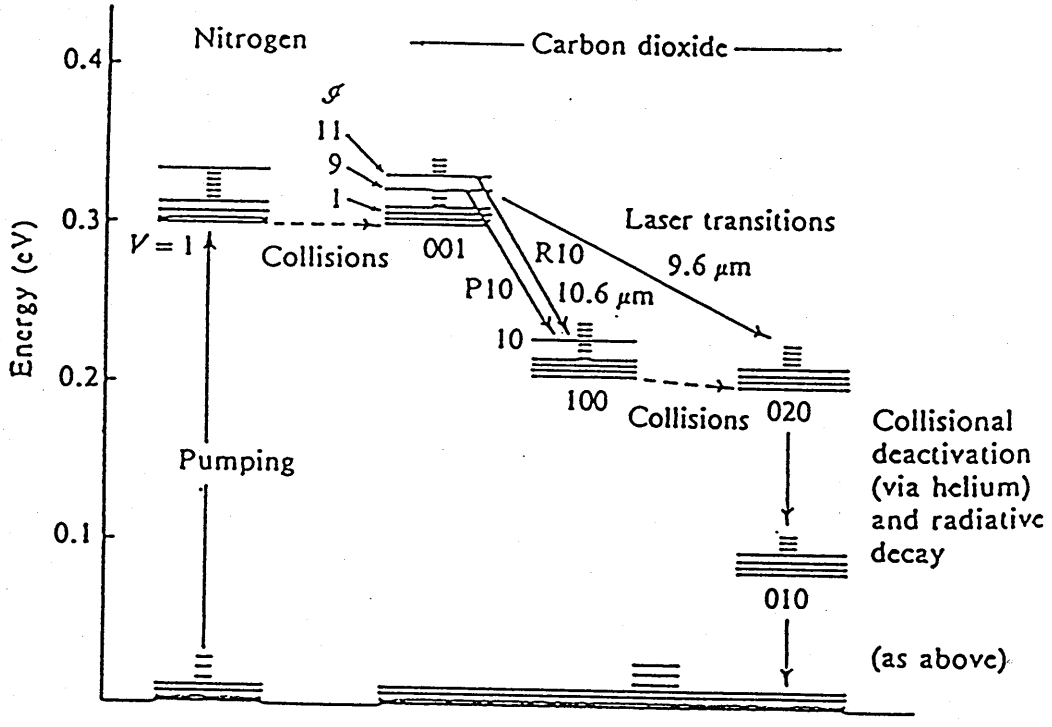

Simplified Energy Level Diagram for CO_2 Laser

Each vibrational level has many rotational levels associated with it. J =1,2, etc.The letters P and R represent transitions where J changes by + 1 and - 1 respectively

FIGURE (A2.I.2)

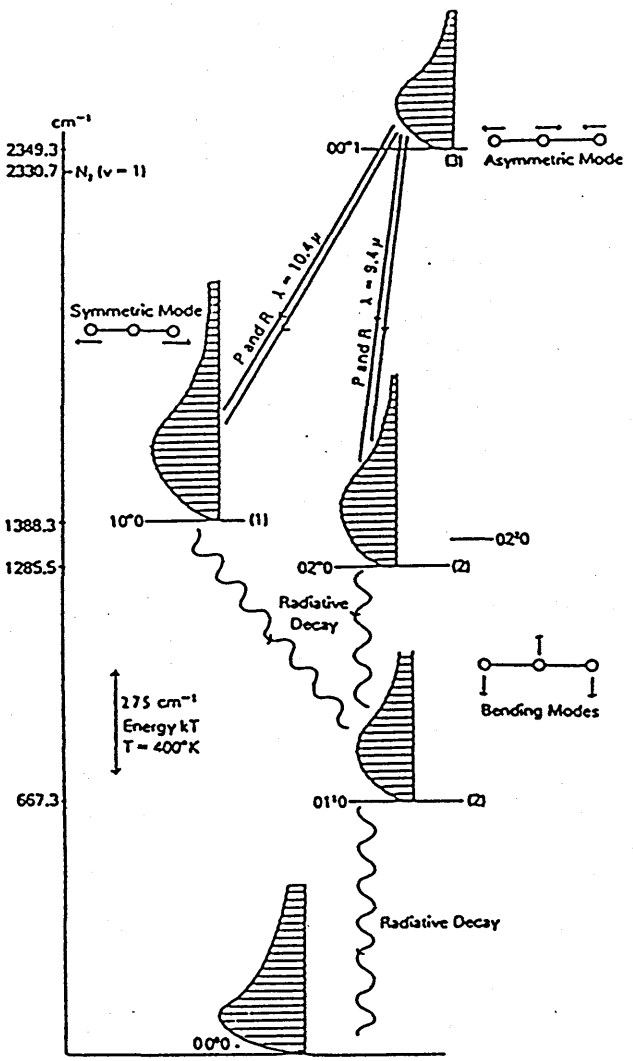

Lower vibrational levels of the electronic ground state of CO_2. Vibrational levels are designated by v_1, v_2^l, v_3, where $l = v_2, v_2-2, \ldots, 0$ for even v_2, and $l = v_2, v_2-2, \ldots, 1$ for odd v_2. The populations of the rotational substates of the vibrational states are indicated by the lengths of the lines specifying the rotational states. Dipole transitions of CO_2 satisfy $\Delta J = \pm 1$, where ΔJ is the change in rotational quantum number, corresponding to the observed R and P branches of the emission spectrum. The lines are designated $P(J)$ or $R(J)$, where J is the rotational quantum number of the lower level.

FIGURE (A2.I.3)

Appendix (2.II)

RELAXATION PROCESSES IN CO_2

A2.II.1 Relaxation of the 01^10 level:

Relaxation of this level is very important for the CO_2 laser since it basically limits population inversion densities associated with the 00^01 -10^00 and 00^01-02^00 laser transitions.Relaxation of the 01^10 level by collision with He,CO_2,CO, and N_2 may be written as:

$$CO_2(01^10) + M \xrightarrow{k} CO_2(00^00) + M + 667\ cm^{-1}$$

where M is a gas molecule in the mixture,

k rate constant in $Torr^{-1}.Sec^{-1}$

and at 300°K k for M=CO_2 is 194 $Torr^{-1}.Sec^{-1}$,

k for M=He is 3.27 X 10^3 $Torr^{-1}.Sec^{-1}$,

k for M=CO is 2.5 x 10^4 $Torr^{-1}.Sec^{-1}$,and

k for M=N_2 is 650 $Torr^{-1}.Sec^{-1}$ [A2.II.1].

It should be noted that CO can relax the 01^10 level of the CO_2 molecule very effectively. Although helium is less efficient in deactivating the 01^10 level ,it yields the highest gain compared with any other single gas additives because the addition of a large amount of helium does not affect the upper laser level, whereas it strongly reduces the 10^00 level relaxation time,[A2.II.2].

A2.II.2 Relaxation of the 00°1 level :

This is a very important process since the upper laser level is coupled to the lower laser level by collisions and by stimulated emission, as:

$$CO_2(00°1) + M \xrightarrow[k]{\text{collisions}} CO_2(v1,v2,0) + M + Et$$

and

$$CO_2(00°1) \xrightarrow[k]{\text{stimulation}} CO_2(10°0) \text{ or } CO_2(02°0) + h\nu$$

where

M gas molecule in the system,

Et translation energy,

hν radiation given out due to stimulated emission,

k rate constant in $Torr^{-1}.Sec^{-1}$.

Cheo [A2.II.3] gives some relaxation rate constants of $CO_2(00°1)$ in various gas mixtures at 300°K and these are:

for $M=CO_2$ k =367 $Torr^{-1}.Sec^{-1}$,

for $M=N_2$ k =110 $Torr^{-1}.sec^{-1}$,

for M=He k =67 $Torr^{-1}.sec^{-1}$,and

for M=CO k =193 $Torr^{-1}.sec^{-1}$.

It can be seen from these values that population of the upper laser level is relatively unaffected upon addition of a large amount of He.

A2.II.3 Relaxation of the $10^{0}0$ and $02^{0}0$ levels:

The two mixed states $(10^{0}0,02^{0}0)'$ and $(10^{0}0,02^{0}0)''$ are in Fermi resonance can decay to the $01^{1}0$ level through resonant processes such as :

$$CO_2(10^{0}0,02^{0}0)' + CO_2(00^{0}0) \xrightarrow{k} 2CO_2(01^{1}0) - 50\ cm^{-1}$$

$$CO_2(10^{0}0,02^{0}0)'' + CO_2(00^{0}0) \xrightarrow{k} 2CO_2(01^{1}0) + 52\ cm^{-1}$$

Values of the effective rate constant k of CO_2 in various gas mixtures are given in Ref[A2.II.1],and these are:

for CO_2 $k=2.2 \times 10^{3}$ $Torr^{-1}.Sec^{-1}$,

for N_2 $k=26$ $Torr^{-1}.sec^{-1}$,

for He $k=4.7 \times 10^{3}$ $Torr^{-1}.sec^{-1}$, and

for CO $k=4.1 \times 10^{3}$ $Torr^{-1}.sec^{-1}$ at 300°K.

REFERENCES

APPENDIX 2.II

A2.II.1 Levine A K - ' A Series of advances in lasers '-, Vol 3,Chap(II) , Marcel Dekker Inc. , New York , 1971.

A2.II.2 Cheo P K -'Effects of CO_2,He and N_2 on the lifetime of the 00°1 and 10°0 CO_2 laser levels and on pulsed gain at 10.6 μ'- J.Appl.Phys.,Vol 38, 1967 (3563).

A2.II.3 Cheo P k -'Relaxation of the 10.6 μ CO_2 laser levels by collisions with H_2 '- Appl. Phys. Lett., Vol 11 ,1967 (38) ;IEEEJ.QE., Vol 4 , 1968(587).

APPENDIX 2.III

EXCITATION

AND RESONANCE ENERGY TRANSFER PROCESSES IN CO

A2.III.1 Direct excitation of CO :

This can be written as:

$$CO(v=0) + e\ (fast) \longrightarrow CO^{-} \longrightarrow CO(v=1) + e\ (slow)$$

This reaction which proceeds via a negatively charged state has a large cross section (in the region of 10^{-16} cm^2 for electrons of about 2 eV energy) as shown in figure (A2.III.1). By comparing this with total cross sections for $N_2(v=1-8)$, as shown in figure(2.3) ,it can be seen that for CO the cross section is broader and has a maximum at about 0.5 eV lower in energy .Hence ,more CO (v=1) molecules are formed in the discharge and available for transferring their vibrational energy to CO_2 molecules. The rate constants for direct excitation of CO have been reported by Pivovar and Leonov [A2.III.2] and these are found to have maximum values at an average energy in the range $0.5 < \bar{U} < 1.5$ eV which falls off slowly with increasing $\bar{U}$.

A2.III.2 Resonance energy transfer :

This is an important process as it involves the transfer of the vibrational energy of excited CO molecules to the upper laser level $CO_2(00°1)$. It can be represented as:

$$CO(v=1) + CO_2(00°0) \longrightarrow CO(v=0) + CO_2(00°1) - 206\ cm^{-1}$$

Cheo [A2.III.3] gives a value of 1.38×10^3 $Torr^{-1}.Sec^{-1}$ at 300°K for the rate constant of this process. Smith and Thomson [A2.III.4] give a more general (i.e temperature dependent) formula for calculating k.At 300° K, $k=3.2 \times 10^3$ $Torr^{-1}.sec^{-1}$. Starr and Hancock [A2.III.5] have measured the rate k at temperatures from 163°K to 406°K ,a value of 2.35×10^3 $Torr^{-1}.Sec^{-1}$ has been given at 301°K.

The resonance energy transfer between N_2 and $CO_2(00°1)$ can be written as:

$$N_2(v=1) + CO_2(00°0) \longrightarrow N_2(v=0) + CO_2(00°1) - 18\ cm^{-1}$$

The rate constant is given by Cheo [A2.III.3] as equal to 1.9×10^4 $Torr^{-1}.Sec^{-1}$. Although this process is more efficient than that for CO molecules,CO can be expected to be both an alternative pumping channel and a vibrational energy reservoir.

REFERENCES

APPENDIX 2.III

A2.III.1 Haddad G N and Milloy H B -'Cross sections for electron-carbon monoxide collisions in the range 1-4 eV '- Aust. J. Phys.,Vol 36, 1983 (473).

A2.III.2 Pivovar VA and Leonov SN -'Rate constants for stepwise excitation of vibrational levels of carbon monoxide by electron impact'- Sov. Phys. Tech. Phys., Vol 22 ,1977 (206).

A2.III.3 Levine AK - ' A Series of advances in lasers ', Vol 3,Chap(II),Marcel Dekker Inc., New York, 1971.

A2.III.4 Smith K and Thomson RM -'Computer Modelling of Gas Lasers'-, Plenum Press, New York, 1978.

A2.III.5 Starr DF and Hancock JK -'Vibrational energy transfer in CO_2-CO mixtures from 163° to 406° K'-J. Chem. Phys.,Vol 63,1975 (4730).

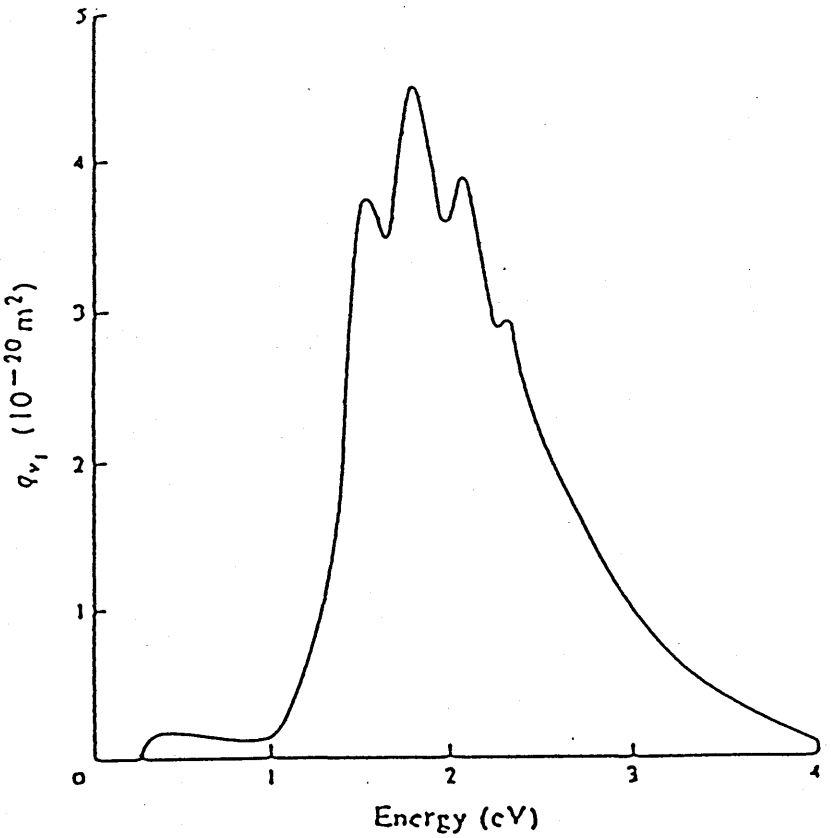

Cross Sections for Vibrational Excitation of CO

by Electron Impact [2.III.1]

FIGURE (A2.III.1)

APPENDIX 2.IV

ELECTRON ENERGY DISTRIBUTION

The behavior of electrons in the electrical discharge is of particular importance because most of the energy transferred from the electrical field is acquired by fast-moving electrons. The electron swarm can be described by its phase-space distribution function through the Boltzmann's transport equation which can be represented by the Legendre series expansion,[A2.IV.1] :

$$f(\bar{r},\bar{v},t) = \sum_{k=0}^{\infty} f_k(\bar{r},v,t)\, P_k(\cos\theta) \qquad \ldots\ldots\ldots\ldots(1)$$

where

$\bar{r}$ and $\bar{v}$ are position and velocity vectors,

t is time, and

$\theta=0$ is in the direction of the electric field.

The electron energy distribution function can be separated into two parts: a large isotropic part, $f_o(\bar{r},v,t)$, and a small anisotropic part, $f_1(\bar{r},v,t)$ which is the first higher order expansion term of $f_k(\bar{r},v,t)$. Numerical calculations of the electron energy distribution function for conditions usually encountered in CO_2 lasers start from the Boltzmann transport equation for the isotropic part f_o of the distribution function. These calculations are based on the following assumptions:

(1) The discharge is set up between infinite parallel electrodes.

(2) The dimensions of the discharge region are large as compared to the mean free path for all types of collisions.

(3) The gas is weakly ionised ; i.e the density of excited molecules is small and therefore , the electron-electron and electron-ion collisions are unimportant.

(4) The electron energy distribution is almost spherically symmetric.

(5) The inelastic collision cross-sections are small with respect to the elastic cross-sections, i.e the electrons lose only a small fraction of their energy upon collisions with neutral particles.

The first basic assumption of the conventional theory of electron transport in a gas in an electric field is that of truncating equation (1) by writing that

$f_k(\bar{r},v,t) = 0$ for $k \geq 2$

therefore, only the first- and zeroth-order terms are retained in the expansion. This so called two-term expansion adequately describes conditions corresponding to a slight degree of anisotropy(i.e low E/N),[A2.IV.2].

The second basic assumption in transport calculations is that of writing $f(\bar{r},\bar{v},t)$ as a separable product of density and velocity distributions, [A2.IV.1],that is

$$f(\bar{r},\bar{v},t) = n_e(\bar{r},t)\ \{f_0(\bar{r},v,t) + f_1(\bar{r},v,t)\} \quad \ldots\ldots\ldots(2)$$

where

$$n_e(\bar{r},t) = \int_0^\infty f_0(r,v,t)\ dv$$

In spatially uniform gas, the distribution function depends on velocity only, i.e

$$f(\bar{v},t) = n_e(t)\ \{f_o(v,t) + f_1(v,t)\} \qquad \ldots\ldots\ldots\ldots(3)$$

By introducing the kinetic energy of electrons

$u=(1/2)mv^2$,so that

$$\partial/\partial v = (\partial u/\partial v)(\partial/\partial u) = mv(\partial/\partial u)$$

hence, equation (3) can be written as,[A2.IV.3] :

$$(E^2/3)[\partial/\partial u\{(u/NQ_m)(\partial f_o/\partial u)\} + (2m/M)\{\partial/\partial u(u^2 NQ_m f_o)\}$$
$$+ (2mkT/Me)\{\partial/\partial u(u^2 N Q_m \partial f_o/\partial u)\}$$
$$+ \sum_j [(u+u_j)f_o(u+u_j)N_o Q_j(u+u_j) - uf_o(u) N_o Q_j(u)]$$
$$+ \sum_j [(u-u_j)f_o(u-u_j)N_o Q_{-j}(u-u_j) - uf_o(u) N_j Q_{-j}(u)]$$
$$= (mu/2e)^{1/2}\ \partial f_o/\partial t \qquad \ldots\ldots\ldots\ldots(4)$$

For a mixture of gases, equation (4) can be written as :

$$(E^2/3)[\partial/\partial u\{u(\textstyle\sum_n N_n Q_m^n)^{-1}(\partial f_o/\partial u)\}] + 2m\partial/\partial u[u^2\{\textstyle\sum_n N_n Q_m^n$$
$$/M_n\}f_o] + (2mkT/e)\partial/\partial u[u^2\{\textstyle\sum_n N_n Q_m^n/M_n\}\partial f_o/\partial u]$$
$$+ \sum_j \sum_n [\{(u+u_{jn})f_o(u+u_{jn})N_n Q_j^n(u+u_{jn})\} - \{uf_o(u)NQ_j^n(u)\}]$$
$$+ \sum_j \sum_n [\{(u-u_{jn})f_o(u-u_{jn})N_{nj} Q_{-j}^n(u-u_{jn})\}$$
$$-\{uf_o(u)N_{nj}Q_{-j}^n(u)\}] = (mu/2e)^{1/2}\ \partial f_o/\partial t \qquad \ldots\ldots(5)$$

For molecular gas discharge conditions (such as that encountered in CO_2 lasers) ,electron energy relaxation is very fast (10^{-9} -10^{-8}) sec owing to the large electron molecule vibrational excitation rates. Hence,the electron energy and density respond in a quasi-steady fashion in the 10^{-7} -10^{-5} sec time range required for a change in charged particle properties. Thus, the time derivative term in equation (5) can be neglected,[A2.IV.4].

By defining δ_n as the fractional concentration of the nth species and $\delta^n{}_j$ as the fractional concentration of the jth vibrational level of species n:

$$\delta_n = N_n/N \quad , \quad \delta^n{}_j = N_{nj}/N$$

and dividing through by N, equation (5) becomes:

$$(1/3)(E/N)^2 d/du\{(udf(u)/du)/\Sigma_n \delta_n Q^n{}_m(u)\}$$
$$+ 2md/du \{u(\Sigma_n (\delta_n Q^n{}_m(u)/M_n) f(u)\}$$
$$+(2mk_bT/e)d/du\{u^2(\Sigma_n(\delta_n Q^n{}_m(u)/M_n))df(u)/du\}$$
$$+ \Sigma_j \Sigma_n \{(u+u_n)f(u+u_{jn})\delta_n Q^n{}_j(u+u_n) - uf(u)\delta_n Q^n{}_j(u)\}$$
$$+ \Sigma_j \Sigma_n \delta^n{}_j\{(u-u_{jn})f(u-u_{jn})\delta_n Q^n{}_{-j}(u-u_{jn}) - uf(u)\delta_n Q^n{}_{-j}(u)\}$$
$$= 0 \qquad \text{.....(6)}$$

The distribution function f(u) is normalised such that the fraction of electrons between energy u and u+du is given by $u^{1/2} f(u)$, hence:

$$\int_0^\infty u^{1/2} f(u)\, du = 1$$

REFERENCES

APPENDIX 2.IV

A2.IV.1 Briglia G L and Romano L - ' Monte Carlo and Boltzmann Two-Term Calculations of Electron Transport in CO_2 ' - Lettere Al Nuovo Cimento, Vol. 40, No. 17, 1984 (513) .

A2.IV.2 Wedding A B - ' Electron swarm parameters in a CO_2 - N_2 -He -CO gas mixture '- J. Phys. D: Appl. Phys. ,18, 1985 (2351) .

A2.IV.3 Smith K and Thomson R M -'Computer Modelling of Gas Lasers'- Plenum Press, New York, 1978.

A2.IV.4 Nighan W L,Wiegand W J,and Haas R A -'Ionisation instability in CO_2 laser discharges '- Appl. Phys. Lett. , Vol 22, 1973 (579) .

APPENDIX (4.I)

ENERGY TRANSFER RATE CONSTANTS

A4.I.1 Collisional Relaxation :

For the important energy transfer processes shown in figure (4.1),the following rate values were obtained from literature:

(i) for relaxation of the $CO_2(01^10)$ level the rate constant is:

$$K_{320}=(K_{CO2} + K_{N2} + K_{He} + K_{CO})x9.657x10^{18}/T \quad ....(A4.I.1)$$

where:

$$K_{CO2} = 6.0x10^{-10}exp(-77/T^{1/3})\ P_{CO2} \quad .....(A4.I.2a)$$

$$K_{N2} = 1.23x10^{-10}exp(-77/T^{1/3})\ P_{N2} \quad .....(A4.I.2b)$$

and

$$K_{He} = 8.4x10^{-11}exp(-45/T^{1/3})\ P_{He} \quad .....(A4.I.2c)$$

are given by Byabagambi [A4.I.1].

For carbon monoxide,K_{CO} is given by Smith and Thomson [A4.I.2] as :

$$K_{CO} = 6.82x10^{-8}exp(-77/T^{1/3})\ P_{CO} \quad .....(A4.I.3)$$

(ii) for relaxation of the upper laser level(00°1), the rate constant is:

$$K_{132} = (K_{CO2} + K_{N2} + K_{He} + K_{CO})x9.657x10^{18}/T \quad ..(A4.I.4)$$

where:

$$K_{CO_2}=6.38X10^{-18}\ \exp(-83/T^{1/3})\ P_{CO_2} \quad ...(A4.I.5a)$$

$$K_{N_2}=1.38X10^{-11}\ \exp(-55.6/T^{1/3})\ P_{N_2} \quad ...(A4.I.5b)$$

and

$$K_{He}=5.07x10^{-10}\ \exp(-83/T^{1/3})\ P_{He} \quad ...(A4.I.5c)$$

are given by Byabagambi [A4.I.1].

For carbon monoxide, the temperature dependence of K_{CO} was obtained from Rosser et al [A4.I.3] where the rate constant is proportional to the exponential of the temperature, hence an equation of the form

$$K = a\ \exp(-b/T^{1/3})$$

is assumed and the constants a and b determined by a least square fit to the data. Thus, K_{CO} is given as:

$$K = 1.94x10^{-13}\ \exp(-21.5/T^{1/3})\ P_{CO} \quad ....(A4.I.6)$$

(iii) due to lack of data, the temperature dependence of the rate constants K_{2131} and K_{2231} was neglected and the values used by Byabagambi [A4.I.1] and Chatwin [Reference 4 in chapter 4] were adopted. Thus,

$$K_{2131} = 6 \times 10^5\ P_{CO_2} \quad .....(A4.I.7)$$

$$K_{2231} = 5.15 \times 10^5\ P_{CO_2} \quad .....(A4.I.8)$$

The factor $(9.657x10^{18}/T)$ was used to convert equations (A4.I.1) and (A4.I.4) into units of $Torr^{-1}.sec^{-1}$ [A4.I.1].

A4.I.2 Resonant Energy Transfer :

Resonant energy transfer process occurs when excited molecules collide with ground state molecules.This process is very important for the excitation of the upper laser level where excited N_2 molecules collide and excite ground state CO_2 molecules as follows:

$$N_2(v=1) + CO_2(00°0) \underset{K_{15}}{\overset{K_{51}}{\rightleftharpoons}} N_2(v=0) + CO_2(00°1) - 18\ cm^{-1} \quad .....(A4.I.9)$$

A similar process takes place when excited CO molecules collide and excite ground state CO_2 molecules as follows:

$$CO(v=1) + CO_2(00°0) \underset{K_{17}}{\overset{K_{71}}{\rightleftharpoons}} CO(v=0) + CO_2(00°1) - 206\ cm^{-1} \quad .....(A4.I.10)$$

In describing these processes, the following values of rate constants given by Byabagambi [A4.I.1] were used:

$$K_{15}=9.657x10^{18}\ exp(-10.7/T^{1/2})\ P_{N2}/T \quad .....(A4.I.11)$$

$$K_{51}=9.657x10^{18}\ exp(-10.7/T^{1/2})\ P_{CO2}/T \quad .....(A4.I.12)$$

For carbon monoxide, the following values of K_{17} and K_{71} were used,

$$K_{17}=1.56x10^{-11}\ exp(-30.1/T^{1/3})x9.657x10^{18}xP_{CO}/T \quad (A4.I.13)$$

$$K_{71}=1.56x10^{-11}\ exp(-30.1/T^{1/3})x9.657x10^{18}xP_{CO}/T \quad (A4.I.14)$$

Moreover,excited CO molecules collide and excite ground state N_2 molecules as follows:

$$CO\ (v=1) + N_2(v=0) \longrightarrow CO\ (v=0) + N_2(v=1) - 187\ cm^{-1} \quad .....(A4.I.15)$$

The rate constant for this process is given as:

$$K_{75}=6.98x10^{-13}\ exp(-25.6/T^{1/3})x9.657x10^{18}xP_{N2}/T \quad (A4.I.16)$$

The temperature dependence of the rate constants for these processes was obtained from Smith and Thomson [A4.I.2].

REFERENCES

APPENDIX (4.1)

A4.I.1 Byabagambi C A - ' Surface Heating in Metals Irradiated by Fast I.R. Laser Pulses ' - Ph.D Thesis , University of Glasgow , 1987.

A4.I.2 Smith and Thomson R M -'Computer Modelling Of Gas Lasers ' - Plenum Press , New York , 1978.

A4.I.3 Rosser W A ,Sharma R D,and Gerry E T -'Deactivation of Vibrationally Excited Carbon Dioxide (00°1) by Collisions with Carbon monoxide ' - J. Chem. Phys. , Vol 54 , 1971 (1196) .

APPENDIX (4.II)

DERIVATION OF THE ABSORPTION COEFFICIENT

A4.II.1 NOMENCLATURE :

n	molecular population (molecules/cm^3).
P_o	total pressure (Torr).
T	temperature (°K).
k	Boltzmann constant =1.38026x10^{-23} (J/°K).
τ_{sp}	radiative lifetime (sec).
σ	absorption coefficient (cm^2).
λ	transition wavelength (cm).
Θ_r	characteristic temperature (°K).
l	rotational quantum number.
α_{N2}	pressure ratio =P_{N2}/P_{CO2} .
V	velocity ratio =$\langle v_{ij} \rangle / \langle v_{jj} \rangle$.
m	molecular weight (kg/kmole).
γ_c	collision frequency (sec^{-1}).
i	species identification (CO_2,N_2,He,CO) .
N_o	Avogadro's number =6.025x10^{26} (molecules/kmole).
σ'	optical broadening collision cross section (cm^2).

A4.II.2 DERIVATION :

The population of species (i) is expressed according to the equation of state for an ideal gas as:

$$n_i = P_i/kT \qquad \text{.....(A4.II.1)}$$

and total pressure for the gas mixture as:

$$P_o = \Sigma P_i = P_{co2}[1+(P_{N2}/P_{co2})+(P_{He}/P_{co2})+(P_{co}/P_{co2})]$$

or $$P_o = P_{co2}[1 + \alpha_{N2} + \alpha_{He} + \alpha_{co}] \qquad \text{.....(A4.II.2)}$$

The absorption coefficient at the line centre for the P(20) transition line can be expressed as:

$$\sigma = (\lambda^2/4_{\Pi}\, \tau_{sp}\, \nu_c) \times (RP) \qquad \text{.....(A4.II.3)}$$

where RP is the rotational population term for the translational-rotational energy transfer process [reference A4.II.1] . The absorption coefficient is that of high pressure (P>10 Torr) collision-broadening where the spectral line of absorption can be approximated by purely homogeneous lineshape function (Lorentz or collisional) , [references A4.II.2 and A4.II.3].

The collision frequency is given by:

$$\nu_c = [\{8kTN_o/_{\Pi}(\tfrac{1}{2}m_{co2})\}^{1/2}\, n_j\sigma_j'\Sigma\, (n_i\sigma_i'\langle v_{ij}\rangle/n_j\sigma_j'\langle v_{jj}\rangle)] \qquad \text{.....(A4.II.4)}$$

The rotational population are given by:

$$n_l/n = [\{2(2l+1)/(T/\Theta_r)\}\, \exp\{-l(l+1)(\Theta_r/T)\}] \qquad \text{...(A4.II.5)}$$

By differentiating equation(A4.II.5) for optimum l:

$$l_{opt.} = \tfrac{1}{2}[(2T/\Theta_r)^{1/2} - 1]$$

and substituting this value into equation (A4.II.5):

$$n_l/n = [\{2^{3/2}/(T/\Theta_r)^{1/2}\}\, \exp(-\tfrac{1}{2}+\tfrac{1}{4}\Theta_r/T) \qquad \text{.....(A4.II.6)}$$

so the populations in the upper laser level (n_{001}) and the lower laser level (n_{I+II}) are expressed in terms of the

vibrational level populations.The lower laser level is designated as (n_{I+II}) to show the Fermi resonance of (10°0,02°0)'≈(10°0,02°0)" levels (see figure 4.1).

The lasing transition populations are:

$$n_2=n_{001}[\{2^{3/2}/(T/\Theta_r)^{1/2}\}\exp(-\tfrac{1}{2}+\Theta_r/T)] \quad ...(A4.II.7\ a)$$

and

$$n_1=n_{I+II}[\{2^{3/2}/(T/\Theta_r)^{1/2}\}\exp(-\tfrac{1}{2}+\Theta_r/T)] \quad ...(A4.II.7\ b)$$

Expanding the exponential terms in equqtions (A4.II.7 a and A4.II.7 b) as a binomial series, the populations become:

$$n_2=n_{001}[\{2^{3/2}/(T/\Theta_r)^{1/2}\}\exp(-\tfrac{1}{2}) \quad .....(A4.II.7\ c)$$

$$n_1=n_{I+II}[\{2^{3/2}/(T/\Theta_r)^{1/2}\}\exp(-\tfrac{1}{2}) \quad .....(A4.II.7\ d)$$

Factoring the rotational occupancy term out and including this into equation (A4.II.3) and considering equations (A4.II.1),(A4.II.2) and (A4.II.4) , the absorption coefficient becomes:

$$\sigma=[\{(\lambda^2/4\pi\tau_{sp})(2^{3/2}\exp(-\tfrac{1}{2}))\}/\{(8kTN_o/\pi(\tfrac{1}{2}m_{CO2}))^{1/2}n_{CO2}\sigma'_{CO2}(1+\alpha_{N2}\sigma^{\sim}_{N2}V_{N2}+\alpha_{He}\sigma^{\sim}_{He}V_{He}+\alpha_{CO}\sigma^{\sim}_{CO}V_{CO})(T/\Theta_r)^{1/2}\}] \quad .....(A4.II.8)$$

where:

$$V=\{(m_1+m_3)/2m_1\}^{1/2} \quad .....(A4.II.9)$$

$\sigma^{\sim}$= cross section ratio = σ'_1/σ'_3

$$\sigma'=\pi\{(\sigma_1+\sigma_3)/2\}^2=\pi[\tfrac{1}{4}\sigma^2+\tfrac{1}{4}\sigma^2_3+\tfrac{1}{2}\sigma_1\sigma_3]$$

$$=\pi\sigma^2_1[\tfrac{1}{4}(1+\sigma^2_3/\sigma^2_1+2\sigma_3/\sigma_1)]$$

$$=\sigma'_1[\tfrac{1}{4}\{1+\sigma'_3/\sigma'_1+2(\sigma'_3/\sigma'_1)^{1/2}\}] \quad ....(A4.II.10)$$

A4.II.3 EVALUATION :

m_{CO2} =44.011 (kg/kmole)

m_{N2} =28.016 (kg/kmole)

m_{He} =4.003 (kg/kmole)

m_{CO} =28.01 (kg/kmole)

λ =10.59 μm

The following values were obtained from [ref. A4.II.2]:

$\sigma'_{CO2}=5.7 \times 10^{-19}$ m^2

$\sigma'_{N2}=5.0 \times 10^{-19}$ m^2

$\sigma'_{He}=1.77 \times 10^{-19}$ m^2

$\sigma'_{CO}=5.6 \times 10^{-19}$ m^2

τ_{sp} =4.7 sec.

From equation (A4.II.9) , the velocity ratio for each species is:

$V_{N2} = \{(m_{N2}+ m_{CO2})/2m^2\}^{1/2} = (28.016+44.011/2x28.016)^{1/2}$

=1.1337821

$V_{He} = \{(m_{He}+ m_{CO2})/2m_{He}\}^{1/2} = (4.003+44.011/2x4.003)^{1/2}$

=2.4489287

$V_{CO} = \{(m_{CO}+ m_{CO2})/2m_{CO}\}^{1/2} = (28.01+44.011/2x28.01)^{1/2}$

=1.1338563

From equation (A4.II.10),the cross section ratio is:

$\bar{\sigma}_{N2} = \frac{1}{4}[1+(5/5.7)+2(5/5.7)^{1/2}] = 0.9375911$

$\bar{\sigma}_{He} = \frac{1}{4}[1+(1.77/5.7)+2(1.77/5.7)^{1/2}] = 0.6062561$

$\bar{\sigma}_{CO} = \frac{1}{4}[1+(5.6/5.7)+2(5.6/5.7)^{1/2}] = 0.9912086$

Substituting these values into equation (A4.II.8), the absorption coefficient becomes:

$$\sigma = [\{(10.59\times10^{-6})^2/4_{\pi}\times4.7\}\{2^{3/2}\ \exp(-\tfrac{1}{2})\}\{2^{1/2}\}] \ /$$
$$[\{(8\times1.38026\times10^{-23}\times6.025\times10^{26})/(_{\pi}\times44.011\times0.565)\}^{1/2} \times$$
$$\{n_{co_2}T\times5.7\times10^{-19}\}\{1+0.9375911\times1.1337821(n_{N_2}/n_{co_2}) +$$
$$0.606256\times2.4489287(n_{He}/n_{co_2}) + 0.9912086\times1.1338563$$
$$(n_{co}/n_{co_2})\}]$$

i.e,

$$\sigma =[692.456/n_{co_2}T\{\ 1 + 1.063(n_{N_2}/n_{co_2}) + 1.4846(n_{He}/n_{co_2})$$
$$+ 1.1238(n_{co}/n_{co_2})\}] \qquad \text{.....(A4.II.11)}$$

REFERENCES

APPENDIX 4.II

A4.II.1 Hoffman A L and Vlases G C -'A simplified model for predicting Gain,Saturation,and Pulse length for Gas Dynamics Lasers'- IEEE J.QE. ,8, 1972(46).

A4.II.2 Gerry E T and Leonard D A -'Measurement of 10.6μ CO_2 Laser Transition Probability and Optical Broadening Cross Sections'- Appl. Phys. Lett.,8 , 1966 (227).

A4.II.3 Shanmugasundaram V and Reddy N M - ' Theoretical gain optimization studies in CO_2-N_2 lasers III. Inclusion of line shape effects '- J.Appl.Phys., Vol 51 ,1980 (5615).